

## U.S. Department of Energy—Grand Junction, Colorado

## Calculation Cover Sheet

Calc. No. MOA-02-03-2006-4-07-00 Discipline: Geotechnical Properties No. of Sheets: 2

Project: Moab UMTRA Project

Site: Crescent Junction, Utah

Feature: Seismic Rippability Investigation

## Sources of Data:

## Sources of Formulas and References:

Hasbrouck Geophysics, Inc., 2005. *Crescent Junction Disposal Site Seismic Rippability Investigation*, Final Report, November.

Mac Lean, H. D., 2005. "Review of Seismic Rippability Investigation Report", November.

Preliminary Calc. ☐Final Calc. ☐

Supersedes Calc. No.

Author:

R. Heydenburg  
Name Date

Checked by:

Mark Hendley 6-9-06  
Name Date

Approved by:

Kurt Karp 6-13-06  
Name DateMark Hendley for Greg Lord 6-9-06  
Name DateK. H. St. 6/12/06  
Name DateP. H. Best 6/13/06  
Name Date

## **Problem Statement:**

Preliminary site selection performed jointly by the U.S. Department of Energy (DOE) and the Contractor has identified a 2,300 acre withdrawal area in the Crescent Flat area just northeast of Crescent Junction, Utah, as a possible site for a final disposal cell for the Moab uranium mill tailings. The proposed disposal cell would cover approximately 300 acres. Based on the preliminary site-selection process, the suitability of the Crescent Junction Disposal Site is being evaluated from several technical aspects, including geomorphic, geologic, hydrologic, seismic, geochemical, and geotechnical. The objective of this calculation set is to present results of the rippability investigation based on seismic refraction activities at the Crescent Junction Disposal Site.

This calculation will be used in the *Remedial Action Plan and Site Design for Stabilization of Moab Title I Uranium Mill Tailings at the Crescent Junction, Utah, Disposal Site* (RAP), and summarized in the appropriate sections of the Remedial Action Selection (RAS) Report for the Moab site.

## **Method of Solution:**

A refraction seismic survey was conducted along 10 seismic lines centered on existing boreholes at the Crescent Junction Site to assist in evaluation of suitability of the site for disposal of the Moab tailings. The purposes of the seismic surveys were to determine the seismic velocities of weathered and unweathered Mancos Shale deposits that underlie the site and relate those velocities to the rippability of the subsurface materials. The refraction seismic method is routinely used for rippability investigations. Data collection and analysis methods for this project were performed in accordance with the *Standard Guide for Using the Seismic Refraction Method for Subsurface Investigation* ASTM Designation: D 5777-00.

The Final Report of the *Crescent Junction Disposal Site Seismic Rippability Investigation* is in Appendix A and a review of this report is in Appendix B.

## **Assumptions:**

N/A

## **Calculation:**

N/A

## **Discussion:**

Seismic velocities and the thickness of layers underlying the proposed disposal cell to a depth of approximately 60 feet, produced by means of a refraction seismic survey, have been provided in the report. This information will be used to determine optimal and economic depths of excavation for construction of the disposal cell at the Crescent Junction Site. The suitability of selecting equipment based on the reported velocities should be based on the excavators experience with ripping machinery where seismic velocities are known. Data in this report will be used in making these determinations during the conceptual design phase of the disposal cell.

## **Conclusion and Recommendations:**

Use of this information in the conceptual design of the disposal cell at the Crescent Junction will be incorporated into appropriate sections of the RAS and other design documentation.

## **Computer Source:**

N/A



**References:**

See Cover Sheet.

## **Appendix A**

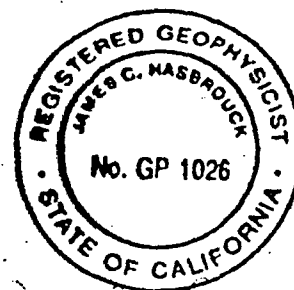
### **Seismic Rippability Investigation Report**

# *Final Report*

## **Crescent Junction Disposal Site Seismic Rippability Investigation**

for

**S. M. Stoller Corporation  
Grand Junction, Colorado**



November 21, 2005

*James C. Hasbrouck*  
*11/21/05*

---

2473 North Leah Lane  
Prescott, Arizona 86301 USA  
928-778-6320 (Telephone and Fax)  
jim@hasgeo.com (E-Mail)  
<http://www.hasgeo.com> (Homepage)

## **TABLE OF CONTENTS**

<b>INTRODUCTION.....</b>	<b>1</b>
<b>DATA ACQUISITION .....</b>	<b>1</b>
<b>DATA PROCESSING .....</b>	<b>3</b>
<b>RESULTS.....</b>	<b>4</b>
<b>LIMITATIONS OF INVESTIGATION .....</b>	<b>6</b>
<b>REFERENCE.....</b>	<b>6</b>

### **Table**

Table 1: Summary of interpreted velocities and depths.....	5
--	---

### **Figures**

Borehole and Seismic Line Locations Map  
Borehole 202 NW to SE Seismic Line Elevation Section  
Borehole 202 SW to NE Seismic Line Elevation Section  
Borehole 204 NW to SE Seismic Line Elevation Section  
Borehole 204 SW to NE Seismic Line Elevation Section  
Borehole 206 NW to SE Seismic Line Elevation Section  
Borehole 206 SW to NE Seismic Line Elevation Section  
Borehole 207 NW to SE Seismic Line Elevation Section  
Borehole 207 SW to NE Seismic Line Elevation Section  
Borehole 208 NW to SE Seismic Line Elevation Section  
Borehole 208 SW to NE Seismic Line Elevation Section  
Borehole 202 NW to SE Seismic Line Depth Section  
Borehole 202 SW to NE Seismic Line Depth Section  
Borehole 204 NW to SE Seismic Line Depth Section  
Borehole 204 SW to NE Seismic Line Depth Section  
Borehole 206 NW to SE Seismic Line Depth Section  
Borehole 206 SW to NE Seismic Line Depth Section  
Borehole 207 NW to SE Seismic Line Depth Section  
Borehole 207 SW to NE Seismic Line Depth Section  
Borehole 208 NW to SE Seismic Line Depth Section  
Borehole 208 SW to NE Seismic Line Depth Section  
Caterpillar D8 Tractor Ripping Chart  
Caterpillar D9 Tractor Ripping Chart  
Caterpillar D10 Tractor Ripping Chart  
Caterpillar D11 Tractor Ripping Chart

### **CD**

Velocity Analysis Tables  
Time-Distance (T-D) Plots  
Modeled elevations and depths beneath each source point and geophone  
Observer Reports

## **INTRODUCTION**

Refraction seismic surveys were conducted for S. M. Stoller Corporation along ten seismic lines centered on existing boreholes at the proposed Crescent Junction Disposal Site to assist in the evaluation of the suitability of the site as a final repository for the Moab uranium mill tailings. The purposes of the seismic surveys were to determine the seismic velocities of weathered and unweathered Mancos Shale deposits that underlie the site and relate those velocities to the rippability of the subsurface materials.

The refraction seismic method is routinely used for rippability investigations. Caterpillar Inc. has prepared charts that relate seismic velocities to different sized rippers. For typical refraction seismic rippability investigations a seismic velocity versus depth or elevation profile is generated along each survey line and then the velocities are related to the Caterpillar charts so that a proper ripper can be selected by the construction contractor. Two types of refraction seismic surveys may be conducted to ascertain the rippability estimates of the subsurface: two-dimensional (2D) tomography and delay-time. The 2D tomography method offers a more detailed and gradational section of the subsurface seismic velocity, but takes a little more time in the field and thus is slightly more expensive. The delay-time method offers only a layered and averaged velocity section, but may be more familiar to construction contractors since it has been in use for a much longer time than 2D tomography. Stoller selected the delay-time method for this project.

This seismic survey was a joint effort between Bird Seismic Service, Inc. of Globe, Arizona and Hasbrouck Geophysics, Inc. of Prescott, Arizona. Bird Seismic acquired the seismic data using the survey design prepared by Hasbrouck Geophysics, while Hasbrouck Geophysics processed and interpreted all the data and prepared the final report. This final report will be reviewed by Mr. H. David MacLean of Grand Junction, Colorado. Ken Bernstein is president of Bird Seismic Services, Inc. and may be reached at [ken@birdseismic.com](mailto:ken@birdseismic.com) or 928-719-1848. Jim Hasbrouck is president of Hasbrouck Geophysics, Inc. and may be contacted at [jim@hasgeo.com](mailto:jim@hasgeo.com) or 928-778-6320. Dave MacLean is available at [107770.3066@compuserve.com](mailto:107770.3066@compuserve.com) or 970-242-1649.

## **DATA ACQUISITION**

Seismic surveys essentially consist of recording seismic waves that have been generated by artificial sources, observing the arrival times of these waves, and producing cross-sections of variations in subsurface seismic wave velocities that can then be related to geology. The source of seismic energy for surface surveys is primarily dependent upon the target depths and local geology, and for relatively shallow surveys is generally either a sledgehammer or weight-drop system. The seismic waves are detected by geophones in surface surveys. A geophone consists of a coil suspended by springs with magnets built into the case. A seismic wave moves the case and the magnets while the coil remains relatively stationary because of its inertia. The relative movement of the magnetic field with respect to the coil generates a voltage across the coil that is proportional to the velocity of the seismic wave. The electrical voltages produced by the geophones are transmitted back to a recording instrument (seismograph) via cables. In refraction seismic surveys it is necessary, according to Snell's Law, that velocities increase with depth so that the refracted seismic waves can be detected on the surface. For refraction seismic surveys in

most sedimentary environments it is typical that velocities increase with depth (i.e., there are no velocity reversals) and it is assumed that this is the case for the Crescent Junction Disposal Site.

According to Stoller, the depth to weathered bedrock in the project area is assumed to vary from two to approximately 25 feet. Unweathered bedrock may be deeper than 50 feet thus the refraction seismic survey is designed to investigate to depths somewhat greater than 50 feet using the standard rule-of-thumb for refraction seismic surveys that the first geophone to "see" a refraction from a layer will be at a distance of three to five times the expected depth. For example, if an investigation depth of 60 feet is desired then the first geophone to see a refraction, if present, from that depth will be at 180 to 300 feet along the line of geophones, or spread, with the larger distance applicable to areas with generally slower velocities. In order to accurately map the deeper horizons, several geophones must be beyond the initial geophone that records the deeper refraction thus a geophone interval of 10 feet with 30 feet far offsets (resulting in a total spread of 500 feet) is used for this project.

The refraction seismic data for this project were acquired with a 48-channel Bison 9048 seismograph with 21-bits of dynamic range, 250 milliseconds (ms) record lengths, and 0.25 ms sample intervals with Mark Products 10-Hz geophones implanted approximately three inches into the ground at intervals of 10 feet along each line. The seismic source was an Elastic Wave Generator (EWG) accelerated weight-drop mounted on the back of a 4x4 pickup and consisted of a 207-pound weight that was lifted hydraulically against large springs and then released resulting in a force much greater than the weight itself. For each seismic line data from a minimum of eleven source points were acquired (seven within the spread nominally between geophones 6 and 7, 12 and 13, 18 and 19, 24 and 25, 30 and 31, 36 and 37, and 42 and 43, and off each end at distances of 10 and 30 feet). The geophone distances were initially measured with either a tape or takeout intervals on the geophone spread cable and after completion of data acquisition every fourth geophone and each offset source point was surveyed to at least centimeter accuracy by a contractor to Stoller. Because the surface topography change was minor and the seismic lines were relatively straight it was only necessary to survey the coordinates and elevations of every fourth geophone and then interpolate values for the intermediate geophones.

The seismic data were stacked nominally four to six times (depending upon offset and noise) at each source point to increase the signal-to-noise ratio. Stacking, or signal enhancement, involved repeated source impacts at the same point into the same set of geophones. For each source point, the stacked data were recorded into the same seismic data file and theoretically the seismic signal arrived at the same time from each impact and thus was enhanced, while noise was random and tended to be reduced or canceled. After recording the data on the hard disk of the seismograph, the seismic records were copied to a personal computer at the end of each field day. These data were e-mailed nightly from the field to Mr. Hasbrouck and copies of the Observer Reports (field notes) were faxed at the same time. The quality of the seismic data ranged from very good to excellent depending primarily upon offset, and identifiable first breaks (first arrivals of seismic energy) were present along all the lines.

## DATA PROCESSING

The refraction seismic data were processed using the *SIPwin* (version 2.77) set of computer programs from Rimrock Geophysics Inc., Lakewood, Colorado. The general processing flow consisted of the initial selection, or "picking", of the seismic first breaks (first arrival of seismic energy) with the *SIPIK* program, creation of data files for input into the interpretation program with the *SIPIN* program, and interpretation of the data using modeling and iterative ray-tracing techniques with the *SIPT2* program. A first break was selected as the initial downward variation of the seismic signal from a horizontal line and was generally accurate to a time between 0.5 and 1 ms. To enhance the accuracy of first break picks, the seismic record was zoomed to a time that only encompassed the breaks themselves (i.e., only the portion of the seismic record where the first breaks were visible). The *SIPT2* program uses the delay-time method to obtain a first-approximation depth model, which is then trimmed by a series of ray-tracing and model adjustment iterations to minimize any discrepancies between the picked arrival times and corresponding times traced through a 2½-dimensional model. Arrival times at two geophones, separated by some variable XY-distance, are used in refractor velocity analyses and time-depth calculations. Using the principle of migration and iterative ray-tracing within the *SIPT2* program, forward and reverse seismic rays emerge from essentially the same point on the reflector, thus requiring the reflector to be plane over only a very small distance. The ray-tracing procedure tests and corrects the estimated migrated position of points representing the locations of ray entry and emergence from the refracting horizon and takes into account the dip of the refracting horizon at those emergence points, therefore enabling accurate representation of steeply dipping horizons.

For any refraction seismic data analysis, it is important to determine accurate velocities. The *SIPT2* program employs several routines for selection of the proper velocities. For the direct arrivals through the first layer, the velocity is computed by dividing the distances from each source point to each geophone by the corresponding arrival times. These individual velocities are averaged for each source point and a weighted average is computed. For layers beneath the first layer, velocities are computed by two methods: 1) Regression, in which a straight line is fit by least squares to the arrival times representing the velocity layer and average velocities are computed by taking the reciprocals of the weighted average of the slopes of the regression lines, and 2) the Hobson-Overton method wherein velocities are computed if there are reciprocal arrivals from two opposing source points at two or more geophones. Final velocities used in the *SIPT2* inversion process are computed by taking an average of the two methods. As quality control measures, time versus distance (T-D) plots (which represent velocities) are inspected along each seismic line relative to reciprocal times, irregularity and parallelism as per ASTM D5777. The refraction seismic data for this project adequately met the requirements of each of these tests.

Included within this report are a borehole and seismic line location map, and elevation and depth versus distance refraction seismic sections for each line with annotated average velocities for each layer. Also included is a CD with output from the *SIPT2* program that includes velocity analysis tables, T-D plots indicating the picked arrival times, and modeled elevations and depths beneath each source point and geophone. Note that the distances in the modeled results have been corrected for horizontal foreshortening (i.e., corrections are made to obtain true horizontal

positions). The modeled results are used to construct the elevation and depth sections, and are in Microsoft Excel format for future client use if desired.

## **RESULTS**

According to Stoller, the geology of the project area consists of essentially three layers. The near surface is alluvial overburden composed of unconsolidated silt, clay, and sandstone fragments. Beneath the alluvium is weathered bedrock, or weathered Mancos Shale, composed of fractured, chemically weathered, siltstone, silty sandstone or clayey siltstone of variable thickness. The weathered layer is often highly fractured with calcite and gypsum fracture coatings. The Mancos Shale is present beneath the weathered layer and is increasingly competent with depth. Although the Mancos Shale appears to be a great shale mass, it is not one homogeneous unit. According to available lithologic logs for the boreholes within the project area, the Mancos Shale seems to be described as consisting not only of shale but also some sandstone layers and what has been termed a silty claystone. The lithologic logs generally indicate variations in the composition of the unweathered Mancos Shale near its top with increasing shale constituents with depth.

Interpretation of the refraction seismic data indicates three layers, representing alluvial overburden, weathered Mancos Shale and competent Mancos Shale. Table 1 indicates the range in velocities and depths for each line. The first layer velocities range from about 1160 to 1330 feet per second and are consistent with typical unsaturated alluvial overburden values. The second layer velocities range from about 4060 to 5220 feet per second and represent typical values for weathered material such as the Mancos Shale. The variation in velocity values for the interpreted weathered Mancos Shale is probably related to the degree of fracturing and the amount of calcite and/or gypsum coating of the fractures. The higher velocities may have less fracturing or the fractures may be coated with an increased amount of calcite and/or gypsum. It is not possible from the seismic results to determine which scenario exists. The third layer, or competent Mancos Shale bedrock, velocities range from about 9000 to as high as 10000 feet per second with the majority of the velocity values in a range from about 9000 to 9400 feet per second. Velocity variations of the interpreted Mancos Shale bedrock are considered relatively minor and probably related to slight changes in composition of the bedrock or some amount of fracturing. Velocity variations are present along the intersecting seismic lines at each borehole, but generally than about 5% which is reasonable given that the velocity values are averages and the subsurface geology is variable (as evidenced by changes in the lithologic logs between boreholes).

The thickness of the overburden layer (or the depth to the top of layer 2 which is interpreted as weathered Mancos Shale) ranges from about 4½ to 18 feet, while the depth to the top of layer 3 (or interpreted unweathered Mancos Shale bedrock) varies from about 24 to 60 feet. The tie point depths between intersecting lines at each borehole are generally less than about 5% which is considered reasonable and quite acceptable for seismic surveys. Depth values at intersecting points from lines oriented in different directions often vary because of anisotropy within the subsurface geological formations. Anisotropy is defined as a variation of a physical property (e.g., velocity) depending upon the direction in which it is measured. In general, surface refraction seismic data have shown a 10% to 15% variation between the actual depths to velocity



layer anomalies, as verified primarily by geophysical borehole logging, and the depth predicted by the models.

Table 1: Summary of interpreted velocities and depths

Line	Layer 1 velocity (ft/s)	Layer 2 velocity (ft/s)	Layer 3 velocity (ft/s)	Depth to top of layer 2 (ft)	Depth to top of layer 3 (ft)
202NW-SE	1230	4218	10005	4.5 - 15.1	34.3 - 58.7
202SW-NE	1305	4305	9353	11.3 - 17.1	31.5 - 53.0
204NW-SE	1334	4674	9035	8.0 - 14.9	40.4 - 61.1
204SW-NE	1206	4705	9399	10.1 - 18.1	40.5 - 59.3
206NW-SE	1305	5221	9380	9.9 - 16.0	29.5 - 46.8
206SW-NE	1281	5169	9479	7.7 - 15.2	25.4 - 47.5
207NW-SE	1159	4195	9011	7.1 - 14.3	26.7 - 49.1
207SW-NE	1228	4061	9021	5.9 - 15.0	28.9 - 45.9
208NW-SE	1260	4430	9676	11.0 - 14.5	33.3 - 48.8
208SW-NE	1191	4633	9805	9.0 - 13.6	23.4 - 48.4

Inspection of either the elevation or depth sections indicates that the subsurface is far from planar, with some areas showing signs of possible incised bedrock channels (e.g., particularly possibly both lines at borehole 208). Because both the first and last approximately 30 to 50 feet, or more, of the sections have less forward and reverse raypath coverage (refer to the T-D plots), results in those areas should be viewed with some caution. Nevertheless, subsurface depth variations are present along each of the seismic lines.

According to Caterpillar's ripping charts, shale is considered rippable at seismic velocities ranging up to about 6000 to 10200 feet per second for tractor models D8 to D11, respectively. Rippable velocities are slightly different if the subsurface material is composed more of a siltstone (up to about 6500 to 9900 for a D8 to D11 tractor, respectively). Referencing the ripping charts from Caterpillar, it is reasonable to assume that all of the interpreted layer 2 or weathered Mancos Shale can be ripped with a tractor as small as a D8 (note that the Caterpillar ripping charts are not available for tractors smaller than a D8). If it is necessary to rip the interpreted competent Mancos Shale bedrock, with velocities interpreted to be greater than 9000 feet per second, it will be necessary to employ a D11 tractor.

Although the seismic survey covered only a very small portion of the proposed Crescent Junction Disposal Site it is reasonable to assume that excavation in the proposed site will be impacted by the variable weathered and unweathered bedrock depths. Although the author of this report is not aware of the design depth of the proposed disposal site excavation, if it is say 40 feet then there will be areas encountered with much higher velocity material at depth which will require either larger rippers or other means of excavation. For example, if material is ripped along the borehole 207 SW to NE seismic line to a depth of 40 feet materials with average velocities of around 4000 and 9000 feet per second will both be encountered. Obviously, a D8 tractor would not be able to rip to a depth of 40 feet along the entire length of this line.

## **LIMITATIONS OF INVESTIGATION**

Although a refraction seismic investigation is the most cost-effective way to determine rippability of material in a project area (versus sporadic boreholes that offer only localized information), it must be realized that according to Caterpillar ripping is still more art than science, and much will depend upon operator skill and experience. Caterpillar states in their Handbook that tooth penetration is often the key to ripping success, regardless of seismic velocity. Low seismic velocities in sedimentary rocks can indicate probable rippability. However, if the fractures and bedding joints do not allow tooth penetration then the material may not be ripped effectively. Pre-blasting or "popping" may induce sufficient fracturing to permit tooth entry.

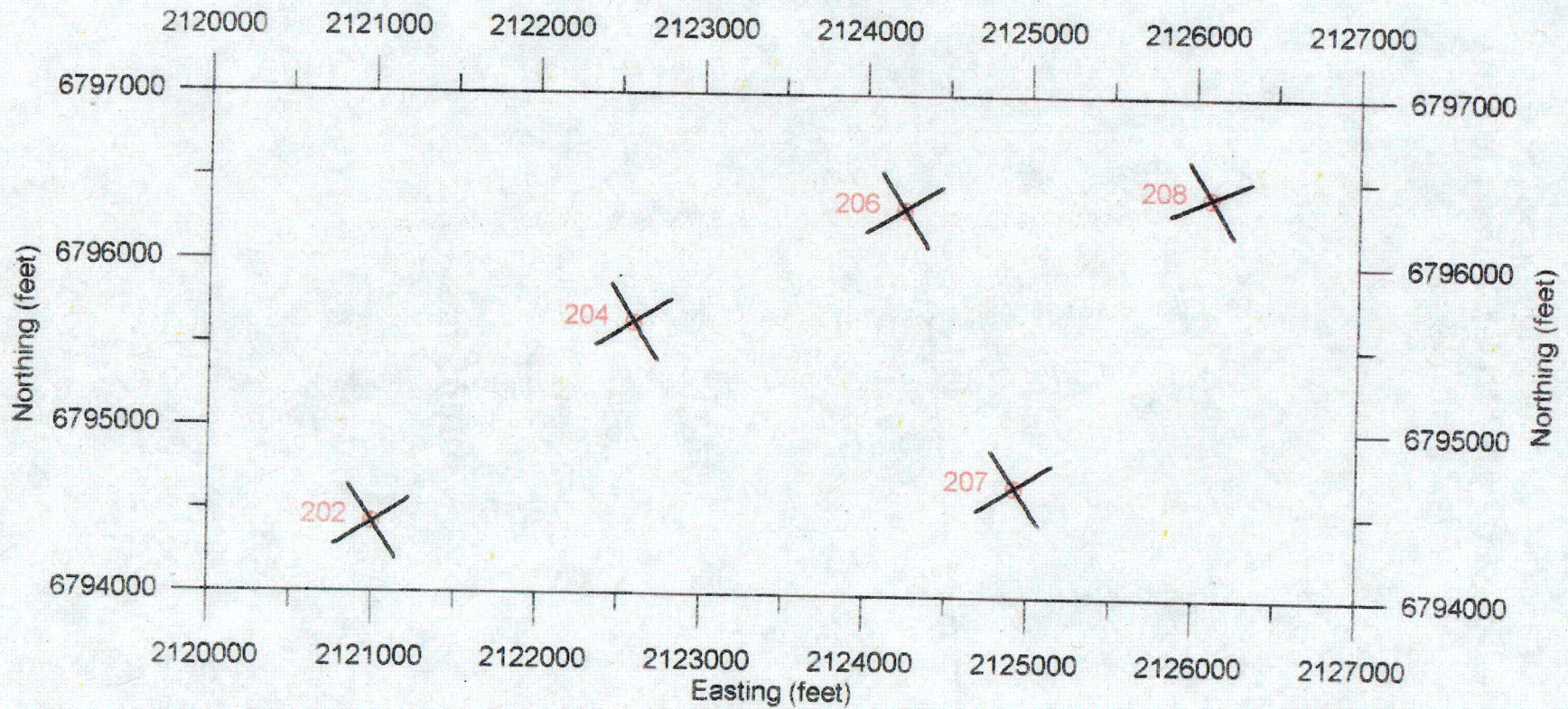
This survey was conducted with state-of-the-art instrumentation operated by experienced geophysicists, the data were processed by an experienced and licensed geophysicist with a commercial software package utilized on projects with similar objectives, and the results were interpreted by an experienced and licensed geophysicist. However, no warranty, either expressed or implied, is made as to the usability of the results of this survey. Additionally, the ripper performance charts developed by Caterpillar are intended for estimating purposes only and neither Caterpillar Inc. nor Hasbrouck Geophysics, Inc. warrant that the tractors will perform as estimated.

## **REFERENCE**

Caterpillar Performance Handbook, Edition 30, October 1999, *Use of Seismic Velocity Charts*, pp. 1-71 to 1-78.



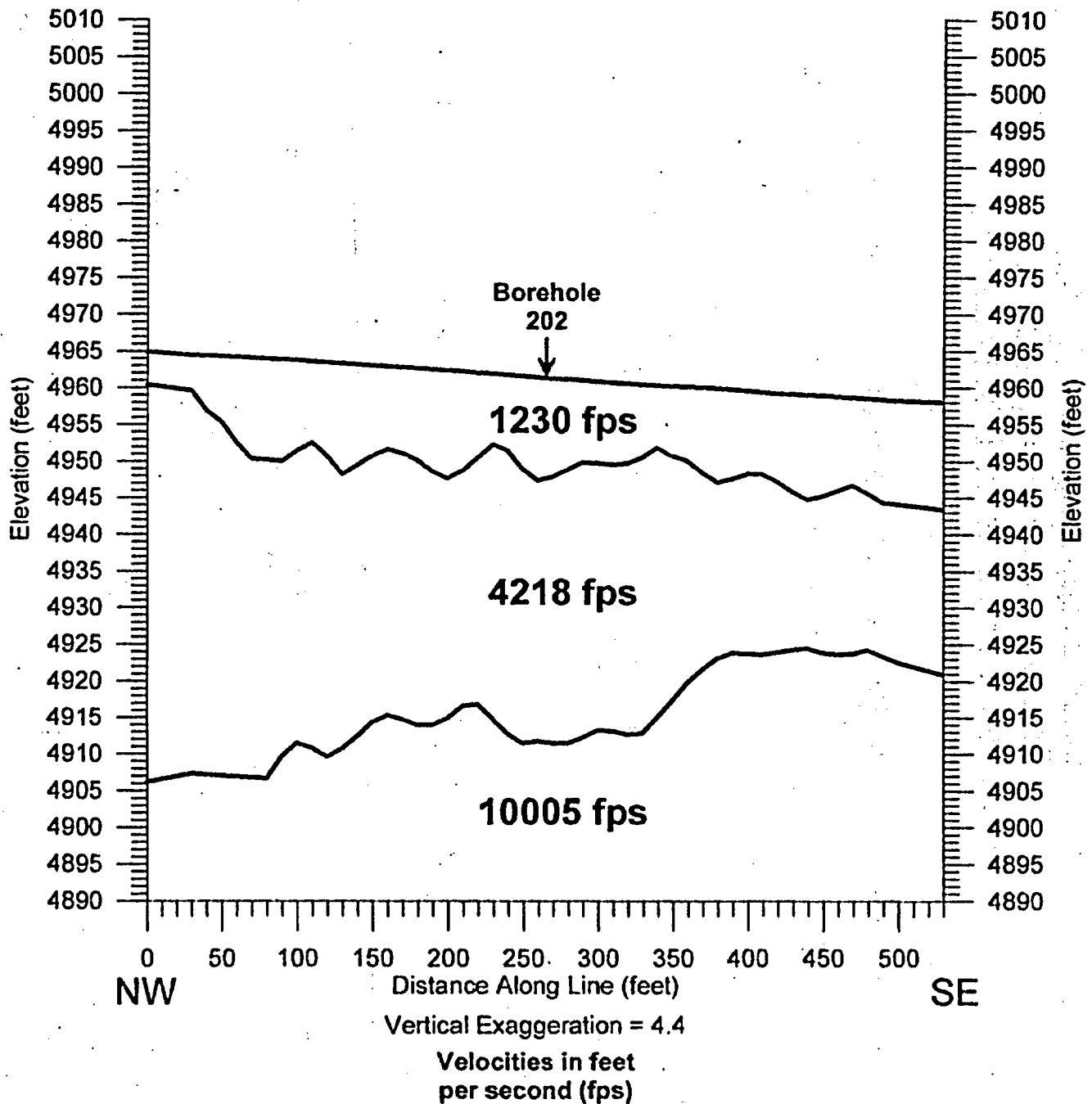
# Seismic Rippability Investigation Crescent Junction Disposal Site Borehole and Seismic Line Locations



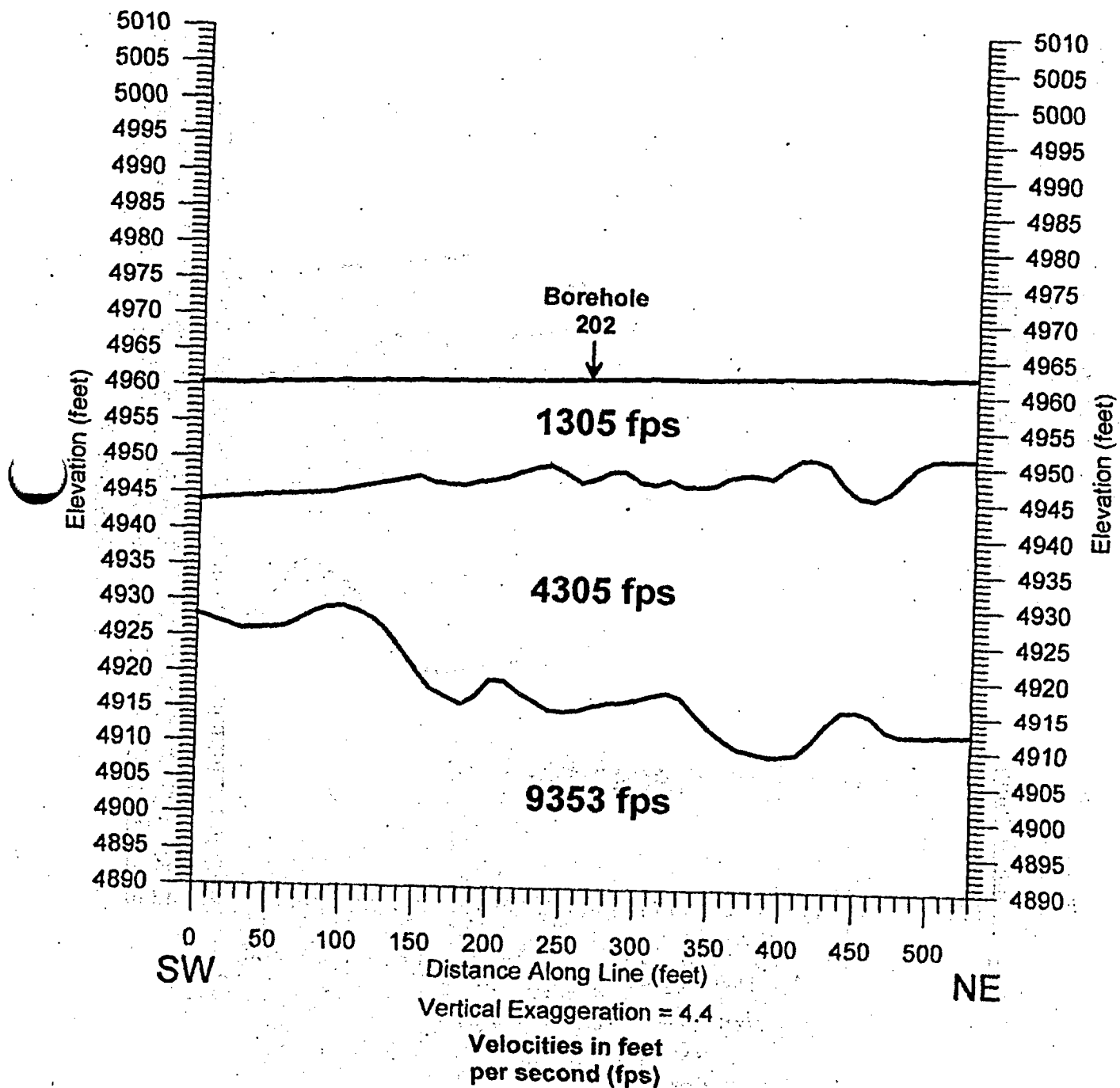
C44



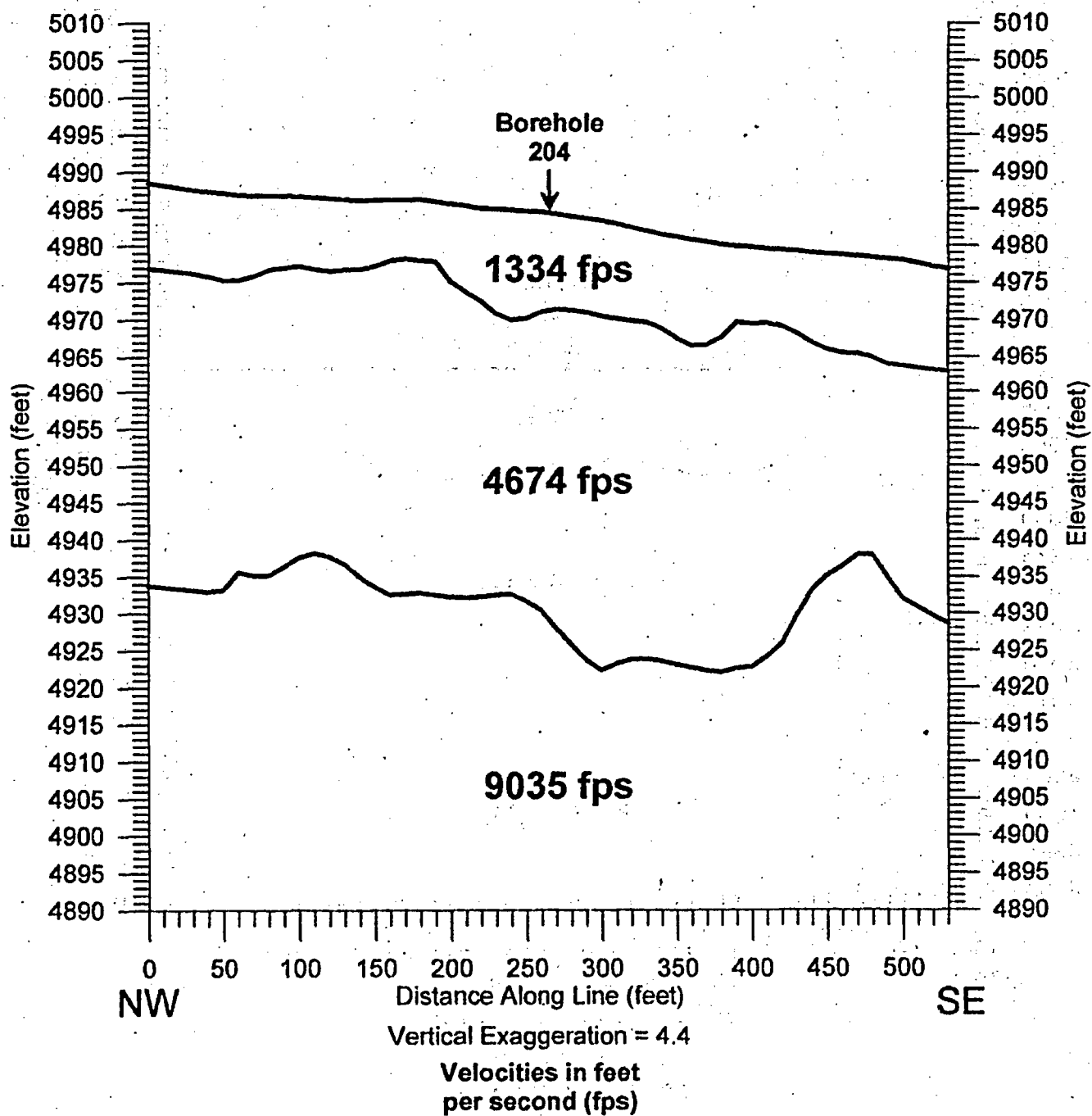
Seismic Rippability Investigation  
Crescent Junction Disposal Site  
**Borehole 202 NW to SE Seismic Line**  
*Elevation Section*



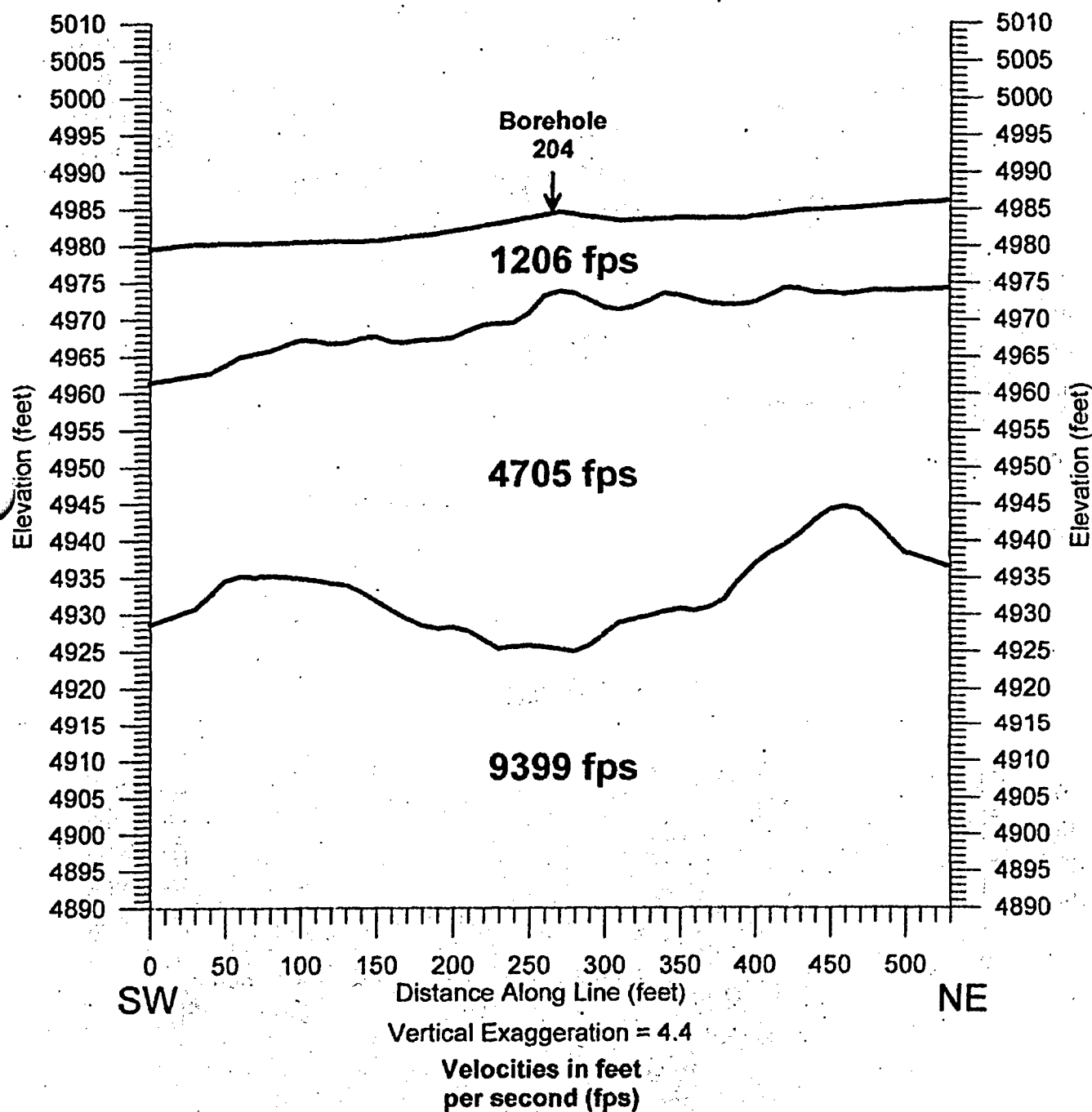
Seismic Rippability Investigation  
Crescent Junction Disposal Site  
Borehole 202 SW to NE Seismic Line  
Elevation Section



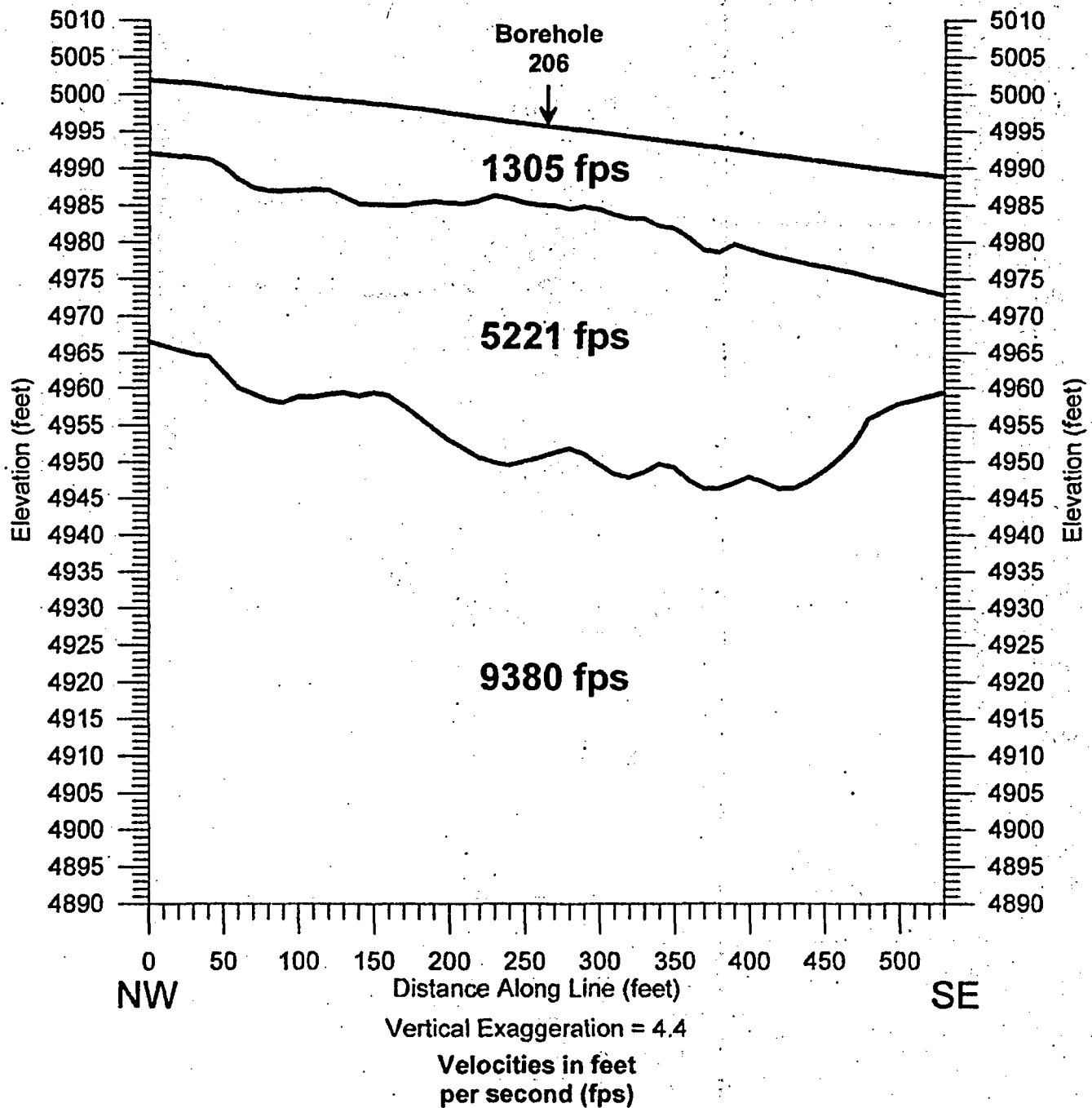
Seismic Rippability Investigation  
Crescent Junction Disposal Site  
**Borehole 204 NW to SE Seismic Line**  
*Elevation Section*



Seismic Rippability Investigation  
Crescent Junction Disposal Site  
**Borehole 204 SW to NE Seismic Line**  
*Elevation Section*

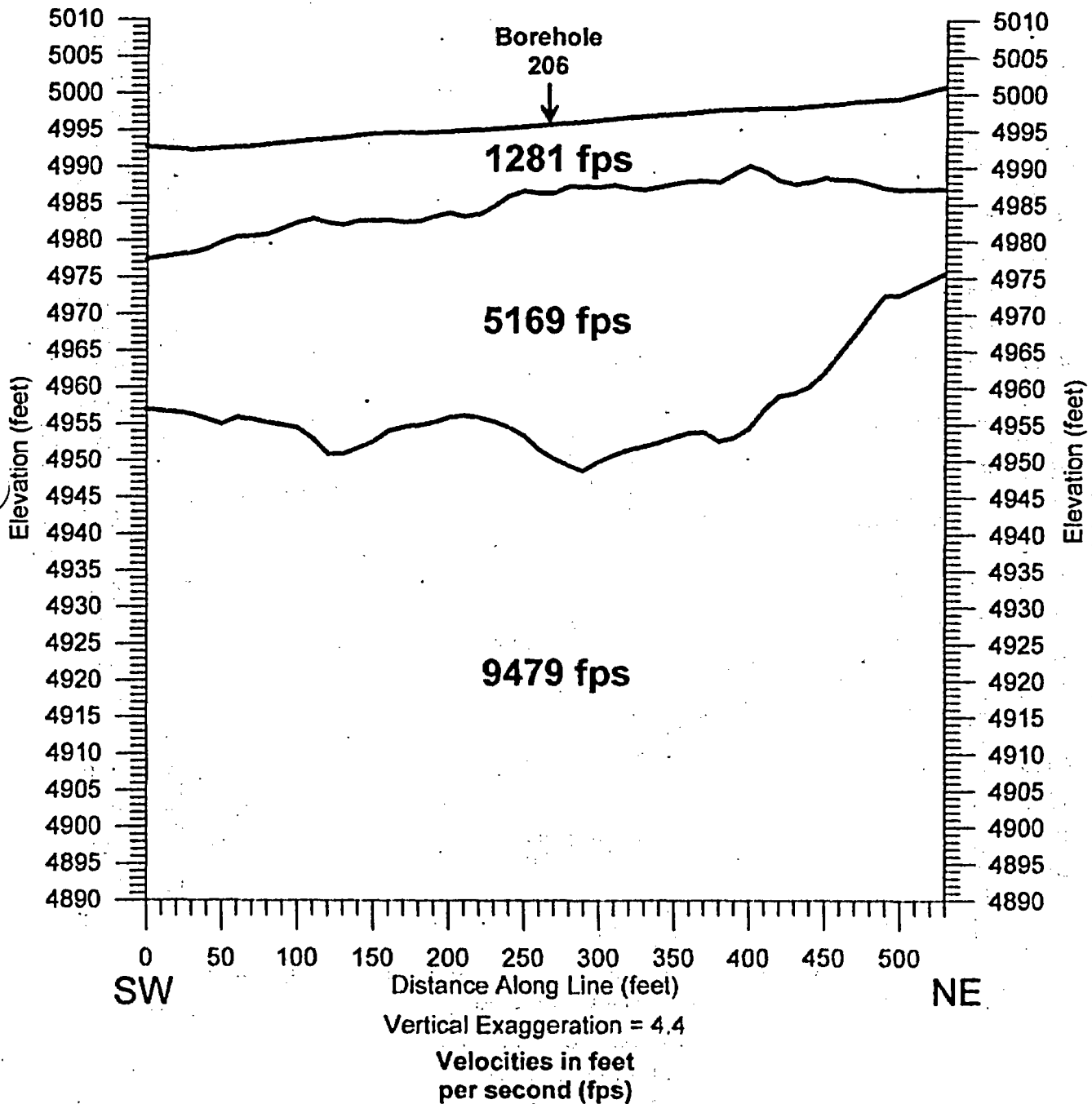


Seismic Rippability Investigation  
Crescent Junction Disposal Site  
**Borehole 206 NW to SE Seismic Line**  
*Elevation Section*

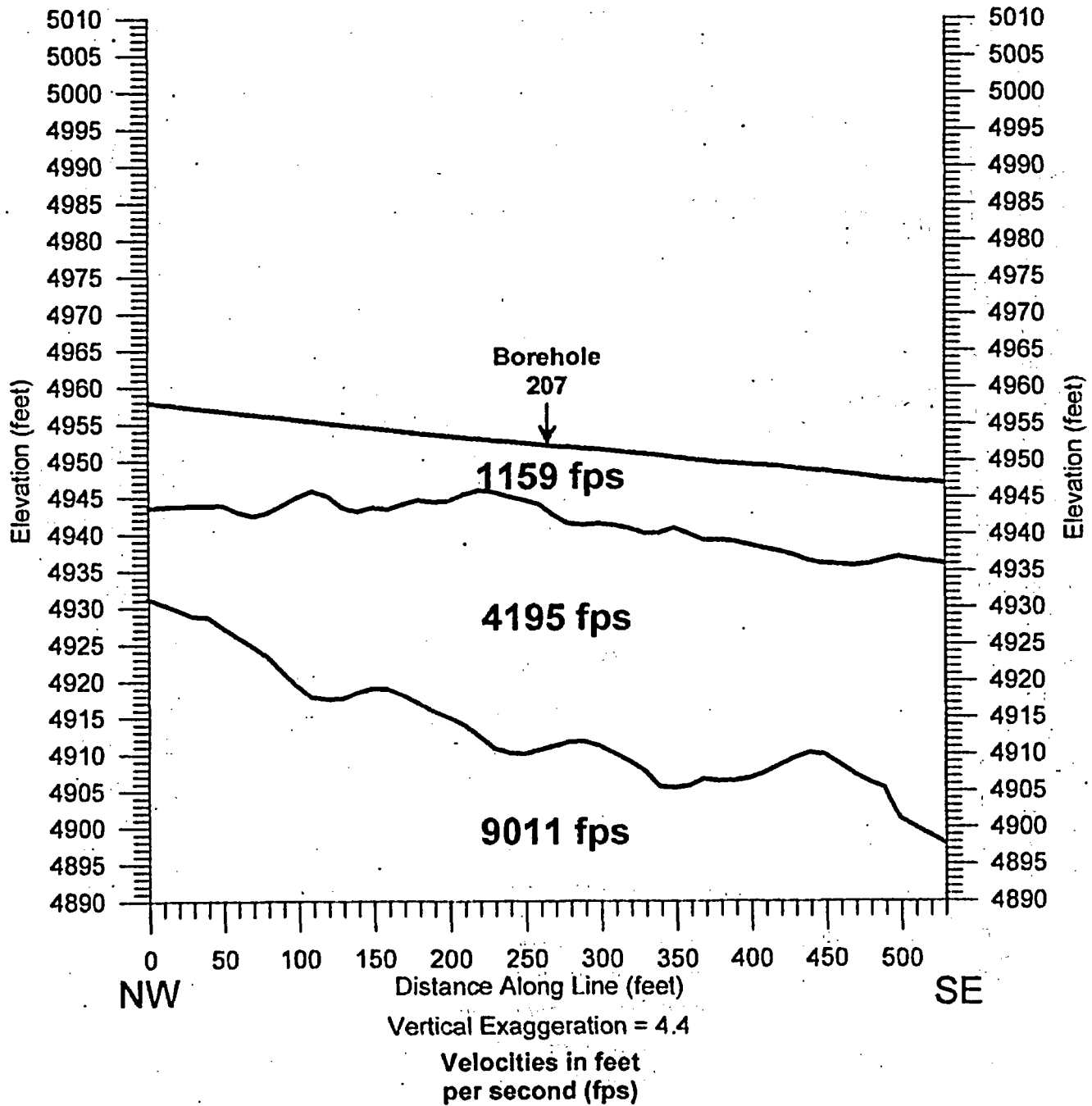




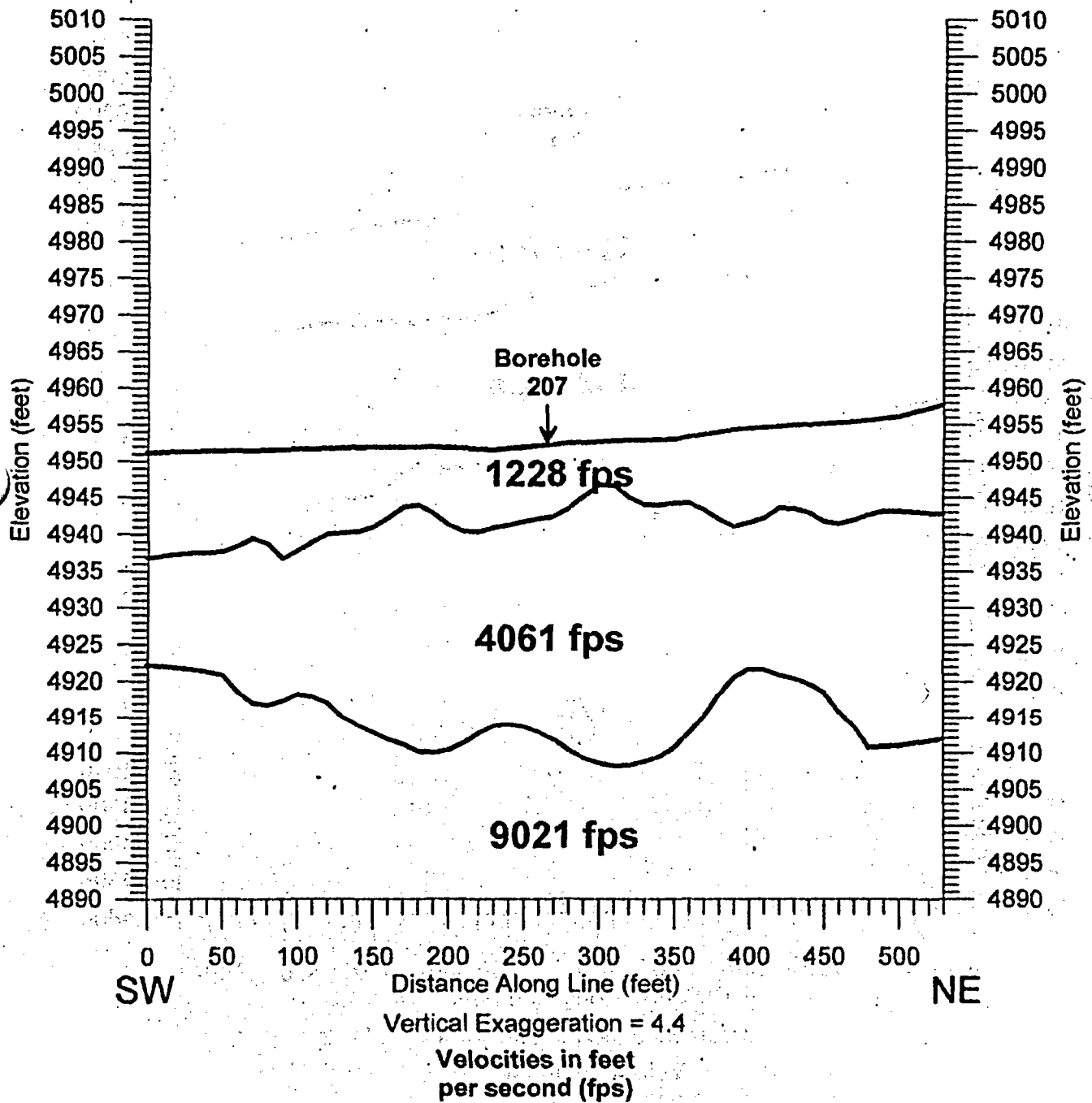
Seismic Rippability Investigation  
Crescent Junction Disposal Site  
Borehole 206 SW to NE Seismic Line  
Elevation Section



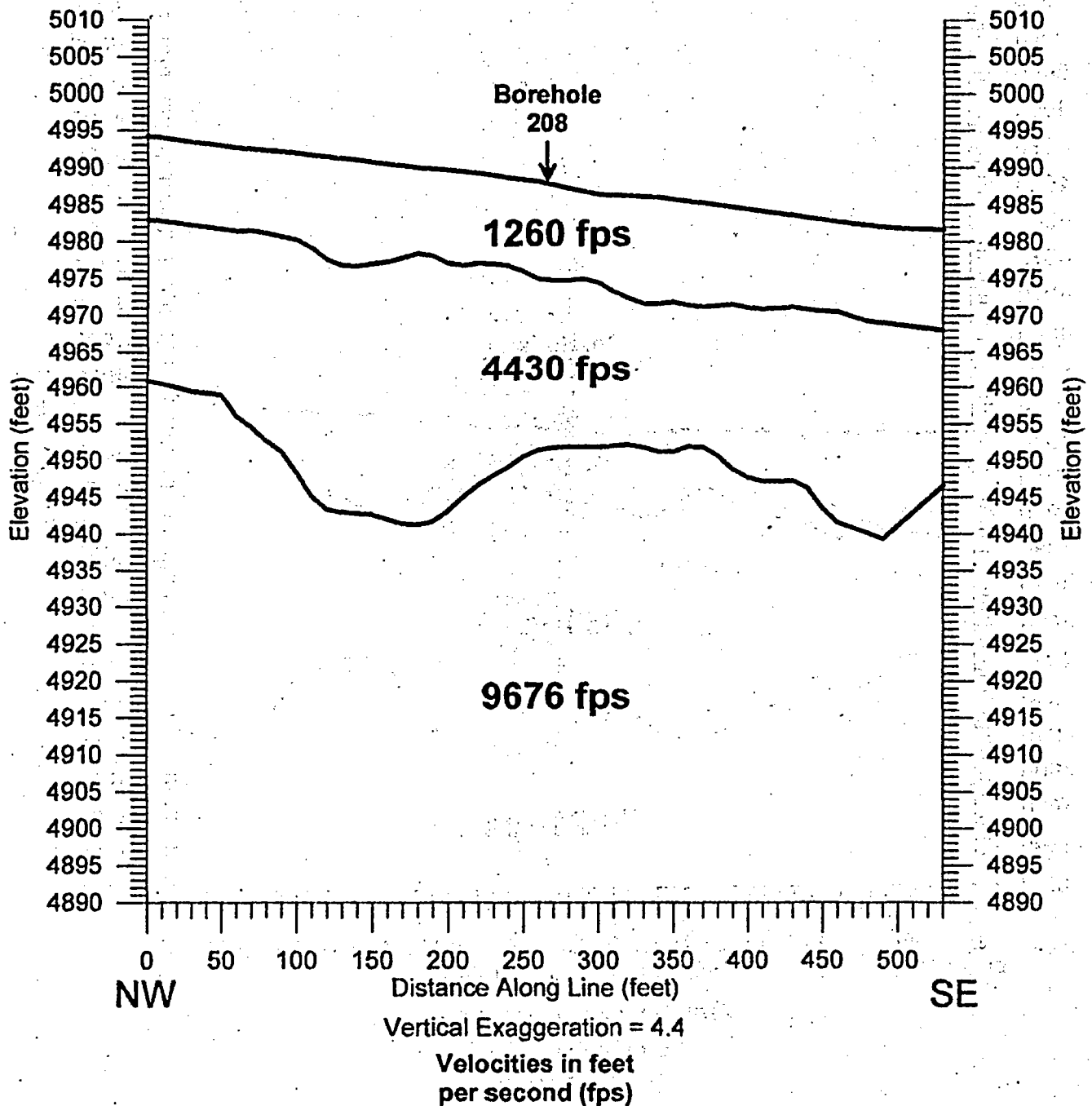
Seismic Rippability Investigation  
Crescent Junction Disposal Site  
**Borehole 207 NW to SE Seismic Line**  
*Elevation Section*



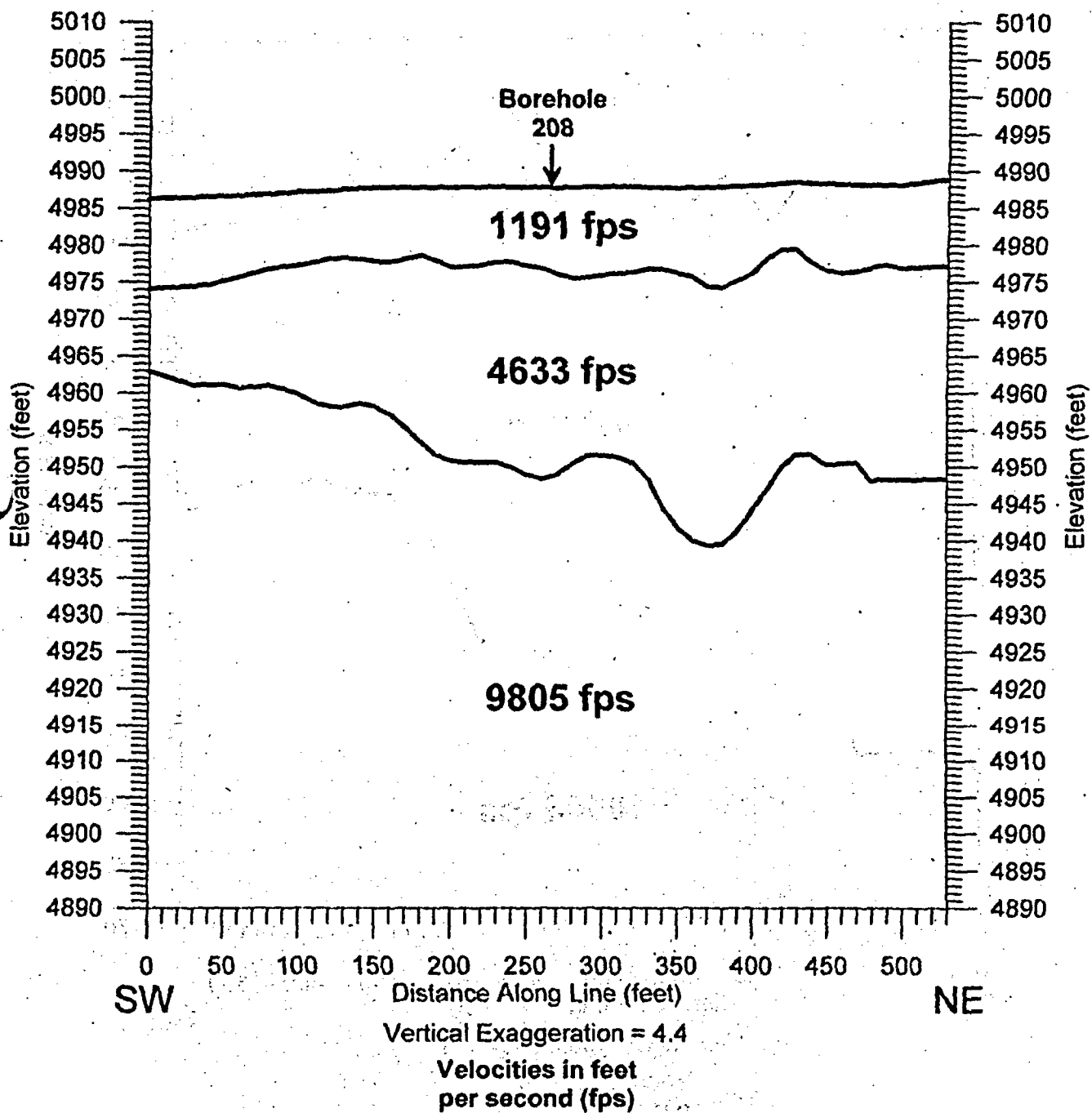
Seismic Rippability Investigation  
Crescent Junction Disposal Site  
**Borehole 207 SW to NE Seismic Line**  
*Elevation Section*



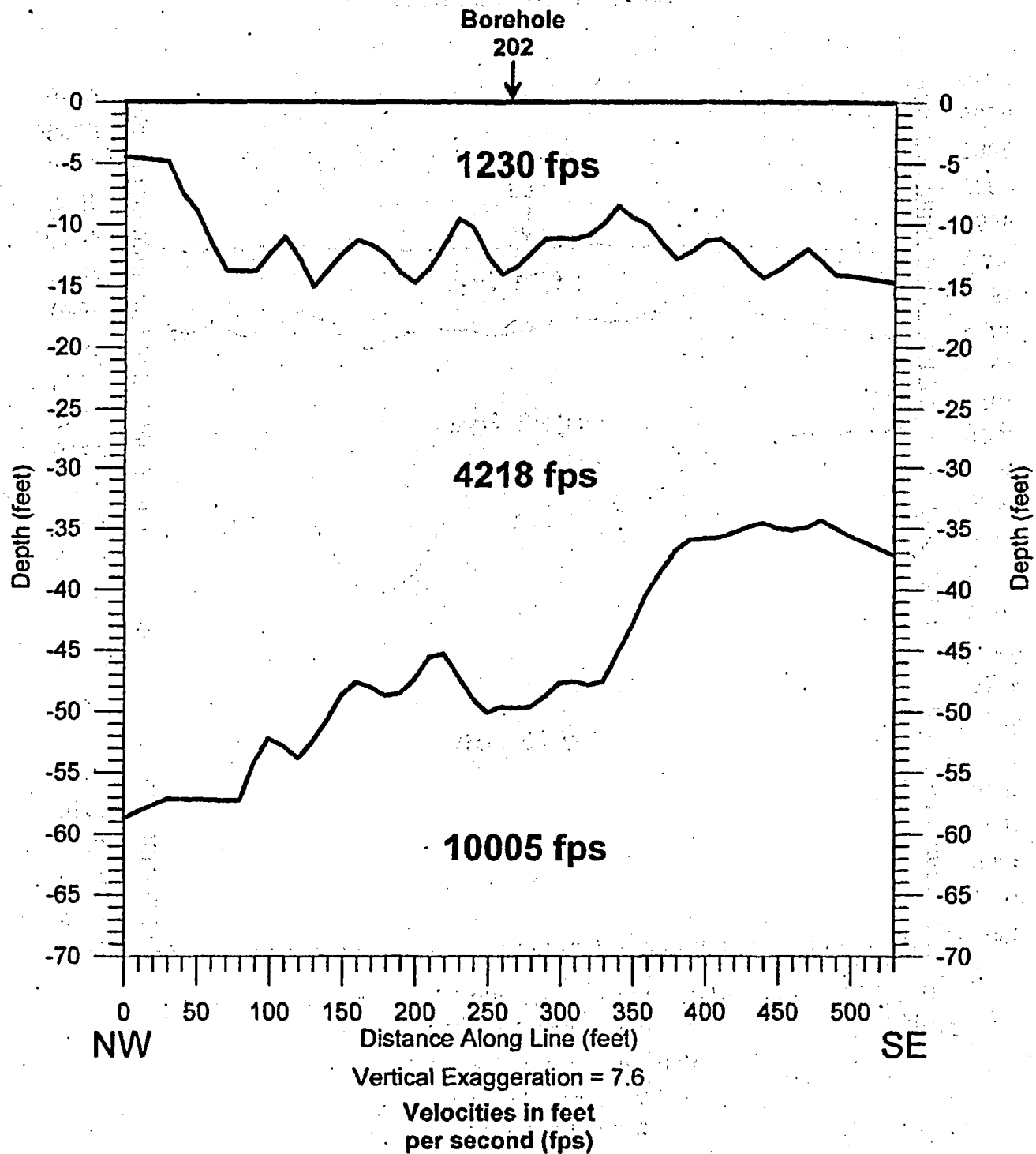
Seismic Rippability Investigation  
Crescent Junction Disposal Site  
**Borehole 208 NW to SE Seismic Line**  
*Elevation Section*



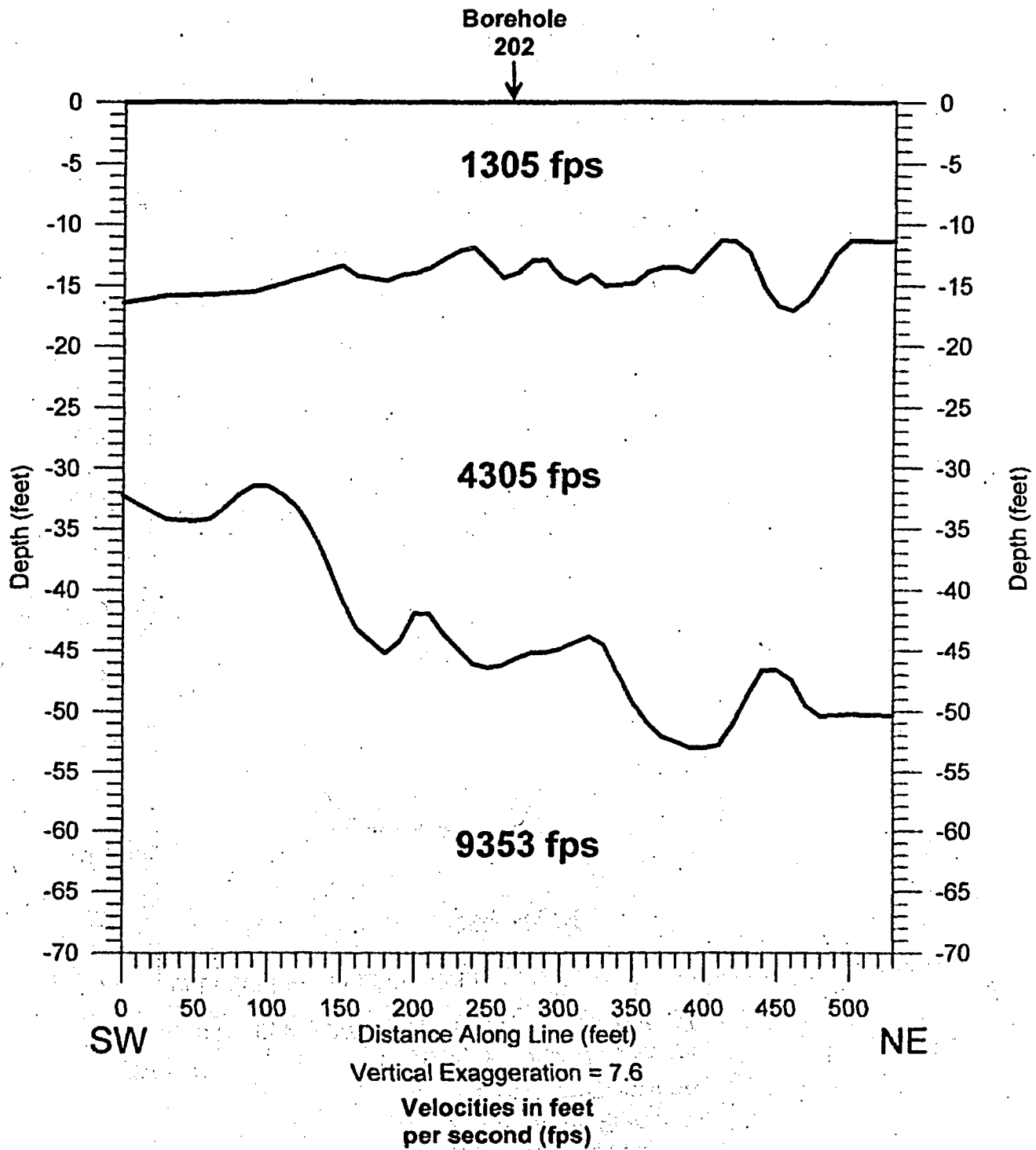
**Seismic Rippability Investigation  
Crescent Junction Disposal Site  
Borehole 208 SW to NE Seismic Line  
Elevation Section**



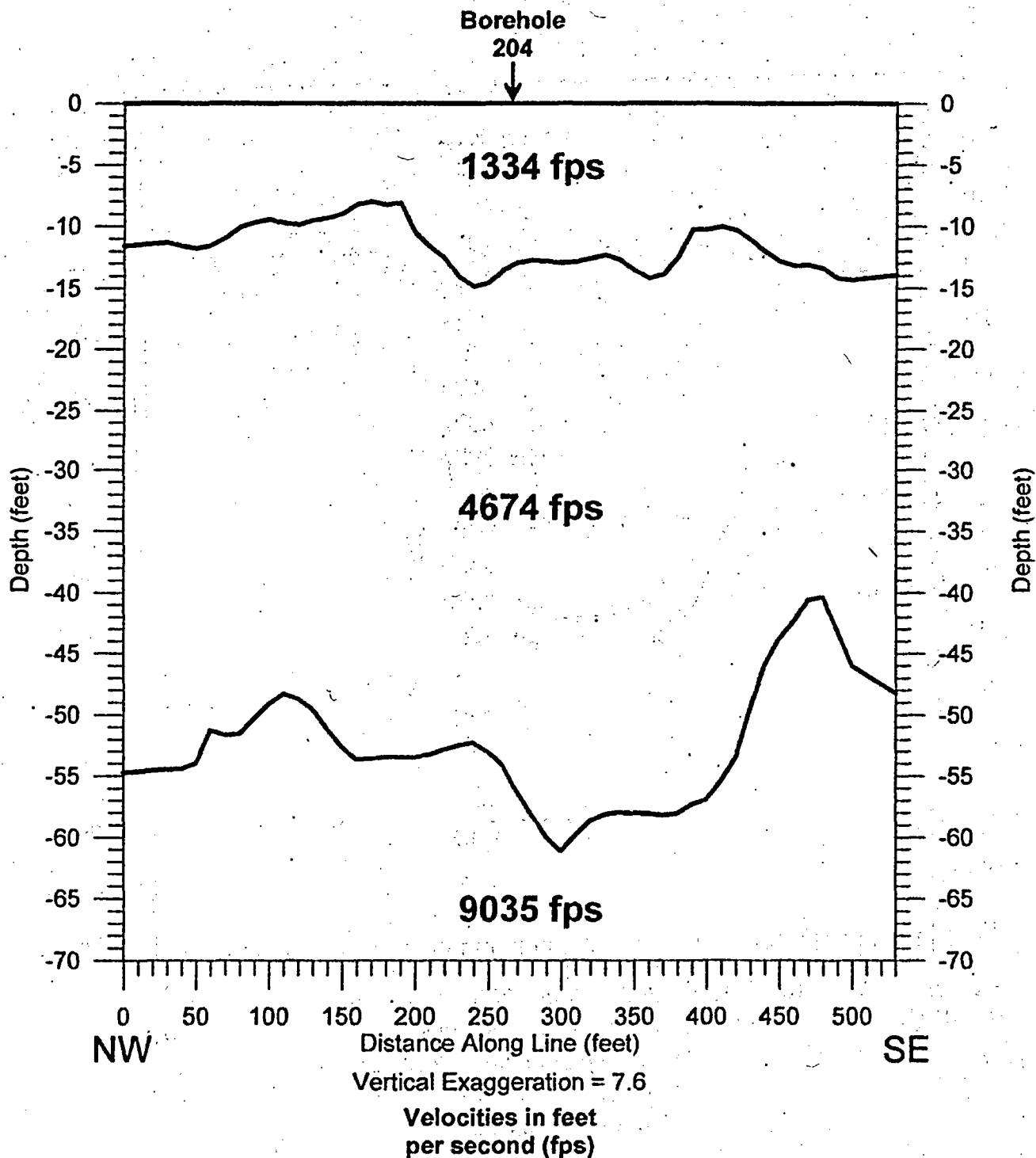
Seismic Rippability Investigation  
Crescent Junction Disposal Site  
**Borehole 202 NW to SE Seismic Line**  
*Depth Section*



Seismic Rippability Investigation  
Crescent Junction Disposal Site  
Borehole 202 SW to NE Seismic Line  
Depth Section

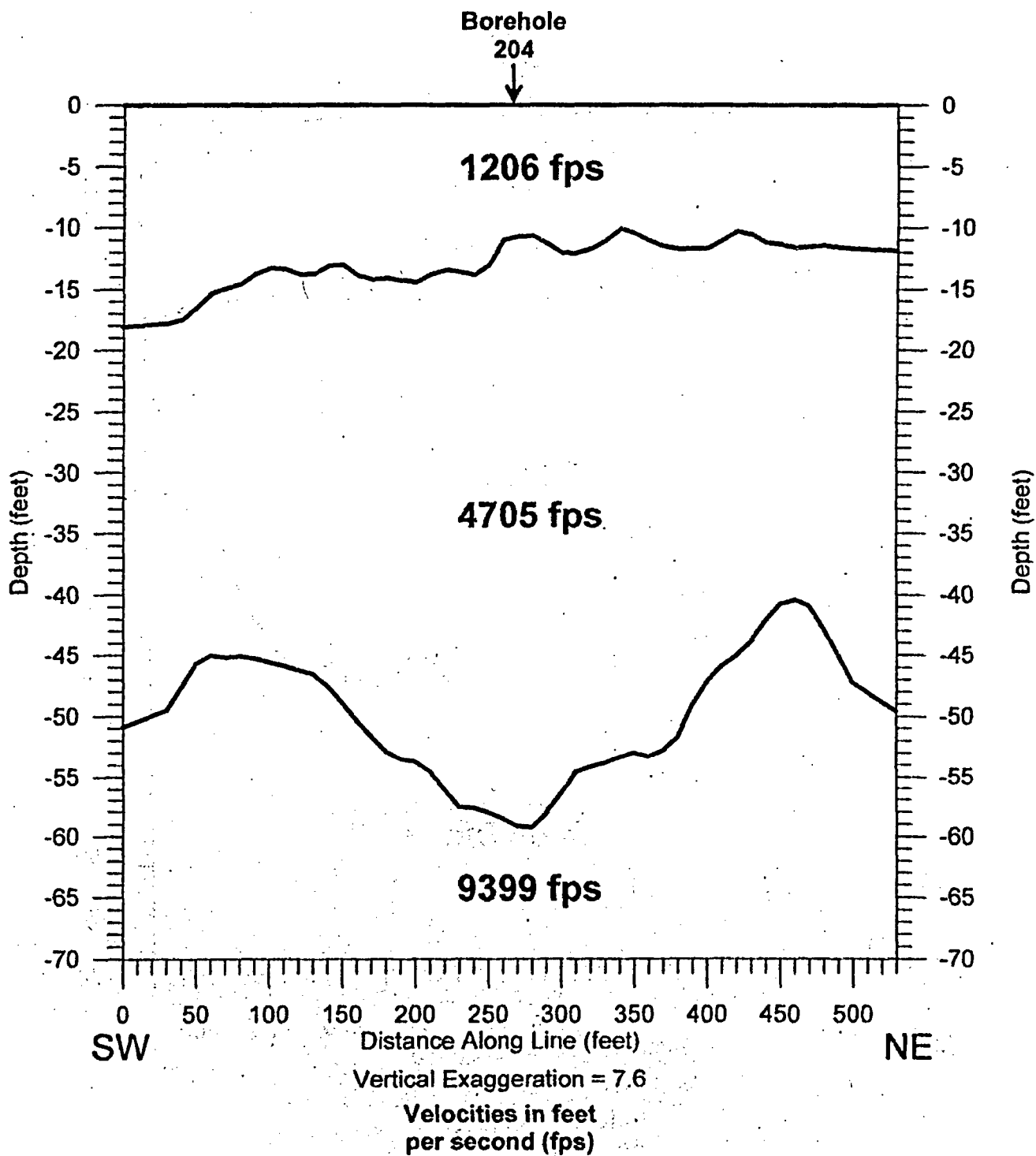


Seismic Rippability Investigation  
Crescent Junction Disposal Site  
**Borehole 204 NW to SE Seismic Line**  
*Depth Section*

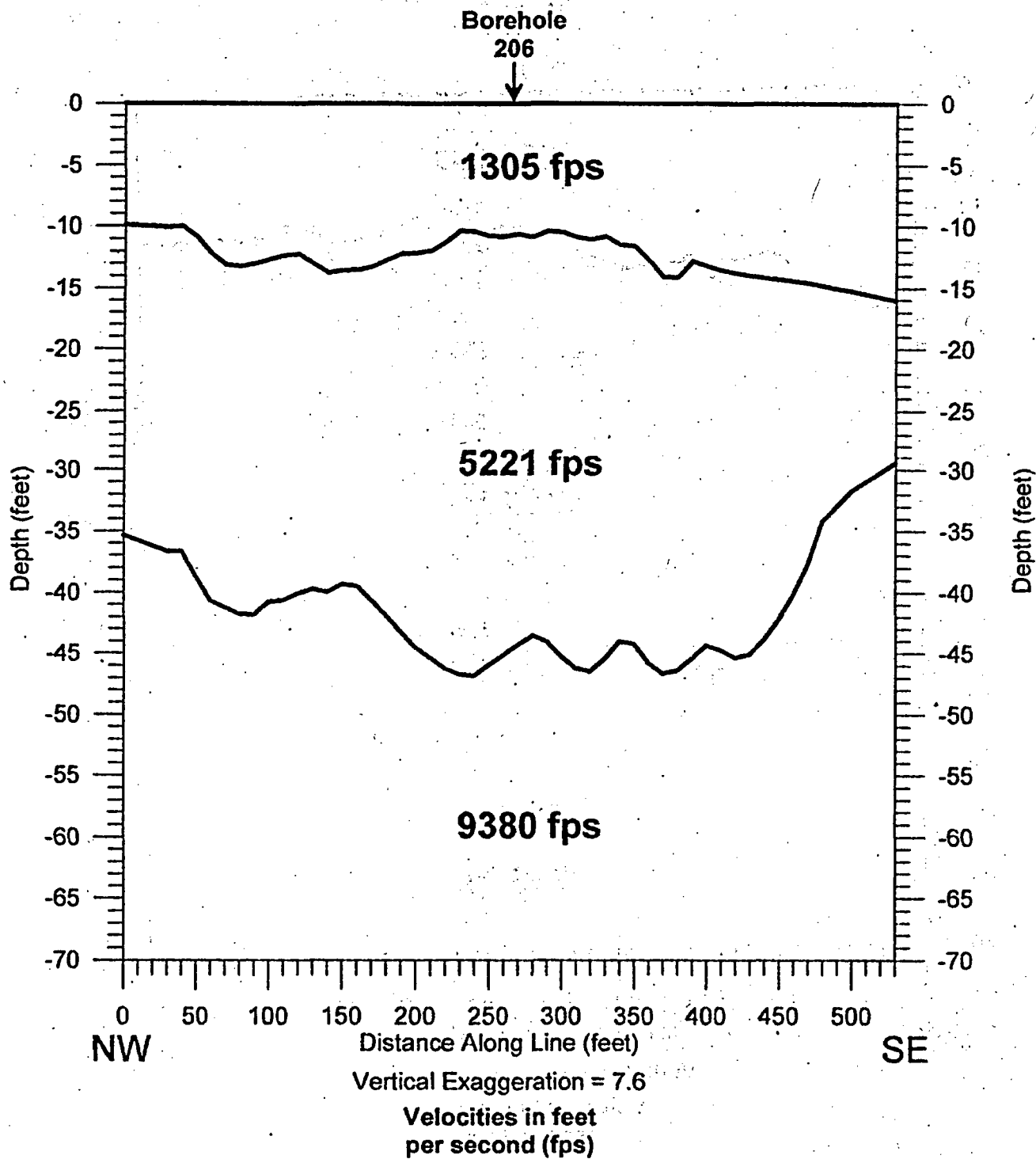




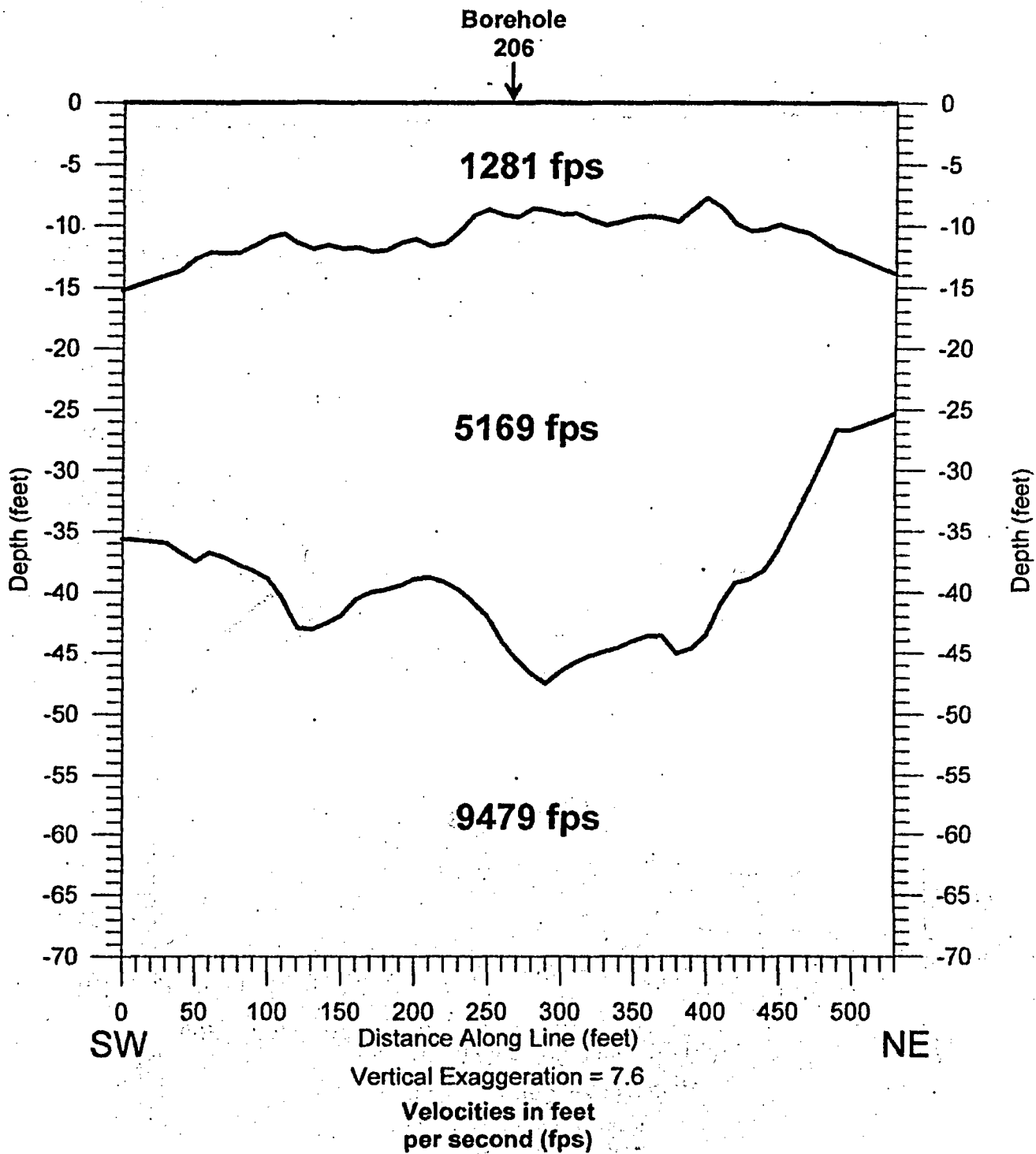
Seismic Rippability Investigation  
Crescent Junction Disposal Site  
**Borehole 204 SW to NE Seismic Line**  
*Depth Section*



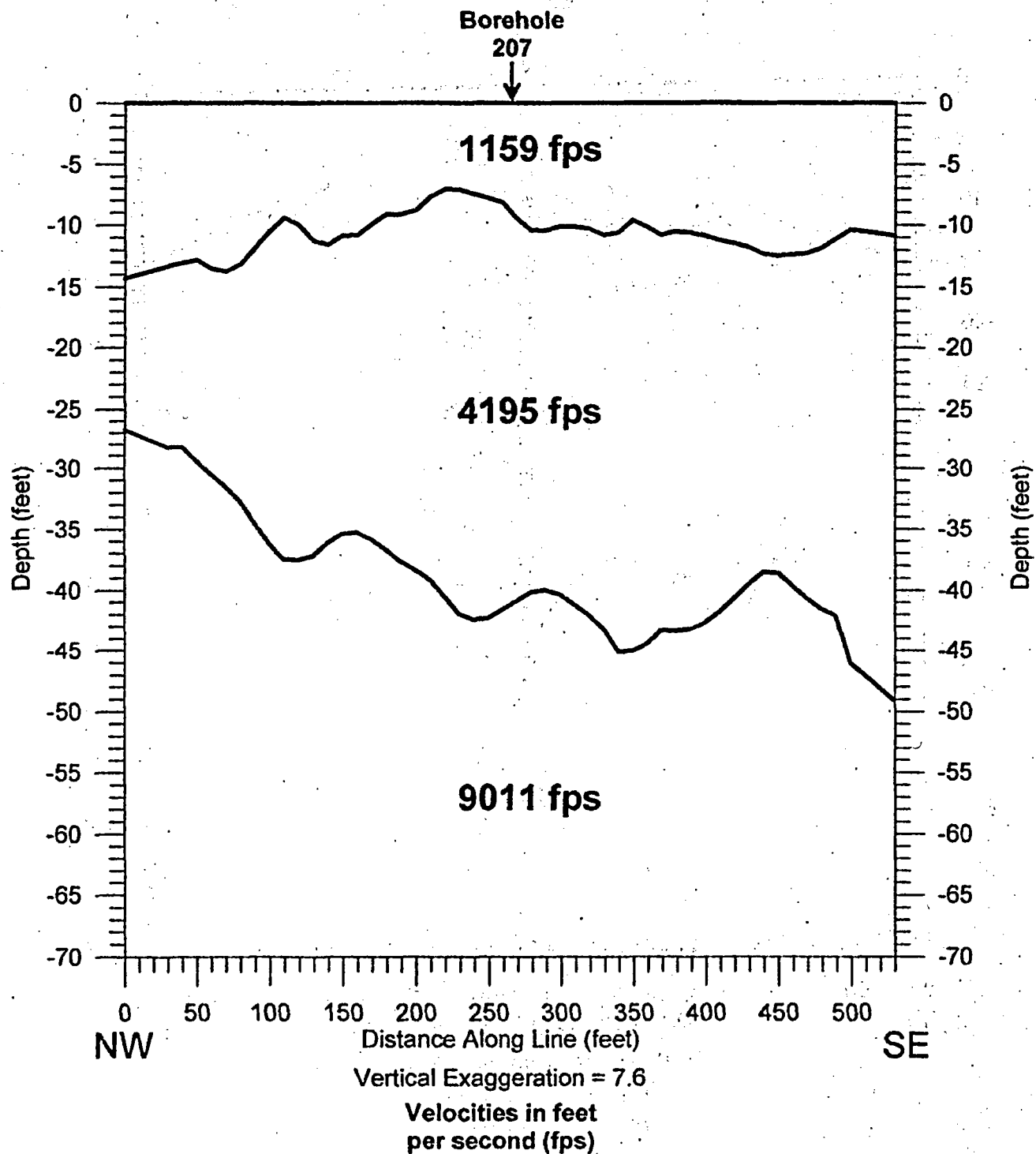
Seismic Rippability Investigation  
Crescent Junction Disposal Site  
**Borehole 206 NW to SE Seismic Line**  
*Depth Section*



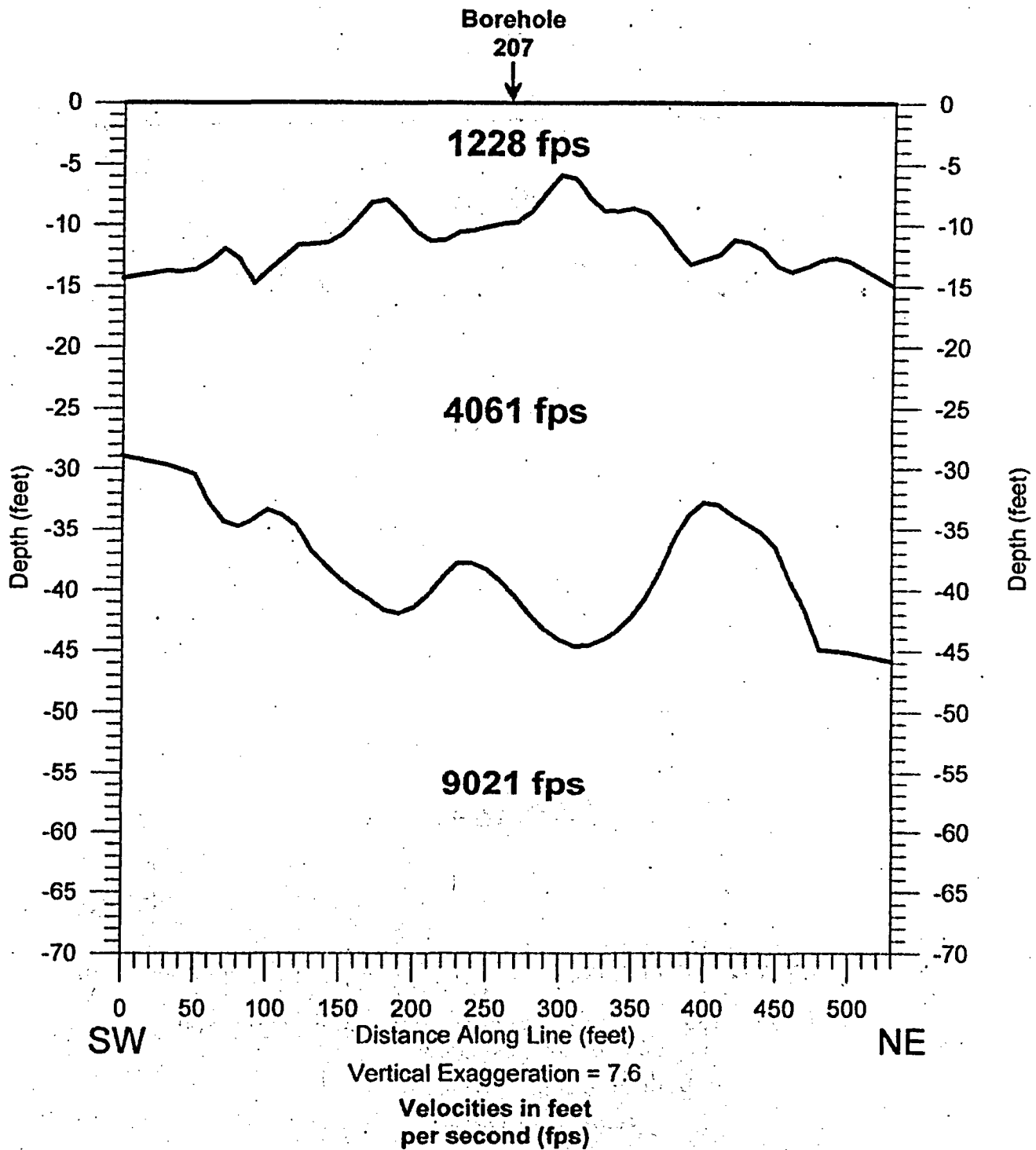
Seismic Rippability Investigation  
Crescent Junction Disposal Site  
**Borehole 206 SW to NE Seismic Line**  
*Depth Section*



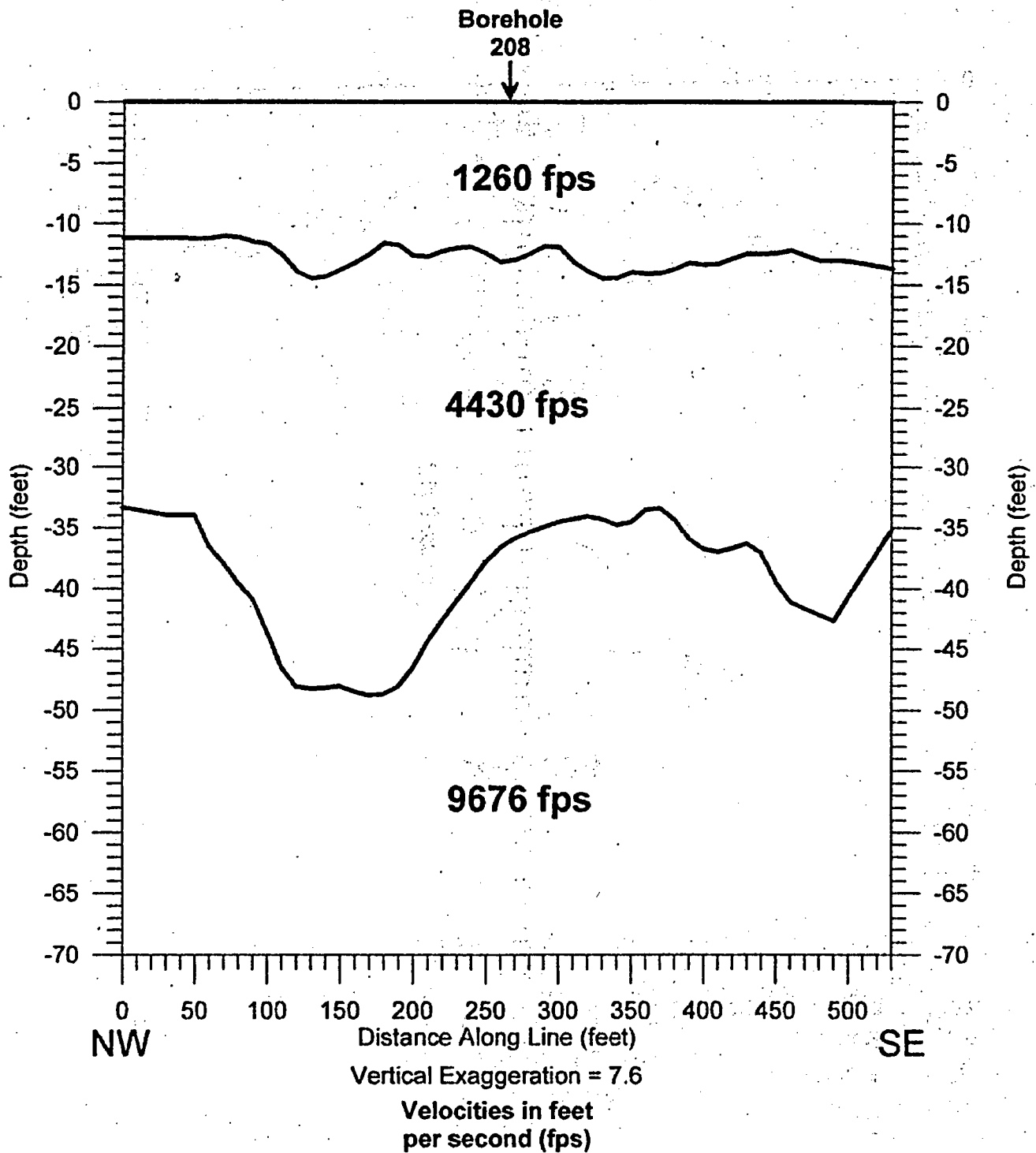
Seismic Rippability Investigation  
Crescent Junction Disposal Site  
**Borehole 207 NW to SE Seismic Line**  
*Depth Section*



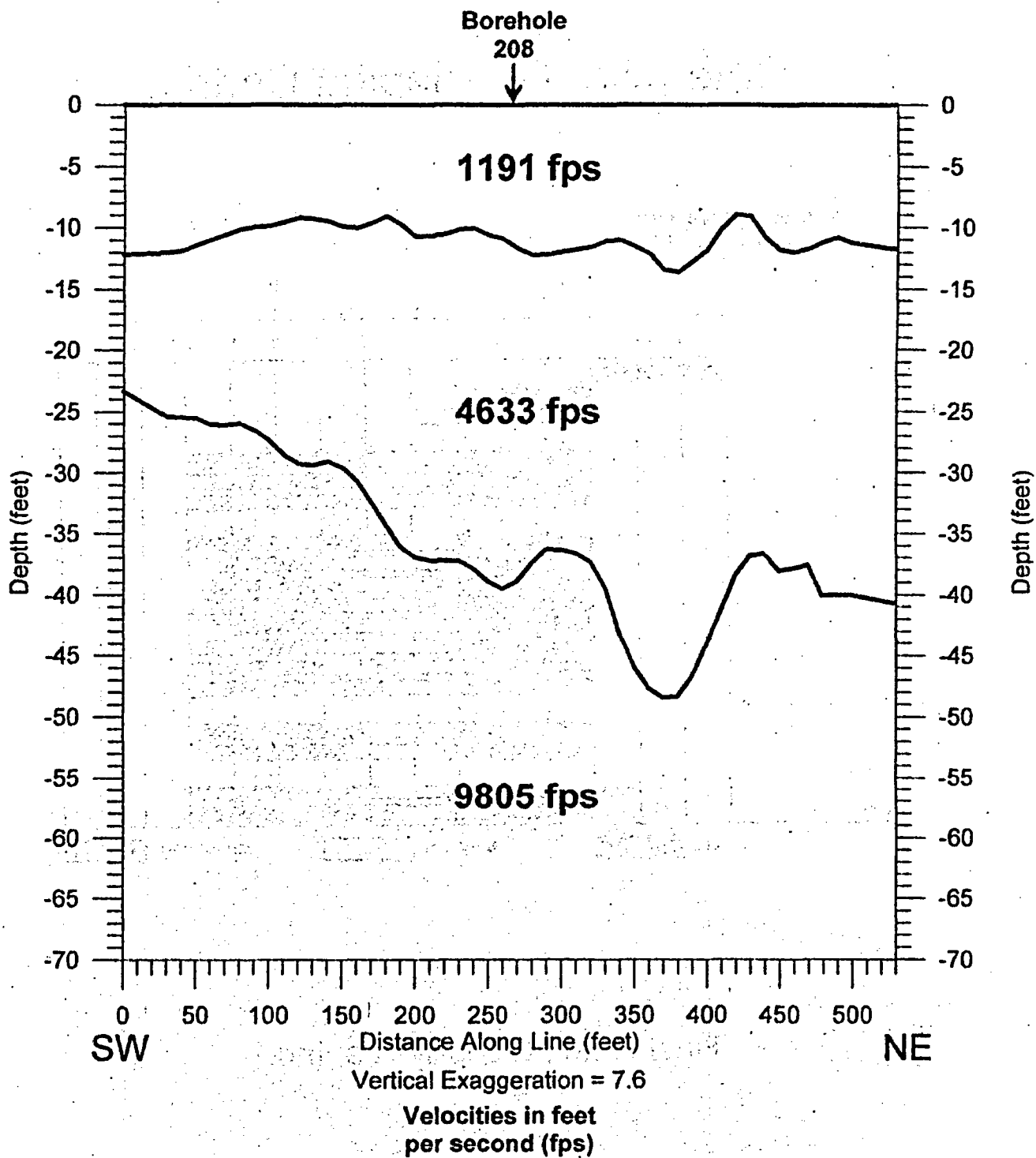
Seismic Rippability Investigation  
Crescent Junction Disposal Site  
**Borehole 207 SW to NE Seismic Line**  
*Depth Section*



Seismic Rippability Investigation  
Crescent Junction Disposal Site  
**Borehole 208 NW to SE Seismic Line**  
*Depth Section*



Seismic Rippability Investigation  
Crescent Junction Disposal Site  
**Borehole 208 SW to NE Seismic Line**  
*Depth Section*



# Caterpillar D8 Ripping Chart

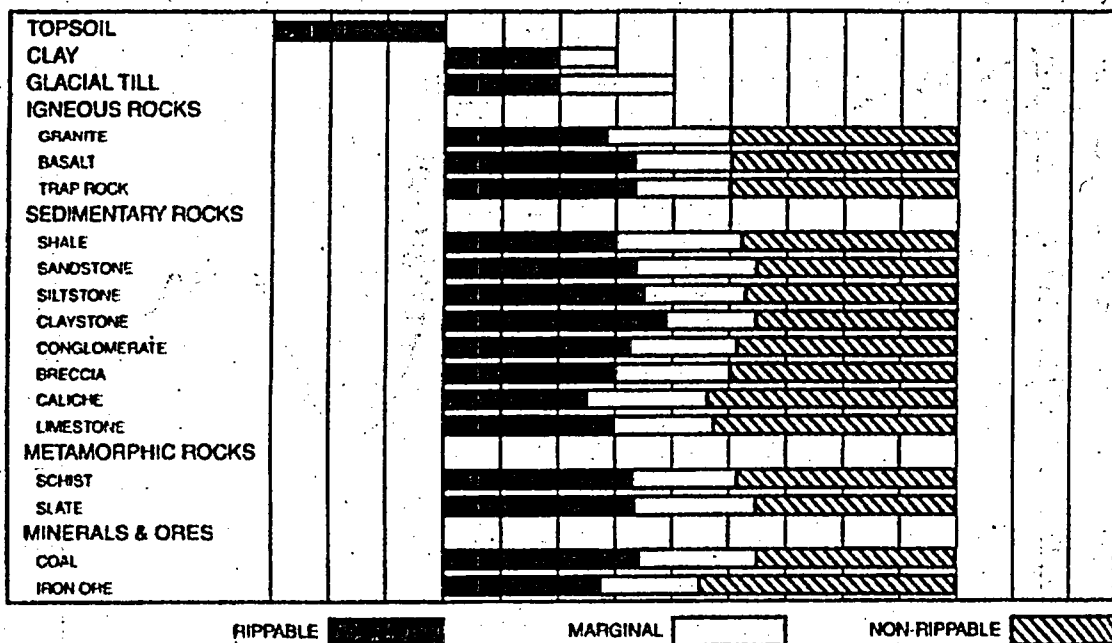
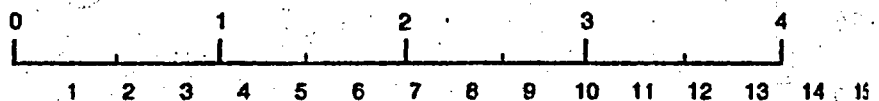
## D8R

- Multi or Single Shank No. 8 Ripper
- Estimated by Seismic Wave Velocities

Seismic Velocity

Meters Per Second  $\times 1000$

Feet Per Second  $\times 1000$



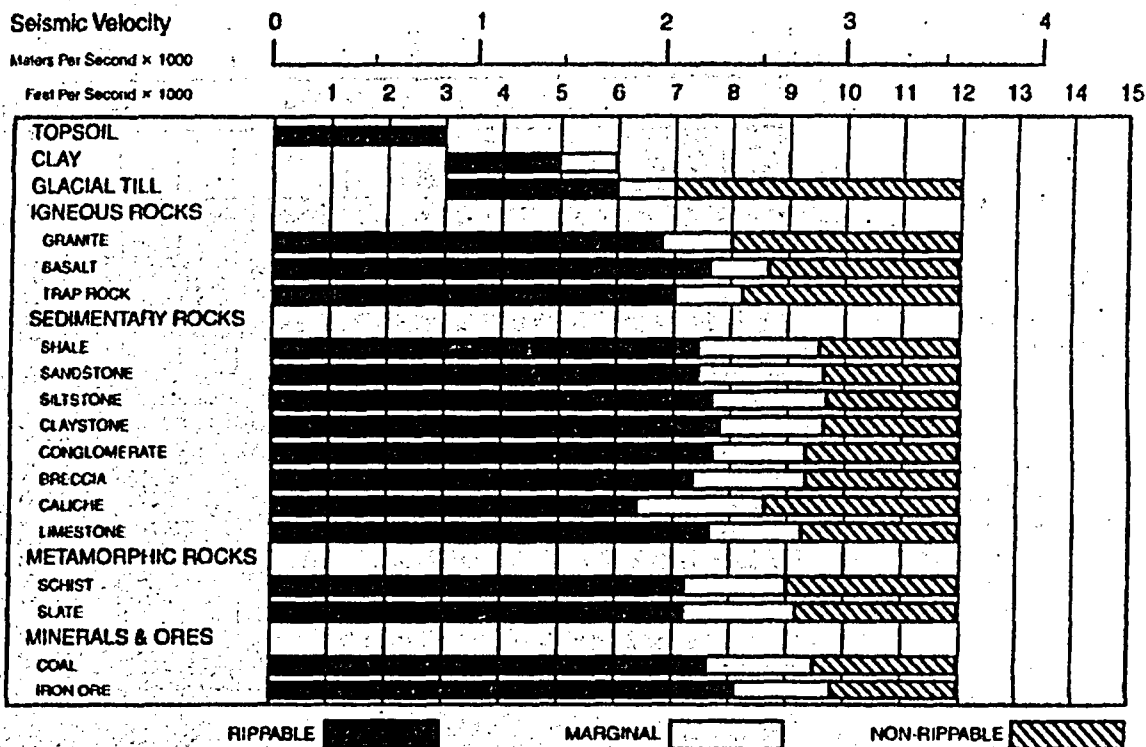
Hasbrouck Geophysics, Inc.



# Caterpillar D9 Ripping Chart

D9R

- Multi or Single Shank No. 9 Ripper
- Estimated by Seismic Wave Velocities



Hasbrouck Geophysics, Inc.

# Caterpillar D10 Ripping Chart

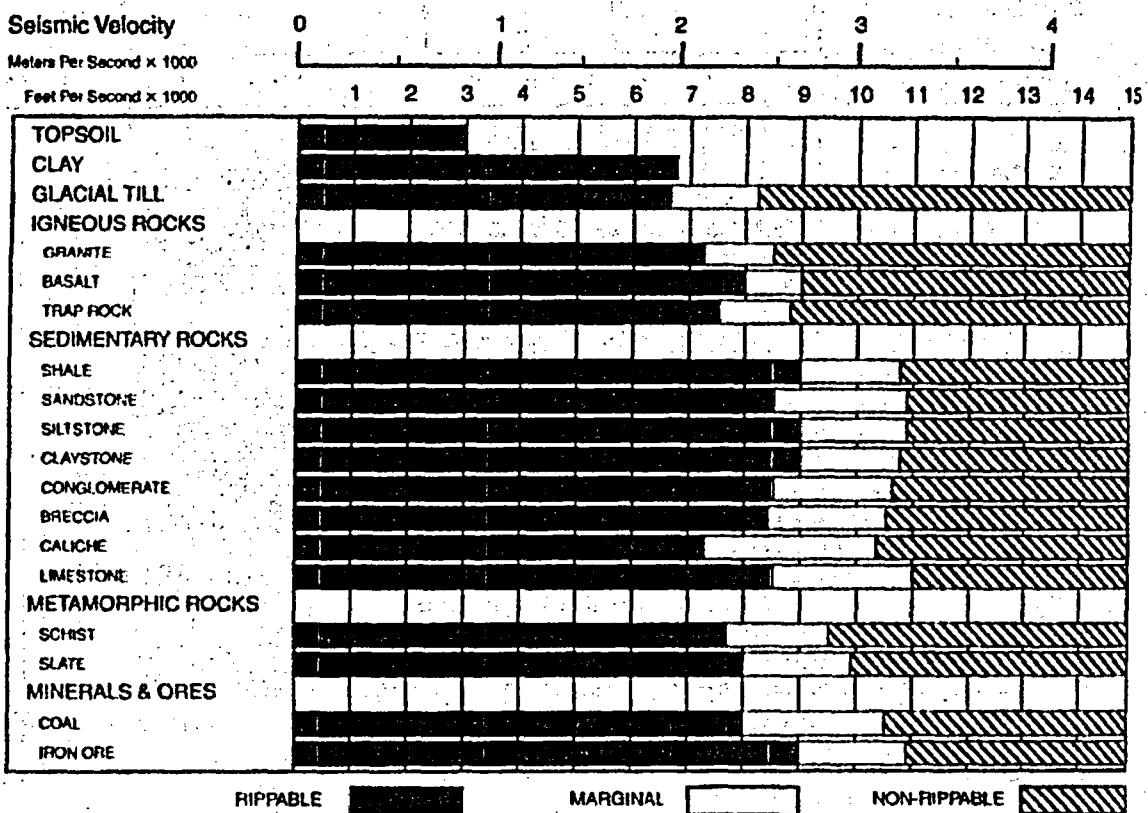
## D10R

- Multi or Single Shank No. 10 Ripper
- Estimated by Seismic Wave Velocities

Seismic Velocity

Meters Per Second x 1000

Feet Per Second x 1000



Hasbrouck Geophysics, Inc.

# Caterpillar D11 Ripping Chart

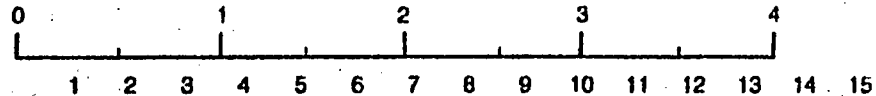
D11R

- Multi or Single Shank No. 11 Ripper
- Estimated by Seismic Wave Velocities

Seismic Velocity

Meters Per Second x 1000

Feet Per Second x 1000



RIPPABLE

MARGINAL

NON-RIPPABLE

Hasbrouck Geophysics, Inc.

## **Appendix B**

### **Review of Seismic Rippability Investigation Report**

The Word Works Inc., dba

**H. David Mac Lean, P. Geoph**

November 23, 2005

Mr. Mark Kautsky  
S.M. Stoller Corp.  
2597 B 1/4 Road  
Grand Junction CO 81503

**Subject: Review of Report; Seismic Rippability Investigations**  
*at the Crescent Junction Disposal Site,*  
*for S.M. Stoller Corp. Grand Junction CO*  
*by Hasbrouck Geophysics.*

202 North Ave., PMB 252  
Grand Junction Co 81501 Phone/fax : 970-242-1649

## **H. David Mac Lean, P. Geoph.**

**Review of Report "Crescent Junction  
Disposal Site Rippability Investigations"  
by Hasbrouck Geophysics**

**November 23, 2005**

In its simplest form, the delay time method involves measurement of the time of arrival of a seismic wave at two geophone locations separated by a distance  $D$ . The description of the method and the procedures employed to accomplish the measurements as set forth in the above reference report are in accordance with standard industry practice. It is a limitation of the method that in order to measure the seismic velocity of successively deeper units, the seismic velocity must increase sequentially with depth, as stated in the report. This is usually the case in the most frequently encountered field situations, but low velocity, or reversal situations are encountered on occasion. Low velocity reversals do not appear to occur at the Crescent Junction site.

The lithologic section and the depth of investigation were specified by Stoller. The near surface section was determined by careful logging of core and cuttings from boreholes located throughout the planned repository. Selected boreholes formed the centers of the seismic refraction spreads as shown in the Borehole and Seismic Line Location Map included with the subject report. The refraction surveys were intended to extend the layer thickness information for approximately 250 ft in four orthogonal directions from the borehole.

### **Field Data Acquisition**

The equipment referenced in the subject report was inspected during a visit to the field operations on October 29. The equipment was found to be as specified, and to be in good working order. Field conditions were less than optimal. Heavy rains had turned the area into a quagmire; nevertheless, the field crew was able to bring equipment into the area and proceeded with the survey with only minimal interruption caused by the adverse road and access conditions.

Field work for the survey was conducted October 29 and 30, 2005. It was observed that all field activities were conducted in a professional and workmanlike manner. Prior to commencement of operations, the field crew was briefed on health and safety issues by a Stoller representative, and a Health and Safety Plan was provided to the crew. The briefing was attended by this reviewer. Requirements of the plan, including clothing specifications were carefully observed by all field personnel. In accordance with plan requirements, any soil that became even slightly contaminated in the course of the field activities was removed from the site and disposed of in accordance with applicable procedures and regulations.

This reviewer participated in one day of the field operations and noted that they were conducted as described in the report. Field work was conducted by a crew provided by Bird Geophysics in accordance with survey design specifications developed by Hasbrouck Geophysics. The crew was obviously well trained and performed all assigned tasks with competence and in a professional manner.

## **H. David Mac Lean, P. Geoph.**

Review of Report "Crescent Junction  
Disposal Site Rippability Investigations"  
by Hasbrouck Geophysics

November 23, 2005

Upon locating the center of the refraction spreads referenced in an expanded version of the "Borehole and Seismic Line Location Map" included in the report, two orthogonal survey lines were extended in a NE-SW direction and a NW-SE direction. The lines were run by chain and compass; markers were placed at 10 foot intervals for a distance of 270 ft in the four directions from the center point. Every fourth marker from the center was identified so that its position could be surveyed later to the required accuracy. Since the terrain was open and unencumbered by vegetation, the entire line could be viewed from vantage points along the line. Lines were visually determined to be straight along the length of the chained interval.

Geophones were placed at each 10 foot marker. All geophones in a linear string were connected to the Bison 48 channel seismograph with Mark Products geophone cables.

Seismic signals were generated by the accelerated weight drop hammer mentioned in the report. A 200 lb metal bar is raised against compressing springs, and is thus accelerated downward to strike an aluminum plate placed on the ground at the shot point. The hammering operation started at one end of the line, and continued at various points along the spread as stated in the report. This is standard "shooting" procedure for seismic refraction surveys. The multiple shot points allow numerous depth and velocity determinations at various points along the spreads, and permit averaging and compensation for anisotropy and dip, since the seismic ray path can be observed in opposite directions. This procedure enables production of a much more detailed and representative velocity-depth section than would be possible if only a single shot point was employed.

Several (up to six) "shots" or hammer blows were taken at each shot point, allowing the seismic signals at each geophone location to be stacked. This procedure increases the signal to noise ratio. As pointed out in the report, seismic waves that arrive at a geophone at the same time following a hammer blow are additive to the signal; random noise or seismic signals for which the strike instant is incorrect are destructive and will not augment or enhance the initial seismic signal. On completion of the stacking activity, a seismogram was printed in the field for inspection and quality assurance purposes.

On the completion of the field survey day, digital data sets were forwarded to Hasbrouck Geophysics for processing and analysis. The data were processed by Hasbrouck Geophysics using the SIPwin software from Rimrock Geophysics. This processing software is state-of-the-technology for Refraction Seismic Data Processing. Given the software capabilities and the field procedures employed, Hasbrouck Geophysics was able to calculate seismic velocities over very short refractor distances. Velocities were calculated using both the regression and Hobson-Overton methods. This processing combination adequately deals with the effects anisotropy, and the distortions introduced by dipping layers. The resulting depth and velocity calculations were then employed to produce the very detailed velocity/depth sections included with the subject report.

## **H. David Mac Lean, P. Geoph.**

Review of Report "Crescent Junction  
Disposal Site Rippability Investigations"  
by Hasbrouck Geophysics

November 23, 2005

### **Analysis**

The velocities for the 3 layers discussed in the report, i.e., alluvium (layer 1) weathered Mancos Shale (layer 2) and Mancos Shale (layer 3) are well within the range expected for these materials. In unconsolidated material such as Layer 1, seismic velocities are often close to acoustic velocities in air (approximately 1100fps). Considerable variation in the measured velocity of Layer 2, (the weathered shale or regolith) can be expected depending on the amount of sand or silt inclusioning and the degree of consolidation within local areas. As pointed out in the report, weathering will not be complete through the entire geologic section and the lithologic material is not uniform. As expected, the seismic velocities increase as a function of depth.

The velocity function for all three layers underlying the planned repository is well illustrated by the time-distance (T-D) plot for one of the survey lines at borehole 204. A copy of the T-D plot is attached hereto. The figure provides a visual indication of the seismic velocity for the various layers. Generally, the flatter the curve on the T-D plot, the higher the velocity. A segment of the T-D plot that is continuous over a measurable interval indicates an identifiable layer. A simple estimate of the velocity associated with this interval can be made by dividing the distance interval D by the difference in arrival time (T) on the T-D plot. Of course the actual final determination of the depth associated with this interval involves a considerably more complex calculation, as has been discussed peripherally in the report.

### **Limitations**

The purpose of measuring the seismic velocities of the layers underlying the proposed mill tailings repository was to estimate the rippability of the underlying lithologic units. Hasbrouck Geophysics has developed depth and velocity sections for all of the surveyed lines that show the lithologic layers to depths of 50 to 60 feet and the measured seismic velocities within these layers to the accuracy that is achievable with the equipment and methodology employed. However, the relationship of these measured seismic velocities to rippability of a particular unit is empirical, not an engineering certainty. Caterpillar Inc. and others involved with heavy equipment operations have observed an apparent relationship and have published charts and graphs showing the ripping capabilities of certain tractor models for various geologic material with a range of seismic velocities. However, there are many other factors that contribute to rippability, such as the degree and orientation of fracturing. Although the rippability charts published by Caterpillar Inc. represent that material with a seismic velocity in a certain range is usually within the ripping capability of certain tractor types, it is not an engineering certainty that this is the case.



## **H. David Mac Lean, P. Geoph.**

Review of Report "Crescent Junction  
Disposal Site Rippability Investigations"  
by Hasbrouck Geophysics

November 23, 2005

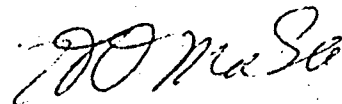
Accordingly, any decision to employ a certain type of equipment based on the velocities provided in the subject report must be taken on the basis of the excavation contractor's own knowledge, and not on statements or implied statements in the report. The velocities and layer thicknesses provided in the report are valid within the accuracy of the seismic refraction method, and are reproducible by similar surveys. Nevertheless, the relationship of these in-situ measured velocities and the suitability of a specific tractor model for ripping a geologic unit with these velocities is strictly empirical and may vary from that presented in the rippability charts provided by Caterpillar Inc.

### **Conclusions**

The subject report provides seismic velocities and the thickness of layers underlying the proposed tailings repository to a depth of about 60 ft or more. The sections showing these depths and velocities provided in the report were produced by means of a refraction seismic survey that was conducted in a professional and workmanlike manner, employing equipment that was suitable to the task. The measured interval velocities, unit thicknesses and variations to be expected are accurate to within the limitations of the current state of refraction seismic technology. The statement in the report that measured velocities are accurate to within 10 per cent is probably overly pessimistic; the accuracy of the measurements is probably much closer to 5% or less. General experience suggests that the unit thicknesses stated in the report are accurate to within 10% or better.

As stated in the report, the suitability of selecting equipment based on the reported velocities is based entirely on the experience of Caterpillar Inc. Nothing in the subject report should be construed as an endorsement of the suitability of a particular tractor model for ripping and excavating applications at the Crescent Junction repository. This decision must be taken on the basis of the excavator's own experience with ripping machinery in applications where seismic velocities are known.

Respectfully Submitted,



H. David Mac Lean, P. Geoph.

HDM/hdm

Enclosures:

Borehole 204 NW to SE Time-Distance plot

**H. David Mac Lean, P. Geoph.**

Review of Report "Crescent Junction  
Disposal Site Rippability Investigations"  
by Hasbrouck Geophysics

November 23, 2005

**References:**

Caterpillar Performance Handbook, Ed 30, October 1999, Use of  
Seismic Velocity Charts pp 1-71-1-78

## **H. David Mac Lean, P. Geoph.**

Review of Report "Crescent Junction  
Disposal Site Rippability Investigations"  
by Hasbrouck Geophysics

November 23, 2005

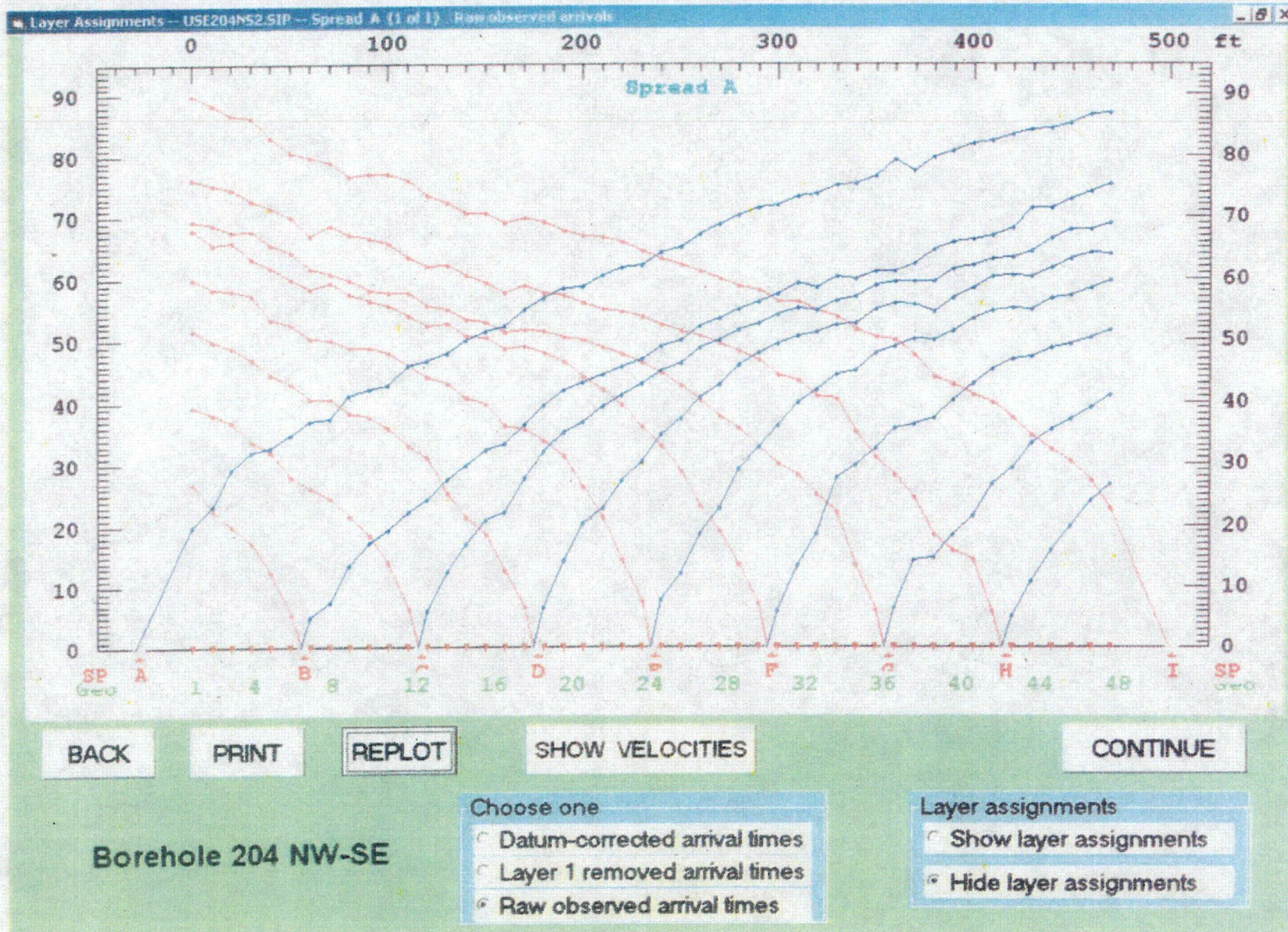
### **Statement of Qualifications**

H. David Mac Lean is a Registered Professional Geophysicist in the State of California, Registration No. 440 and in the Province of Alberta, Canada, Registration no.M15724. Mr. Mac Lean has been a practicing geophysicist for over 35 years.

Mr. Mac Lean has gained experience with the seismic refraction method while engaged in aggregate mapping activities in the Beaufort Sea, and in laying out seismic surveys for oil exploration in Alberta, Canada.

Mr. Mac Lean is an emeritus member of the Society of Exploration Geophysicists, the Canadian Exploration Geophysical Society, The Australian Society of Exploration Geophysicist, the Society for Mining and Metallurgy of the American Institute Mining Engineering and other technical and professional societies dedicated to the advancement of geophysics. Mr. MacLean is a frequent attendee at conventions, trade shows and seminars dedicated to geophysical technologies.







## U.S. Department of Energy—Grand Junction, Colorado

## Calculation Cover Sheet

Calc. No. MOA-02-03-2006-4-07-00 Discipline: Geotechnical Properties No. of Sheets: 2

Project: Moab UMTRA Project

Site: Crescent Junction, Utah

Feature: Seismic Rippability Investigation

## Sources of Data:

## Sources of Formulae and References:

Hasbrouck Geophysics, Inc., 2005. *Crescent Junction Disposal Site Seismic Rippability Investigation*, Final Report, November.

Mac Lean, H. D., 2005. "Review of Seismic Rippability Investigation Report", November.

Preliminary Calc. ☐Final Calc. ☐

Supersedes Calc. No.

Author:

R. Heydenburg  
Name Date

Checked by:

Mark Kautsky 6-9-06  
Name Date

Approved by:

Kurt Kays 6-13-06  
Name DateMark Kautsky P. Grayson 6-9-06  
Name DateR. H. St. 6/12/06  
Name DateP. H. Burk 6/13/06  
Name Date

## **Problem Statement:**

Preliminary site selection performed jointly by the U.S. Department of Energy (DOE) and the Contractor has identified a 2,300 acre withdrawal area in the Crescent Flat area just northeast of Crescent Junction, Utah, as a possible site for a final disposal cell for the Moab uranium mill tailings. The proposed disposal cell would cover approximately 300 acres. Based on the preliminary site-selection process, the suitability of the Crescent Junction Disposal Site is being evaluated from several technical aspects, including geomorphic, geologic, hydrologic, seismic, geochemical, and geotechnical. The objective of this calculation set is to present results of the rippability investigation based on seismic refraction activities at the Crescent Junction Disposal Site.

This calculation will be used in the *Remedial Action Plan and Site Design for Stabilization of Moab Title I Uranium Mill Tailings at the Crescent Junction, Utah, Disposal Site* (RAP), and summarized in the appropriate sections of the Remedial Action Selection (RAS) Report for the Moab site.

## **Method of Solution:**

A refraction seismic survey was conducted along 10 seismic lines centered on existing boreholes at the Crescent Junction Site to assist in evaluation of suitability of the site for disposal of the Moab tailings. The purposes of the seismic surveys were to determine the seismic velocities of weathered and unweathered Mancos Shale deposits that underlie the site and relate those velocities to the rippability of the subsurface materials. The refraction seismic method is routinely used for rippability investigations. Data collection and analysis methods for this project were performed in accordance with the *Standard Guide for Using the Seismic Refraction Method for Subsurface Investigation* ASTM Designation: D 5777-00.

The Final Report of the *Crescent Junction Disposal Site Seismic Rippability Investigation* is in Appendix A and a review of this report is in Appendix B.

## **Assumptions:**

N/A

## **Calculation:**

N/A

## **Discussion:**

Seismic velocities and the thickness of layers underlying the proposed disposal cell to a depth of approximately 60 feet, produced by means of a refraction seismic survey, have been provided in the report. This information will be used to determine optimal and economic depths of excavation for construction of the disposal cell at the Crescent Junction Site. The suitability of selecting equipment based on the reported velocities should be based on the excavators experience with ripping machinery where seismic velocities are known. Data in this report will be used in making these determinations during the conceptual design phase of the disposal cell.

## **Conclusion and Recommendations:**

Use of this information in the conceptual design of the disposal cell at the Crescent Junction will be incorporated into appropriate sections of the RAS and other design documentation.

## **Computer Source:**

N/A

**References:**

See Cover Sheet.

## **Appendix A**

### **Seismic Rippability Investigation Report**





**Hasbrouck Geophysics, Inc.**  
*Groundwater, Engineering, Environmental & Mining*

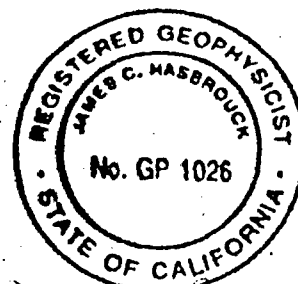
---

## *Final Report*

### **Crescent Junction Disposal Site Seismic Rippability Investigation**

for

**S. M. Stoller Corporation  
Grand Junction, Colorado**



**November 21, 2005**

*James C. Hasbrouck*  
*11/21/05*

---

2473 North Leah Lane  
Prescott, Arizona 86301 USA  
928-778-6320 (Telephone and Fax)  
jim@hasgeo.com (E-Mail)  
<http://www.hasgeo.com> (Homepage)

## TABLE OF CONTENTS

INTRODUCTION.....	1
DATA ACQUISITION .....	1
DATA PROCESSING .....	3
RESULTS.....	4
LIMITATIONS OF INVESTIGATION .....	6
REFERENCE.....	6

### Table

Table 1: Summary of interpreted velocities and depths.....	5
--	---

### Figures

Borehole and Seismic Line Locations Map
Borehole 202 NW to SE Seismic Line Elevation Section
Borehole 202 SW to NE Seismic Line Elevation Section
Borehole 204 NW to SE Seismic Line Elevation Section
Borehole 204 SW to NE Seismic Line Elevation Section
Borehole 206 NW to SE Seismic Line Elevation Section
Borehole 206 SW to NE Seismic Line Elevation Section
Borehole 207 NW to SE Seismic Line Elevation Section
Borehole 207 SW to NE Seismic Line Elevation Section
Borehole 208 NW to SE Seismic Line Elevation Section
Borehole 208 SW to NE Seismic Line Elevation Section
Borehole 202 NW to SE Seismic Line Depth Section
Borehole 202 SW to NE Seismic Line Depth Section
Borehole 204 NW to SE Seismic Line Depth Section
Borehole 204 SW to NE Seismic Line Depth Section
Borehole 206 NW to SE Seismic Line Depth Section
Borehole 206 SW to NE Seismic Line Depth Section
Borehole 207 NW to SE Seismic Line Depth Section
Borehole 207 SW to NE Seismic Line Depth Section
Borehole 208 NW to SE Seismic Line Depth Section
Borehole 208 SW to NE Seismic Line Depth Section
Caterpillar D8 Tractor Ripping Chart
Caterpillar D9 Tractor Ripping Chart
Caterpillar D10 Tractor Ripping Chart
Caterpillar D11 Tractor Ripping Chart

### CD

Velocity Analysis Tables
Time-Distance (T-D) Plots
Modeled elevations and depths beneath each source point and geophone
Observer Reports

## INTRODUCTION

Refraction seismic surveys were conducted for S. M. Stoller Corporation along ten seismic lines centered on existing boreholes at the proposed Crescent Junction Disposal Site to assist in the evaluation of the suitability of the site as a final repository for the Moab uranium mill tailings. The purposes of the seismic surveys were to determine the seismic velocities of weathered and unweathered Mancos Shale deposits that underlie the site and relate those velocities to the rippability of the subsurface materials.

The refraction seismic method is routinely used for rippability investigations. Caterpillar Inc. has prepared charts that relate seismic velocities to different sized rippers. For typical refraction seismic rippability investigations a seismic velocity versus depth or elevation profile is generated along each survey line and then the velocities are related to the Caterpillar charts so that a proper ripper can be selected by the construction contractor. Two types of refraction seismic surveys may be conducted to ascertain the rippability estimates of the subsurface: two-dimensional (2D) tomography and delay-time. The 2D tomography method offers a more detailed and gradational section of the subsurface seismic velocity, but takes a little more time in the field and thus is slightly more expensive. The delay-time method offers only a layered and averaged velocity section, but may be more familiar to construction contractors since it has been in use for a much longer time than 2D tomography. Stoller selected the delay-time method for this project.

This seismic survey was a joint effort between Bird Seismic Service, Inc. of Globe, Arizona and Hasbrouck Geophysics, Inc. of Prescott, Arizona. Bird Seismic acquired the seismic data using the survey design prepared by Hasbrouck Geophysics, while Hasbrouck Geophysics processed and interpreted all the data and prepared the final report. This final report will be reviewed by Mr. H. David MacLean of Grand Junction, Colorado. Ken Bernstein is president of Bird Seismic Services, Inc. and may be reached at [ken@bridseismic.com](mailto:ken@bridseismic.com) or 928-719-1848. Jim Hasbrouck is president of Hasbrouck Geophysics, Inc. and may be contacted at [jim@hasgeo.com](mailto:jim@hasgeo.com) or 928-778-6320. Dave MacLean is available at [107770.3066@compuserve.com](mailto:107770.3066@compuserve.com) or 970-242-1649.

## DATA ACQUISITION

Seismic surveys essentially consist of recording seismic waves that have been generated by artificial sources, observing the arrival times of these waves, and producing cross-sections of variations in subsurface seismic wave velocities that can then be related to geology. The source of seismic energy for surface surveys is primarily dependent upon the target depths and local geology, and for relatively shallow surveys is generally either a sledgehammer or weight-drop system. The seismic waves are detected by geophones in surface surveys. A geophone consists of a coil suspended by springs with magnets built into the case. A seismic wave moves the case and the magnets while the coil remains relatively stationary because of its inertia. The relative movement of the magnetic field with respect to the coil generates a voltage across the coil that is proportional to the velocity of the seismic wave. The electrical voltages produced by the geophones are transmitted back to a recording instrument (seismograph) via cables. In refraction seismic surveys it is necessary, according to Snell's Law, that velocities increase with depth so that the refracted seismic waves can be detected on the surface. For refraction seismic surveys in

most sedimentary environments it is typical that velocities increase with depth (i.e., there are no velocity reversals) and it is assumed that this is the case for the Crescent Junction Disposal Site.

According to Stoller, the depth to weathered bedrock in the project area is assumed to vary from two to approximately 25 feet. Unweathered bedrock may be deeper than 50 feet thus the refraction seismic survey is designed to investigate to depths somewhat greater than 50 feet using the standard rule-of-thumb for refraction seismic surveys that the first geophone to "see" a refraction from a layer will be at a distance of three to five times the expected depth. For example, if an investigation depth of 60 feet is desired then the first geophone to see a refraction, if present, from that depth will be at 180 to 300 feet along the line of geophones, or spread, with the larger distance applicable to areas with generally slower velocities. In order to accurately map the deeper horizons, several geophones must be beyond the initial geophone that records the deeper refraction thus a geophone interval of 10 feet with 30 feet far offsets (resulting in a total spread of 500 feet) is used for this project.

The refraction seismic data for this project were acquired with a 48-channel Bison 9048 seismograph with 21-bits of dynamic range, 250 milliseconds (ms) record lengths, and 0.25 ms sample intervals with Mark Products 10-Hz geophones implanted approximately three inches into the ground at intervals of 10 feet along each line. The seismic source was an Elastic Wave Generator (EWG) accelerated weight-drop mounted on the back of a 4x4 pickup and consisted of a 207-pound weight that was lifted hydraulically against large springs and then released resulting in a force much greater than the weight itself. For each seismic line data from a minimum of eleven source points were acquired (seven within the spread nominally between geophones 6 and 7, 12 and 13, 18 and 19, 24 and 25, 30 and 31, 36 and 37, and 42 and 43, and off each end at distances of 10 and 30 feet). The geophone distances were initially measured with either a tape or takeout intervals on the geophone spread cable and after completion of data acquisition every fourth geophone and each offset source point was surveyed to at least centimeter accuracy by a contractor to Stoller. Because the surface topography change was minor and the seismic lines were relatively straight it was only necessary to survey the coordinates and elevations of every fourth geophone and then interpolate values for the intermediate geophones.

The seismic data were stacked nominally four to six times (depending upon offset and noise) at each source point to increase the signal-to-noise ratio. Stacking, or signal enhancement, involved repeated source impacts at the same point into the same set of geophones. For each source point, the stacked data were recorded into the same seismic data file and theoretically the seismic signal arrived at the same time from each impact and thus was enhanced, while noise was random and tended to be reduced or canceled. After recording the data on the hard disk of the seismograph, the seismic records were copied to a personal computer at the end of each field day. These data were e-mailed nightly from the field to Mr. Hasbrouck and copies of the Observer Reports (field notes) were faxed at the same time. The quality of the seismic data ranged from very good to excellent depending primarily upon offset, and identifiable first breaks (first arrivals of seismic energy) were present along all the lines.

## DATA PROCESSING

The refraction seismic data were processed using the *SIPwin* (version 2.77) set of computer programs from Rimrock Geophysics Inc., Lakewood, Colorado. The general processing flow consisted of the initial selection, or "picking", of the seismic first breaks (first arrival of seismic energy) with the *SIPK* program, creation of data files for input into the interpretation program with the *SIPIN* program, and interpretation of the data using modeling and iterative ray-tracing techniques with the *SIPT2* program. A first break was selected as the initial downward variation of the seismic signal from a horizontal line and was generally accurate to a time between 0.5 and 1 ms. To enhance the accuracy of first break picks, the seismic record was zoomed to a time that only encompassed the breaks themselves (i.e., only the portion of the seismic record where the first breaks were visible). The *SIPT2* program uses the delay-time method to obtain a first-approximation depth model, which is then trimmed by a series of ray-tracing and model adjustment iterations to minimize any discrepancies between the picked arrival times and corresponding times traced through a 2½-dimensional model. Arrival times at two geophones, separated by some variable XY-distance, are used in refractor velocity analyses and time-depth calculations. Using the principle of migration and iterative ray-tracing within the *SIPT2* program, forward and reverse seismic rays emerge from essentially the same point on the reflector, thus requiring the reflector to be plane over only a very small distance. The ray-tracing procedure tests and corrects the estimated migrated position of points representing the locations of ray entry and emergence from the refracting horizon and takes into account the dip of the refracting horizon at those emergence points, therefore enabling accurate representation of steeply dipping horizons.

For any refraction seismic data analysis, it is important to determine accurate velocities. The *SIPT2* program employs several routines for selection of the proper velocities. For the direct arrivals through the first layer, the velocity is computed by dividing the distances from each source point to each geophone by the corresponding arrival times. These individual velocities are averaged for each source point and a weighted average is computed. For layers beneath the first layer, velocities are computed by two methods: 1) Regression, in which a straight line is fit by least squares to the arrival times representing the velocity layer and average velocities are computed by taking the reciprocals of the weighted average of the slopes of the regression lines, and 2) the Hobson-Overton method wherein velocities are computed if there are reciprocal arrivals from two opposing source points at two or more geophones. Final velocities used in the *SIPT2* inversion process are computed by taking an average of the two methods. As quality control measures, time versus distance (T-D) plots (which represent velocities) are inspected along each seismic line relative to reciprocal times, irregularity and parallelism as per ASTM D5777. The refraction seismic data for this project adequately met the requirements of each of these tests.

Included within this report are a borehole and seismic line location map, and elevation and depth versus distance refraction seismic sections for each line with annotated average velocities for each layer. Also included is a CD with output from the *SIPT2* program that includes velocity analysis tables, T-D plots indicating the picked arrival times, and modeled elevations and depths beneath each source point and geophone. Note that the distances in the modeled results have been corrected for horizontal foreshortening (i.e., corrections are made to obtain true horizontal

positions). The modeled results are used to construct the elevation and depth sections, and are in Microsoft Excel format for future client use if desired.

## **RESULTS**

According to Stoller, the geology of the project area consists of essentially three layers. The near surface is alluvial overburden composed of unconsolidated silt, clay, and sandstone fragments. Beneath the alluvium is weathered bedrock, or weathered Mancos Shale, composed of fractured, chemically weathered, siltstone, silty sandstone or clayey siltstone of variable thickness. The weathered layer is often highly fractured with calcite and gypsum fracture coatings. The Mancos Shale is present beneath the weathered layer and is increasingly competent with depth. Although the Mancos Shale appears to be a great shale mass, it is not one homogeneous unit. According to available lithologic logs for the boreholes within the project area, the Mancos Shale seems to be described as consisting not only of shale but also some sandstone layers and what has been termed a silty claystone. The lithologic logs generally indicate variations in the composition of the unweathered Mancos Shale near its top with increasing shale constituents with depth.

Interpretation of the refraction seismic data indicates three layers, representing alluvial overburden, weathered Mancos Shale and competent Mancos Shale. Table 1 indicates the range in velocities and depths for each line. The first layer velocities range from about 1160 to 1330 feet per second and are consistent with typical unsaturated alluvial overburden values. The second layer velocities range from about 4060 to 5220 feet per second and represent typical values for weathered material such as the Mancos Shale. The variation in velocity values for the interpreted weathered Mancos Shale is probably related to the degree of fracturing and the amount of calcite and/or gypsum coating of the fractures. The higher velocities may have less fracturing or the fractures may be coated with an increased amount of calcite and/or gypsum. It is not possible from the seismic results to determine which scenario exists. The third layer, or competent Mancos Shale bedrock, velocities range from about 9000 to as high as 10000 feet per second with the majority of the velocity values in a range from about 9000 to 9400 feet per second. Velocity variations of the interpreted Mancos Shale bedrock are considered relatively minor and probably related to slight changes in composition of the bedrock or some amount of fracturing. Velocity variations are present along the intersecting seismic lines at each borehole, but generally than about 5% which is reasonable given that the velocity values are averages and the subsurface geology is variable (as evidenced by changes in the lithologic logs between boreholes).

The thickness of the overburden layer (or the depth to the top of layer 2 which is interpreted as weathered Mancos Shale) ranges from about 4½ to 18 feet, while the depth to the top of layer 3 (or interpreted unweathered Mancos Shale bedrock) varies from about 24 to 60 feet. The tie point depths between intersecting lines at each borehole are generally less than about 5% which is considered reasonable and quite acceptable for seismic surveys. Depth values at intersecting points from lines oriented in different directions often vary because of anisotropy within the subsurface geological formations. Anisotropy is defined as a variation of a physical property (e.g., velocity) depending upon the direction in which it is measured. In general, surface refraction seismic data have shown a 10% to 15% variation between the actual depths to velocity

layer anomalies, as verified primarily by geophysical borehole logging, and the depth predicted by the models.

Table 1: Summary of interpreted velocities and depths

Line	Layer 1 velocity (ft/s)	Layer 2 velocity (ft/s)	Layer 3 velocity (ft/s)	Depth to top of layer 2 (ft)	Depth to top of layer 3 (ft)
202NW-SE	1230	4218	10005	4.5 - 15.1	34.3 - 58.7
202SW-NE	1305	4305	9353	11.3 - 17.1	31.5 - 53.0
204NW-SE	1334	4674	9035	8.0 - 14.9	40.4 - 61.1
204SW-NE	1206	4705	9399	10.1 - 18.1	40.5 - 59.3
206NW-SE	1305	5221	9380	9.9 - 16.0	29.5 - 46.8
206SW-NE	1281	5169	9479	7.7 - 15.2	25.4 - 47.5
207NW-SE	1159	4195	9011	7.1 - 14.3	26.7 - 49.1
207SW-NE	1228	4061	9021	5.9 - 15.0	28.9 - 45.9
208NW-SE	1260	4430	9676	11.0 - 14.5	33.3 - 48.8
208SW-NE	1191	4633	9805	9.0 - 13.6	23.4 - 48.4

Inspection of either the elevation or depth sections indicates that the subsurface is far from planar, with some areas showing signs of possible incised bedrock channels (e.g., particularly possibly both lines at borehole 208). Because both the first and last approximately 30 to 50 feet, or more, of the sections have less forward and reverse raypath coverage (refer to the T-D plots), results in those areas should be viewed with some caution. Nevertheless, subsurface depth variations are present along each of the seismic lines.

According to Caterpillar's ripping charts, shale is considered rippable at seismic velocities ranging up to about 6000 to 10200 feet per second for tractor models D8 to D11, respectively. Rippable velocities are slightly different if the subsurface material is composed more of a siltstone (up to about 6500 to 9900 for a D8 to D11 tractor, respectively). Referencing the ripping charts from Caterpillar, it is reasonable to assume that all of the interpreted layer 2 or weathered Mancos Shale can be ripped with a tractor as small as a D8 (note that the Caterpillar ripping charts are not available for tractors smaller than a D8). If it is necessary to rip the interpreted competent Mancos Shale bedrock, with velocities interpreted to be greater than 9000 feet per second, it will be necessary to employ a D11 tractor.

Although the seismic survey covered only a very small portion of the proposed Crescent Junction Disposal Site it is reasonable to assume that excavation in the proposed site will be impacted by the variable weathered and unweathered bedrock depths. Although the author of this report is not aware of the design depth of the proposed disposal site excavation, if it is say 40 feet then there will be areas encountered with much higher velocity material at depth which will require either larger rippers or other means of excavation. For example, if material is ripped along the borehole 207 SW to NE seismic line to a depth of 40 feet materials with average velocities of around 4000 and 9000 feet per second will both be encountered. Obviously, a D8 tractor would not be able to rip to a depth of 40 feet along the entire length of this line.

## LIMITATIONS OF INVESTIGATION

Although a refraction seismic investigation is the most cost-effective way to determine rippability of material in a project area (versus sporadic boreholes that offer only localized information), it must be realized that according to Caterpillar ripping is still more art than science, and much will depend upon operator skill and experience. Caterpillar states in their Handbook that tooth penetration is often the key to ripping success, regardless of seismic velocity. Low seismic velocities in sedimentary rocks can indicate probable rippability. However, if the fractures and bedding joints do not allow tooth penetration then the material may not be ripped effectively. Pre-blasting or "popping" may induce sufficient fracturing to permit tooth entry.

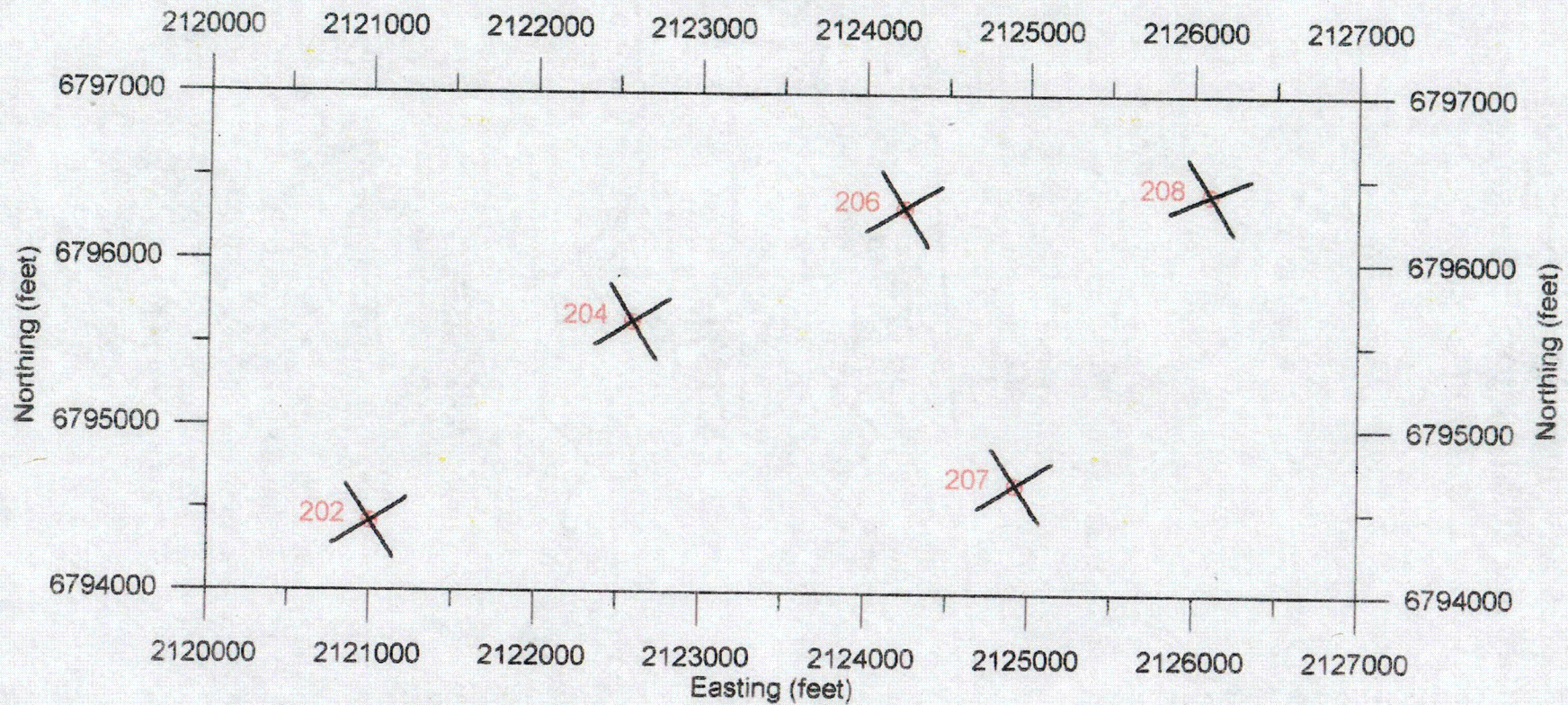
This survey was conducted with state-of-the-art instrumentation operated by experienced geophysicists, the data were processed by an experienced and licensed geophysicist with a commercial software package utilized on projects with similar objectives, and the results were interpreted by an experienced and licensed geophysicist. However, no warranty, either expressed or implied, is made as to the usability of the results of this survey. Additionally, the ripper performance charts developed by Caterpillar are intended for estimating purposes only and neither Caterpillar Inc. nor Hasbrouck Geophysics, Inc. warrant that the tractors will perform as estimated.

## REFERENCE

Caterpillar Performance Handbook, Edition 30, October 1999, *Use of Seismic Velocity Charts*, pp. 1-71 to 1-78.



Seismic Rippability Investigation  
Crescent Junction Disposal Site  
Borehole and Seismic Line Locations



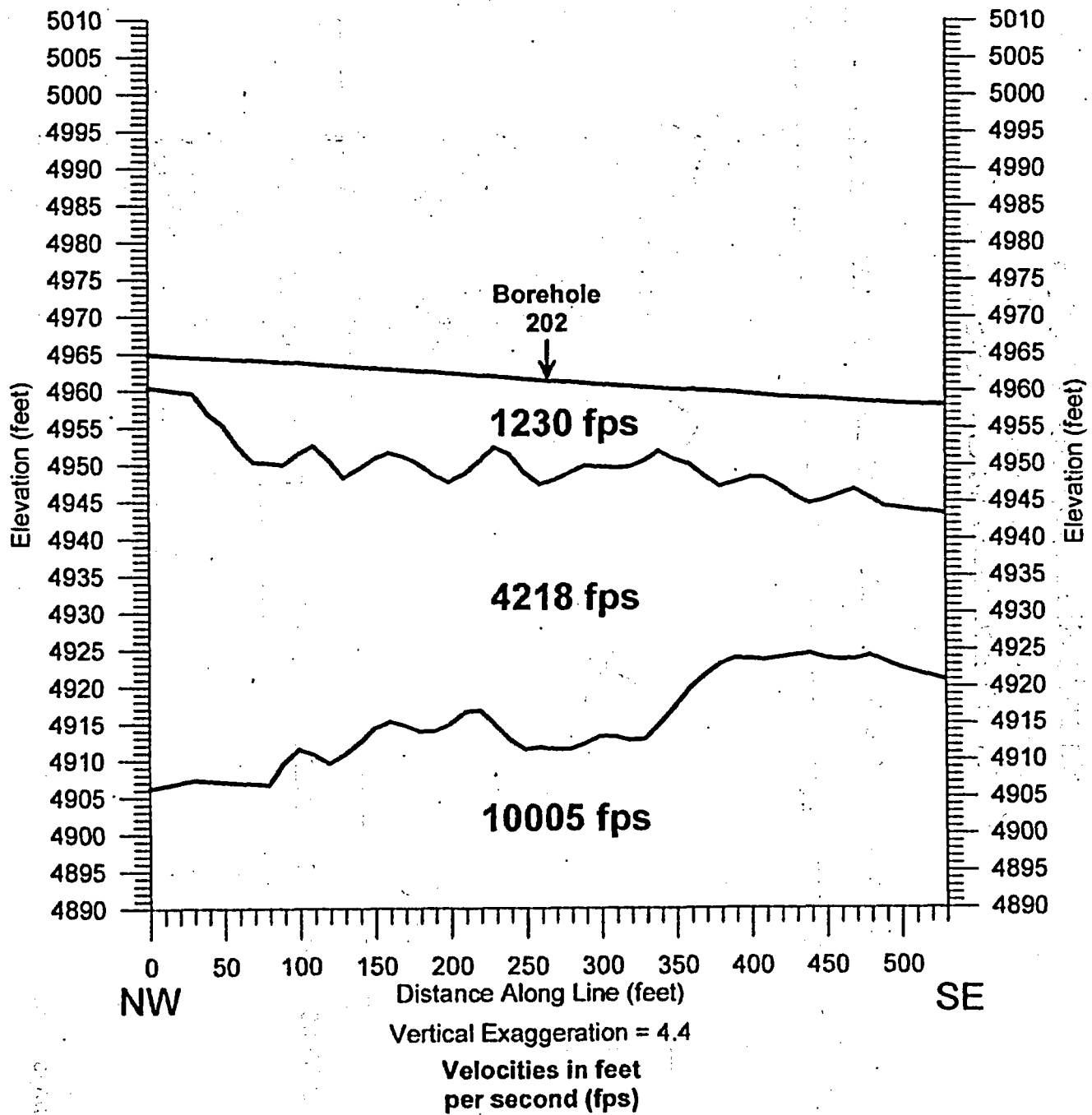
Borehole  
⊕



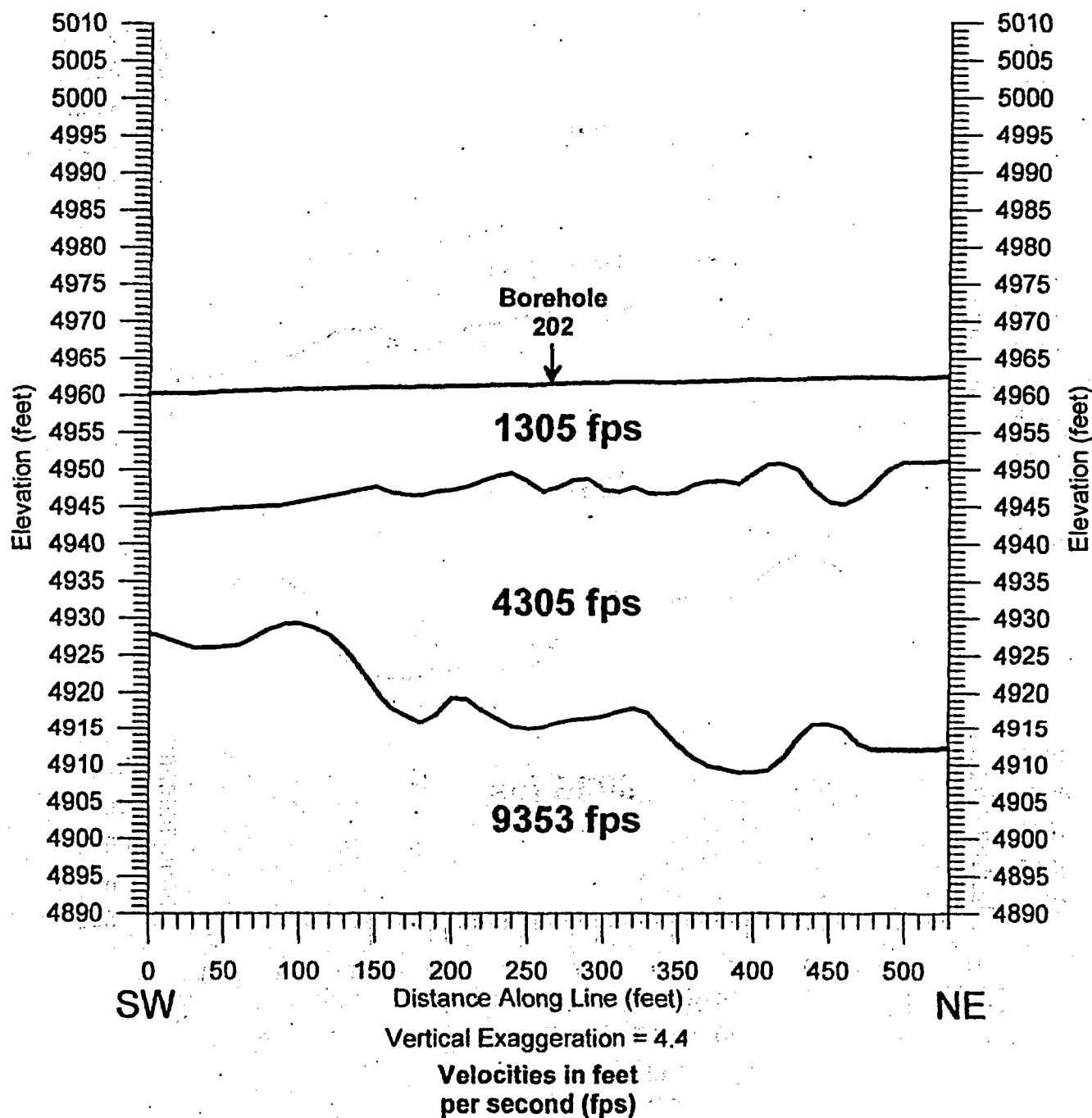
Seismic Line  
—



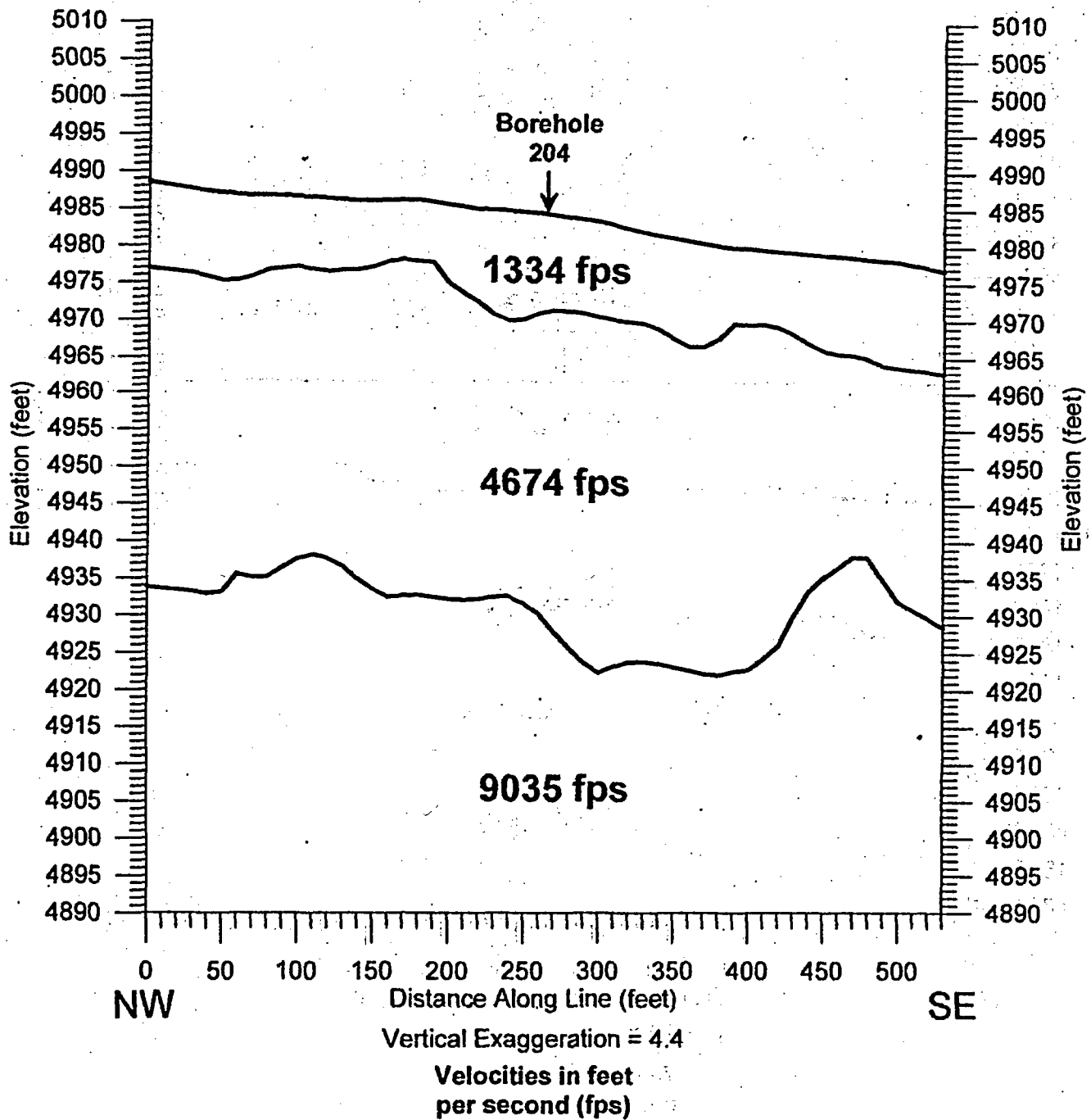
Seismic Rippability Investigation  
Crescent Junction Disposal Site  
**Borehole 202 NW to SE Seismic Line**  
*Elevation Section*



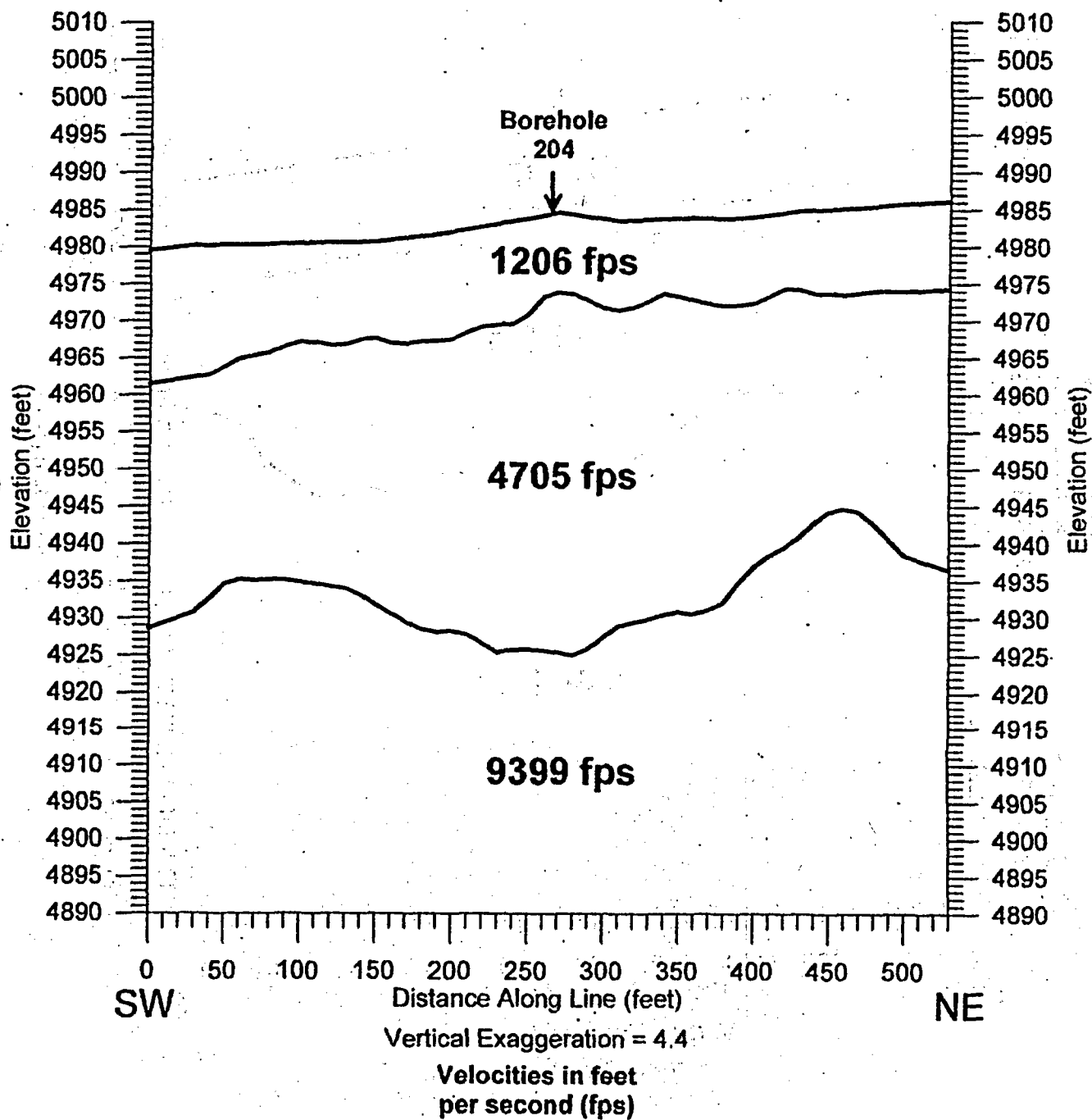
Seismic Rippability Investigation  
Crescent Junction Disposal Site  
**Borehole 202 SW to NE Seismic Line**  
*Elevation Section*



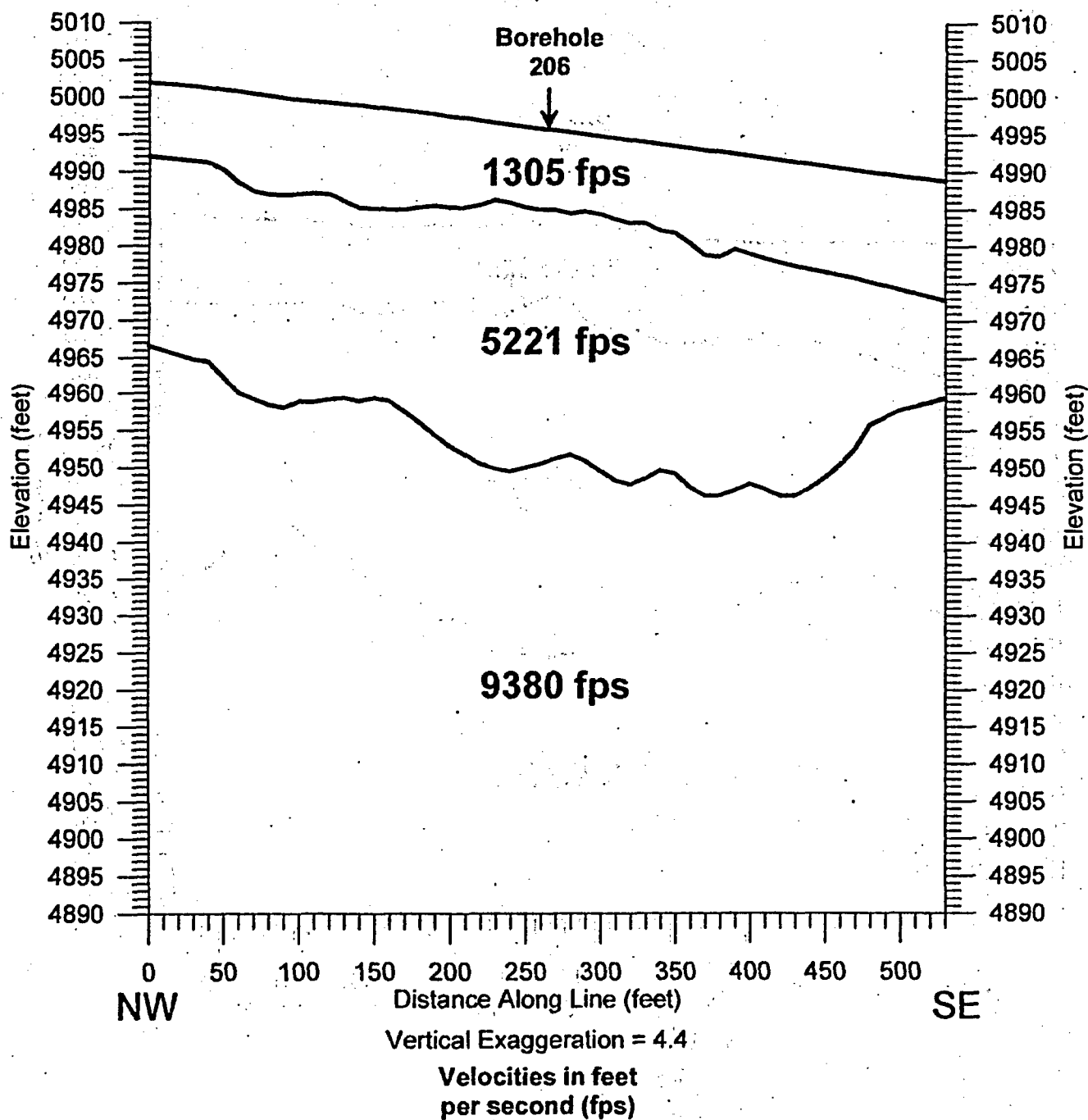
Seismic Rippability Investigation  
Crescent Junction Disposal Site  
**Borehole 204 NW to SE Seismic Line**  
*Elevation Section*



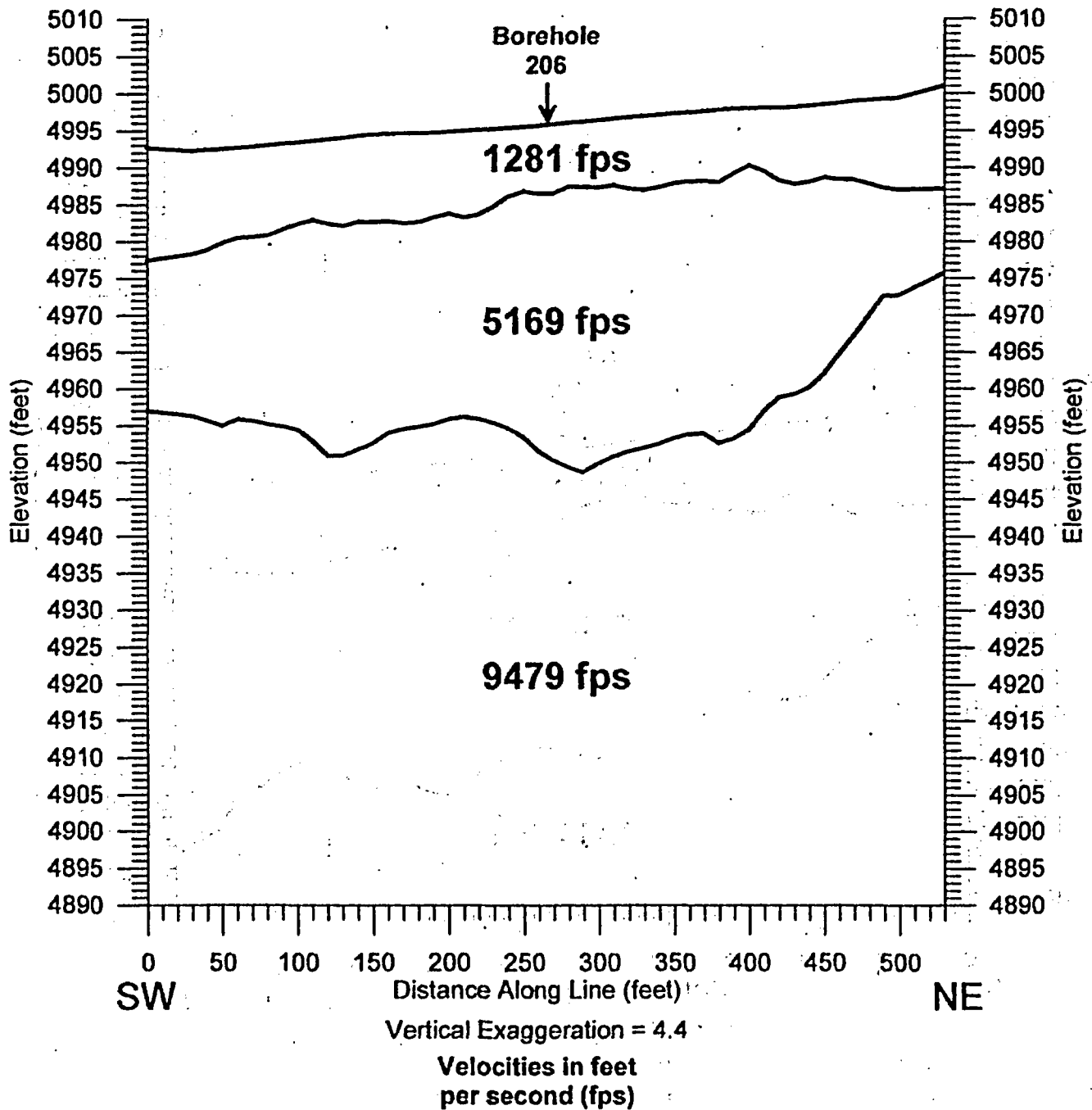
Seismic Rippability Investigation  
Crescent Junction Disposal Site  
**Borehole 204 SW to NE Seismic Line**  
*Elevation Section*



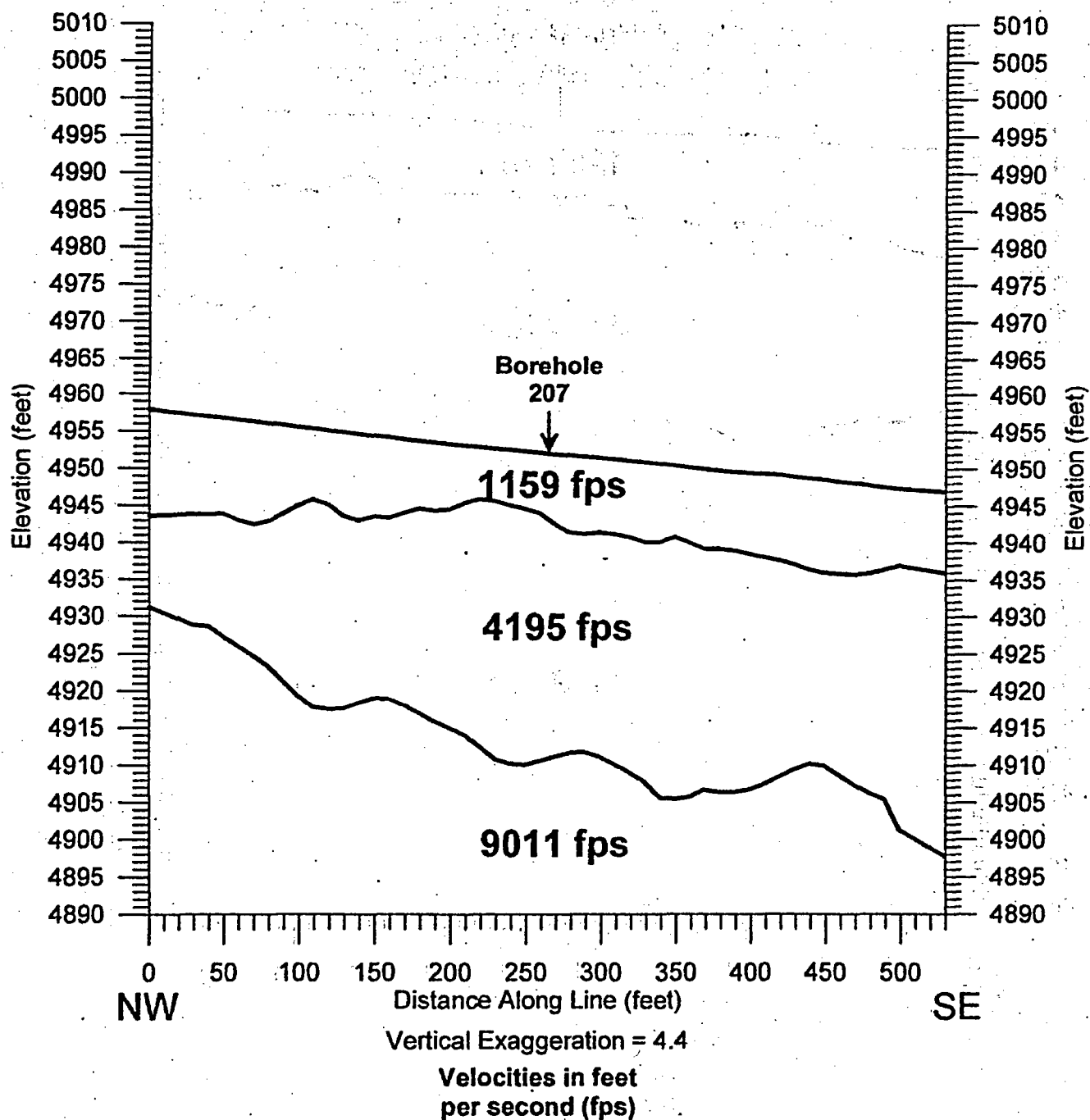
Seismic Rippability Investigation  
Crescent Junction Disposal Site  
Borehole 206 NW to SE Seismic Line  
Elevation Section



**Seismic Rippability Investigation  
Crescent Junction Disposal Site  
Borehole 206 SW to NE Seismic Line  
Elevation Section**

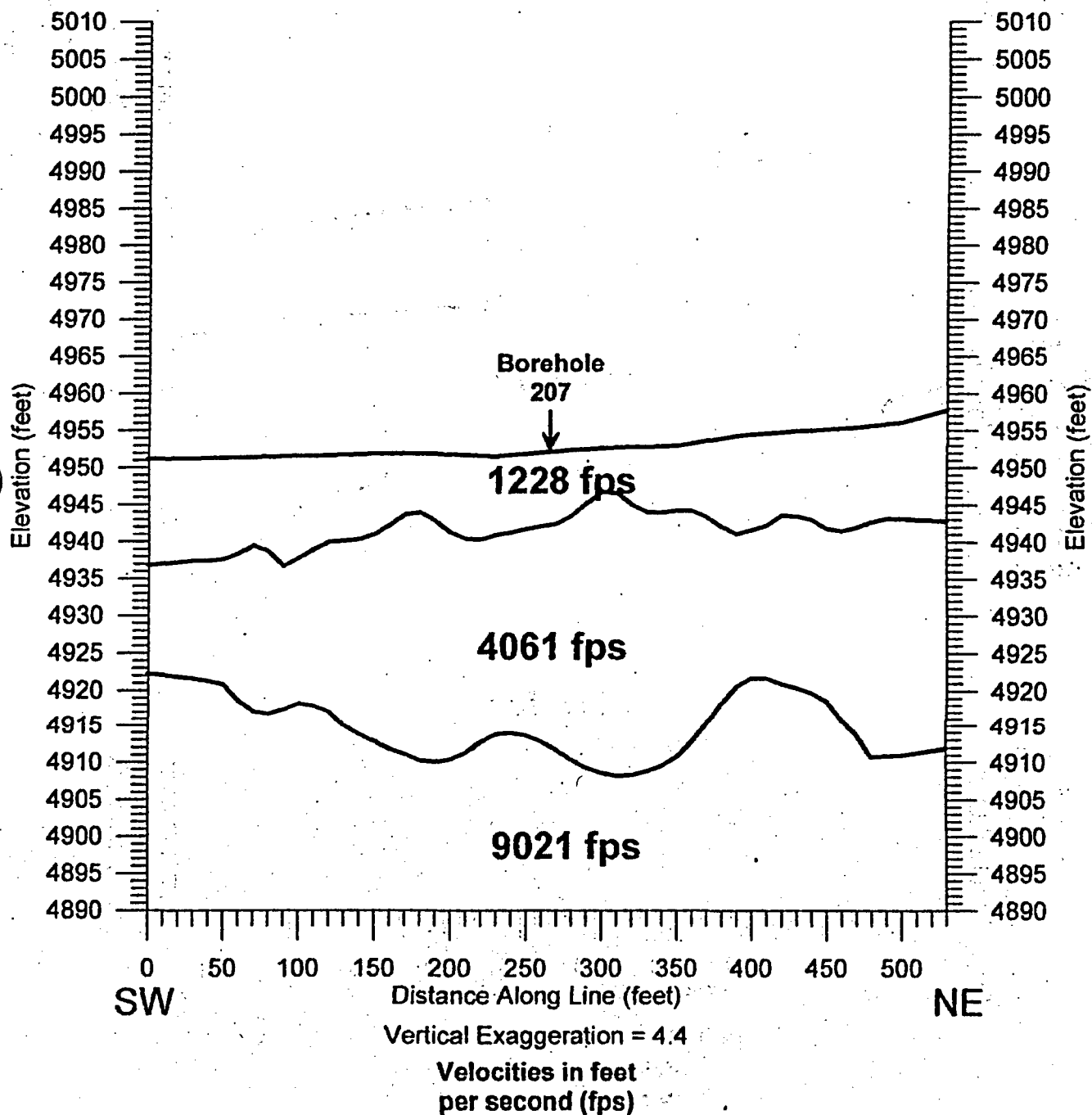


Seismic Rippability Investigation  
Crescent Junction Disposal Site  
**Borehole 207 NW to SE Seismic Line**  
*Elevation Section*

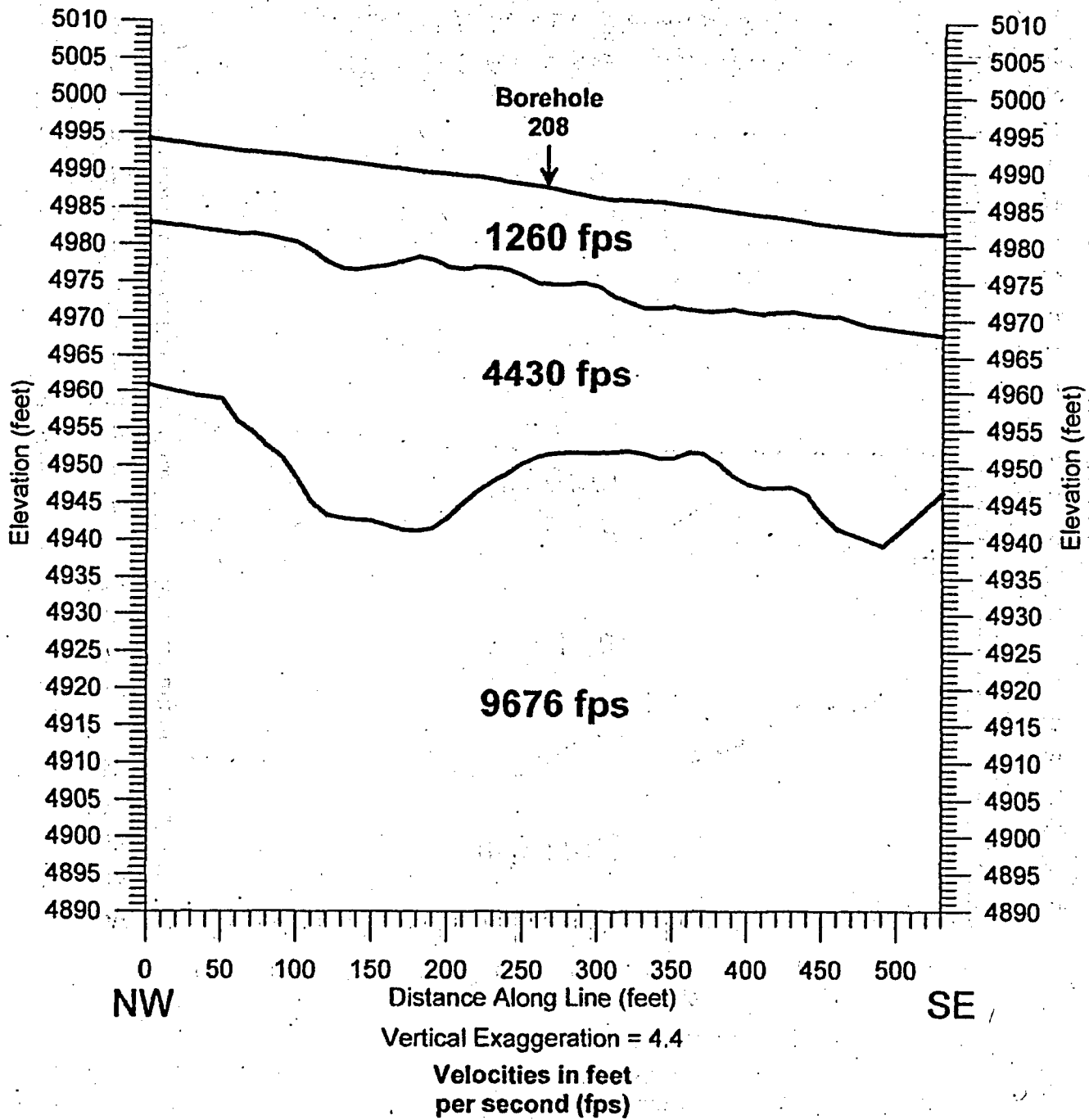




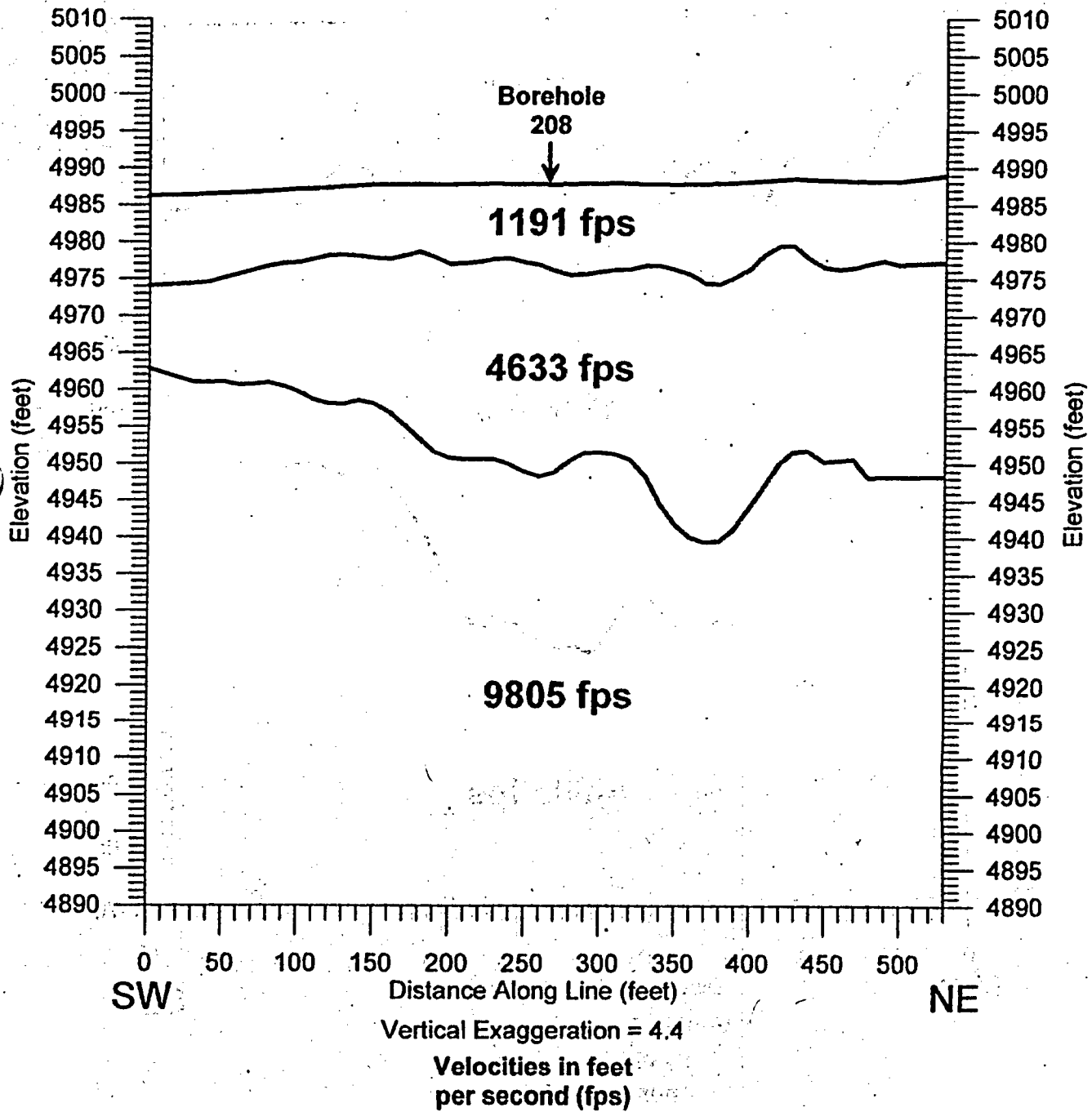
Seismic Rippability Investigation  
Crescent Junction Disposal Site  
**Borehole 207 SW to NE Seismic Line**  
*Elevation Section*



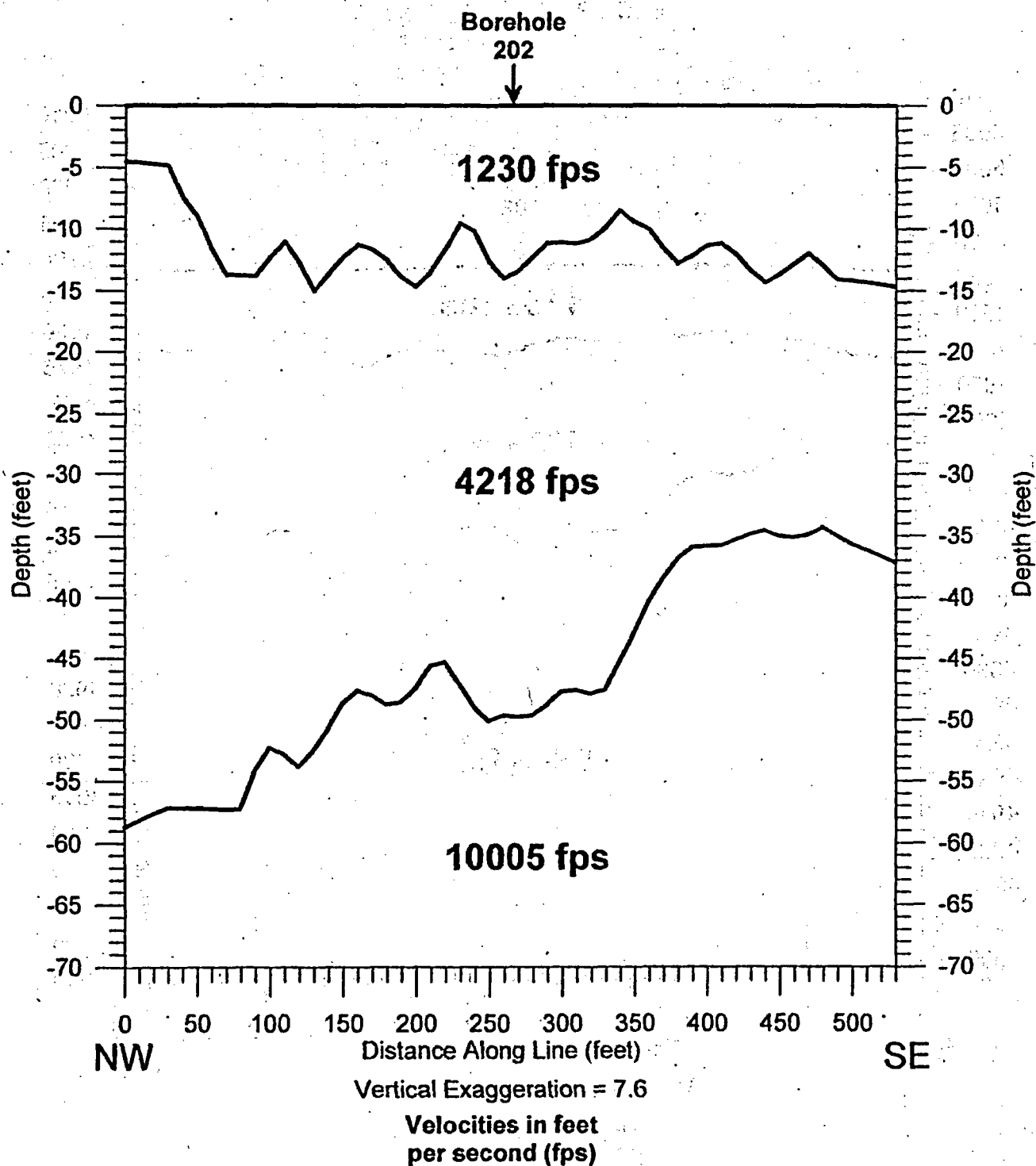
Seismic Rippability Investigation  
Crescent Junction Disposal Site  
Borehole 208 NW to SE Seismic Line  
Elevation Section



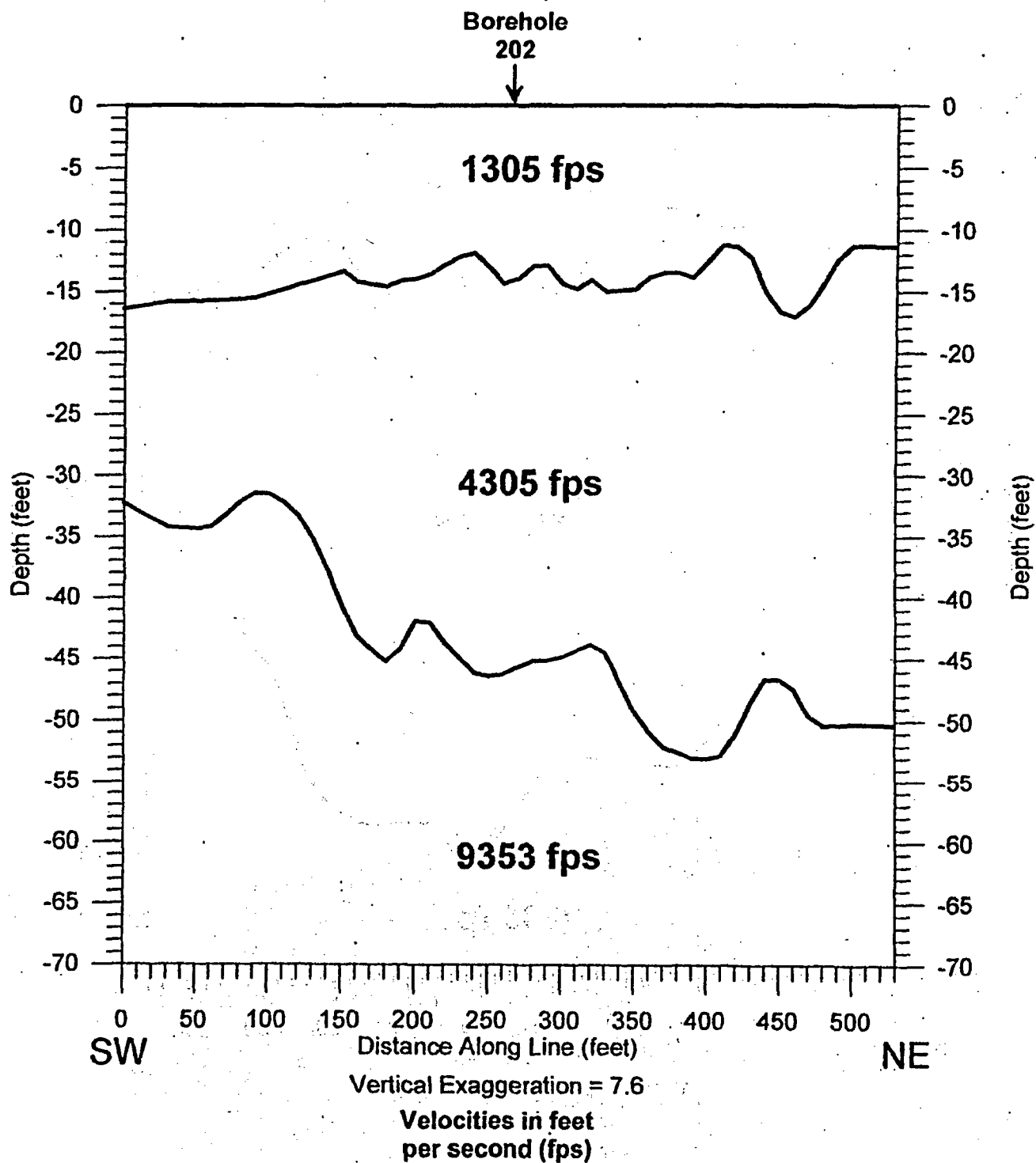
Seismic Rippability Investigation  
Crescent Junction Disposal Site  
**Borehole 208 SW to NE Seismic Line**  
*Elevation Section*



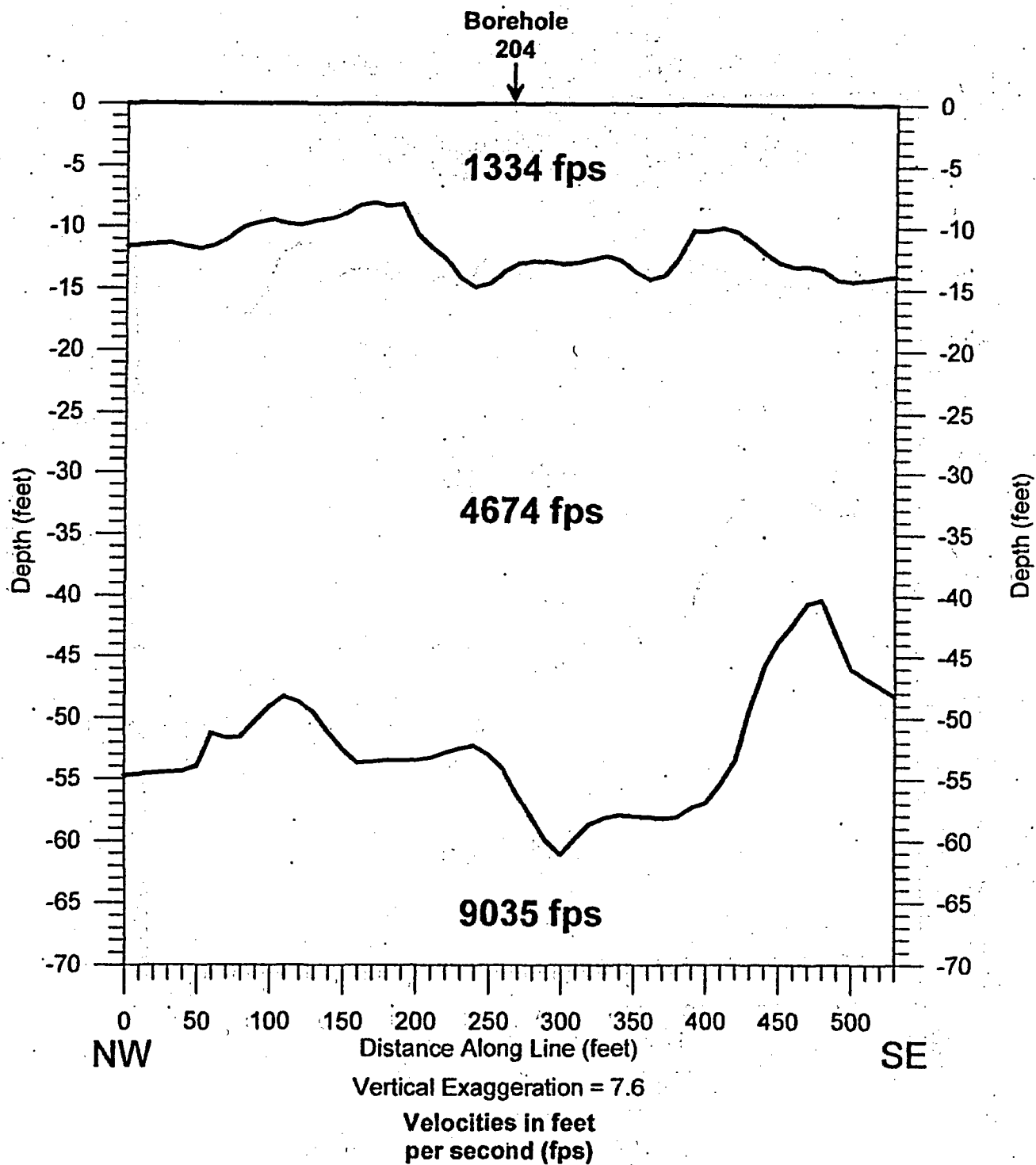
Seismic Rippability Investigation  
Crescent Junction Disposal Site  
**Borehole 202 NW to SE Seismic Line**  
*Depth Section*



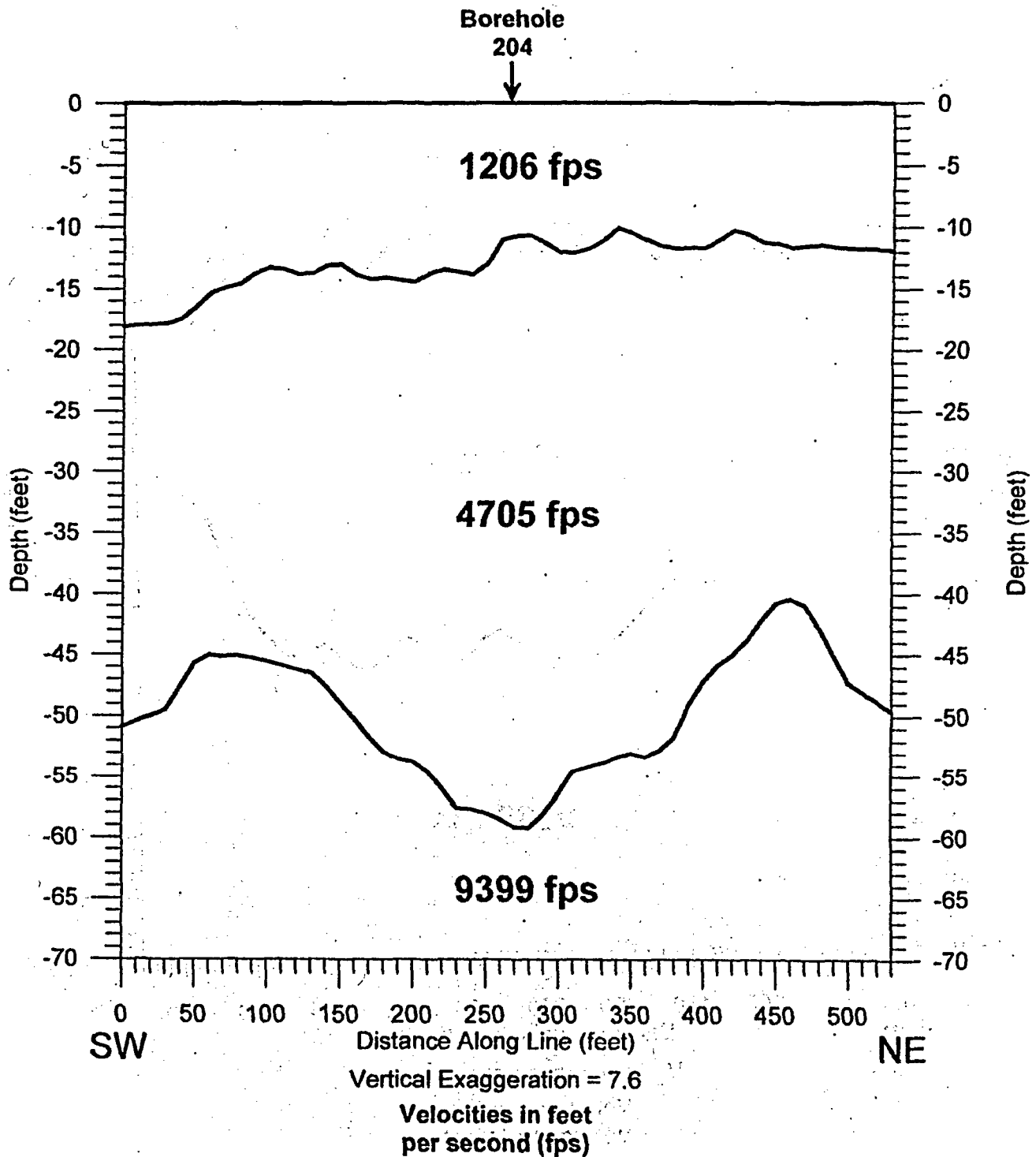
Seismic Rippability Investigation  
Crescent Junction Disposal Site  
**Borehole 202 SW to NE Seismic Line**  
*Depth Section*



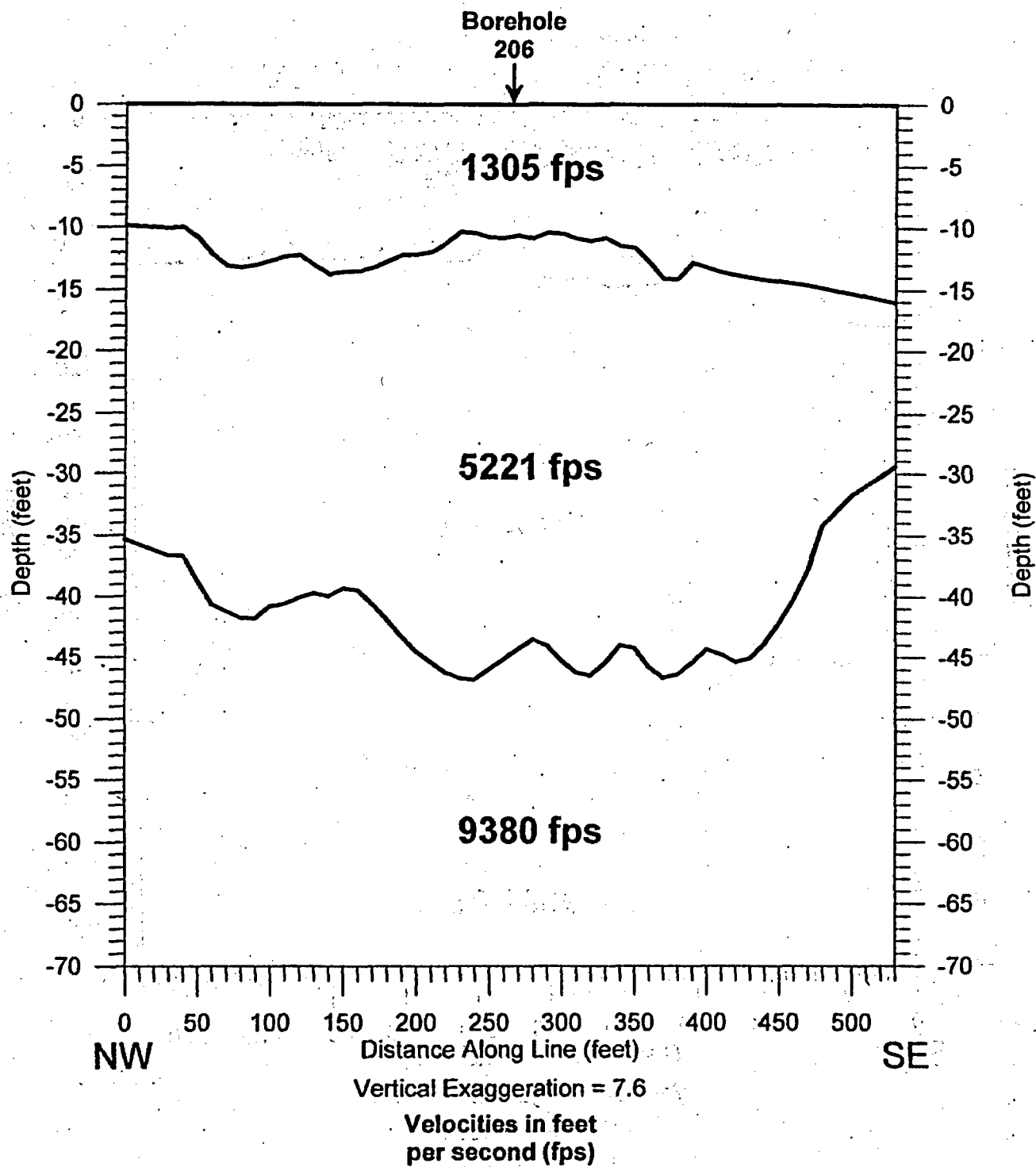
Seismic Rippability Investigation  
Crescent Junction Disposal Site  
**Borehole 204 NW to SE Seismic Line**  
*Depth Section*



Seismic Rippability Investigation  
Crescent Junction Disposal Site  
**Borehole 204 SW to NE Seismic Line**  
*Depth Section*

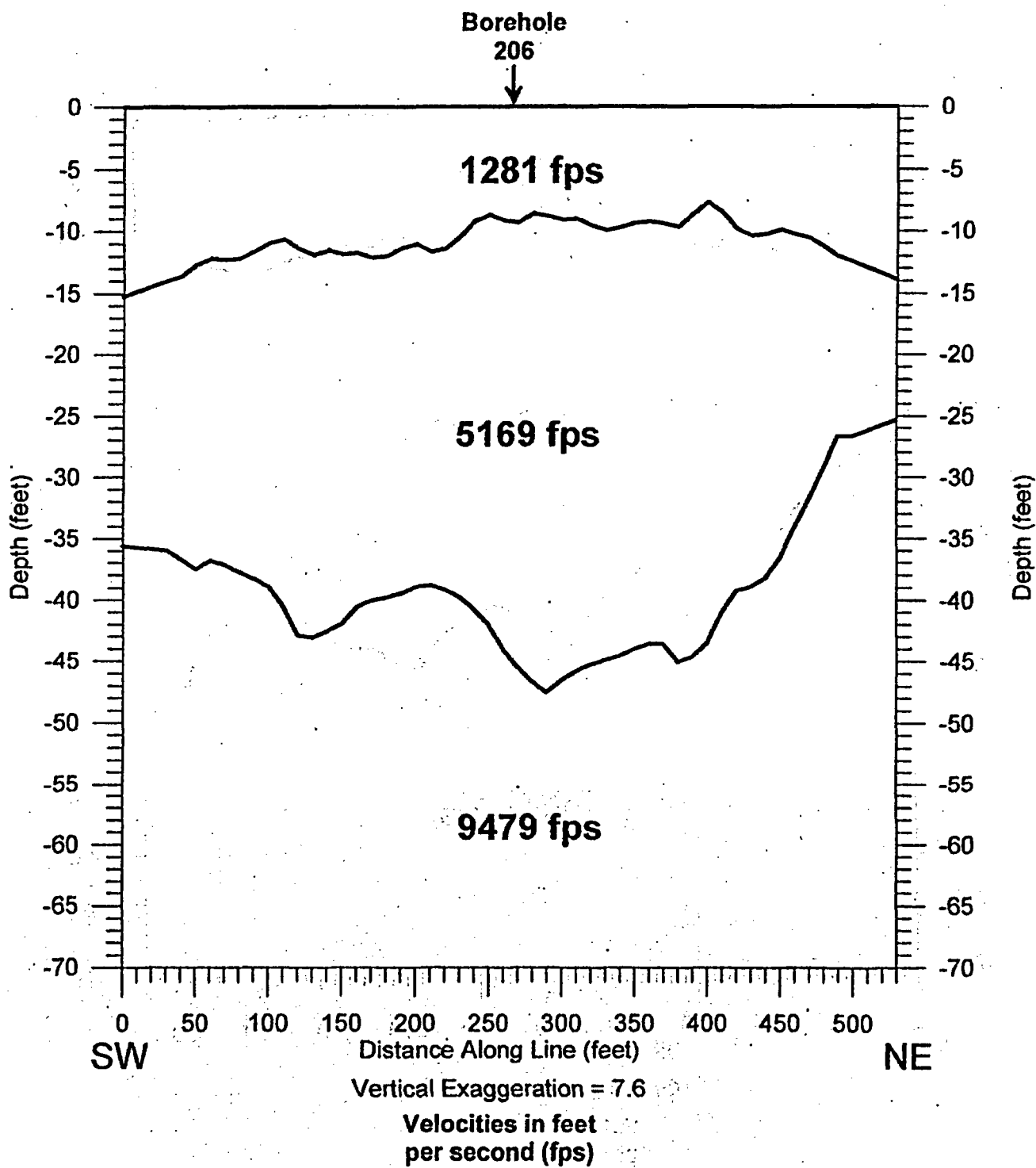


Seismic Rippability Investigation  
Crescent Junction Disposal Site  
**Borehole 206 NW to SE Seismic Line**  
*Depth Section*

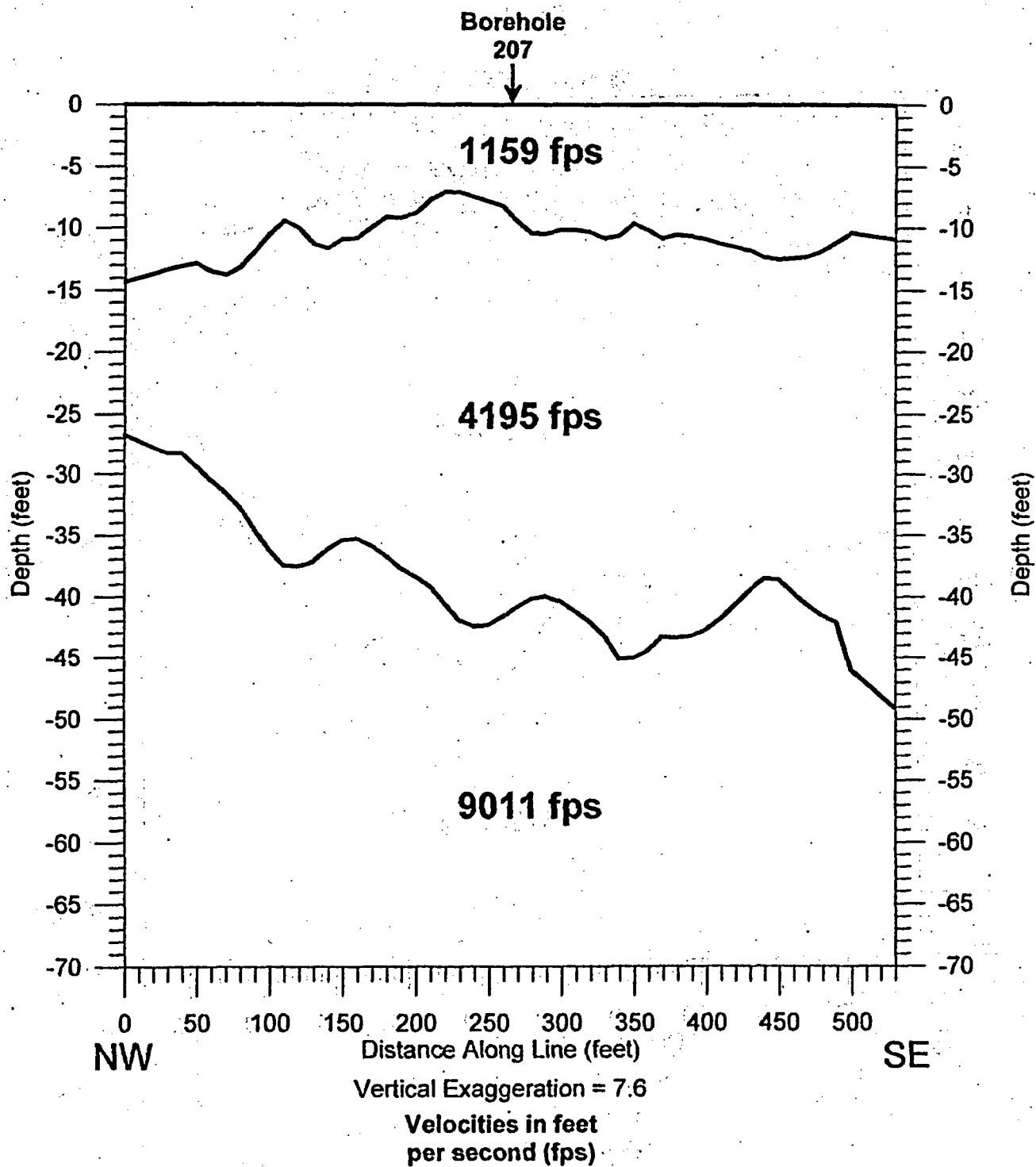




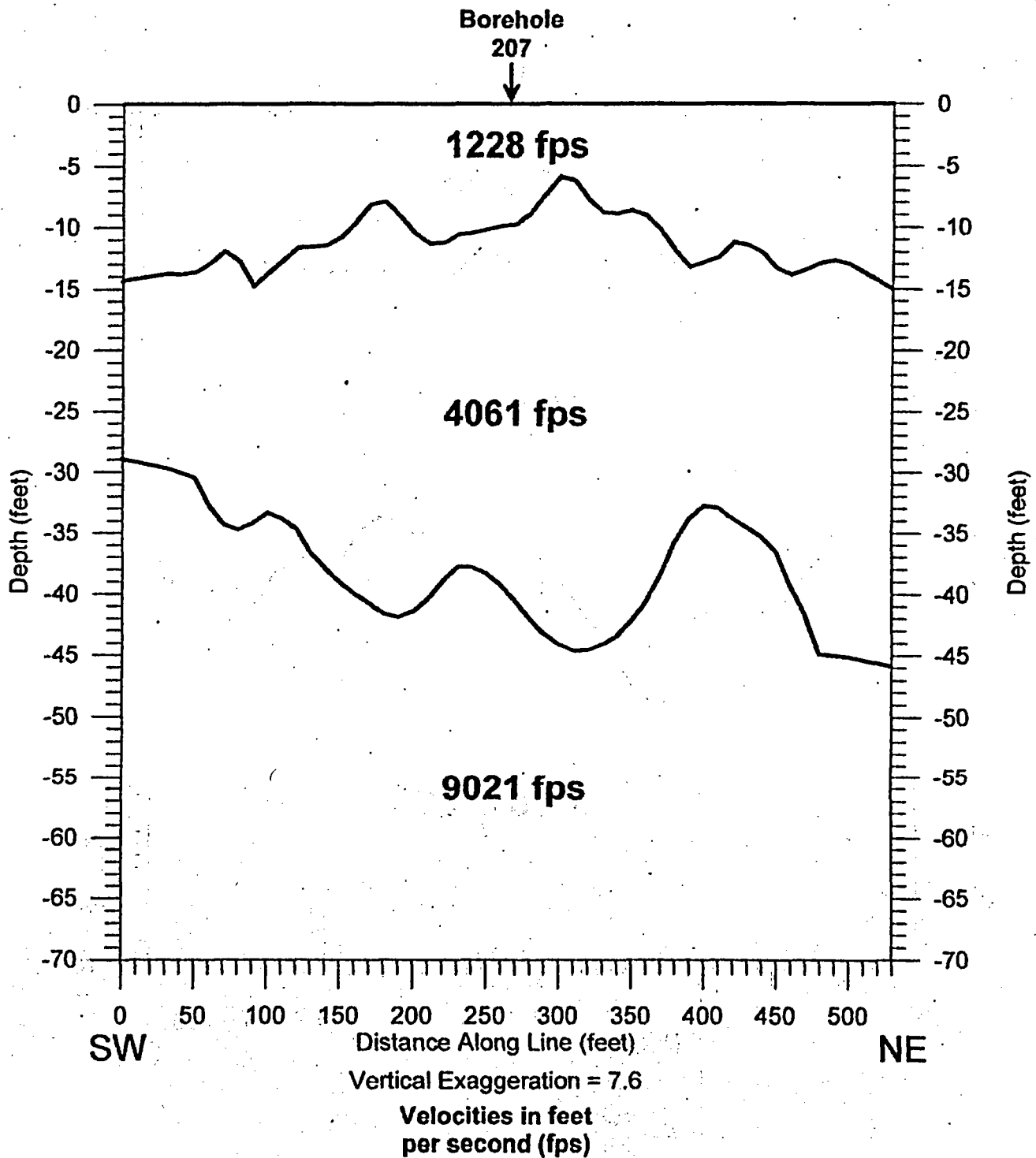
Seismic Rippability Investigation  
Crescent Junction Disposal Site  
**Borehole 206 SW to NE Seismic Line**  
*Depth Section*



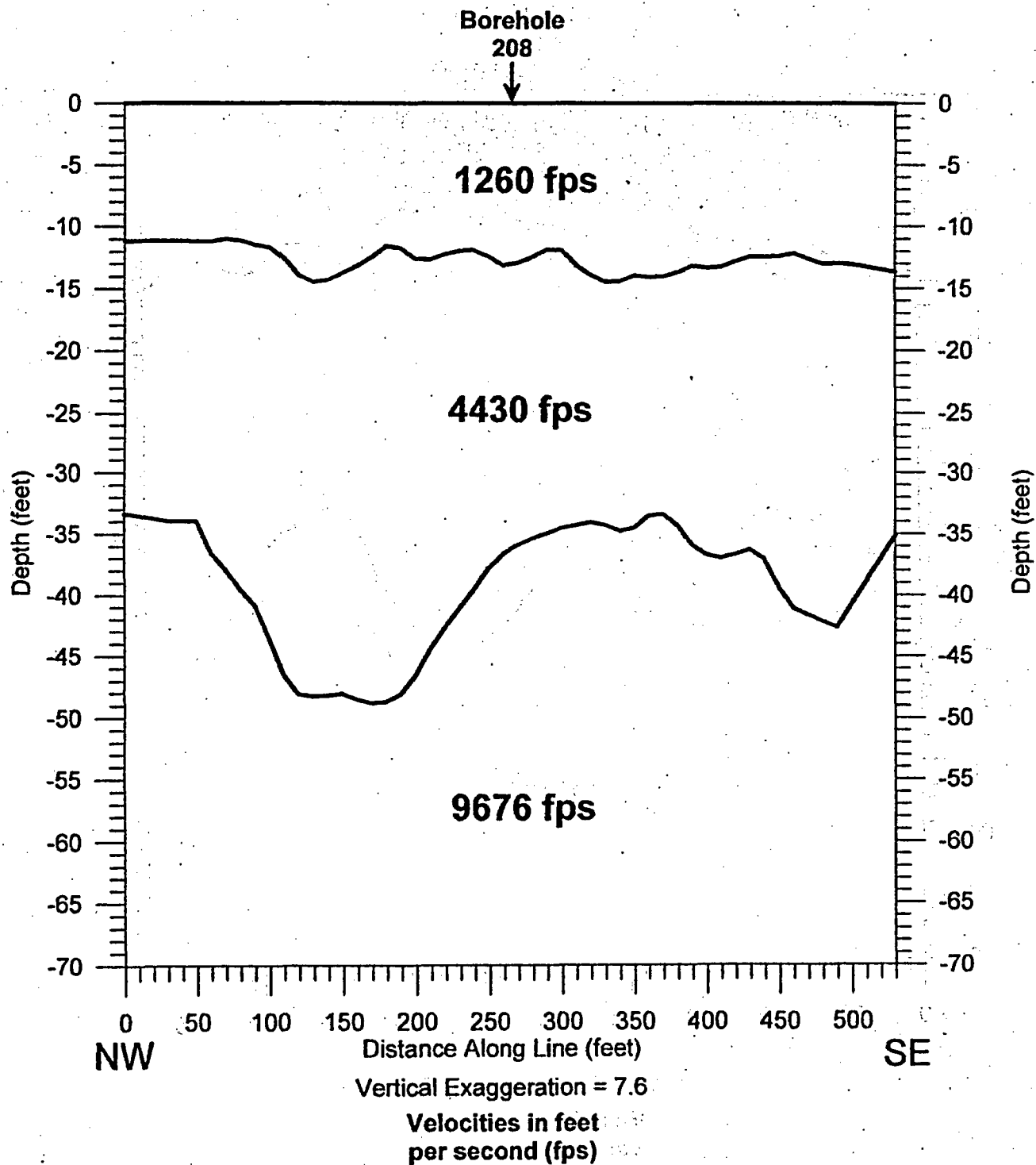
Seismic Rippability Investigation  
Crescent Junction Disposal Site  
**Borehole 207 NW to SE Seismic Line**  
*Depth Section*



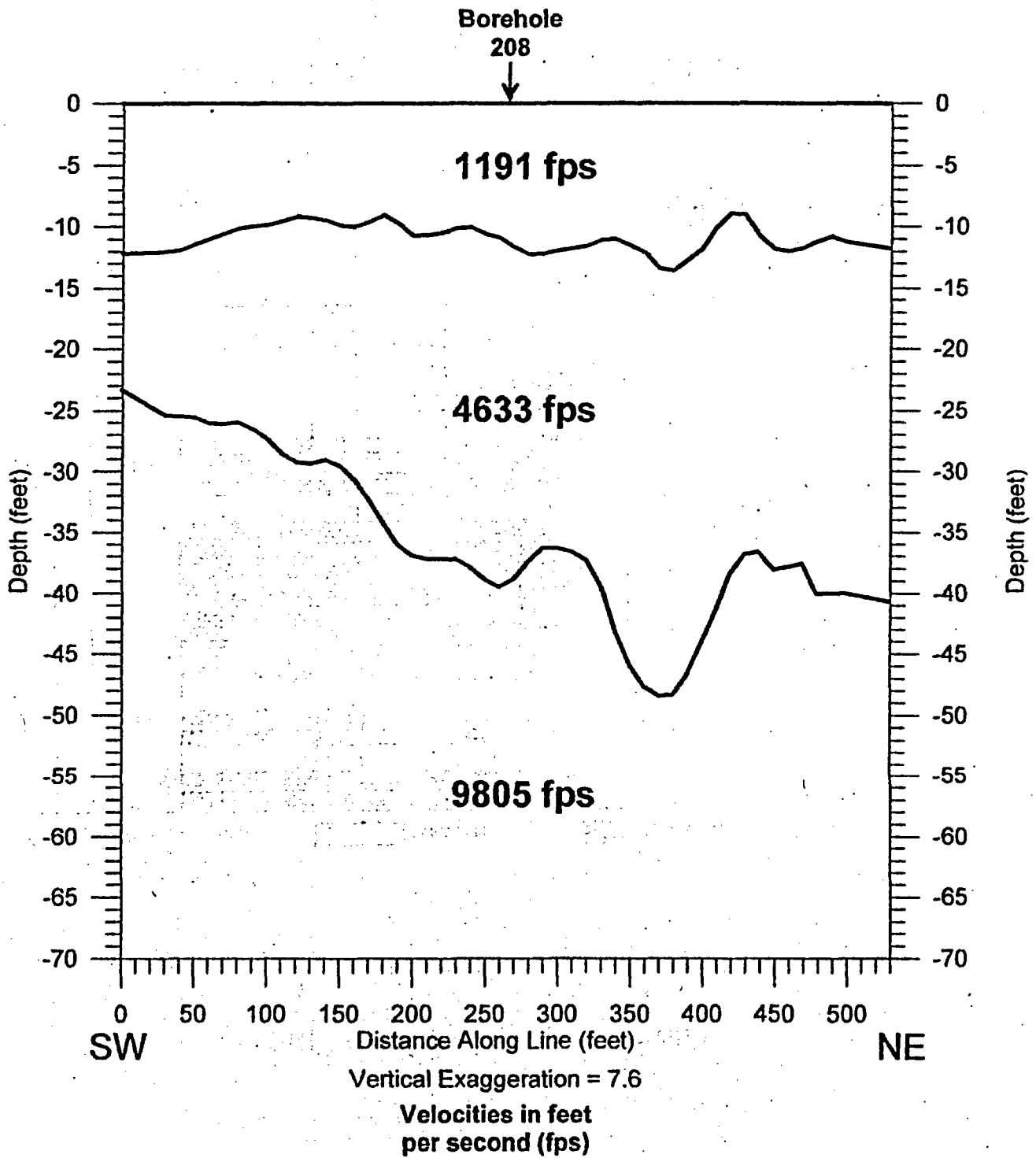
Seismic Rippability Investigation  
Crescent Junction Disposal Site  
**Borehole 207 SW to NE Seismic Line**  
*Depth Section*



Seismic Rippability Investigation  
Crescent Junction Disposal Site  
**Borehole 208 NW to SE Seismic Line**  
*Depth Section*



Seismic Rippability Investigation  
Crescent Junction Disposal Site  
**Borehole 208 SW to NE Seismic Line**  
*Depth Section*



# Caterpillar D8 Ripping Chart

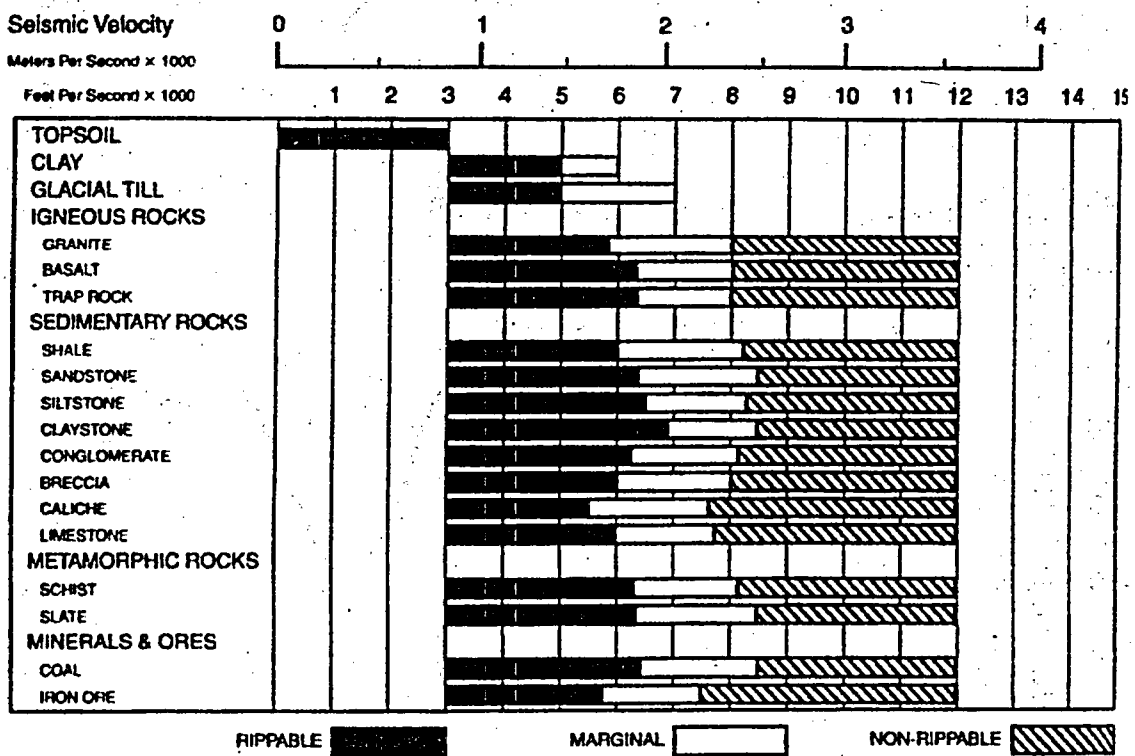
**D8R**

- Multi or Single Shank No. 8 Ripper
- Estimated by Seismic Wave Velocities

**Seismic Velocity**

Meters Per Second x 1000

Feet Per Second x 1000

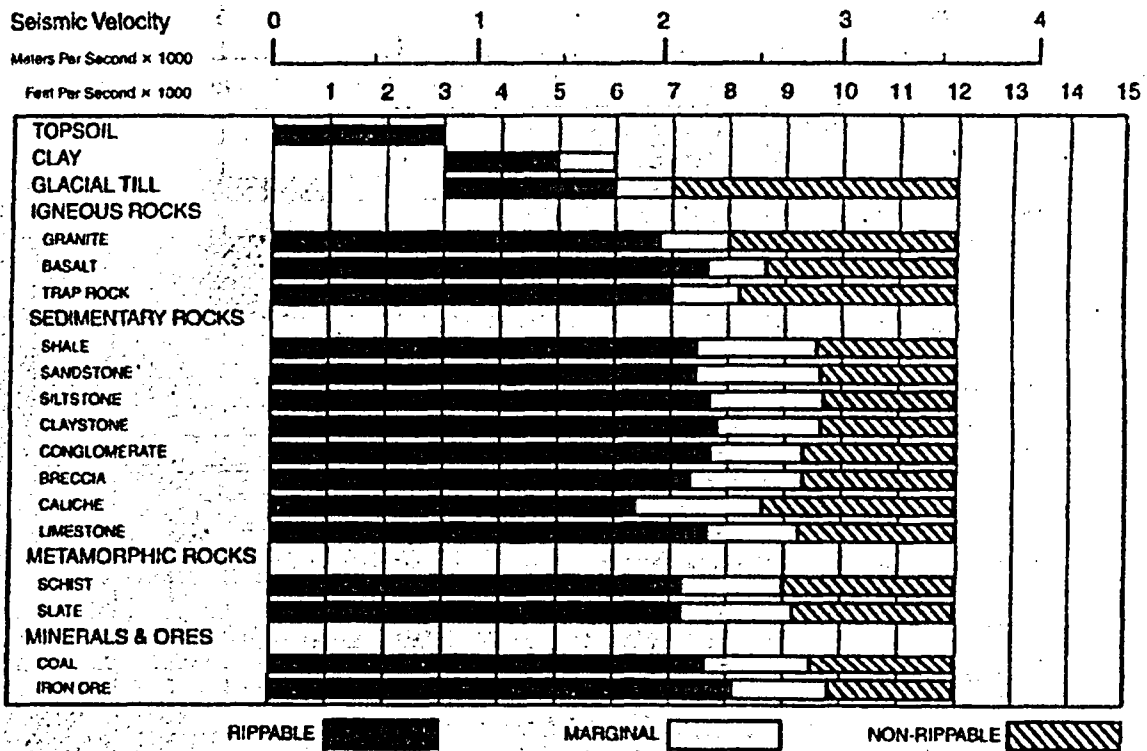


Hasbrouck Geophysics, Inc.

# Caterpillar D9 Ripping Chart

D9R

- Multi or Single Shank No. 9 Ripper
- Estimated by Seismic Wave Velocities



Hasbrouck Geophysics, Inc.

# Caterpillar D10 Ripping Chart

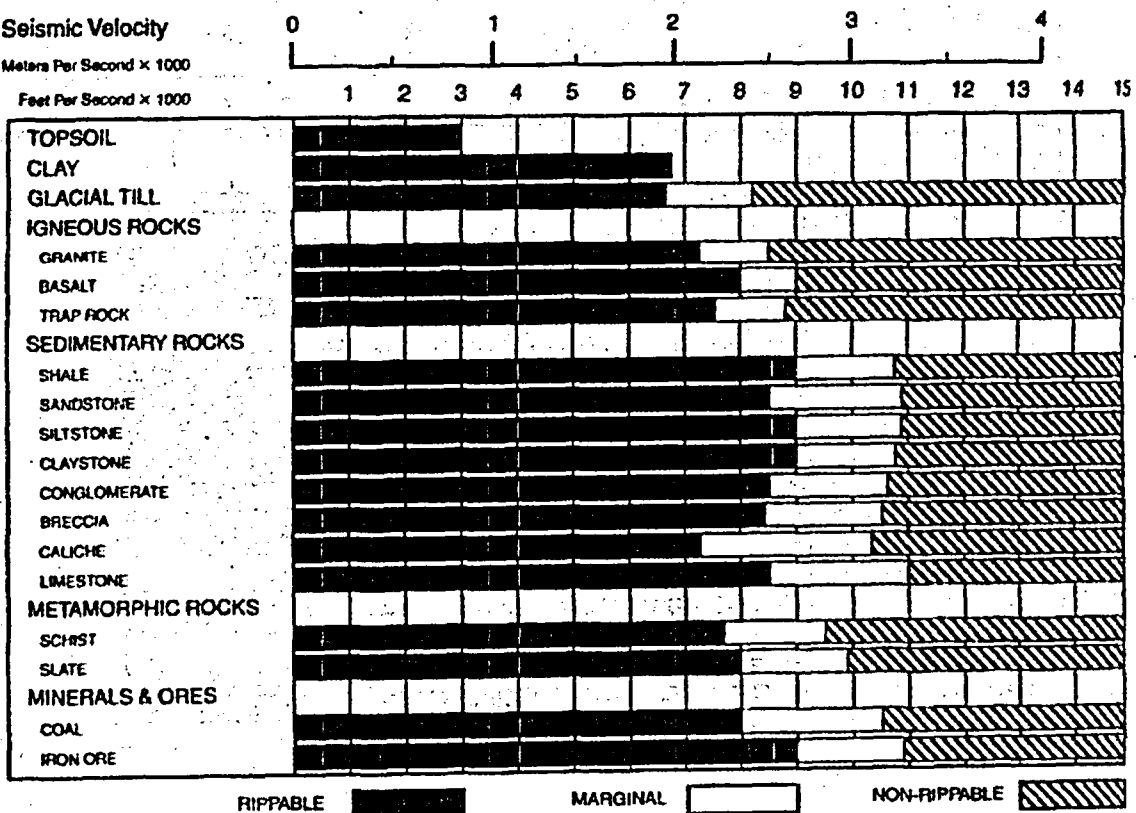
## D10R

- Multi or Single Shank No. 10 Ripper
- Estimated by Seismic Wave Velocities

Seismic Velocity

Meters Per Second x 1000

Feet Per Second x 1000



Hasbrouck Geophysics, Inc.



# Caterpillar D11 Ripping Chart

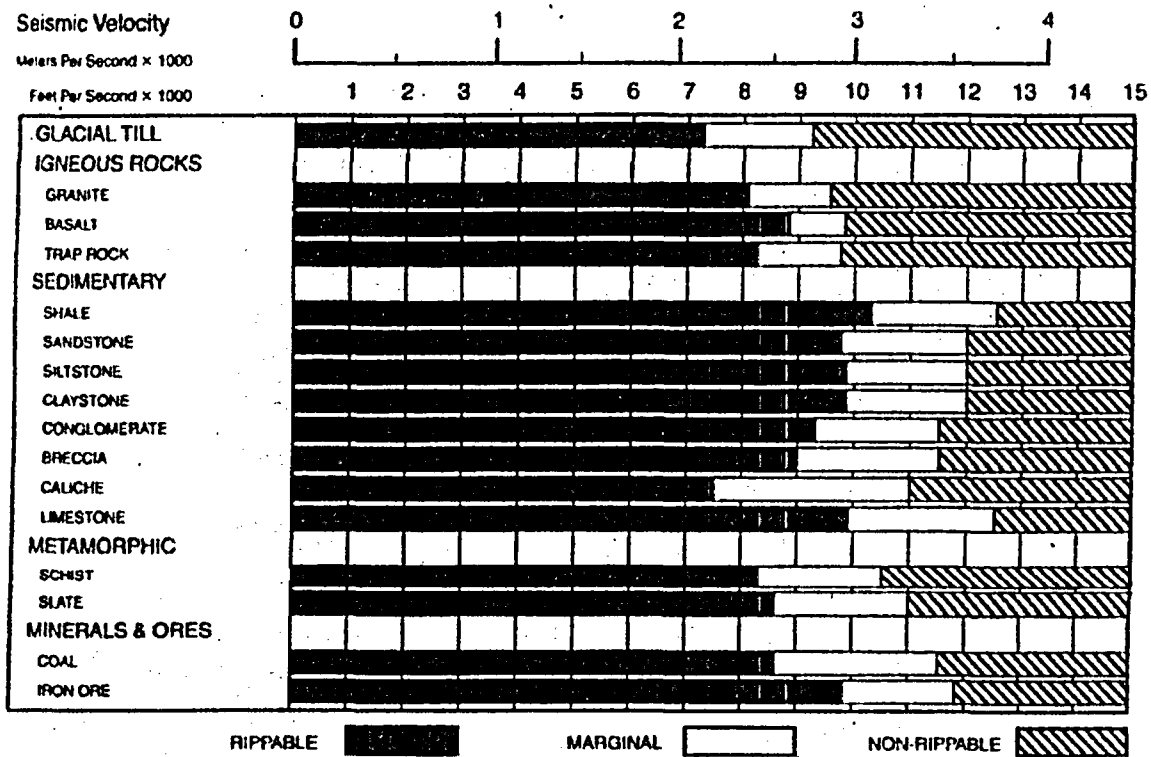
D11R

- Multi or Single Shank No. 11 Ripper
- Estimated by Seismic Wave Velocities

Seismic Velocity

Meters Per Second x 1000

Feet Per Second x 1000



Hasbrouck Geophysics, Inc.

## **Appendix B**

### **Review of Seismic Rippability Investigation Report**

The Word Works Inc., dba

**H. David Mac Lean, P. Geoph**

November 23, 2005

Mr. Mark Kautsky  
S.M. Stoller Corp.  
2597 B 1/4 Road  
Grand Junction CO 81503

**Subject: Review of Report; Seismic Rippability Investigations  
at the Crescent Junction Disposal Site,  
for S.M. Stoller Corp. Grand Junction CO  
by Hasbrouck Geophysics.**

202 North Ave., PMB 252  
Grand Junction Co 81501 Phone/fax : 970-242-1649

## **H. David Mac Lean, P. Geoph.**

Review of Report "Crescent Junction  
Disposal Site Rippability Investigations"  
by Hasbrouck Geophysics

November 23, 2005

In its simplest form, the delay time method involves measurement of the time of arrival of a seismic wave at two geophone locations separated by a distance  $D$ . The description of the method and the procedures employed to accomplish the measurements as set forth in the above reference report are in accordance with standard industry practice. It is a limitation of the method that in order to measure the seismic velocity of successively deeper units, the seismic velocity must increase sequentially with depth, as stated in the report. This is usually the case in the most frequently encountered field situations, but low velocity, or reversal situations are encountered on occasion. Low velocity reversals do not appear to occur at the Crescent Junction site.

The lithologic section and the depth of investigation were specified by Stoller. The near surface section was determined by careful logging of core and cuttings from boreholes located throughout the planned repository. Selected boreholes formed the centers of the seismic refraction spreads as shown in the Borehole and Seismic Line Location Map included with the subject report. The refraction surveys were intended to extend the layer thickness information for approximately 250 ft in four orthogonal directions from the borehole.

### **Field Data Acquisition**

The equipment referenced in the subject report was inspected during a visit to the field operations on October 29. The equipment was found to be as specified, and to be in good working order. Field conditions were less than optimal. Heavy rains had turned the area into a quagmire; nevertheless, the field crew was able to bring equipment into the area and proceeded with the survey with only minimal interruption caused by the adverse road and access conditions.

Field work for the survey was conducted October 29 and 30, 2005. It was observed that all field activities were conducted in a professional and workmanlike manner. Prior to commencement of operations, the field crew was briefed on health and safety issues by a Stoller representative, and a Health and Safety Plan was provided to the crew. The briefing was attended by this reviewer. Requirements of the plan, including clothing specifications were carefully observed by all field personnel. In accordance with plan requirements, any soil that became even slightly contaminated in the course of the field activities was removed from the site and disposed of in accordance with applicable procedures and regulations.

This reviewer participated in one day of the field operations and noted that they were conducted as described in the report. Field work was conducted by a crew provided by Bird Geophysics in accordance with survey design specifications developed by Hasbrouck Geophysics. The crew was obviously well trained and performed all assigned tasks with competence and in a professional manner.

## **H. David Mac Lean, P. Geoph.**

Review of Report "Crescent Junction  
Disposal Site Rippability Investigations"  
by Hasbrouck Geophysics

November 23, 2005

Upon locating the center of the refraction spreads referenced in an expanded version of the "Borehole and Seismic Line Location Map" included in the report, two orthogonal survey lines were extended in a NE-SW direction and a NW-SE direction. The lines were run by chain and compass; markers were placed at 10 foot intervals for a distance of 270 ft in the four directions from the center point. Every fourth marker from the center was identified so that its position could be surveyed later to the required accuracy. Since the terrain was open and unencumbered by vegetation, the entire line could be viewed from vantage points along the line. Lines were visually determined to be straight along the length of the chained interval.

Geophones were placed at each 10 foot marker. All geophones in a linear string were connected to the Bison 48 channel seismograph with Mark Products geophone cables.

Seismic signals were generated by the accelerated weight drop hammer mentioned in the report. A 200 lb metal bar is raised against compressing springs, and is thus accelerated downward to strike an aluminum plate placed on the ground at the shot point. The hammering operation started at one end of the line, and continued at various points along the spread as stated in the report. This is standard "shooting" procedure for seismic refraction surveys. The multiple shot points allow numerous depth and velocity determinations at various points along the spreads, and permit averaging and compensation for anisotropy and dip, since the seismic ray path can be observed in opposite directions. This procedure enables production of a much more detailed and representative velocity-depth section than would be possible if only a single shot point was employed.

Several (up to six) "shots" or hammer blows were taken at each shot point, allowing the seismic signals at each geophone location to be stacked. This procedure increases the signal to noise ratio. As pointed out in the report, seismic waves that arrive at a geophone at the same time following a hammer blow are additive to the signal; random noise or seismic signals for which the strike instant is incorrect are destructive and will not augment or enhance the initial seismic signal. On completion of the stacking activity, a seismogram was printed in the field for inspection and quality assurance purposes.

On the completion of the field survey day, digital data sets were forwarded to Hasbrouck Geophysics for processing and analysis. The data were processed by Hasbrouck Geophysics using the SIPwin software from Rimrock Geophysics. This processing software is state-of-the-technology for Refraction Seismic Data Processing. Given the software capabilities and the field procedures employed, Hasbrouck Geophysics was able to calculate seismic velocities over very short refractor distances. Velocities were calculated using both the regression and Hobson-Overton methods. This processing combination adequately deals with the effects anisotropy, and the distortions introduced by dipping layers. The resulting depth and velocity calculations were then employed to produce the very detailed velocity/depth sections included with the subject report.

## **H. David Mac Lean, P. Geoph.**

Review of Report "Crescent Junction  
Disposal Site Rippability Investigations"  
by Hasbrouck Geophysics

November 23, 2005

### **Analysis**

The velocities for the 3 layers discussed in the report, i.e., alluvium (layer 1) weathered Mancos Shale (layer 2) and Mancos Shale (layer 3) are well within the range expected for these materials. In unconsolidated material such as Layer 1, seismic velocities are often close to acoustic velocities in air (approximately 1100fps). Considerable variation in the measured velocity of Layer 2, (the weathered shale or regolith) can be expected depending on the amount of sand or silt inclusioning and the degree of consolidation within local areas. As pointed out in the report, weathering will not be complete through the entire geologic section and the lithologic material is not uniform. As expected, the seismic velocities increase as a function of depth.

The velocity function for all three layers underlying the planned repository is well illustrated by the time-distance (T-D) plot for one of the survey lines at borehole 204. A copy of the T-D plot is attached hereto. The figure provides a visual indication of the seismic velocity for the various layers. Generally, the flatter the curve on the T-D plot, the higher the velocity. A segment of the T-D plot that is continuous over a measurable interval indicates an identifiable layer. A simple estimate of the velocity associated with this interval can be made by dividing the distance interval D by the difference in arrival time (T) on the T-D plot. Of course the actual final determination of the depth associated with this interval involves a considerably more complex calculation, as has been discussed peripherally in the report.

### **Limitations**

The purpose of measuring the seismic velocities of the layers underlying the proposed mill tailings repository was to estimate the rippability of the underlying lithologic units. Hasbrouck Geophysics has developed depth and velocity sections for all of the surveyed lines that show the lithologic layers to depths of 50 to 60 feet and the measured seismic velocities within these layers to the accuracy that is achievable with the equipment and methodology employed. However, the relationship of these measured seismic velocities to rippability of a particular unit is empirical, not an engineering certainty. Caterpillar Inc. and others involved with heavy equipment operations have observed an apparent relationship and have published charts and graphs showing the ripping capabilities of certain tractor models for various geologic material with a range of seismic velocities. However, there are many other factors that contribute to rippability, such as the degree and orientation of fracturing. Although the rippability charts published by Caterpillar Inc. represent that material with a seismic velocity in a certain range is usually within the ripping capability of certain tractor types, it is not an engineering certainty that this is the case.

## **H. David Mac Lean, P. Geoph.**

Review of Report "Crescent Junction  
Disposal Site Rippability Investigations"  
by Hasbrouck Geophysics

November 23, 2005

Accordingly, any decision to employ a certain type of equipment based on the velocities provided in the subject report must be taken on the basis of the excavation contractor's own knowledge, and not on statements or implied statements in the report. The velocities and layer thicknesses provided in the report are valid within the accuracy of the seismic refraction method, and are reproducible by similar surveys. Nevertheless, the relationship of these in-situ measured velocities and the suitability of a specific tractor model for ripping a geologic unit with these velocities is strictly empirical and may vary from that presented in the rippability charts provided by Caterpillar Inc.

### **Conclusions**

The subject report provides seismic velocities and the thickness of layers underlying the proposed tailings repository to a depth of about 60 ft or more. The sections showing these depths and velocities provided in the report were produced by means of a refraction seismic survey that was conducted in a professional and workmanlike manner, employing equipment that was suitable to the task. The measured interval velocities, unit thicknesses and variations to be expected are accurate to within the limitations of the current state of refraction seismic technology. The statement in the report that measured velocities are accurate to within 10 per cent is probably overly pessimistic; the accuracy of the measurements is probably much closer to 5% or less. General experience suggests that the unit thicknesses stated in the report are accurate to within 10% or better.

As stated in the report, the suitability of selecting equipment based on the reported velocities is based entirely on the experience of Caterpillar Inc. Nothing in the subject report should be construed as an endorsement of the suitability of a particular tractor model for ripping and excavating applications at the Crescent Junction repository. This decision must be taken on the basis of the excavator's own experience with ripping machinery in applications where seismic velocities are known.

Respectfully Submitted,



H. David Mac Lean, P. Geoph.

HDM/hdm

Enclosures:

Borehole 204 NW to SE Time-Distance plot

## **H. David Mac Lean, P. Geoph.**

Review of Report "Crescent Junction  
Disposal Site Rippability Investigations"  
by Hasbrouck Geophysics

November 23, 2005

### **References:**

                    . Caterpillar Performance Handbook, Ed 30, October 1999. *Use of  
Seismic Velocity Charts* pp 1-71-1-78



## **H. David Mac Lean, P. Geoph.**

Review of Report "Crescent Junction  
Disposal Site Rippability Investigations"  
by Hasbrouck Geophysics

November 23, 2005

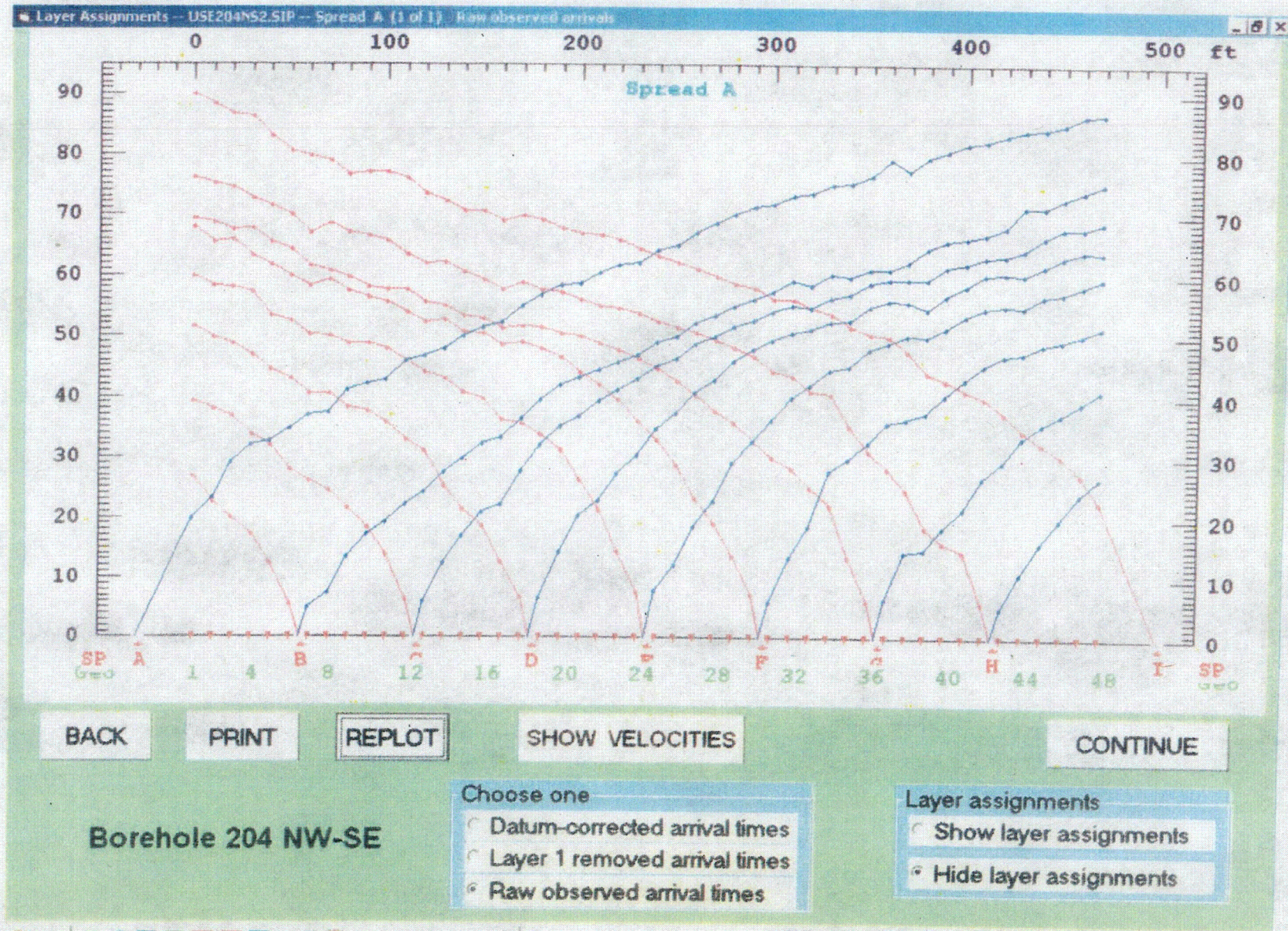
### **Statement of Qualifications**

H. David Mac Lean is a Registered Professional Geophysicist in the State of California, Registration No. 440 and in the Province of Alberta, Canada, Registration no.M15724. Mr. Mac Lean has been a practicing geophysicist for over 35 years.

Mr. Mac Lean has gained experience with the seismic refraction method while engaged in aggregate mapping activities in the Beaufort Sea, and in laying out seismic surveys for oil exploration in Alberta, Canada.

Mr. Mac Lean is an emeritus member of the Society of Exploration Geophysicists, the Canadian Exploration Geophysical Society, The Australian Society of Exploration Geophysicist, the Society for Mining and Metallurgy of the American Institute Mining Engineering and other technical and professional societies dedicated to the advancement of geophysics. Mr. MacLean is a frequent attendee at conventions, trade shows and seminars dedicated to geophysical technologies.





C47



## **Contents**

**Appendix A    Material Placement in the Disposal Cell**

**Appendix B    Geochemical Attenuation and Performance Assessment Modeling**

# U.S. Department of Energy—Grand Junction, Colorado

## Calculation Cover Sheet

Calc. No.: MOA-02-05-2006-3-05-00

Discipline: Geochemical  
Properties

No. of Sheets: 38

Project: Moab UMTRA Project

Site: Crescent Junction Disposal Site

Feature:  
Geochemical Attenuation and Performance Assessment Modeling

Sources of Data:

Sources of Formulae and References:

List of actual references reviewed.

Preliminary Calc. ☐

Final Calc. ☐

Supersedes Calc. No.

Author:

J. Morrison 6/13/06  
Name Date

Checked by:

[Signature] 6/14/06  
Name Date

Approved  
by:

[Signature] 6-14-06  
Name Date

[Signature] 6-14-06  
Name Date

[Signature] 6-14-06  
Name Date

Name Date

# **Crescent Junction Disposal Site Geochemical Characterization of Mancos Shale and Reaction-Transport Modeling of Contaminant Attenuation**

## **Executive Summary**

The purpose of this work was to develop a robust one-dimensional reaction-transport model that could be used by site personnel to help evaluate the attenuation of contaminants in ground water that may migrate from a proposed uranium mill tailings disposal cell at Crescent Junction, Utah. Although it is unlikely that contaminated water from the disposal cell will penetrate the thick Mancos Shale, contaminant attenuation by bedrock affords increased protection for deep ground water systems. Data for the model were derived from laboratory characterization of the bedrock beneath the proposed disposal cell. The disposal cell will contain tailings from the Moab, Utah, (Atlas) uranium mill and is underlain by Mancos Shale Formation. Samples of Mancos Shale were collected from 10 cores that were evenly distributed in the area of the proposed disposal cell. Five samples were collected from each of the 10 cores for a total of 50 samples, at depths of 40 to 300 ft.

The chemistry of the water-soluble fractions of the samples was determined and used to help estimate the proportions and types of water-soluble minerals. Based on these results it is estimated that the water-soluble mineral assemblage is dominated by nahcolite ( $\text{NaHCO}_3$ ) with major amounts of Ca-Na exchange and gypsum ( $\text{CaSO}_4 \cdot 2\text{H}_2\text{O}$ ). Halite, sylvite, and dolomite occur in lesser amounts and calcite is present. Gypsum and dolomite are more dominant in the shallow samples, while nahcolite and halite are more concentrated in the deeper samples. The mineral abundances were used as initial conditions for the ground-water reaction-transport model.

Cation exchange capacity (CEC) was measured on 20 core samples of Mancos Shale. CEC ranged from 0.54 to 36.29 meq/100 g with a mean of 11.23 meq/100 g. These values are consistent with shale composed of kaolinite, illite, and smectitic interlayered clay minerals as determined by x-ray diffraction analysis. In the reaction-transport modeling, the mean CEC value is used to specify the number of cation exchange sites. Cation exchange was used to model retardation of  $\text{NH}_4$ .

X-ray diffraction (XRD) analysis on 10 samples of Mancos Shale was used to further identify minerals present in the core samples. The bulk mineralogy is dominated by quartz, with lesser amounts of dolomite and calcite, small amounts of feldspar, and traces of gypsum. The clay mineral fraction is dominated by mixed-layer (mostly illite/smectite) clays, illite, and kaolinite, with illite layers dominating the mixed-layer clays. The mineralogy was used to help estimate initial mineral composition for the reaction-transport model.

Particle surface area was determined by BET analysis on 10 Mancos Shale samples. Surface areas range from 8.81 to 13.22  $\text{m}^2/\text{g}$  with a mean of 11.02  $\text{m}^2/\text{g}$ . Surface area measured on a powdered split is consistent with surface areas measured on the 1- to 2-mm fractions, indicating that the BET method is probably accounting for intraparticle surface area. Surface area was used as an input to the surface-complexation adsorption algorithm in the reaction-transport model.

Distribution ratios ( $R_d$ ) are a measure of the partitioning of a contaminant between the ground water and the solid fraction of the aquifer. The higher the  $R_d$ , the more partitioning to the solids and the more retardation of the contaminant. The  $R_d$  value can vary significantly with solution chemistry. For example, Davis et al. (2004) showed that  $R_d$  values for uranium in a sample of alluvium varied by more than a factor of 10 depending on dissolved carbonate concentration and pH value. For the reaction-transport modeling, a surface-complexation approach is used instead of using constant  $R_d$  values to simulate retardation of U. Using the surface-complexation approach, the  $R_d$  value changes as chemical conditions (especially pH and

pCO<sub>2</sub>) change in the aquifer. The results of the R<sub>d</sub> determinations were complicated by the analytical imprecision associated with relatively small concentration differences between tests containing sediment and controls without sediment. However, the data indicate that R<sub>d</sub> values for uranium adsorption on Mancos Shale are relatively low, ranging from essentially 0 to 0.84 mL/g. The main use of the R<sub>d</sub> values was to test and calibrate the surface-complexation module used for U transport in the reaction-transport modeling.

Two sequential batch-leaching tests were conducted to observe chemical evolution of tailings leachate as it interacted with Mancos Shale. One test simulated vertical transport and the other horizontal transport through the Mancos Shale. Chemical changes that occurred in the tailings leachate as it reacted with progressively more Mancos Shale in the horizontal simulation include slightly increasing values of pH, Cl, K, Na, SO<sub>4</sub>, and U. Similar to the simulation of horizontal transport, pH values in the vertical simulation progressively increased with increased reaction. Progressive increases also occurred in the Cl, Na, SO<sub>4</sub>, and U concentrations, but decreasing trends in alkalinity and possibly NH<sub>4</sub> occurred. The results of the sequential batch tests were used to help calibrate the reaction-transport models.

The laboratory data discussed above were used to develop a one dimensional reaction-transport model of tailings fluid interaction with the Mancos Shale to simulate transport of contaminants beneath the Crescent Junction disposal cell. Two simulations were run, one simulation representing horizontal flow through shallow Mancos Shale and the other representing vertically downward flow through progressively deeper Mancos Shale. The only difference in input parameters between the horizontal and vertical simulations is the initial abundances of minerals, the deeper Mancos Shale having more nahcolite and less gypsum than the shallow Mancos Shale. The simulations were calculated with the transport algorithm embedded in the PHREEQC geochemical computer program.

In both the horizontal and vertical transport simulations, NH<sub>4</sub> is retarded for about 3.5 pore volumes, after which concentrations rise rapidly to the influent concentration. Retardation of NH<sub>4</sub> was caused by the exchange of dissolved NH<sub>4</sub> cations for solid-phase exchangeable Ca, K, Mg, and Na. Most of the exchange involves Na ion because Na dominates the cations in Mancos Shale ground water at the Crescent Junction site. Effluent U concentrations in the horizontal simulation are retarded for slightly less than one pore volume during which the U concentration is less than about 0.075 mg/L. After one pore volume, U concentrations increase rapidly and reach the influent value (4 mg/L) after about 3 pore volumes. In the vertical simulation, U concentrations are never less than 2.4 mg/L; however, U concentrations remain less than the influent until about 4 pore volumes. In the horizontal simulation, K<sub>d</sub> values were initially 0.26 mL/g and decreased to 0.19 mL/g after about 2 pore volumes. In the vertical simulation, K<sub>d</sub> values were negligible initially and increased to 0.15 mL/g after about 4 pore volumes. The differences in K<sub>d</sub> values and dissolved U concentrations between the two simulations result from variation in the ionic composition of the solutions resulting from equilibration with minerals and cation exchange sites. A critical factor was the presence of a higher concentration of gypsum in the horizontal simulation than in the vertical simulation. Calcium released from dissolution of gypsum in the horizontal simulation caused precipitation of calcite, which resulted in decreased pH. These conditions led to increased partitioning of U to the specific adsorption sites on the Mancos Shale and increased retardation in the horizontal simulation.

In summary, the transport results suggest that NH<sub>4</sub> migration is retarded by several pore volumes. Uranium is retarded by about 1 pore volume, but only if Ca is released from gypsum dissolution. To evaluate the effects of this analysis on contaminant transport beneath the proposed Crescent Junction disposal cell, it is necessary to know the flux of contaminated water from the cell. The effective porosity of the Mancos Shale must also be known; attenuation would be much less in a system dominated by fracture flow than one dominated by porous media flow. Evaluation of the flow regime was beyond the scope of this investigation; thus, results of the model simulations are provided in terms of pore volumes. To maximize the benefit of these results in the field setting, project personnel will need to couple these results with results of hydrologic investigations to convert units of pore volume to more useful units of travel time and distance. Alternatively, a sensitivity analysis that uses reasonable bounds for the hydrologic parameters may be appropriate to assess the impact of chemical attenuation at the Crescent Junction site.

Much of the work presented in this paper on U adsorption uses an approach recently developed by Dr. James Davis and co-workers at the U. S. Geological Survey. Davis et al. were funded by the U.S. Nuclear Regulatory Commission specifically to advance the state-of-the-art in geochemical methods used for the transport of U at uranium milling sites. Their model of surface complexation adsorption is well suited to the work presented here.

## Introduction

This work was conducted to characterize the geochemistry of the bedrock beneath and adjacent to the proposed disposal cell location at Crescent Junction, Utah. The disposal cell will be constructed to contain tailings from the former Moab, Utah, (Atlas) uranium-ore processing mill and will be underlain by the Mancos Shale Formation. The purpose of this work is to provide data to help evaluate the potential for ground water contamination and transport of tailings constituents at the disposal site. The basis for this work is provided in Section 4.5 of the "Work Plan for Characterization of Crescent Junction Disposal Site" (Appendix A) and was modified based on discussions with Moab Uranium Mill Tailings Remedial Action (UMTRA) Project personnel. The scope, which includes laboratory investigations and reaction-transport modeling, is defined in Appendix A.

The geochemical approach involves collecting site-specific data and using these data to model geochemical interactions between tailings pore fluid and the Mancos Shale. Results of the laboratory investigations provide the following information about the Mancos Shale: (1) abundance and mineralogy of water-soluble minerals; (2) mineralogy of water-insoluble minerals, including clays; (3) cation exchange capacity (CEC); (4) surface area; and (5) chemical distribution ratios ( $R_d$ ). These data were used to construct a one-dimensional reaction-transport model of tailings water transport through the Mancos Shale. The model includes equations governing aqueous speciation, mineral dissolution, mineral precipitation, mixing with other ground water, cation exchange, and adsorption. In addition, two sequential batch-leaching tests were conducted, and the results were used to help calibrate the geochemical model. Numerous analyses of tailings pore fluids have been made previously, and no additional analyses were made for this study.

Samples of Mancos Shale were collected from 10 cores that were evenly distributed in the area of the proposed disposal cell (see Appendix A for locations). Samples were obtained from the Prairie Canyon and Blue Gate Shale Members of the Mancos Formation, the geologic units that directly underlie the proposed disposal cell (Table 1). Five samples were collected from each of the 10 cores for a total of 50 samples. The disposal cell excavation will extend approximately 20 feet (ft) below the ground surface; thus, the uppermost sample of each core was collected from a depth of 40 ft. The remaining four samples per core were collected at equal intervals below 40 ft; with the deepest samples obtained at 300 ft. Evaluation of these samples provided a reasonable set of data to assess lateral and vertical distributions of geochemical properties in the Mancos Shale underlying the location of the proposed disposal cell.

*Table 1. Geologic Members of Mancos Shale in Samples Used in this Study<sup>a</sup>*

Boring Number	40-ft Depth	105-ft Depth	170-ft Depth	235-ft Depth	300-ft Depth
CJ-201	PC	PC	BG	BG	BG
CJ-202	BG	BG	BG	BG	BG
CJ-203	PC	PC	BG	BG	BG
CJ-204	PC	BG	BG	BG	BG
CJ-205	BG	BG	BG	BG	BG
CJ-206	PC/BG	BG	BG	BG	BG
CJ-207	BG	BG	BG	BG	BG
CJ-208	PC	PC	BG	BG	BG
CJ-209	BG	BG	BG	BG	BG
CJ-210	PC	PC	BG	BG	BG

<sup>a</sup>PC = Prairie Canyon Member. BG = Blue Gate Shale Member.

The water-soluble chemistry of all 50 samples was measured. Samples from the 40-ft depth (and some from the 105-ft depth) were used for additional analyses because these samples are representative of rock directly beneath the proposed tailings disposal cell and are most likely to contact migrating tailings fluids. All 40-ft-deep samples were analyzed for surface area, mineralogy by X-ray diffraction (XRD), CEC, and uranium (U) distribution ratios. In addition, all 105-ft-deep samples were measured for U, uranium  $R_d$ , and CEC values.

This report is divided into 10 sections. Section 0 describes the general methods used for acquisition of samples and analyses. Sections 0 through 0 present methods and results for each characterization activity, and Section 0 provides the laboratory results of two sequential batch-leaching tests. Section 0 develops each module of a reaction-transport model and presents reaction-transport simulations for the sequential batch-leaching tests and the Crescent Junction Site. Section 0 provides a summary and conclusions.

Much of the work presented in this paper on U adsorption uses an approach recently developed by Dr. James Davis and co-workers at the U.S. Geological Survey. Davis et al. present a sophisticated method to evaluate U adsorption using detailed data collected at a former uranium milling site at Naturita, Colorado, a site administered by the U.S. Department of Energy Office of Legacy Management. The U.S. Nuclear Regulatory Commission funded the recent work by Davis and others specifically to advance the state-of-the-art in geochemical methods used for the transport of U at uranium milling sites.

## General Methods

### Sample Collection and Preparation

Five samples were collected from each of the 10 cores. The samples were collected at depths of 40, 105, 170, 235, and 300 ft. Sample numbers are in the format CJ-201-40, where CJ is Crescent Junction, 201 is the boring number, and 40 is the depth measured in feet. Samples were 2 inches in diameter and contained approximately 2.5 linear inches of core. Samples were air dried and stored in plastic containers until used for the tests. Dried samples were lightly crushed with a hammer or pestle, sieved, and split using a riffle splitter as needed for the tests. Bulk sample weights ranged from 238 grams (g) to 615 g. Moisture contents range from 0.76 percent to 3.01 percent and have no obvious relationship to sample depth or lithology. Laboratory notes are presented in Appendix B and a complete set of raw data and Excel calculations are presented in Appendix C.

### Analytical Methods

The laboratory portion of the work was conducted in the DOE Environmental Sciences Laboratory at Grand Junction, Colorado. A subcontract was procured with Dr. William Hood, Grand Junction, Colorado, to conduct XRD analysis. Micromeritics Analytical Services, Norcross, Georgia, measured particle surface areas using the standard Brunauer, Emmett, and Teller (BET) method. Table 2 presents analytical methods used for water chemistry measurements.

Table 2. Analytical Methods

Constituent	Procedure Number DOE (STO 210)	Procedure Description
Alkalinity	AP (Alk-1)	Titration with H <sub>2</sub> SO <sub>4</sub>
Ammonia	AP (NH <sub>3</sub> -1)	Spectrometry-Salicylate
Calcium	AP (Ca-1)	Flame Atomic Absorption
Chloride	AP (Cl-2)	Ion Chromatography
Magnesium	AP (Mg-1)	Flame Atomic Absorption
Nitrate	AP (NO <sub>3</sub> -4)	Ion Chromatography
Oxidation-Reduction Potential (ORP)	AP (ORP-1)	Electrode
pH	AP (pH-1)	Electrode
Potassium	AP (K-1)	Flame Atomic Absorption
Sodium	AP (Na-1)	Flame Atomic Absorption
Specific Conductance	AP (EC-1)	Electrode
Sulfate	AP (SO <sub>4</sub> -4)	Ion Chromatography
Uranium	AP (U-2)	Kinetic Phosphorescence



# Analysis of Water-Soluble Extracts

## Introduction

This portion of the work scope was designed to identify and estimate abundances of minerals present in the water-soluble fraction of the Mancos Shale. The water-soluble fraction is the most reactive portion of the aquifer and will likely have a significant effect on chemical evolution of the ground water system. Appendix C contains a complete set of chemical results for the water-soluble extractions.

## Methods

Samples were crushed, air dried, and sieved to  $-10 +18$  mesh (1 to 2 millimeters [mm] nominal diameter). This size fraction was selected because it (1) is likely to have sufficient material to accomplish the tests, (2) is uniform enough so that surface area is relatively constant and easy to determine, (3) is efficient to work with in the laboratory (testing apparatus can be relatively small), and (4) should be reasonably representative of the bulk rock encountered in the field.

The leaching procedure was modified from procedure CB (BT-1) (STO 210). Two grams of the sieved sample was placed in a plastic centrifuge tube with 100 milliliters (mL) of deionized water at room temperature. The tube was agitated end over end for 4 hours. The solids were separated from the water by centrifuging and decanting to produce a clear solution. The solutions were analyzed for pH, oxidation-reduction potential (ORP), specific conductance, alkalinity, ammonium ( $\text{NH}_4$ ), calcium (Ca), chloride (Cl), magnesium (Mg), nitrate ( $\text{NO}_3$ ), potassium (K), sodium (Na), sulfate ( $\text{SO}_4$ ), and U.

## Results and Discussion

All 50 samples were analyzed by the water-extraction method. Analyses included major ions that constitute most water-soluble minerals as well as the mill tailings contaminants  $\text{NH}_4$  and U. Mass balance calculations made using the computer program NETPATH (Plummer et al. 1994) were used to estimate the mineralogy of the water-soluble fraction. Mineral identifications were aided by XRD analyses (Section 5), but XRD is limited in its ability to detect small amounts (typically less than 10 percent) of minerals and does not provide quantitative information on mineral abundance. This section reports the concentrations of the constituents in the water-soluble fractions of the Mancos Shale samples and the mineral assemblages calculated using NETPATH.

### Masses of Constituents in the Water-Soluble Extracts

The solid-phase concentration of each constituent (Table 3) was calculated from the measured concentration and the solids-to-solution ratio (2 g in 100 mL). The total water-soluble fraction ranged from 0.40 to 2.85 percent (by weight) of the sample, with a mean value of 0.72 percent (Table 3; 1 percent is equivalent to 1,000 micrograms per gram [ $\mu\text{g/g}$ ]). Only two samples (CJ-203-40 and CJ-204-40) exceeded 1 percent, and both were from the 40-ft depth. Values of pH in the solutions after agitation ranged from 6.17 to 9.88, with a mean pH value of 9.50. Only five samples, all from the 40-ft depth, had pH values less than 9.00.

The water-soluble fractions are dominated by carbonate (alkalinity), Na, and  $\text{SO}_4$ , with lesser amounts of Ca, Cl, K, and Mg (see "Mean" in Table 3). Data in Table 3, show that Ca and  $\text{SO}_4$  are more dominant in the shallow (40-ft) samples than in the samples obtained from deeper depths, suggesting the presence of more gypsum ( $\text{CaSO}_4 \cdot 2\text{H}_2\text{O}$ ) in the shallow horizon. Alkalinity and Na appear to increase in the deeper horizons, suggesting the presence of nahcolite ( $\text{NaHCO}_3$ ) in the deeper horizons.

Concentrations of  $\text{NO}_3\text{-N}$  were less than the detection limit of 5.5  $\mu\text{g/g}$  in all but three samples. The three samples with higher  $\text{NO}_3\text{-N}$  values were collected at the 40-ft depth. Ammonia-N ( $\text{NH}_3\text{-N}$ ) values ranged from less than the detection limit of 4  $\mu\text{g/g}$  to 36  $\mu\text{g/g}$  and had no obvious correlation with depth. Water-soluble U concentrations ranged from 0.006 to 0.519  $\mu\text{g/g}$ . Only one sample (CJ-208-40) had a U concentration more than 0.1  $\mu\text{g/g}$ , and that sample was from the 40-ft depth. These U values are low compared to an average total concentration of U reported for the Earth's crust (1.8  $\mu\text{g/g}$ ; Mason and Moore

1982) and an average value (20  $\mu\text{g/g}$ ) reported by Wedepohl (1974) for marine black shale such as the Mancos Shale. Part of the reason for the lower results is that the literature crustal and marine black shale averages were analyzed on total digestions of the rock rather than the water-soluble fractions.

### Mineralogy of the Water-Soluble Fraction

The geochemical computer program NETPATH was used to calculate possible mineral assemblages dissolved from the Mancos Shale samples by the deionized water. The most common use of NETPATH is to model mineral-phase reactions that could occur as ground water flows through an aquifer, based on the water chemistry data of two ground water samples collected along a flow path. In this study, we used NETPATH to help evaluate the mineralogy of the water-soluble fractions. To do this, deionized water was used as the initial solution composition and the analytical results of the water after reaction with solid samples was used as the final water composition. Water-soluble concentrations of  $\text{NH}_3$  and U were also measured, but the identification of the mineral phases containing these constituents was not pursued because of low concentrations of these contaminants. Results of XRD analysis helped to identify mineral phases that are most likely to contain the water-soluble components (Section 0).

#### *Primer on NETPATH*

To run NETPATH, the solution chemistry is entered into a database. From the database, dissolved species, mineral saturation indices, dissolved inorganic carbon concentration (from alkalinity), and electrical balance were calculated for each solution. The molal concentrations of the constituent elements were then imported to NETPATH for mass balance calculations. Combinations of mineral phases were specified, and the program calculated the amount of each phase that must precipitate or dissolve to meet the compositional constraints.

NETPATH solves a set of mass balance chemical equations and can determine a set of mineral assemblages to account for the chemical differences between two water compositions. For example, if water A has 10 millimoles (mmol) of Ca and evolves to water B that has 2 mmol of Ca, then 8 mmol of Ca was lost. Several chemical processes can account for the loss, including (1) precipitation of calcite ( $\text{CaCO}_3$ ), (2) precipitation of gypsum, (3) exchange of Ca for Na on an exchanger, and other processes. Clearly, each process will produce other changes in the water chemistry; for example, calcite precipitation will cause carbon (C) loss, gypsum precipitation will cause  $\text{SO}_4$  loss, etc. Thus, NETPATH models for this example are also constrained by mass balances for C and  $\text{SO}_4$ .

The user selects *constraints* and *permissible phases* for use with a simulation. *Constraints* are elements and *permissible phases* are minerals, exchange sites, or gases. Given the number of *constraints*, there must be enough *permissible phases* to afford a solution and there must be a phase for each *constraint* (for example if Ca is a *constraint*, there must be a phase that contains Ca).

Important points to remember about NETPATH models are (1) models are not unique, (2) models are not supported by thermodynamic principles (for example, a NETPATH model can have calcite precipitating, even though precipitation is impossible because of undersaturation), (3) the final water composition must have evolved from the initial composition (e.g., two water samples from the same stream tube in a flow system or water reacted with rock in a laboratory batch test such as was done in this study), and (4) the models are strongly a function of the *constraints* and *permissible phases* selected by the user. The user selects *constraints* and *permissible phases* by evaluating the data available about the site and applying geochemical principles.

Table 3. Results of Water Extractions Expressed as Micrograms of Constituent Per Gram of Rock

Sample	pH	Alk	Cl	NO <sub>3</sub> -N	SO <sub>4</sub>	NH <sub>3</sub> -N	U	Ca	Na	Mg	K	Total
CJ-201-40	7.97	450	399	10.95	3964	5.5	0.014	695	1040	170	485	7219
CJ-202-40	9.26	1800	494	25.73	816	6	0.047	22.5	1000	38	755	4957
CJ-203-40	6.17	600	159	15.24	20645	10	0.065	6120	450	400	100	28499
CJ-204-40	8.46	750	137	<5.50	8552.5	21	0.071	1840	1300	350	106	13062
CJ-205-40	9.16	1850	231	<5.50	785.5	20	0.073	12.5	1225	18.5	325	4473
CJ-206-40	8.78	1750	259	<5.50	1111.5	11.5	0.050	62.5	1075	36	115	4426
CJ-207-40	9.64	4050	210	<5.50	1492	36	0.040	4.5	2500	7	240	8545
CJ-208-40	9.29	1600	322	<5.50	835.5	7.5	0.519	52.5	1050	19	80	3972
CJ-209-40	8.49	1000	123.5	<5.50	4098.5	<4	0.043	250	1550	180	195	7407
CJ-210-40	9.72	3650	249.5	<5.50	780	16.5	0.041	9.5	1900	6.5	155	6773
CJ-201-105	9.39	1950	344	<5.50	366.5	4	0.010	38	1200	8	140	4056
CJ-202-105	9.78	4150	868.5	<5.50	216	16.5	0.035	9	1800	6	860	7932
CJ-203-105	9.52	2450	886.5	<5.50	377	13	0.055	22.5	1450	6.5	815	6026
CJ-204-105	9.85	4350	261	<5.50	254.5	17.5	0.055	5	2000	5.5	280	7179
CJ-205-105	9.73	4650	369	<5.50	330	23.5	0.041	3	2050	6	230	7667
CJ-206-105	9.29	2200	322.5	<5.50	429.5	14.5	0.011	34.5	1150	39.5	110	4306
CJ-207-105	9.61	3400	274	<5.50	215.5	15	0.066	14.5	1350	5.5	115	5395
CJ-208-105	9.31	1950	330.5	<5.50	581	12.5	0.051	34.5	1200	9.5	105	4229
CJ-209-105	9.77	4650	255	<5.50	371.5	21	0.035	7	2150	5.5	145	7611
CJ-210-105	9.32	1950	355.5	<5.50	478	10	0.047	51	1000	11.5	95	3957
CJ-201-170	9.78	3850	358	<5.50	249	15	0.036	7.5	1825	6	220	6536
CJ-202-170	9.79	4450	225.5	<5.50	269	21.5	0.057	5.5	2050	5	175	7207
CJ-203-170	9.75	3800	345	<5.50	276.5	14	0.054	11	1800	6.5	165	6424
CJ-204-170	9.81	4150	401.5	<5.50	264.5	24	0.062	4.5	1850	5.5	230	6936
CJ-205-170	9.68	4800	301.5	<5.50	274.5	23.5	0.040	3.5	2100	5	235	7749
CJ-206-170	9.76	4600	315.5	<5.50	223.5	22	0.010	5	1950	5	150	7277
CJ-207-170	9.63	3800	289.5	<5.50	276.5	23	0.013	8	1650	5.5	150	6208
CJ-208-170	9.8	5050	302	<5.50	287	19	0.052	4	2200	4.5	165	8037
CJ-209-170	9.51	2950	343.5	<5.50	333.5	18.5	0.033	16.5	1750	6	120	5544
CJ-210-170	9.77	3950	315.5	<5.50	282.5	20.5	0.026	8.5	1800	4.5	115	6502
CJ-201-235	9.81	4100	337.5	<5.50	168	20	0.077	5	1925	5.5	220	6787
CJ-202-235	9.8	4050	306	<5.50	223.5	16.5	0.024	6	1800	5	160	6573
CJ-203-235	9.8	4450	333.5	<5.50	295	25.5	0.031	4	2050	5	240	7409
CJ-204-235	9.74	3250	378	<5.50	301.5	23.5	0.040	9	1600	4.5	165	5737
CJ-205-235	9.67	4500	259.5	<5.50	452	27	0.040	5.5	2200	4.5	130	7584
CJ-206-235	9.71	4200	336.5	<5.50	252.5	26	0.010	6	1850	4.5	145	6826
CJ-207-235	9.75	4550	271	<5.50	269	24	0.013	5.5	2000	4	125	7254
CJ-208-235	9.81	4850	275.5	<5.50	212.5	25.5	0.008	3.5	2100	4	145	7622
CJ-209-235	9.78	4400	303.5	<5.50	297	17	0.043	6.5	1900	4	120	7054
CJ-210-235	9.81	4500	302	<5.50	228.5	19	0.017	5	1950	3.5	115	7129
CJ-201-300	9.86	4650	412	<5.50	180.5	20.5	0.006	4.5	2150	5.5	330	7759
CJ-202-300	9.81	4300	555.5	<5.50	198	16	0.048	8.5	1900	4	540	7528
CJ-203-300	9.7	3800	347.5	<5.50	189	19	0.013	5.5	1800	5	160	6332
CJ-204-300	9.85	4550	270	<5.50	217	22	0.022	1.5	2000	5	160	7231
CJ-205-300	9.73	4250	258.5	<5.50	293.5	23	0.040	6.5	1900	4	125	6866
CJ-206-300	9.63	4300	333	<5.50	103.5	20.5	0.037	6	1850	4.5	125	6748
CJ-207-300	9.76	4700	252	<5.50	292	23	0.007	4	2050	3.5	125	7455
CJ-208-300	9.64	3600	323.5	<5.50	235.5	17.5	0.036	11.5	1550	4	100	5848
CJ-209-300	9.88	5200	252.5	<5.50	172.5	30	0.034	4	2150	4	110	7929
CJ-210-300	9.83	4950	275	<5.50	256	20.5	0.038	4.5	2150	3.5	110	7775
Mean	9.50	3555	329	<6.21	1085	18.5	0.044	189	1726	29	213	7151

pH values in final solution; alkalinity as CaCO<sub>3</sub>

### *Estimated Mineralogy of the Crescent Junction Core Samples Based on NETPATH Calculations*

Seven elements (C, Ca, Cl, K, Mg, Na, and S) were used to constrain the NETPATH models. After trial and error using a wide range of phase assemblages in NETPATH, seven permissible phases were selected because they produced a reasonable set of results. The selection of permissible phases was aided by XRD (see Section 5), and hand-lens observations, and literature on soluble mineral phases that are likely to be present in the Mancos Shale. The minerals selected as permissible phases are calcite, gypsum, thenardite ( $\text{Na}_2\text{SO}_4$ ), nahcolite, halite ( $\text{NaCl}$ ), sylvite ( $\text{KCl}$ ), and dolomite [ $\text{CaMg}(\text{CO}_3)_2$ ]. Cation exchange of Ca and Na was also permitted. Because eight phases (including exchange) were permitted and only seven constraints were used, each sample analysis produced two to three models that exactly match the mass balance constraints. Selection of the model for each sample was somewhat arbitrary, but the major phases are similar among all the models.

The NETPATH results are given in millimole per liter (mmol/L) of test solution (water-soluble extractions). The tests used 2 g of rock in 0.10 L of water. Assuming a porosity of 0.25 and a mineral density of 2500 grams per liter (g/L) for the Mancos Shale at the Crescent Junction Site, a conversion factor of 0.375 is used to convert the NETPATH results to input values for the geochemical modeling program PHREEQC used in Section 9 (Parkhurst and Appelo 1999):

$$\frac{0.75 \text{ L}_{(\text{rock})} \times 2500 \text{ g}_{(\text{rock})}}{0.25 \text{ L}_{(\text{gw})}} = \frac{7500 \text{ g}_{(\text{rock})}}{\text{L}_{(\text{gw})}}$$

$$\frac{0.1 \text{ L}_{(\text{test soln})} \times 7500 \text{ g}_{(\text{rock})}}{2 \text{ g}_{(\text{rock})} \times \text{L}_{(\text{gw})}} \times \frac{1 \text{ mol}_{(\text{mineral})}}{1000 \text{ mmol}_{(\text{mineral})}} = \frac{0.375 \text{ mmol}_{(\text{mineral})}}{1 \text{ mol}_{(\text{mineral})}} \frac{\text{L}_{(\text{test soln})}}{\text{L}_{(\text{gw})}}$$

where "gw" is ground water and "test soln" is test solution.

The results of the mineral abundances calculated by NETPATH are presented in units of mmol/L of ground water (Table 4). Although thenardite was included in the list of permissible phases, it was not present in any of the selected mineral assemblages (Table 4).

On the basis of the means presented in Table 4, the mineral assemblage is dominated by nahcolite with major amounts of Ca-Na exchange and gypsum. Halite, sylvite, and dolomite occur in lesser amounts. Potassium is contained only in sylvite, thus the concentration of sylvite is constrained by the K concentration. Similarly, the concentration of Mg dictates the concentration of dolomite. All other constraints are contained in more than one phase, and mass balance equations must be solved. Calcite constitutes to 24.23 percent of the soluble mineral mass, but in some simulations calcite had to precipitate to meet the mass balance constraints.

Gypsum and dolomite are more dominant in the samples from the 40-ft depth than in samples from deeper depths (Table 4). Nahcolite and halite are more concentrated in the samples from deeper depths than in the samples from 40-ft depths. Sylvite is concentrated more in the 40-ft and 105-ft samples. The results presented in Table 4 are used in Section 9.3 to designate initial mineral concentrations for a ground water reaction-transport model.

*Table 4. Water-Soluble Mineralogy Estimates Based on Mass Balance Approach  
(expressed as millimole per liter of ground water; negative values indicate precipitation)*

Sample	Calcite	Gypsum	Nahcolite	Halite	Sylvite	Ca-Na Exchange	Dolomite
CJ-201-40	-0.07875	0.3075	0.04125	-0.0075	0.09375	0.15375	0.0525
CJ-202-40	0.0075	0.06375	0.20625	-0.0412	0.14625	0.07875	0.01125
CJ-203-40	-1.0125	1.6125	0.975	0.015	0.01875	-0.42	0.12375
CJ-204-40	-0.345	0.6675	0.24375	0.0075	0.01875	0.08625	0.10875
CJ-205-40	0.045	0.06	0.19125	-0.015	0.06375	0.1125	0.0075

Table 4 (continued). Water-Soluble Mineralogy Estimates Based on Mass Balance Approach  
(expressed as millimole per liter of ground water; negative values indicating precipitation)

Sample	Calcite	Gypsum	Nahcolite	Halite	Sylvite	Ca-Na Exchange	Dolomite
CJ-206-40	-0.0825	0.08625	0.31125	0.03375	0.0225	0.00375	0.01125
CJ-207-40	0.105	0.11625	0.37125	-0.0037	0.045	0.225	0.00375
CJ-208-40	-0.03	0.06375	0.22875	0.0525	0.015	0.03	0.0075
CJ-209-40	-0.1725	0.31875	0.21	-0.0112	0.0375	0.15375	0.05625
CJ-210-40	0.05625	0.06	0.36375	0.0225	0.03	0.11625	0.00375
CJ-201-105	0.0525	0.03	0.195	0.045	0.02625	0.075	0.00375
CJ-202-105	0.0675	0.015	0.40125	0.01875	0.165	0.0825	0.00375
CJ-203-105	0.09	0.03	0.21	0.03	0.1575	0.11625	0.00375
CJ-204-105	0.135	0.01875	0.34125	0.00375	0.0525	0.15375	0.00375
CJ-205-105	0.045	0.02625	0.49125	0.03375	0.045	0.07125	0.00375
CJ-206-105	-0.015	0.03375	0.28125	0.045	0.0225	0.0225	0.01125
CJ-207-105	-0.0375	0.015	0.44625	0.0375	0.0225	-0.01875	0.00375
CJ-208-105	0.0075	0.045	0.24	0.04875	0.01875	0.04875	0.00375
CJ-209-105	0.08625	0.03	0.43875	0.02625	0.02625	0.11625	0.00375
CJ-210-105	-0.04125	0.0375	0.28875	0.05625	0.01875	-0.01125	0.00375
CJ-201-170	0.09	0.01875	0.345	0.03375	0.04125	0.10875	0.00375
CJ-202-170	0.1125	0.0225	0.39	0.015	0.03375	0.13125	0.00375
CJ-203-170	0.07125	0.0225	0.36375	0.04125	0.03	0.09	0.00375
CJ-204-170	0.06	0.0225	0.40125	0.04125	0.045	0.0825	0.00375
CJ-205-170	0.0525	0.0225	0.51375	0.01875	0.045	0.07875	0.00375
CJ-206-170	0.0375	0.01875	0.4875	0.0375	0.03	0.05625	0.00375
CJ-207-170	0.0075	0.0225	0.44625	0.03375	0.03	0.03	0.00375
CJ-208-170	0.0675	0.0225	0.49875	0.03375	0.03	0.09375	0.00375
CJ-209-170	0.105	0.02625	0.255	0.04875	0.0225	0.13125	0.00375
CJ-210-170	0.0525	0.0225	0.39375	0.045	0.0225	0.075	0.00375
CJ-201-235	0.11625	0.01125	0.34125	0.03	0.04125	0.13125	0.00375
CJ-202-235	0.06375	0.01875	0.39	0.03375	0.03	0.0825	0.00375
CJ-203-235	0.10125	0.0225	0.3975	0.0225	0.045	0.12375	0.00375
CJ-204-235	0.06	0.0225	0.3075	0.04875	0.03	0.0825	0.00375
CJ-205-235	0.08625	0.03375	0.44625	0.03	0.02625	0.12	0.00375
CJ-206-235	0.03375	0.01875	0.45375	0.045	0.02625	0.0525	0.00375
CJ-207-235	0.0525	0.0225	0.465	0.03375	0.0225	0.075	0.00375
CJ-208-235	0.07875	0.015	0.465	0.03	0.02625	0.09375	0.00375
CJ-209-235	0.03375	0.0225	0.465	0.04125	0.0225	0.05625	0.00375
CJ-210-235	0.05625	0.01875	0.45	0.04125	0.0225	0.07125	0.00375
CJ-201-300	0.13875	0.015	0.3675	0.0225	0.06375	0.15375	0.00375
CJ-202-300	0.09375	0.015	0.38625	0.015	0.105	0.10875	0.00375
CJ-203-300	0.07125	0.015	0.3675	0.04125	0.03	0.08625	0.00375
CJ-204-300	0.09	0.01875	0.40875	0.02625	0.03	0.10875	0.00375
CJ-205-300	0.0525	0.0225	0.43875	0.03	0.0225	0.075	0.00375
CJ-206-300	0.0225	0.0075	0.495	0.045	0.0225	0.03	0.00375
CJ-207-300	0.05625	0.0225	0.48375	0.03	0.0225	0.07875	0.00375
CJ-208-300	-0.0075	0.01875	0.435	0.04875	0.01875	0.01125	0.00375
CJ-209-300	0.07875	0.015	0.4875	0.03375	0.0225	0.09	0.00375
CJ-210-300	0.17625	0.01875	0.27	0.0375	0.0225	0.19875	0.00375
Mean	0.0199	0.0847	0.3779	0.0287	0.0406	0.0781	0.0109

# Cation Exchange Capacity

## Introduction

CEC is the ability of a solid substance to freely exchange one cation for another. For example, cations in smectite clay minerals are able to readily enter and exit the interlayer (exchangeable) sites. Cations are selective in their ability to occupy exchange sites, and selectivity is often influenced by the hydration state of the dissolved cation. CEC can be dependent on other solution variables such as pH values. CEC is commonly expressed in units of milliequivalents per 100 grams (meq/100 g). Typical values of CEC for pure clays are 3 to 15 meq/100 g for kaolinite, 80 to 150 meq/100 g for smectite, and 10 to 40 meq/100 g for illite (Grim 1953). Mancos Shale samples analyzed in this study contain mostly kaolinite, illite, and smectitic interlayered clay minerals (Section 5).

Because clay minerals are abundant, the Mancos Shale may have a large CEC that can cause significant changes to ground water chemistry. Knowledge of the CEC is required to develop a geochemical model of water-rock interactions. It is assumed that most of the CEC in the Crescent Junction samples is due to the clay minerals. In the reaction-transport modeling, presented in Section 9.5, the CEC is considered a fixed property of the rock, but selectivity of cations occupying the exchange sites is controlled by solution chemistry. The laboratory results presented in this section are used to specify the number of exchange sites in the models.

## Methods

CEC was measured on 20 core samples of Mancos Shale collected from 40-ft and 105-ft depths. Samples were crushed, air dried, and sieved to -10 +18 mesh (1- to 2-mm nominal diameter) in the same manner as for the other tests. This size fraction was selected because it is easy to work with in small-scale CEC tests and has a reasonably constant surface area (Section 6). The results could be scaled to field conditions by normalizing to the surface area. CEC was also measured on a powdered Mancos Shale sample to provide information on maximum CEC.

Various methods have been used to measure CEC. Most methods rely on saturation of the exchange sites with a single composition of cation; subsequently the cation is removed from the fully saturated mineral and its mass is measured to determine CEC. No general method exists that can be reliably used for all clay-bearing samples (Bain and Smith 1987). Methods include saturation with Ba, Ca, K, Na, or  $\text{NH}_4$ , (Jackson 1969; Bain and Smith 1987).

In this study, CEC was determined using the ammonium saturation method (Chapman 1965 as described in Bain and Smith 1987). This method was selected largely because the saturating solution (ammonium acetate) is highly buffered and maintains its near-neutral pH value throughout the test (Chapman 1965). Another advantage is that  $\text{NH}_4$  concentrations are easily measured in the sodium-chloride extracts. Accuracy of the method was checked by measuring the CEC of a calcium-montmorillonite clay standard (sample number STx-1) from the Source Clay collection of the Clay Minerals Society. CEC values published by Borden and Giese (2001) for this specimen were 89 meq/100 g with a standard deviation of 2 meq/100 g. CEC values of nine repetitions in our laboratory ranged from 71.4 to 85.7 meq/100 g with a mean of 77.0 and a standard deviation of 6.6. Although slightly lower than the Borden and Giese (2001) results, our values are reasonably similar and probably within the range of analytical uncertainty.

For the ammonium saturation method, the clay sample was first saturated with  $\text{NH}_4$  ions using 1 molar (M) ammonium acetate followed by exchange with sodium chloride (STO 210, method CB [CEC-1]). For a CEC measurement, an exact weight of clay ranging from 20 milligrams (mg) to 200 mg was combined with 20 mL of 1 M ammonium acetate and agitated end over end for 2 hours. The solids were separated from the liquid phase by centrifugation, and the saturation process with ammonium acetate was repeated five times. Isopropyl alcohol (20 mL) was then added to the solids, the mixture was agitated by hand, and centrifuged. Five additional washings with isopropyl alcohol were conducted, after which 20 mL of 100 g/L sodium chloride solution was added to the solid phases to initiate removal of the  $\text{NH}_4$  cations from the exchange sites. The sodium chloride solution was agitated by hand seven times. The  $\text{NH}_4$  concentration in the resultant solution was measured spectrophotometrically and was used to calculate the CEC.

## Results and Discussion

CEC measurements ranged from 0.54 to 36.29 meq/100 g with a mean of 11.23 meq/100 g (Table 5). The mean is within the range published by Grim (1953) for pure kaolinite (3 to 15 meq/100 g) and pure illite (10 to 40 meq/100 g) but is significantly less than pure smectite (80 to 150 meq/100 g). The values for these Mancos Shale samples are reasonable for the clay mineral compositions as determined by XRD analysis (Section 5).

One sample (CJ-205-40) was ground to a powder to compare CEC values for a finer grain size. The CEC measurements of the powder (10.29 and 10.43 meq/100 g for duplicate samples) were similar to the 1- to 2-mm grain size. Although limited to one analysis, this result provides confidence for applying the laboratory CEC values to the field in the reaction-transport models (Section 9.5). The CECs are used in the reaction-transport models to simulate cation exchange of Ca, K,  $\text{NH}_4$ , and Na. Retardation of  $\text{NH}_4$  in the model is assumed to be caused by the cation exchange with the Mancos Shale.

*Table 5. Results of Cation Exchange Measurements*

Sample ID <sup>a</sup>	Size Fraction	CEC (meq/100 g)
CJ-201-40	1 to 2 mm	9.29
CJ-202-40	1 to 2 mm	11.71
CJ-203-40	1 to 2 mm	36.29
CJ-204-40	1 to 2 mm	10.71
CJ-205-40	1 to 2 mm	10.71
CJ-205-40-Dup	1 to 2 mm	12.71
CJ-205-40-P	<1 mm	10.29
CJ-205-40-P-Dup	<1 mm	10.43
CJ-206-40	1 to 2 mm	5.86
CJ-207-40	1 to 2 mm	15.43
CJ-208-40	1 to 2 mm	7.00
CJ-209-40	1 to 2 mm	17.00
CJ-210-40	1 to 2 mm	11.43
CJ-201-105	1 to 2 mm	5.29
CJ-202-105	1 to 2 mm	11.43
CJ-203-105	1 to 2 mm	7.00
CJ-204-105	1 to 2 mm	12.86
CJ-204-105-Dup	1 to 2 mm	13.14
CJ-205-105	1 to 2 mm	12.43
CJ-206-105	1 to 2 mm	7.43
CJ-207-105	1 to 2 mm	8.57
CJ-208-105	1 to 2 mm	7.14
CJ-209-105	1 to 2 mm	14.71
CJ-210-104	1 to 2 mm	0.54
Minimum		0.54
Maximum		36.29
Mean		11.23

<sup>a</sup>P = Powdered Sample, Dup = Duplicate

A brief literature search was conducted to determine if the CEC values of Crescent Junction Mancos Shale samples are comparable to CEC measurements of Mancos Shale samples from other areas. Evangelou et al. (1984) collected samples of partially weathered and unweathered outcrop samples of Mancos Shale from the West Salt Creek Watershed near Grand Junction, Colorado, and analyzed the CEC using the calcium/barium exchange method. They reported CEC values ranging from 13.25 to 19.96 meq/100 g. These values are similar to the Crescent Junction values and suggest that the CEC for Mancos Shale may be relatively constant.

## X-Ray Diffraction Analysis

### Introduction

XRD was used to identify minerals present in the core samples. XRD is capable of defining the internal arrangement of atoms in a crystalline lattice, thus making it possible to positively identify minerals. Identification of mineralogy based on chemical methods (Section 3.3.2) is more ambiguous because often minerals have similar chemical compositions and, in some cases, identical compositions. Unlike chemical methods, XRD analysis is not able to detect small quantities of minerals (XRD is generally limited to detection of approximately 10 percent, but detection is dependent on mineral crystallinity) and only semi-quantitative estimates of mineral abundances are possible. XRD analyses were conducted at Mesa State College in Grand Junction, Colorado, by Dr. William Hood (Appendix D).

Chemical interaction between ground water and Mancos Shale is likely to occur mostly at the surfaces of clay minerals. Therefore, clay mineral chemistry is important to the transport of contaminants by the ground water. XRD is one of the best analytical tools to identify clay minerals. For this study, 10 core samples, all from the 40-ft depth, were analyzed by XRD.

For XRD analysis, the sample is subjected to an x-ray beam. The atomic lattice within the individual mineral crystals diffracts (reflects) the x-ray beam, and the angle of diffraction is measured. The angle of diffraction and the intensity of the diffracted x-rays produce a "fingerprint" that can be used to identify the minerals (Jackson 1969).

### Methods

A random powder mount was used for identification of major minerals (Appendix D). Samples were finely powdered with a mortar and pestle, and placed in a sample holder, and scanned from 4.2 to 50 degrees 2 $\theta$  using a Rigaku Miniflex x-ray diffractometer (Appendix D). The Jade computer program was used to calculate spacings and to compare diffraction patterns of the samples with diffraction patterns of known minerals.

Splits of the samples were analyzed for clay mineralogy (Appendix D). Analysis of clay mineralogy is more complex than for the major minerals because the sample requires four separate preparation methods and an XRD analysis of each. To prepare the clay mineral splits, the clays were segregated into fine particles and not flocculated. The bulk sample was first placed in water overnight to remove readily soluble material and initiate disaggregation of the clays. Calgon (sodium metaphosphate) was added to further disperse clay minerals and the mixture was allowed to sit for 8 hours. Magnesium was added to the suspension to saturate the clay mineral interlayers (to produce a constant d spacing of this lattice plane). A small quantity of the suspension was smeared on a glass microscope slide and allowed to dry. The four methods used to treat the clay mineral separates are (1) air drying, (2) glycolating, (3) heating to 300 °C, and (4) heating to 550 °C. More details on the preparation and analysis methods are available in Appendix D. XRD patterns from these four treatments were used to positively identify the clay minerals and to estimate the amount of smectite layers in interlayered illite/smectite clays.

Estimates of the mineral abundance of non-phylosilicate minerals were made by a process including background removal, normalizing the peak intensities to a quartz standard, and summing the peak intensities. Estimates of clay mineral abundance used the glycolated diffractograms and employed a series of computer enhancements, including background removal and peak assessment. The ratio of illite to smectite layers in the mixed-layer clays was estimated from a comparison of the Mg-saturated and



glycolated diffractograms. More details on the methods used to estimate mineral abundances are presented in Appendix D. X-ray diffraction methods provide only a semi-quantitative estimate of the mineral abundances. According to Schultz (1964) based on his work with Pierre Shale (a Mancos Shale equivalent), the abundance estimates are adversely affected by sampling, sample preparation, machine response, and, most importantly, interpretation. Schultz (1964) also states that if a mineral makes up more than 15 percent of the sample, the precision of the abundance estimate is usually within about 10 percent. At lower mineral concentrations, the uncertainty increases.

## Results and Discussion

XRD analysis was conducted on the 10 samples of Mancos Shale collected from the 40-ft depth. The mineralogical composition of these samples is dominated by quartz, with lesser amounts of dolomite and calcite, small amounts of feldspar, and traces of gypsum (Table 6.). Orthoclase and plagioclase feldspar occur in approximately equal amounts.

*Table 6. Non-Phyllosilicate Mineral Abundance Estimates in Percent Based on XRD Analysis of Bulk Samples*

Sample ID	Quartz	Calcite	Dolomite	Orthoclase	Plagioclase	Gypsum
CJ-201-40	32	3	5	1	1	Tr <sup>a</sup>
CJ-202-40	29	3	4	1	1	1
CJ-203-40	36	4	5	1	2	1
CJ-204-40	33	2	3	1	1	
CJ-205-40	28	3	6	1	1	
CJ-206-40	39	4	6	1	2	
CJ-207-40	25	3	3	1	1	
CJ-208-40	38	3	5	1	1	
CJ-209-40	27	1	3	2	1	Tr
CJ-210-40	24	4	3	1	1	

<sup>a</sup>Tr = trace.

The clay mineral fraction is dominated by mixed-layer (mostly illite/smectite) clays, illite, and kaolinite (Table 7.). The mixed-layer clays are dominated by illite layers. A small amount of mixed-layer chlorite/vermiculite is probably present.

*Table 7. Estimates of Clay Mineral Abundance in Percent of Total Clay Based on XRD Analysis*

Sample ID	Mixed Layer <sup>a</sup>	Illite	Kaolinite	Percent Illite in Mixed-Layer Clays
CJ-201-40	43	29	28	70
CJ-202-40	38	36	26	60
CJ-203-40	43	31	25	60
CJ-204-40	40	30	29	60
CJ-205-40	46	31	23	60
CJ-206-40	37	34	29	60
CJ-207-40	27	36	37	50
CJ-208-40	35	36	29	60
CJ-209-40	39	31	29	60
CJ-210-40	39	37	25	60

<sup>a</sup>Mostly mixed-layer illite/smectite with minor chlorite/vermiculite.

A brief literature survey was conducted to determine if the XRD results for the Mancos Shale at Crescent Junction are typical of other Mancos Shale localities. Schultz (1997) reported that clays in the Mancos Shale from the Colorado Plateau region contain 50 to 60 percent mixed-layer illite/smectite, 12 to 15 percent poorly ordered kaolinite, and 30 to 35 percent illite; however, no source of data is provided in that publication. Nadeau and Reynolds (1981b) discuss clay mineral XRD results of 77 bentonite-shale paired samples collected from the Mancos Shale throughout the Western Interior of North America. They determined that the clays are primarily randomly mixed-layer illite/smectite with illite compositions ranging from 0 to 85 percent. They attribute the origin of the clays to volcanic ash. The illitic component increases in response to increased burial metamorphism, as does the ordering of the illite/smectite.

Nadeau and Reynolds (1981a) discuss XRD clay mineralogy results of 690 samples of Mancos Shale collected from 154 sites in the four-state region of Colorado, Utah, Arizona, and New Mexico. These clays are dominated by mixed-layer illite/smectite, with 20 to 60 percent illite layers. The regional distribution of ordering in the mixed-layer illite/smectite is attributed to differences in burial metamorphism of the Mancos Shale. Evangelou et al. (1984) collected samples of partially weathered and unweathered outcrop samples of Mancos Shale from the West Salt Creek Watershed near Grand Junction, Colorado, and analyzed the clay fractions by XRD. These clay fractions contain mica, kaolin, smectite, and randomly interstratified mixed-layer clay, possibly mica/vermiculite. These studies generally indicate that the clays identified in the Crescent Junction samples (kaolinite, illite, and mixed-layer illite/smectite) are typical of the Mancos Shale throughout much of its depositional basin.

## Surface Area

### Introduction

Knowledge of the surface area of the Mancos Shale samples is needed to relate the results to the transport of contaminants through the subsurface. Processes such as cation exchange and adsorption are directly related to the surface area that the ground water contacts. For example, for the same travel distance, interaction of dissolved contaminants with the rock will be less in a fracture-dominated matrix (small surface area) than in a porous-media (higher surface area) flow. It is beyond the scope of this study to determine the nature of the flow (fracture versus porous media) in the subsurface at the Crescent Junction Site. However, to properly use the data collected during this study in site models, these data will need to be normalized to surface area. Therefore, it is important to measure the surface area of the samples used in the tests. Surface area was determined for 10 core samples from the 40-ft depth.

### Methods

Samples were crushed, air dried, and sieved to -10 +18 mesh (1- to 2-mm nominal diameter) in the same manner as for other tests. Surface area was determined by the standard BET method. This method is the most widely used method for determining particle surface area. Samples were prepared by heating while simultaneously evacuating to remove impurities. The prepared samples were then cooled with liquid nitrogen and analyzed by measuring the volume of  $N_2$  gas adsorbed at specific pressures (Micromeritics 2006; Jackson 1969). Multiple-point isotherm measurements were conducted. The multiple point tests are more accurate than single point tests. Micromeritics Analytical Services, Norcross, Georgia, conducted the surface area measurements (Appendix E).

### Results and Discussion

Measured surface areas of the 10 samples from the 40-ft depth range from 8.81 to 13.22 square meters per gram ( $m^2/g$ ) with a mean of  $11.02 m^2/g$  (Table 8.). These values are reasonably comparable to surface areas measured by Davis and Curtis (2003) on alluvial aquifer samples obtained from the former Naturita, Colorado, uranium-ore processing site. Surface areas measured on the 16 Naturita samples range from 5.2 to  $20.0 m^2/g$  with a mean of  $12.43 m^2/g$  and standard deviation of  $3.77 m^2/g$ . Surface area was used as an input to the surface-complexation algorithm in the transport model presented in Section 0.

Surface area was also measured on a powdered split of Crescent Junction sample CJ-205-40. The surface area of the powdered sample ( $10.7 \text{ m}^2/\text{g}$ ) is consistent with surface areas measured on the 1- to 2-mm fractions, indicating that the BET method is probably accounting for intraparticle surface area.

*Table 8. Results of BET Surface Area Analysis of 1- to 2-mm Size Fraction*

Sample ID	Surface Area ( $\text{m}^2/\text{g}$ )
CJ-201-40	10.65
CJ-202-40	12.21
CJ-203-40	8.81
CJ-204-40	12.92
CJ-205-40	9.95
CJ-206-40	9.46
CJ-207-40	13.12
CJ-208-40	9.39
CJ-209-40	10.46
CJ-210-40	13.22
Minimum	8.81
Maximum	13.22
Mean	11.02

## Distribution Ratios

### Introduction

Distribution ratios ( $R_d$ ) are a measure of the partitioning of a contaminant between the ground water and the solid fraction of the aquifer. The higher the  $R_d$  value, the more partitioning to the solids and the more retardation of the contaminant. The  $R_d$  value is empirical and is simply the ratio of the measured concentration in the solids (milligrams per kilogram [ $\text{mg}/\text{kg}$ ]) to the measured concentration in the ground water (milligrams per liter [ $\text{mg}/\text{L}$ ]), and has units of milliliters per gram ( $\text{mL}/\text{g}$ ).  $R_d$  values are often used to simulate retardation of contaminants in ground water models. When used in these models, an implicit assumption exists that chemical retardation occurs by the process of adsorption under equilibrium conditions. For the equilibrium assumption, the  $R_d$  value is often referred to as a distribution coefficient ( $K_d$ ). Many models also assume that  $K_d$  does not vary with the concentration of the contaminant, but research has shown that it often does, and algorithms such as the Langmuir or Freundlich equations are used to produce a better fit to  $R_d$  data. To test if  $R_d$  values vary with contaminant concentrations, multiple points using various concentrations are measured, and plots of these "adsorption isotherms" are fitted with the various models. If the plot is reasonably linear, then models using a constant  $K_d$  value (also termed linear isotherm) will produce satisfactory results.

The  $R_d$  value can vary significantly with solution chemistry. For example, Davis et al. (2004) show that  $R_d$  values for U in a sample of alluvium vary by more than a factor of 10, depending on dissolved carbonate concentrations and pH values. Also, the  $R_d$  approach is only valid for contaminants that occur in trace concentrations.

For the reaction-transport modeling, a surface-complexation approach is employed instead of using  $R_d$  values to simulate retardation of U (Section 0). With the surface-complexation approach, the  $R_d$  value changes as chemical conditions (especially pH and  $\text{pCO}_2$ ) change in the aquifer. The main use of the  $R_d$  values determined in this study is to test and calibrate the surface-complexation module used in the reaction-transport modeling.

## Methods

Uranium  $R_d$  values were determined using procedure CB (Rd-1) in STO 210. In summary, a sample of Mancos Shale was crushed and sieved to -10 +18 mesh (1- to 2-mm nominal diameter). The sample (5 g for a single-point  $R_d$  value) was placed in a plastic centrifuge tube with 100 mL of pH value-adjusted synthetic pore fluid (SPF) that simulates tailings or evolved pore fluid. The tubes were agitated end over end for 24 hours and then centrifuged, decanted, and filtered through a 0.45-micrometer ( $\mu\text{m}$ ) filter. Filtrates were analyzed for electrical conductivity, pH value, alkalinity, and U concentration. Controls included SPF without solids and duplicates. The concentration of U in the solid phase was determined from the loss of U from the SPF solution.  $R_d$  values were determined from the calculated concentration of U in the solid phase and the measured U concentration in the solution.

Uranium  $R_d$  values were determined using three different SPF compositions designed to simulate ground water that could be present in the Mancos Shale after construction of the disposal cell. One solution (SPF-1) simulates pore fluids that currently exist in the tailings. Another solution (SPF-2) simulates tailings pore water mixed with 50 percent Mancos Shale ground water. A third solution (SPF-3) simulates water that results from the sequential batch-leaching testing (Section 0). Table 9 provides compositions of the SPF fluids. The SPF solutions were spiked with 1 mg/L U to enable measurement of the  $R_d$  values.

Table 9. Composition (milligrams per liter) of SPF Used in Uranium  $R_d$  Tests

Constituent	SPF-1	SPF-2	SPF-3
Sodium	5781.41	5888.61	7806.64
Potassium	112.23	76.31	166.10
Calcium	209.62	148.48	195.65
Magnesium	315.71	197.32	179.56
Ammonium	2181.82	1036.36	900.00
Sulfate	17454.37	14606.17	17913.58
Chloride	910.26	<sup>a</sup> 309.49	1365.38
Inorganic Carbon	271.43	314.29	78.57
pH Value	6.63	6.96	7.97

<sup>a</sup>The value for Cl for SPF-2 should have been approximately 4541 mg/L. The low value (309.49) resulted from an error in designing the SPF-2 solution.

Single-point  $R_d$  measurements for U were determined for 20 samples, and 6-point isotherms were determined for five samples of SPF-1. For the five samples used for isotherms, single-point  $R_d$  values were also determined using SPF-2 and SPF-3 to evaluate sensitivity to solution chemistry.

## Results and Discussion

$R_d$  values were corrected for the amount of "labile" U contained in the Mancos Shale samples. The labile U fraction is defined as U in the solid fraction capable of being released to the solution during a test (Davis et al. 2004). Release of labile U is usually a function of time with longer agitation periods resulting in higher concentrations of labile U. A constant value of 0.0436  $\mu\text{g/g}$  for the labile U fraction was used in our study. This value is the mean of eight measurements of the sequential batch-leaching tests (Section 0). In the sequential batch tests, U-free SPF was reacted for various time periods with Mancos Shale samples, and U concentrations were measured in the final solutions. For comparison, Davis et al. (2004) used a value of 0.21  $\mu\text{g/g}$  for labile U in uncontaminated alluvial aquifer sediment from the Naturita Site.

Despite making corrections for the labile U, some tests produced negative  $R_d$  values (Table 11). Negative  $R_d$  values are a combination of (1) analytical uncertainty, (2) relatively low  $R_d$  values, and (3) variable contribution from labile U. Minimum and maximum  $R_d$  values presented in the tables in this section are

based on analytical imprecision of  $\pm 2.5$  percent in all  $U$  measurements. Many of the  $R_d$  determinations were fairly sensitive to the analytical imprecision.

Single-point determinations of  $R_d$  using SPF-1 (tailings fluid) ranged from negative values to 0.84 mL/g (Table 10). The maximum  $R_d$  value, accounting for 2.5 percent error in all measurements, is 1.9 mL/g. These values are reasonably similar to  $R_d$  values measured on alluvial aquifer material from other uranium-ore milling sites. For example,  $R_d$  values for samples collected at the DOE New Rifle, Colorado, Site, for alluvium and Wasatch Formation, range from negative values to 3.7 mL/g and 1.6 mL/g, respectively (DOE 1999).

Table 10. Final Concentrations of  $U$  in Liquid ( $U_l$ ) and Solid ( $U_s$ ) Phases and  $R_d$  for Single-Point Determination with SPF-1<sup>a</sup>

Sample ID	$U_l$ ( $\mu\text{g/L}$ ) Measured	$U_s$ ( $\mu\text{g/g}$ ) Calculated	$R_d$ (mL/g)	$R_d$ (mL/g) Minimum	$R_d$ (mL/g) Maximum
CJ-201-40	898.0	-1.33	-1.48	-2.38	-0.53
CJ-202-40	805.4	0.28	0.34	-0.65	1.39
CJ-203-40	892.2	-1.21	-1.36	-2.27	-0.40
CJ-204-40	890.9	-1.19	-1.33	-2.24	-0.38
CJ-205-40	793.9	0.51	0.64	-0.37	1.70
CJ-206-40	906.1	-1.49	-1.64	-2.54	-0.70
CJ-207-40	811.6	0.15	0.19	-0.79	1.22
CJ-208-40	753.6	0.54	0.72	-0.29	1.78
CJ-209-40	926.6	-1.90	-2.05	-2.93	-1.13
CJ-210-40	757.6	0.46	0.61	-0.39	1.67
CJ-201-105	850.1	-0.37	-0.44	-1.39	0.57
CJ-202-105	839.4	-0.16	-0.19	-1.15	0.83
CJ-203-105	821.2	0.21	0.25	-0.73	1.29
CJ-204-105	822.4	0.18	0.22	-0.76	1.26
CJ-205-105	839.3	-0.15	-0.18	-1.15	0.83
CJ-206-105	852.1	-0.41	-0.48	-1.43	0.52
CJ-207-105	798	0.67	0.84	-0.17	1.91
CJ-208-105	805.6	0.52	0.64	-0.36	1.70
CJ-209-105	813.6	0.36	0.44	-0.55	1.49
CJ-210-105	819.4	0.24	0.30	-0.69	1.34
SPF-1	829.4				

<sup>a</sup>Test conditions: pH 7.57, alkalinity 570 mg/L  $\text{CaCO}_3$ , 50 g/L. Minimum and maximum  $R_d$  values based on  $\pm 2.5$  percent for  $U$  analyses on final solutions and SPF-1.

Single-point  $R_d$  values for samples from the 40-ft depth using SPF-2 (simulated tailings pore water mixed with 50 percent Mancos Shale ground water) range from -0.46 to 0.51 mL/g with one negative value (Table 11). Single-point  $R_d$  values for samples from the 40-ft depth using SPF-3 (simulated water that results from the sequential batch-leaching testing) ranged from 0.41 to 1.92 mL/g (Table 12). Maximum  $R_d$  values for SPF-2 and SPF-3 are 1.56 and 3.04 mL/g, respectively. The  $R_d$  values for SPF-3 are slightly higher than those of the SPF-1 and SPF-2 solutions, indicating increased partitioning to the solid phase. This might be expected for SPF-3, as it has a much lower dissolved carbon concentration and a higher pH value (Table 9).

Table 11. Final Concentrations of U in Liquid ( $U_l$ ) and Solid ( $U_s$ ) Phases and  $R_d$  for Single-Point Determination with SPF-2<sup>a</sup>

Sample ID	$U_l$ (μg/L) Measured	$U_s$ (μg/g) Calculated	$R_d$ (mL/g)	$R_d$ (mL/g) Minimum	$R_d$ (mL/g) Maximum
CJ-202-40	760.4	0.22	0.29	-0.70	1.33
CJ-205-40	765.0	0.13	0.17	-0.82	1.20
CJ-207-40	756.1	0.31	0.40	-0.59	1.45
CJ-208-40	789.5	-0.36	-0.46	-1.41	0.54
CJ-208-40D	752.1	0.39	0.51	-0.49	1.56
CJ-210-40	761.0	0.21	0.27	-0.71	1.31
SPF-2	769.2				

<sup>a</sup>Test conditions: pH 7.69, alkalinity 907 mg/L CaCO<sub>3</sub>, 50 g/L. Minimum and maximum  $R_d$  values are based on  $\pm 2.5$  percent for U analyses on final solutions and SPF-2. D in sample ID number indicates duplicate analysis.

Table 12. Final Concentrations of U in Liquid ( $U_l$ ) and Solid ( $U_s$ ) Phases and  $R_d$  for Single-Point Determination with SPF-3<sup>a</sup>

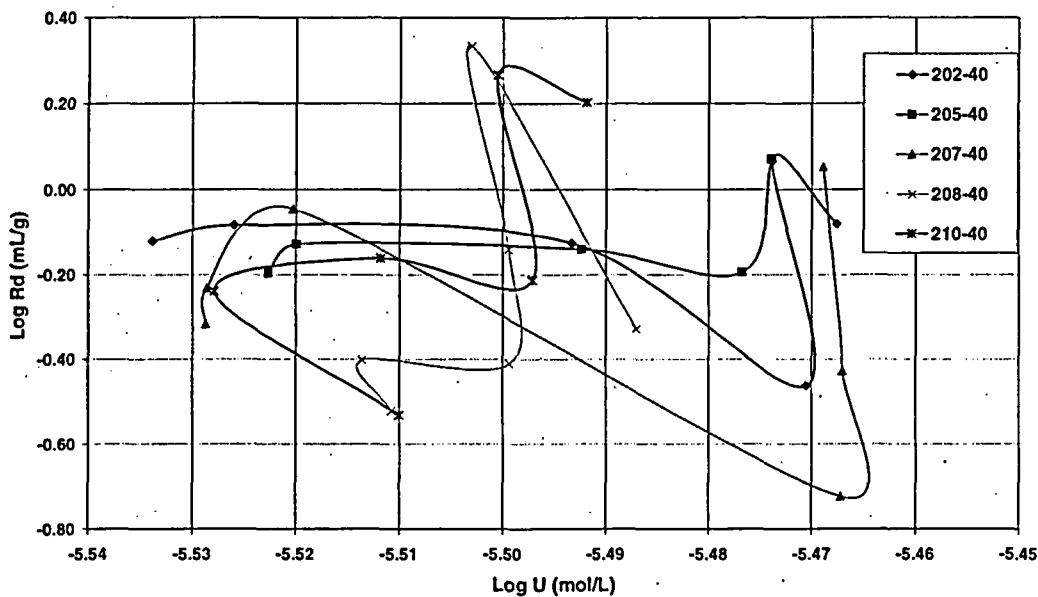
Sample ID	$U_l$ (μg/L) Measured	$U_s$ (μg/g) Calculated	$R_d$ (mL/g)	$R_d$ (mL/g) Minimum	$R_d$ (mL/g) Maximum
CJ-202-40	742.2	1.42	1.92	0.85	3.04
CJ-205-40	756.7	1.13	1.50	0.45	2.60
CJ-207-40	783.4	0.60	0.77	-0.25	1.83
CJ-208-40	797.0	0.33	0.41	-0.58	1.46
CJ-210-40	793.9	0.39	0.49	-0.51	1.54
SPF-3	811.2				

<sup>a</sup>Test conditions: pH 7.91, alkalinity 313 mg/L CaCO<sub>3</sub>, 50 g/L. Minimum and maximum  $R_d$  values are based on  $\pm 2.5$  percent for U analyses on final solutions and SPF-3.

Isotherm tests using mass-to-water ratios of 10, 20, 50, 100, 200, and 250 g/L were conducted on five Mancos Shale samples from the 40-ft depth using SPF-1. For a linear isotherm, the results should plot as a straight line on a log-log plot such as shown on Figure 1a. The lack of linearity of these plots is likely due in large part to analytical imprecision. The analytical uncertainty is greatest at the highest values of dissolved U (Figure 1b). Better definition would result if the tests had spanned a larger range of U concentrations and used larger masses of solids. Although these data are scattered, it is apparent that the uranium  $R_d$  values of the Crescent Junction Mancos Shale samples are relatively low.

The same data shown on Figure 1a are plotted on Figure 2 at a larger scale, along with the Naturita uranium  $R_d$  results from Davis et al. (2004). Data from Crescent Junction form a relatively tight group near the dissolved U concentration of  $10^{-5.50}$  mol/L. Many of the Crescent Junction sample uranium  $R_d$  values are lower than any of the Naturita results. The lowest Naturita  $R_d$  values were measured on solutions with high CO<sub>2</sub> partial pressures and a near-neutral pH value of 6.88 (Davis1 on Figure 2). The Crescent Junction SPFs also have high CO<sub>2</sub> concentrations and near-neutral pH (Table 9), which accounts for their low  $R_d$  values. The mineralogy of the Mancos Shale (e.g., low in iron oxyhydroxide) compared to alluvial samples may also be partly responsible for the lower  $R_d$  values.

a.



b.

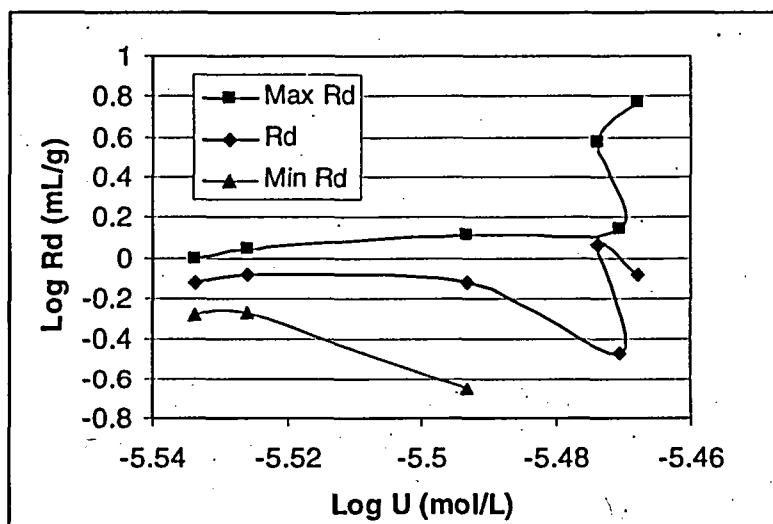
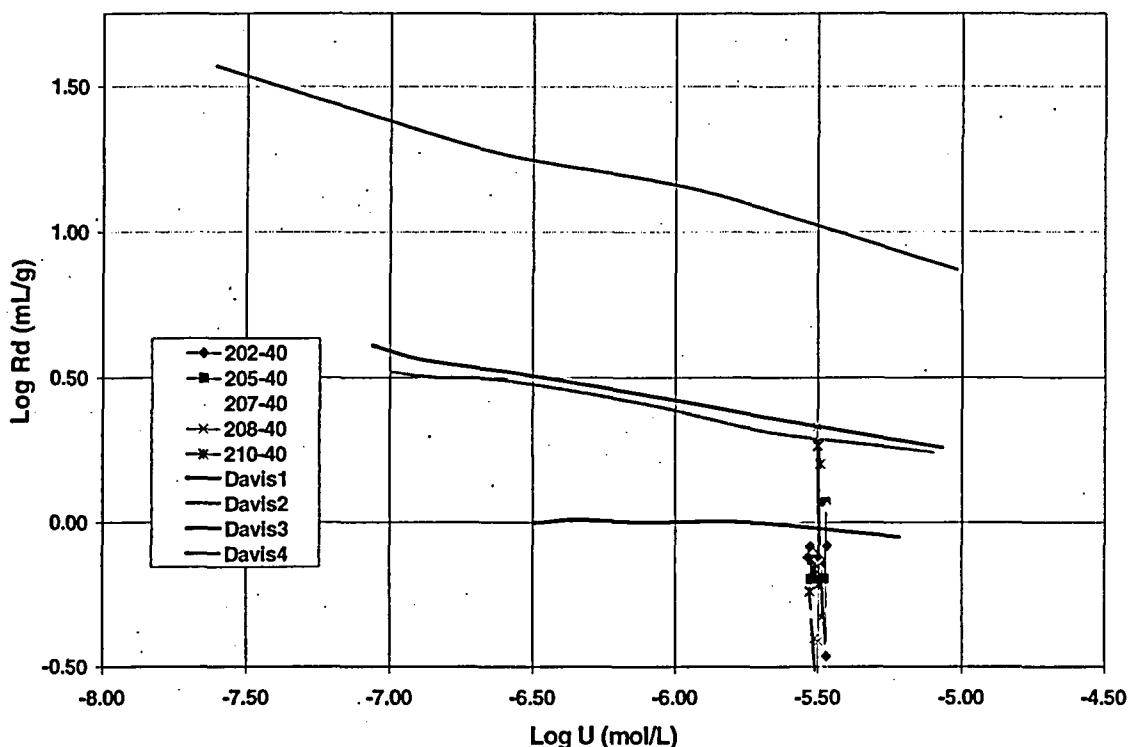


Figure 1. a. Isotherm Plot of Uranium  $R_d$  Determinations Made on Crescent Junction Mancos Shale Sample Using SPF-1,

b. Isotherm Plot of Sample 202-40 Showing Effect of Analytical Imprecision on Calculated Uranium  $R_d$  Values; Maximum and Minimum  $R_d$  Values are Calculated Using  $\pm 2.5\%$  Uncertainty on all Analytical Measurements.



Davis1 = AGW-6, pH 6.88, 6.8 percent CO<sub>2</sub>, 820 g/L  
 Davis2 = AGW-5, pH 7.18, 1.57 percent CO<sub>2</sub>, 250 g/L  
 Davis3 = AGW-7, pH 7.58, 0.47 percent CO<sub>2</sub>, 125 g/L  
 Davis4 = AGW-3 (laboratory air), pH 7.94, 0.05 percent CO<sub>2</sub>, 25 g/L

*Figure 2. Comparison of Uranium  $R_d$  Determinations Made on Crescent Junction Mancos Shale Samples Using SPF-1 to Data from the Naturita Site by Davis et al. (2004)*

The uranium  $R_d$  values from our testing are more scattered than the results measured by Davis et al. (2004) on the Naturita samples. The scatter is largely due to the lower rock-to-water ratios used in our tests. Davis et al. (2004) used up to 820 g/L, whereas, we used a maximum of 250 g/L. Because of the low  $R_d$  values, a higher rock-to-water ratio would have reduced the scatter in our data. However, we believe that additional measurements at higher rock-to-water ratios are unnecessary because the results are not likely to change the conclusion that the parameters used in the Davis et al. (2004) model are a reasonable approximation for use at the Crescent Junction site.

## Sequential Batch-Leaching Tests

### Introduction

Two sequential batch-leaching tests were conducted to measure evolution of tailings leachate chemistry as it interacts with Mancos Shale. Results of these tests were used to help calibrate the reaction transport models presented in Section 0. In the sequential batch-leaching tests, the test fluid (SPF-1) was not spiked with U as it was for the  $R_d$  tests (Section 7.27). Rather, any U in the solution was released from the Mancos Shale samples. The evolution of major-ion chemistry and pH were monitored to determine the effects of these changes on U partitioning.

### Methods



A 100-g sample of Mancos Shale was crushed, air dried, and sieved to -10 +18 mesh (1- to 2-mm nominal diameter). The sample was combined with 400 mL of SPF-1 in a 500-mL glass Erlenmeyer flask, agitated on an orbital shake table for 24 hours, and then centrifuged, decanted, and filtered (0.45  $\mu$ m) to separate solids from the solution. A 50-mL split was retained and analyzed for pH, ORP, specific conductance, alkalinity, Ca, Cl, K, Mg, Na, NH<sub>3</sub>, NO<sub>3</sub>, SO<sub>4</sub>, and U. The remaining solution was placed with approximately 87.5 g of the next Mancos Shale sample. The exact amount of the Mancos Shale sample was calculated so that the water-to-rock ratio remained constant. The procedure was repeated to monitor the changing solution composition as the fluid reacted with progressively more Mancos Shale.

## Results and Discussion

Two sequential batch-leaching tests were conducted, one to simulate vertical transport and one to simulate horizontal transport through the Mancos Shale. To simulate horizontal transport, the 40-ft-depth samples from borings CJ-203, -204, and -206 were used, in that order. Chemical changes that occurred in the solution as it reacted with progressively more Mancos Shale include slightly increasing values of pH, Cl, K, Na, SO<sub>4</sub>, and U. Small decreases occurred in ORP and NH<sub>3</sub>-N, while alkalinity, Ca, and Mg remained fairly stable (Table 13). The increase in U may be caused by longer reaction times with the sediment or by decreasing R<sub>d</sub> values because of increasing pH values and nearly constant dissolved carbonate concentration.

To simulate vertical transport, SPF-1 (Table 9) was reacted sequentially with samples from boring CJ-205 from the 40-, 105-, 170-, 235- and 300-ft depths. Similar to the simulation of horizontal transport, pH values progressively increase with increased reaction. Progressive increases also occurred in the Cl, Na, SO<sub>4</sub>, and U concentrations. Decreasing trends occur in alkalinity and possibly NH<sub>3</sub>-N. Dissolved U concentrations increased despite lowered concentrations of dissolved carbonate (alkalinity). Some carbonate was apparently lost from the solution because of outgassing and/or mineral precipitation. The progressively higher U concentrations may simply be caused by desorption from fresh adsorption sites at each reaction step, or may be caused by variable pH and pCO<sub>2</sub> values.

Table 13. Results of Sequential Batch-Leaching Tests

Depth (ft)	pH	ORP (mV) <sup>a</sup>	Cond. <sup>b</sup> ( $\mu$ S/cm)	Ca (mg/L)	Na (mg/L)	Mg (mg/L)	K (mg/L)	Alk <sup>c</sup> (mg/L)	Cl (mg/L)	NO <sub>3</sub> (mg/L)	SO <sub>4</sub> (mg/L)	NH <sub>3</sub> -N (mg/L)	U ( $\mu$ g/L)
<b>CJ-203, -204, and -206</b>													
40	7.66	196.7	29400	320	5700	440	141	560	1026	764	18676	1700	5.5
40	7.79	186.3	30100	350	5400	510	156	450	1096	828	19872	1500	19.3
40	7.83	175.2	29900	349	6300	300	177	560	1120	820	19910	1300	25.4
<b>CJ-205</b>													
40	7.73	187.3	29200	236	5700	210	141	620	1106	756	18504	1600	3.0
105	7.85	171.4	29800	220	6400	200	168	560	1116	770	18828	1400	19.5
170	7.96	171.5	29600	199	6500	250	157	520	1196	776	19032	1100	29.0
235	7.85	173.3	29700	203	7000	180	167	400	1284	804	19700	1800	44.9
300	7.97	173.5	30600	196	7800	180	166	330	1336	794	19492	900	54.5

<sup>a</sup>mV = millivolt.

<sup>b</sup>Cond. = electrical conductivity in microsiemens per centimeter ( $\mu$ S/cm).

<sup>c</sup>Alk = alkalinity in milligrams per liter as CaCO<sub>3</sub>.

Another outcome of the sequential batch-leaching tests was an estimate of the amount of labile U in the Mancos Shale. The labile U concentration is the readily releasable portion and is needed to calculate uranium R<sub>d</sub> values as discussed in Section 0. Labile U should be measured using a solution that strongly favors partitioning of U into the liquid phase, such as the strong carbonate solution used by Davis and Curtis (2003). SPF-1 has a relatively high carbonate concentration and should produce a reasonable estimate of labile U; however, our results should be considered as minimum values. The labile U concentrations range from 0.0120 to 0.0660  $\mu$ g/g, with a mean of 0.0436  $\mu$ g/g (Table 14).

Table 14. Labile U Concentrations

Sample ID	SPF-1 (mL)	Mass (g)	U (µg/L)	Labile U (µg/g)
CJ-203-40	400	100	5.5	0.0220
CJ-204-40	315	78.75	19.3	0.0552
CJ-206-40	240	60	25.4	0.0244
CJ-205-40	400	100	3	0.0120
CJ-205-105	315	78.75	19.5	0.0660
CJ-205-170	240	60	29	0.0380
CJ-205-235	165	41.25	44.9	0.0636
CJ-205-300	100	25	54.5	0.0384
Mean				0.0436

## Reaction-Transport Modeling

### Introduction

This task consists of developing a reaction transport model using the PHREEQC code (Parkhurst and Appelo 1999). Ion exchange is modeled using data from the CEC determinations (Section 0) and surface area measurements (Section 0). Initial conditions include concentrations of minerals as estimated from the soluble chemistry results (Section 0) and XRD results (Section 0). A surface-complexation model (SCM) for U was developed and calibrated against the uranium  $R_d$  measurements provided in Section 0.

The reaction-transport model includes one-dimension transport of tailings water through the Mancos Shale. Aqueous speciation reactions are typically fast with respect to ground water flow and were modeled at chemical equilibrium. Water-to-rock interaction includes mineral precipitation and dissolution, adsorption, and cation exchange. For the models used in this study, it is assumed that the system is oxidized; no reduced species were included. Results from the sequential batch reaction tests were used to test and calibrate the reaction-transport model. Input files for the sequential batch models are presented in Appendix F. Input files for the Crescent Junction models are presented in Appendix G, and the thermodynamic database is presented in Appendix H.

The reaction-transport model is adaptable to allow inclusion of such factors as (1) mixing with ground water, (2) reaction kinetics, and (3) changing oxidation-reduction state (e.g., due to biologic activity). Thus, sensitivity of the transport to various parameters can be readily estimated with additional model simulations. In this section, each "module" of the reaction-transport model is discussed separately, and input parameters used in the reaction-transport modeling are specified.

### Aqueous Speciation Module

The aqueous speciation reactions used in this study are identical to those used by Davis and Curtis (2003), supplemented with reactions in the PHREEQC.dat thermodynamic database provided with the PHREEQC program (Parkhurst and Appelo 1999). All aqueous U species are from Davis and Curtis (2003). Table 15 and Table 16 provide lists of the non-U-bearing and U-bearing aqueous speciation reactions respectively, used in this study.

Table 15. Non-U-Bearing Aqueous Speciation Reactions and Logarithmic Equilibrium Constants Used in the Reaction-Transport Modeling<sup>a</sup>

Reaction	Log K
$\text{CO}_3^{2-} + \text{H}^+ = \text{HCO}_3^-$	10.329
$\text{SO}_4^{2-} + \text{H}^+ = \text{HSO}_4^-$	1.98
$\text{NH}_4^+ = \text{NH}_3(\text{aq}) + \text{H}^+$	-9.252
$\text{Ca}^{+2} + \text{H}_2\text{O} = \text{CaOH}^+ + \text{H}^+$	-12.78
$\text{Ca}^{+2} + \text{CO}_3^{2-} + \text{H}^+ = \text{CaHCO}_3^+$	11.435
$\text{Mg}^{+2} + \text{H}_2\text{O} = \text{MgOH}^+ + \text{H}^+$	-11.44
$\text{Mg}^{+2} + \text{H}^+ + \text{CO}_3^{2-} = \text{MgHCO}_3^+$	11.399
$\text{Na}^+ + \text{H}_2\text{O} = \text{NaOH}(\text{aq}) + \text{H}^+$	-14.18
$\text{Na}^+ + \text{HCO}_3^- = \text{NaHCO}_3(\text{aq})$	-0.25
$\text{K}^+ + \text{H}_2\text{O} = \text{KOH}(\text{aq}) + \text{H}^+$	-14.46
$\text{CO}_3^{2-} + 2\text{H}^+ = \text{CO}_2(\text{aq}) + \text{H}_2\text{O}$	16.683
$\text{H}_2\text{O} = \text{OH}^- + \text{H}^+$	-14.0
$\text{NH}_4^+ + \text{SO}_4^{2-} = \text{NH}_4\text{SO}_4^-$	1.11
$\text{Ca}^{+2} + \text{CO}_3^{2-} = \text{CaCO}_3(\text{aq})$	3.224
$\text{Ca}^{+2} + \text{SO}_4^{2-} = \text{CaSO}_4(\text{aq})$	2.3
$\text{Mg}^{+2} + \text{CO}_3^{2-} = \text{MgCO}_3(\text{aq})$	2.98
$\text{Mg}^{+2} + \text{SO}_4^{2-} = \text{MgSO}_4(\text{aq})$	2.37
$\text{Na}^+ + \text{CO}_3^{2-} = \text{NaCO}_3^-$	1.27
$\text{Na}^+ + \text{SO}_4^{2-} = \text{NaSO}_4^-$	0.7
$\text{K}^+ + \text{SO}_4^{2-} = \text{KSO}_4^-$	0.85

<sup>a</sup>From Davis and Curtis (2003) and Parkhurst and Appelo (1999).

Table 16. U-Bearing Aqueous Speciation Reactions and Logarithmic Equilibrium Constants Used in the Reaction-Transport Modeling<sup>a</sup>

Reaction	Log K
$\text{UO}_2^{+2} + \text{H}_2\text{O} = \text{UO}_2\text{OH}^+ + \text{H}^+$	-5.20
$\text{UO}_2^{+2} + 2\text{H}_2\text{O} = \text{UO}_2(\text{OH})_2(\text{aq}) + 2\text{H}^+$	-11.50
$\text{UO}_2^{+2} + 3\text{H}_2\text{O} = \text{UO}_2(\text{OH})_3^- + 3\text{H}^+$	-20.00
$\text{UO}_2^{+2} + 4\text{H}_2\text{O} = \text{UO}_2(\text{OH})_4^{2-} + 4\text{H}^+$	-33.0
$2\text{UO}_2^{+2} + \text{H}_2\text{O} = (\text{UO}_2)_2\text{OH}^{+3} + \text{H}^+$	-2.70
$2\text{UO}_2^{+2} + 2\text{H}_2\text{O} = (\text{UO}_2)_2(\text{OH})_2^{+2} + 2\text{H}^+$	-5.62
$3\text{UO}_2^{+2} + 4\text{H}_2\text{O} = (\text{UO}_2)_3(\text{OH})_4^{+2} + 4\text{H}^+$	-11.90
$3\text{UO}_2^{+2} + 5\text{H}_2\text{O} = (\text{UO}_2)_3(\text{OH})_5^+ + 5\text{H}^+$	-15.55
$3\text{UO}_2^{+2} + 7\text{H}_2\text{O} = (\text{UO}_2)_3(\text{OH})_7^- + 7\text{H}^+$	-31.00
$4\text{UO}_2^{+2} + 7\text{H}_2\text{O} = (\text{UO}_2)_4(\text{OH})_7^+ + 7\text{H}^+$	-21.90
$\text{UO}_2^{+2} + \text{CO}_3^{2-} = \text{UO}_2\text{CO}_3(\text{aq})$	9.67
$\text{UO}_2^{+2} + 2\text{CO}_3^{2-} = \text{UO}_2(\text{CO}_3)_2^{2-}$	16.94
$\text{UO}_2^{+2} + 3\text{CO}_3^{2-} = \text{UO}_2(\text{CO}_3)_3^{4-}$	21.60
$3\text{UO}_2^{+2} + 6\text{CO}_3^{2-} = (\text{UO}_2)_3(\text{CO}_3)_6^{6-}$	54.0
$2\text{UO}_2^{+2} + \text{CO}_3^{2-} + 3\text{H}_2\text{O} = (\text{UO}_2)_2\text{CO}_3(\text{OH})_3^- + 3\text{H}^+$	-0.86
$3\text{UO}_2^{+2} + \text{CO}_3^{2-} + 3\text{H}_2\text{O} = (\text{UO}_2)_3\text{CO}_3(\text{OH})_3^+ + 3\text{H}^+$	0.66
$11\text{UO}_2^{+2} + 6\text{CO}_3^{2-} + 12\text{H}_2\text{O} = (\text{UO}_2)_{11}(\text{CO}_3)_6(\text{OH})_{12}^{2-} + 12\text{H}^+$	36.43
$\text{UO}_2^{+2} + \text{NO}_3^- = \text{UO}_2\text{NO}_3^+$	0.3
$\text{UO}_2^{+2} + \text{Cl}^- = \text{UO}_2\text{Cl}^+$	0.17
$\text{UO}_2^{+2} + 2\text{Cl}^- = \text{UO}_2\text{Cl}_2(\text{aq})$	-1.1
$\text{UO}_2^{+2} + \text{SO}_4^{2-} = \text{UO}_2\text{SO}_4(\text{aq})$	3.15
$\text{UO}_2^{+2} + 2\text{SO}_4^{2-} = \text{UO}_2(\text{SO}_4)_2^{2-}$	4.14

<sup>a</sup>From Davis and Curtis (2003).

For this study, it was assumed that the reactions among all aqueous chemical species are at equilibrium. This assumption is reasonable because reaction rates among dissolved aqueous species are relatively fast. Numerically, this is accomplished by solving the set of Log K expressions. For example, the numerical expression for the first reaction in Table 15 is

$$\text{Log } K = \text{Log } a_{(\text{HCO}_3^-)} - \text{Log } a_{(\text{CO}_3^{2-})} - \text{Log } a_{(\text{H}^+)} \quad \text{Equation 1}$$

where  $a$  is the activity of the dissolved species. Activities are related to concentrations using activity coefficients calculated using the Debye-Hückle theory; for example:

$$a_{(\text{HCO}_3^-)} = \gamma_{(\text{HCO}_3^-)} m_{(\text{HCO}_3^-)} \quad \text{Equation 2}$$

where  $\gamma$  is the Debye-Hückle activity coefficient and  $m_{(\text{HCO}_3^-)}$  is the molality of the bicarbonate ion.

### Mineral Precipitation/Dissolution and Gas-Phase Module

Four minerals (calcite, gypsum, halite, and nahcolite) were allowed to equilibrate with the aqueous solution during the reaction-transport simulations. Table 17 presents these mineral reactions and their associated equilibrium constants. Similar to the aqueous speciation reactions in the previous section, equilibrium was forced between the aqueous solution and each of these minerals. Numerically, this means that the following condition must hold for each mineral, using calcite as an example:

$$\text{Log } K = \text{Log } a_{(\text{CO}_3^{2-})} - \text{Log } a_{(\text{Ca}^{2+})} - \text{Log } a_{(\text{CaCO}_3)} \quad \text{Equation 3}$$

where  $a_{(\text{CaCO}_3)}$  is the activity of calcite, which is assumed to be in the pure phase and, thus, has unit activity.

Table 17. Reactions and Logarithmic Equilibrium Constants for Minerals Allowed to Equilibrate During Reaction-Transport Simulations<sup>a</sup>

Mineral Name	Mineral Reaction	Log K
Calcite	$\text{CaCO}_3 = \text{CO}_3^{2-} + \text{Ca}^{+2}$	-8.48
Gypsum	$\text{CaSO}_4 \cdot 2\text{H}_2\text{O} = \text{Ca}^{+2} + \text{SO}_4^{2-} + 2\text{H}_2\text{O}$	-4.58
Nahcolite	$\text{NaHCO}_3 = \text{Na}^+ + \text{HCO}_3^-$	-0.548
Halite	$\text{NaCl} = \text{Na}^+ + \text{Cl}^-$	1.582

<sup>a</sup>From Wateq4f.dat database supplied with the PHREEQC program (Parkhurst and Appelo 1999).

Minerals present were allowed to dissolve; therefore, the initial concentration of a mineral is an important input parameter. The initial concentrations of minerals were estimated from the NETPATH results of the water-soluble chemistry results (Table 4). The mineral compositions of samples from the 40-ft depth were distinctly different from samples from deeper depths in that they contained more gypsum and less nahcolite. Because calcite was not completely dissolved during the water extraction tests, its composition was set at 1 weight percent [0.75 mol/L<sub>(gw)</sub>], considered to be a reasonable value for the Mancos Shale based on hand-lens observations of core samples and identification by XRD analysis. Table 18 presents the estimated mineral abundances; these values were used in the reaction-transport modeling.

Table 18. Estimated Mineral Abundances (in mole per liter of ground water) Used in Reaction-Transport Modeling

Mineral	Abundance (vertical transport)	Abundance (horizontal transport)
Calcite	0.75	0.75
Gypsum	0.02	0.50
Nahcolite	0.50	0.20
Halite	0.02	0.02

Though only the minerals listed in Table 17 were allowed to react during the transport simulations, other minerals were included in the thermodynamic database to track the saturation indices (SI). Saturation index (SI) is defined as

$$SI = \frac{IAP}{Log K} \quad \text{Equation 4}$$

where IAP is the ion activity product. If the SI is positive, the solution is oversaturated, and the mineral will tend to precipitate. If the SI is negative, the solution is undersaturated, and the mineral, if present, would tend to dissolve. By tracking the mineral SIs, the modeler is aware of additional mineral precipitation that may need to be included. Table 19 provides the minerals included only for information on the SI.

Table 19. Reactions and Logarithmic Equilibrium Constants for Minerals Included in Reaction-Transport Modeling but Not Allowed to Equilibrate<sup>a</sup>

Mineral Name	Mineral Reaction	Log K
Aragonite	$\text{CaCO}_3 = \text{CO}_3^{-2} + \text{Ca}^{+2}$	-8.336
Dolomite	$\text{CaMg}(\text{CO}_3)_2 = \text{Ca}^{+2} + \text{Mg}^{+2} + 2\text{CO}_3^{-2}$	-17.09
Anhydrite	$\text{CaSO}_4 = \text{Ca}^{+2} + \text{SO}_4^{-2}$	-4.36
Thenardite	$\text{Na}_2\text{SO}_4 = 2\text{Na}^+ + \text{SO}_4^{-2}$	-0.179
Trona	$\text{NaHCO}_3:\text{Na}_2\text{CO}_3:2\text{H}_2\text{O} = 2\text{H}_2\text{O} + 3\text{Na}^+ + \text{CO}_3^{-2} + \text{HCO}_3^-$	-0.795
Natron	$\text{Na}_2\text{CO}_3:10\text{H}_2\text{O} = 2\text{Na}^+ + \text{CO}_3^{-2} + 10\text{H}_2\text{O}$	-1.311
Thermonatrite	$\text{Na}_2\text{CO}_3:\text{H}_2\text{O} = 2\text{Na}^+ + \text{CO}_3^{-2} + \text{H}_2\text{O}$	0.125
Schoepite	$\text{UO}_2(\text{OH})_2:\text{H}_2\text{O} + 2\text{H}^+ = \text{UO}_2^{+2} + 3\text{H}_2\text{O}$	4.93
Rutherfordine	$\text{UO}_2\text{CO}_3 = \text{UO}_2^{+2} + \text{CO}_3^{-2}$	-14.49
Gummite	$\text{UO}_3 + 2\text{H}^+ = \text{UO}_2^{+2} + \text{H}_2\text{O}$	10.403
Gamma $\text{UO}_3$	$\text{UO}_3 + 2\text{H}^+ = \text{UO}_2^{+2} + \text{H}_2\text{O}$	7.719
Unnamed	$\text{Na}_4\text{UO}_2(\text{CO}_3)_3 = 4\text{Na}^+ + \text{UO}_2^{+2} + 3\text{CO}_3^{-2}$	-16.290
$\beta\text{-UO}_2(\text{OH})_2$	$\text{UO}_2(\text{OH})_2 + 2\text{H}^+ = \text{UO}_2^{+2} + 2\text{H}_2\text{O}$	5.544

<sup>a</sup>From Davis and Curtis (2003) and Parkhurst and Appelo (1999).

Several gas phases were also included in the thermodynamic database. The SI for a gas-phase reaction is the logarithm of its partial pressure (measured in atmospheres). Thus, by tracking the partial pressures the modeler can be aware of unusual situations, such as a partial pressure that exceeds 1 atmosphere, which could result in separation of a gas phase. Table 20 provides the three gas phases included in the modeling.

*Table 20. Reactions and Logarithmic Equilibrium Constants for Gases Included in Reaction-Transport Modeling but not Allowed to Equilibrate<sup>a</sup>*

Gas	Reaction	Log K
CO <sub>2</sub> (gas)	CO <sub>2</sub> (gas) = CO <sub>2</sub> (aq)	-1.472
H <sub>2</sub> O (gas)	H <sub>2</sub> O (gas) = H <sub>2</sub> O (aq)	1.51
NH <sub>3</sub> (gas)	NH <sub>3</sub> (gas) = NH <sub>3</sub> (aq)	1.7966

<sup>a</sup>CO<sub>2</sub> from Davis and Curtis (2003); H<sub>2</sub>O and NH<sub>3</sub> from Parkhurst and Appelo (1999).  
aq = aqueous

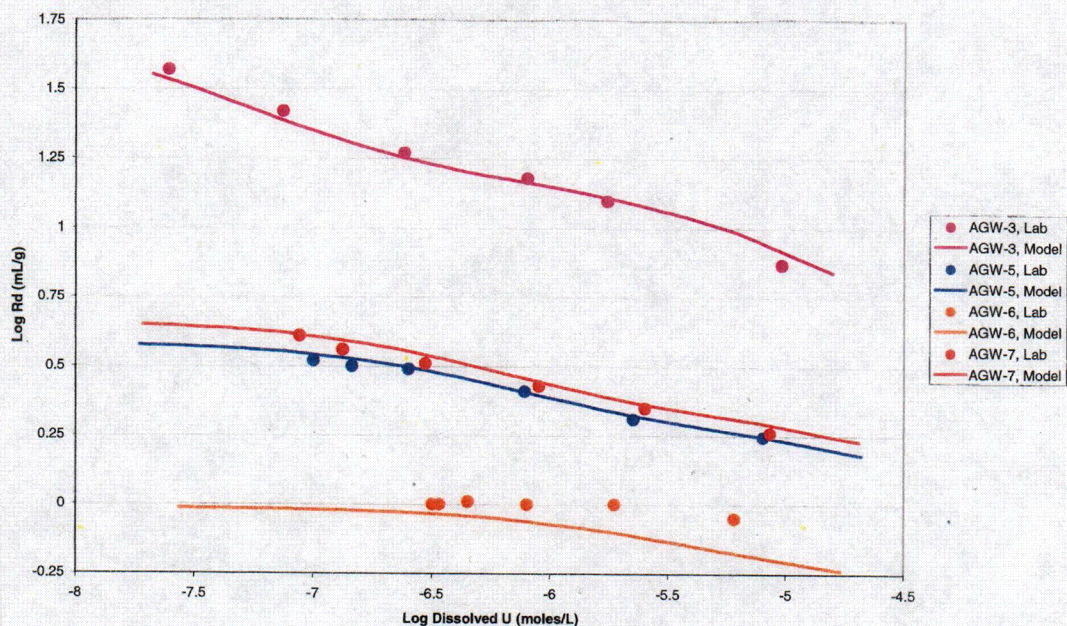
## Uranium Adsorption Module

Uranium adsorption is simulated using an SCM (Davis et al. 1978). In an SCM, adsorption is a function of the electrostatic potential and the species complexation configuration at a mineral surface; these parameters vary with solution composition. The SCM approach has been widely used to model adsorption of U(VI) to pure phase minerals, in particular, iron oxyhydroxide (Davis 2001, Hsi and Langmuir 1985, Tripathi 1984, Morrison et al. 1995). Naturally occurring sediments are more complicated because of the presence of a mixture of many minerals. To simplify the use of the SCM approach in modeling field situations, Davis et al. (2004) developed an approach they called the Generalized Composite Model (GCM). In a GCM, the rock is treated as a composite of mineral phases, and surface-complexation constants for the composite are calibrated from laboratory measurements. As with the SCM, adsorption processes in a GCM vary with ground water composition. Thus, instead of treating the distribution of contaminant between solids and water as a constant (the so-called  $K_d$  approach), the  $K_d$  values vary throughout a transport simulation. To simplify computations, Davis et al. (2004) elected not to consider the effects of surface charge potential on adsorption, and we also omit this effect. Thus, the adsorption module is solved numerically using equilibrium expressions in a manner similar to the aqueous-speciation module. Three types of adsorption sites (weak, strong, and very strong) were required to produce an acceptable fit to the laboratory data.

Davis and Curtis (2003) provide thermodynamic data and model parameters for a GCM. Because they used data different from that in the PHREEQC database and a different numerical processor, we started by entering their data and parameters into PHREEQC and checking the accuracy of the calculated results. The results shown on Figure 3 indicate a good match between our modeled results using PHREEQC and the laboratory results of Davis and Curtis (2003). The small differences between the PHREEQC and laboratory results for AGW-6 (Davis and Curtis 2003, label synthetic ground water as AGW) probably arise because the model is sensitive to solution parameters in this range; some of the aqueous thermodynamic data were not provided by Davis and Curtis 2003. However, the small deviation should not significantly affect the adsorption calculations for the Crescent Junction reaction-transport model.

The uranium  $R_d$  data reported in Section 0 were used to check the calibration of the GCM for U adsorption to Mancos Shale. By comparison with the data of Davis and Curtis (2003), the laboratory measurements from our study grouped tightly at relatively low values of  $R_d$  (Figure 4). Models of the Crescent Junction  $R_d$  measurements using the GCM, without any changes to the surface-complexation constants, are also presented on Figure 4 (SPF-1, SPF-2, and SPF-3). The  $R_d$  measurements generally plot above the models. As discussed in Section 0, many of the  $R_d$  measurements were negative because of variable amounts of labile U and analytical imprecision. Thus, the measured  $R_d$  values are maximum values, and the actual  $R_d$  values may be lower, as indicated by the SPF models on Figure 4. Therefore, as a first approximation, we elected to use the Davis and Curtis (2003) GCM as it is without attempting to modify the surface-complexation constants. With this approach, the uranium  $R_d$  values used for the SPF fluid migration are kept quite low, consistent with results of the  $R_d$  tests. Table 21 provides the GCM uranium adsorption surface complex reactions and associated equilibrium constants. Other input parameters needed for the GCM are proportions of weak, strong, and very strong sites = 0.9879, 0.012, and 0.0001, respectively; site density = 1.92  $\mu\text{mol}/\text{m}^2$  (Davis and Kent 1990); surface area for Mancos Shale = 11.02  $\text{m}^2/\text{g}$  (mean value of 10 BET measurements, Section 0); and rock-to-water ratio = 7500 g (based on 25 percent porosity and 2.5 g/mL rock density).





Compositions of solutions AGW-3, AGW-5, AGW-6, and AGW-7 are provided in Davis and Curtis (2003).

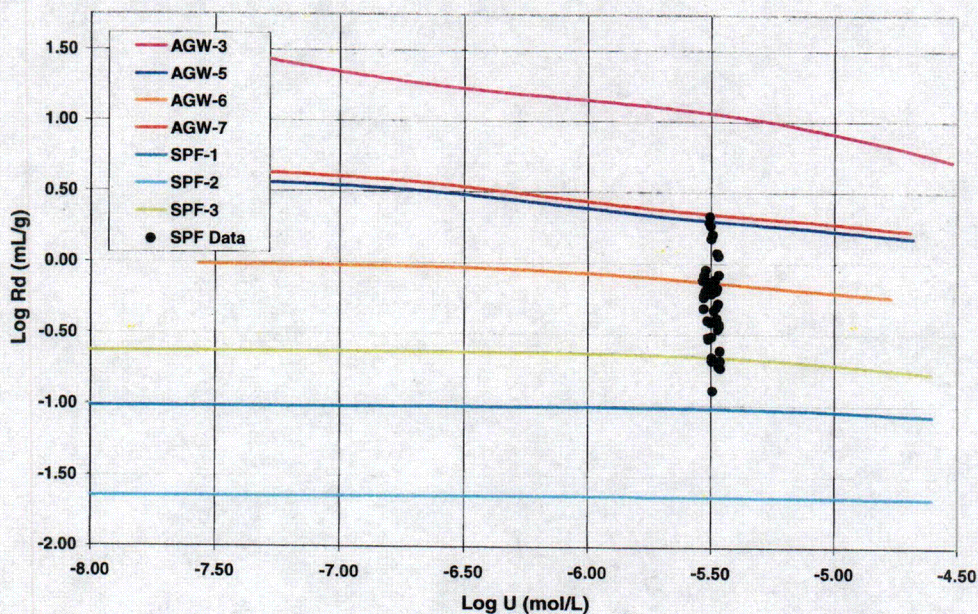
AGW-3: pH 7.94, 0.05 percent CO<sub>2</sub> (lab air), 25 g/L

AGW-5: pH 7.22, 1.24 percent CO<sub>2</sub>, 125 g/L

AGW-6: pH 6.88, 6.8 percent CO<sub>2</sub>, 820 g/L

AGW-7: pH 7.58, 0.47 percent CO<sub>2</sub>, 125 g/L

Figure 3. Comparison of PHREEQC Uranium Adsorption Model With Data From Davis and Curtis (2003)



SPF models use the Davis and Curtis (2003) GCM without modification.

Figure 4. Comparison of Uranium  $R_d$  Measurements (black dots) Made in This Study With Naturita Sediment Models (AGW plots) from Davis and Curtis (2003)

c400



Table 21. Uranium Surface-Complexation Reactions and Logarithmic Equilibrium Constants Used in Reaction-Transport Modeling<sup>a</sup>

Reaction	Log K
$\text{Hfo\_wOH} + \text{UO}_2^{+2} + \text{H}_2\text{O} = \text{Hfo\_wOUO}_2\text{OH} + 2\text{H}^+$	-6.74
$\text{Hfo\_sOH} + \text{UO}_2^{+2} + \text{CO}_2 + \text{H}_2\text{O} = \text{Hfo\_sOUO}_2\text{CO}_3^- + 3\text{H}^+$	-8.00
$\text{Hfo\_vOH} + \text{UO}_2^{+2} + \text{H}_2\text{O} = \text{Hfo\_vOUO}_2\text{OH} + 2\text{H}^+$	-2.06
$\text{Hfo\_vOH} + \text{UO}_2^{+2} + \text{CO}_2 + \text{H}_2\text{O} = \text{Hfo\_vOUO}_2\text{CO}_3^- + 3\text{H}^+$	-6.36

<sup>a</sup>From Davis et al. (2004); w, s, v = weak, strong, and very strong sites.  
Hfo represents an adsorption site.

## Cation Exchange Module

Cation exchange was considered to be a prominent chemical mechanism for ground water transport in the Mancos Shale. The Mancos Shale contains a high proportion of clay minerals that include a significant fraction of smectite (Section 0). Smectites are layered silicate minerals with freely exchangeable cations within the interlayer space. The CEC was used in the reaction-transport modeling as a measure of the total amount of exchangeable sites present in the rock.

The mean CEC value of 11.23 meq/100 g (Section 0) was used for the modeling. The number of exchange sites in equivalents per liter (eq/L) of ground water (0.842 eq/L) was calculated as the product of the mass of rock per liter of ground water and the CEC:

$$\text{Exchange Sites} = 7500 \text{ g}_{(\text{rock})}/\text{L}_{(\text{gw})} * 11.23 \text{ meq}/100 \text{ g}_{(\text{rock})} * 1 \text{ eq}/1000 \text{ meq} = 0.842 \text{ eq/L} \quad \text{Equation 5}$$

Calculations of cation exchange by PHREEQC are accomplished by solving equilibrium expressions for each exchange reaction. For example, the exchange reaction and logarithmic equilibrium expression for Ca is



$$\text{Log}(0.8) = \text{Log } a_{(\text{CaX}_2)} - \text{Log } a_{(\text{Ca}^{+2})} - 2\text{Log } a_{(\text{X}^-)} \quad \text{Equation 6}$$

where X is on the exchange site.

Table 22 presents the exchange reactions and associated logarithmic equilibrium constants used in the modeling. Some cations have a higher selectivity for exchange sites than other cations; this selectivity is accounted for in the equilibrium constants. Retardation of  $\text{NH}_4$  contamination from the tailings is likely to be largely a function of cation exchange.

Table 22. Exchange Reactions and Logarithmic Equilibrium Constants Used in Reaction-Transport Modeling<sup>a</sup>

Reaction	Log K
$\text{H}^+ + \text{X}^- = \text{HX}$	1.0
$\text{NH}_4^+ + \text{X}^- = \text{NH}_4\text{X}$	0.6
$\text{Ca}^{+2} + 2\text{X}^- = \text{CaX}_2$	0.8
$\text{Mg}^{+2} + 2\text{X}^- = \text{MgX}_2$	0.6
$\text{Na}^+ + \text{X}^- = \text{NaX}$	0.0
$\text{K}^+ + \text{X}^- = \text{KX}$	0.7

<sup>a</sup>From Parkhurst and Appelo (1999).  
X represents an exchange site.



## Model Calibration Using Sequential Batch-Leaching Results

The sequential batch-leaching results (Section 0) were modeled to calibrate the release of background U from the Mancos Shale and to compare modeled major-ion concentrations with experimental results. Appendix F provides the PHREEQC input files for the sequential batch-leaching simulations.

The rock-to-water ratio used in the sequential batch-leaching tests was 250 g/L (100 g of rock to 400 mL of water). Because input parameters for the models are normalized to a liter of water, the parameters for the sequential batch-leaching models are different from the field models that used a rock-to-water ratio of 7,500 g/L. Table 23 provides the normalized parameters for the sequential batch-leaching models.

Table 23. Parameters Used in Sequential Batch-Leaching Models

Parameter	Value
Rock-to-Water Ratio	250 g/L
Cation Exchange Capacity	11.23 meq/100 g
Rock Surface Area	11.02 m <sup>2</sup> /g
Exchange Sites	0.028 eq/L
Adsorption Site Density	5290 $\mu$ mol/L
Very Strong Sites	0.53 $\mu$ mol/L
Strong Sites	63.5 $\mu$ mol/L
Weak Sites	5226 $\mu$ mol/L
Calcite Concentration	0.025 mol/L
Gypsum Concentration (40 ft)	0.01 mol/L
Gypsum Concentration (>40 ft)	0.000667 mol/L
Nahcolite Concentration (40 ft)	0.00667 mol/L
Nahcolite Concentration (>40 ft)	0.017 mol/L
Halite Concentration	0.000667 mol/L

The initial distributions of cations on the exchange sites were determined by assuming the rock sample was in equilibrium with the ground water sample collected at the Crescent Junction Site (ground water sample from Borehole 210 collected November 7, 2005). The composition of this water (Table 24) was equilibrated with the solid sample to fix the initial distribution of cations on the exchange sites.

Table 24. Composition of Borehole 210 Ground Water Collected November 7, 2005

Parameter	Value
pH	7.23
Alkalinity (mg/L as CaCO <sub>3</sub> )	634
Calcium (mg/L)	180
Sodium (mg/L)	12,000
Magnesium (mg/L)	140
Potassium (mg/L)	58
Sulfate (mg/L)	1,700
Chloride (mg/L)	23,000

To calibrate the distribution of U-bearing surface adsorption complexes, the U concentration in the Borehole 210 ground water sample was adjusted until the U concentration in the model matched reasonably well with the labile U released (Table 14) during the sequential batch-leaching tests. The concentration of U required to match well with the labile U release was 0.2 mg/L. To achieve the same concentrations of U-bearing adsorption sites for the Crescent Junction reaction-transport modeling, this U concentration was scaled to 6.7 µg/L to account for the 30-fold difference in rock-to-water ratio.

After initializing the cation exchange sites and adsorption sites, a sequential batch-leaching test was simulated by reacting SPF-1 fluid with appropriate mineral phases in a step-wise fashion. For the horizontal sequential batch-leaching scenario, three reaction steps were conducted using minerals representing samples collected from the 40-ft depth Mancos Shale. For the vertical scenario, SPF-1 was first reacted with the 40-ft mineral assemblage followed by four additional reaction steps with the mineral phases representing progressively deeper Mancos Shale.

As discussed in Section 0, the results of the horizontal sequential batch-leaching tests showed several distinctive concentration trends: For example, concentrations of Na, SO<sub>4</sub>, and U increased, while NH<sub>4</sub> decreased and Ca remained constant. These trends are simulated well with the model (Table 25). Modeled pH values were less than measured results and had a reverse trend (Table 25). Modeled alkalinity values (not listed in the table) were higher than the measured values. The inconsistencies in pH and alkalinity values are attributed largely to addition of bicarbonate ion to the solution from the dissolution of nahcolite in the model. As the bicarbonate component increases, calcite precipitates, causing pH values to decrease.

Comparison of modeled and measured results of the vertical sequential batch-leaching test shows trends similar to the horizontal scenario (Table 26). Unlike the horizontal model, pH values show an increasing trend after reaction step 3, and Ca has a decreasing trend. In both the horizontal and the vertical models, the observed trends result from interactions among several chemical processes that transfer mass between the solid and liquid phases, including mineral precipitation/dissolution, cation exchange, and specific adsorption for U. Considering the complexity of the system, the ability to simulate the measured results is quite good.

*Table 25. Comparison of Measured and Modeled Results of Sequential Batch-Leaching Test for Horizontal Transport<sup>a</sup>*

Reaction Step	pH	Ca (mg/L)	Na (mg/L)	SO <sub>4</sub> (mg/L)	NH <sub>4</sub> -N (mg/L)	U (µg/L)
1	7.66 (7.01)	320 (342)	5700 (5941)	18676 (19392)	1700 (1707)	5.5 (8.7)
2	7.79 (6.87)	350 (344)	5400 (6401)	19872 (19517)	1500 (1494)	19.3 (17.1)
3	7.83 (6.78)	349 (345)	6300 (6836)	19910 (19670)	1300 (1301)	25.4 (25.5)

<sup>a</sup>Modeled results in parentheses.

*Table 26. Comparison of Measured and Modeled Results of Sequential Batch-Leaching Test for Vertical Transport<sup>a</sup>*

Reaction Step	pH	Ca (mg/L)	Na (mg/L)	SO <sub>4</sub> (mg/L)	NH <sub>4</sub> -N (mg/L)	U (µg/L)
1	7.73 (6.81)	236 (347)	5700 (5941)	18505 (19123)	1600 (1807)	3.0 (8.9)
2	7.85 (6.74)	220 (255)	6400 (6631)	18828 (19190)	1400 (1580)	19.5 (17.9)
3	7.96 (6.74)	199 (185)	6500 (7284)	19032 (19248)	1100 (1376)	29.0 (27.0)
4	7.85 (6.76)	203 (137)	7000 (7905)	19700 (19315)	1800 (1194)	44.9 (36.1)
5	7.97 (6.78)	196 (105)	7800 (8494)	19492 (19382)	900 (1033)	54.5 (45.3)

<sup>a</sup>Modeled results in parentheses.

## Transport Modeling

Two modeling scenarios of the Crescent Junction Site are presented: (1) horizontal flow through the upper Mancos Shale (depths of less than 40-ft below ground surface) and (2) vertical flow through deeper Mancos Shale (depths greater than 40-ft below ground surface). Input files for the two scenarios are provided in Appendix G. Parameters used for the transport models are similar to those used for the sequential batch-leaching models (Section 0) but are scaled to account for the different rock-to-water ratio. Table 27 presents a summary of the parameter values. Modeling was conducted using the PHREEQC code (Parkhurst and Appelo 1999).

Table 27. Parameters Used in the Crescent Junction Reaction-Transport Models

Parameter	Value
Rock-to-Water Ratio	7500 g/L
Cation Exchange Capacity	11.23 meq/100 g
Rock Surface Area	11.02 m <sup>2</sup> /g
Exchange Sites	0.842 eq/L
Adsorption Site Density	0.1587 mol/L
Very Strong Sites	15.87 $\mu$ mol/L
Strong Sites	1904 $\mu$ mol/L
Weak Sites	0.1568 mol/L
Calcite Concentration	0.75 mol/L
Gypsum Concentration (40 ft)	0.5 mol/L
Gypsum Concentration (>40 ft)	0.02 mol/L
Nahcolite Concentration (40 ft)	0.2 mol/L
Nahcolite Concentration (>40 ft)	0.5 mol/L
Halite Concentration	0.02 mol/L

### Transport Model Setup

The horizontal flow simulation involves the flow of tailings pore fluid, represented by SPF-1 (Table 9), through shallow Mancos Shale, represented by the mineralogy of the 40-ft samples. For the vertical transport simulation, SPF-1 water flows through deeper Mancos Shale, represented by the mineralogy of samples deeper than 40 ft. For both simulations, the compositions of cation exchange sites and specific adsorption sites were set by equilibration with Borehole 210 (BH210) ground water. BH210 ground water was equilibrated with calcite and gypsum prior to equilibrating the exchange/adsorption sites. Sufficient U (6.7  $\mu$ g/L) was added to BH210 ground water to match the calibration condition for composition of U-bearing surface-complexation sites determined from the sequential batch model (Section 0).

Transport was simulated in one dimension (similar to flow through a laboratory column or flow along a flow system streamline). The model domain consisted of 20 equally spaced cells and water flows through the domain by invoking 200 "shifts." Each shift transports water through a cell; thus, a total of 10 pore volumes (a pore volume being the volume of water within the fully saturated domain) were modeled. Pore volume is related to ground-water travel time or distance, if the ground water flow velocity is known. For simplicity, dispersion and diffusion were not included in the simulations although PHREEQC includes these capabilities.

### Transport Model Results

For both simulations, NH<sub>4</sub> is retarded for about 3.5 pore volumes, after which concentrations increase rapidly to the influent concentration (Figure 5 and Figure 6). Retardation of NH<sub>4</sub> is caused by the exchange of dissolved NH<sub>4</sub> cations for solid-phase Ca, K, Mg, and Na. Most of the exchange involves Na ions because Na dominates the cations in BH210 ground water (Table 24). Thus, the cation exchange sites on the model Mancos Shale are initially dominated by Na. The compositional variation in the cation exchange

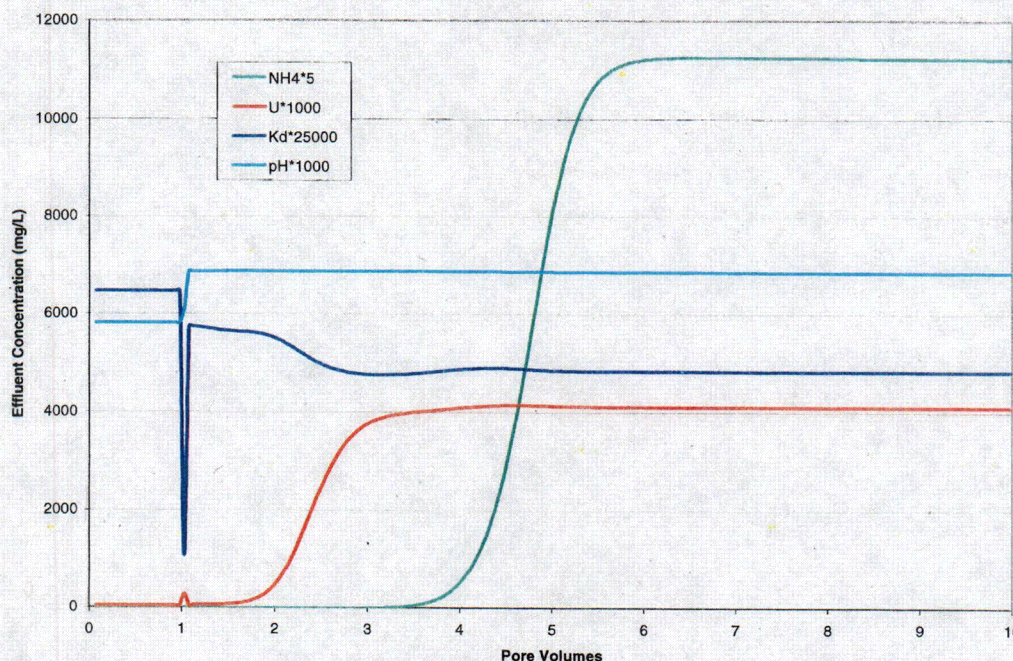


sites caused by the different mineral assemblages in the horizontal and vertical simulations did not significantly effect retardation of  $\text{NH}_4$ .

Effluent U concentrations in the horizontal simulation are retarded for slightly less than a pore volume during which the U concentration is less than about 0.075 mg/L (Figure 5). After 1 pore volume, U concentrations increase rapidly and reach the influent value (4.0 mg/L) after about 3 pore volumes. In the vertical simulation, U concentrations are never less than 2.4 mg/L (Figure 6). However, U concentrations in the vertical simulation remain less than the influent until about 4 pore volumes.

Uranium retardation is simulated by specific adsorption to the Mancos Shale. Specific adsorption is modeled using the U surface complexes listed in Table 21. Using this approach, the distribution coefficient ( $K_d$ ) is not held constant but varies throughout a simulation.  $K_d$  values are not used explicitly in the simulations but were computed and are plotted on Figure 5 and Figure 6.

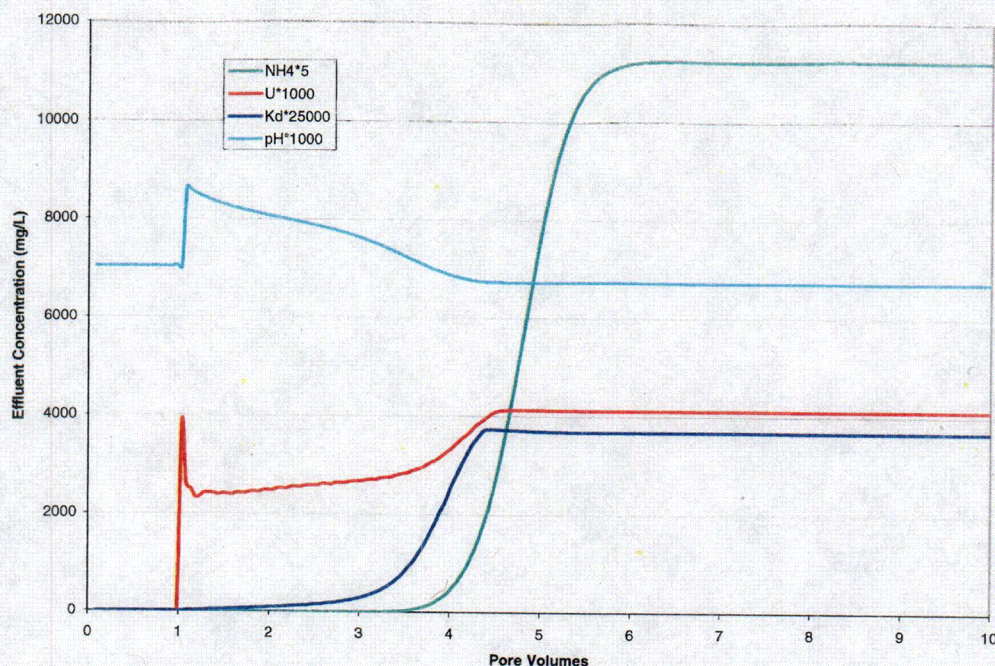
In the horizontal simulation,  $K_d$  values were initially 0.26 mL/g and decreased to 0.19 mL/g after about 2 pore volumes. In the vertical simulation,  $K_d$  values were negligible initially and increased to 0.15 mL/g after about 4 pore volumes. The differences in  $K_d$  values and dissolved U concentrations between the two simulations are products of the variation in the ionic composition of the solutions resulting from equilibration with minerals and cation exchange sites. A critical factor was the presence of a higher concentration of gypsum in the horizontal simulation than in the vertical simulation. Calcium released from dissolution of gypsum in the horizontal simulation caused precipitation of calcite, which resulted in decreased pH values. Initial Ca concentrations in the horizontal simulation were about 850 mg/L compared to only 9 mg/L in the vertical simulation (Figure 7 and Figure 8). These conditions led to increased partitioning of U to specific adsorption sites and increased retardation.



Values are scaled for plotting purposes using the multipliers shown in the legend.  $K_d$  values (mL/g) are calculated as the ratio of adsorbed concentration to dissolved concentration.

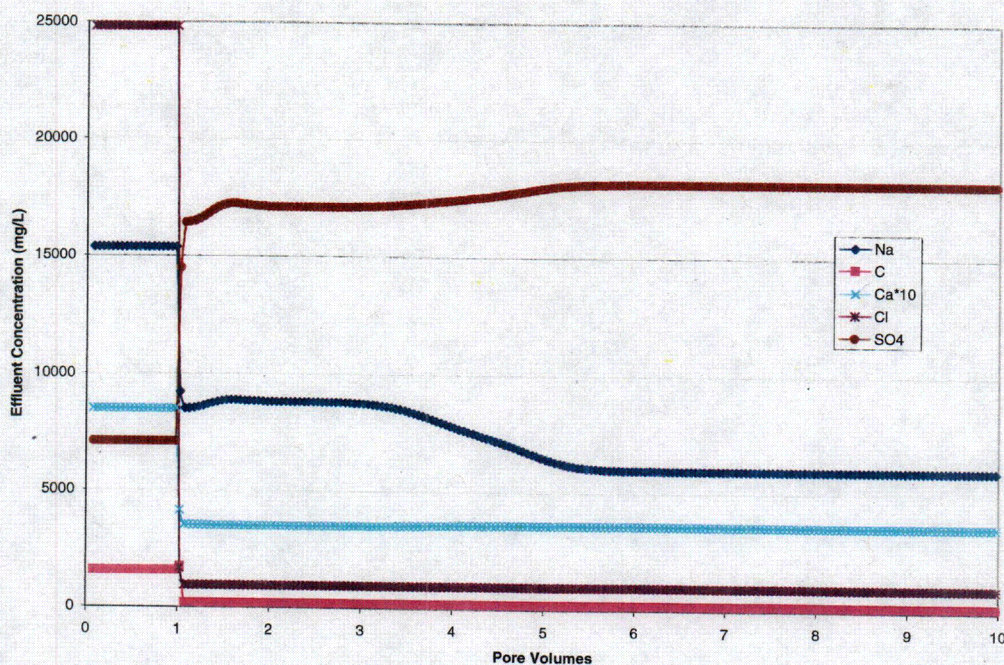
Figure 5. Effluent (Cell 20) Concentrations of U (mg/L),  $\text{NH}_4$  (mg/L), and Uranium  $K_d$  (mL/g) and pH Values for the Horizontal Transport Simulation





Values are scaled for plotting purposes using the multipliers shown in the legend.  $K_d$  values (mL/g) are calculated as the ratio of adsorbed concentration to dissolved concentration.

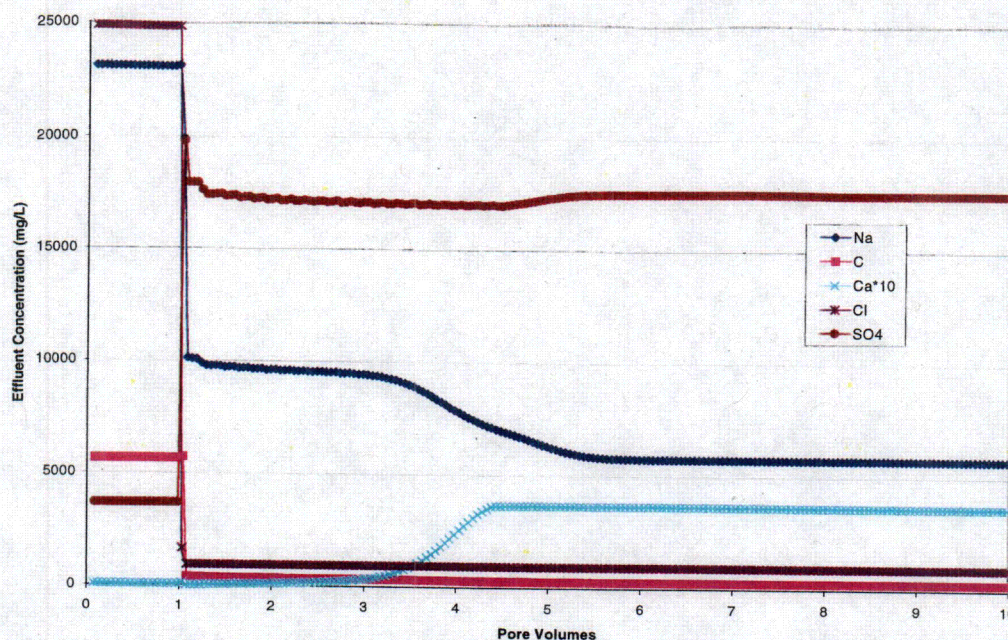
Figure 6. Effluent (Cell 20) Concentrations of U (mg/L),  $\text{NH}_4$  (mg/L), and Uranium  $K_d$  (mL/g) and pH Values for the Vertical Transport Simulation



Calcium values are multiplied by 10 for plotting purposes.

Figure 7. Effluent (Cell 20) Concentrations of Major Ions for the Horizontal Transport Simulation





Calcium values are multiplied by 10 for plotting purposes.

Figure 8. Effluent (Cell 20) Concentrations of Major Ions for the Vertical Transport Simulation

Elevated initial  $\text{SO}_4$  concentrations in the horizontal simulation are caused by gypsum dissolution, and lower initial dissolved carbon (IV) concentrations result from calcite precipitation. Chloride concentrations are similar between the two simulations because it was treated as a conservative ion with no chemical reactions to affect it.

In summary, the transport results suggest that  $\text{NH}_4$  migration is retarded by several pore volumes. Uranium is retarded by about 1 pore volume but only if Ca is released from gypsum dissolution.

It is beyond the scope of this investigation to estimate ground water velocity beneath the proposed disposal cell at the Crescent Junction Site; thus, results of the model simulations were provided in terms of pore volumes. To use these results in a field setting, units of pore volume must be converted to more useful units of travel time and distance. The conversion is straightforward if the ground water velocity is known. For example, if the ground water flows horizontally from the disposal cell at 10 ft per year, the projected concentrations of U and  $\text{NH}_4$  at a distance of 10 ft after 1 year are equivalent to the values at 1 pore volume on Figure 5. For the same ground water flow velocity at a distance of 5 ft, the projected concentrations are equivalent to 2 pore volumes after 1 year. After 2 years, the concentrations at the 10-ft and 5-ft distances are equivalent to 2 and 4 pore volumes, respectively, and so on. If the porosity of the Mancos Shale aquifer is significantly different than the value (0.25) used in the simulations, then model input would need to be reformulated. Thus, if ground water moves dominantly by fracture flow, some modifications will likely be required.

## Model Limitations

The models presented in the previous section couple many of the chemical processes that are likely to affect transport of constituents at the Crescent Junction Site. Model limitations include both hydrologic and chemical factors. Importantly, the model is *not* limited by an assumption of a constant distribution coefficient ( $K_d$ ) for U, an assumption that has been questioned by Davis et al. (2004).

Ground water flow modeling with PHREEQC is limited to one dimension. Thus, models are constrained to a single streamline. Although the modeling code is able to simulate dispersion and diffusion, these processes were not included for simplification purposes. Because of the low-bulk hydraulic conductivity, much of the



ground water transport through the Mancos Shale is likely to be through fractures or other large-scale features. Such features are not explicitly considered in the models presented in this study. Rather, the flow regime is implicit by the values used to assign concentrations of minerals, exchange sites, and adsorption sites. Because we based these values on the results of laboratory determinations of surface area and bulk density, we made an implicit assumption of pseudo porous-media flow. Adaptation of the model to fracture flow would be accomplished by decreasing the concentrations of sites and minerals (normalizing to a liter of ground water).

The ionic strength of the tailings pore fluids is higher than is commonly prescribed as a limit for use of the Debye-Hückle theory used in PHREEQC to calculate activity coefficients. The ionic strength limitation could be improved by employing empirical activity coefficient algorithms, such as the Pitzer equations (Mariner 2001). Unfortunately, these activity models exist for some of the major ions but are not available for U.

As a first approximation, oxidation-reduction (redox) processes were ignored in the transport models. Although the PHREEQC code is capable of calculating redox equilibria, many redox processes are rate limited. Rate-limited processes can be incorporated in PHREEQC, but universally applicable kinetic data needed to apply these processes are currently unavailable. Another reason for omitting redox processes in the models is that no data are available to confirm that redox processes are occurring in the Mancos Shale at the Crescent Junction Site. Scattered occurrences of pyrite and carbonaceous material suggest that redox processes could be occurring. However, some data suggest relatively oxidized conditions as deep as 300 ft (the depth of the boreholes at the site). Ground water collected from six of these boreholes has redox potentials ranging from 234 to 442 millivolt (mv) with one exception of 15 mV (SEEPPro database). The two values of dissolved oxygen that were determined on these same ground water samples have values (2.41 mg/L and 2.8 mg/L) consistent with oxidized conditions. Also, scattered occurrences of oxidized iron (limonite) staining are present in the upper portion of the Mancos Shale. If data collected later confirm the presence of redox processes, these processes are readily stimulated by the reaction-transport model.

Other chemical factors that limit the modeling are omission of solid solutions and rate-limited processes. These are omitted from the working model because of lack of data to support a viable analysis rather than lack of model capabilities.

## Conclusions

The water-soluble mineral assemblage of the Mancos Shale at the Crescent Junction site is likely dominated by nahcolite with major amounts of Ca-Na exchange and gypsum. Halite, sylvite, and dolomite occur in lesser amounts and calcite is present. Gypsum and dolomite are more dominant in the shallow samples, while nahcolite and halite are more concentrated in the deeper samples. Cation exchange capacity of the Mancos Shale ranges from 0.54 to 36.29 meq/100 g with a mean of 11.23 meq/100 g. The bulk mineral assemblage in the Mancos is dominated by quartz, with lesser amounts of dolomite and calcite, small amounts of feldspar, and traces of gypsum. The clay mineral fraction is dominated by mixed-layer (mostly illite/smectite) clays, illite, and kaolinite with illite layers dominating the mixed-layer clays. Particle surface area ranges from 8.81 to 13.22 m<sup>2</sup>/g with a mean of 11.02 m<sup>2</sup>/g. Distribution ratios for uranium adsorption on Mancos Shale are low, ranging from essentially 0 to 0.84 mL/g.

As tailings fluids reacted with progressively more Mancos Shale in sequential batch tests, slight increases were observed in pH, and concentrations of Na, K, Cl, SO<sub>4</sub>, and U. Results of a reaction-transport model of sequential batch tests showed reasonably good agreement with observed concentrations for Na, Ca, SO<sub>4</sub>, NH<sub>4</sub>, and U; but the modeled pH values were slightly less than the observed values. Considering the complexity of the chemical interactions, these results were considered favorable; thus, this model was used in a one-dimensional simulation of contaminant transport beneath the Crescent Junction disposal cell. The transport results suggest that NH<sub>4</sub> migration is retarded by several pore volumes. Uranium is retarded by about 1 pore volume, but only if Ca is released from gypsum dissolution. To evaluate the effects of this analysis on contaminant transport beneath the proposed Crescent Junction disposal cell, it is necessary to know the flux of contaminated water from the cell and the effective porosity of the Mancos Shale. Evaluation of the flow regime was beyond the scope of this investigation; thus, results of the model simulations are provided in terms of pore volumes. To maximize the benefit of these results in the field setting, project personnel will need to couple these results given in units of pore volume, with the results from hydrologic investigations to yield more useful units of travel time and distance. Alternatively, a sensitivity analysis that

uses reasonable bounds for the hydrologic parameters may be appropriate to assess the impact of chemical attenuation at the Crescent Junction site.

## References

- Bain, D.C., and B.F.L. Smith, 1987. Chemical Analysis, in *A Handbook of Determinative Methods in Clay Mineralogy*, Wilson, M.J. (Ed.), Chapman and Hall, New York, pp. 248–274.
- Border, D. and Giese, R.F., 2001. Baseline Studies of the Clay Minerals Society Source Clays: Cation Exchange Capacity Measurements by the Electrode Method, *Clays and Clay Minerals*, vol. 49, pp. 444–445.
- Chapman, H.D., 1965. Cation Exchange Capacity, in *Methods of Soil Analysis. (Agronomy)*, C.A. Black et al. (Eds.), vol. 9, Amer. Soc. Agron, Madison, Wisconsin, pp. 891–901.
- Davis, J.A., 2001. *Surface Complexation Modeling of Uranium(VI) Adsorption on Natural Mineral Assemblages*, NUREG/CR-6708, U.S. Nuclear Regulatory Commission, Rockville, Maryland.
- Davis, J.A., and G.P. Curtis, 2003. *Application of Surface Complexation Modeling to Describe Uranium (VI) Adsorption and Retardation at the Uranium Mill Tailings Site at Naturita, Colorado*, NUREG/CR-6820, U.S. Nuclear Regulatory Commission, Washington D.C.
- Davis, J.A., and D.B. Kent, 1990. Surface Complexation Modeling in Aqueous Geochemistry, Mineral-Water Interface Geochemistry, *Reviews in Mineralogy Series*, Mineralogical Society of America, vol. 23, pp. 177–260.
- Davis, J.A., R.O. James, and J.O. Leckie, 1978. Surface Ionization and Complexation at the Oxide/Water Interface, *J. Colloid and Interface Sci.*, vol. 63, pp. 480–499.
- Davis, J.A., D.E. Meece, M. Kohler, and G.P. Curtis, 2004. Approaches to Surface Complexation Modeling of Uranium (IV) Adsorption on Aquifer Sediments, *Geochim. et Cosmochim. Acta*, vol. 68, pp. 3621–3641.
- Evangelou, V. P., L.D. Whittig, and K.K. Tanji, 1984. *Dissolved Mineral Salts Derived from Mancos Shale*, *J. Environ. Qual*, vol. 13, pp. 146–150.
- Grim, R.E., 1953. *Clay Mineralogy*, McGraw Hill, New York.
- Hsi, C.D., and D. Langmuir, 1985. Adsorption of Uranyl Onto Ferric Oxyhydroxide: Application of the Surface Complexation Site-Binding Model, *Geochim. Cosmochim. Acta*, vol. 49, pp. 1931–1941.
- Jackson, M.L., 1969. *Soil Chemical Analysis – Advanced Course*, Madison, Wisconsin.
- Mariner, P.E., 2001. Performance of a Pitzer Database Developed for In-Drift Evaporation Calculations, *2001 International High Level Radioactive Waste Management Conference*.
- Mason, B., and C.B. Moore, 1982. *Principles of Geochemistry, Fourth Edition*, John Wiley & Sons, New York, NY.
- Micromeritics Analytical Services, 2006. Surface Area, Website material, [www.particletesting.com](http://www.particletesting.com).
- Morrison, S.J., R.R. Spangler, and V.S. Tripathi, 1995. Adsorption of Uranium(VI) on Amorphous Ferric Oxyhydroxide at High Concentrations of Dissolved Carbon(IV) and Sulfur(VI), *J. Contam. Hydrol.*, vol. 17, pp. 333–346.
- Nadeau, P.H., and R.C. Reynolds, Jr., 1981a. Burial and Contact Metamorphism in the Mancos Shale, *Clays and Clay Minerals*, vol. 28, pp. 249–259.



Nadeau, P.H., and R.C. Reynolds, Jr., 1981b. Volcanic Components in Pelitic Sediments, *Nature*, vol. 294, pp. 72-74.

Parkhurst, D.L., and C.A.J. Appelo, 1999. *User's Guide to PHREEQC (Version 2) – A Computer Program for Speciation, Batch-Reaction, One-Dimensional Transport, and Inverse Geochemical Calculations*, Water-Resources Investigations Report 99-4259, U.S. Geological Survey.

Plummer, L.N., E.C. Prestemon, and D.L. Parkhurst, 1994. *An Interactive Code (NETPATH) for Modeling Net Geochemical Reactions Along a Flow Path*, Water Resources Investigations Report 91-4078, U.S. Geological Survey.

Schultz, L.G., 1964. *Quantitative interpretation of mineralogical composition from X-ray and chemical data for the Pierre Shale*, Professional Paper 391-C, U.S. Geological Survey, Washington, D.C.

Schultz, L.G., 1997. in *Minerals of Colorado*, E.B. Eckel (Ed), Friends of Mineralogy Edition, Fulcrum Publishers, Golden, Colorado.

Tripathi, V.S., 1984. *Uranium(VI) transport modeling: geochemical data and submodels*, Ph.D. Dissertation, Stanford University, Stanford, California.

U.S. Department of Energy (DOE), 1999. *Final Site Observational Work Plan for the UMTRA Project New Rifle Site*, GJO99-112-TAR, Rev. 1, Grand Junction, Colorado.

STO 210. *Environmental Sciences Laboratory Procedures Manual*, continuously updated, prepared by S.M. Stoller Corporation for the U.S. Department of Energy, Grand Junction, Colorado.

Wedepohl, K.H. (editor), 1974. *Handbook of Geochemistry*, Springer Verlag, Berlin.

## **Appendix A**

**Copy of "Work Plan Geochemical Analysis of  
Mancos Shale Cores from the Crescent Junction Disposal  
Cell Site"**

**Work Plan  
Geochemical Analysis of Mancos Shale Cores  
from the  
Crescent Junction Disposal Cell Site,  
Moab UMTRA Project**

January 2006

Work Performed by S.M. Stoller Corporation under DOE Contract No. DE-AC01-02GJ79491  
for the U.S. Department of Energy Office of Environmental Management,  
Grand Junction, Colorado

## Contents

1.0	Introduction .....	1
2.0	Task Descriptions .....	1
2.1	Task 1 – Preparation and Sample Collection.....	2
2.2	Task 2 – Analysis of Water Soluble Fractions .....	2
2.3	Task 3 – Measurements of Cation Exchange Capacity (CEC).....	3
2.4	Task 4 – X-ray Diffraction Analysis .....	4
2.5	Task 5 – Determine Surface Area of Mancos Shale.....	4
2.6	Task 6 – Determination of Distribution Ratios.....	4
2.7	Task 7 – Sequential Batch Leaching Test.....	5
2.8	Task 8 – Coupled Hydrogeochemical Transport Modeling .....	6
2.9	Task 9 – Reporting.....	6
3.0	Schedule .....	6
4.0	References .....	6

## Tables

Table 1. Analytical Methods.....	2
----------------------------------	---

## 1.0 Introduction

This work plan details work that will be done to characterize the geochemistry of the bedrock beneath and adjacent to the proposed disposal cell at Crescent Junction, Utah. The disposal cell will contain tailings from the Moab, Utah, (Atlas) uranium mill and will be underlain by Mancos Shale Formation. The purpose of the work is to provide data that will help evaluate the potential for ground water contamination and transport by constituents in the tailings. The basis for this work is provided in Section 4.5 of Department of Energy (DOE) (2005) and has been modified based on discussions with Moab UMTRA Project personnel. The scope includes laboratory investigation and geochemical modeling, and is presented as nine individual tasks.

The geochemical approach involves collecting site-specific data that can be used to model geochemical interactions between tailings pore fluid and the Mancos Shale. Results from this work will provide the following information about the Mancos Shale:

- Abundance and mineralogy of water soluble minerals
- Mineralogy of water insoluble minerals, including clay mineralogy
- Cation exchange capacity
- Surface area
- Chemical distribution ratios ( $R_d$ )

The data will be used to construct a one-dimensional coupled hydrogeochemical model of tailings water transport through the Mancos. The model will include equations governing aqueous speciation, mineral dissolution, mineral precipitation, mixing with other ground water, oxidation/reduction, cation exchange, and adsorption. In addition, a sequential batch-leaching test will be conducted and the results used to help calibrate the geochemical model. Numerous analyses of tailings pore fluids have been made previously and no additional analyses will be made for the current work scope.

Samples of Mancos Shale will come from 10 cores that were collected from borings evenly distributed in the area of the proposed disposal cell (see DOE 2005 for locations). Samples will primarily consist of the Blue Gate Shale Member of the Mancos Formation because this unit is the most likely to receive contaminated drainage from the disposal cell. Some samples may also be collected from the Prairie Canyon Member of the Mancos. Approximately five samples will be collected from each of the 10 cores for a total of 50 samples. The disposal cell will be excavated approximately 20 ft into the ground; thus, the uppermost sample will be collected from a depth of about 40 ft. The remaining four samples (per core) will be collected at equal intervals below 40 ft. These samples should provide a reasonable set of data to evaluate lateral and vertical distribution of geochemical properties in the Mancos.

## 2.0 Task Descriptions

This section provides details of the nine individual laboratory and modeling tasks. The laboratory portion of the work will be conducted in the Applied Sciences and Technology (AST) testing

facility at the Grand Junction site. Equipment available in the AST facility that will be used for this work include:

- Ion chromatograph
- PH/ORP/conductivity probes and meters
- Balances
- Shaker tables
- Atomic absorption spectrometer
- Solids/liquid separation equipment
- Drying ovens
- Specialized spectrometers and other sample analysis equipment

A subcontract will be procured with Mesa State College to conduct X-ray diffraction (XRD) analysis. Particle surface areas using BET will be measured by a contract laboratory. Analytical methods are presented in Table 1.

*Table 1. Analytical Methods*

Constituent	Procedure Number DOE (2005b)	Procedure Description
Alkalinity	AP(Alk-1)	Titration with H <sub>2</sub> SO <sub>4</sub>
Ammonia	AP(NH <sub>3</sub> -1)	Spectrometry - Salicylate
Calcium	AP(Ca-1)	Flame Atomic Absorption
Chloride	AP(Cl-2)	Ion Chromatography
Magnesium	AP(Mg-1)	Flame Atomic Absorption
Nitrate	AP(NO <sub>3</sub> -4)	Ion Chromatography
Oxidation/Reduction Potential	AP(ORP-1)	Electrode
pH	AP(pH-1)	Electrode
Potassium	AP(K-1)	Flame Atomic Absorption
Sodium	AP(Na-1)	Flame Atomic Absorption
Specific Conductance	AP(EC-1)	Electrode
Sulfate	AP(SO <sub>4</sub> -4)	Ion Chromatography
Uranium	AP(U-2)	Kinetic Phosphorescence

## 2.1 Task 1 – Preparation and Sample Collection

Task 1 includes procurement of chemicals and supplies, many of which are already available in the AST testing facility. Subcontracts with Mesa State College for XRD analysis and a contract laboratory for BET analysis will be procured.

Five samples will be collected from each of the 10 cores. The samples will be collected at depths of 40 ft, 105 ft, 170 ft, 235 ft, and 300 ft. Each sample will contain approximately 3 linear inches of core. Samples will be air-dried and stored in plastic containers until used for the tests. A sample log will be prepared that contains sample numbers, bulk weights, and moisture contents. Dried samples will be lightly crushed with a hammer or pestle, sieved, and split using a riffle splitter as needed for the tests.

## 2.2 Task 2 – Analysis of Water Soluble Fractions

Task 2 is designed to identify and estimate abundance of minerals present in the water-soluble fraction of the Mancos. Mineral identification will be aided by the XRD work in Task 4; however, XRD is limited in its ability to detect small amounts (less than about 5 percent) of

mineral and does not provide information on mineral abundance. All 50 samples will be analyzed. Water-soluble minerals are likely to include thenardite ( $\text{Na}_2\text{SO}_4$ ), halite ( $\text{NaCl}$ ), gypsum ( $\text{CaSO}_4 \cdot 2\text{H}_2\text{O}$ ), and other Na-Ca-K-Mg- $\text{SO}_4$ - $\text{CO}_2$ - $\text{NO}_3$ -Cl-bearing salts. Analyses will include major ions that make up these minerals as well as mill tailings contaminants  $\text{NH}_3$  and U.

Samples will be crushed, air dried, and sieved to -10 +18 mesh (1 to 2 mm nominal diameter). The size fraction was selected because: (1) it is likely to have sufficient material to accomplish the testing, (2) it is uniform enough so that surface area is relatively constant and easy to determine, and (3) it is efficient to work with in the laboratory (testing apparatus can be relatively small).

The leaching procedure is modified from DOE 2005b, procedure CB (BT-1). Two grams of the sieved sample is placed in a plastic centrifuge tube with 100 mL of deionized water at room temperature. The tube is agitated end-over-end for four hours. The solids are separated from the water by centrifuging and decanting, and/or filtering to produce a clear solution. The solution is then analyzed for pH, ORP, specific conductance, alkalinity, Ca, Na, Mg, K,  $\text{SO}_4$ , Cl,  $\text{NO}_3$ ,  $\text{NH}_3$ , and U.

The solid-phase concentration of each leachable major ion will be calculated from the measured concentration and the solid/solution masses used. These solid-phase concentrations will be cast in mole units and mineral stoichiometry will be used to estimate abundances of soluble minerals. The geochemical computer program NETPATH (Plummer et al., 1994) may be used to help determine possible mineral mixtures. In NETPATH, the user can define the initial solution by the composition of the test leachate and the final solution as pure water. Various combinations of mineral phases can be specified and the program calculates the amount of each phase that must precipitate to meet the compositional constraints. Results of X-ray diffraction will help to identify possible mineral phases. Solid-phase concentrations of the contaminants  $\text{NH}_3$  and U will also be calculated; however, concentrations are expected to be small and identification of the mineral phases containing these constituents will not likely be possible.

### 2.3 Task 3 – Measurements of Cation Exchange Capacity (CEC)

The Mancos Shale contains abundant clay minerals. Many types of clay have large CEC that can cause significant changes to ground water chemistry. Knowledge of the CEC is required to develop a geochemical model of water rock interactions. Therefore, CEC will be measured on 20 core samples of Mancos.

Samples will be crushed, air dried, and sieved to -10 +18 mesh (1 to 2 mm nominal diameter) in the same manner as for other tests. The CEC will be determined using a standard method such as the Ca/Mg exchange method (Jackson, 1969) or the ammonium saturation method (Chapman, 1965 as described in Bain and Smith, 1987). The choice of method will be determined after a thorough review of the applicability to the Mancos cores. For the Ca/Mg exchange method, approximately 0.5 to 2 g (exact weight depends on expected CEC) of Mancos is saturated with  $\text{Ca}^{2+}$  using 0.5 N  $\text{CaCl}_2$  solution. The  $\text{Ca}^{2+}$  ion is then replaced with  $\text{Mg}^{2+}$  using 0.5N  $\text{MgCl}_2$ , and the concentration of  $\text{Ca}^{2+}$  released is used to calculate CEC. For the ammonium saturation method, the clay sample is first saturated with ammonium ion using one molar ammonium acetate followed by exchange with sodium chloride. CEC will also be measured on one powdered Mancos sample to provide information on maximum CEC.

## 2.4 Task 4 – X-ray Diffraction Analysis

Chemical interaction between ground water and Mancos Shale is likely to occur mostly at the surfaces of clay minerals. Therefore, clay mineral chemistry is important to the transport of contaminants by the ground water. XRD is one of the best analytical tools to identify the mineralogy of the clay mineral fraction of the Mancos. Ten core samples will be selected for XRD analysis.

Mancos samples will be finely powdered with a mortar and pestle and fractions will be separated by suspension in Calgon solution to concentrate the clay minerals. These clay-mineral separates will be treated in four different ways prior to XRD analysis (Wilson, 1987): (1) air dried, (2) glycolated, (3) heated 300 °C, and (4) heated 550 °C. XRD patterns from these runs will be used to identify clay minerals such as illite (I), smectite (S), interlayered I/S, chlorite, and kaolinite.

X-ray diffraction (XRD) will also be used to determine the major minerals present in the core samples. For these analyses, the 10 core samples will be powdered and oriented randomly.

## 2.5 Task 5 – Determine Surface Area of Mancos Shale

Knowledge of the surface area of the Mancos Shale samples used in the testing is needed to relate the results to the transport of contaminants through the subsurface. Processes such as cation exchange and adsorption are directly related to the surface area that the ground water contacts. For example, for the same travel distance, interaction of dissolved contaminants with the rock will be much less in a fracture-dominated matrix than for porous-media flow. It is beyond the scope of this work plan to determine the nature of the flow (fracture-verses-porous media) in the subsurface at the Crescent Junction site; however, to properly use the data collected during this study in site models, they will need to be normalized to surface area. Therefore, it is important to measure the surface area of the samples used in the testing.

Surface area will be determined for a subset of 10 core samples. Samples will be crushed, air dried, and sieved to -10 +18 mesh (1 to 2 mm nominal diameter) in the same manner as for other tests. Surface area will also be measured on a powdered Mancos sample to provide information on maximum surface area. Surface area will be determined by the standard Brunauer, Emmett, and Teller (BET) method. This method uses N<sub>2</sub> gas adsorption isotherms at -183 °C to measure surface area (Jackson 1969).

## 2.6 Task 6 – Determination of Distribution Ratios

Distribution ratios ( $R_d$ ) provide a measure of the partitioning of a contaminant between the ground water and the solid constituents that comprise the aquifer. The higher the  $R_d$ , the more partitioning to the solids and the more retardation. The  $R_d$  value is an empirical value that is simply the ratio of the measured concentration in the solids (mg/kg) to the measured concentration in the ground water (mg/L) and has units of mL/g. The  $R_d$  values are often used to simulate retardation of contaminants in ground water models. When used in these models there is an implicit assumption that chemical retardation occurs by the process of adsorption under equilibrium conditions. For the equilibrium assumption, the  $R_d$  value is often referred to as a



$K_d$  value. Many models also assume that  $K_d$  does not vary with the concentration of the contaminant. However, research has shown that this variation sometimes exists and algorithms such as the Langmuir or Freundlich equations are used to produce a better fit to the  $R_d$  data. To test if  $R_d$  varies with contaminant concentration, multiple points using various concentrations are measured and plots of these "adsorption isotherms" are fitted with the various models. If the plot is reasonably linear, then a  $K_d$  (also termed linear isotherm) will produce satisfactory results.

$R_d$  values will be determined using DOE (2005b) procedure CB (Rd-1). In summary, a sample of Mancos Shale is crushed and sieved to -10 +18 mesh (1 to 2 mm nominal diameter) as in Task 2. The sample (5 g) is placed in a plastic centrifuge tube with 100 mL of synthetic pore fluid (SPF) that simulates tailings pore fluid. The  $R_d$  value can vary significantly with solution chemistry. For example, Davis et al. (2004) showed that  $R_d$  values for U in a sample of alluvium varied by more than a factor of 10 depending on dissolved carbonate concentration and pH value.  $R_d$  values will be determined using three SPF compositions that are designed to simulate ground water that could be present in the Mancos Shale after construction of the disposal cell. One solution (SPF-1) will simulate pore fluids that currently exist in the tailings. Another solution (SPF-2) will simulate tailing pore water mixed with 50% Mancos ground water. A third solution (SPF-3) will simulate water that results from the sequential batch-leaching test discussed in Task 7.

Single-point  $R_d$  measurements for U will be made on 20 samples and 6-point isotherms will be measured on five of these using SPF-1. For the five samples used for isotherms, single-point  $R_d$  values will also be determined using SPF-2 and SPF-3 to evaluate sensitivity to solution chemistry. The  $R_d$  approach is only valid for contaminants that occur in trace concentrations. Due to the high concentrations present in the pore fluid, modeling the transport of  $\text{NH}_3$  by adsorption is not valid; thus,  $R_d$  values for  $\text{NH}_3$  will not be measured.

## 2.7 Task 7 – Sequential Batch Leaching Test

Two sequential batch-leaching tests will be conducted to "measure evolution of tailings leachate", chemistry as it interacts with Mancos Shale. For this study, it is assumed that the major transport path is either vertically downward beneath the tailings pile or subhorizontal through the weathered zone. Results of this test will be used to help validate the coupled hydrogeochemical transport model presented in the next section.

For the vertical scenario, a 100-g sample of Mancos (40-ft depth) will be crushed, air dried, and sieved to -10 +18 mesh (1 to 2 mm nominal diameter). The sample will be combined with 400 mL of SPF-1 in a 500-mL glass Erlenmeyer flask. The mixture will be agitated on an orbital shake table for 24 hours. At that time, the solids will be separated from the liquid by centrifugation, decantation, and/or filtering. A 50-mL split will be retained and analyzed for pH, ORP, specific conductance, alkalinity, Ca, Na, Mg, K,  $\text{SO}_4$ , Cl,  $\text{NO}_3$ ,  $\text{NH}_3$ , and U. The remaining solution will be placed with approximately 87.5 g of Mancos sample from 105-ft depth. The exact amount of Mancos sample will be calculated so the water-to-rock ratio remains constant. The procedure will be repeated three times with progressively deeper samples.

For the horizontal scenario, a 3-step leach will be conducted using the 40-ft deep samples from cores 203, 204, and 206.

## 2.8 Task 8 – Coupled Hydrogeochemical Transport Modeling

This task consists of developing a coupled hydrogeochemical transport model using the PHREEQC code (Parkhurst and Appelo, 1999). Ion exchange will be modeled using data from the CEC tests in Task 3 and surface area measurements in Task 5. Initial conditions will include concentrations of minerals as estimated from the results of Tasks 2 and 4. A surface complexation model for U, based on  $R_d$  measurements (Task 6) will be incorporated.

The model will include one-dimension transport of tailings water through the Mancos Shale. Aqueous speciation reactions are typically fast with respect to ground water flow and will be modeled at chemical equilibrium. Water-rock interaction will include mineral precipitation and dissolution, adsorption, and cation exchange. The model will be adaptable to allow inclusion of such factors as: (1) mixing with ground water, (2) reaction kinetics, and (3) changing redox state (e.g., due to biologic activity). Thus, sensitivity of the transport to various parameters can be readily estimated with additional model simulations. Two model simulations will be conducted to simulate the vertical and horizontal scenarios described in Section 2.7. The model can be used to simulate other transport paths with minor changes.

## 2.9 Task 9 – Reporting

Results of the testing and modeling will be presented as Moab Calculation Sets.

## 3.0 Schedule

Completion Date	Activity
January 13, 2006	Task 1. Preparation and Sample Collection
March 4, 2006	Task 2. Analysis of Water Soluble Fractions
March 4, 2006	Task 3. Measurements of Cation Exchange Capacity
March 4, 2006	Task 4. X-Ray Diffraction Analysis
March 4, 2006	Task 5. Determine Surface Area of Mancos Shale
March 4, 2006	Task 6. Determination of Distribution Ratios
March 4, 2006	Task 7. Sequential Batch Leaching Test
May 10, 2006	Task 8. Coupled Hydrogeochemical Transport Modeling
June 1, 2006	Task 9. Draft Report

## 4.0 References

Bain, D.C.; Smith, B.F.L., 1987. Chemical analysis, in Wilson, M.J. (Ed.) *A Handbook of Determinative Methods in Clay Mineralogy*, Chapman and Hall, New York, pp. 248-274.

Chapman, H.D., 1965. Cation exchange capacity, in C.A. Black et al. (Eds.), *Methods of Soil Analysis. (Agronomy)*, vol. 9, Amer. Soc. Agron, Madison, Wisconsin, pp. 891-901.

Davis, J.A.; Meece, D.E.; Kohler, M.; Curtis, G.P., 2004. Approaches to surface complexation modeling of uranium (IV) adsorption on aquifer sediments, *Geochim. et Cosmochim. Acta*, 68, pp. 3621-3641.

Jackson, M.L. 1969. *Soil Chemical Analysis – Advanced Course*, published by author, Madison, WI, 895 pp.

Parkhurst, D.L.; Appelo, C.A.J. 1999. *User's Guide to PHREEQC (Version 2) – A Computer Program for Speciation, Batch-Reaction, One-Dimensional Transport, and Inverse Geochemical Calculations*, Water-Resources Investigations Report 99-4259, U.S. Geol. Survey, 312 p.

Plummer, L.N.; Prestemon, E.C.; Parkhurst, D.L. 1994. *An Interactive Code (NETPATH) for Modeling Net Geochemical Reactions Along a Flow Path*, Water Resources Investigations Report 91-4078, U.S. Geol. Survey, 227 p.

U.S. Department of Energy (DOE), 2005a. *Work Plan for Characterization of Crescent Junction Disposal Site*, DOE-EM/GJ912-2005.

U.S. Department of Energy (DOE), 2005b (regularly updated). *Environmental Sciences Laboratory Procedures Manual*, STO210, U.S. Department of Energy Office of Legacy Management, Grand Junction, CO.

Wilson, M.J., 1987. X-ray powder diffraction methods, in Wilson, M.J. (Ed.) *A Handbook of Determinative Methods in Clay Mineralogy*, Chapman and Hall, New York, pp. 26-98.

**Appendix B**  
**Laboratory Notes**

Crescent Jctn. Ark 1 Sample Collection

1/9/06

Travel to Crescent Junction site to obtain core samples with Sherrison and C. Goodnight.

Appropriate core boxes retrieved from sea-land storage. An approx 3" piece of core was obtained @ the level noted with the top of the core starting at the level noted e.g. 201-40 = 201-40 to 40'9".

Larger Appl of CT285-40 obtained for adtlg testing

Samples were split off w/ chisel and hammer when there was no natural weak line. Spacers were placed in core boxes to indicate sample locations.

Samples were double bagged and labeled for return to GTO.

Samples were delivered to Geotech Engineering Group for prep with following instructions

1. Do not pulverize.
2. Gently disaggregate to -10/+18 (-2mm nominal diameter)
3. Avoid (as much as possible) generating heat.
4. Once disaggregated, place in Calvetta, sealed polylock bags to avoid cooling, moisture content.

Samples returned to G5. Placed in pans for air drying. LOD calculated.  
Samples then sieved into 3 size fractions to obtain the 1-2 mm split for analysis.

+10 mesh	=	> 2mm
-10/+18	=	1-2mm
-18	=	< 1mm

CJ01-01-02

[illegible]

# Crescent Open Task 2

CS01-01-03

2

1/18/06

Place 2g of each of the following into 50 ml centrifuge tubes.

Add

Sample

Size

Sample

Size

CS 205-40

1-2mm

CS 207-40

1-2mm

105

105

170

170

235

235

300

300

CS 206-40

CS 208-40

105

105

170

170

235

235

300

300

Place on end over end stir bar @ 8 RPM x 4 hours

Remove from stir bar. Centrifuge 30" x 3500 RPM

Decant into individual 100ml Volumetric flasks

Refill Cent. tubes w 50ml Mullig H<sub>2</sub>O

Place on end over end stir bar x 30" @ 8 RPM

Remove from stir bar. Centrifuge 30" x 3500 RPM

Add supernatant to respective vol. flasks. Fill to vol w Mullig

Filter through 0.45 um vac. filter. Measure parameters, analyze. See attached Spreadsheet

# Crescent Jan. Task 2

CJ01-01-04<sup>3</sup>

1/19/06

Place 2g of each of the following into 50ml centrifuge tubes. Add

Sample Size

Sample Size

CJ209- 40 1-2 mm

CJ-202-40D 1-2 mm

105

204-40D

170

206-40D

235

208-40D

300

CJ210- 40

105

170

235

300

Place on end over end stir bar @ 8RPM x 4 hours

Remove from stir bar. Centrifuge 30" x 3500RPM

Decant into individual 100mL vol. flasks

Refill cent. tubes w 50mL Mullig H<sub>2</sub>O

Place on end over end stir bar @ 8RPM x 30"

Remove from stir bar, centrifuge 30" x 3500RPM

Add supernatant to respective vol flask. Fill to Vol w Mullig

Filter through 0.4um Vac filter. Measure parameters, analyze. See attached spreadsheet



# Crescent Junction CEC Task 3

CJ01-01-05

1	2	3	4	5	6	7	8	9	10	11	12	13
2/4/06	Place 100mg of the following samples in 30ml cent. tubes. Follow CB AP(CEC) $\Sigma$ 10. Exposure to amacetate & 4 then overnight for 5th. AOK.											
	Sample	NH <sub>3</sub> -N (mg/L)		CEC (meg/100g)								
2/4/06	CJ001-40	0.65		9.286								
date	202-40	0.82		11.714								
	203-40	2.54		36.286								
	204-40	0.75		10.714								
	205-40	0.75		10.714								
	206-40	0.41		5.857								
	207-40	1.08		15.429								
	208-40	0.49		7.000								
	209-40	1.19		17.000								
	210-40	0.80		11.429								
	205-40P	0.72		10.286								
	205-40P-D	<del>0.89</del> 0.73		<del>12.714</del> 10.429								
2/5/06	201-105	0.37		5.286								
date	202-105	0.80		11.429								
	203-105	0.49		7.000								
	204-105	0.90		12.857								
	205-105	0.87		12.429								
	206-105	0.52		7.429								
	207-105	0.60		8.571								
	208-105	0.50		7.143								
	209-105	1.03		14.714								
	210-105	0.38		5.429								
	204-105D	0.92		13.143								
	205-40D	0.89		12.714								

Task 4 XRD

CJ01-01-06

1/17/06 Place ~~an~~ approx 15g split of the following samples in individual 30ml centrifuge tubes. Samples are of the <1mm size fraction, air dried. All are from the 40' depth.

Sample

CJ-201-40

202-40

203-40

204-40

205-40

206-40

207-40

208-40

209-40

210-40

Delivered to Dr. Bill Hood for XRD analysis

Crescent Jctn. Task 5 - BET Surface Area.

CJ01-01-07

1/17/06 Prepare the following samples for shipment to Micromeritics for BET method multipoint surface analysis. All are air dried from 40' below surface. Place 150g of the following in 30ml cent tubes.

Sample	Particle size (mm)	
CJ201-40	1-2	
202-40	1-2	
203-40	1-2	
204-40	1-2	
205-40	1-2	
205-40 P	<1	(powdered)
206-40	1-2	
207-40	1-2	
208-40	1-2	
209-40	1-2	
210-40	1-2	

Send to Micromeritics Analytical Services via Fedex  
One Micromeritics Dr  
Norcross, GA 30093-1877  
1-770-662-3630

Request Cat#005-01 Multipoint surface area analysis =  $N_2$  gas

2/4/06 Call Micromeritics re analysis - 1-2mm frac <sup>results</sup> comparable to powdered sample. Confirmed samples run as submitted (not powdered) w/ phone conversation with analyst that performed tests. He suggested  $N_2$  molecule was smaller than interstitial space of the 1-2mm fraction and was seeing "inside" the particles.

**Sarah Morris**

---

**From:** Stan Morrison  
**Sent:** Thursday, February 02, 2006 9:35 AM  
**To:** Sarah Morris  
**Subject:** FW: Micromeritics Analytical Services - Analysis Results

Sarah,

Surface Area results. I've included an Excel sheet ("Results\_Surface Area") with the results tabulated (in the format your original data table). Of interest, the powdered sample was very similar to the coarser sample. Could you contact them and confirm that the samples were not powdered prior to analysis.

Thanks,

Stan

-----Original Message-----

**From:** michael.poston@micromeritics.com [mailto:michael.poston@micromeritics.com]  
**Sent:** Thursday, February 02, 2006 7:49 AM  
**To:** Stan Morrison  
**Cc:** mark.talarico@micromeritics.com  
**Subject:** Micromeritics Analytical Services - Analysis Results

Dear Stan Morrison,

Thank you for submitting your samples to Micromeritics Analytical Services. We appreciate the opportunity to serve you. Attached below, please find the results for your samples and a copy of the submission form (for future submissions). If you have any questions, comments or concerns please contact us at 770-662-3630.

Sincerely,

Michael Poston - Lab Analyst  
Micromeritics Analytical Services  
1 Micromeritics Dr.  
Norcross, GA 30093  
770.662.3630

[www.particletesting.com](http://www.particletesting.com)

*This e-mail is intended for the use of the addressee(s) only and may contain privileged, confidential, or proprietary information that is exempt from disclosure under law. If you have received this message in error, please inform us promptly by reply e-mail, then delete the e-mail and destroy any printed copy. Thank you.*

2/2/2006

**Sarah Morris**

---

**From:** Stan Morrison  
**Sent:** Thursday, February 02, 2006 1:02 PM  
**To:** Sarah Morris  
**Subject:** RE: Micromeritics Info

Sarah,

Thanks. That satisfied my concern. Please put the response in the project file.

Stan

-----Original Message-----

**From:** Sarah Morris  
**Sent:** Thursday, February 02, 2006 11:16 AM  
**To:** Stan Morrison  
**Subject:** Micromeritics Info

I just called and talked to the person that did the surface area analysis. He confirmed that the samples were analyzed as instructed, that the samples were not powdered prior.

When I told him your concern that the surface area of the 1-2 mm fraction was comparable to the powdered split, his response was that "it is possible that the N<sub>2</sub> molecule was smaller than the interstitial space of the 1-2 mm fraction and was seeing "inside" the particles." He said that he was probably not the one to converse with about that possibility. If you wanted to call and discuss, the best person would be Greg Fields, their business manager who would probably be knowledgeable, but if he didn't, would know who to put you in contact with. Their number is 770-662-3630.

Sarah

CJ01-01-09

CJ01-01-10

## Crescent Junction Task 6 Kd

2/9/2006 Prepare 2L SPF1 = Batch 1

2/10/2006 Spike soln 2 mg/L U std. pH = 7.56

adjust pH to 6.57  $\pm$  1.55 mL conc  $\text{HNO}_3$   $\mu$  = 920.8  $\mu\text{g/L}$  Cond = 27800 alk = 4801000 add 100 mL SPF1  $\pm$   $\mu$  to the following then place on rotating bar @ 8 RPM

	Mass	On	Off	SPF1 $\pm$ $\mu$	pH	Cond ( $\mu\text{S/cm}$ )	alk ( $\mu\text{g/L}$ )	$\mu$ ( $\mu\text{g/L}$ )
CJ 201e40	5g	2/10/06	2/11/06	Batch 1	7.51	29400	650	898.0
201e40 D	5g				7.53	29400	580	925.2
203e40	5				7.47	29400	560	892.2
204e40	5				7.49	29200	600	890.9
206e40 <del>5g</del>	5				7.53	29400	540	906.1
207e40 D	5				7.55	29400	610	823.9
208e40 D	5				7.58	29400	570	831.4
209e40	5				7.50	29400	460	926.6
201e105	5				7.65	29500	640	850.1
202e105	5				7.65	29500	550	839.4
203e105	5				7.58	29400	610	821.2
204e105	5				7.61	29400	550	822.4
205e105	5				7.67	29400	560	839.3
205e105 D	5				7.54	29500	570	820.2
206e105	5				7.52	29700	560	852.1
207e105	5				7.58	29700	610	798.0
208e105	5				7.57	29800	530	805.6
209e105	5				7.60	29600	600	813.6
210e105	5				7.56	29600	530	819.4
Batch Blank SPF	0				7.46	29500	440	829.4

2/11/06 <sup>0930</sup> Remove above from bar. Cent 20" x 300 RPM. Filter thru 0.45  $\mu\text{m}$  filter. Analyze

Task 6 Ed

[illegible]

CJ01-01-12

Task 6 KD

1	2	3	4	5	6	7	8	9	10	11	12	13
2/11/2006	1000	Place following in	rotating stir bar @	8 RPM	after adding	100 mL	SPFI-U (Batch 2)					
	SPFI-U (Batch 2)	4L	= pH 6.63	alk = 690 mg/L as CaCO <sub>3</sub>	U = 942.3 (measured 2/12/06)							
	Sample	Mem	on	H <sub>2</sub> O	SPFI-U	pH	Cond (µS/cm)	Alk (mg/L as CaCO <sub>3</sub> )	U (µg/L)			
CJ202e 40	1	2/11/06	2/12/06	Batch 2 day 1	7.47	29200	780	810.8				
	2				7.51	29000	840	799.3				
	5				7.52	29000	900	805.4				
	10				7.53	28900	930	764.3				
	20				7.53	28900	870	708.8				
	25				7.58	28800	870	696.2				
CJ205e 40	1				7.53	28900	830	821.4				
	2				7.54	29000	830	799.1				
	5				7.54	28900	850	793.9				
	10				7.56	29000	900	766.0				
	20				7.58	28900	890	718.8				
	25				7.60	28900	880	714.4				
CJ207e 40	1				7.54	29100	860	808.4				
	2				7.50	29200	820	811.9				
	5				7.48	29100	890	811.6				
Blank SPFI-U Batch 2					7.39	29100	710	817.1				
Blank 2												
2/12/2006	Remove from stir bar	Cent 20" x 3000 rpm.	Filter through 0.45 µm filter.	Analyze								



Crescent Jctn. Task 6 Kd

2/12/06 1 Prepare 1 L SPF2. Spike = 0.1 mL 10,000 mg/L. Concentration should measure 1000 ug/L  
 2  
 3 Start pH = 7.84 adjust pH to 6.98  $\pm$  0.3 mL conc  $\text{HNO}_3$   $\text{U} = 893.9 \text{ ug/L}$   
 4 alk = 1000 cond = 22500 ORP = 203.9  
 5  
 6 2/13/06 CK stability of SPF2 = U. pH  $\uparrow$  7.54. Add 0.2 mL conc  $\text{HNO}_3$  pH = 6.94  
 7 cond 22300 ORP 226.3. alk 880  $\frac{1}{4} \text{ U} = 765.0 \text{ ug/L}$  (set overnight prior to analysis)  
 8  
 9 1H add 100 mL SPF2 = U to the following  
 10  
 11

	Mass	on	off	SPF2 = U	pH	Cond (u/cm)	Alk (meq/L)	U (ug/L)
CJ 202e40	5g	2/13/06	2/14/06	Batch 1	7.59	22200	910	760.4
205e40	5				7.67	22400	880	765.0
207e40	5				7.76	22600	900	756.1
208e40	5				7.75	22700	900	789.5
208e40D	5				7.67	22600	930	752.1
210e40	5				7.69	24600	920	761.0
Blank 1 SPF2	0				7.55	24600	880	769.2

0930 Remove above from stir bar. Centrifuge 20" x 3500 RPM. Filter through 0.45 um filter and analyze  
 2/14/2006 Prepare SPF3, will add U and pH adjust in AM  
 2/22/2006 SPF3 no U = 7.79 Add 0.11 mL 10K U (ug/L). Use 100 uL extra due to  $\uparrow$  Vol of "1L recipe"  
 pH = 7.75, Cond = 28200 uS/cm, ORP = 193.5 mV, alk = 280 mg/L as  $\text{CaCO}_3$   $\text{U} = 799.3 \text{ ug/L}$   
 0930 add 100 mL SPF3 = U to the following

CJ01-01-14

Crescent Jtn. Task 6 Kd's

	1	2	3	4	5	6	7	8	9	10	11	12	13
2/22/06	1	SPF3 EU	100 mL	to the following									
0930	2		Mass	m	off	pH	Cond us/cm	Alk	U (ug/L)				
	3					(end)	(end)	(end)	end.				
	4	CJ002040	5g	2/22/06	2/23/06	7.88	28700	270	742.2				
	5	205e40	5			7.90	28900	270	756.7				
	6	207e40	5			7.91	28800	370	783.4				
	7	208e40	5			7.91	28700	270	797.0				
	8	210e40	5			7.93	29000	330	793.9				
	9	210e40D	5			7.92	28700	370	766.4				
	10	SPF3-	0			7.81	28600	250	807.8	811.2			
2/23/06	11	Remove from rotating still vac. Centrifuge 3500 RPM x 20' filter through 0.45um filter											
	12	analyze											
	13	Check SPF3 parent soln - day 2											
	14												
	15												
	16												
	17												
	18												
	19												
	20												
	21												
	22												
	23												
	24												
	25												
	26												
	27												
	28												
	29												
	30												
	31												

pH = 7.75

Cond = 28500

ORP = 187.3

alk = 290

U = 818.1 ug/L  
827.7





501-01-17

	A	B	C	D	E	F	G	H	I	J	K	L
2			Solids									
3		mL per	mg per									
4		L of	L of	Na	K	Ca	Mg	NH4	SO4	Cl	NO3	C
5		Soln	Soln	mg/L	mg/L	mg/L	mg/L	mg/L	mg/L	mg/L	mg/L	mg/L
6	Liquid Components											
7	V2O5, V=998mg/L, 2%HNO3	0.00									0.00	
8	V2O5, V=1000mg/L, 5%HNO3	0.00									0.00	
9	V2O5, V=1000mg/L, 1.4%HNO3	0.00									0.00	
10	V2O5, V=1000mg/L, 2%HNO3	0.00									0.00	
11	Na2MoO4.2H2O, Mo=925mg/L	0.00		0.00								
12	Na2MoO4.2H2O, Mo=1000 mg/L	0.00		0.00								
13	(NH4)2MoO4, 1006 mg/L Mo	0.00						0.00				
14	U3O8, U=10000mg/L, 3.5%HNO3	0.10									3.38	
15	U3O8, U=10000mg/L, 5.2%HNO3	0.00									0.00	
16	U Std, U=1000mg/L, 2% HNO3	0.00									0.00	
17	Ra Std, Ra=68.7pCi/mL, 2% HNO3	0.00									0.00	
18	As Std, As=999mg/L, 5%HNO3	0.00									0.00	
19	As Std, As=1000mg/L, 1.4%HNO3	0.00									0.00	
20	Sa =998 mg/L 5% HNO3	0.00									0.00	
21	Cd Std = 1000mg/L, -2% HNO3	0.00									0.00	
22												
23	100g/L K2CO3	0.00	0.00		0.00							0.00
24	10g/L KCl	0.00	0.00		0.00					0.00		
25	50g/L NaHCO3	11.00	550.00	150.60								76.57
26	100g/L Na2SO4.10H2O	474.00	47400.00	6771.43					14131.68			
27	100g/L Na2SO4 (0.89 H2O)	0.00	0.00	0.00					0.00			
28	500g/L (NH4)2SO4	6.60	3300.00					900.00	2400.00			
29	1.5g/L CaSO4.2H2O	560.00	840.00			195.65			468.62			
30	1.2 g/L CaSO4	0.00	0.00			0.00			0.00			
31	200g/L MgSO4.7H2O	9.10	1820.00				179.56		709.38			
32	100g/L K2SO4	3.70	370.00		166.10				203.90			
33	conc H2SO4(36N)	0.00							0.00			
34	927.2 g/L CaCl2.2H2O	0.00	0.00			0.00				0.00		
35	92.72 g/L CaCl2.2H2O	0.00	0.00			0.00				0.00		
36	300g/L NaCl	7.50	2250.00	884.62						1365.38		
37	100g/L MgCl2.8H2O	0.00	0.00				0.00			0.00		
38	100g/L NH4Cl	0.00	0.00					0.00		0.00		
39	100g/L NaNO3	0.00	0.00	0.00							0.00	
40	2% HNO3	0.00									0.00	
41	mL 1N NaOH needed to neutralize	0.00		0.00								
42	66.67 g/L NaN3	0.00	0.00	0.00								
43												
44												
45	Totals (mg/L)	1072.00		7806.64	166.10	195.65	179.56	900.00	17913.58	1365.38	3.38	76.57
46	ACTUAL (mg/L)			7800.00	166.00	196.00	180.00	900	19492.00	1336.00	?	79.20
47	Totals (mol/L)			3.40E-01	4.25E-03	4.88E-03	7.39E-03	5.00E-02	1.87E-01	3.85E-02	5.46E-05	8.55E-03
48												
49	ACTUAL pH	7.97										
50	Measured pH (no acid or base)	?										
51	Measured pH ( added)											
52	ACTUAL Alk (mg/L CaCO3)	330.00										
53	Measured Alk (no acid or base)	?										
54	Measured Alk ( added)											
55	EQ Acid per Liter	8.004E-05										
56												
57												



# CS Task 7

CJO1-01-19

2/13/2006 0745 Remove from orbital shaker. Divide Vol & Solids between 2 ea 250ml vials  
Place in centrifuge @3500 RPM x 20"  
Decant and filter through 0.45um filter. Vol = 215 ml (start 240-215 ml = 25 ml retained in solids)  
Horizontal test is complete. Retain all for analysis  
Vertical test continues. Retain 50ml 205 & 176 for analysis  
CT 205 & 235 - 2/11 4.25 g in 165 ml residual SPF1  
Return to orbital shaker.

2/14/06 0900 Remove from orbital shaker. Divide vol & solids between 2 ea 175 ml vials  
Place in centrifuge @3500 RPM x 20"  
Decant and filter through 0.45um filter. Vol = 145 ml (start 165 ml - 145 = 20 ml retained in solids)  
Retain 40ml CT 205 & 235 for analysis  
CT 205 & 300 - 2/11 25 g in 100 ml residual SPF1  
Return to orbital shaker  
Measure SPF1 prep 2/9/06 pH, ORP, alk conc

2/15/05 0830 Remove from orbital shaker. Decant and filter thru 0.45um filter.  
Retain all for analysis



## Crescent Jctn. Tank 7 Sequential Batch Leach CJOI-01-20

Sample	1 Vol SPFI	2 Mass	3 pH	4 ORP	5 Cond	6 Alk	7 Cl	8 NO <sub>3</sub>	9 SO <sub>4</sub>	10 NH <sub>3</sub> -N	11 U	12	13
	mo U (mL)	(g)		(mv)	(uS/cm)	(mg/L as CaCO <sub>3</sub> )	(mg/L)	(mg/L)	(mg/L)	(mg/L)	(ug/L)		
CJ 203e40	400	100	7.66	196.7	29400	560	1026	764	18676	1700	5.5		
204e40	315	78.75	7.79	186.3	30100	450	1096	828	19872	1500	19.3		
206e40	240	60	7.83	175.2	29900	560	1120	820	19910	1300	25.4		
CJ 205e40	400	100	7.73	187.3	29200	620	1106	756	18504	1600	3.0		
e105	315	78.75	7.85	171.4	29800	560	1116	770	18828	1400	19.5		
e170	240	60	7.96	171.5	29600	520	1196	776	19032	1100	29.0		
e235	165	41.25	7.85	173.3	29700	400	1284	804	19700	1800	44.9		
e300	100	25	7.97	173.5	30600	330	1336	794	19492	900	54.5		
Plant Dbln	2/10	0	6.62	197.4	26800	560	1018	738	18272	2000	<0.1		
SPFI mol		0											
SPFI mol	2/4		7.85	191.9	29600	510	1018	738	18272	2000			

note -  
samples are  
yellow tinged



## Crescent Jtn Task 7 Sequential Batch Leach (Data cont)

CJ01-01-21

Sample	Vol SPFI	Mass	#	Ca	Na	Mg	K						
	ml	(g)		(mg/L)	(mg/L)	(mg/L)	(mg/L)						
1													
2													
3													
4													
5													
6													
7													
8													
9													
10													
11													
12													
13													
14													
15													
16													
17													
18													
19													
20													
21													
22													
23													
24													
25													
26													
27													
28													
29													
30													
31													
32													
33													
34													
35													
36													
37													
38													
39													
40													
41													
42													
43													
44													
45													
46													
47													
48													
49													
50													
51													
52													
53													
54													
55													
56													
57													
58													
59													
60													
61													
62													
63													
64													
65													
66													
67													
68													
69													
70													
71													
72													
73													
74													
75													
76													
77													
78													
79													
80													
81													
82													
83													
84													
85													
86													
87													
88													
89													
90													
91													
92													
93													
94													
95													
96													
97													
98													
99													
100													
101													
102													
103													
104													
105													
106													
107													
108													
109													
110													
111													
112													
113													
114													
115													
116													
117													
118													
119													
120													
121													
122													
123													
124													
125													
126													
127													
128													
129													
130													
131													
132													
133													
134													
135													
136													
137													
138													
139													
140													
141													
142													
143													
144													
145													
146													
147													
148													
149													
150													
151													
152													
153													
154													
155													
156													
157													
158													
159													
160													
161													
162													
163													
164													
165													
166													
167													
168													
169													
170													
171													
172													
173													
174													
175													
176													
177													
178													
179													
180													
181													
182													
183													
184													
185													
186													
187													
188													

## **Appendix C**

### **Complete Chemical Results and Computations**

- (1) *Loss on Drying*
- (2) *Size Fraction Analysis*
- (3) *X-Ray Diffraction Results*
- (4) *Surface Area Results*
- (5) *Cation Exchange Capacity Results*
- (6) *Water Soluble Minerals – Raw Data*
- (7) *Water Soluble Minerals – NETPATH Results*
- (8) *Water Soluble Minerals – PHREEQC Input*
- (9) *Distribution Ratios: Single-Point, SPF1*
- (10) *Distribution Ratios: Single-Point, SPF2*
- (11) *Distribution Ratios: Single-Point, SPF3*
- (12) *Distribution Ratios: Multiple-Point Isotherms*
- (13) *Results of Sequential Batch Tests*



Sample	Tare	Gross Wet	Gross Dry	Net Wet	Net Dry	LOD (g)	LOD (%)	Comments			
CJ-209-235	6.7	390.1	385.3	383.4	378.6	4.8	1.25%				
CJ-209-300	6.7	521.4	516.6	514.7	509.9	4.8	0.93%	299'10"			
CJ-210-40	6.7	376.6	369.9	369.9	363.2	6.7	1.81%				
CJ-210-105	6.7	299	296.2	292.3	289.5	2.8	0.96%				
CJ-210-170	6.7	391.1	386.1	384.4	379.4	5	1.30%				
CJ-210-235	6.7	392.1	386.3	385.4	379.6	5.8	1.50%				
CJ-210-300	6.7	415.1	409.6	408.4	402.9	5.5	1.35%				

S.M.Stoller													
Point of Contact:													
Sarah Morris													
248-6514													
Crescent Junction Core Analysis													
01/09/06													
Samples returned from Geotech Engineering Group													
Disaggregated prior to LOD, some samples powdered easily, so greater >1mm fraction than anticipated													
Splits are function of mild disaggregation, not indicative of true particle size													
Air Dried, Sieved													
+10 mesh = >2mm													
-10/+18 = 1-2mm													
-18 = <1mm													
Sample	Net Total	+2mm	+2mm	+2mm	1-2mm	1-2mm	1-2mm	<1mm	<1mm	<1mm			Frac >1
	Mass	gross (g)	(g)	(%)	gross (g)	(g)	(%)	gross (g)	(g)	(%)			(g)
CJ-201-40	335.8	21.3	14.6	4.35%	147.8	141.1	42.02%	184.6	177.9	52.98%	99.34%		155.7
CJ-201-105	370.9	23.8	17.1	4.61%	159.1	152.4	41.09%	206.8	200.1	53.95%	99.65%		169.5
CJ-201-170	310.9	38.5	31.8	10.23%	131.5	124.8	40.14%	159.4	152.7	49.12%	99.49%		156.6
CJ-201-235	349.2	103.3	96.6	27.66%	112.7	106	30.36%	151.6	144.9	41.49%	99.51%		202.6
CJ-201-300	354.1	101	94.3	26.63%	122.9	116.2	32.82%	148.7	142	40.10%	99.55%		210.5
CJ-202-40	331.6	93	86.3	26.03%	104.8	98.1	29.58%	152.5	145.8	43.97%	99.58%		184.4
CJ-202-105	332.3	102.4	95.7	28.80%	102.6	95.9	28.86%	146.3	139.6	42.01%	99.67%		191.6
CJ-202-170	238	71.9	65.2	27.39%	85.9	79.2	33.28%	98.7	92	38.66%	99.33%		144.4
CJ-202-235	347	90.5	83.8	24.15%	119	112.3	32.36%	156.4	149.7	43.14%	99.65%		196.1
CJ-202-300	291.2	95.5	88.8	30.49%	97.2	90.5	31.08%	116.3	109.6	37.64%	99.21%		179.3
CJ-203-40	380.1	68.3	61.6	16.21%	120.8	114.1	30.02%	210.1	203.4	53.51%	99.74%		175.7
CJ-203-105	434	110.4	103.7	23.89%	138.2	131.5	30.30%	203.8	197.1	45.41%	99.61%		235.2
CJ-203-170	431.7	152.1	145.4	33.68%	138.5	131.8	30.53%	159.3	152.6	35.35%	99.56%		277.2
CJ-203-235	361.8	151.1	144.4	39.91%	99.4	92.7	25.62%	124.3	117.6	32.50%	98.04%		237.1
CJ-203-300	431.4	155	148.3	34.38%	118.7	112	25.96%	168.3	161.6	37.46%	97.80%		260.3
CJ-204-40	343.6	100.8	94.1	27.39%	90.8	84.1	24.48%	160.7	154	44.82%	96.68%		178.2
CJ-204-105	302.4	122.7	116	38.36%	79.7	73	24.14%	112.7	106	35.05%	97.55%		189
CJ-204-170	389.1	188.9	182.2	46.83%	90.4	83.7	21.51%	122	115.3	29.63%	97.97%		265.9
CJ-204-235	299.4	124.7	118	39.41%	78.4	71.7	23.95%	109.5	102.8	34.34%	97.70%		189.7
CJ-204-300	404.2	175.4	168.7	41.74%	113	106.3	26.30%	128.1	121.4	30.03%	98.07%		275
CJ-205-40	624.3	171.3	164.6	26.37%	186.6	179.9	28.82%	274.2	267.5	42.85%	98.03%		344.5
CJ-205-105	371.6	116	109.3	29.41%	123.2	116.5	31.35%	144	137.3	36.95%	97.71%		225.8
CJ-205-170	408.1	120.2	113.5	27.81%	135.8	129.1	31.63%	163.6	156.9	38.45%	97.89%		242.6
CJ-205-235	318	120.8	114.1	35.88%	97.4	90.7	28.52%	112	105.3	33.11%	97.52%		204.8
CJ-205-300	389.6	147.8	141.1	36.22%	112.9	106.2	27.26%	142.2	135.5	34.78%	98.25%		247.3
CJ-206-40	421	154	147.3	34.99%	104.9	98.2	23.33%	172.1	165.4	39.29%	97.60%		245.5
CJ-206-105	458.9	148.1	141.4	30.81%	130.5	123.8	26.98%	191.2	184.5	40.20%	98.00%		265.2
CJ-206-170	395.1	153	146.3	37.03%	121.7	115	29.11%	133.1	126.4	31.99%	98.13%		261.3
CJ-206-235	304.3	100.8	94.1	30.92%	101.3	94.6	31.09%	115.7	109	35.82%	97.83%		188.7
CJ-206-300	449.3	181.6	174.9	38.93%	129	122.3	27.22%	150.6	143.9	32.03%	98.17%		297.2
CJ-207-40	407.3	161.3	154.6	37.96%	108.6	101.9	25.02%	149.8	143.1	35.13%	98.11%		256.5
CJ-207-105	373.9	154.4	147.7	39.50%	100.2	93.5	25.01%	131.1	124.4	33.27%	97.78%		241.2
CJ-207-170	347.7	145.6	138.9	39.95%	96.8	90.1	25.91%	119.6	112.9	32.47%	98.33%		229
CJ-207-235	369.9	140.6	133.9	36.20%	117	110.3	29.82%	125.7	119	32.17%	98.19%		244.2
CJ-207-300	378.1	119.3	112.6	29.78%	135.5	128.8	34.07%	136.4	129.7	34.30%	98.15%		241.4
CJ-208-40	380.7	106.7	100	26.27%	114.8	108.1	28.40%	175.1	168.4	44.23%	98.90%		208.1
CJ-208-105	357.5	107	100.3	28.06%	112.5	105.8	29.59%	151.9	145.2	40.62%	98.27%		206.1
CJ-208-170	438.7	164	157.3	35.86%	139.7	133	30.32%	146.1	139.4	31.78%	97.95%		290.3
CJ-208-235	386.8	142.7	136	35.16%	122.7	116	29.99%	133.9	127.2	32.89%	98.04%		252
CJ-208-300	387.5	72.6	65.9	17.01%	146.2	139.5	36.00%	182.6	175.9	45.39%	98.40%		205.4
CJ-209-40	313.7	65.6	58.9	18.78%	107.5	100.8	32.13%	152.5	145.8	46.48%	97.39%		159.7

Sample	Net Total	+2mm	+2mm	+2mm	1-2mm	1-2mm	1-2mm	<1mm	<1mm	<1mm		Frac >1
	Mass	gross (g)	(g)	(%)	gross (g)	(g)	(%)	gross (g)	(g)	(%)		(g)
CJ-209-105	386.1	123.7	117	30.30%	130.3	123.6	32.01%	145.1	138.4	35.85%	98.16%	240.6
CJ-209-170	469	89.4	82.7	17.63%	169.9	163.2	34.80%	222.2	215.5	45.95%	98.38%	245.9
CJ-209-235	383.4	95.3	88.6	23.11%	135.6	128.9	33.62%	166.5	159.8	41.68%	98.41%	217.5
CJ-209-300	514.7	100.2	93.5	18.17%	198.9	192.2	37.34%	227.8	221.1	42.96%	98.47%	285.7
CJ-210-40	369.9	128.4	121.7	32.90%	115.3	108.6	29.36%	138.1	131.4	35.52%	97.78%	230.3
CJ-210-105	292.4	65.3	58.6	20.04%	102	95.3	32.59%	141	134.3	45.93%	98.56%	153.9
CJ-210-170	384.4	98.4	91.7	23.86%	139.3	132.6	34.50%	159.7	153	39.80%	98.15%	224.3
CJ-210-235	385.4	110.7	104	26.98%	140.1	133.4	34.61%	147.3	140.6	36.48%	98.08%	237.4
CJ-210-300	408.4	96.2	89.5	21.91%	153.4	146.7	35.92%	171.8	165.1	40.43%	98.26%	236.2

XRD Analysis						
Bill Hood						
SM Stoller						
Point of Contact: Stan Morrison 248-6373						
Dr. Hood received 1/17/2006						
Samples sent to Bill are <1mm fraction						
Bill Hood provided a report to Stan on February 6, 2006						
Summary: (1) non-phylosilicate minerals identified include quartz, calcite, dolomite, orthoclase, plagioclase, and gypsum						
(2) Clay minerals (in order of abundance) include: mixed-layer illite smectite (at least 60% illite layers),						
discrete illite, kaolinite, and mixed-layer chlorite-vermiculite.						
Samples						
Estimated Abundances (%) of Non-Phyllosilicates in Bulk Samples						
	Quartz	Calcite	Dolomite	Orthoclase	Plagioclase	Gypsum
CJ-201-40	32	3	5	1	1	Tr
CJ-202-40	29	3	4	1	1	1
CJ-203-40	36	4	5	1	2	1
CJ-204-40	33	2	3	1	1	
CJ-205-40	28	3	6	1	1	
CJ-206-40	39	4	6	1	2	
CJ-207-40	25	3	3	1	1	
CJ-208-40	38	3	5	1	1	
CJ-209-40	27	1	3	2	1	Tr
CJ-210-40	24	4	3	1	1	
Samples						
Estimated Abundances (%) of Clays						
	Mixed-Layer	Illite	Kaolinite	I/S	%Illite	
CJ-201-40	43	29	28		70	
CJ-202-40	38	36	26		60	
CJ-203-40	43	31	25		60	
CJ-204-40	40	30	29		60	
CJ-205-40	46	31	23		60	
CJ-206-40	37	34	29		60	
CJ-207-40	27	36	37		50	
CJ-208-40	35	36	29		60	
CJ-209-40	39	31	29		60	
CJ-210-40	39	37	25		60	

Micromeritics Analytical Services			
One Micromeritics Drive			
Norcross, GA 30093-1877			
1-770-662-3630			
Multi-point Surface Area Analysis, BET Method			
Catalog #005-01			
Sample	Particle	Surface	
	size	Area	
		m <sup>2</sup> /g	
CJ-201-40	1 to 2 mm	10.6561	
CJ-202-40	1 to 2 mm	12.2117	
CJ-203-40	1 to 2 mm	8.8087	
CJ-204-40	1 to 2 mm	12.9162	
CJ-205-40	1 to 2 mm	9.9511	
CJ-206-40	1 to 2 mm	9.4615	
CJ-207-40	1 to 2 mm	13.1245	
CJ-208-40	1 to 2 mm	9.3897	
CJ-209-40	1 to 2 mm	10.456	
CJ-210-40	1 to 2 mm	13.2247	
	Mean =	11.02002	
	min =	8.8087	
	max =	13.2247	
CJ-205-40-P	<1 mm	10.6955	



Cation Exchange Capacity			
Samples	Size	NH3-N (mg/L)	CEC (meq/100g)
CJ-201-40	1-2 mm	0.65	9.29
CJ-202-40	1-2 mm	0.82	11.71
CJ-203-40	1-2 mm	2.54	36.29
CJ-204-40	1-2 mm	0.75	10.71
CJ-205-40	1-2 mm	0.75	10.71
CJ-205-40-Dup	1-2 mm	0.89	12.71
CJ-205-40-P	<1 mm	0.72	10.29
CJ-205-40-P-Dup	<1 mm	0.73	10.43
CJ-206-40	1-2 mm	0.41	5.86
CJ-207-40	1-2 mm	1.08	15.43
CJ-208-40	1-2 mm	0.49	7.00
CJ-209-40	1-2 mm	1.19	17.00
CJ-210-40	1-2 mm	0.8	11.43
CJ-201-105	1-2 mm	0.37	5.29
CJ-202-105	1-2 mm	0.8	11.43
CJ-203-105	1-2 mm	0.49	7.00
CJ-204-105	1-2 mm	0.9	12.86
CJ-204-105-Dup	1-2 mm	0.92	13.14
CJ-205-105	1-2 mm	0.87	12.43
CJ-206-105	1-2 mm	0.52	7.43
CJ-207-105	1-2 mm	0.6	8.57
CJ-208-105	1-2 mm	0.5	7.14
CJ-209-105	1-2 mm	1.03	14.71
CJ-210-104	1-2 mm	0.038	0.54
	min=	0.04	0.54
	Max =	2.54	36.29
	Mean	0.79	11.23

Water Soluble Fractions: Used 2 g of sample leached with 100 mL of deionized water														
Sample	Depth	pH	Cond	ORP	Alk	Cl	NO3-N	SO4	U	NH3-N	Ca	Na	Mg	K
	ft		(uS/cm)	(mV)	(mg/L as)	(mg/L)	(mg/L)	(mg/L)	(ug/L)	(mg/L)	(mg/L)	(mg/L)	(mg/L)	(mg/L)
CJ-201-40	40	7.97	258	136	9	7.98	0.22	79.28	0.27	0.11	13.9	20.8	3.4	9.7
CJ-201-105	105	9.39	147	104	39	6.88	0.11	7.33	0.95	0.08	0.76	24	0.16	2.8
CJ-201-170	170	9.78	212	95	77	7.16	0.11	4.98	1.29	0.3	0.15	36.5	0.12	4.4
CJ-201-235	235	9.81	220	87	82	6.75	0.11	3.36	1.42	0.4	0.1	38.5	0.11	4.4
CJ-201-300	300	9.86	254	98	93	8.24	0.11	3.61	1.47	0.41	0.09	43	0.11	6.6
CJ-202-40	40	9.26	170	113	36	9.88	0.51	16.32	1.01	0.12	0.45	20	0.76	15.1
CJ-202-40-D	40	9.12	135	56	38	4.25	0.49	16.18	0.36	0.09	0.48	20.5	0.81	3.6
CJ-202-105	105	9.78	267	116	83	17.37	0.11	4.32	0.81	0.33	0.18	36	0.12	17.2
CJ-202-170	170	9.79	238	99	89	4.51	0.11	5.38	10.37	0.43	0.11	41	0.1	3.5
CJ-202-235	235	9.8	214	88	81	6.12	0.11	4.47	0.87	0.33	0.12	36	0.1	3.2
CJ-202-300	300	9.81	251	105	86	11.11	0.11	3.96	0.81	0.32	0.17	38	0.08	10.8
CJ-203-40	40	6.17	800	89	12	3.18	0.30	412.9	0.19	0.2	122.4	9	8	2
CJ-203-105	105	9.52	217	113	49	17.73	0.11	7.54	0.69	0.26	0.45	29	0.13	16.3
CJ-203-170	170	9.75	207	96	76	6.9	0.11	5.53	1.11	0.28	0.22	36	0.13	3.3
CJ-203-235	235	9.8	237	92	89	6.67	0.11	5.9	1.11	0.51	0.08	41	0.1	4.8
CJ-203-300	300	9.7	201	85	76	6.95	0.11	3.78	0.82	0.38	0.11	36	0.1	3.2
CJ-204-40	40	7.81	431	85	15	2.74	0.11	171.05	0.23	0.42	36.8	26	7	2.12
CJ-204-40-D	40	8.46	383	65	19	2.69	0.11	146.47	0.20	0.41	30.4	27	6.2	2.2
CJ-204-105	105	9.85	232	84	87	5.22	0.11	5.09	1.32	0.35	0.1	40	0.11	5.6
CJ-204-170	170	9.81	221	84	83	8.03	0.11	5.29	1.02	0.48	0.09	37	0.11	4.6
CJ-204-235	235	9.74	193	84	65	7.56	0.11	6.03	0.69	0.47	0.18	32	0.09	3.3
CJ-204-300	300	9.85	232	79	91	5.4	0.11	4.34	0.94	0.44	0.03	40	0.1	3.2
CJ-205-40	40	9.16	146	97	37	4.62	0.11	15.71	0.72	0.4	0.25	24.5	0.37	6.5
CJ-205-105	105	9.73	247	95	93	7.38	0.11	6.6	1.13	0.47	0.06	41	0.12	4.6
CJ-205-170	170	9.68	246	85	96	6.03	0.11	5.49	1.07	0.47	0.07	42	0.1	4.7
CJ-205-235	235	9.67	257	84	90	5.19	0.11	9.04	1.24	0.54	0.11	44	0.09	2.6
CJ-205-300	300	9.73	224	78	85	5.17	0.11	5.87	0.81	0.46	0.13	38	0.08	2.5
CJ-206-40	40	8.78	143	77	35	5.18	0.11	22.23	0.21	0.23	1.25	21.5	0.72	2.3
CJ-206-40-D	40	9.07	144	62	29	5.02	0.11	21.28	0.17	0.25	1.37	21.5	0.76	2.2
CJ-206-105	105	9.29	153	76	44	6.45	0.11	8.59	0.26	0.29	0.69	23	0.79	2.2
CJ-206-170	170	9.76	237	75	92	6.31	0.11	4.47	1.04	0.44	0.1	39	0.1	3
CJ-206-235	235	9.71	219	74	84	6.73	0.11	5.05	0.65	0.52	0.12	37	0.09	2.9
CJ-206-300	300	9.63	214	72	86	6.66	0.11	2.07	0.52	0.41	0.12	37	0.09	2.5
CJ-207-40	40	9.64	273	75	81	4.2	0.11	29.84	1.53	0.72	0.09	50	0.14	4.8
CJ-207-105	105	9.61	171	68	68	5.48	0.11	4.31	0.47	0.3	0.29	27	0.11	2.3
CJ-207-170	170	9.63	201	71	76	5.79	0.11	5.53	0.61	0.46	0.16	33	0.11	3
CJ-207-235	235	9.75	241	71	91	5.42	0.11	5.38	0.80	0.48	0.11	40	0.08	2.5
CJ-207-300	300	9.76	247	70	94	5.04	0.11	5.84	0.81	0.46	0.08	41	0.07	2.5
CJ-208-40	40	9.29	138	69	32	6.44	0.11	16.71	0.20	0.15	1.05	21	0.38	1.6
CJ-208-40-D	40	9.27	134	80	35	5.97	0.11	16.63	0.16	0.2	1.42	27.5	0.46	1.8
CJ-208-105	105	9.31	156	71	39	6.61	0.11	11.62	0.26	0.25	0.69	24	0.19	2.1
CJ-208-170	170	9.8	261	71	101	6.04	0.11	5.74	0.15	0.38	0.08	44	0.09	3.3
CJ-208-235	235	9.81	251	69	97	5.51	0.11	4.25	0.87	0.51	0.07	42	0.08	2.9
CJ-208-300	300	9.64	192	66	72	6.47	0.11	4.71	0.34	0.35	0.23	31	0.08	2
CJ-209-40	40	8.49	254	89	20	2.47	0.11	81.97	0.12	0.08	5	31	3.6	3.9
CJ-209-105	105	9.77	250	75	93	5.1	0.11	7.43	0.95	0.42	0.14	43	0.11	2.9
CJ-209-170	170	9.51	179	72	59	6.87	0.11	6.67	0.25	0.37	0.33	35	0.12	2.4
CJ-209-235	235	9.78	226	72	88	6.07	0.11	5.94	0.45	0.34	0.13	38	0.08	2.4
CJ-209-300	300	9.88	254	66	104	5.05	0.11	3.45	0.81	0.6	0.08	43	0.08	2.2
CJ-210-40	40	9.72	221	63	73	4.99	0.11	15.6	0.75	0.33	0.19	38	0.13	3.1
CJ-210-105	105	9.32	138	59	39	7.11	0.11	9.56	0.14	0.2	1.02	20	0.23	1.9
CJ-210-170	170	9.77	212	60	79	6.31	0.11	5.65	0.72	0.41	0.17	36	0.09	2.3
CJ-210-235	235	9.81	230	59	90	6.04	0.11	4.57	0.67	0.38	0.1	39	0.07	2.3
CJ-210-300	300	9.83	249	58	99	5.5	0.11	5.12	0.76	0.41	0.09	43	0.07	2.2

Water Soluble Fraction Results from NETPATH output files										
Sample	Depth	pH	Calcite	Gypsum	Nahcolite	Halite	Sylvite	Exchange	Dolomite	Total
			CaCO <sub>3</sub>	CaSO <sub>4</sub>	NaHCO <sub>3</sub>	NaCl	KCl	Ca/Na	CaMg(CO <sub>3</sub> ) <sub>2</sub>	
			mmol/L	mmol/L	mmol/L	mmol/L	mmol/L	mmol/L	mmol/L	mmol/L
CJ-201-40	40	7.97	-0.21	0.82	0.11	-0.02	0.25	0.41	0.14	1.50
CJ-202-40	40	9.26	0.02	0.17	0.55	-0.11	0.39	0.21	0.03	1.26
CJ-203-40	40	6.17	-2.70	4.30	2.60	0.04	0.05	-1.12	0.33	3.50
CJ-204-40	40	7.81	-0.92	1.78	0.65	0.02	0.05	0.23	0.29	2.10
CJ-205-40	40	9.16	0.12	0.16	0.51	-0.04	0.17	0.30	0.02	1.24
CJ-206-40	40	8.78	-0.22	0.23	0.83	0.09	0.06	0.01	0.03	1.03
CJ-207-40	40	9.64	0.28	0.31	0.99	-0.01	0.12	0.60	0.01	2.30
CJ-208-40	40	9.29	-0.08	0.17	0.61	0.14	0.04	0.08	0.02	0.98
CJ-209-40	40	8.49	-0.46	0.85	0.56	-0.03	0.10	0.41	0.15	1.58
CJ-210-40	40	9.72	0.15	0.16	0.97	0.06	0.08	0.31	0.01	1.74
CJ-201-105	105	9.39	0.14	0.08	0.52	0.12	0.07	0.20	0.01	1.14
CJ-202-105	105	9.78	0.18	0.04	1.07	0.05	0.44	0.22	0.01	2.01
CJ-203-105	105	9.52	0.24	0.08	0.56	0.08	0.42	0.31	0.01	1.70
CJ-204-105	105	9.85	0.36	0.05	0.91	0.01	0.14	0.41	0.01	1.89
CJ-205-105	105	9.73	0.12	0.07	1.31	0.09	0.12	0.19	0.01	1.91
CJ-206-105	105	9.29	-0.04	0.09	0.75	0.12	0.06	0.06	0.03	1.07
CJ-207-105	105	9.61	-0.10	0.04	1.19	0.10	0.06	-0.05	0.01	1.25
CJ-208-105	105	9.31	0.02	0.12	0.64	0.13	0.05	0.13	0.01	1.10
CJ-209-105	105	9.77	0.23	0.08	1.17	0.07	0.07	0.31	0.01	1.94
CJ-210-105	105	9.32	-0.11	0.10	0.77	0.15	0.05	-0.03	0.01	0.94
CJ-201-170	170	9.78	0.24	0.05	0.92	0.09	0.11	0.29	0.01	1.71
CJ-202-170	170	9.79	0.30	0.06	1.04	0.04	0.09	0.35	0.01	1.89
CJ-203-170	170	9.75	0.19	0.06	0.97	0.11	0.08	0.24	0.01	1.66
CJ-204-170	170	9.81	0.16	0.06	1.07	0.11	0.12	0.22	0.01	1.75
CJ-205-170	170	9.68	0.14	0.06	1.37	0.05	0.12	0.21	0.01	1.96
CJ-206-170	170	9.76	0.10	0.05	1.30	0.10	0.08	0.15	0.01	1.79
CJ-207-170	170	9.63	0.02	0.06	1.19	0.09	0.08	0.08	0.01	1.53
CJ-208-170	170	9.80	0.18	0.06	1.33	0.09	0.08	0.25	0.01	2.00
CJ-209-170	170	9.51	0.28	0.07	0.68	0.13	0.06	0.35	0.01	1.58
CJ-210-170	170	9.77	0.14	0.06	1.05	0.12	0.06	0.20	0.01	1.64
CJ-201-235	235	9.81	0.31	0.03	0.91	0.08	0.11	0.35	0.01	1.80
CJ-202-235	235	9.80	0.17	0.05	1.04	0.09	0.08	0.22	0.01	1.66
CJ-203-235	235	9.80	0.27	0.06	1.06	0.06	0.12	0.33	0.01	1.91
CJ-204-235	235	9.74	0.16	0.06	0.82	0.13	0.08	0.22	0.01	1.48
CJ-205-235	235	9.67	0.23	0.09	1.19	0.08	0.07	0.32	0.01	1.99
CJ-206-235	235	9.71	0.09	0.05	1.21	0.12	0.07	0.14	0.01	1.69
CJ-207-235	235	9.75	0.14	0.06	1.24	0.09	0.06	0.20	0.01	1.80
CJ-208-235	235	9.81	0.21	0.04	1.24	0.08	0.07	0.25	0.01	1.90
CJ-209-235	235	9.78	0.09	0.06	1.24	0.11	0.06	0.15	0.01	1.72
CJ-210-235	235	9.81	0.15	0.05	1.20	0.11	0.06	0.19	0.01	1.77
CJ-201-300	300	9.86	0.37	0.04	0.98	0.06	0.17	0.41	0.01	2.04
CJ-202-300	300	9.81	0.25	0.04	1.03	0.04	0.28	0.29	0.01	1.94
CJ-203-300	300	9.70	0.19	0.04	0.98	0.11	0.08	0.23	0.01	1.64
CJ-204-300	300	9.85	0.24	0.05	1.09	0.07	0.08	0.29	0.01	1.83
CJ-205-300	300	9.73	0.14	0.06	1.17	0.08	0.06	0.20	0.01	1.72
CJ-206-300	300	9.63	0.06	0.02	1.32	0.12	0.06	0.08	0.01	1.67
CJ-207-300	300	9.76	0.15	0.06	1.29	0.08	0.06	0.21	0.01	1.86
CJ-208-300	300	9.64	-0.02	0.05	1.16	0.13	0.05	0.03	0.01	1.41
CJ-209-300	300	9.88	0.21	0.04	1.30	0.09	0.06	0.24	0.01	1.95
CJ-210-300	300	9.83	0.47	0.05	0.72	0.10	0.06	0.53	0.01	1.94
Means			0.05	0.23	1.01	0.08	0.11	0.21	0.03	1.71

Water Soluble Minerals: For entry to PHREEQE; From NETPATH results							
Based on 7500 g rock/L (multiplier is 0.375)							
Calcite	Gypsum	Nahcolite	Halite	Sylvite	Exchange	Dolomite	Total
CaCO3	CaSO4	NaHCO3	NaCl	KCl	Ca/Na	CaMg(CO3)2	
mol/Lgw	mol/Lgw	mol/Lgw	mol/Lgw	mol/Lgw	mol/Lgw	mol/Lgw	mol/Lgw
-0.0788	0.3075	0.0413	-0.0075	0.0938	0.1538	0.0525	0.5625
0.0075	0.0638	0.2063	-0.0413	0.1463	0.0788	0.0113	0.4725
-1.0125	1.6125	0.9750	0.0150	0.0188	-0.4200	0.1238	1.3125
-0.3450	0.6675	0.2438	0.0075	0.0188	0.0863	0.1088	0.7875
0.0450	0.0600	0.1913	-0.0150	0.0638	0.1125	0.0075	0.4650
-0.0825	0.0863	0.3113	0.0338	0.0225	0.0038	0.0113	0.3863
0.1050	0.1163	0.3713	-0.0038	0.0450	0.2250	0.0038	0.8625
-0.0300	0.0638	0.2288	0.0525	0.0150	0.0300	0.0075	0.3675
-0.1725	0.3188	0.2100	-0.0113	0.0375	0.1538	0.0563	0.5925
0.0563	0.0600	0.3638	0.0225	0.0300	0.1163	0.0038	0.6525
0.0525	0.0300	0.1950	0.0450	0.0263	0.0750	0.0038	0.4275
0.0675	0.0150	0.4013	0.0188	0.1650	0.0825	0.0038	0.7538
0.0900	0.0300	0.2100	0.0300	0.1575	0.1163	0.0038	0.6375
0.1350	0.0188	0.3413	0.0038	0.0525	0.1538	0.0038	0.7088
0.0450	0.0263	0.4913	0.0338	0.0450	0.0713	0.0038	0.7163
-0.0150	0.0338	0.2813	0.0450	0.0225	0.0225	0.0113	0.4013
-0.0375	0.0150	0.4463	0.0375	0.0225	-0.0188	0.0038	0.4688
0.0075	0.0450	0.2400	0.0488	0.0188	0.0488	0.0038	0.4125
0.0863	0.0300	0.4388	0.0263	0.0263	0.1163	0.0038	0.7275
-0.0413	0.0375	0.2888	0.0563	0.0188	-0.0113	0.0038	0.3525
0.0900	0.0188	0.3450	0.0338	0.0413	0.1088	0.0038	0.6413
0.1125	0.0225	0.3900	0.0150	0.0338	0.1313	0.0038	0.7088
0.0713	0.0225	0.3638	0.0413	0.0300	0.0900	0.0038	0.6225
0.0600	0.0225	0.4013	0.0413	0.0450	0.0825	0.0038	0.6563
0.0525	0.0225	0.5138	0.0188	0.0450	0.0788	0.0038	0.7350
0.0375	0.0188	0.4875	0.0375	0.0300	0.0563	0.0038	0.6713
0.0075	0.0225	0.4463	0.0338	0.0300	0.0300	0.0038	0.5738
0.0675	0.0225	0.4988	0.0338	0.0300	0.0938	0.0038	0.7500
0.1050	0.0263	0.2550	0.0488	0.0225	0.1313	0.0038	0.5925
0.0525	0.0225	0.3938	0.0450	0.0225	0.0750	0.0038	0.6150
0.1163	0.0113	0.3413	0.0300	0.0413	0.1313	0.0038	0.6750
0.0638	0.0188	0.3900	0.0338	0.0300	0.0825	0.0038	0.6225
0.1013	0.0225	0.3975	0.0225	0.0450	0.1238	0.0038	0.7163
0.0600	0.0225	0.3075	0.0488	0.0300	0.0825	0.0038	0.5550
0.0863	0.0338	0.4463	0.0300	0.0263	0.1200	0.0038	0.7463
0.0338	0.0188	0.4538	0.0450	0.0263	0.0525	0.0038	0.6338
0.0525	0.0225	0.4650	0.0338	0.0225	0.0750	0.0038	0.6750
0.0788	0.0150	0.4650	0.0300	0.0263	0.0938	0.0038	0.7125
0.0338	0.0225	0.4650	0.0413	0.0225	0.0563	0.0038	0.6450
0.0563	0.0188	0.4500	0.0413	0.0225	0.0713	0.0038	0.6638
0.1388	0.0150	0.3675	0.0225	0.0638	0.1538	0.0038	0.7650
0.0938	0.0150	0.3863	0.0150	0.1050	0.1088	0.0038	0.7275
0.0713	0.0150	0.3675	0.0413	0.0300	0.0863	0.0038	0.6150
0.0900	0.0188	0.4088	0.0263	0.0300	0.1088	0.0038	0.6863
0.0525	0.0225	0.4388	0.0300	0.0225	0.0750	0.0038	0.6450
0.0225	0.0075	0.4950	0.0450	0.0225	0.0300	0.0038	0.6263
0.0563	0.0225	0.4838	0.0300	0.0225	0.0788	0.0038	0.6975
-0.0075	0.0188	0.4350	0.0488	0.0188	0.0113	0.0038	0.5288
0.0788	0.0150	0.4875	0.0338	0.0225	0.0900	0.0038	0.7313
0.1763	0.0188	0.2700	0.0375	0.0225	0.1988	0.0038	0.7275
Means							
0.0199	0.0847	0.3779	0.0287	0.0406	0.0781	0.0109	0.6406

Single Point Kd's												
Volume of SPF1 = 100 mL												
Mean Labile U (from Sequential Batch Tests) = 0.0436 ug/g												
Sample	Mass	U	U	U	Cs	Cs	Cs	Rd	Rd	Rd	Log U	Log Rd
	(g)	(ug/L)	(ug/L)	(ug/L)	(ug/g)	(ug/g)	(ug/g)	mL/g	mL/g	mL/g	(mol/L)	(mL/g)
		Meas.	Max	Min	Meas.	Min	Max	Meas.	Min	Max	Meas.	Meas.
			2.5% Error	2.5% Error		2.5% Error	2.5% Error		2.5% Error	2.5% Error		
CJ 201-40	5	898	920.45	875.55	-1.3284	-2.1920	-0.4646	-1.48	-2.38	-0.53	-5.423301	#NUM!
CJ 203-40	5	892.2	914.51	869.90	-1.2124	-2.0731	-0.3515	-1.36	-2.27	-0.40	-5.426115	#NUM!
CJ 204-40	5	890.9	913.17	868.63	-1.1864	-2.0465	-0.3261	-1.33	-2.24	-0.38	-5.426748	#NUM!
CJ 206-40	5	906.1	928.75	883.45	-1.4904	-2.3581	-0.6226	-1.64	-2.54	-0.70	-5.419401	#NUM!
CJ 209-40	5	926.6	949.77	903.44	-1.9004	-2.7783	-1.0223	-2.05	-2.93	-1.13	-5.409685	#NUM!
CJ 201-105	5	850.1	871.35	828.85	-0.3704	-1.2101	0.4695	-0.44	-1.39	0.57	-5.447107	#NUM!
CJ 202-105	5	839.4	860.39	818.42	-0.1564	-0.9907	0.6781	-0.19	-1.15	0.83	-5.452608	#NUM!
CJ 203-105	5	821.2	841.73	800.67	0.2076	-0.6176	1.0330	0.25	-0.73	1.29	-5.462128	-0.682773
CJ 204-105	5	822.4	842.96	801.84	0.1836	-0.6422	1.0096	0.22	-0.76	1.26	-5.461494	-0.736127
CJ 205-105	5	839.3	860.28	818.32	-0.1544	-0.9886	0.6801	-0.18	-1.15	0.83	-5.45266	#NUM!
CJ 206-105	5	852.1	873.40	830.80	-0.4104	-1.2511	0.4304	-0.48	-1.43	0.52	-5.446086	#NUM!
CJ 207-105	5	798	817.95	778.05	0.6716	-0.1420	1.4854	0.84	-0.17	1.91	-5.474574	-0.172889
CJ 208-105	5	805.6	825.74	785.46	0.5196	-0.2978	1.3372	0.64	-0.36	1.70	-5.470457	-0.284331
CJ 209-105	5	813.6	833.94	793.26	0.3596	-0.4618	1.1812	0.44	-0.55	1.49	-5.466166	-0.44418
CJ 210-105	5	819.4	839.89	798.92	0.2436	-0.5807	1.0681	0.30	-0.69	1.34	-5.463081	-0.613323
SPF1	0	829.4	850.14	808.67								

Single Point Kd's SPF 2												
Mean Labile U (from Sequential Batch Tests) = 0.0436 ug/g												
Sample	Mass	U	U	U	Cs	Cs	Cs	Rd	Rd	Rd	Log U	Log Rd
	(g)	(ug/L)	(ug/L)	(ug/L)	(ug/g)	(ug/g)	(ug/g)	mL/g	mL/g	mL/g	(mol/L)	(mL/g)
		Meas.	Max	Min	Meas.	Min	Max	Meas.	Min	Max	Meas	Meas.
			2.5% Error	2.5% Error		2.5% Error	2.5% Error		2.5% Error	2.5% Error		
CJ-202-40	5	760.4	779.41	741.39	0.2196	-0.5452	0.9844	0.29	-0.70	1.33	-5.49553	-0.65837
CJ-205-40	5	765	784.13	745.88	0.1276	-0.6395	0.8947	0.17	-0.82	1.20	-5.49292	-0.89415
CJ-207-40	5	756.1	775.00	737.20	0.3056	-0.4571	1.0683	0.40	-0.59	1.45	-5.498	-0.51485
CJ-208-40	5	789.5	809.24	769.76	-0.3624	-1.1418	0.4169	-0.46	-1.41	0.54	-5.47922	#NUM!
CJ-208-40Dup	5	752.1	770.90	733.30	0.3856	-0.3751	1.1463	0.51	-0.49	1.56	-5.5003	-0.41386
CJ-210-40	5	761	780.03	741.98	0.2076	-0.5575	0.9727	0.27	-0.71	1.31	-5.49519	-0.68277
SPF2	0	769.2	788.43	749.97								

Single Point Kd's SPF 3												
Mean Labile U (from Sequential Batch Tests) = 0.0436 ug/g												
Sample	Mass	U	U	U	Cs	Cs	Cs	Rd	Rd	Rd	Log U	Log Rd
	(g)	(ug/L)	(ug/L)	(ug/L)	(ug/g)	(ug/g)	(ug/g)	mL/g	mL/g	mL/g	(mol/L)	mL/g
		Meas	Max	Min	Meas.	Min	Max	Meas.	Min	Max	Meas.	Meas.
			2.5% Error	2.5% Error		2.5% Error	2.5% Error		2.5% Error	2.5% Error		
CJ-202-40	5	742.2	760.76	723.65	1.4236	0.6469	2.2003	1.92	0.85	3.04	-5.50606	0.282867
CJ-205-40	5	756.7	775.62	737.78	1.1336	0.3496	1.9176	1.50	0.45	2.60	-5.49765	0.175536
CJ-207-40	5	783.4	802.99	763.82	0.5996	-0.1977	1.3969	0.77	-0.25	1.83	-5.48259	-0.11612
CJ-208-40	5	797	816.93	777.08	0.3276	-0.4765	1.1317	0.41	-0.58	1.46	-5.47512	-0.38611
CJ-210-40	5	793.9	813.75	774.05	0.3896	-0.4130	1.1922	0.49	-0.51	1.54	-5.47681	-0.30915
SPF 3	0	811.2	831.48	790.92								

Six point Isotherms												
SPF 1 w/U; prepared 2/10/06, Spiked with U on 2/11/06, pH adjusted												
Volume SPF 1 = 100 mL												
Mean Labile U (from Sequential Batch Tests) = 0.0436 ug/g												
0.0436												
Sample	Mass	U	U	U	Cs	Cs	Cs	Rd	Rd	Rd	U	Rd
	(g)	(ug/L)	(ug/L)	(ug/L)	(ug/g)	(ug/g)	(ug/g)	mL/g	mL/g	mL/g	Log mol/L	Log mL/g
		Meas.	Max	Min	Meas.	Min	Max	Meas.	Min	Max	meas	meas
			2.5% Error	2.5% Error		2.5% Error	2.5% Error		2.5% Error	2.5% Error		
SPF 1	0	942.30	965.86	918.74								
	0	942.30	965.86	918.74								
CJ 202-40	1	810.80	831.07	790.53	0.67	-3.40	4.74	0.83	-4.09	6.00	-5.467663	-0.080512
	2	799.30	819.28	779.32	0.93	-1.09	2.95	1.17	-1.33	3.79	-5.473867	0.067451
	5	805.40	825.54	785.27	0.28	-0.53	1.09	0.34	-0.65	1.39	-5.470565	-0.462592
	10	764.30	783.41	745.19	0.57	0.18	0.97	0.75	0.22	1.30	-5.493313	-0.126172
	20	708.80	726.52	691.08	0.59	0.39	0.78	0.83	0.54	1.12	-5.526053	-0.083294
	25	696.20	713.61	678.80	0.53	0.38	0.68	0.76	0.53	1.00	-5.533843	-0.120759
CJ 205-40	1	821.40	841.94	800.87	-0.39	-4.48	3.71	-0.47	-5.32	4.63	-5.462022	
	2	799.10	819.08	779.12	0.94	-1.08	2.96	1.18	-1.31	3.80	-5.473976	0.072187
	5	793.90	813.75	774.05	0.51	-0.30	1.31	0.64	-0.37	1.70	-5.476811	-0.194244
	10	766.00	785.15	746.85	0.55	0.16	0.95	0.72	0.20	1.27	-5.492348	-0.140249
	20	718.80	736.77	700.83	0.54	0.34	0.73	0.74	0.47	1.04	-5.519969	-0.128173
	25	714.40	732.26	696.54	0.45	0.30	0.61	0.64	0.41	0.87	-5.522636	-0.196503
CJ 207-40	1	808.40	828.61	788.19	0.91	-3.15	4.98	1.13	-3.80	6.32	-5.468951	0.05313
	2	811.90	832.20	791.60	0.30	-1.73	2.34	0.37	-2.08	2.96	-5.467074	-0.427201
	5	811.60	831.89	791.31	0.15	-0.66	0.97	0.19	-0.79	1.22	-5.467235	-0.722951
SPF1	0	817.10	837.53	796.67							-5.464302	
	10	718.20	736.16	700.25	0.65	0.27	1.02	0.90	0.37	1.46	-5.520332	-0.044939
	20	704.60	722.22	686.99	0.41	0.23	0.60	0.59	0.32	0.87	-5.528634	-0.231362
	25	704.40	722.01	686.79	0.34	0.19	0.49	0.48	0.27	0.71	-5.528758	-0.31583
CJ 208-40	1	775.40	794.79	756.02	0.36	-3.52	4.25	0.47	-4.43	5.62	-5.487051	-0.328902
	2	747.30	765.98	728.62	1.61	-0.30	3.52	2.15	-0.39	4.83	-5.503082	0.332953
	5	753.60	772.44	734.76	0.54	-0.22	1.31	0.72	-0.29	1.78	-5.499436	-0.141861
	10	753.70	772.54	734.86	0.29	-0.09	0.68	0.39	-0.12	0.92	-5.499378	-0.410924
	20	729.40	747.64	711.17	0.29	0.10	0.48	0.40	0.14	0.67	-5.513611	-0.401167
	25	734.20	752.56	715.85	0.22	0.07	0.37	0.30	0.09	0.52	-5.510763	-0.521029
CJ 210-40	1	766.80	785.97	747.63	1.22	-2.64	5.09	1.60	-3.36	6.80	-5.491895	0.202957
	2	751.70	770.49	732.91	1.39	-0.52	3.30	1.85	-0.68	4.50	-5.500532	0.266533
	5	757.60	776.54	738.66	0.46	-0.30	1.23	0.61	-0.39	1.67	-5.497137	-0.213297
	10	732.40	750.71	714.09	0.51	0.13	0.88	0.69	0.17	1.24	-5.511829	-0.160941
	20	705.80	723.45	688.16	0.41	0.22	0.59	0.58	0.31	0.86	-5.527895	-0.238447
	25	735.40	753.79	717.02	0.22	0.07	0.37	0.29	0.09	0.51	-5.510053	-0.531266
SPF1	0	778.60	798.07	759.14								



Sequential Batch leaching															
Leach solution is SPF1															
Placed on orbital shaker table X 24 hours															
Centrifuge 20" X 3500RPM															
Filtered through 0.45um filter															
50 mL split retained, balance placed with same proportion of next soil to be tested (4:1)															
Sample	Vol	Mass	pH	ORP	Conducti	Alkalini	Chloride	Nitrate	Sulfate	NH3-N	U	Ca	Na	Mg	K
	SPF1	(g)		mV	(uS/cm)	(mg/L)	(mg/L)	(mg/L)	(mg/L)	(mg/L)	(ug/L)	(mg/L)	(mg/L)	(mg/L)	(mg/L)
	(mL)					CaCO3)									
CJ 203-40	400	100	7.66	196.7	29400	560	1026	764	18676	1700	5.5	320	5700	440	141
CJ 204-40	315	78.75	7.79	186.3	30100	450	1096	828	19872	1500	19.3	350	5400	510	156
CJ 206-40	240	60	7.83	175.2	29900	560	1120	820	19910	1300	25.4	349	6300	300	177
CJ 205-40	400	100	7.73	187.3	29200	620	1106	756	18504	1600	3	236	5700	210	141
CJ 205-105	315	78.75	7.85	171.4	29800	560	1116	770	18828	1400	19.5	220	6400	200	168
CJ 205-170	240	60	7.96	171.5	29600	520	1196	776	19032	1100	29	199	6500	250	157
CJ 205-235	165	41.25	7.85	173.3	29700	400	1284	804	19700	1800	44.9	203	7000	180	167
CJ 205-300	100	25	7.97	173.5	30600	330	1336	794	19492	900	54.5	196	7800	180	166
SPF1 (start)			6.62	197.4	26800	560				2000	<0.1				
SPF1 (Final)			7.85	191.9	29600	510	1018	738	18272			196	5300	310	129

**Appendix D**

**Dr. William C. Hood, 2006**

**X-Ray Diffraction Analysis Determination of the Mineralogy of  
10 Mancos Shale Samples**

**Prepared for S.M. Stoller Corporation, February 3, 2006  
Grand Junction, Colorado**

**X-ray determination of the mineralogy of 10 Mancos Shale samples**

A report prepared by:

William C. Hood, PhD  
AAPG Certified Professional Geologist No. 2185  
February 3, 2006

## **X-ray determination of the mineralogy of 10 Mancos Shale samples**

### **Introduction**

At the request of Stan Morrison, ten samples of Mancos Shale from the proposed Atlas Mill tailings disposal site near Crescent Junction were examined by x-ray diffraction techniques. The purpose of the examination was to identify the minerals present in the shale, with special emphasis on the clay mineralogy.

### **Summary and Conclusions**

The mineralogy of the ten samples is quite similar, as might be expected in a marine environment such as the Mancos Shale. The non-phylllosilicate minerals identified include quartz, calcite, dolomite, orthoclase, plagioclase and gypsum. These minerals are estimated to comprise from a third to one-half of the total sample. The clay minerals identified, in order of abundance, are mixed-layer illite/smectite (a little less than 38 percent, discrete illite (about 33 percent), kaolinite (about 28 percent) and mixed-layer chlorite/vermiculite (perhaps 2 or 3 percent). The mixed-layer illite/smectite contains at least 60 percent illitic layers, but the actual amount could not be determined with accuracy. Kaolinite crystallites are the largest clay minerals in the samples at an average grain size of 297 Å, followed by illite at 152 Å and mixed-layer illite/smectite at 67 Å.

### **Methods**

The samples were supplied in pulverized form. A portion of each of the 10 original samples was ground for several minutes using a porcelain mortar and pestle. A five-gram sample of this material was removed for clay analysis. The technique used to separate clay minerals is described in Appendix 1. About two grams of the remaining material was ground for several more minutes to obtain a powdered sample for determining the bulk mineralogy.

The powdered bulk samples were loaded into sample holders and scanned from 4.2 to 50 degrees two-theta using the Rigaku Miniflex x-ray diffractometer at Mesa State College.

Clay samples were scanned over the same interval so that direct comparisons of the clay patterns to the bulk samples could be made. Four scans were made of each clay sample: untreated, glycol solvated, heat treated to 300° C and heat treated to 550° C. Glycol solvation is accomplished by putting the samples into a desiccator that contains ethylene glycol and heating the desiccator in an oven at 60° C overnight. The purpose of this treatment is to expand the mineral smectite or smectite layers within mixed-layer clays to approximately 17 Angstroms d-spacing, facilitating the identification of clays containing an expandable smectitic component. The two heat treatments were accomplished by placing the samples into a muffle furnace and heating to the appropriate temperature, as indicated by a thermocouple thermometer. The 300° C heat treatment collapses the expandable layers to 9.2 Angstroms but does not destroy chlorite, chlorite layers in mixed-layer clays or kaolinite. The 550° C heat treatment destroys kaolinite, facilitating its distinction from chlorite.

## Results

**Bulk samples.** The minerals identified in the bulk samples are, in order of general abundance, quartz, dolomite, calcite, plagioclase, orthoclase and gypsum. The estimated abundances of these minerals are given in Table 1 and the method of estimating the abundances is explained in Appendix 2, which also includes diffraction patterns for quartz, calcite, dolomite, albite and gypsum standards.

Table 1. Estimated abundances (in percent) of non-phyllsilicate minerals in bulk Mancos Shale samples.

Sample	Quartz	Calcite	Dolomite	Orthoclase	Plagioclase	Gypsum
CJ201-40	32	3	5	1	1	Tr
CJ202-40	29	3	4	1	1	1
CJ203-40	36	4	5	1	2	1
CJ204-40	33	2	3	1	1	
CJ205-40	28	3	6	1	1	
CJ206-40	39	4	6	1	2	
CJ207-40	25	3	3	1	1	
CJ208-40	38	3	5	1	1	
CJ209-40	27	1	3	2	1	Tr
CJ210-40	24	4	3	1	1	

Minerals were identified using the diffraction peaks listed in Appendix 3. The x-ray patterns for the bulk samples themselves are in Appendix 4. For each sample, two copies of the x-ray diffraction patterns are included, one with d-spacings for most of the peaks and one with most of the peaks identified as to which mineral they result from.

To verify the presence of the carbonate minerals, calcite and dolomite, a small amount of sample CJ-205-40 was placed in a small container, mixed with water and then several drops of dilute hydrochloric acid were added. The sample effervesced vigorously, confirming the presence of carbonate minerals. After the effervescence stopped, the sample was washed twice to remove the dissolved constituents, dried and x-rayed. The peaks associated with calcite disappeared and the dolomite peak was considerably reduced in intensity, confirming the presence of both minerals (Figure 1).

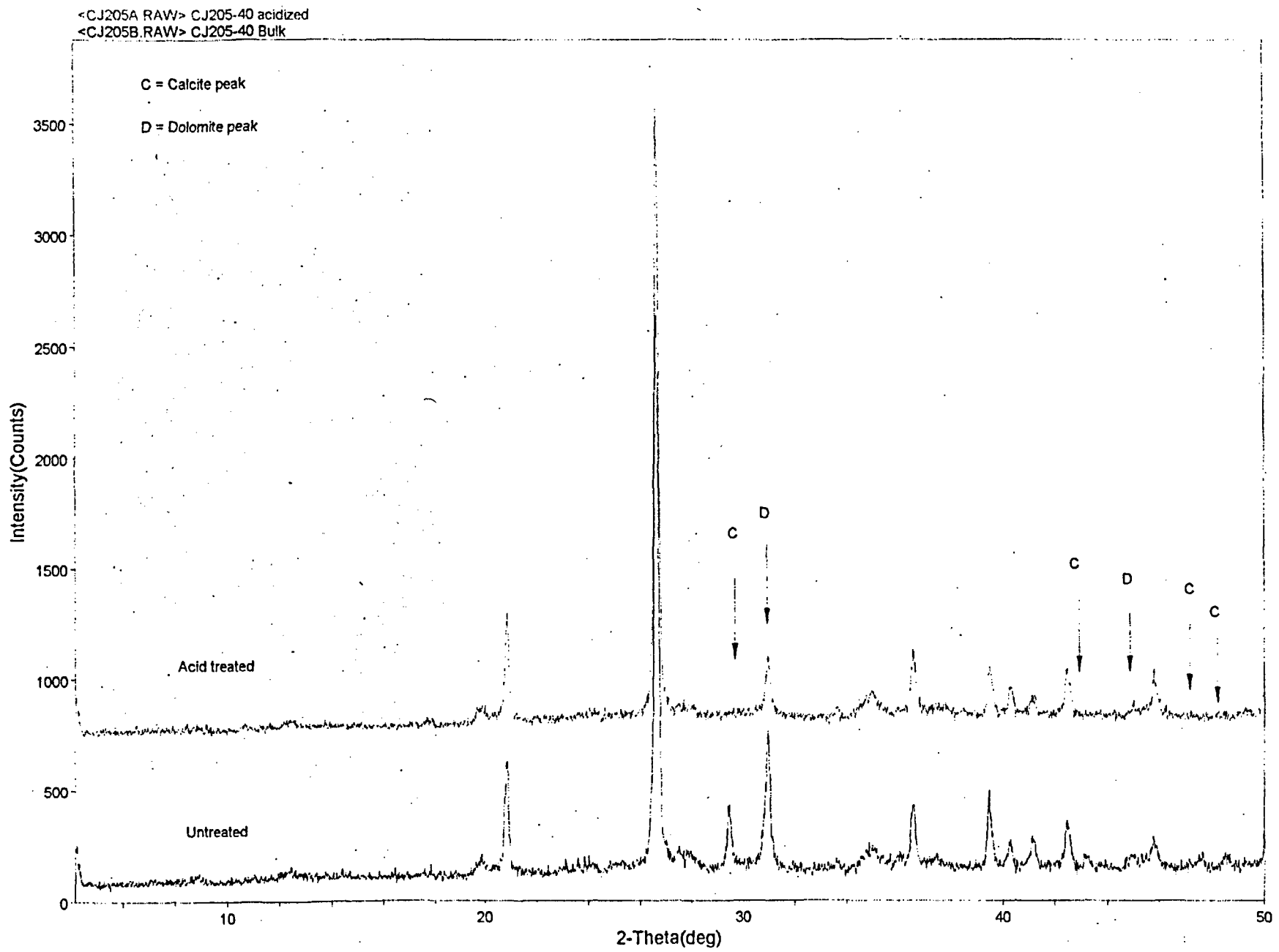


Fig. 1. Comparison of sample CJ201-40 before and after acid treatment.

## Clay separates.

### Identification of clay minerals.

Examination of a typical x-ray diffraction pattern reveals the presence of four phyllosilicate and two non-phyllosilicate minerals in these samples. The two non-phyllosilicates are quartz and dolomite. The phyllosilicate minerals identified are kaolinite, illite, mixed-layer illite/smectite and mixed-layer chlorite/vermiculite. The following paragraphs explain how these minerals were identified.

Kaolinite is recognized by peaks at approximately 7.14 Angstroms, 3.57 Angstroms and 2.38 Angstroms. These correspond to the first, second and third order diffractions from the (001) plane. These spacings do not change when the sample is glycol-solvated or heated to 300° C. They disappear upon heating the sample to 550° C, indicating that the kaolinite has been destroyed. Kaolinite is present in all of the samples

Illite is recognized by peaks at approximately 10 Angstroms, 5.0 Angstroms, 3.3 Angstroms, 2.5 Angstroms and 2.0 Angstroms. These represent the first, second, third, fourth and fifth order diffractions from the (001) plane. Peak intensities are strongest for the odd orders, with the third order peak being the strongest, as is typical for a dioctahedral phyllosilicate. In the case of the CJ sample set, the peak at 3.3 Angstroms (3<sup>rd</sup> order) is quite strong because it is combined with the most intense peak for quartz. The fourth order peak at 2.5 Angstroms is very weak, hardly rising above background in most of the samples. Glycol solvation shifts the peak of expandable minerals, making the 10 Angstrom peak quite obvious. Heat treatments bring about slight peak shifts and significant increases in intensity. These changes are not so much due to changes in the illite itself, but are mainly a result of the collapse of mixed-layer clays to 9.9 Angstroms or slightly less and the diffraction from that material being added to that of the discrete illite.

Mixed-layer illite/smectite is recognized by a broad peak between about 11.2 and 11.9 Angstroms in the untreated sample. The peak is broad and there is enough "chatter" in the background that it is difficult to pick the center of the peak with any certainty. Another complication is that the peak overlaps the peaks from illite and chlorite. The additive effects of these peaks can cause the apparent peak position to shift. In the glycol-solvated sample, the peak shifts to higher d-spacing (lower angle 2-theta or left on the diffraction pattern), indicating expansion of smectitic layers. In these samples, the shift does not usually result in a well-developed peak, but rather a significant drop in intensity near the 10 Angstrom illite peak and a smeared-out low hump between 14 and 17 Angstroms. Heating to 300° C collapses the expandable layers to approximately 9.9 Angstroms, resulting in a marked increase in intensity of the peak at approximately 10 Angstroms. This peak is asymmetric toward low angles, suggesting that not all of the layers are totally collapsed. Heating to 550° C collapses these layers and sharpens the peak at approximately 10 Angstroms.

The presence of small amounts of a chlorite component in the CJ samples is recognized by a low, broad peak about 14.3 Angstroms and a sharper, third order peak, at 4.8 Angstroms, which appears as a shoulder or small peak on the high angle side of the second-order illite peak. The 14.3 Angstrom peak is small and sometimes is just a shoulder on the mixed-layer

illite smectite peak. It persists through glycol solvation and low heat and does not seem to change position, although interference from mixed-layer illite/smectite makes the peak position indeterminate. The peak remains after heating to 550° C but shifts to lower d-spacings, typically about 13.5 angstroms. The shift indicates that the material is not a pure chlorite, but rather a mixed-layer material. To summarize its characteristics, it does not seem to expand upon glycol salvation and collapses somewhat with high heat. Based on the material presented in Moore and Reynolds (1997) the mineral is probably a mixed-layer chlorite/vermiculite.

Figure 2 shows the results of the various treatments for sample CJ201-40 combined into one display to show how the patterns change with various treatments. Stacked patterns for all ten of the samples are contained in Appendix 5. The individual x-ray patterns are located in Appendix 6.

#### Estimating the relative amounts of clay minerals.

To estimate the relative amounts of the various clay minerals, the patterns of the glycol-solvated samples were used. By expanding the smectitic layers in mixed-layer clay, this treatment separates peaks of clays with expandable components from the 10 Angstrom peak of illite. Although the glycol-solvated pattern allows the separation of discrete illite, it does not allow the separation of the mixed-layer illite/smectite from the mixed-layer chlorite/vermiculite.

The first step is to draw a smooth background through the low-angle portion of the x-ray pattern. Figure 3 shows what this looks like. Once the background curve is established, the Jade computer program was used to eliminate the background. Appendix 7 contains the patterns after this step. The next step was to use the peak-painting module within Jade to determine the area under the peak for each of the first-order peaks of mixed-layer clay, discrete illite and kaolinite. Figure 4 shows the painted peaks of a typical sample and Table 2 gives the results of these measurements.

Table 2. Areas under the peaks, as calculated by the Jade computer program.

Sample	Mixed-layer	Illite	Kaolinite	Total
CJ201-40	330	223	214	767
CJ202-40	208	198	141	547
CJ203-40	329	239	194	762
CJ204-40	302	225	220	747
CJ205-40	267	181	134	582
CJ206-40	253	235	200	688
CJ207-40	127	170	177	474
CJ208-40	263	275	216	754
CJ209-40	215	172	160	547
CJ210-40	191	181	123	495



<CJ201HH RAW> CJ201-40 H550  
 <CJ201H RAW> CJ201-40 H300  
 <CJ201G RAW> CJ201-40 glycol  
 <CJ201C RAW> CJ201-40 Clay

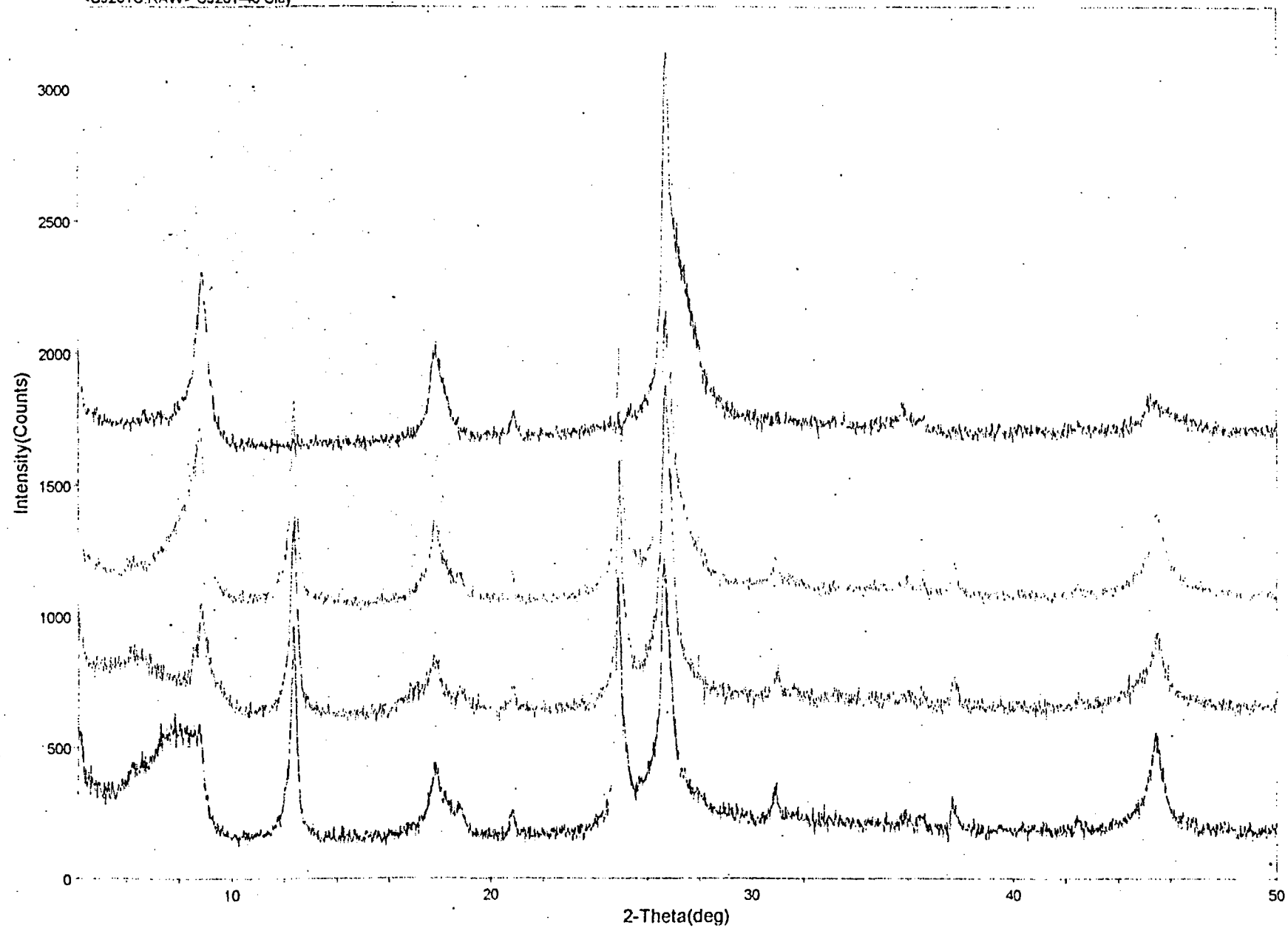


Fig 2 Stacked x-ray patterns showing effects of various treatments, sample CJ201-40.

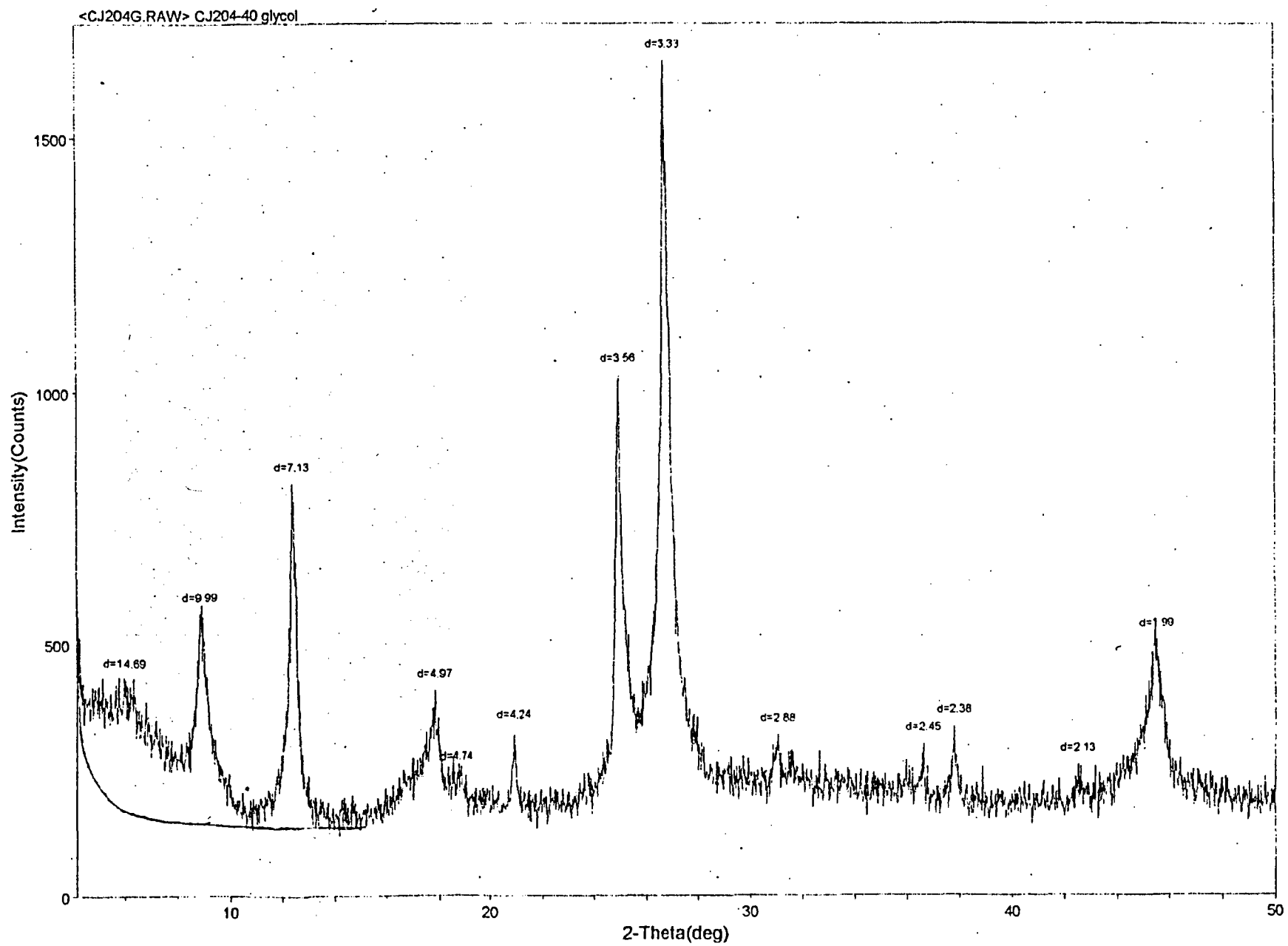


Fig. 3 Estimated low-angle background shown in red, sample CJ204-40.

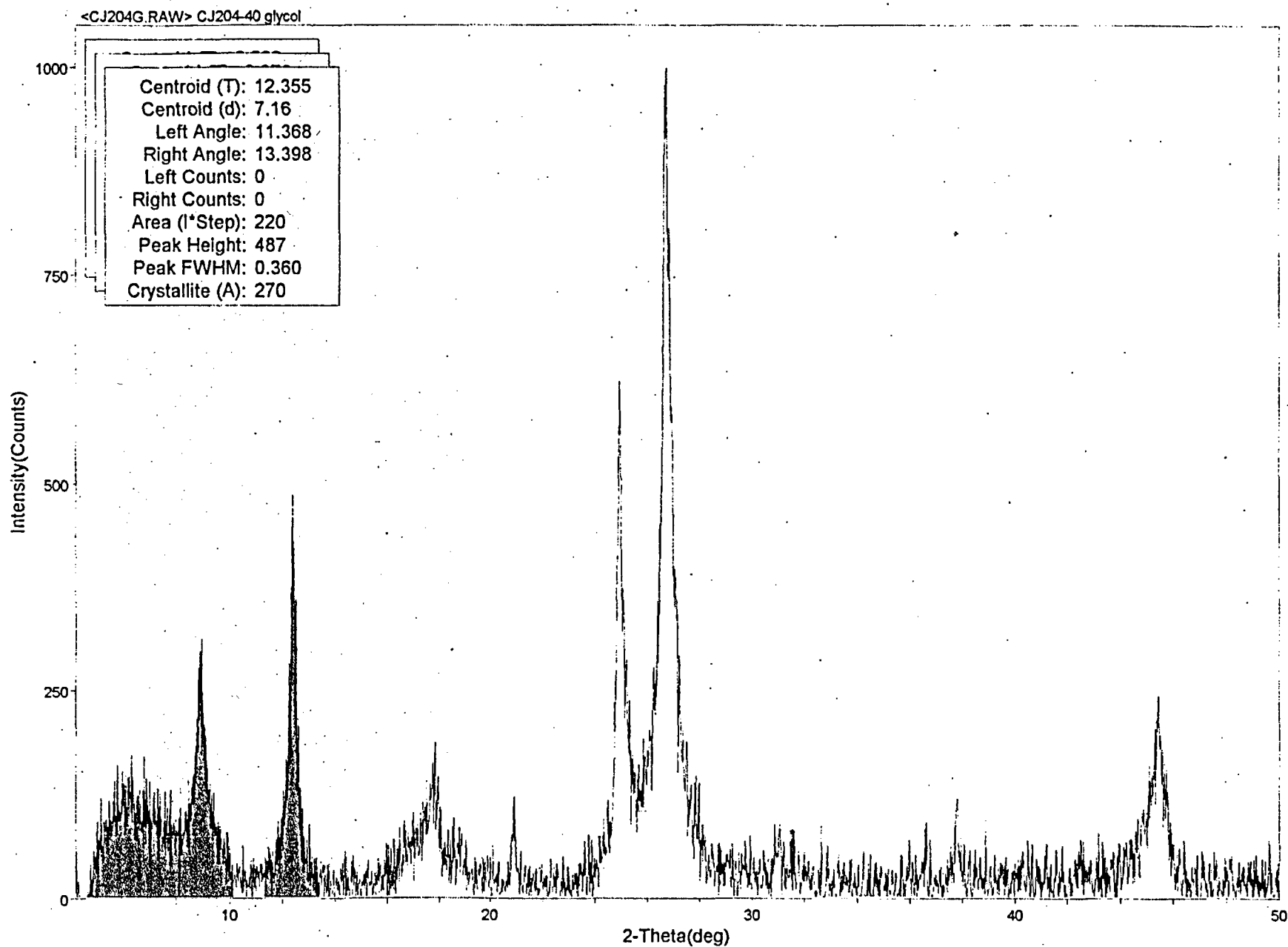


Fig. 4. Measured areas under the peaks, sample CJ204-40.

Finally, the areas under the peaks of the three minerals were added and the relative amounts of the components calculated as a percentage of the total. These values are given in Table 3.

Table 3. Estimated abundance of individual clays, derived from areas under the peaks.

Sample	Mixed-layer	Illite	Kaolinite
CJ201-40	43	29	28
CJ202-40	38	36	26
CJ203-40	43	31	25
CJ204-40	40	30	29
CJ205-40	46	31	23
CJ206-40	37	34	29
CJ207-40	27	36	37
CJ208-40	35	36	29
CJ209-40	39	31	29
CJ210-40	39	37	25

Note. Mixed-layer includes both mixed-layer illite/smectite plus a much smaller amount of mixed-layer chlorite/vermiculite. Mixed-layer chlorite/vermiculite makes up perhaps 5 percent of the mixed-layer component.

The values in Table 3 should be taken only as semi-quantitative approximations. To obtain more quantitative values, standards of similar grain size and crystallinity would have to be mixed in various amounts and x-rayed under the same conditions as the Mancos Shale samples. Such standards were not available. The values that were obtained in this study are, however, useful for inter-sample comparisons.

Little published work exists on the clay mineralogy of the Mancos Shale in the Colorado Plateau region. L. G. Schultz, cited in Eckel, (p. 276) reports that the clays consist of 50 to 60 percent mixed-layer illite/smectite, 12 to 15 percent poorly ordered kaolinite, and 30 to 35 percent discrete illite. No information was given about the method used to determine these amounts. The CJ samples contain more kaolinite and less mixed-layer illite/smectite than reported by Schultz.

#### Amount of illite in mixed-layer illite/smectite

The amount of illitic and smectitic components in the mixed-layer illite/smectite is very difficult to determine in this sample set due to interference among the peaks of the various minerals. The usual procedure for determining the amount of illite and smectite in a mixed-layered illite/smectite is to use the glycol solvated pattern and determine the peak positions for the (001)/(002) and (002)/(003) peaks. Unfortunately in the CJ sample set, the (001)/(002) peak (between 10.3 and 9.0° 2-theta) lies on the flank of a much stronger illite peak and cannot be resolved. Likewise, the (002)/(003) peak (between 15.8 and 17.4° 2-theta) lies on the flank of the second order illite peak and just appears as a broadening of the illite peak and not as a distinct peak itself. However, this fact by itself suggests that the material is richer in the illite component than the smectite component. Materials with large amounts of smectite have peaks at the low angle end of the range, whereas peaks with a large

amount of illite component have peaks at the high end of the range, close to the peak for pure illite

In order to get an independent approximation as to the amount of illite layers in the mixed-layer illite/smectite, I examined the position of the (001)/(001) peak in the Mg-saturated but otherwise untreated sample. Pure smectite would have a peak at 14 Angstroms and pure illite a peak at 10 Angstroms. The assumption this method makes is that there is complete randomness in the mixing of illitic and smectitic components and that the peak position varies in a straight-line manner from 14 to 10 Angstroms. Table 4 presents the results of this analysis. The values are rounded to the nearest 10 percent because of the difficulty in picking the peak position.

Table 4. Estimated amounts of illitic layers in mixed-layer illite/smectite.

Sample	d-spacing	% illitic layers
CJ201-40	11.3	70
CJ202-40	11.6	60
CJ203-40	11.6	60
CJ204-40	11.5	60
CJ205-40	11.7	60
CJ206-40	11.8	60
CJ207-40	11.9	50
CJ208-40	11.8	60
CJ209-40	11.6	60
CJ210-40	11.6	60

The average amount of illitic layers in the material is 60 percent. This should probably be considered to be a minimum estimation, because the (002)/(003) peak of the glycol solvated samples suggest a value that would probably be more on the order of 80 percent illitic layers.

### Crystallite size.

The Jade computer program contains an algorithm for determining crystallite size of crystallites smaller than 1 micron. This information is produced as a by-product of measuring the area under a peak and became available by determining the relative amounts of the various clay minerals. In general, kaolinite has the largest grains with an average size of 297 Å, followed by illite at 152 Å and the mixed-layer material at 67 Å (Table 5).

Table 5. Crystallite size of clay minerals in the CJ sample set.

Samples	Mixed-layer	Illite	Kaolinite
CJ201-40	58	159	334
CJ202-40	74	159	337
CJ203-40	54	133	391
CJ204-40	58	149	270
CJ205-40	57	153	281
CJ206-40	65	171	332
CJ207-40	97	171	231
CJ208-40	71	120	274
CJ209-40	76	160	220
CJ210-40	57	148	295

### References

- Eckel, E. B. (1997) Minerals of Colorado: Friends of Mineralogy Edition, Fulcrum Publishers.
- Moore, D. M., and R. C. Reynolds (1997) X-ray diffraction and the identification and analysis of clay minerals, 2<sup>nd</sup> ed.: Oxford University Press, New York, 378 p.
- Nadeau, P. H. and R. C. Reynolds (1981) Burial and contact metamorphism in the Mancos Shale: Clays and Clay Minerals, 29, 249-259.

## **Appendix 1.**

**Method used to separate and prepare clay minerals for x-ray diffraction**

## **Appendix 1. Method used to separate and prepare clay minerals for x-ray diffraction**

1. Place bulk sample in water overnight to remove any easily soluble material and to partially disaggregate clay. Remove as much of the water as practical without losing the sample.
2. Add fresh water and ¼ tsp. of sodium metaphosphate (Calgon). Agitate vigorously to get the material into suspension.
3. Allow to sit undisturbed for 8 hrs. With a turkey baster or some other large pipette, remove the upper 10 cm. of the suspension. Place this in a separate container. This suspension contains clay (less than 2 micron particles).
4. Re-suspend the bulk material to collect additional clay. If the original suspension yielded little clay or if it flocculated, add additional Calgon. Otherwise, do not add Calgon.
5. Add ¼ tsp. of magnesium chloride or magnesium sulfate to the clay suspension. This does two things; it flocculates the clay and begins the magnesium saturation process. When the flocculated particles have settled to the bottom of the container, remove as much water as you can with the pipette.
6. After re-suspending the bulk sample, repeat step 3. Add the clay suspension to the container with the flocculated clay. Repeat step 5.
7. Repeat steps 4 and 5, but do not add more Calgon to the bulk sample. If there is insufficient clay to do the required analysis, steps 4 & 5 can be repeated as necessary.
8. When sufficient clay has been collected and step 5 has been completed on the accumulated clay, the clay should by now be Mg saturated. At this point, centrifuge the sample to concentrate the clay and remove as much of the water as possible.
9. Add distilled water and get the flocculated clay into suspension. Centrifuge and remove the water.
10. Repeat step 9 until you are confident that you have removed the excess Mg. This usually takes 3 washings, but it depends on the size of the centrifuge tube. When the excess Mg salt is gone, it will take much longer to clear the sample because the finest fraction of clay will start staying in suspension.
11. Add enough water to make a rather thick suspension of clay and agitate vigorously. Allow to sit for a couple of hours so that clumps of clay will settle out. With a pipette, collect the clay from the top centimeter (to obtain only <2 micron material and not the larger flocs), put it onto a glass slide and allow to dry.

If the sample contains a lot of smectite or if it too thick, it may curl up off of the slide. There are two things that can be done if this happens. Make another slide using less material or frost the glass slide lightly and remake the sample.



## **Appendix 2.**

### **Estimating the abundance of non-phyllosilicate minerals in Mancos Shale**

## Appendix 2. Estimating the abundance of non-phyllsilicate minerals in Mancos Shale

The amounts of non-phyllsilicate minerals in the Mancos Shale samples were estimated using the following technique. First, diffraction patterns of pure samples of quartz, calcite, dolomite and albite were obtained under the same conditions as the bulk samples of Mancos Shale. Because the intensities of the most intense peak of the minerals were not identical, the next step was to obtain a normalization factor so that each of the other minerals could be compared to quartz. This was done by first removing the background from the patterns and determining the peak intensity, then dividing the peak intensity of each of the minerals into the peak intensity of quartz. A pure sample of orthoclase was not available, so the intensity of the main peak of this mineral was assumed to be the same as that of albite. This most likely gives an incorrect normalization factor, but because this mineral is present in amounts just slightly above the detection limit, it makes little difference in the interpretation.

The second step is to normalize the peak intensities to quartz and sum the various peak intensities. This gives an approximation of what the quartz peak intensity would be if only quartz plus phyllsilicate minerals were present in the samples. The ratio of intensities of the normalized peaks to the pure quartz standard is a measure of the amount of non-phyllsilicate minerals present in the sample. This assumes that the presence of phyllsilicate minerals suppresses the quartz peak in an amount directly proportional to their abundance. The total amount of non-phyllsilicate minerals is estimated from 33 to 52 percent in the 10 Mancos Shale samples.

The final step is to compare the intensities of the various normalized peaks to the total intensity values and multiply that by the percent of non-phyllsilicate minerals obtained in the preceding step. This gives an approximation of the abundance of each mineral in the bulk sample.

The mineral gypsum was not included in the calculation just described because it was detected in only 4 samples. By comparison with the values for the other minerals, the amount of gypsum is estimated to be 1 percent or less.

The data and results of calculations are shown on the next page. Diffraction patterns for quartz, calcite, dolomite, albite and gypsum follow the calculations page.

# Method for calculating abundance of non-phyllsilicate minerals in bulk samples

Normalize calcite, dolomite and feldspar standards to quartz (background removed)

	Pk. Height	Factor
Quartz	6528	1.000
Calcite	7154	0.912
Dolomite	8683	0.752
Albite	7647	0.854

Measured peak heights (in counts/second) after background removed

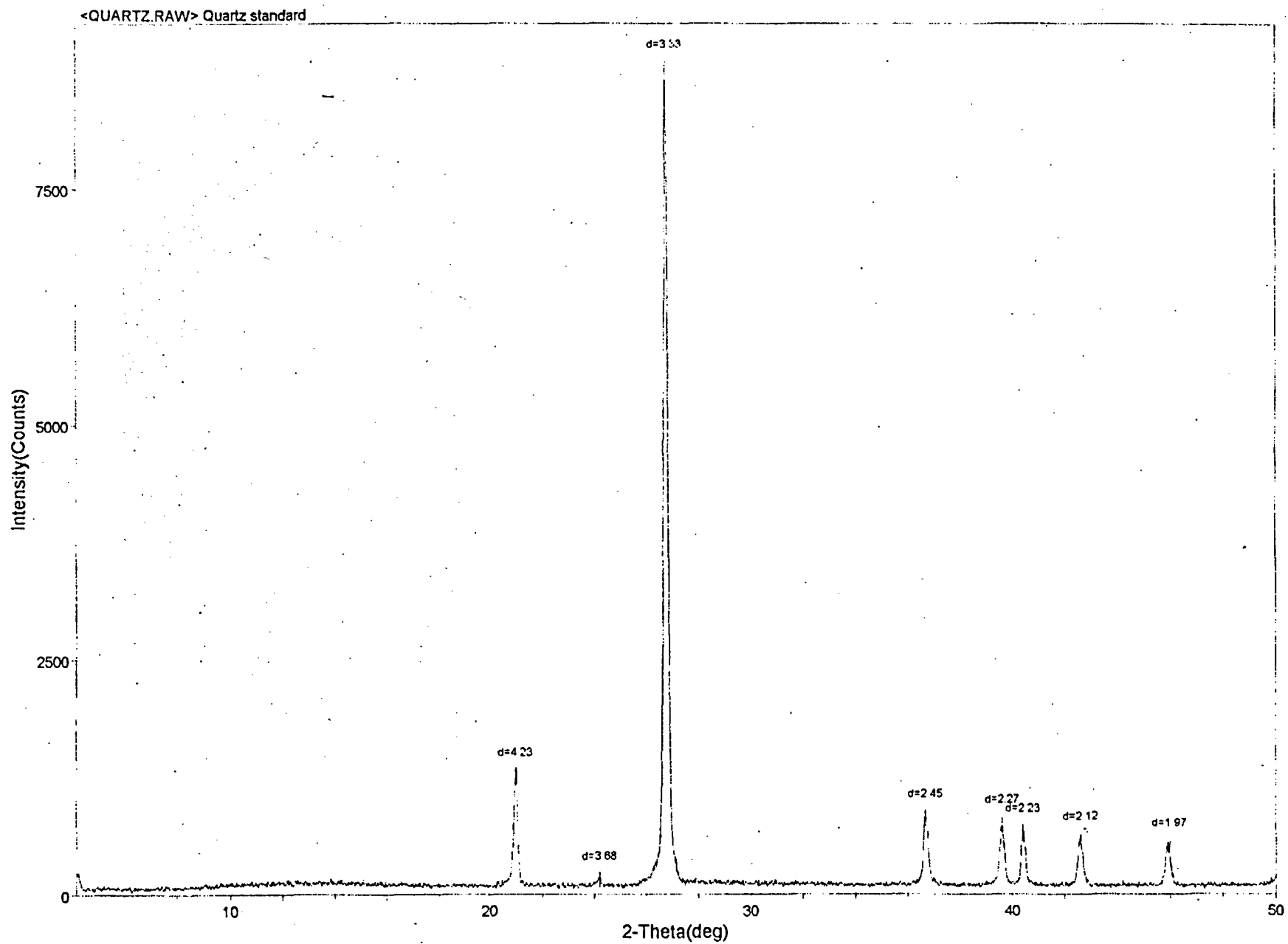
Sample	Quartz	Calcite	Dolomite	Orthoclase	Plagioclase
CJ201-40	2091	199	395	96	68
CJ202-40	1866	240	365	87	86
CJ203-40	2334	283	424	113	121
CJ204-40	2145	178	277	56	102
CJ205-40	1850	233	496	86	90
CJ206-40	2535	251	559	90	128
CJ207-40	1606	213	222	79	104
CJ208-40	2495	241	408	94	94
CJ209-40	1768	88	288	138	114
CJ210-40	1566	268	293	113	93

Peak heights (in counts/second) normalized to quartz

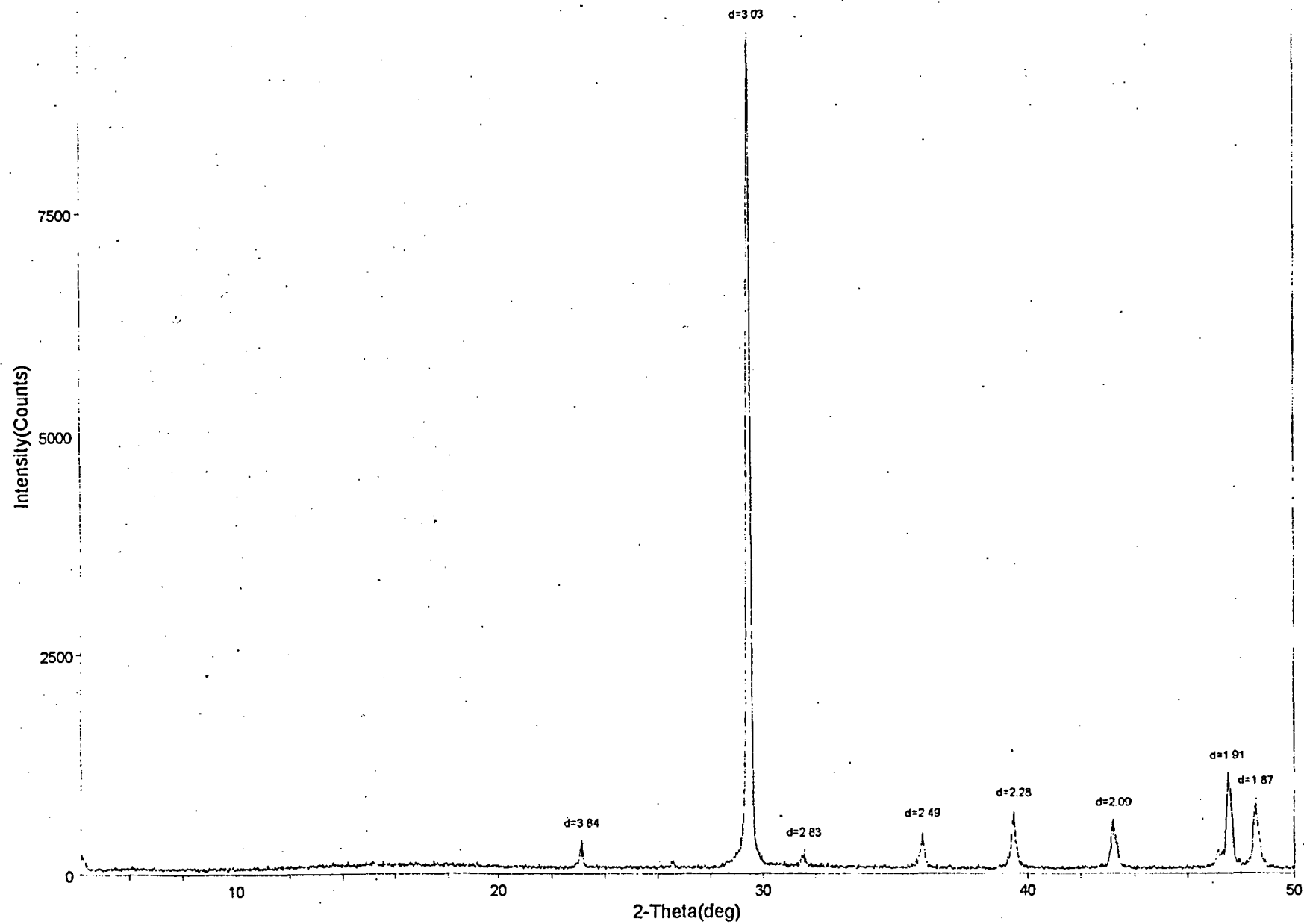
Sample	Quartz	Calcite	Dolomite	Orthoclase	Plagioclase	Total	Percent Non-clay
CJ201-40	2091	182	297	82	58	2710	42
CJ202-40	1866	219	274	74	73	2507	38
CJ203-40	2334	258	319	96	103	3111	48
CJ204-40	2145	162	208	48	87	2651	41
CJ205-40	1850	213	373	73	77	2586	40
CJ206-40	2535	229	420	77	109	3370	52
CJ207-40	1606	194	167	67	89	2123	33
CJ208-40	2495	220	307	80	80	3182	49
CJ209-40	1768	80	217	118	97	2280	35
CJ210-40	1566	245	220	96	79	2207	34

Estimated Percentages of Non-phyllsilicate minerals

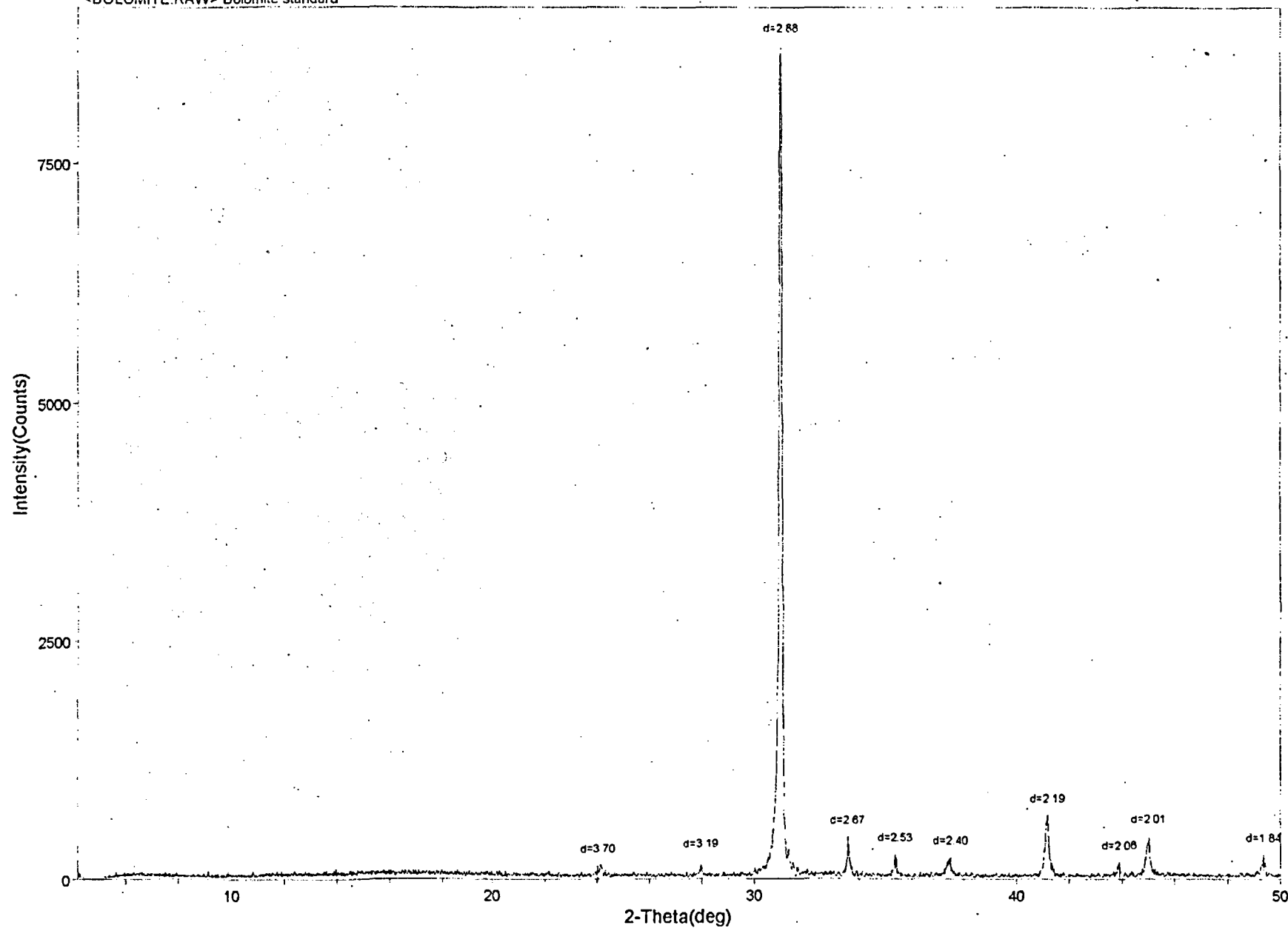
Sample	Quartz	Calcite	Dolomite	Orthoclase	Plagioclase	Gypsum
CJ201-40	32	3	5	1	1	Tr
CJ202-40	29	3	4	1	1	1
CJ203-40	36	4	5	1	2	1
CJ204-40	33	2	3	1	1	
CJ205-40	28	3	6	1	1	
CJ206-40	39	4	6	1	2	
CJ207-40	25	3	3	1	1	
CJ208-40	38	3	5	1	1	
CJ209-40	27	1	3	2	1	Tr
CJ210-40	24	4	3	1	1	

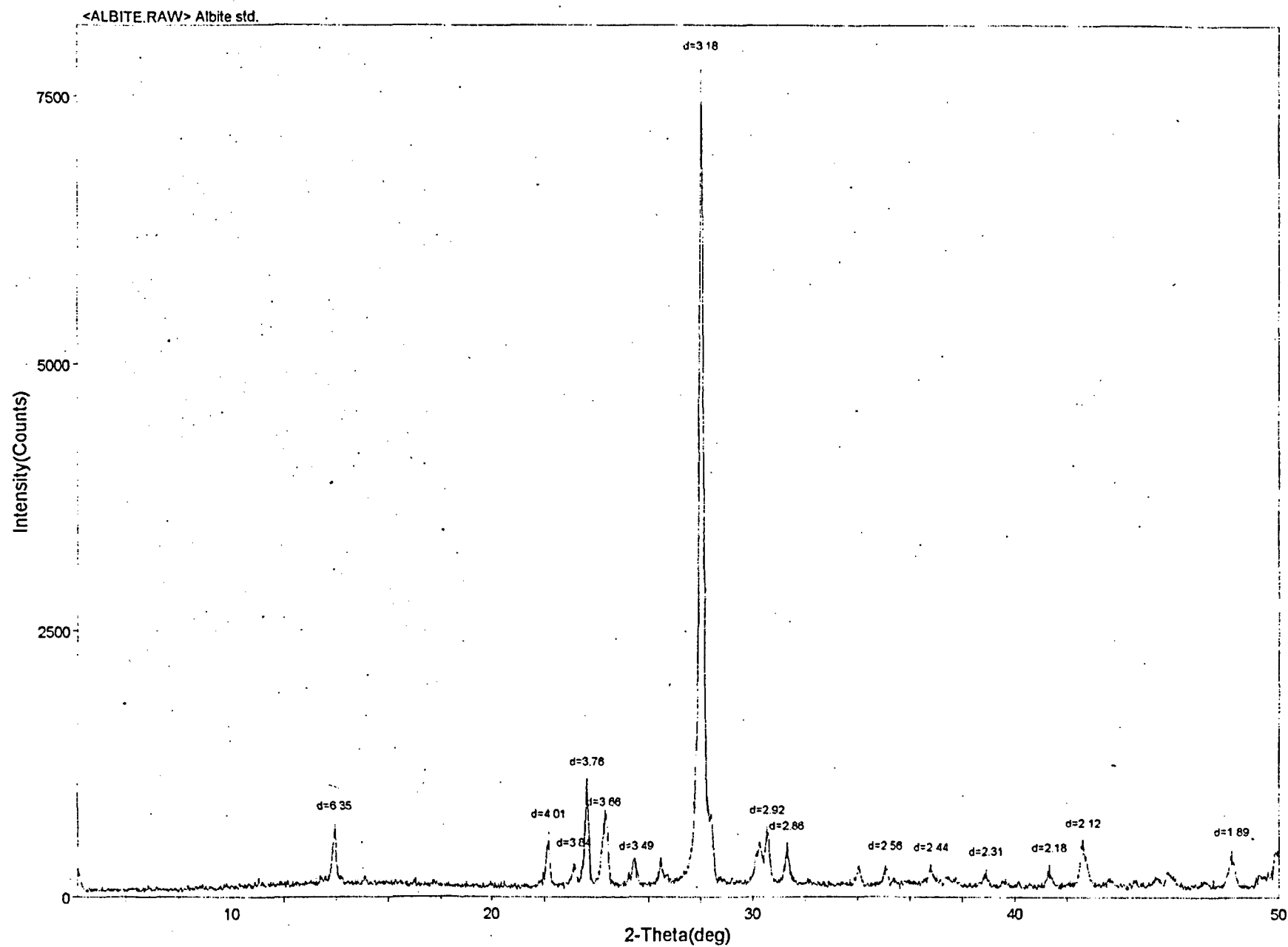


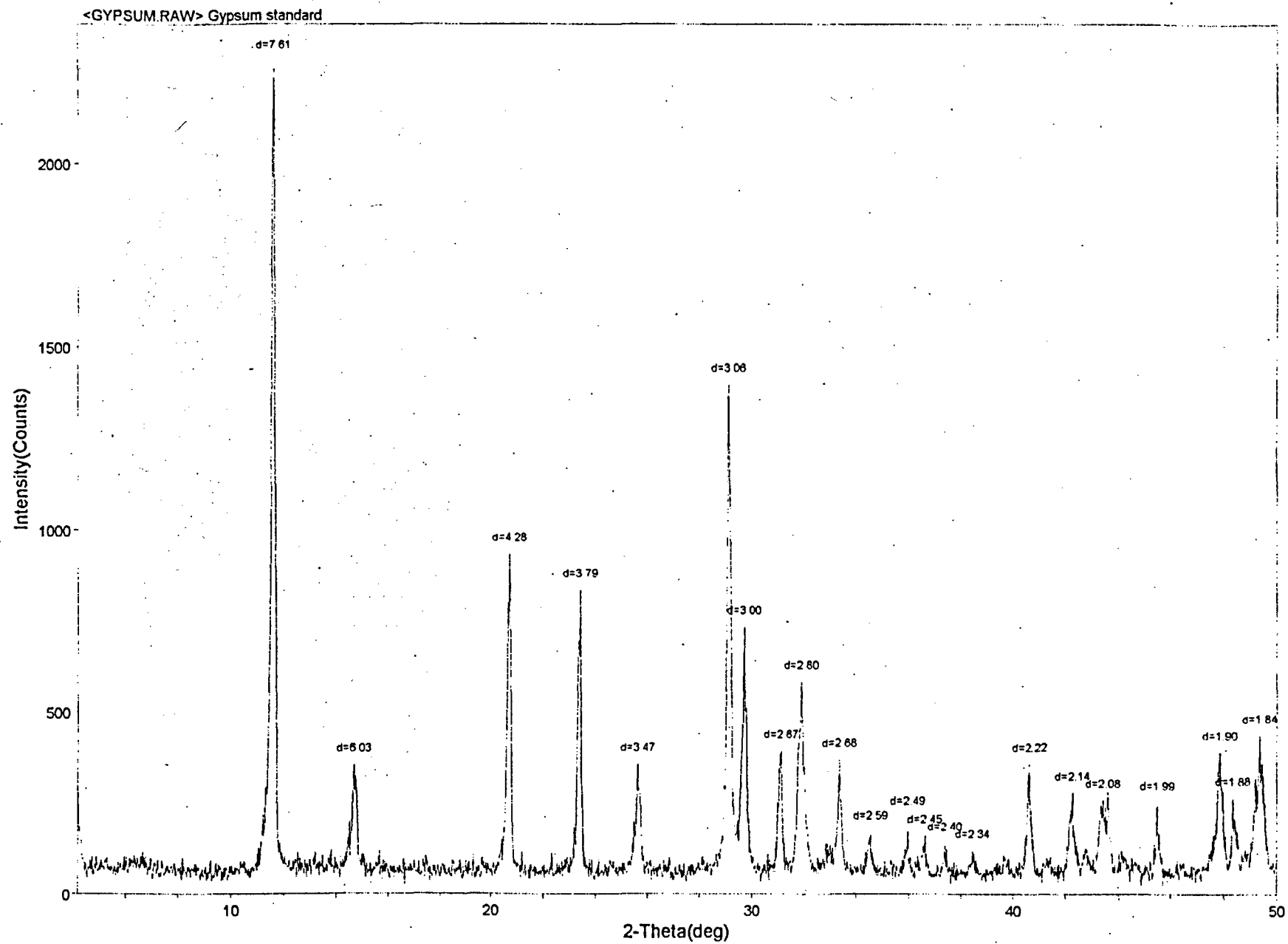
<CALCITE.RAW> Calcite std.



<DOLOMITE.RAW> Dolomite standard









### **Appendix 3.**

**X-ray diffraction peaks used to identify minerals present in bulk samples**

### Appendix 3. X-ray diffraction peaks used to identify minerals present in bulk samples.

14.00	Smectite or chlorite
14-10	Mixed-layer clays
10.00	Illite
7.61	Gypsum
7.14	Kaolinite
6.03	Gypsum
4.48	Kaolinite
4.28	Gypsum
4.26	Quartz
3.86	Calcite
3.80	Gypsum
3.58	Kaolinite
3.47	Gypsum
3.34	Quartz
3.33	Illite
3.29-3.24	Orthoclase
3.18	Plagioclase
3.07	Gypsum
3.04	Calcite
3.00	Gypsum
2.88	Dolomite
2.67	Dolomite
2.57	Kaolinite
2.50	Kaolinite
2.50	Calcite
2.46	Quartz
2.39	Kaolinite
2.34	Kaolinite
2.29	Calcite
2.28	Quartz
2.24	Quartz
2.19	Dolomite
2.13	Quartz
2.10	Calcite
2.01	Illite
1.99	Kaolinite
1.98	Quartz
1.91	Calcite
1.88	Calcite
1.82	Quartz

Notes: Not all of the peaks listed in the ASTM data file of x-ray diffraction peaks were observed for these minerals. Except for quartz, most were present in too small amounts for

any peaks except for those of high intensity to appear

Not all peaks appear at their ideal position. In mixtures of several minerals such as these samples, interference of peaks from different minerals can cause the resulting peak to shift. Also, it is difficult to determine exactly the position of the top of a peak when the peaks are of low intensity such as most of the peaks that appear on these samples.

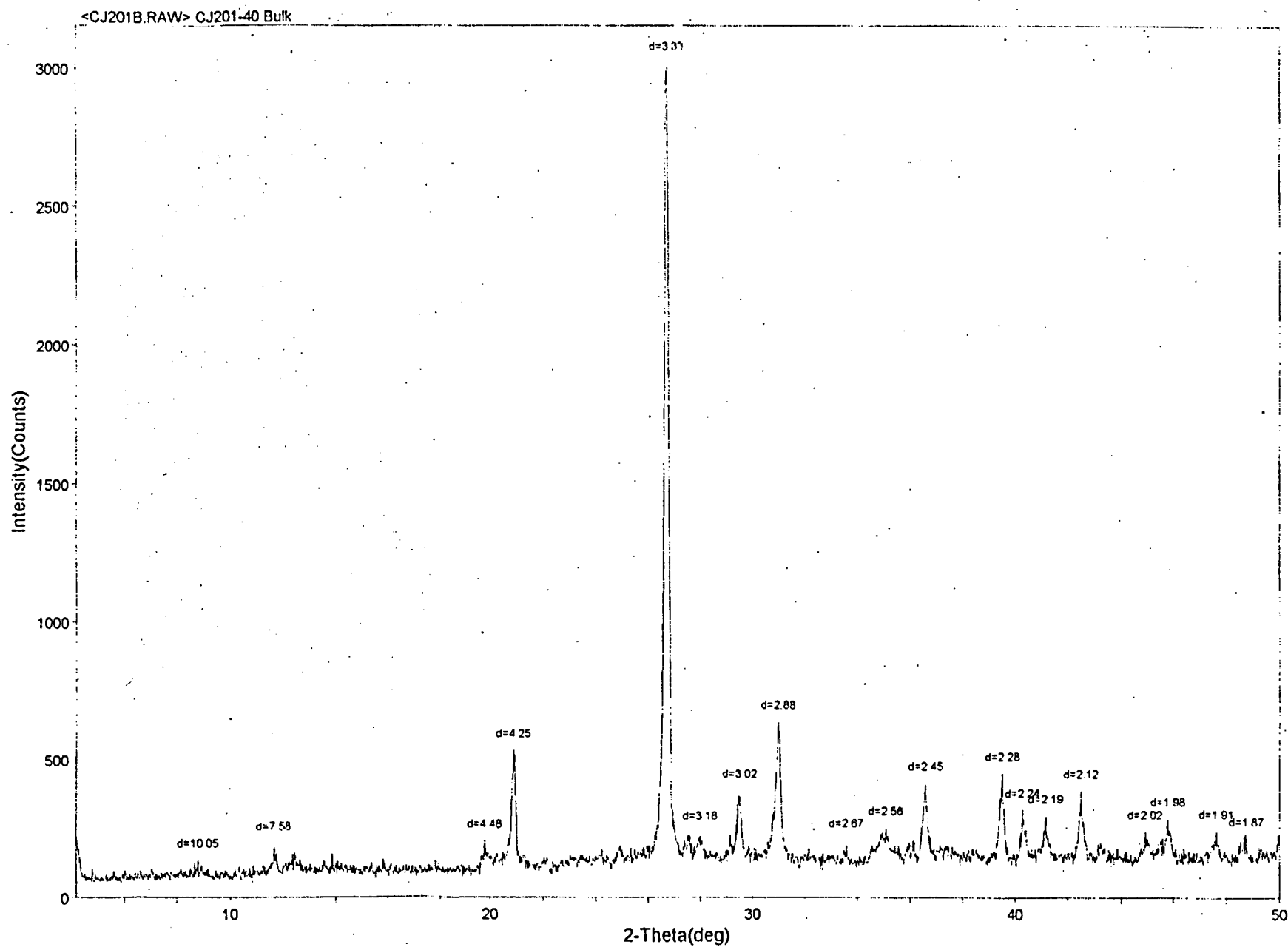
#### **Appendix 4.**

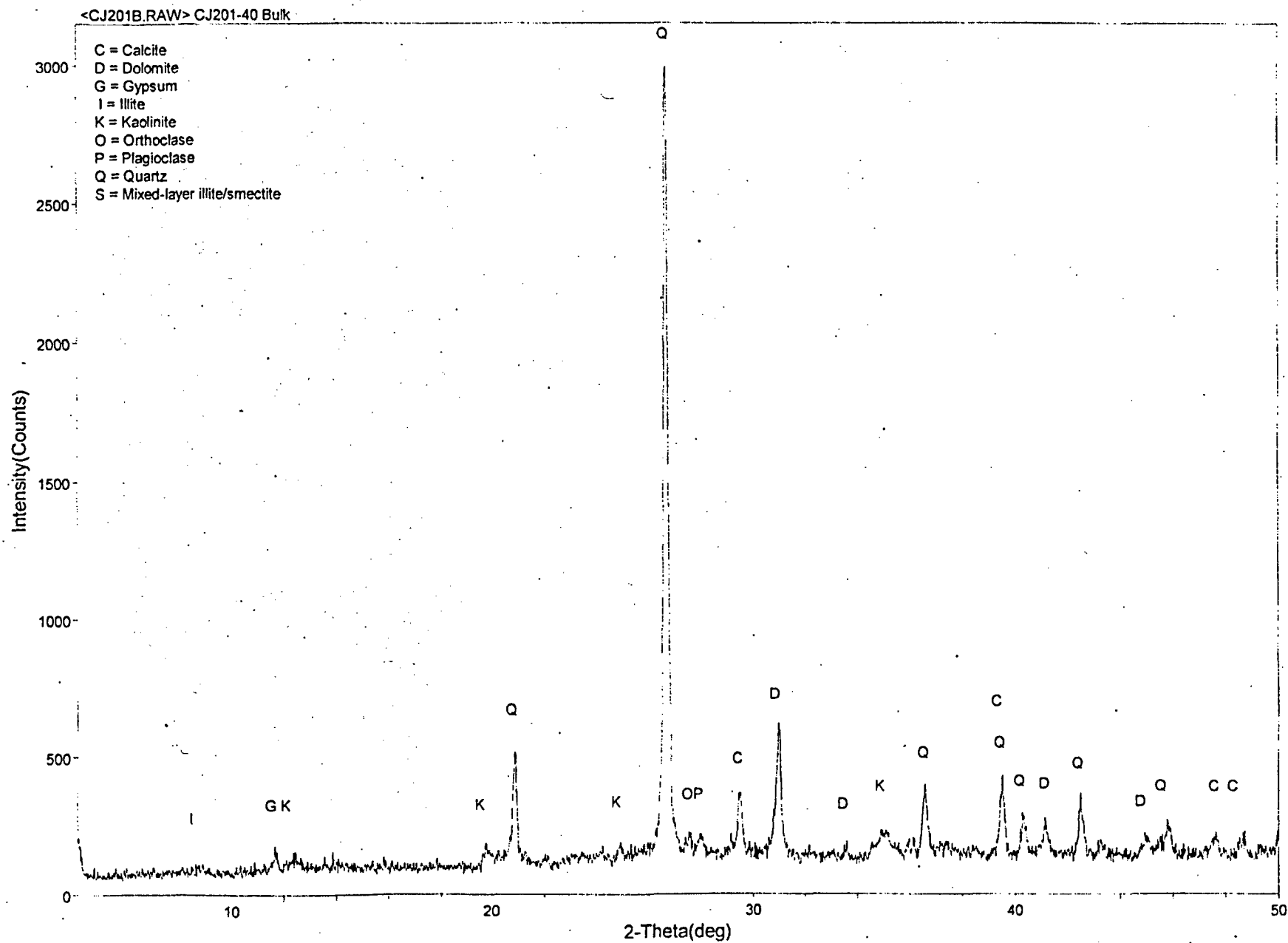
#### **X-ray diffraction patterns of bulk samples**

#### **Appendix 4. X-ray diffraction patterns of bulk samples.**

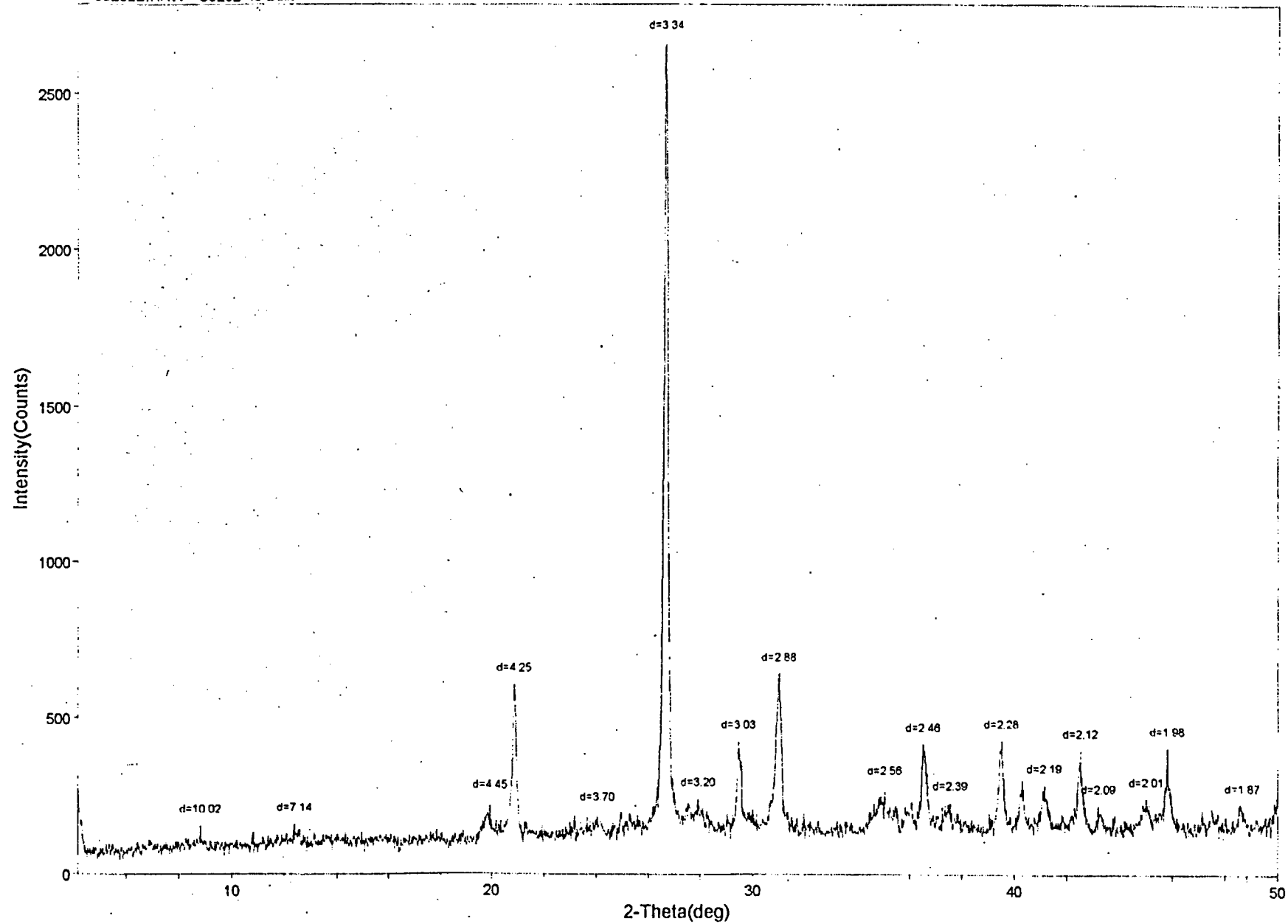
Two copies of each diffraction pattern are presented. The first of each pair is annotated with the d-spacings of most diffraction peaks. A few were not annotated because the closeness of other peaks would make the annotations unreadable.

The second of each pair is annotated with letters showing the identities of the most intense peaks. Not all of the minor peaks were annotated, although they were accounted for.

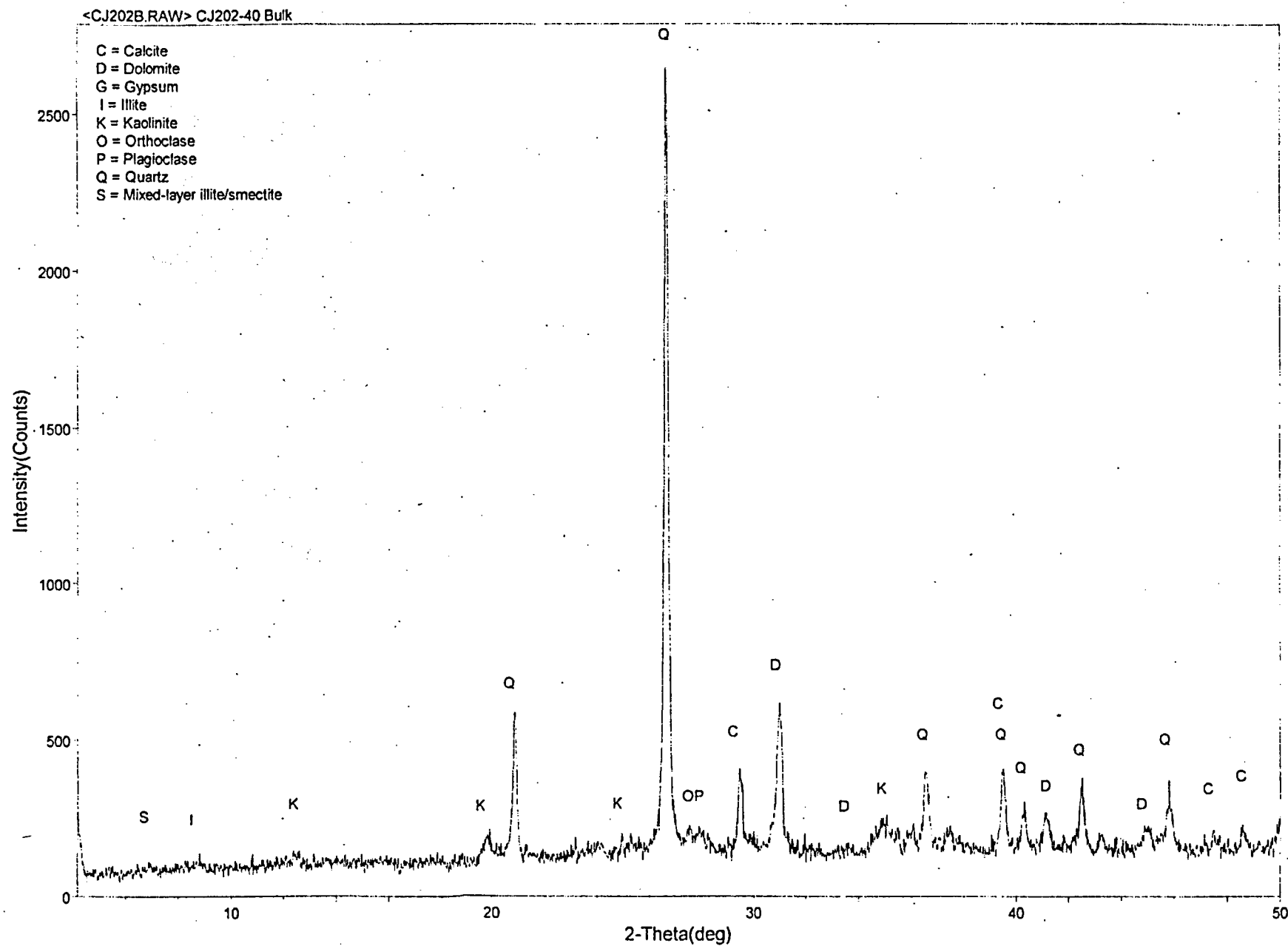


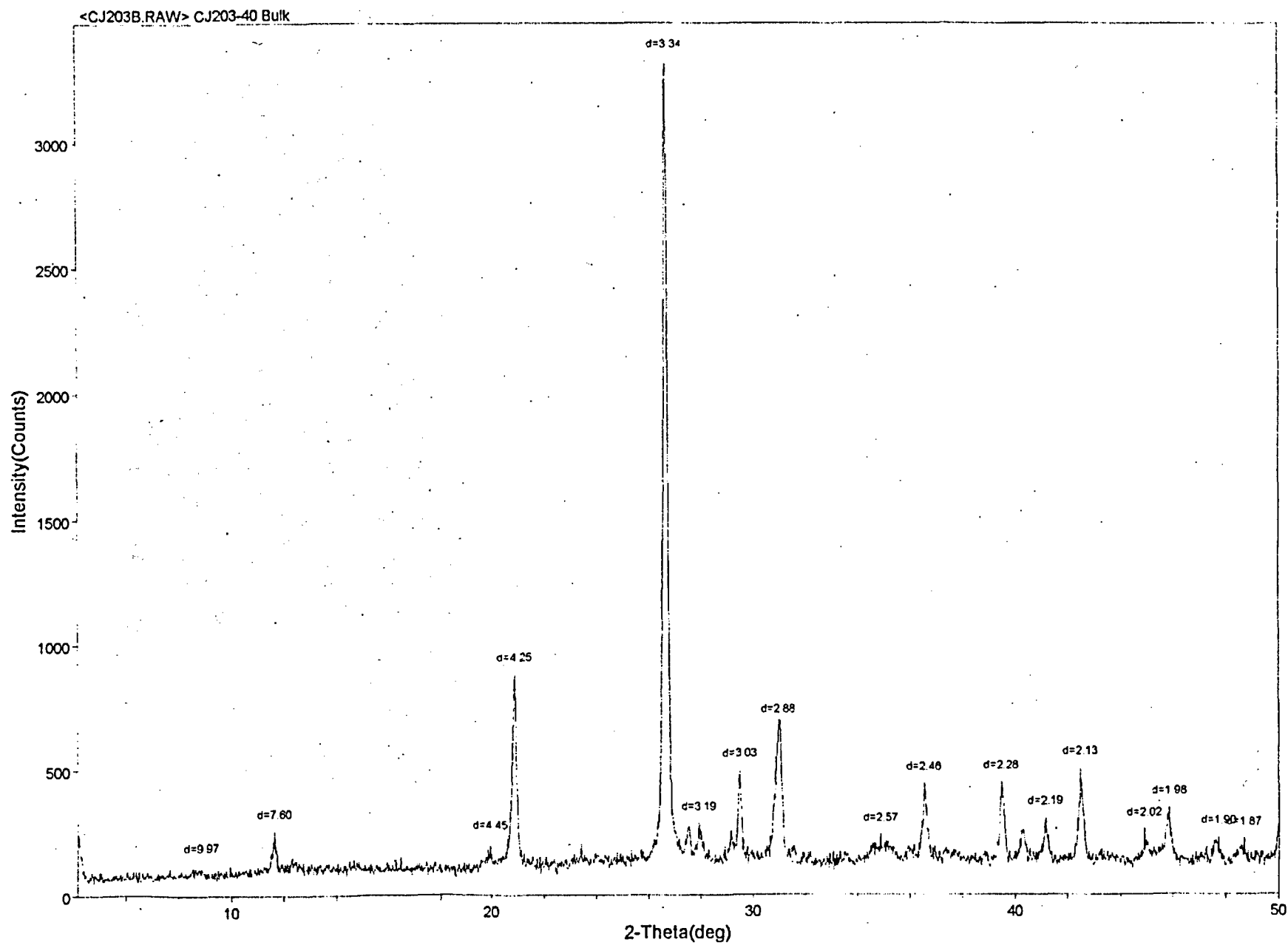


<CJ202B.RAW> CJ202-40 Bulk

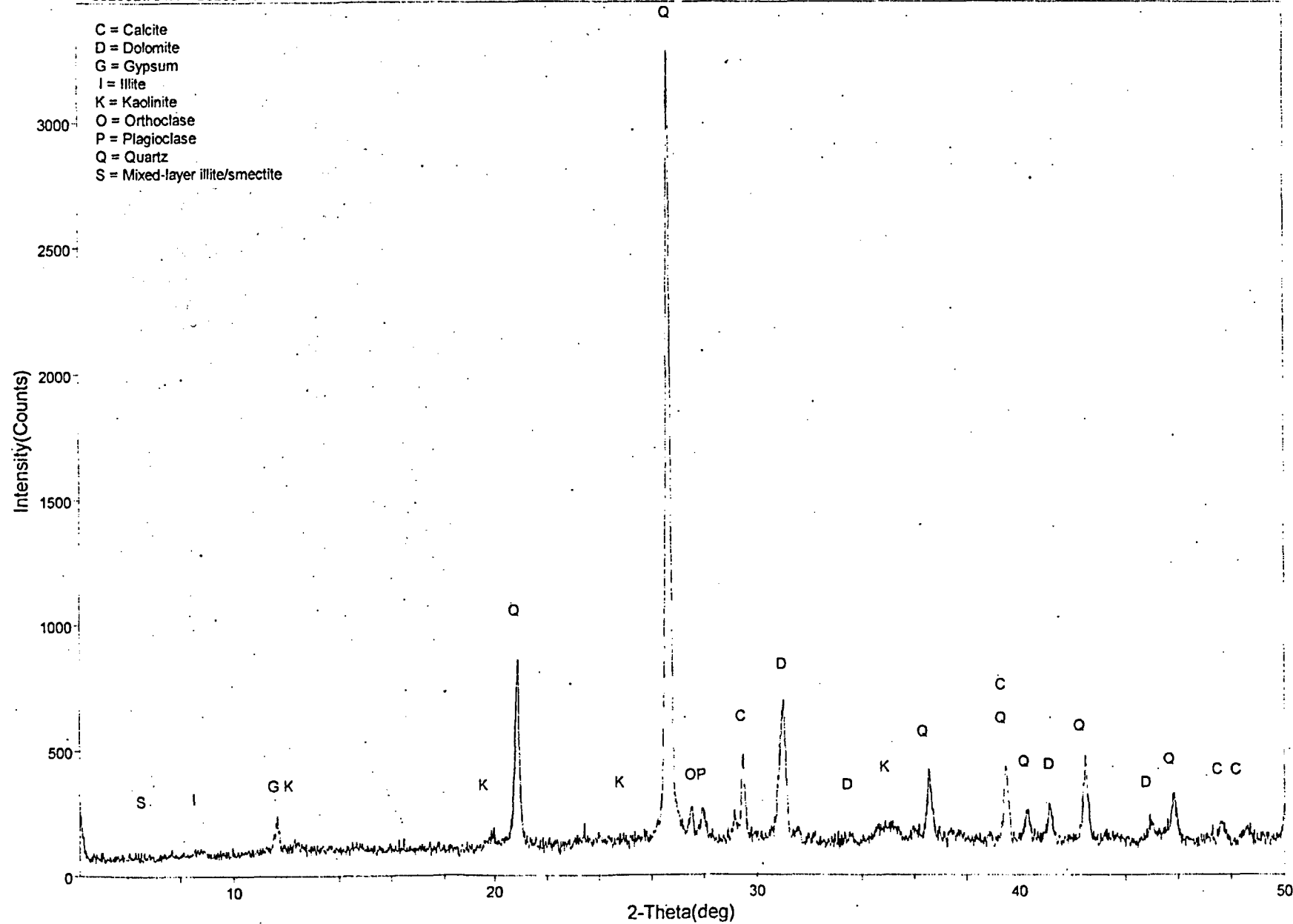


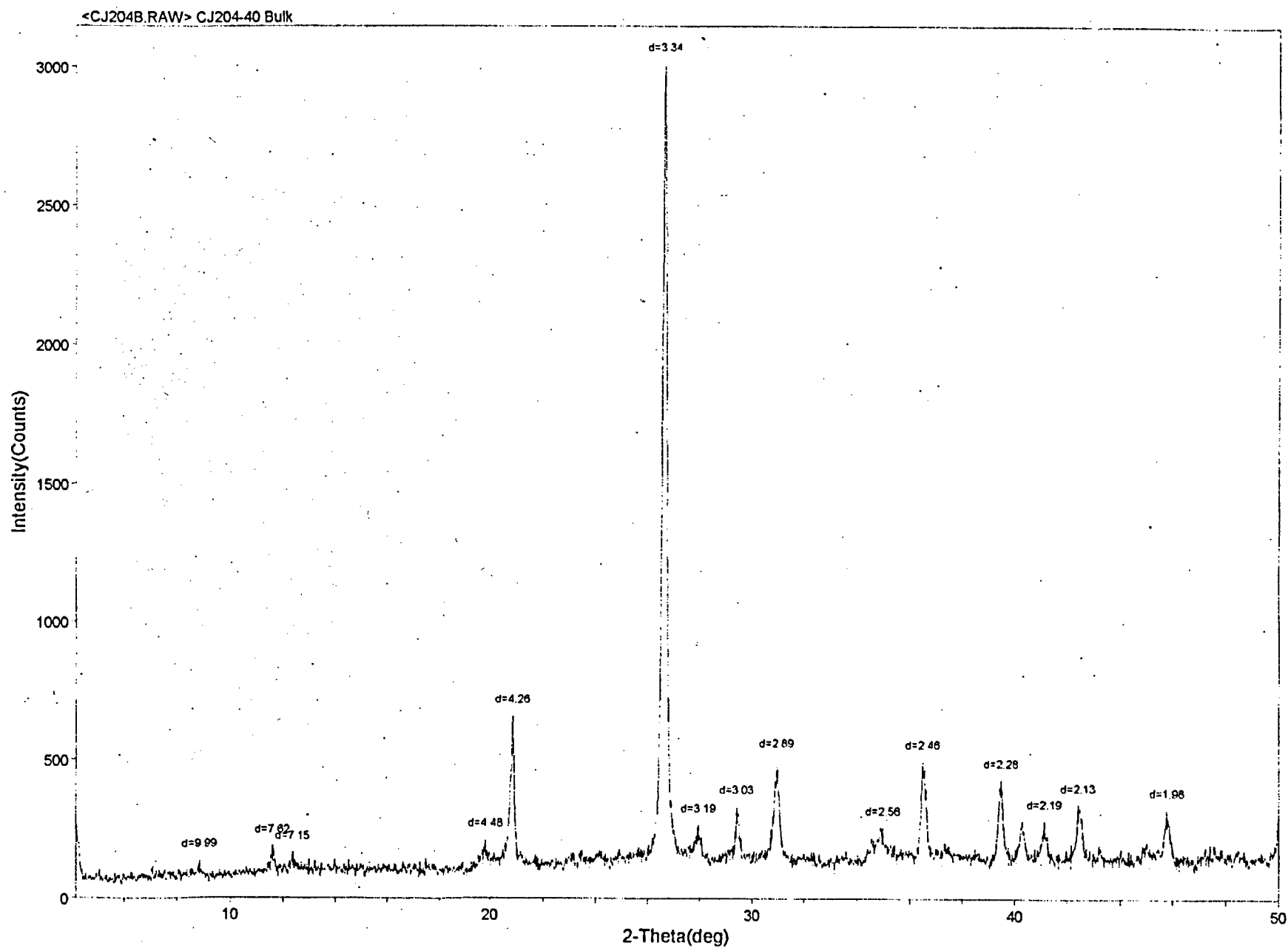


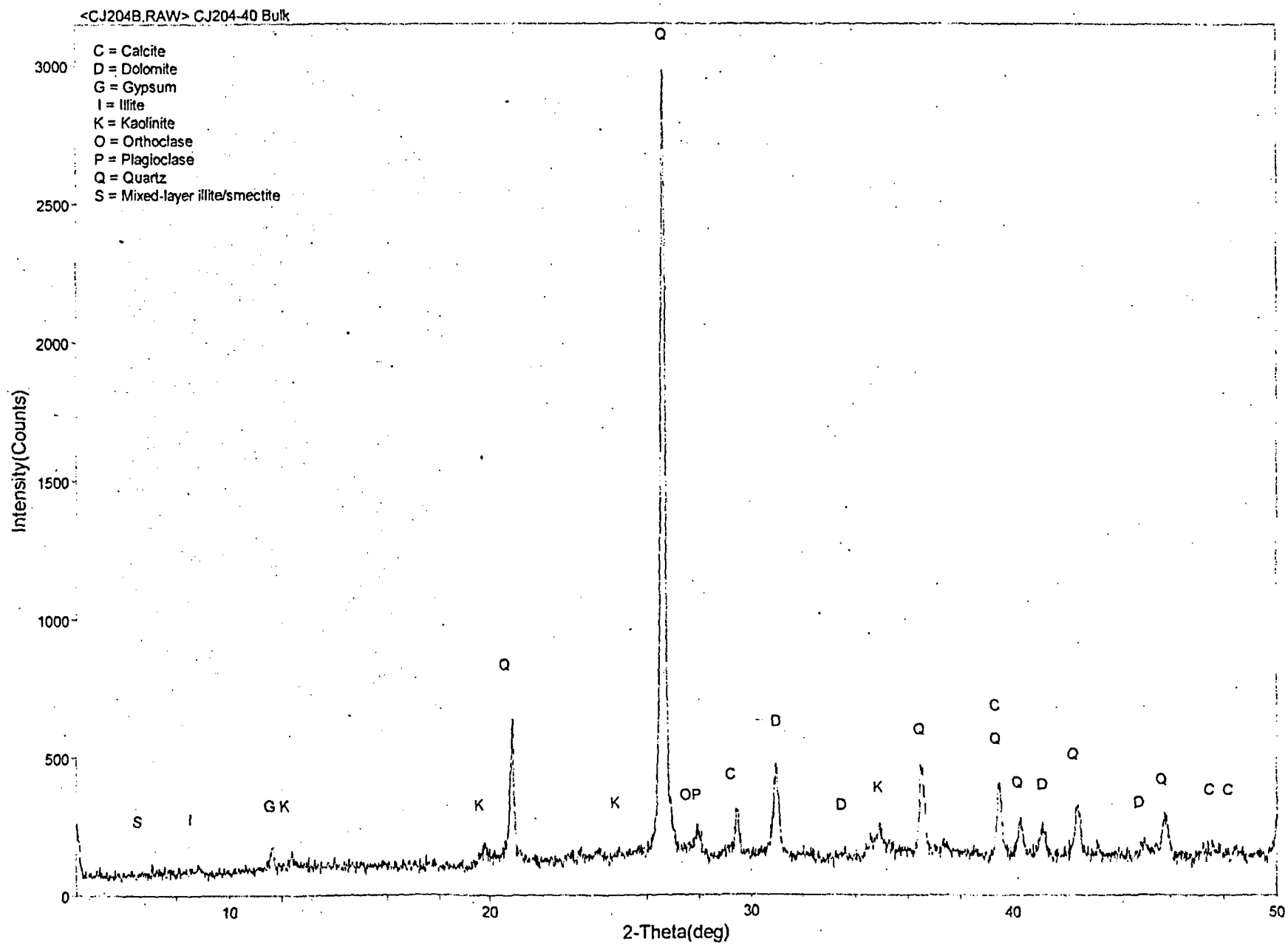


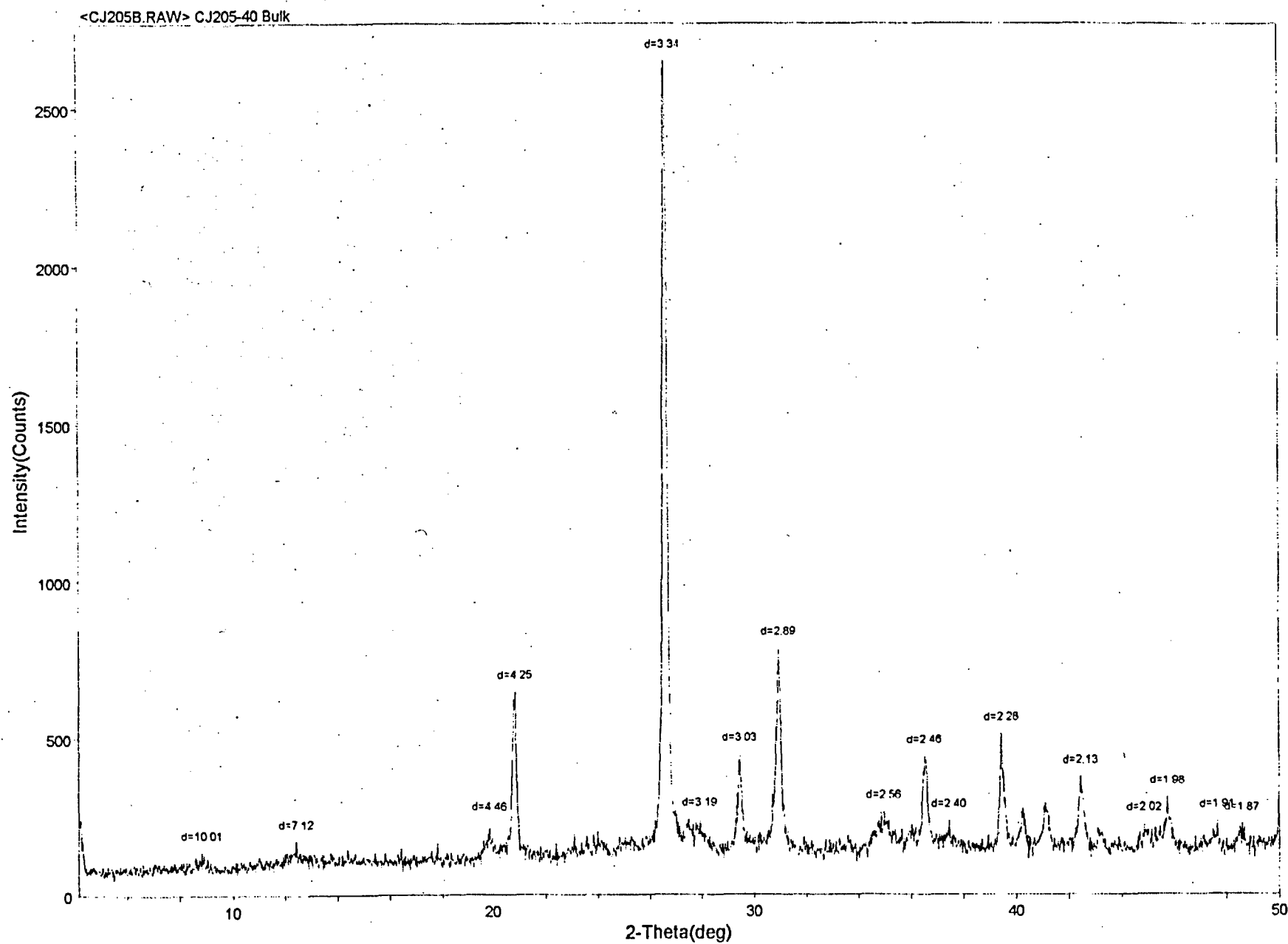


<CJ203B.RAW> CJ203-40 Bulk

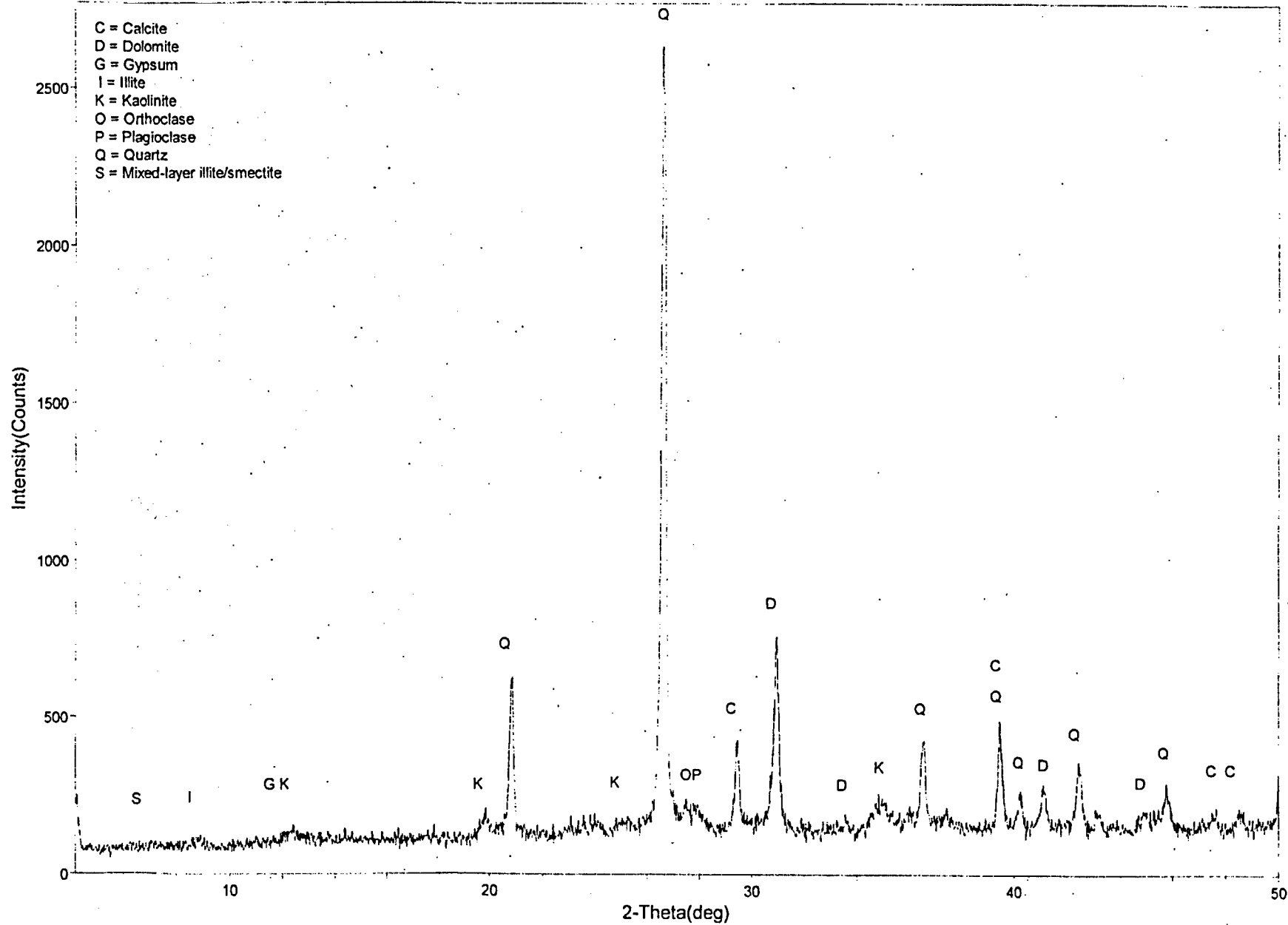


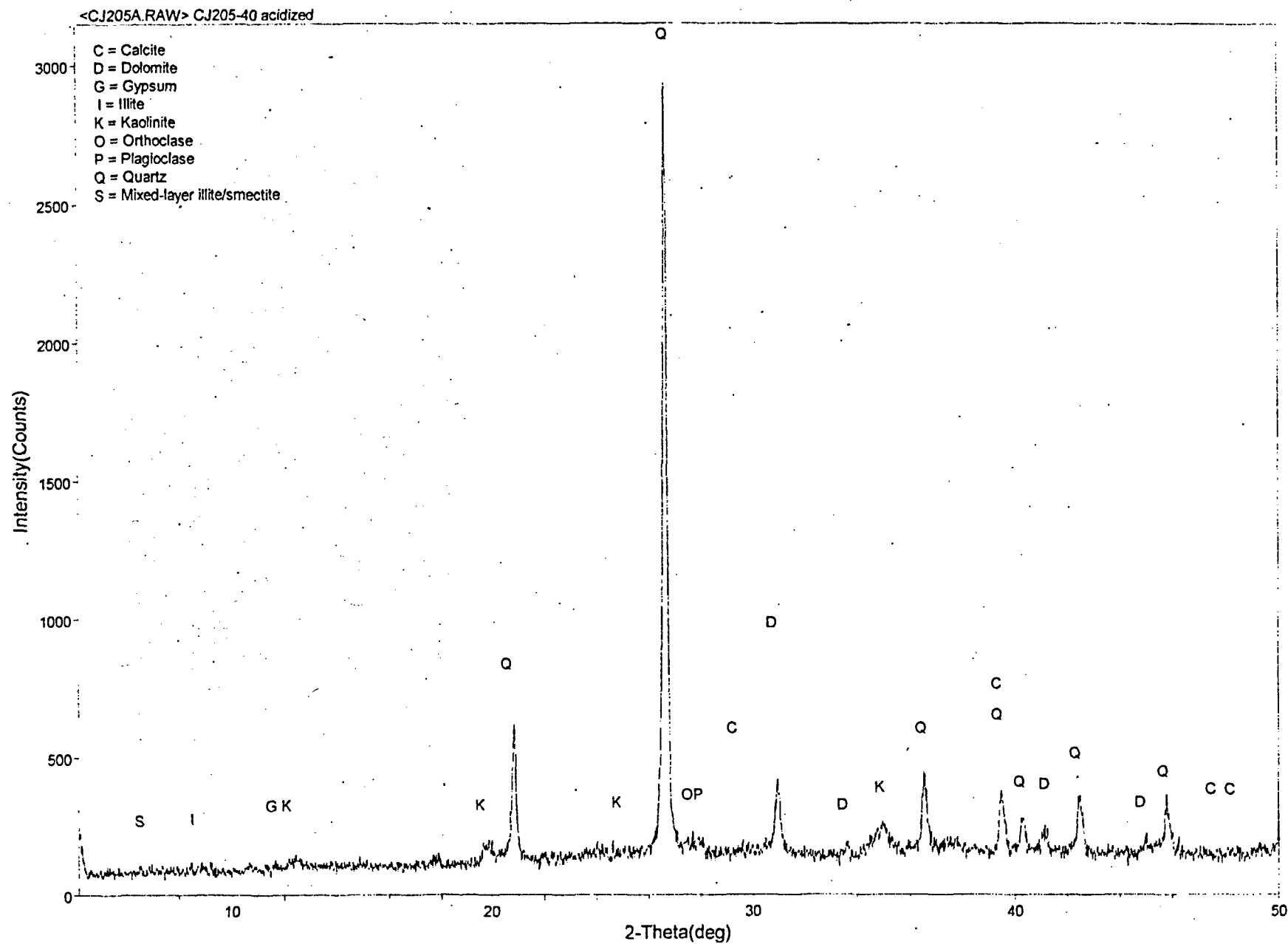




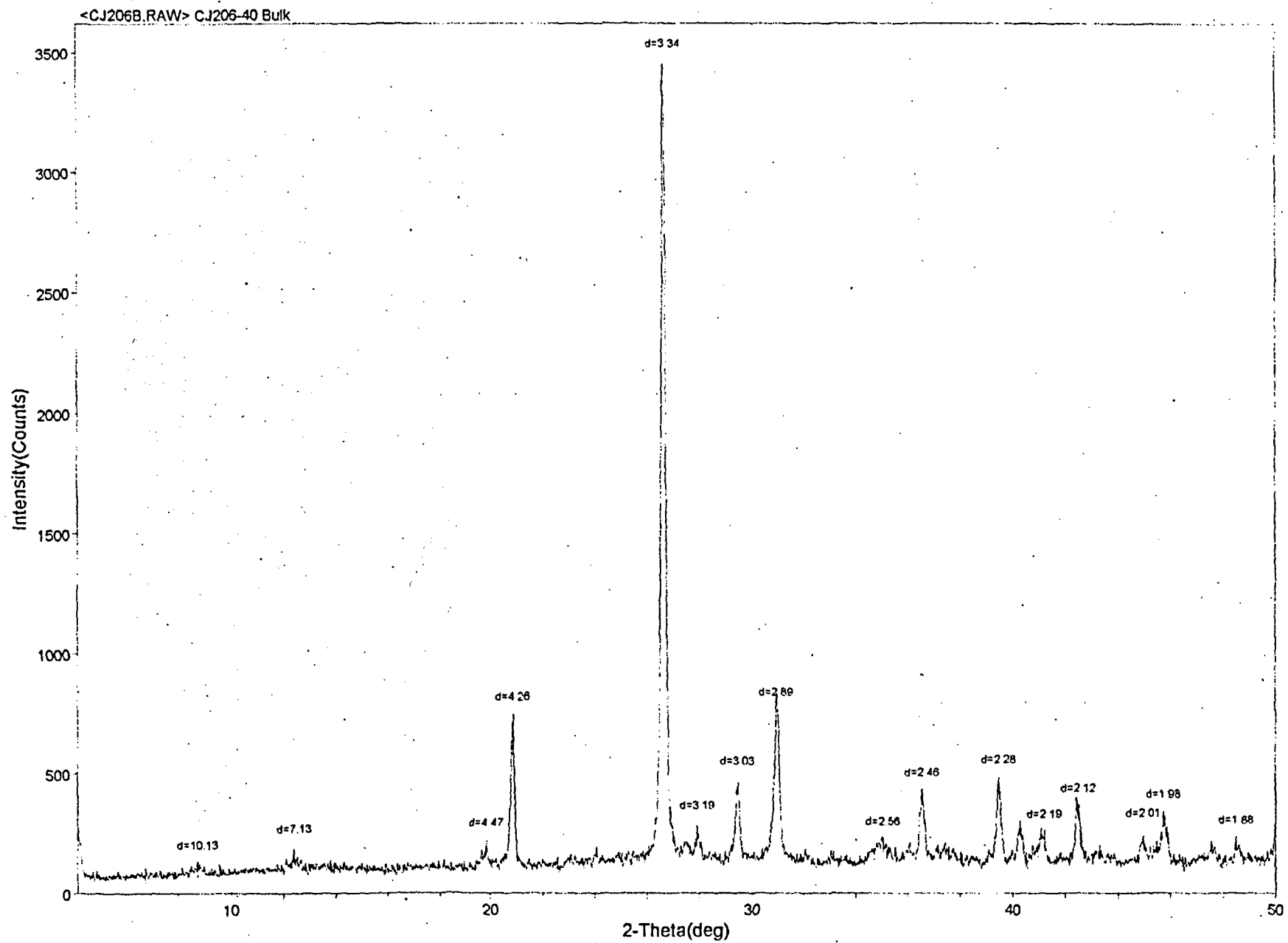


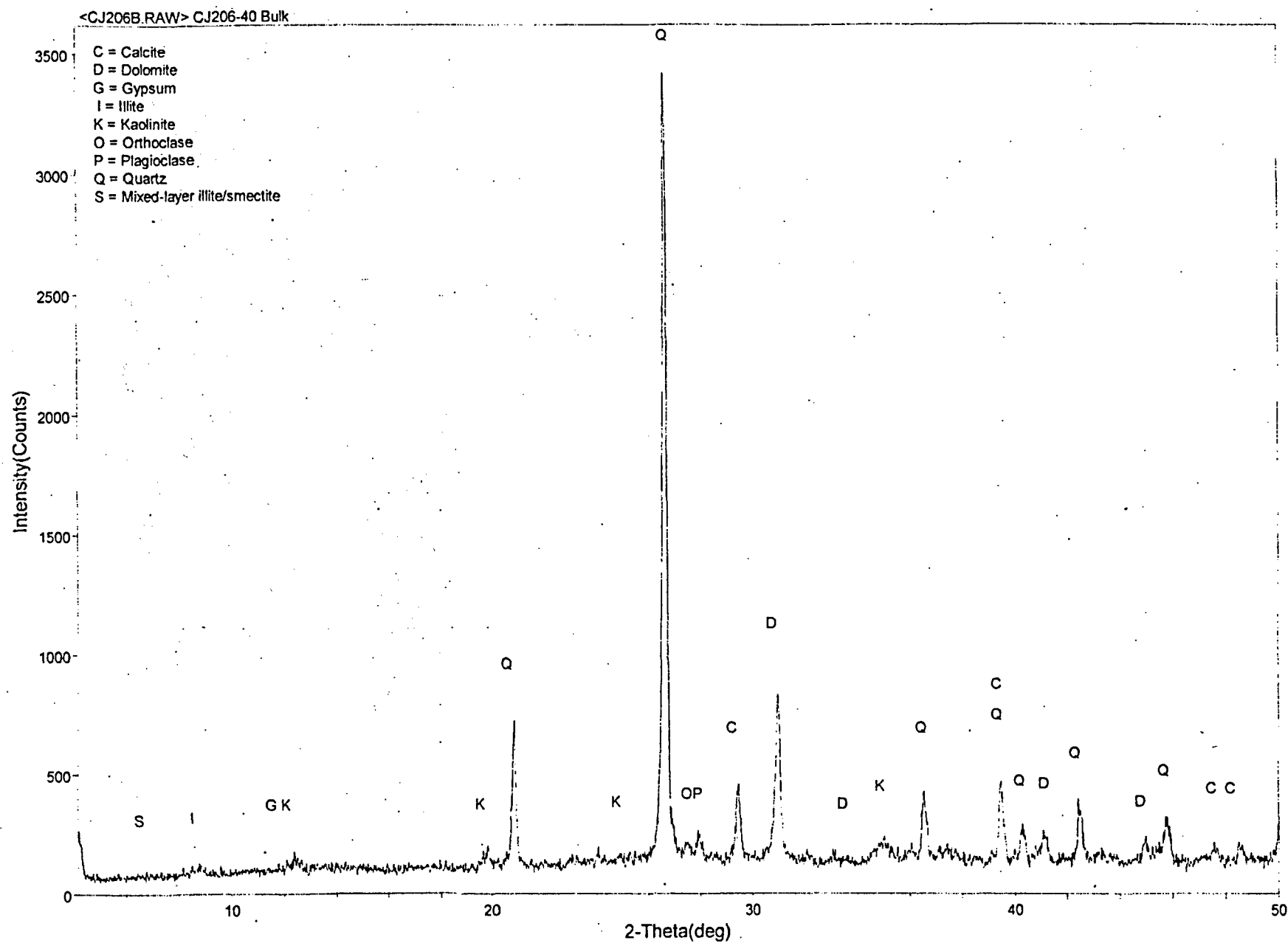
<CJ205B.RAW> CJ205-40 Bulk

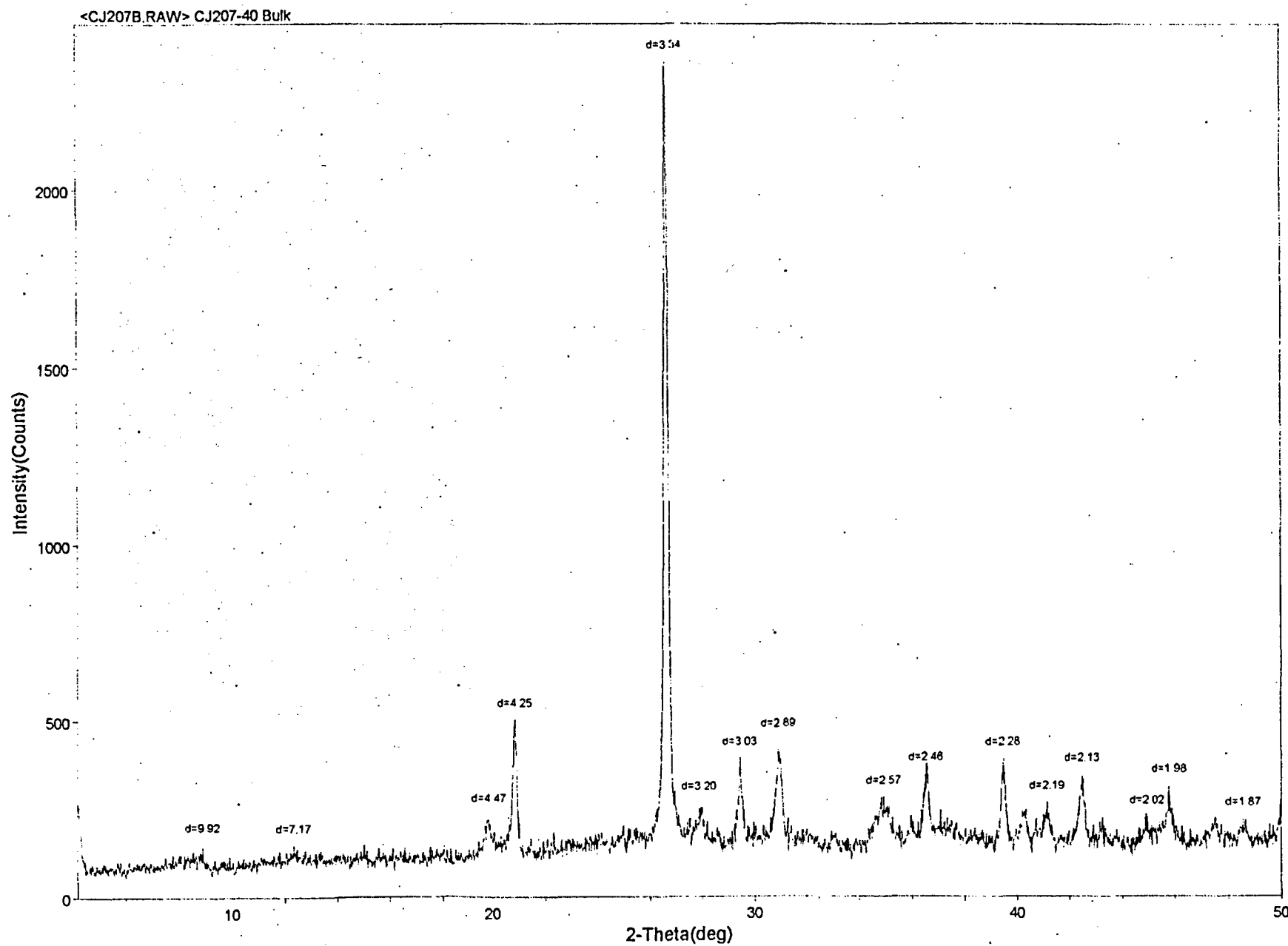




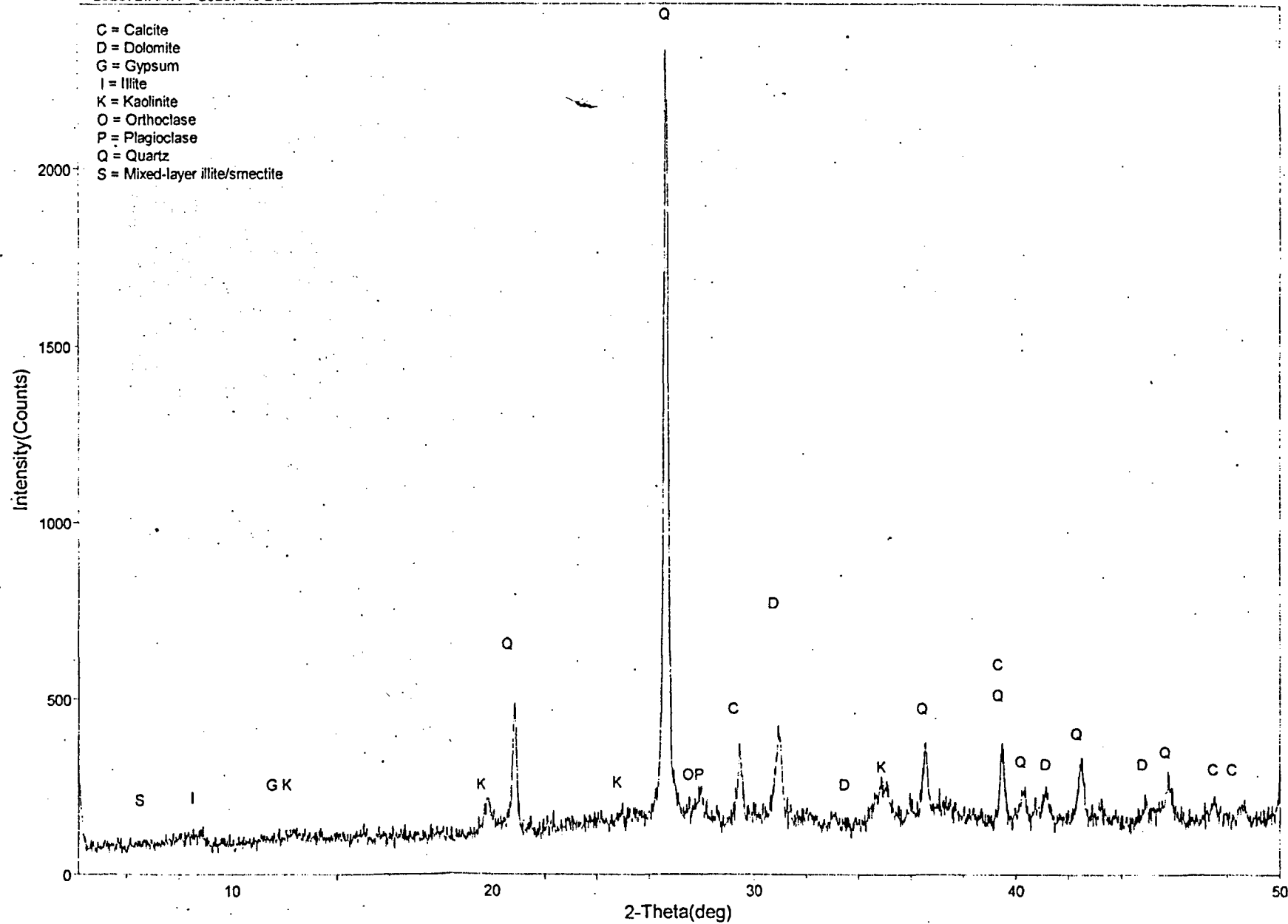


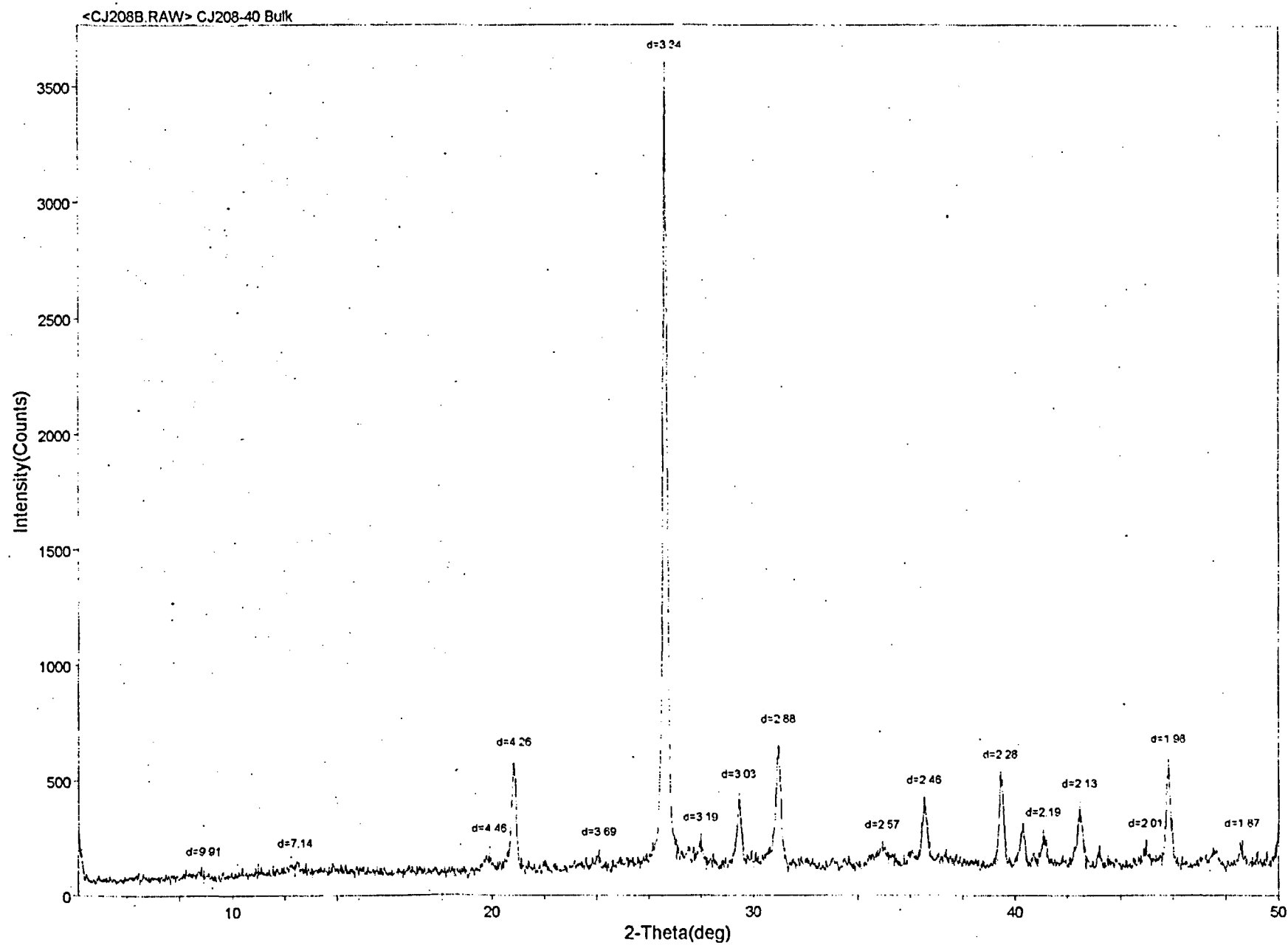




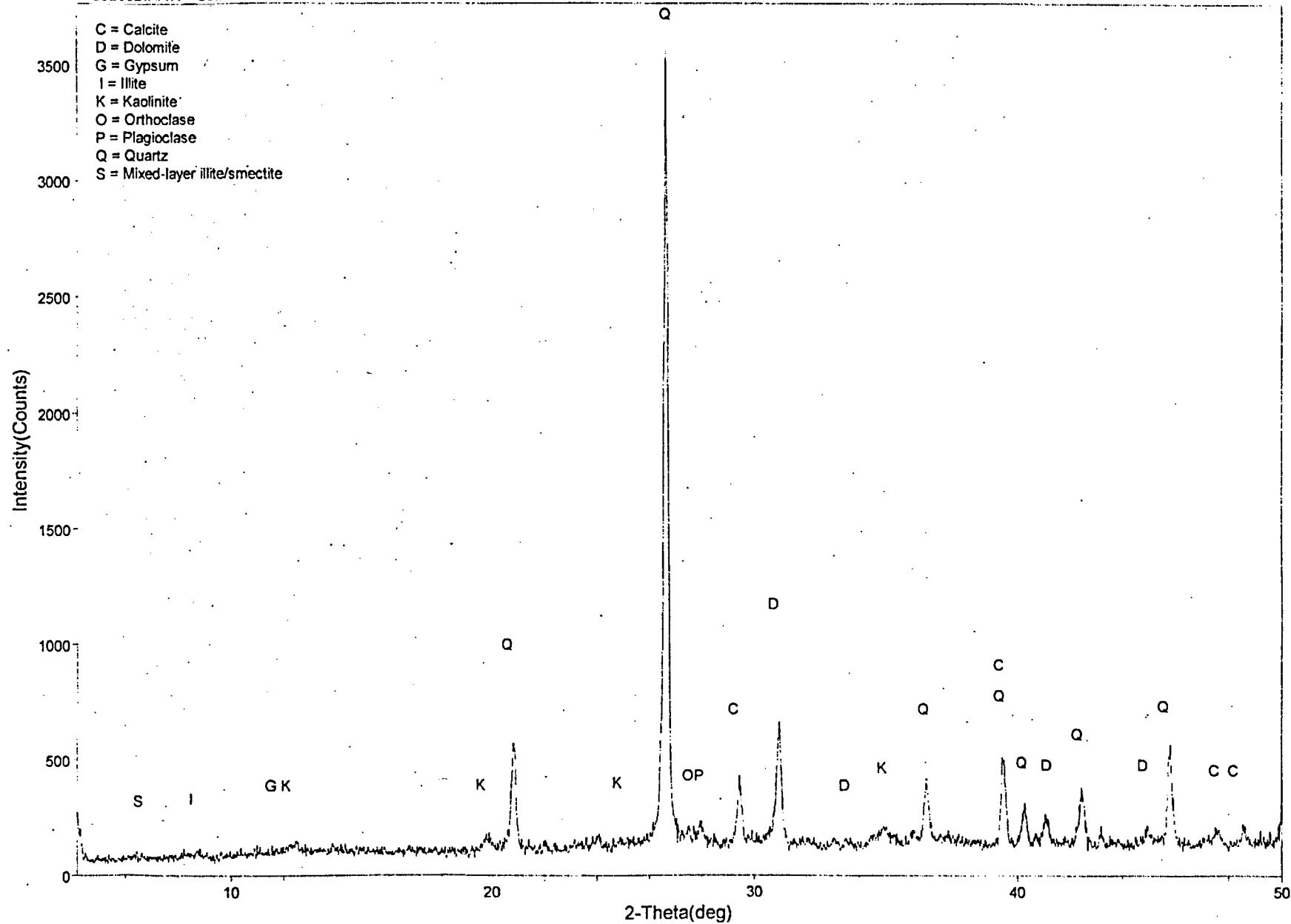


<CJ207B.RAW> CJ207-40 Bulk

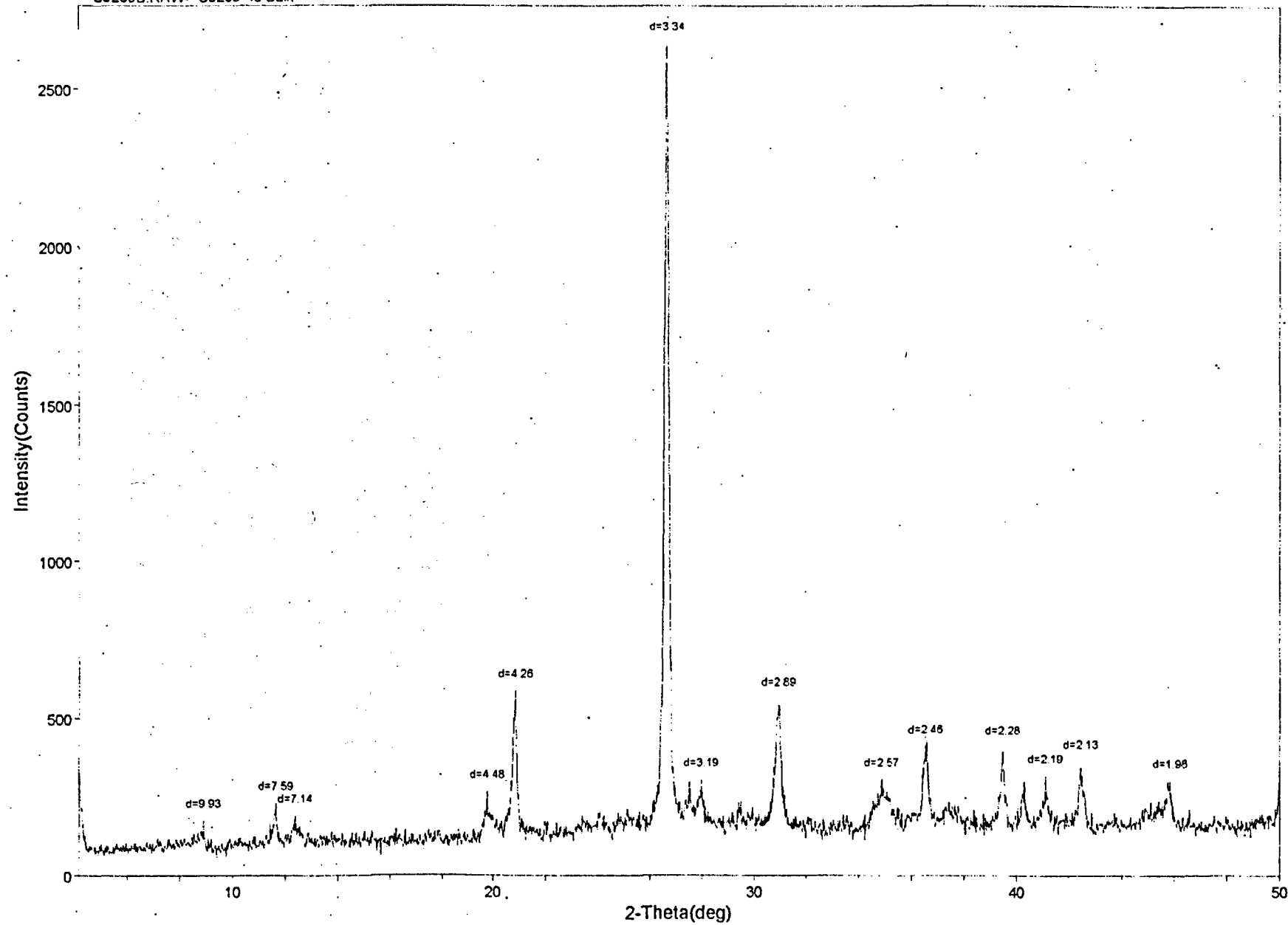




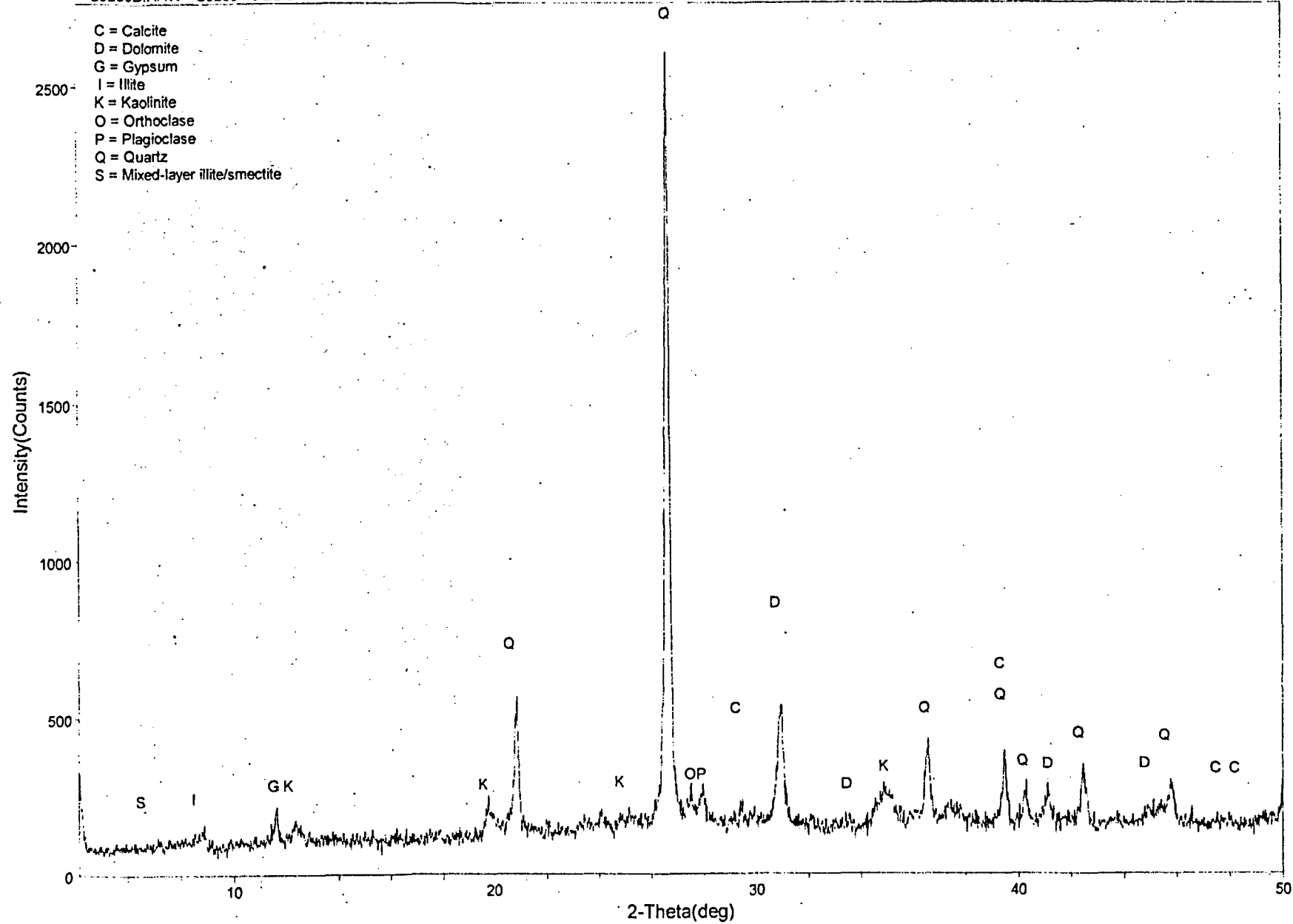
<CJ208B.RAW> CJ208-40 Bulk



<CJ209B.RAW> CJ209-40 Bulk

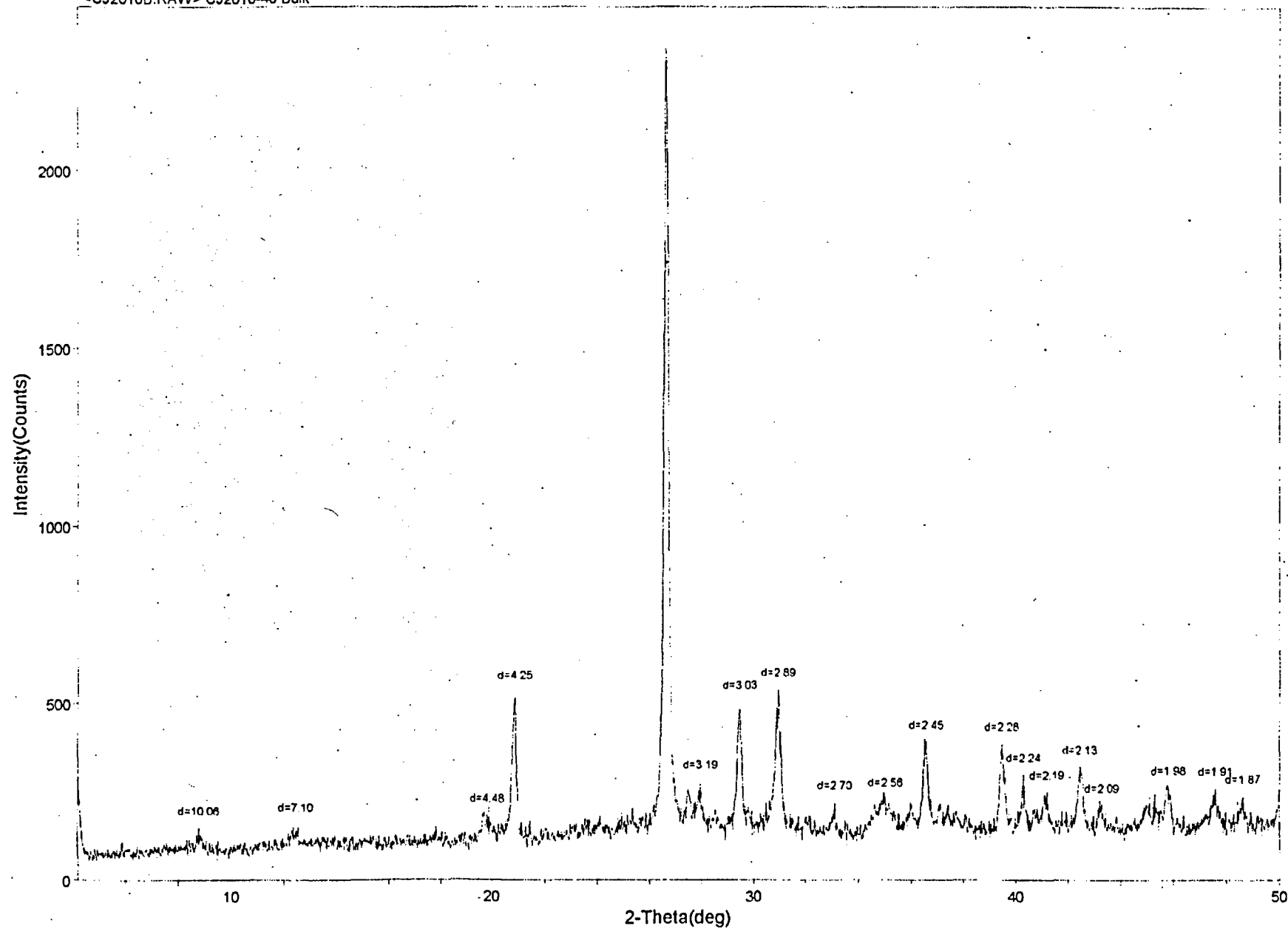


<CJ209B.RAW> CJ209-40 Bulk

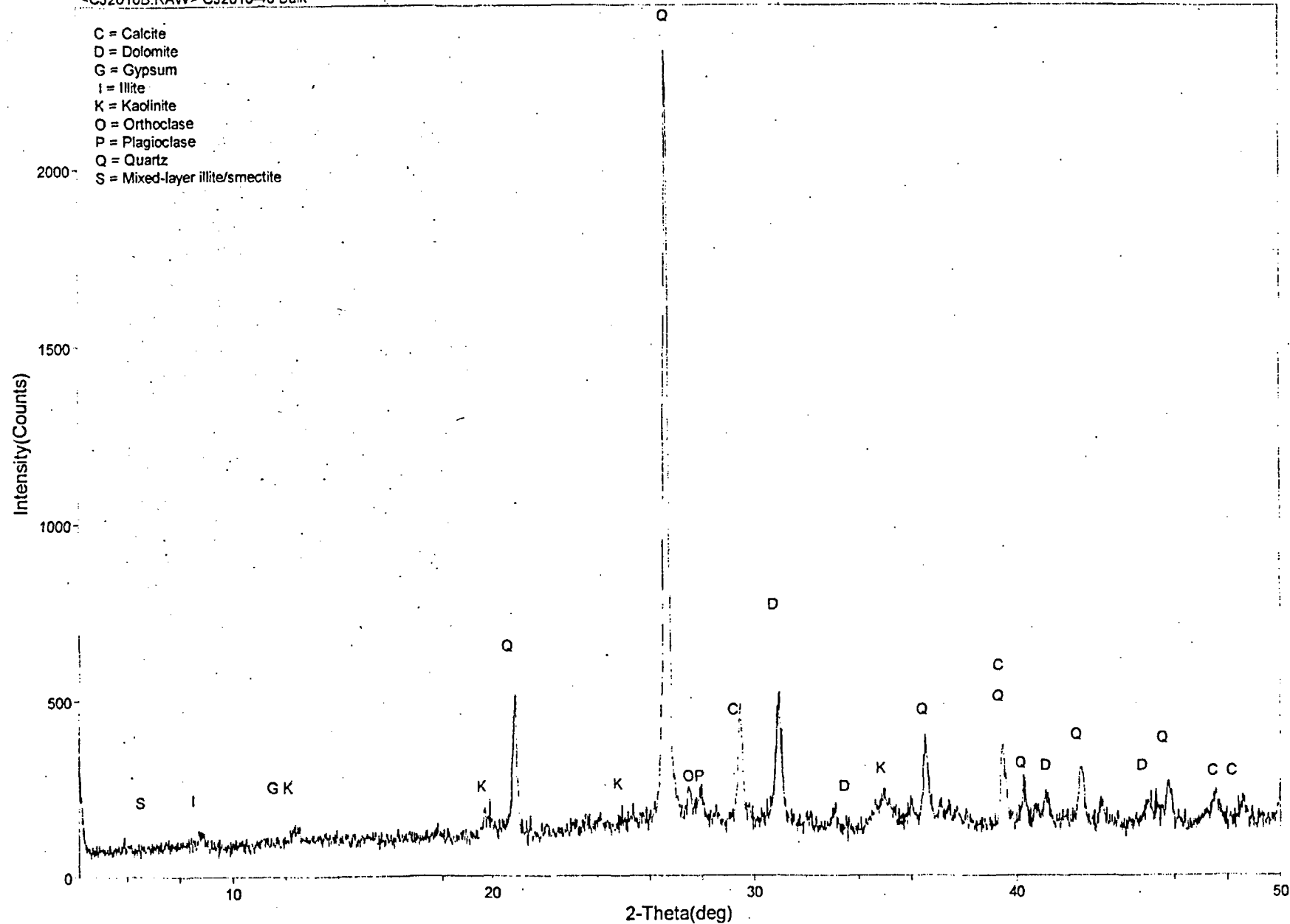




<CJ2010B.RAW> CJ2010-40 Bulk



<CJ2010B.RAW> CJ2010-40 Bulk

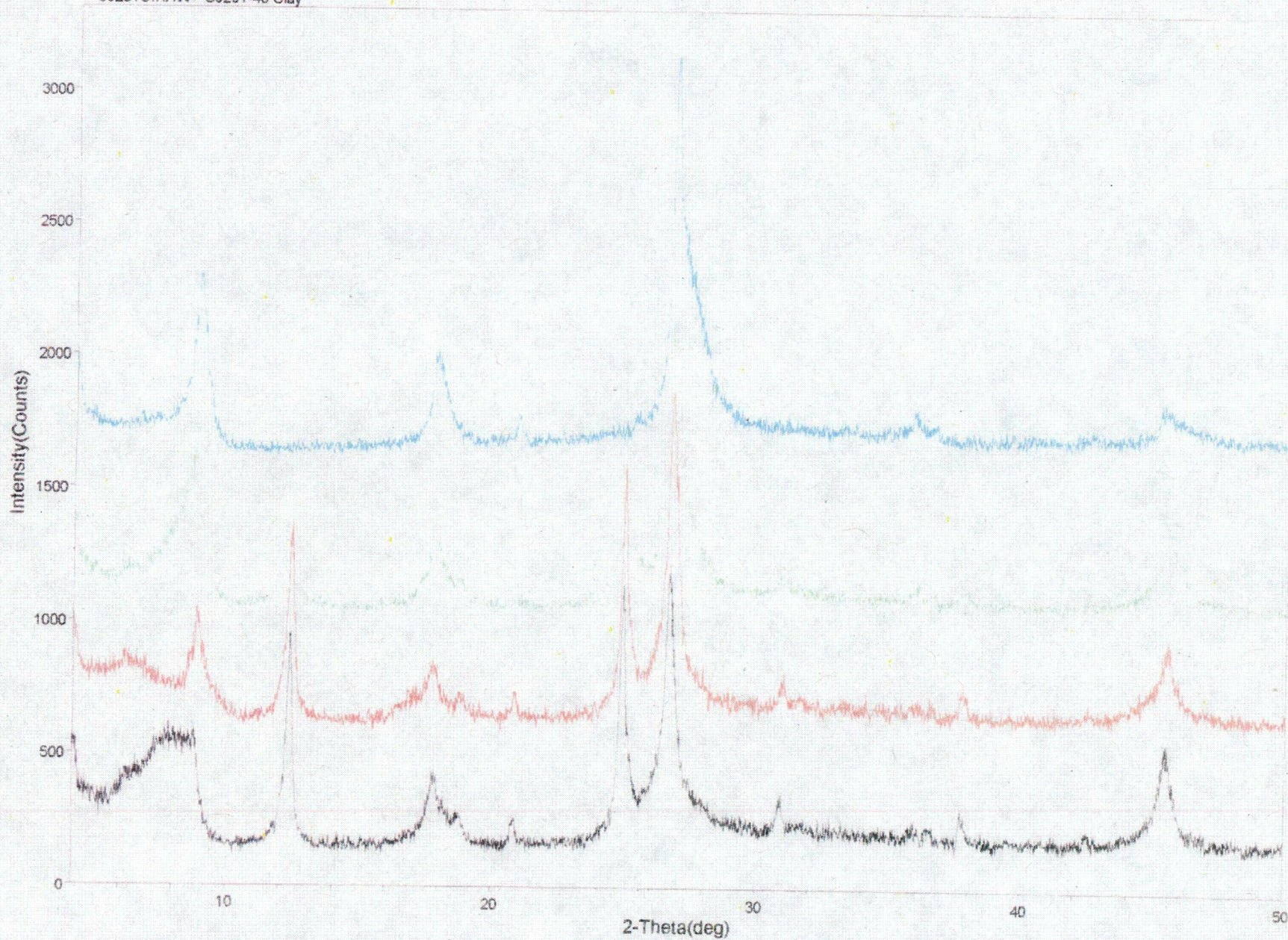


**Appendix 5.**

**Stacked x-ray diffraction patterns of clay minerals in CJ sample set**

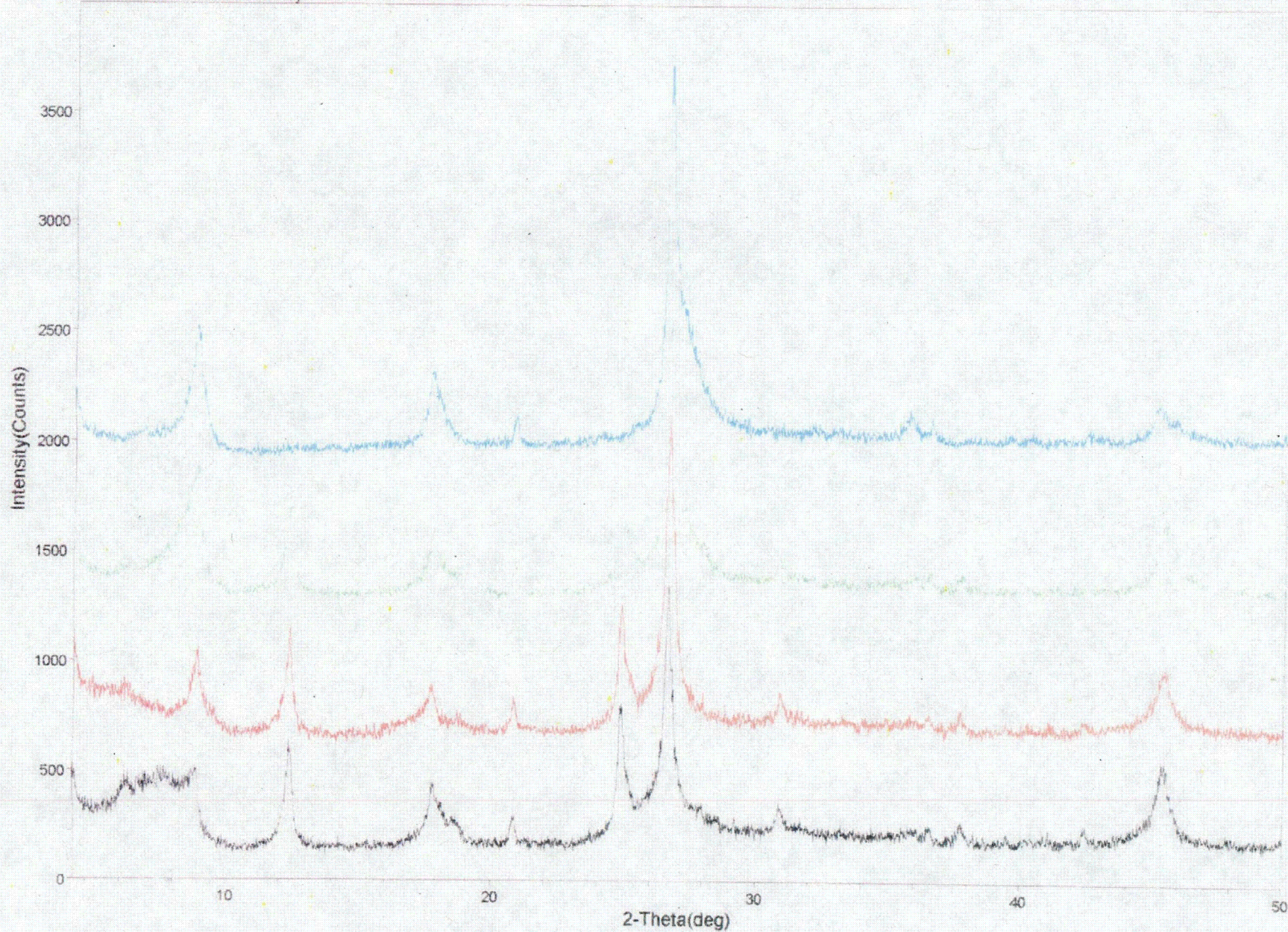


<CJ201HH.RAW> CJ201-40 H550  
<CJ201HI.RAW> CJ201-40 H200  
<CJ201G.RAW> CJ201-40 glycol  
<CJ201C.RAW> CJ201-40 Clay





<CJ202HH RAW> CJ202-40 H550  
<CJ202HL RAW> CJ202-40 H300  
<CJ202G RAW> CJ202-40 glycol  
<CJ202C RAW> CJ 202-40 Clay



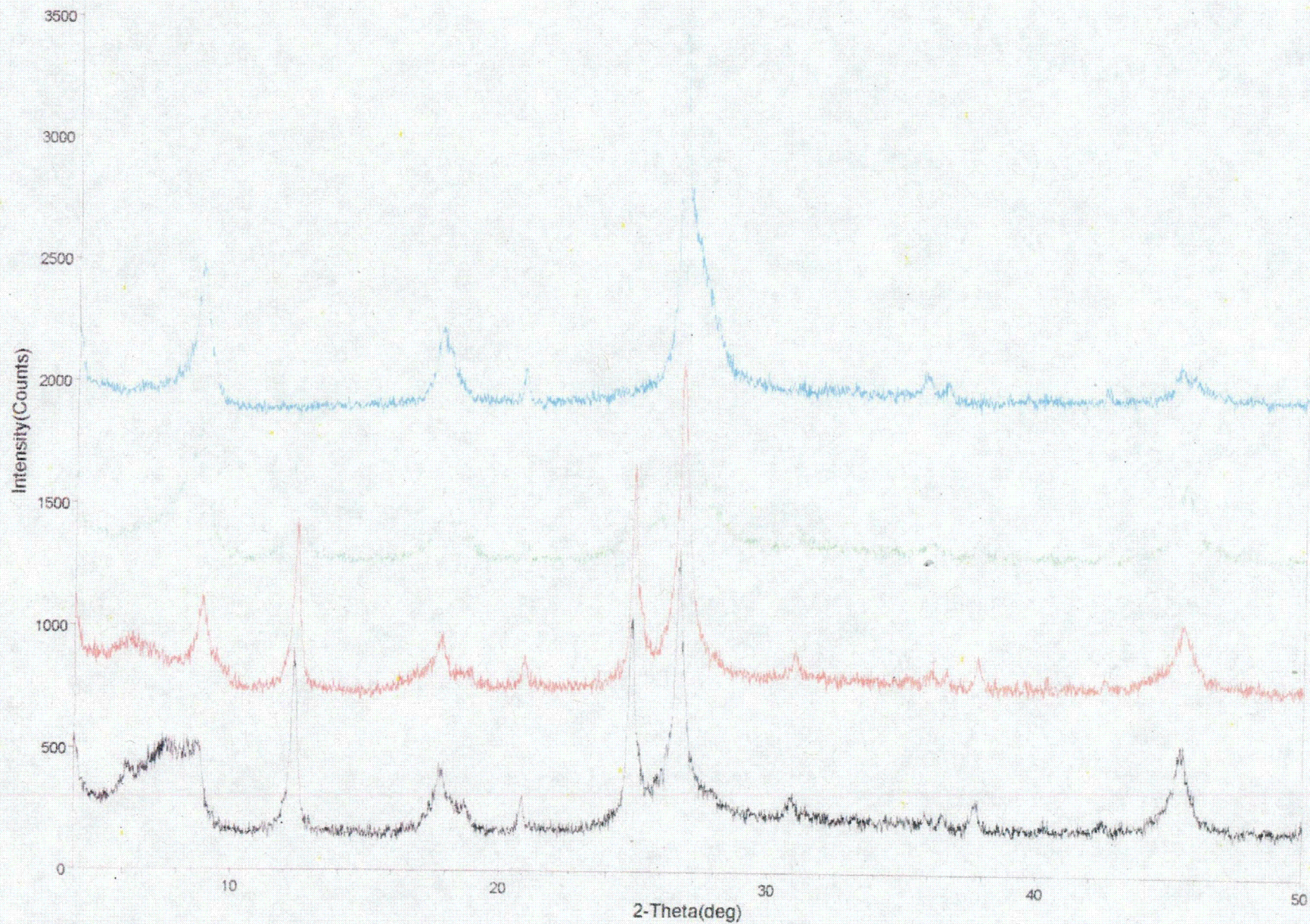


<CJ203HH RAW> CJ203-40 H550

<CJ203HL RAW> CJ203-40 H300

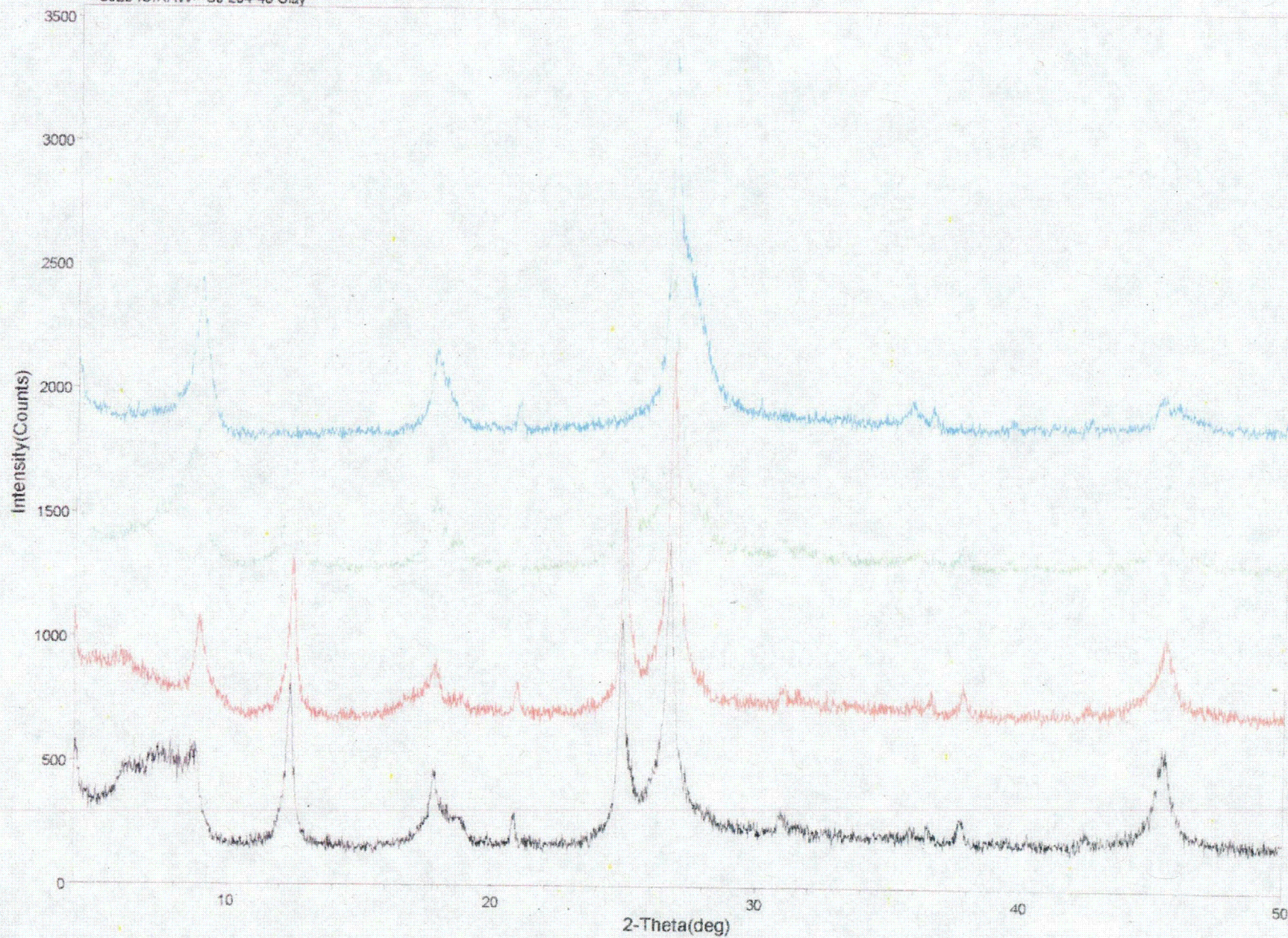
<CJ203G RAW> CJ203-40 glycol

<CJ203C RAW> CJ 203-40 Clay



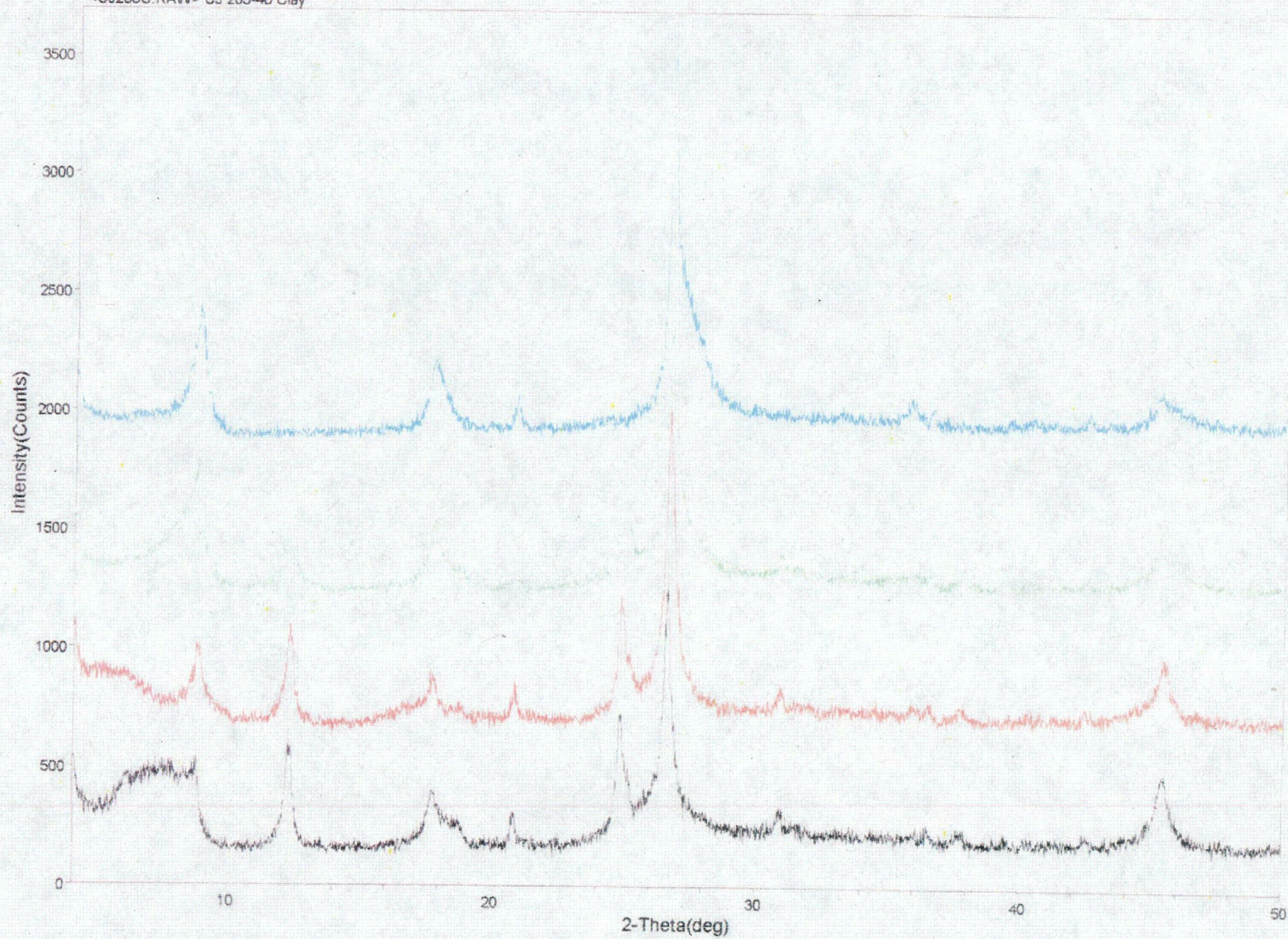


<CJ204HH RAW> CJ204-40 H550  
<CJ204HL RAW> CJ204-40 H-300  
<CJ204G RAW> CJ204-40 glycol  
<CJ204C.RAW> CJ 204-40 Clay



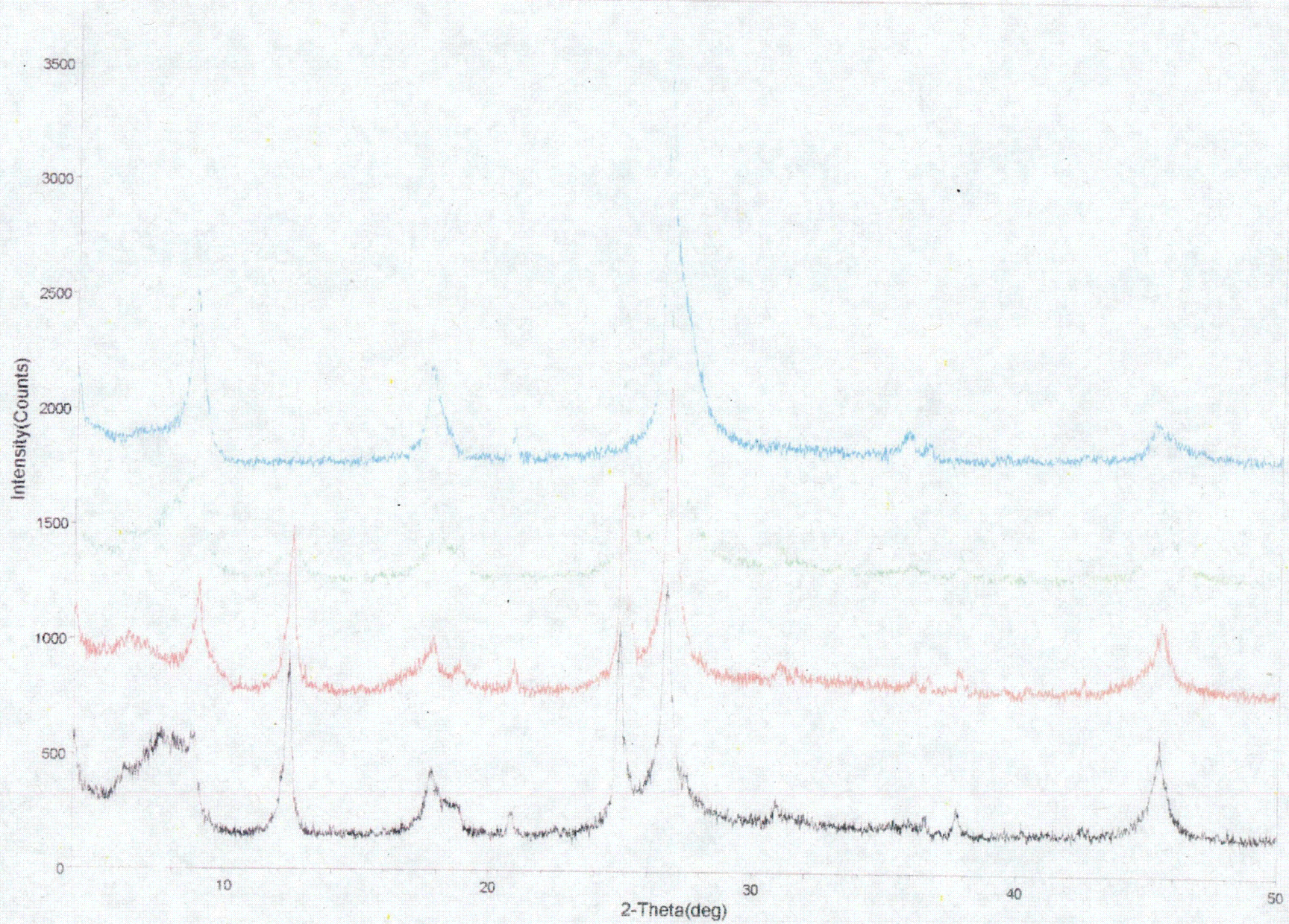


<CJ205HH.RAW> CJ205-40 H550  
<CJ205HL.RAW> CJ205-40 H300  
<CJ205G.RAW> CJ205-40 glycol  
<CJ205C.RAW> CJ 205-40 Clay



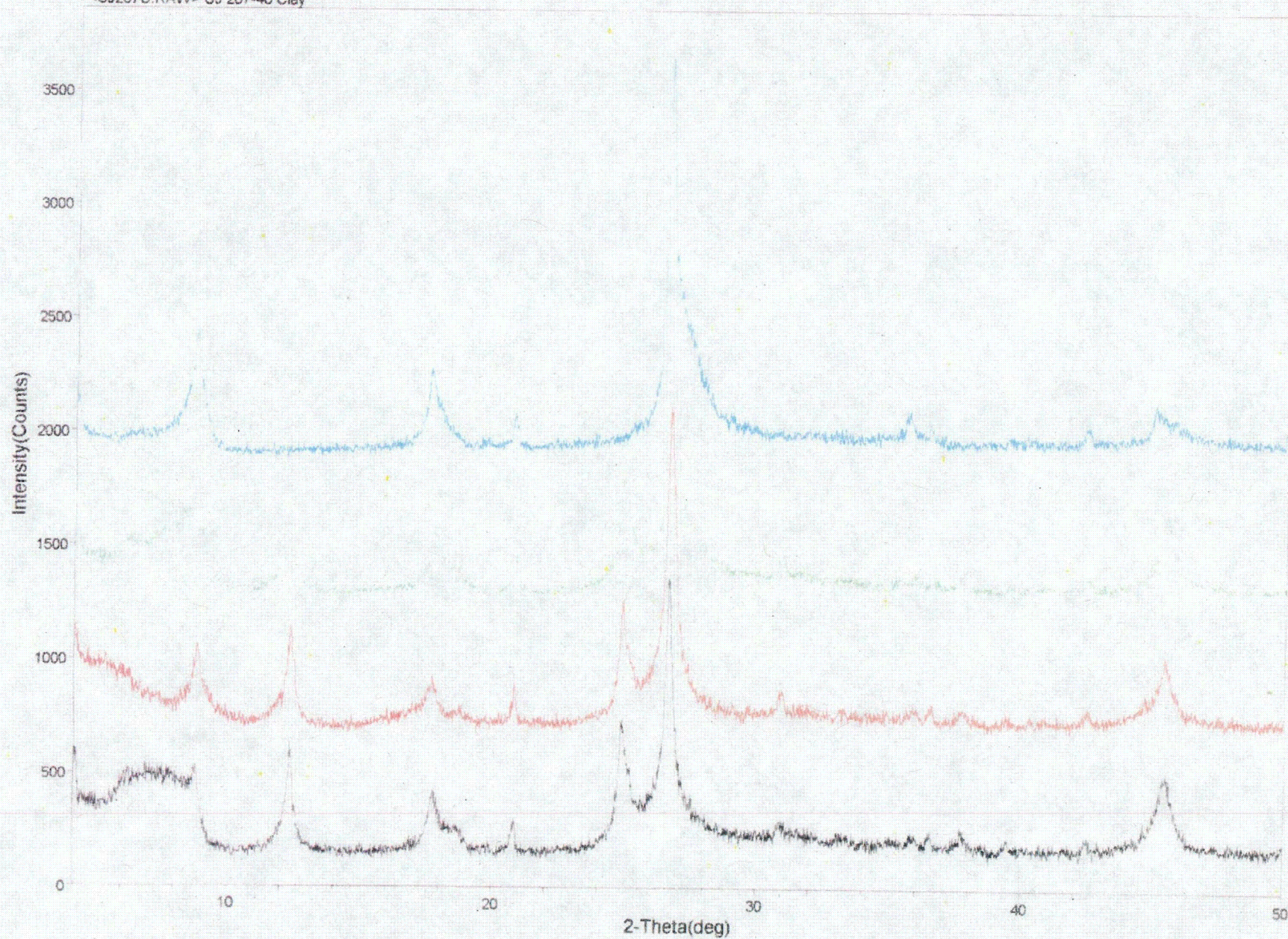


<CJ206HH.RAW> CJ206-40 H550  
<CJ206HL.RAW> CJ206-40 H300  
<CJ206G.RAW> CJ206-40 glycol  
<CJ206C.RAW> CJ 206-40 Clay



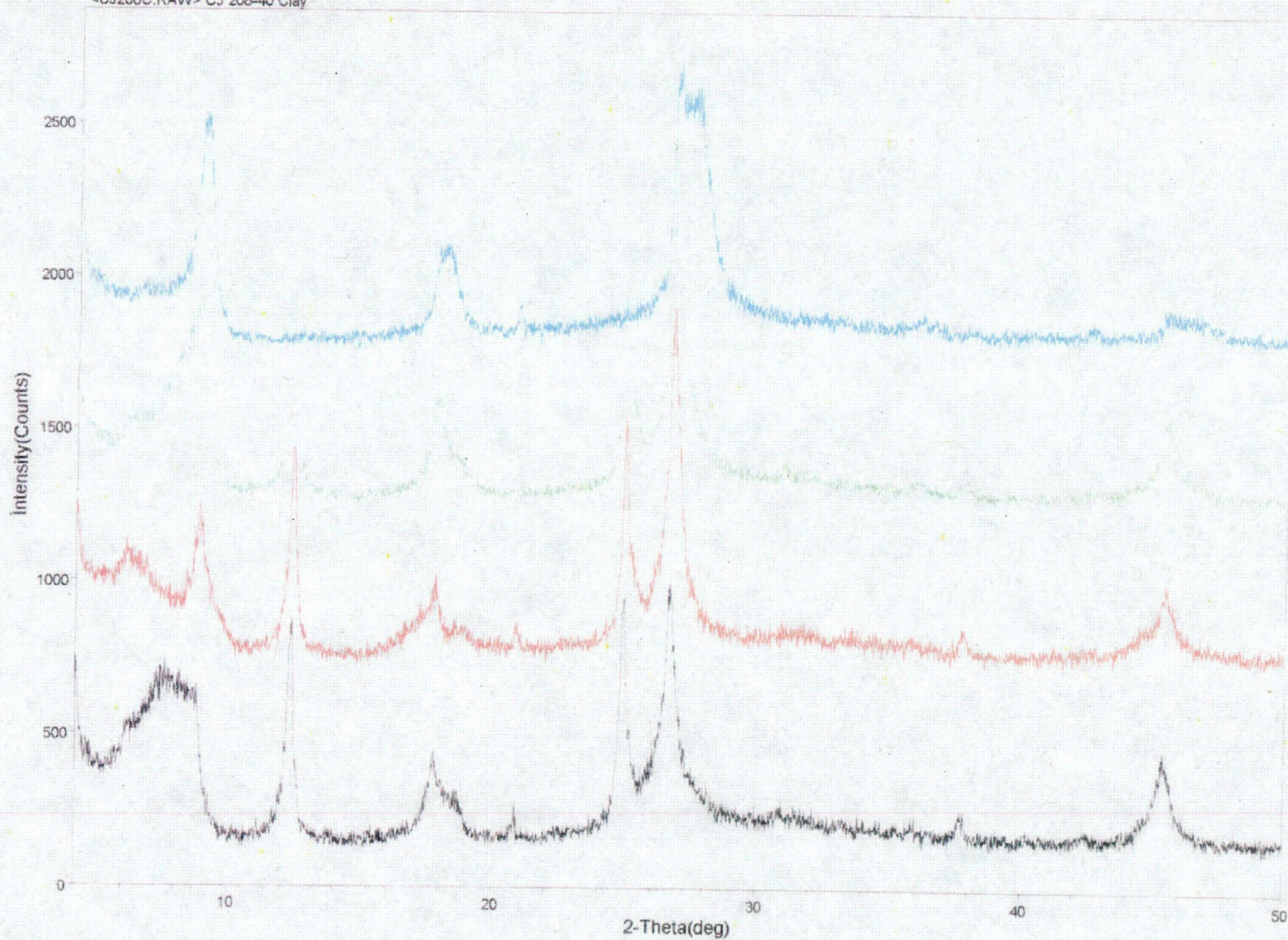


<CJ207HH RAW> CJ207-40 H550  
<CJ207HL RAW> CJ207-40 H300  
<CJ207G RAW> CJ207-40 glycol  
<CJ207C RAW> CJ 207-40 Clay



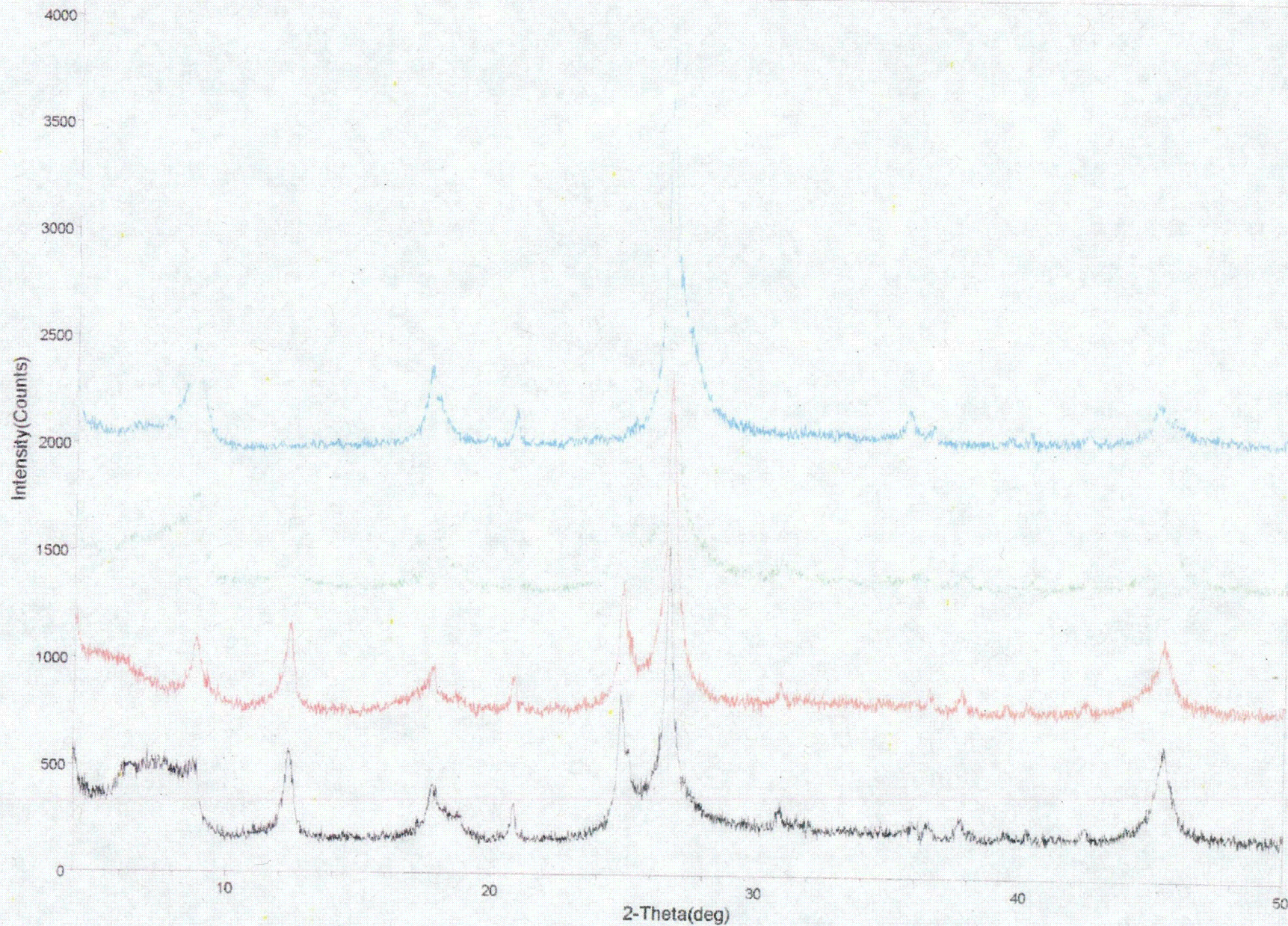


<CJ208HH.RAW> CJ208-40 H550  
<CJ208G.RAW> CJ208-40 glycol  
<CJ208C.RAW> CJ 208-40 Clay



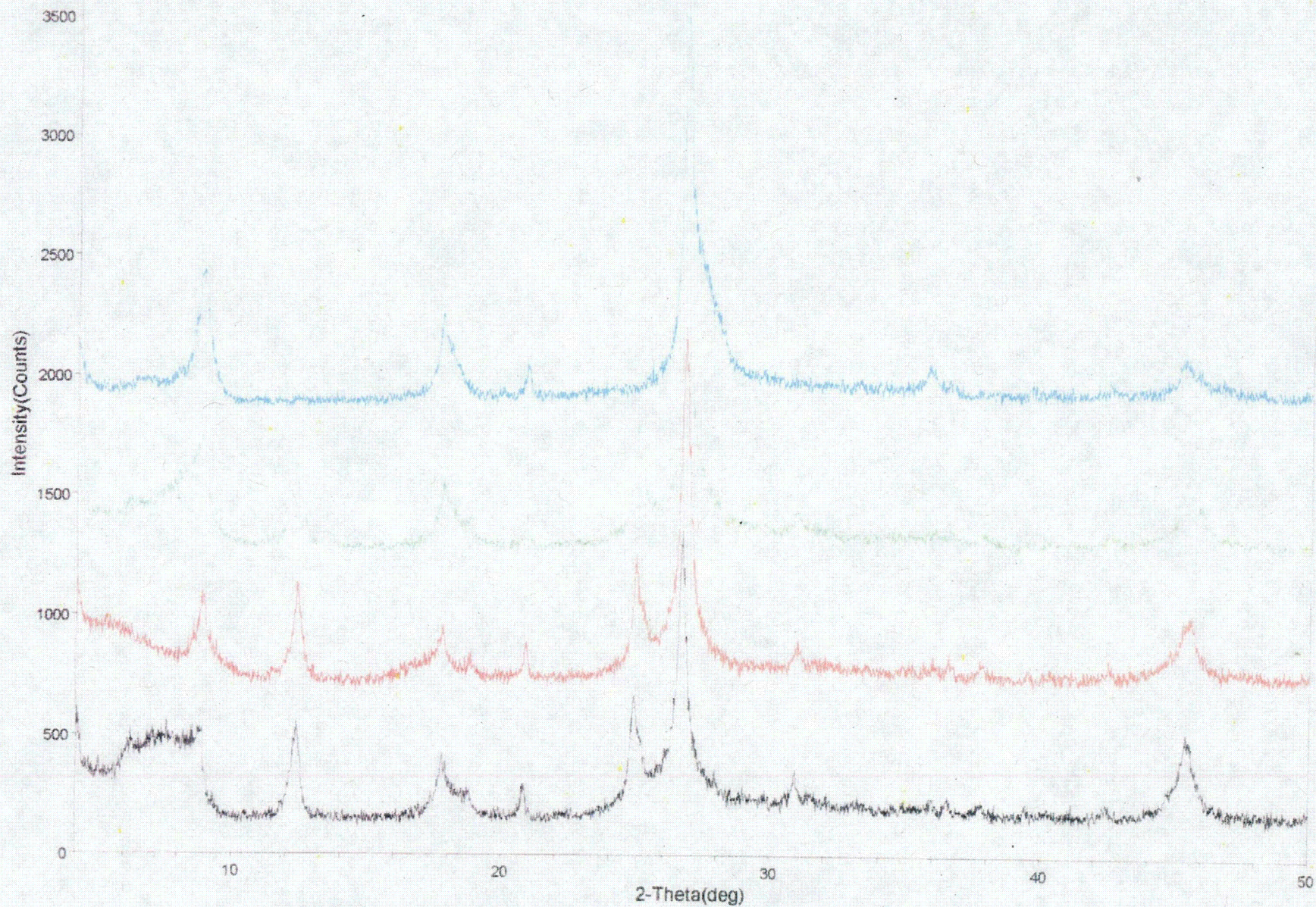


<CJ209HH.RAW> CJ209-40 H550  
<CJ209G.RAW> CJ209-40 glycol  
<CJ209C.RAW> CJ 209-40 Clay





<CJ2010HH.RAW> CJ2010-40 H550  
<CJ2010HL.RAW> CJ2010-40 H300  
<CJ2010G.RAW> CJ2010-40 glycol  
<CJ2010C.RAW> CJ 2010-40 Clay

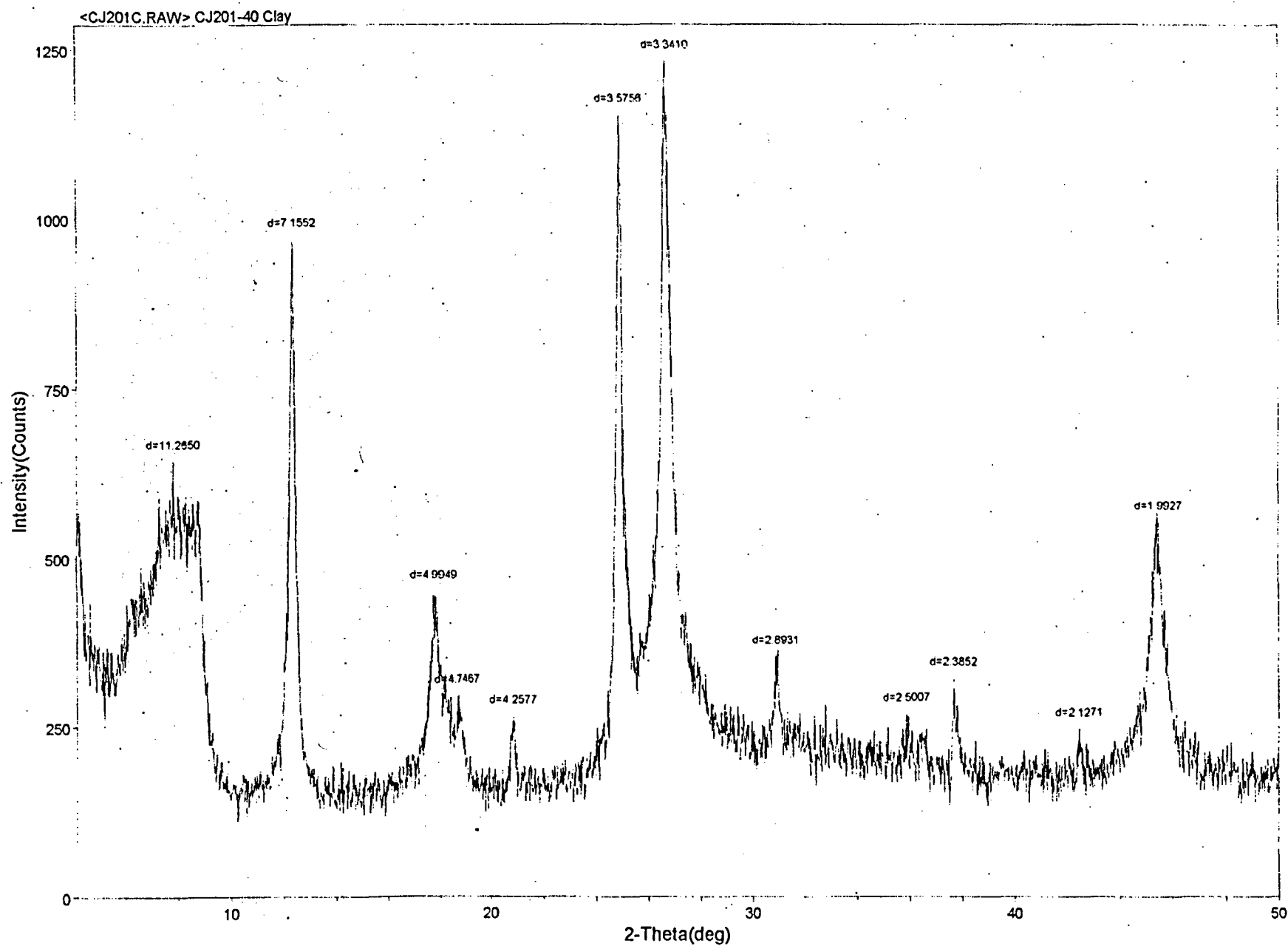


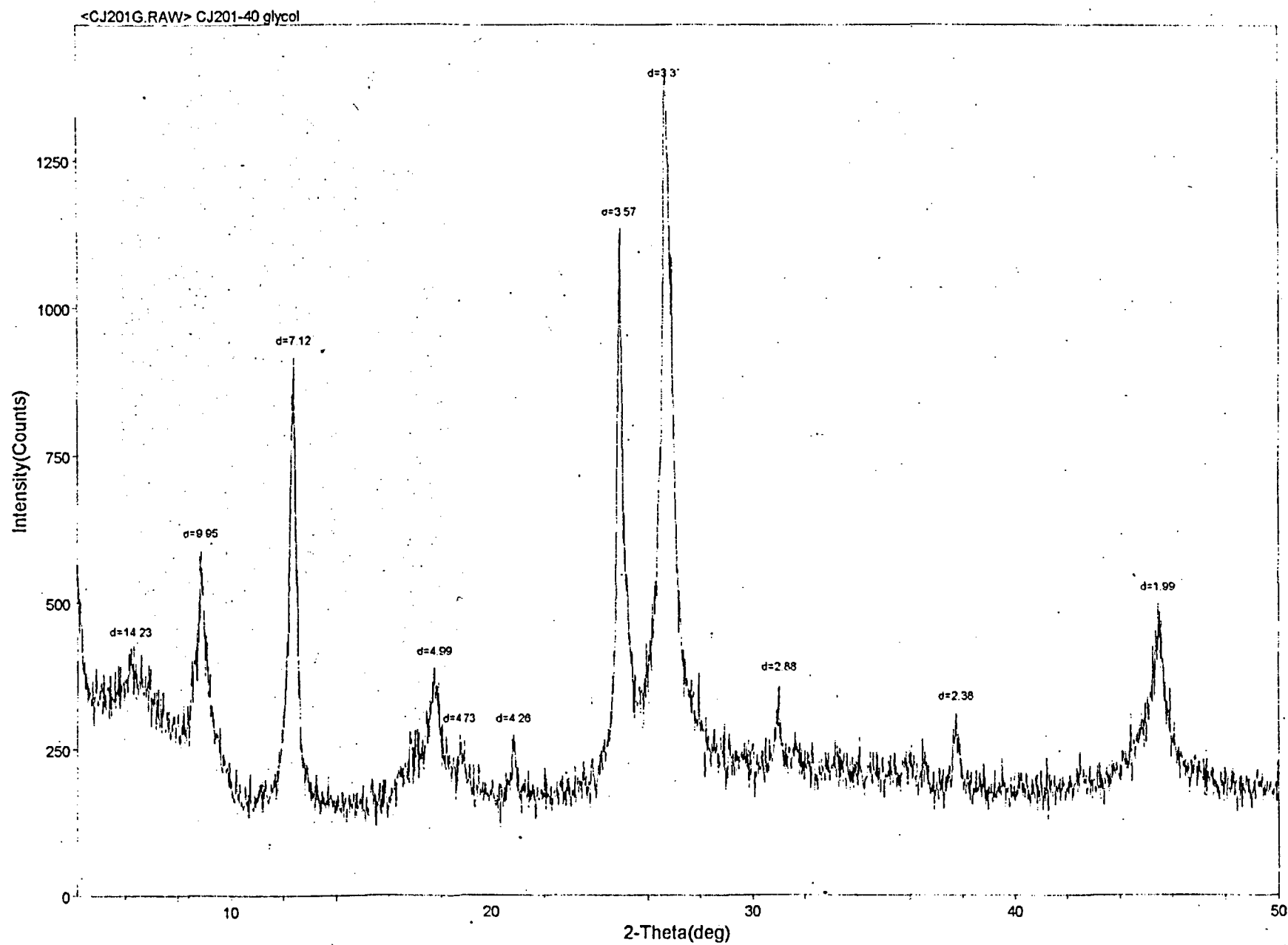


## **Appendix 6.**

### **X-ray diffraction patterns of clay minerals in CJ sample set**

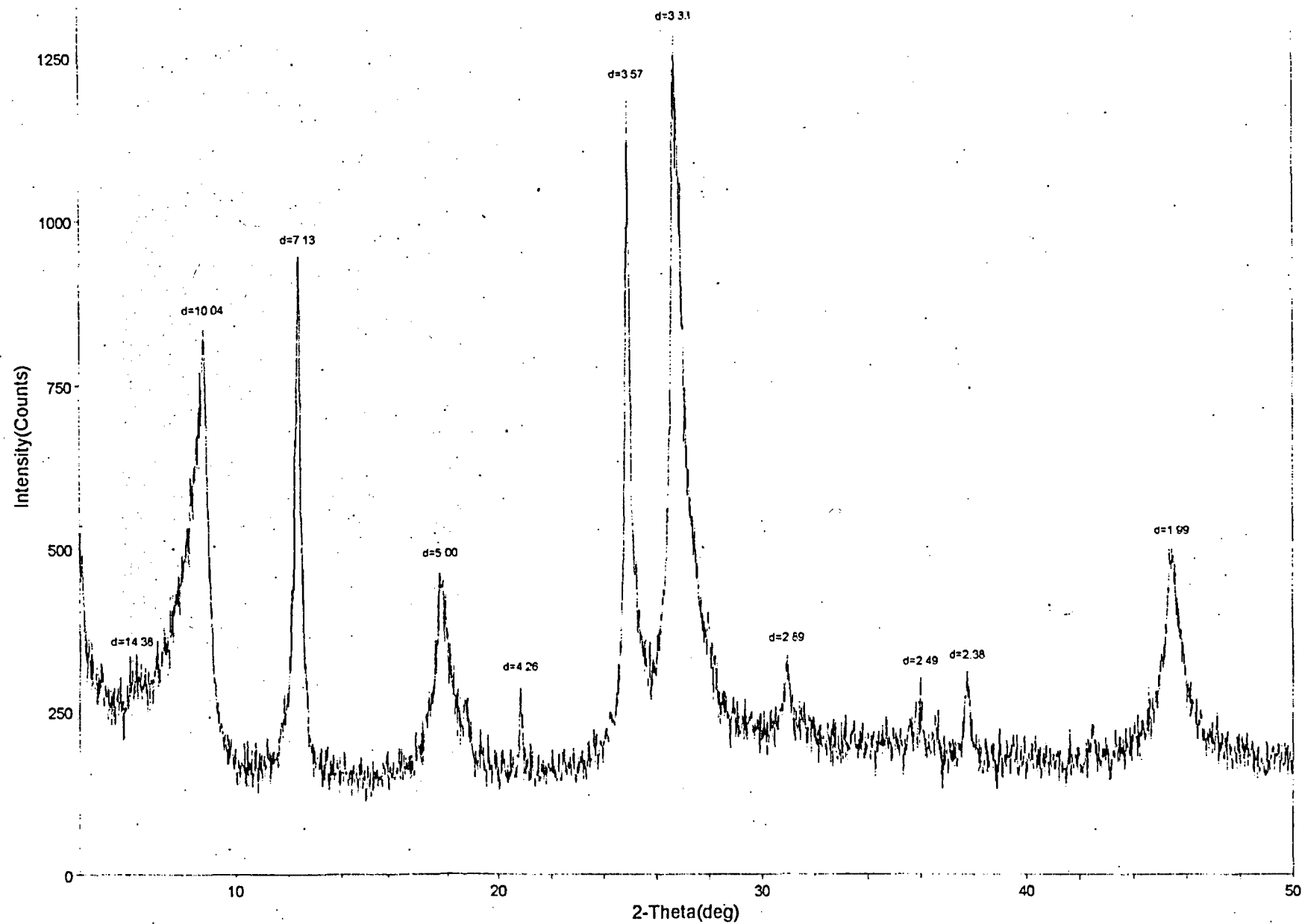
**Patterns are arranged in the sequence: untreated, glycol solvated, heated to 300° C and heated to 500° C for each sample.**

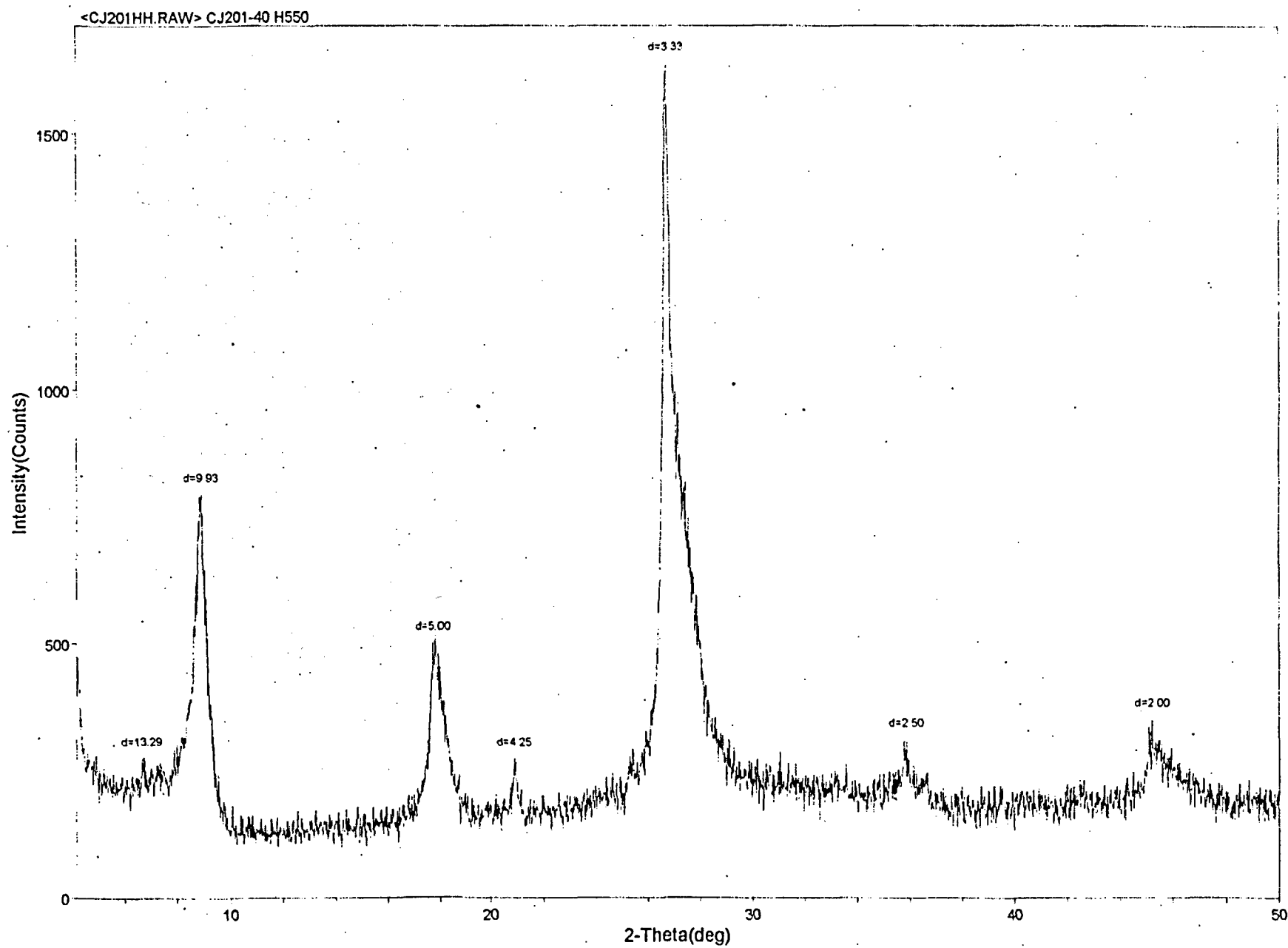


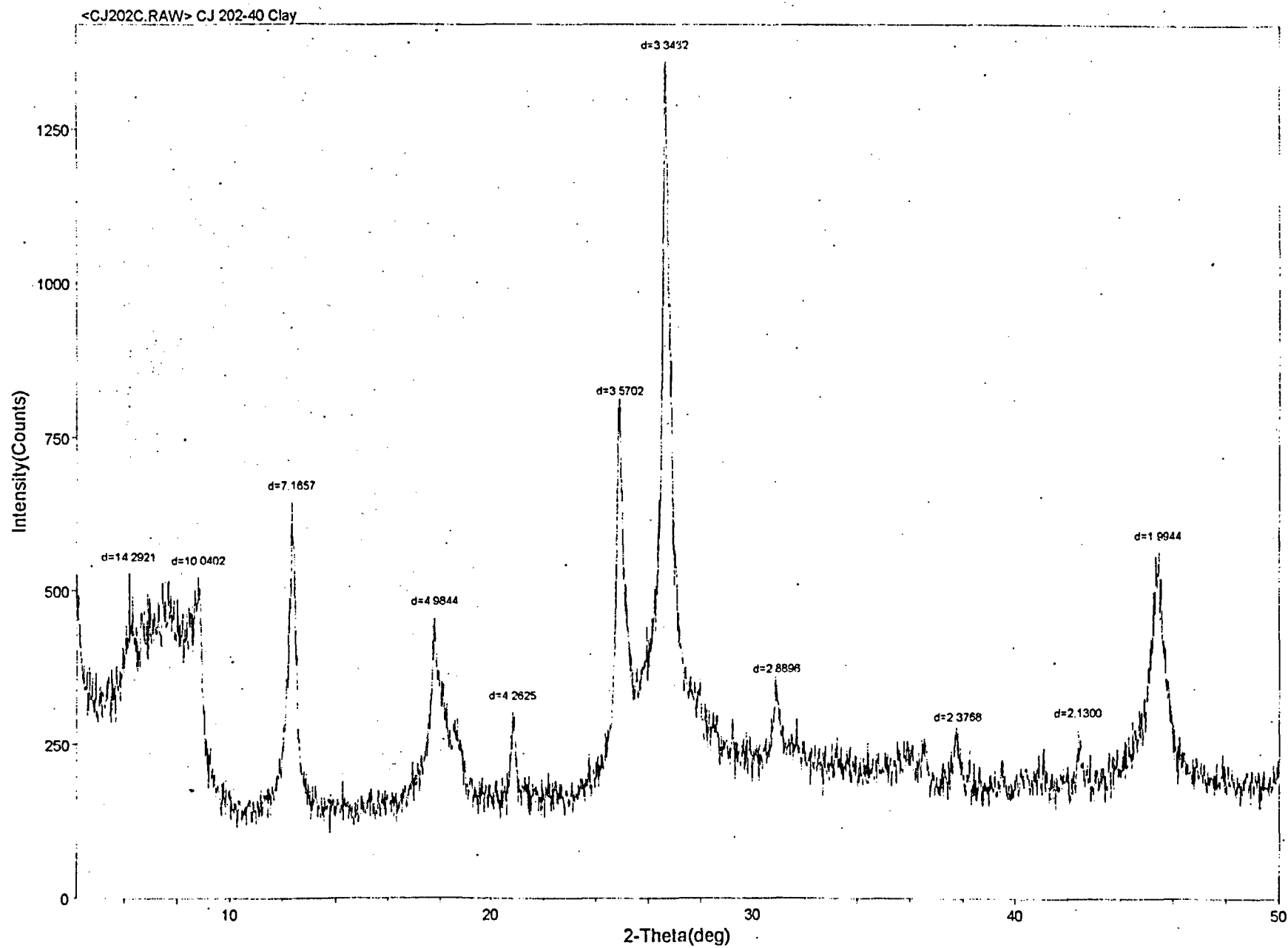




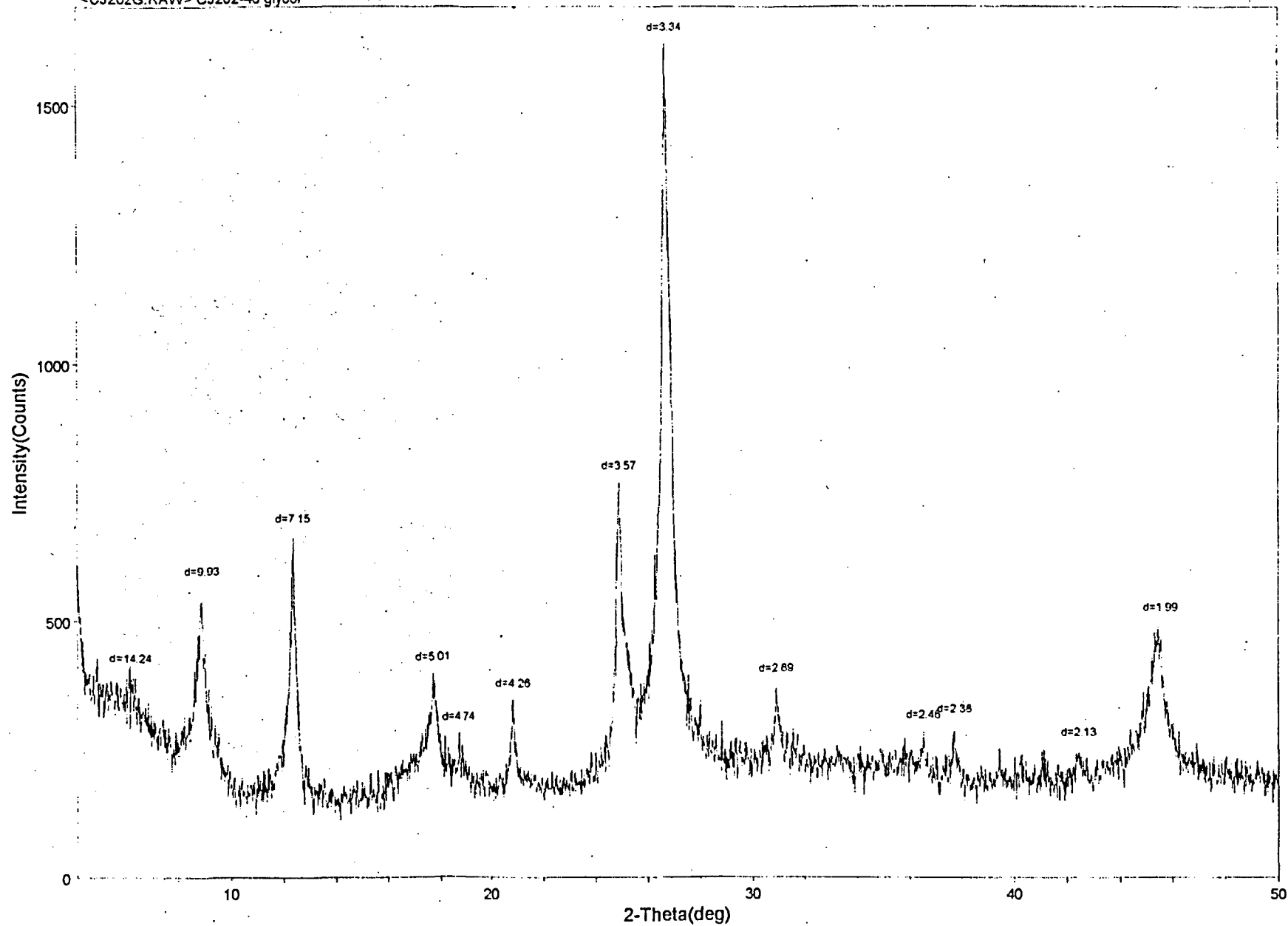
<CJ201HL.RAW> CJ201-40 H300

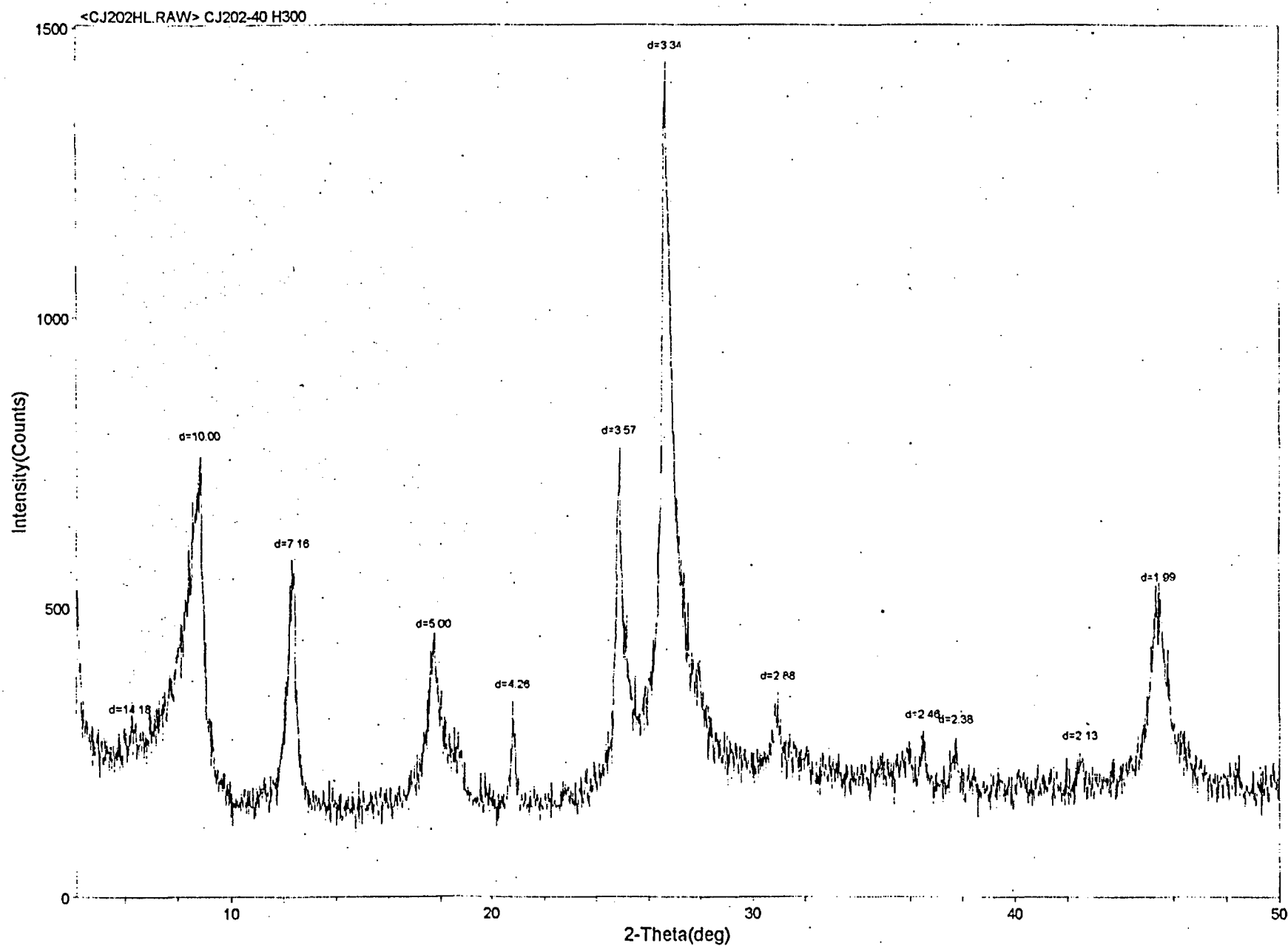


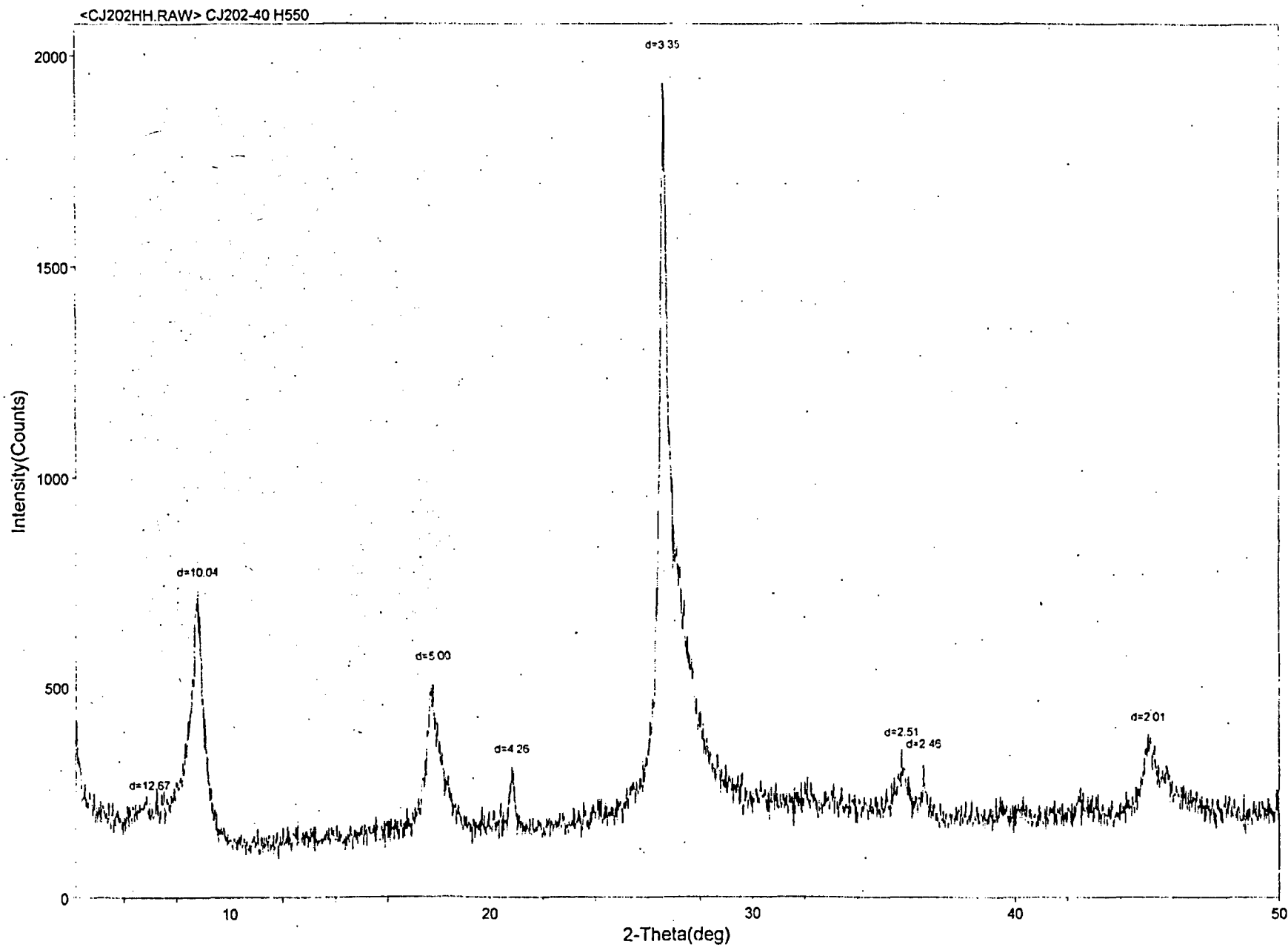




<CJ202G.RAW> CJ202-40 glycol

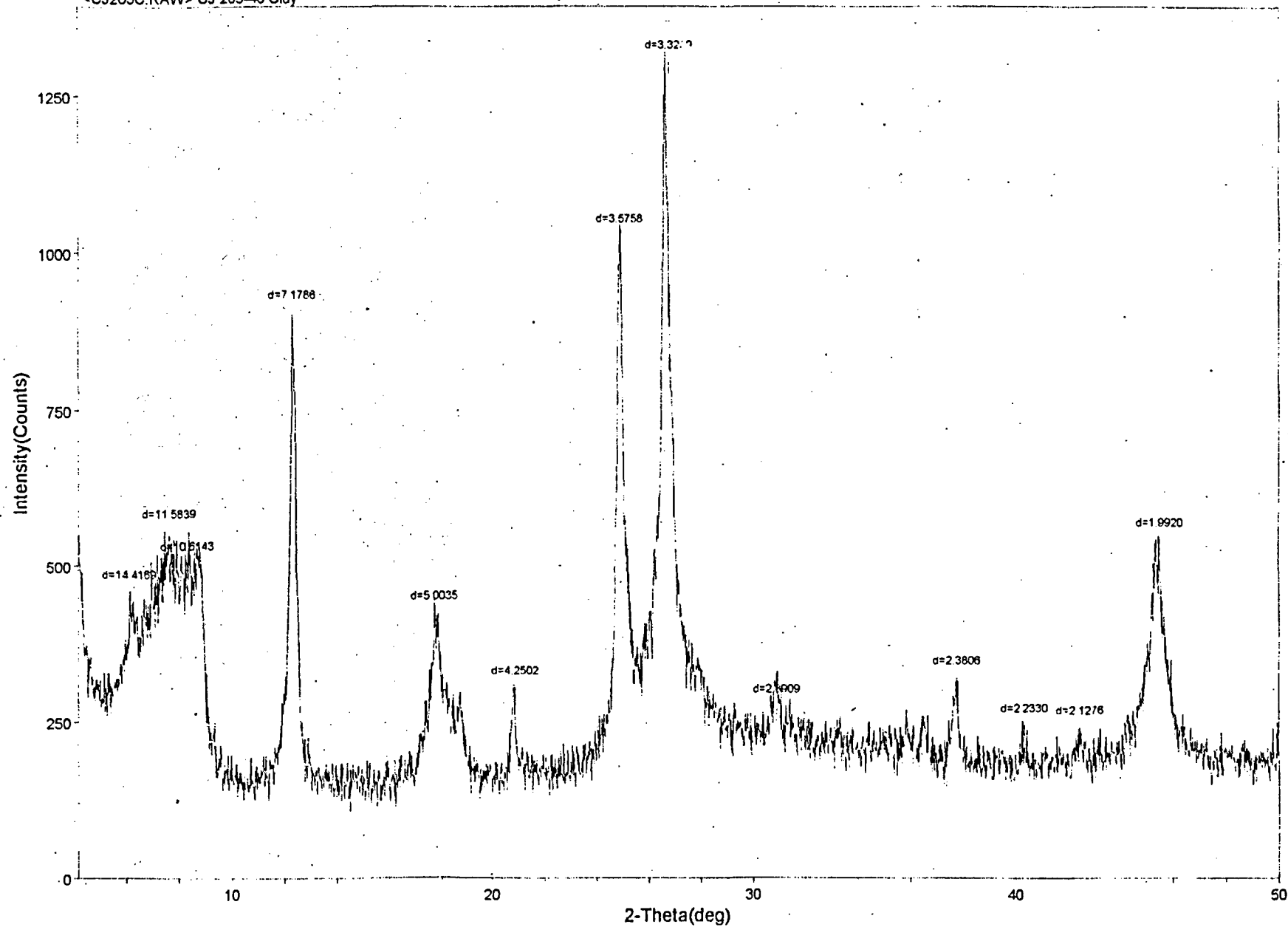




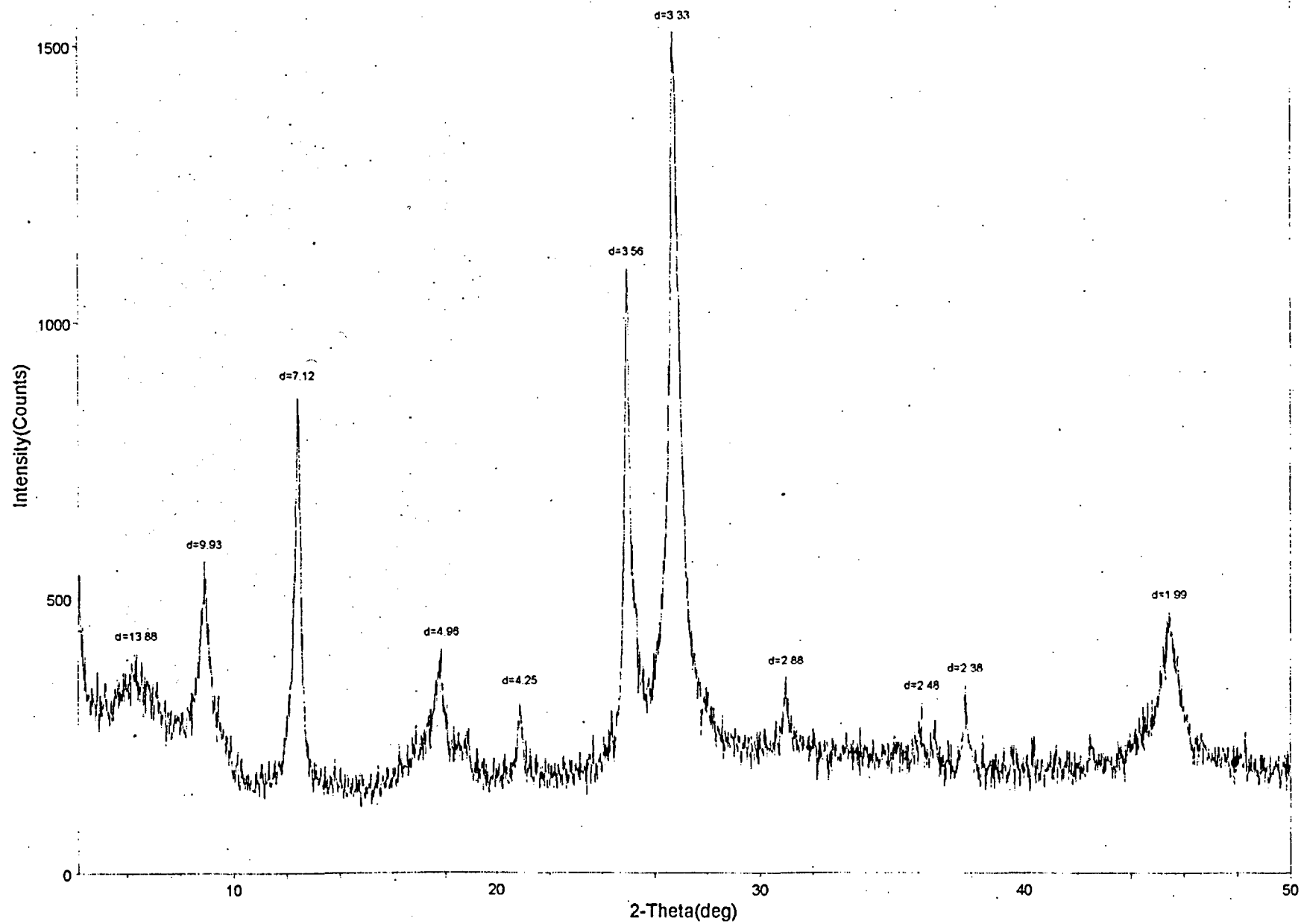


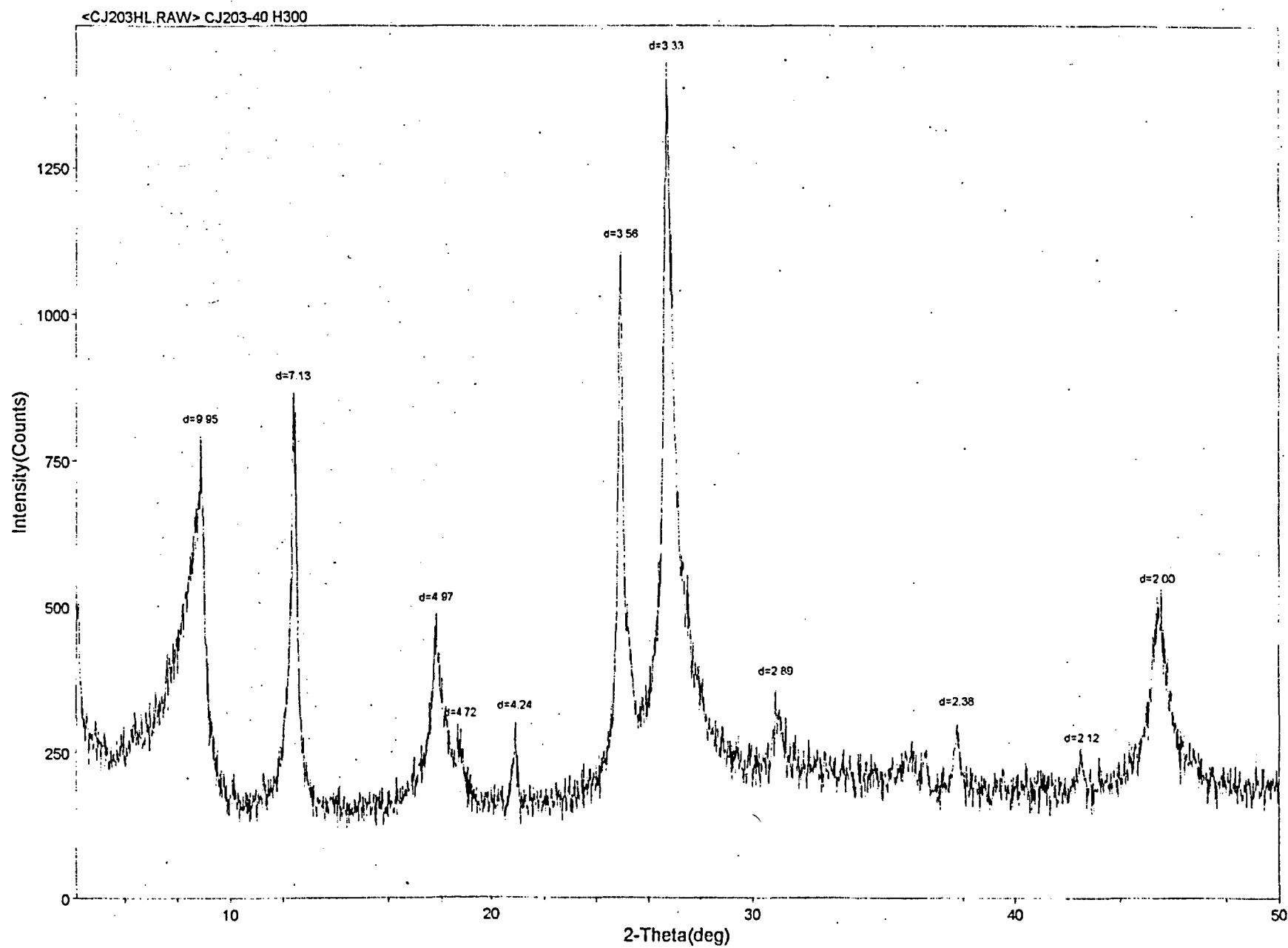


<CJ203C.RAW> CJ 203-40 Clay

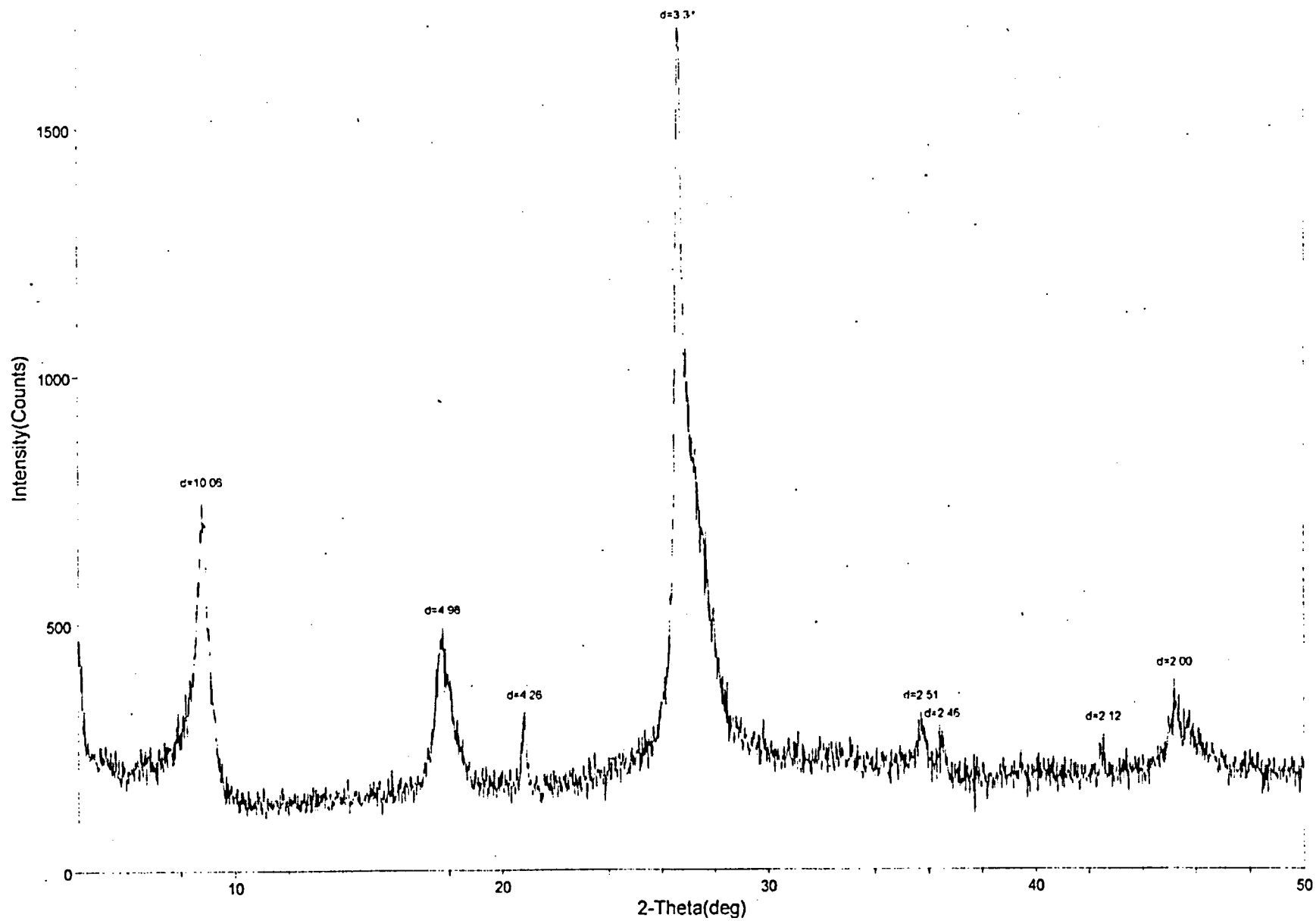


<CJ203G.RAW> CJ203-40 glycol

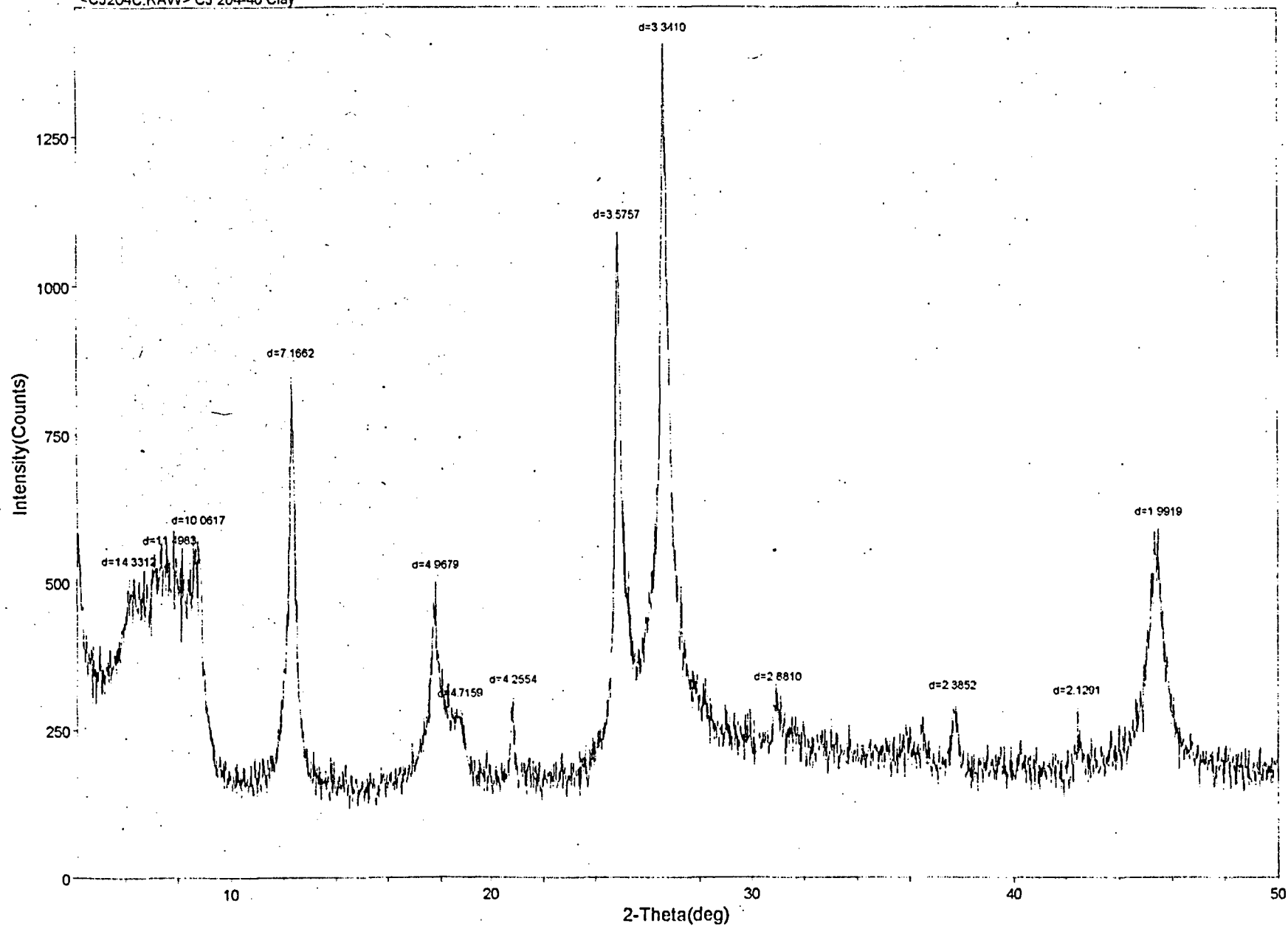




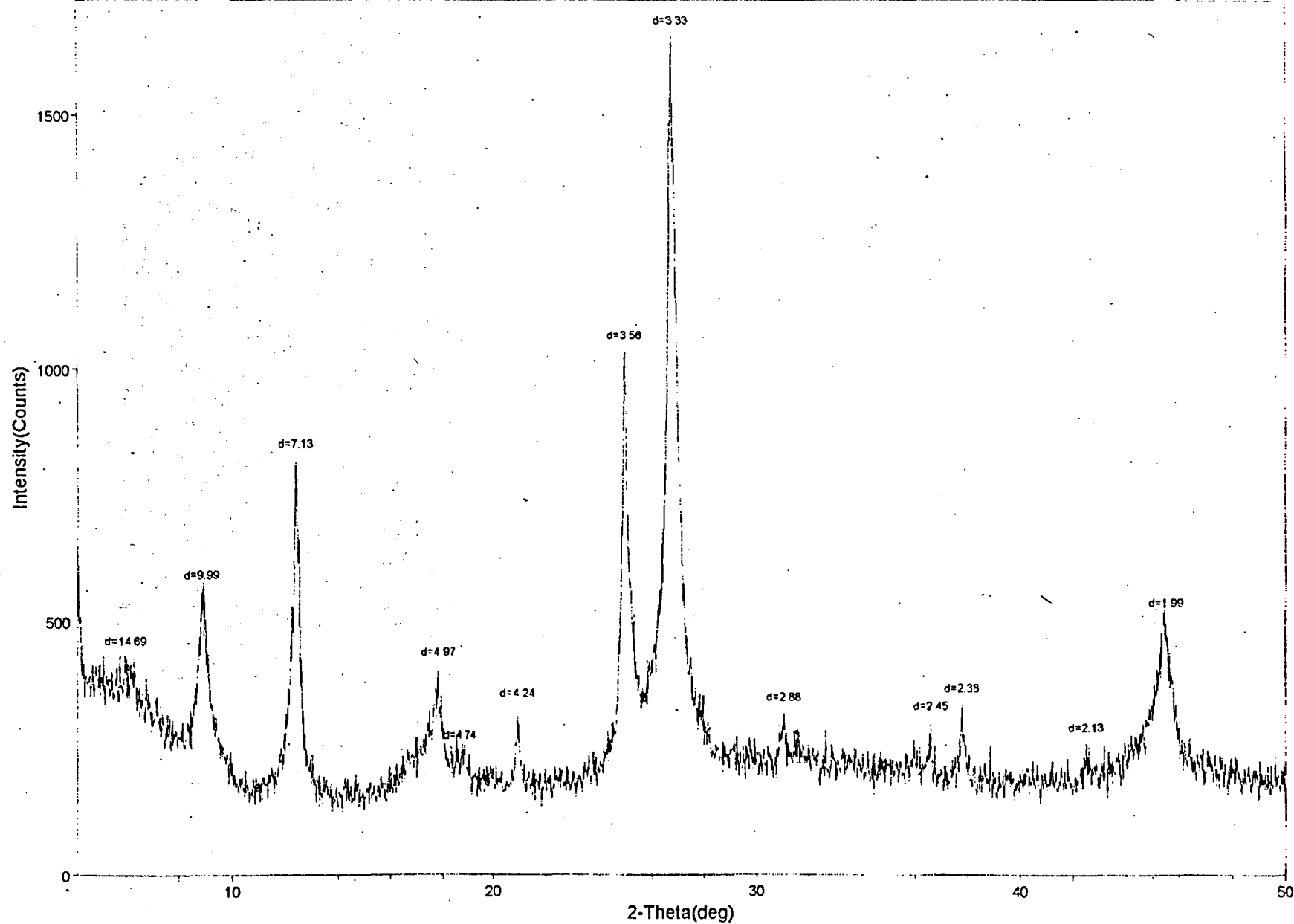
<CJ203HH.RAW> CJ203-40 H550



<CJ204C.RAW> CJ 204-40 Clay

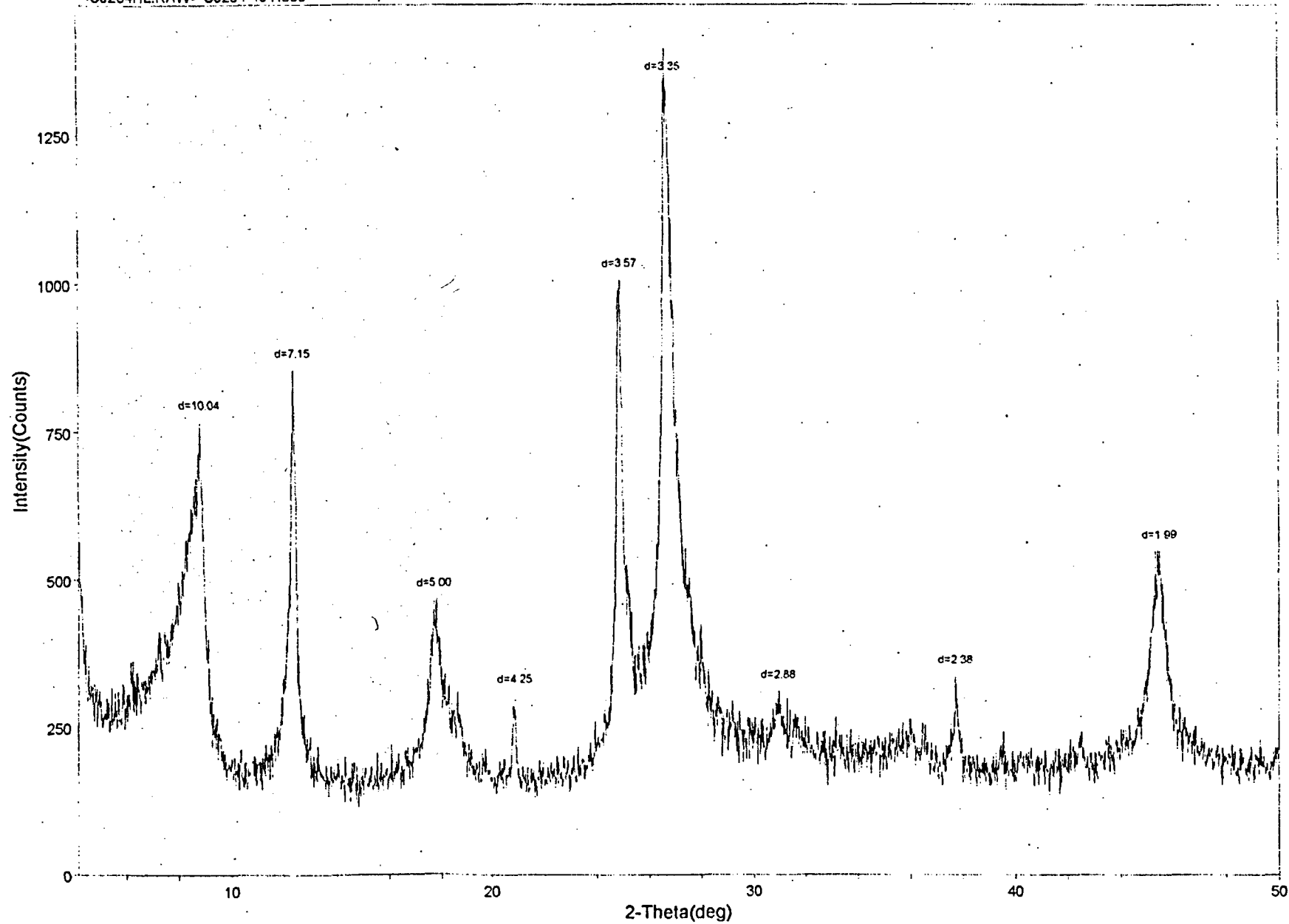


<CJ204G.RAW> CJ204-40 glycol

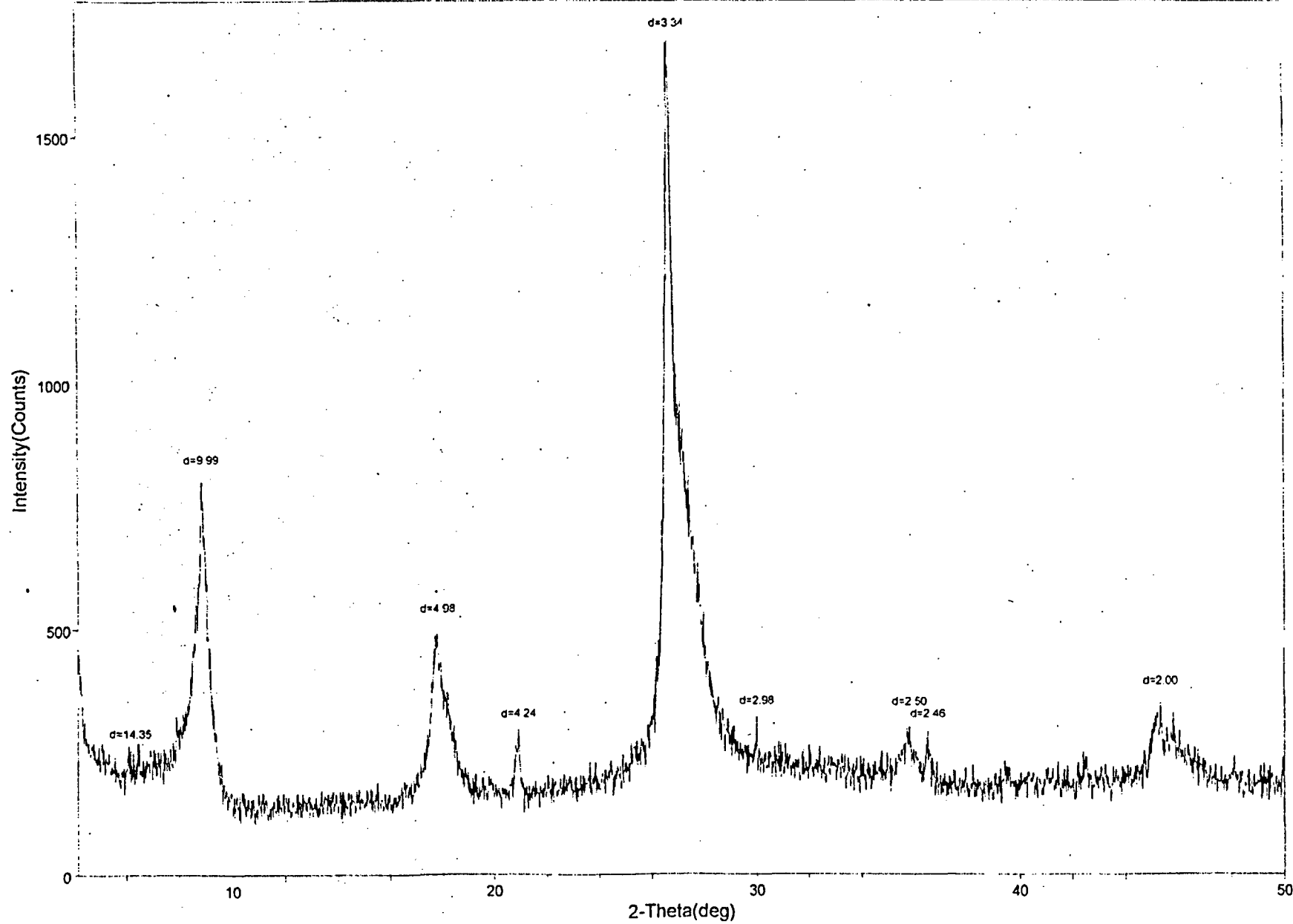


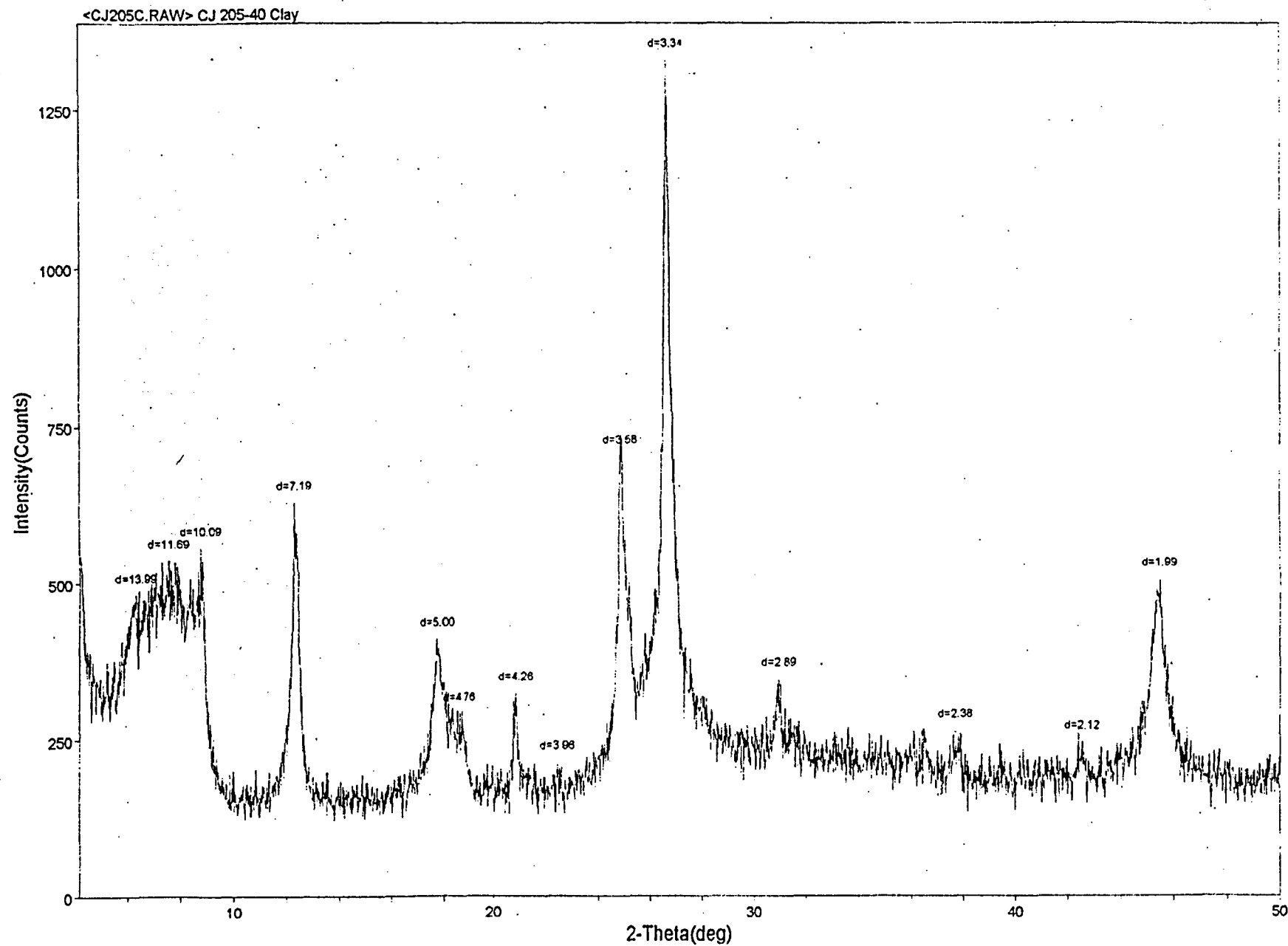


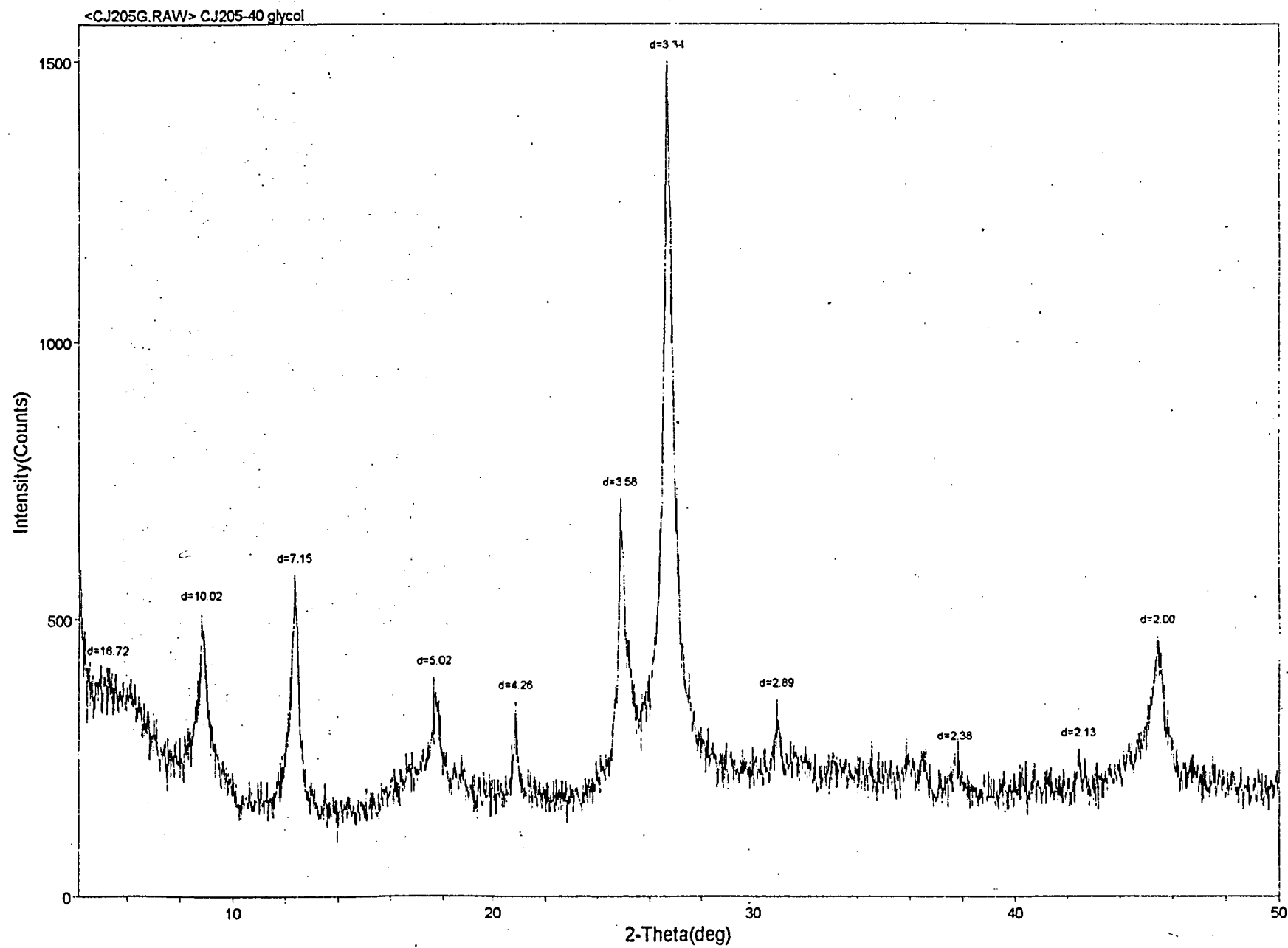
<CJ204HL.RAW> CJ204-40 H300

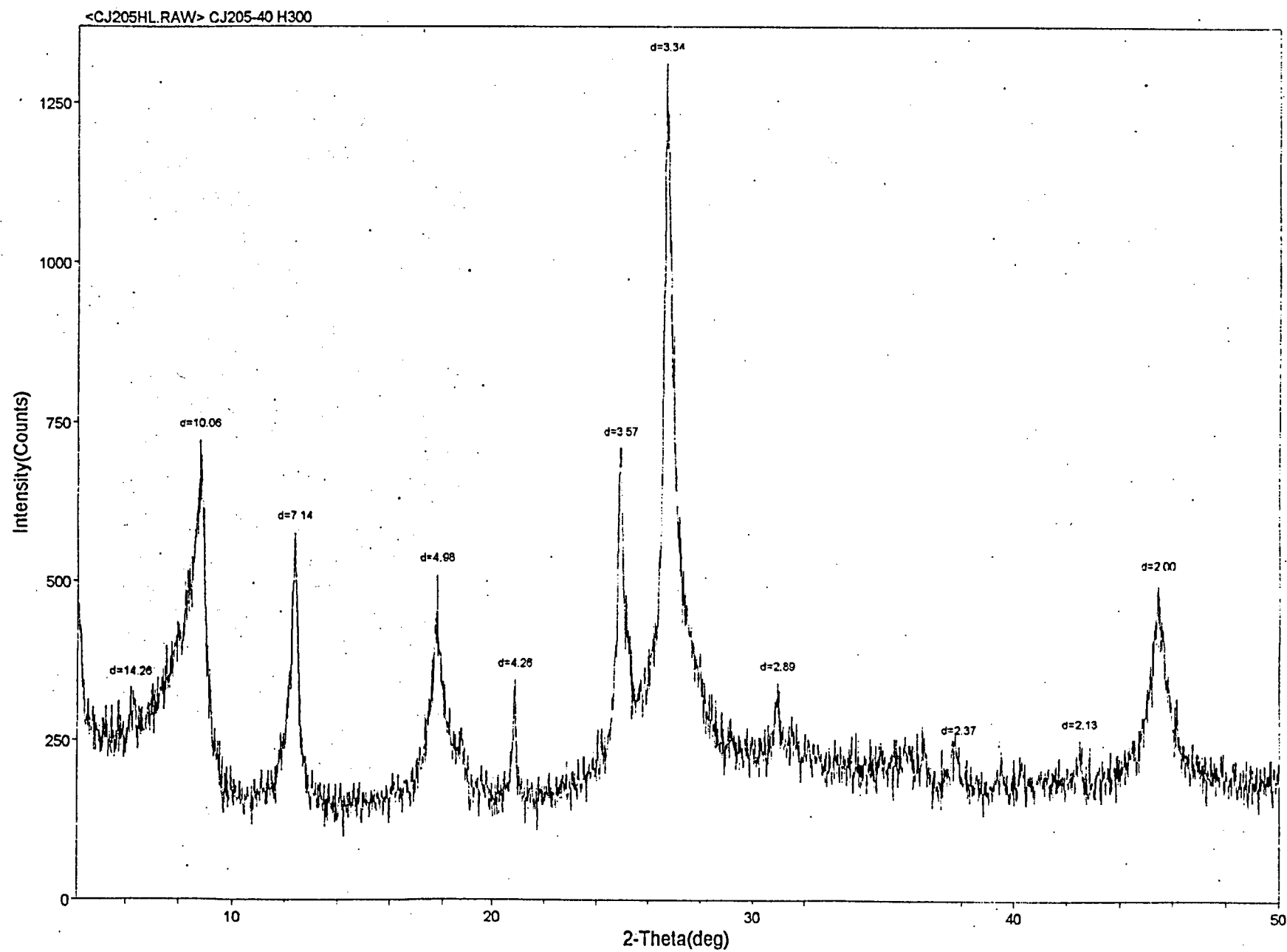


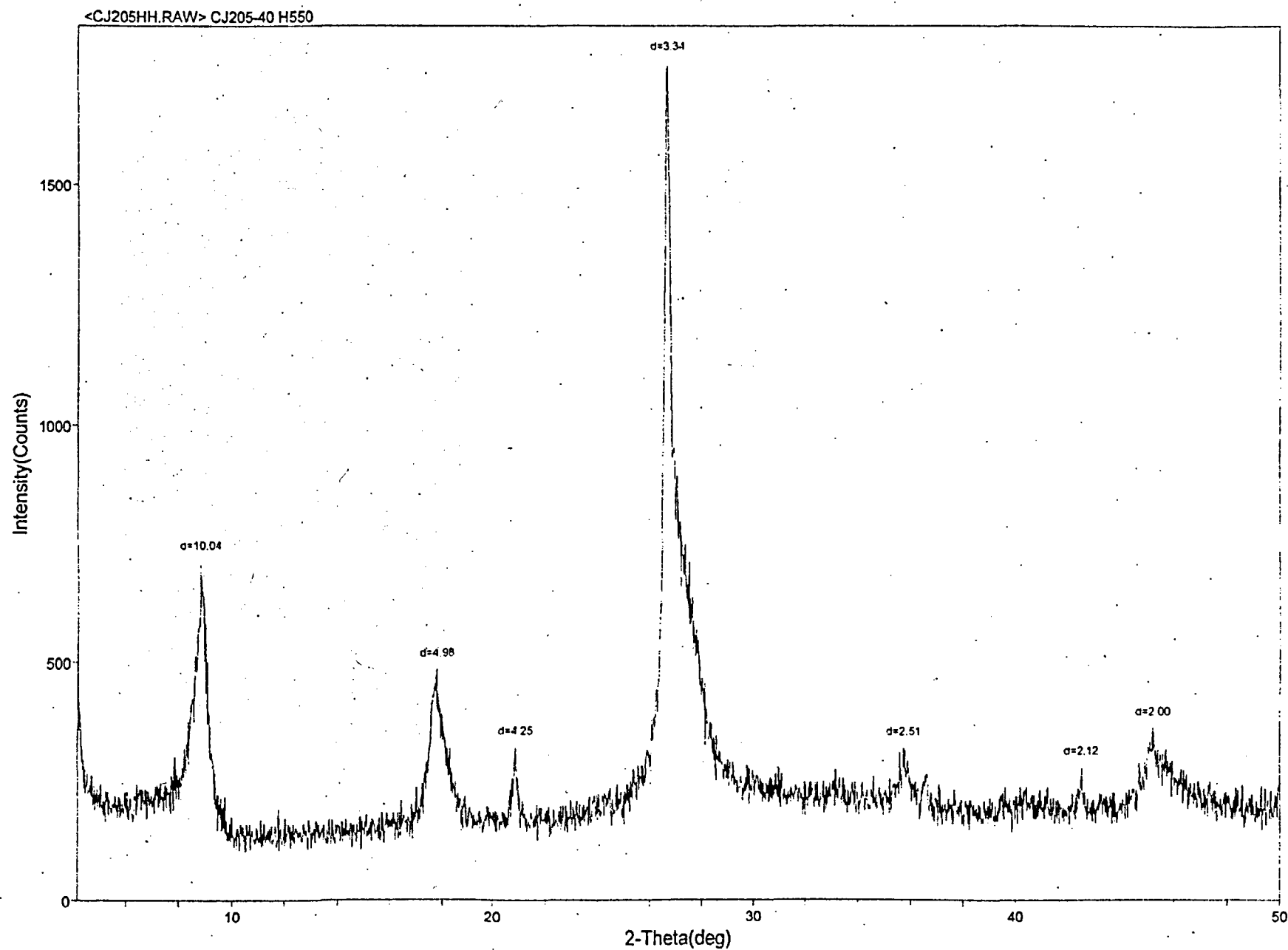
<CJ204HH.RAW> CJ204-40 H550



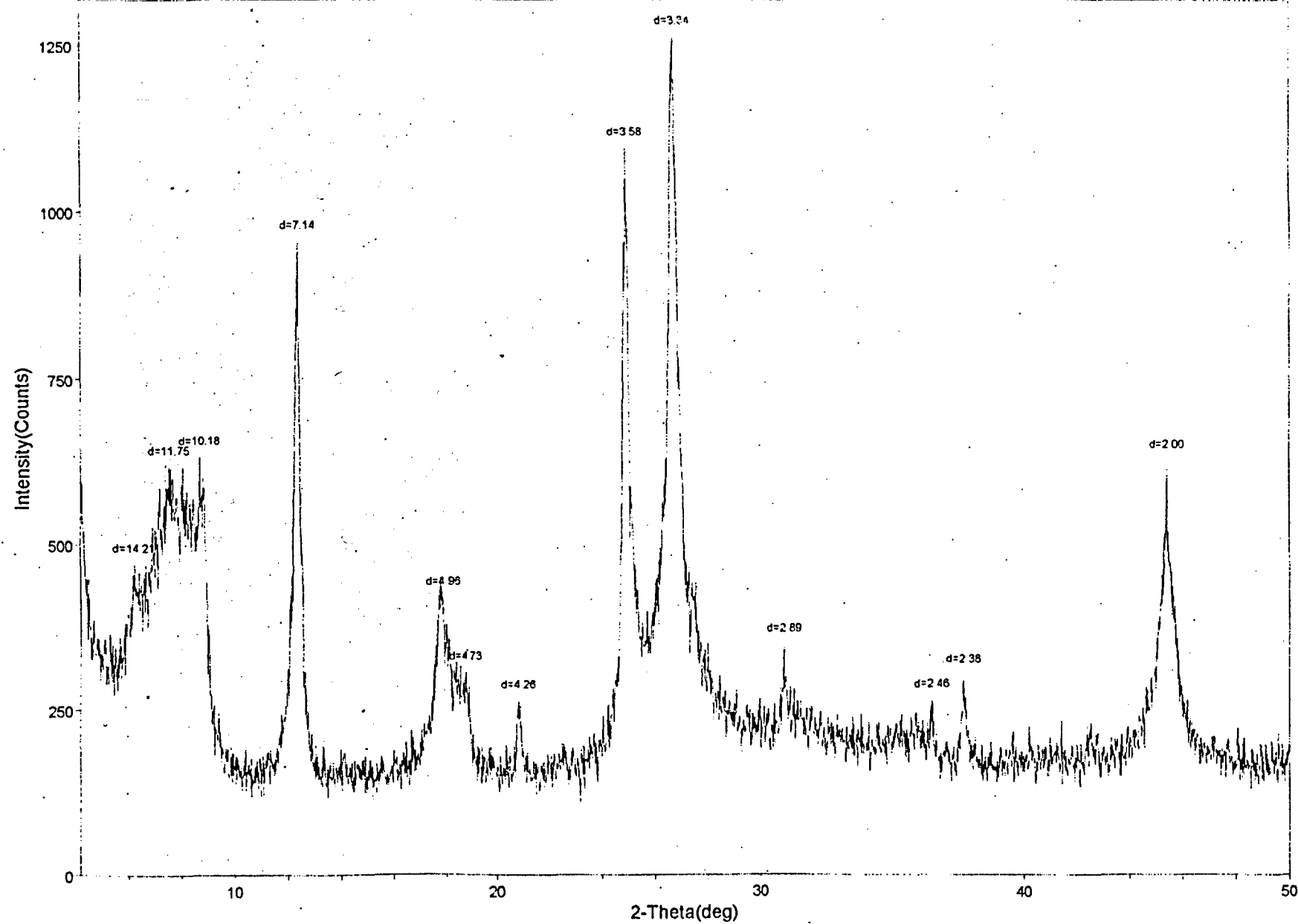




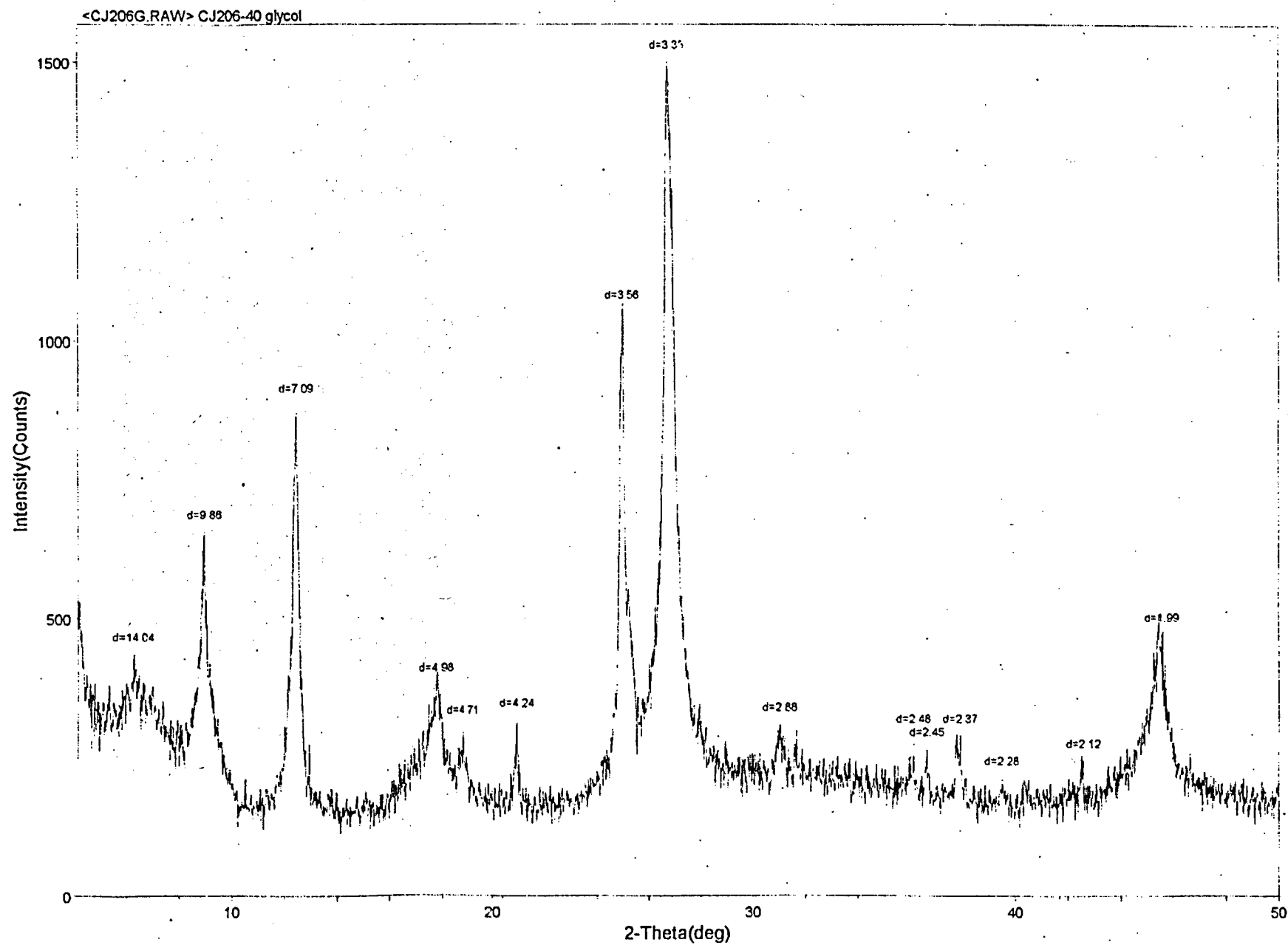


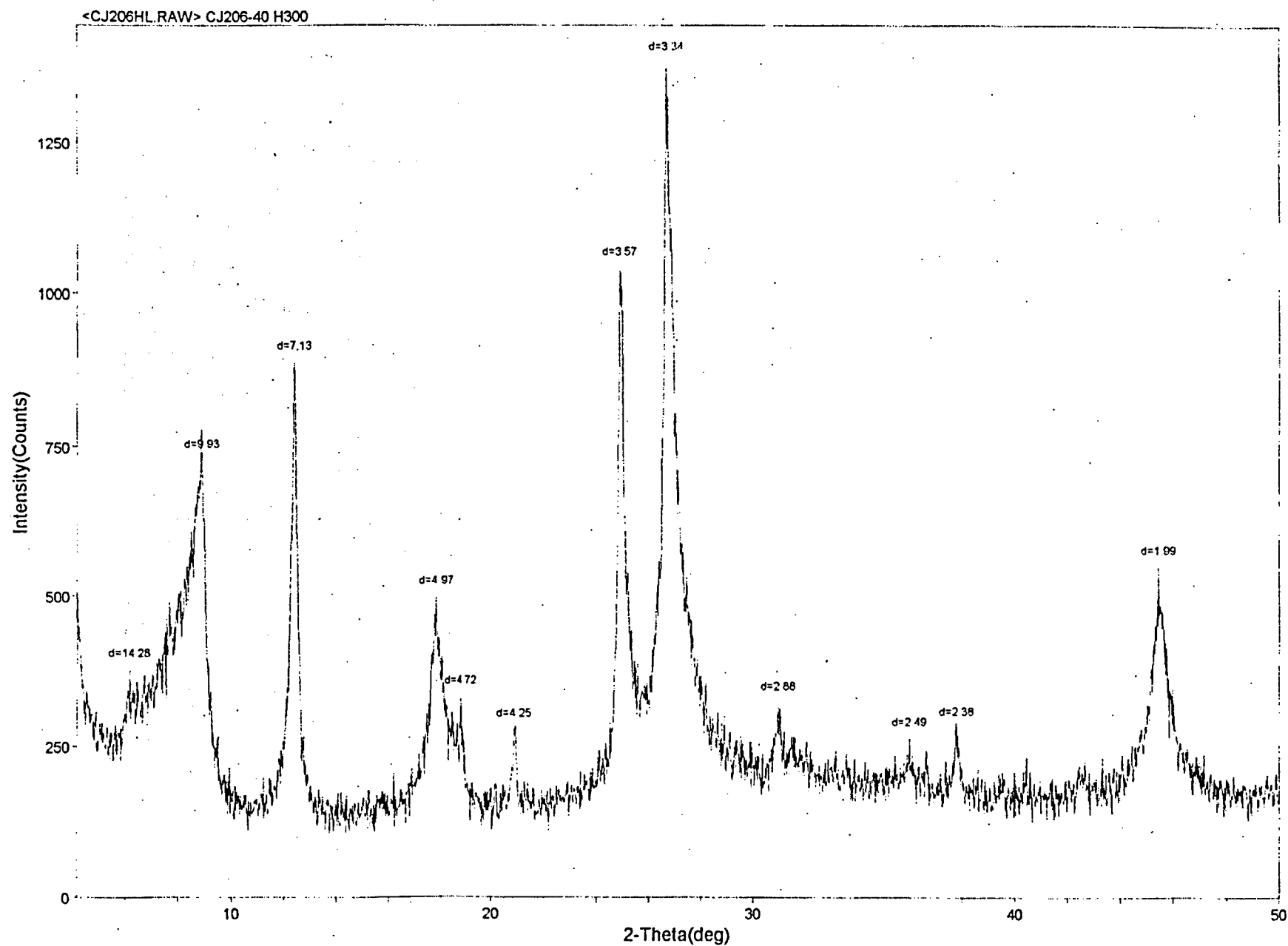


<CJ206C.RAW> CJ 206-40 Clay

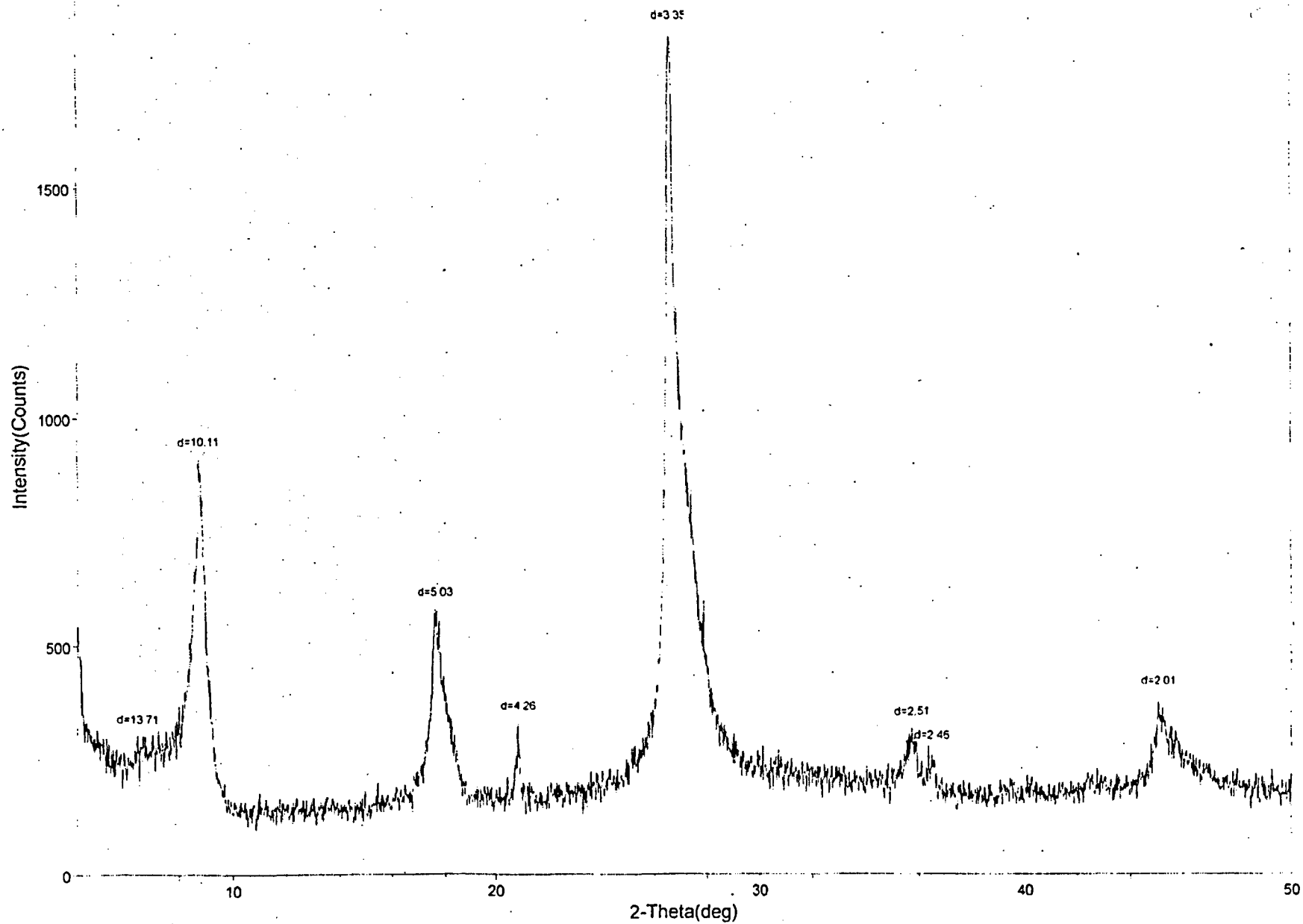


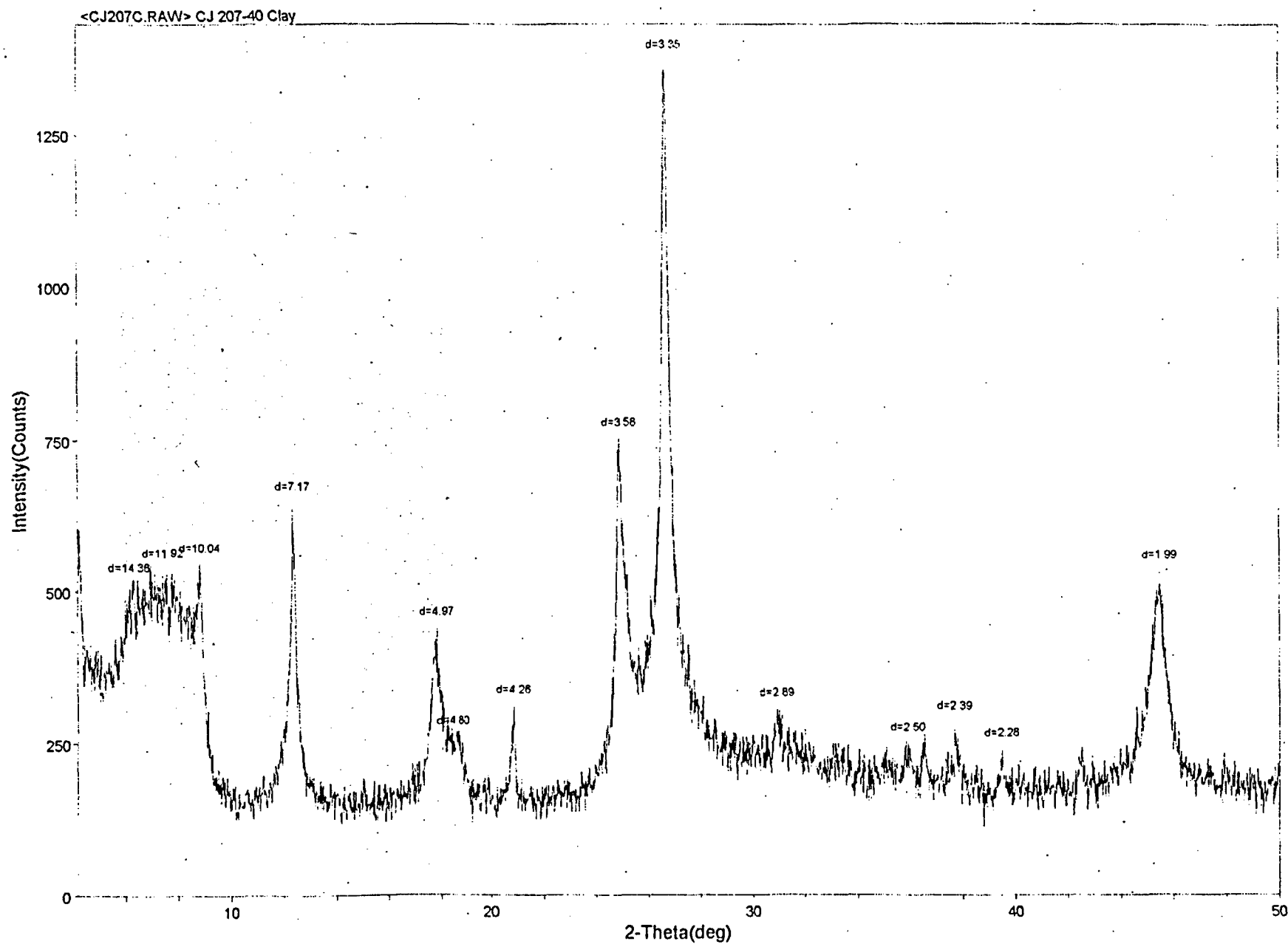


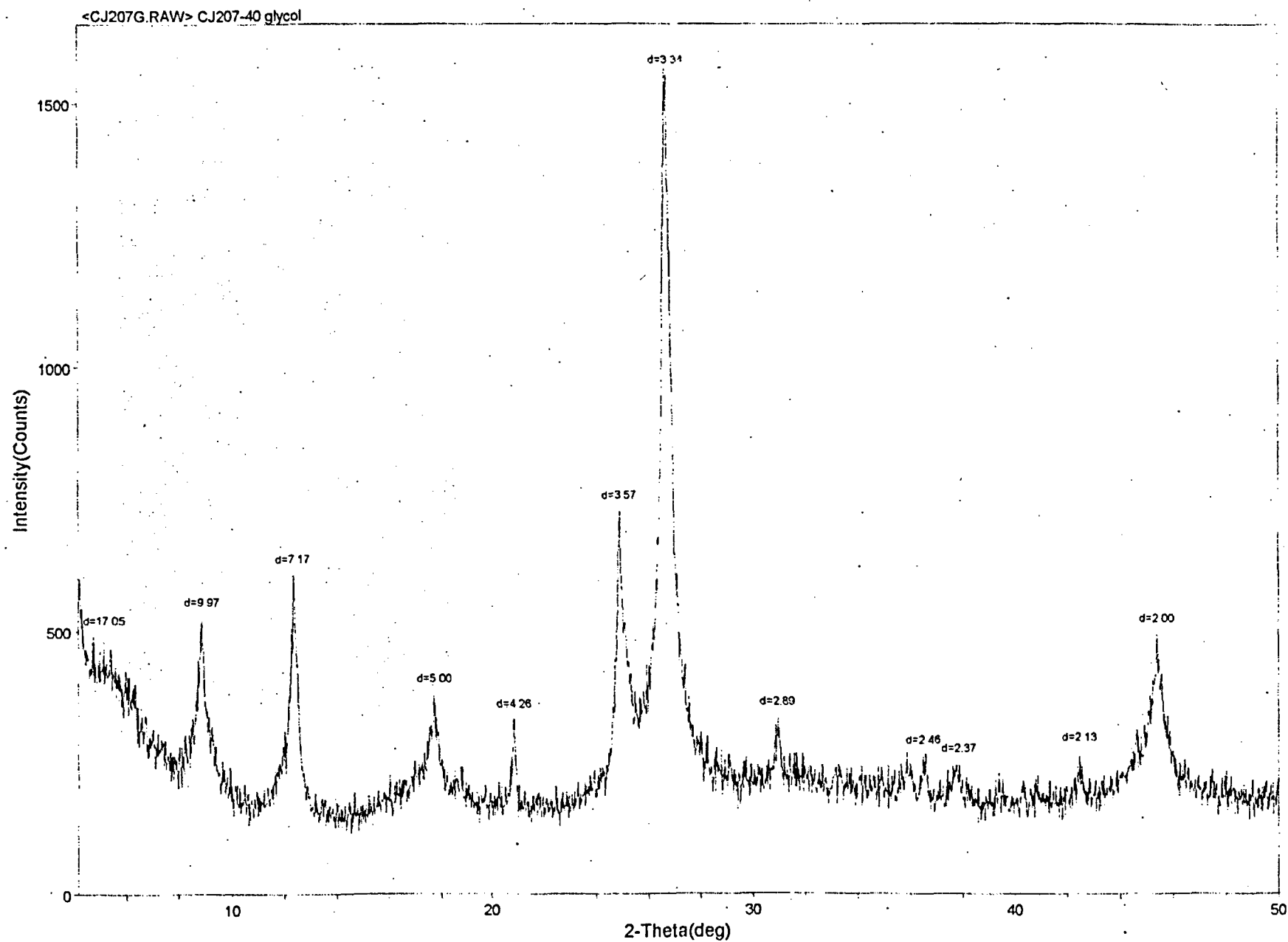


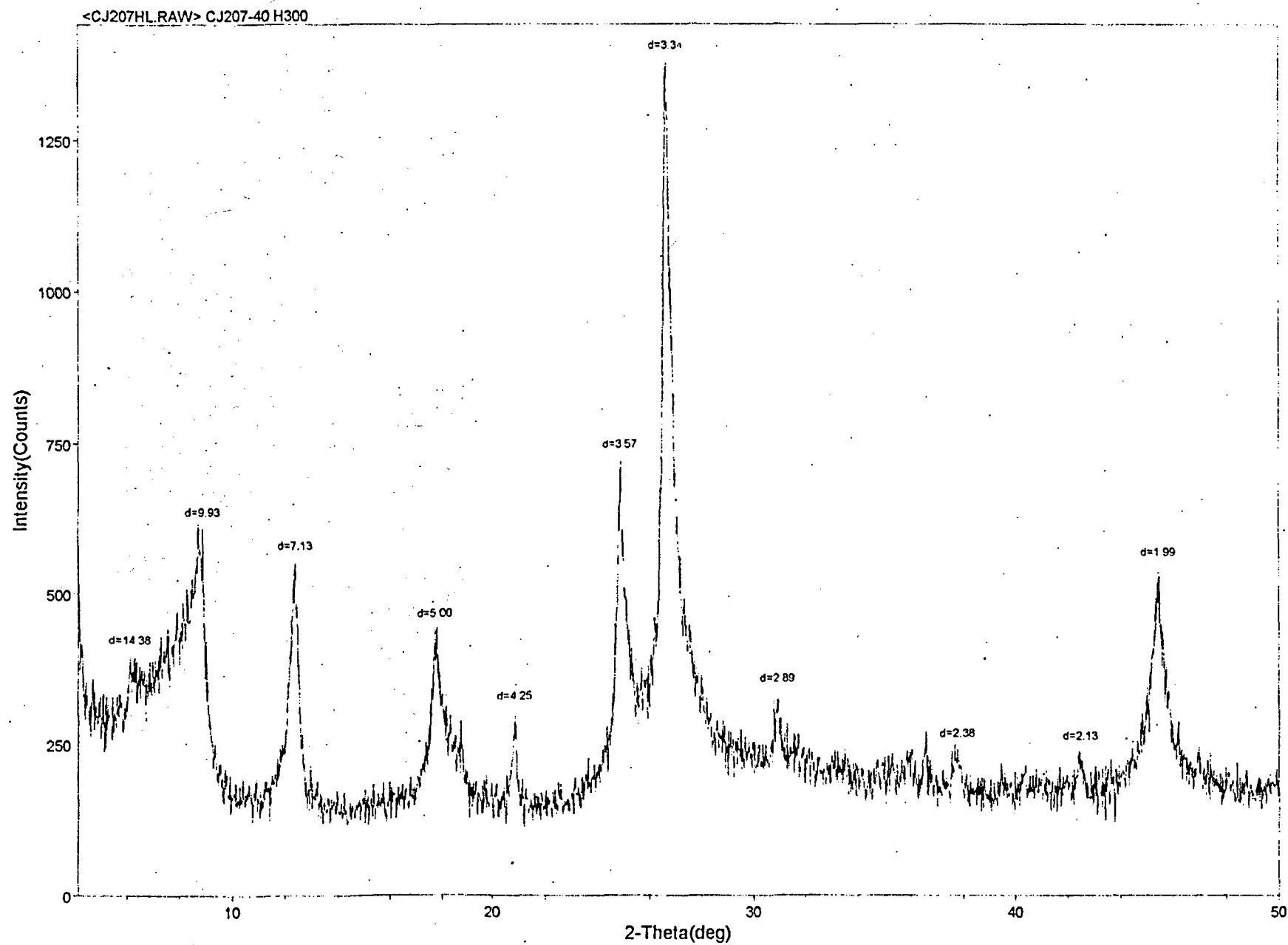


<CJ206HH.RAW> CJ206-40 H550

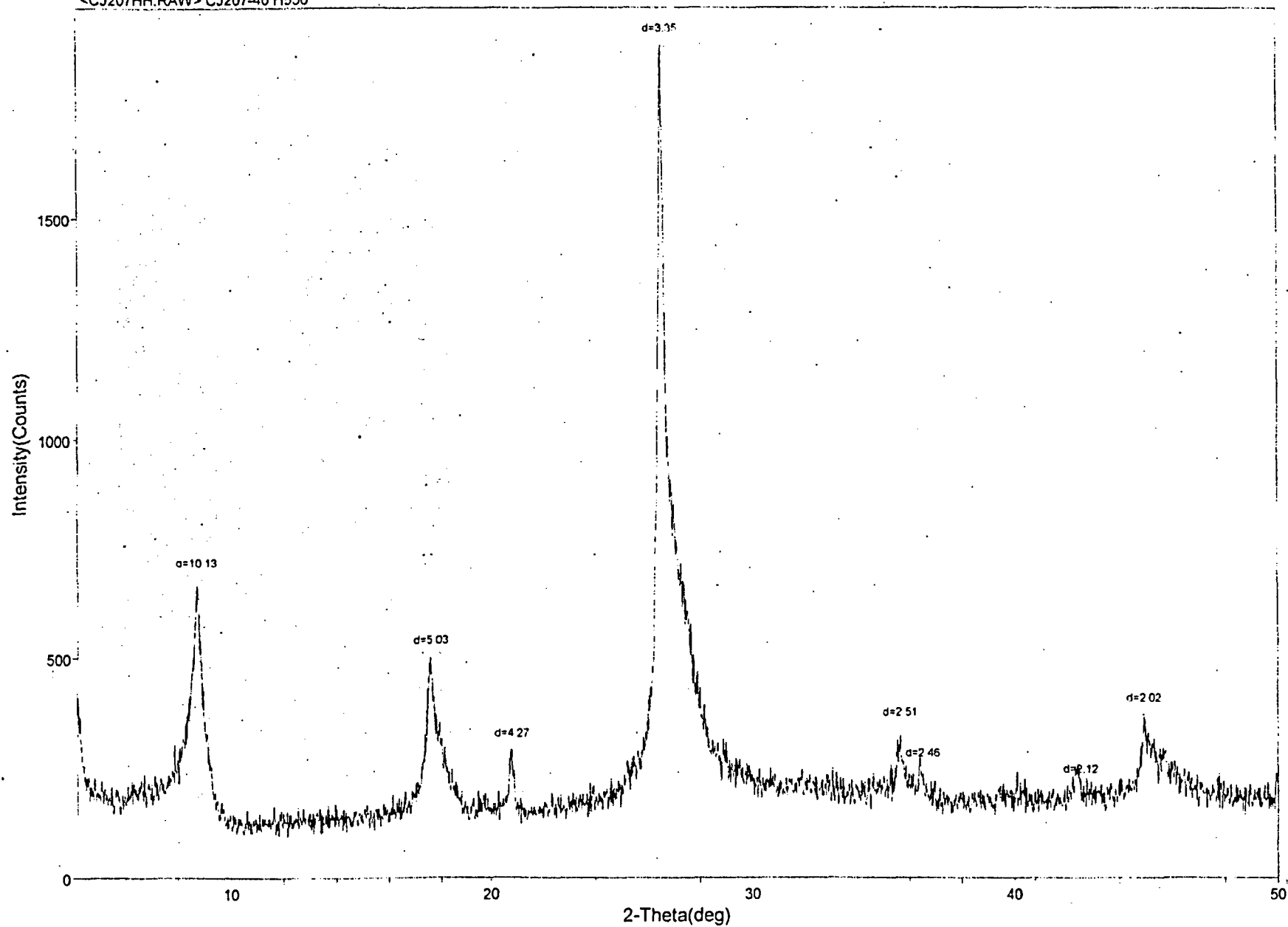




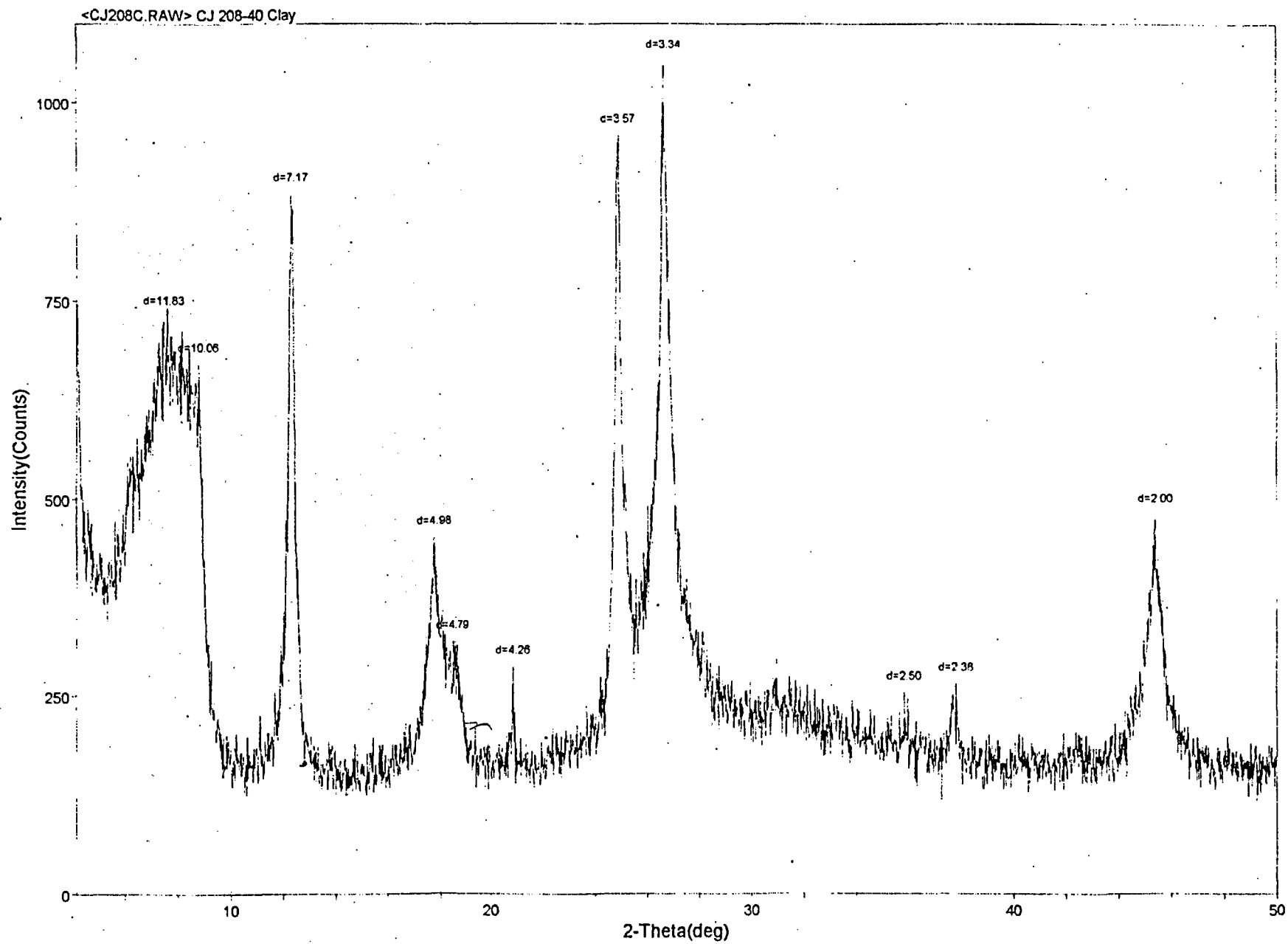


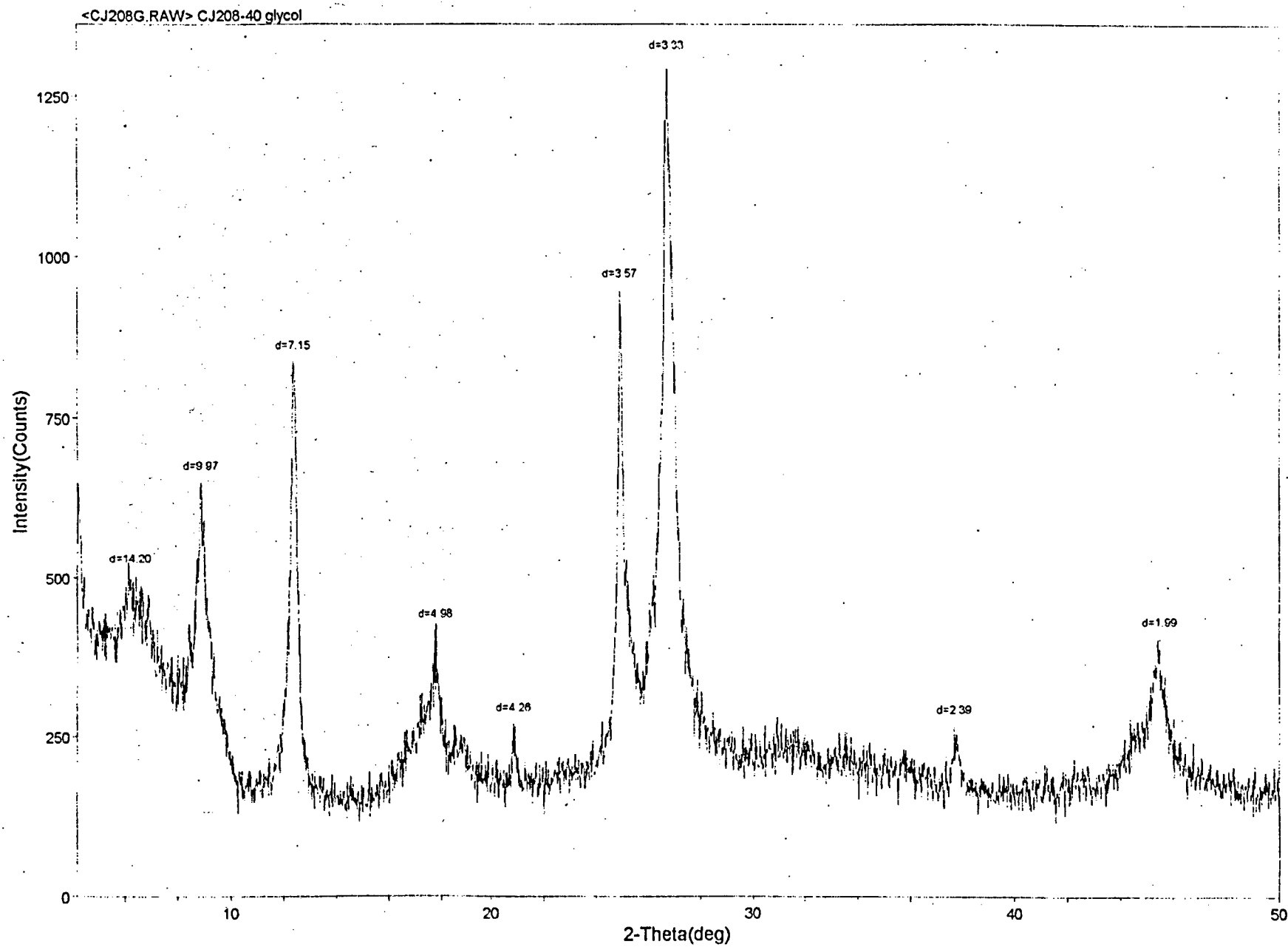


<CJ207HH.RAW> CJ207-40 H550

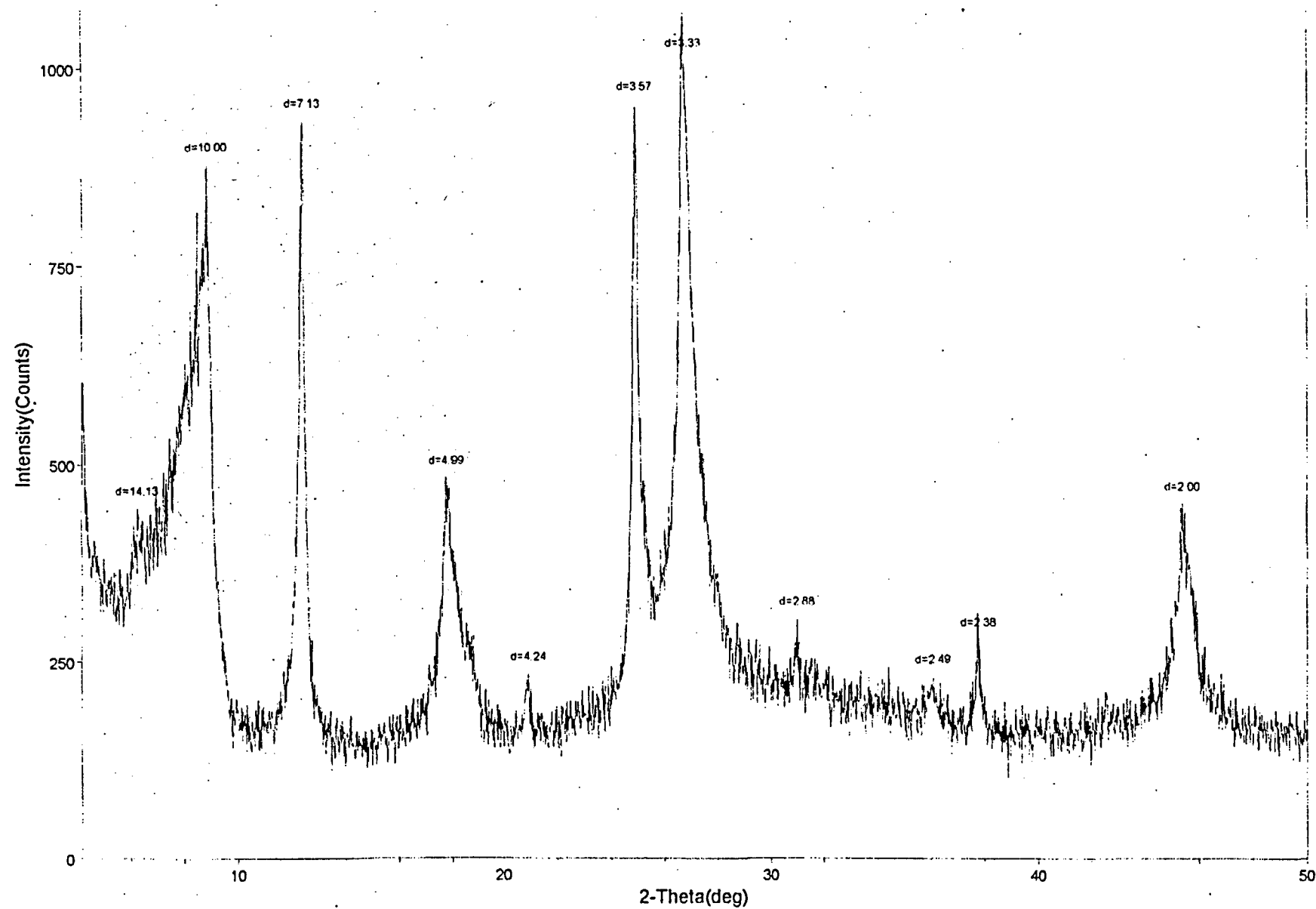


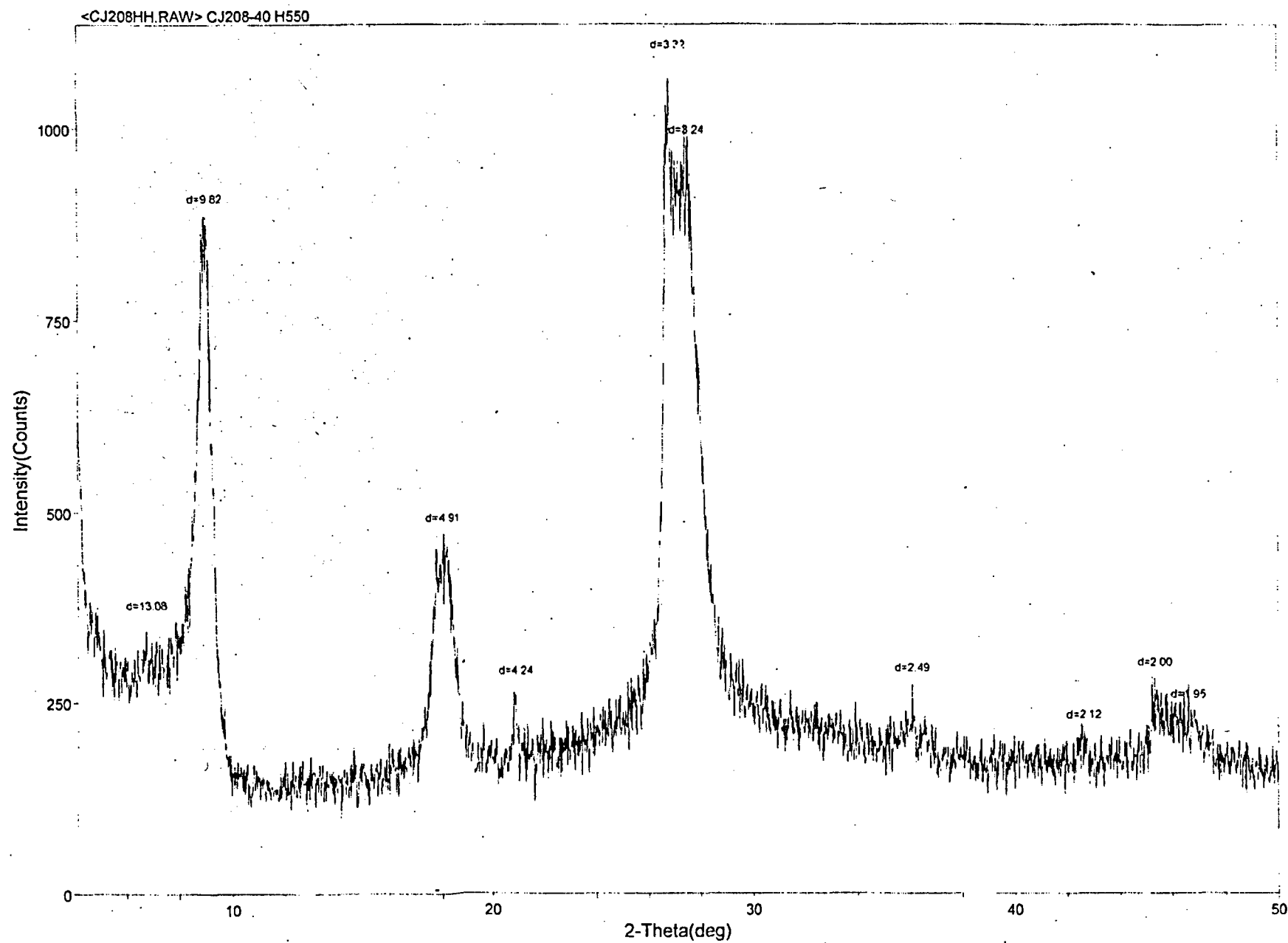




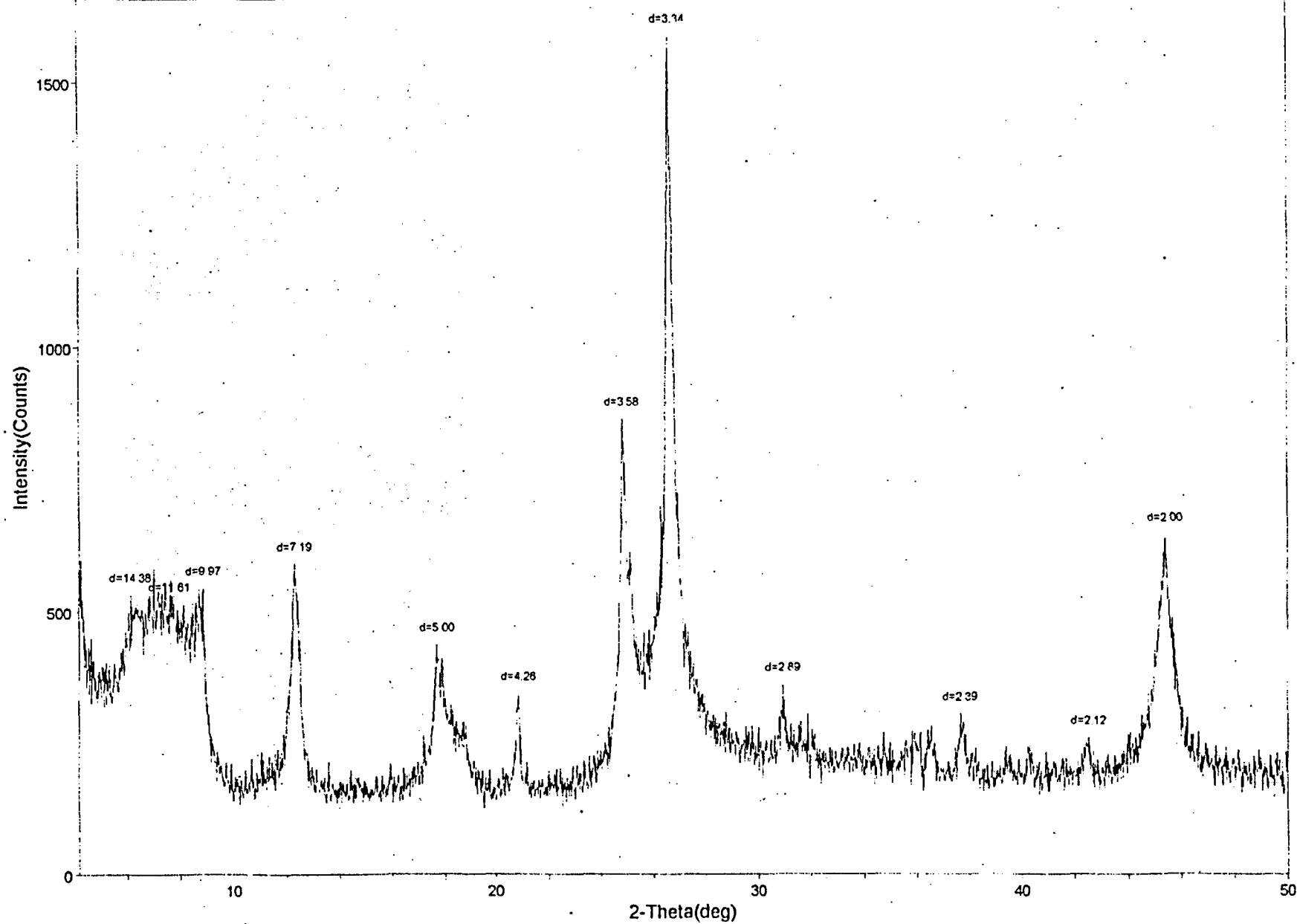


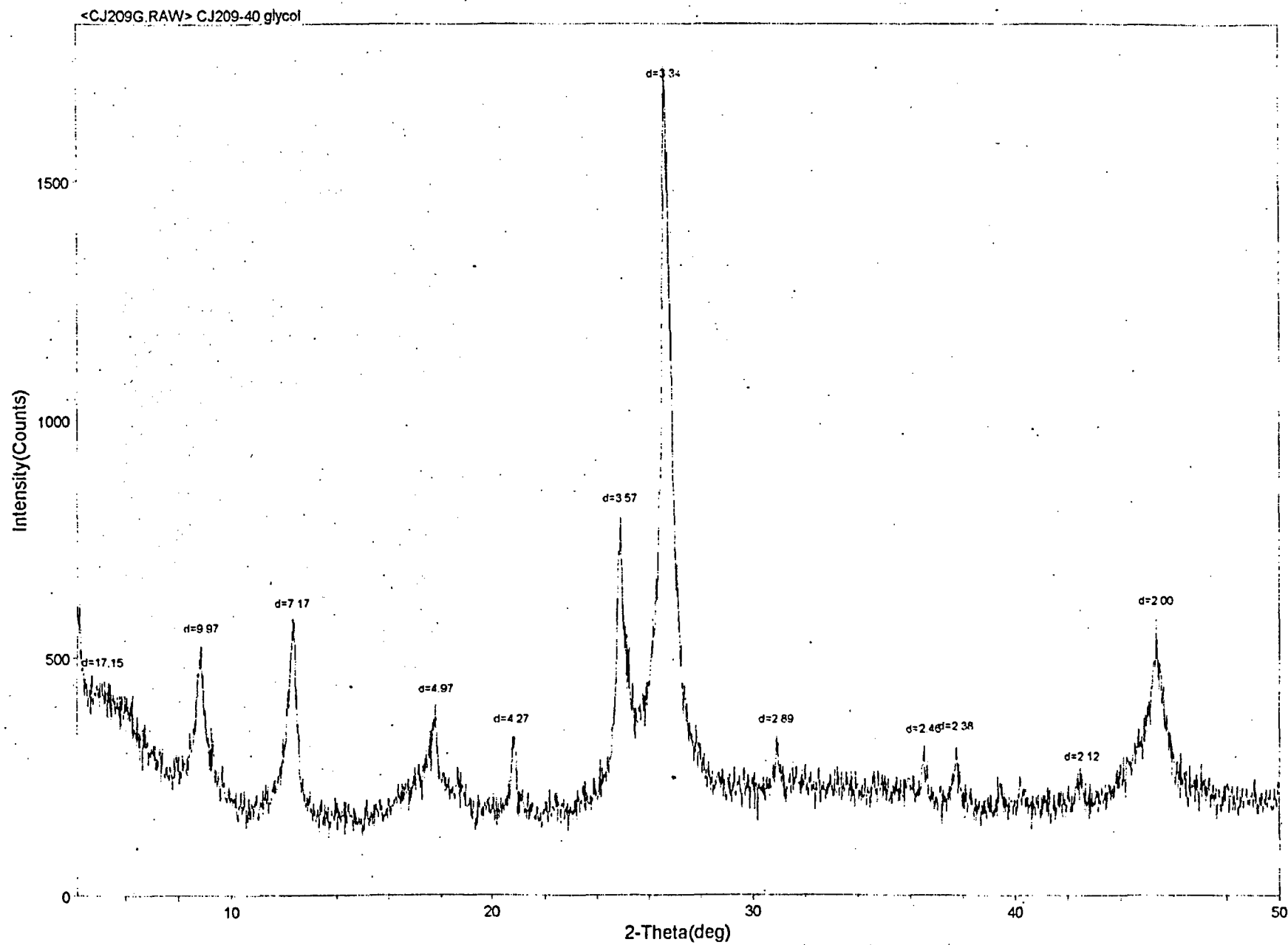
<CJ208HL.RAW> CJ208-40 H300



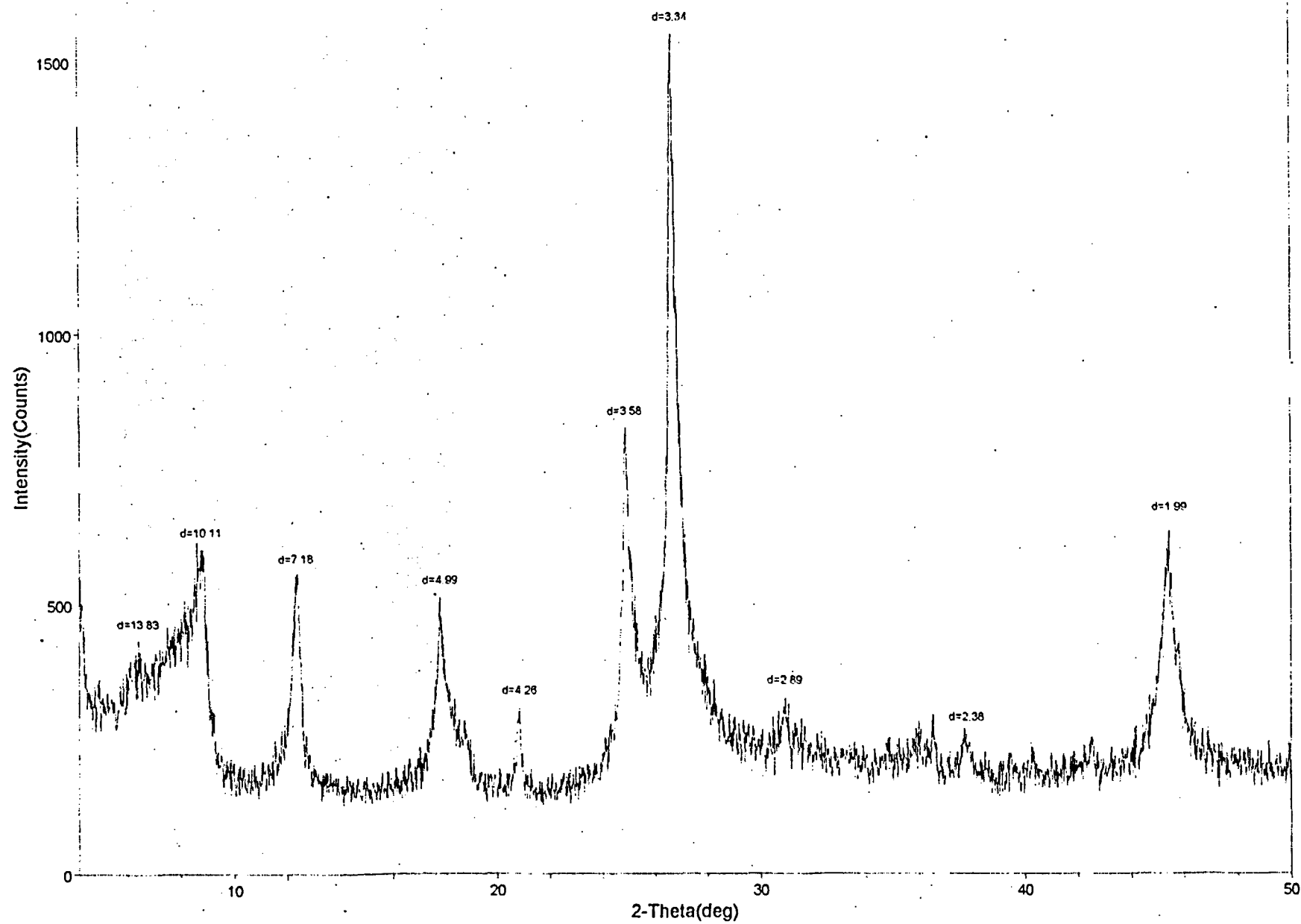


<CJ209C.RAW> CJ 209-40 Clay



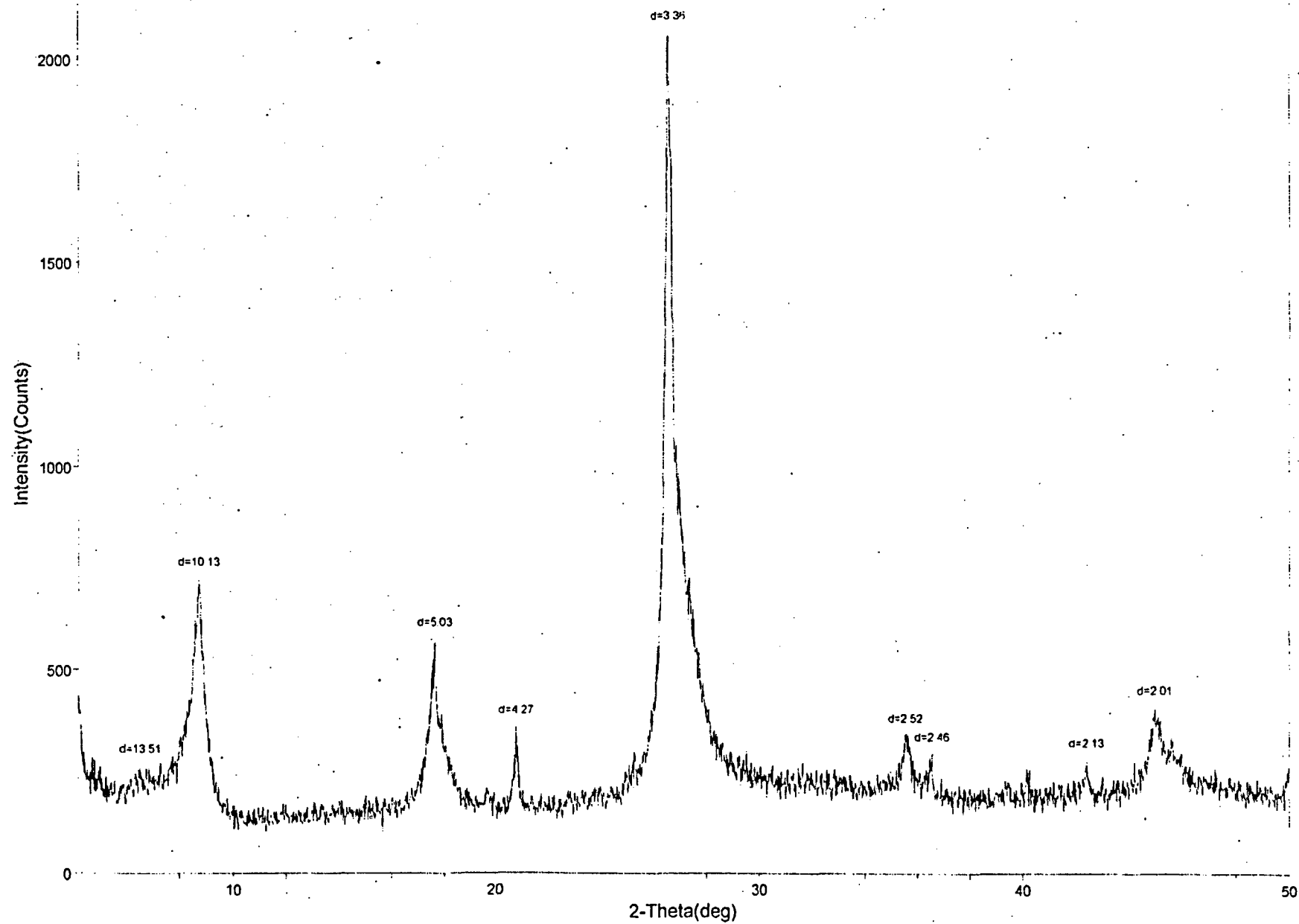


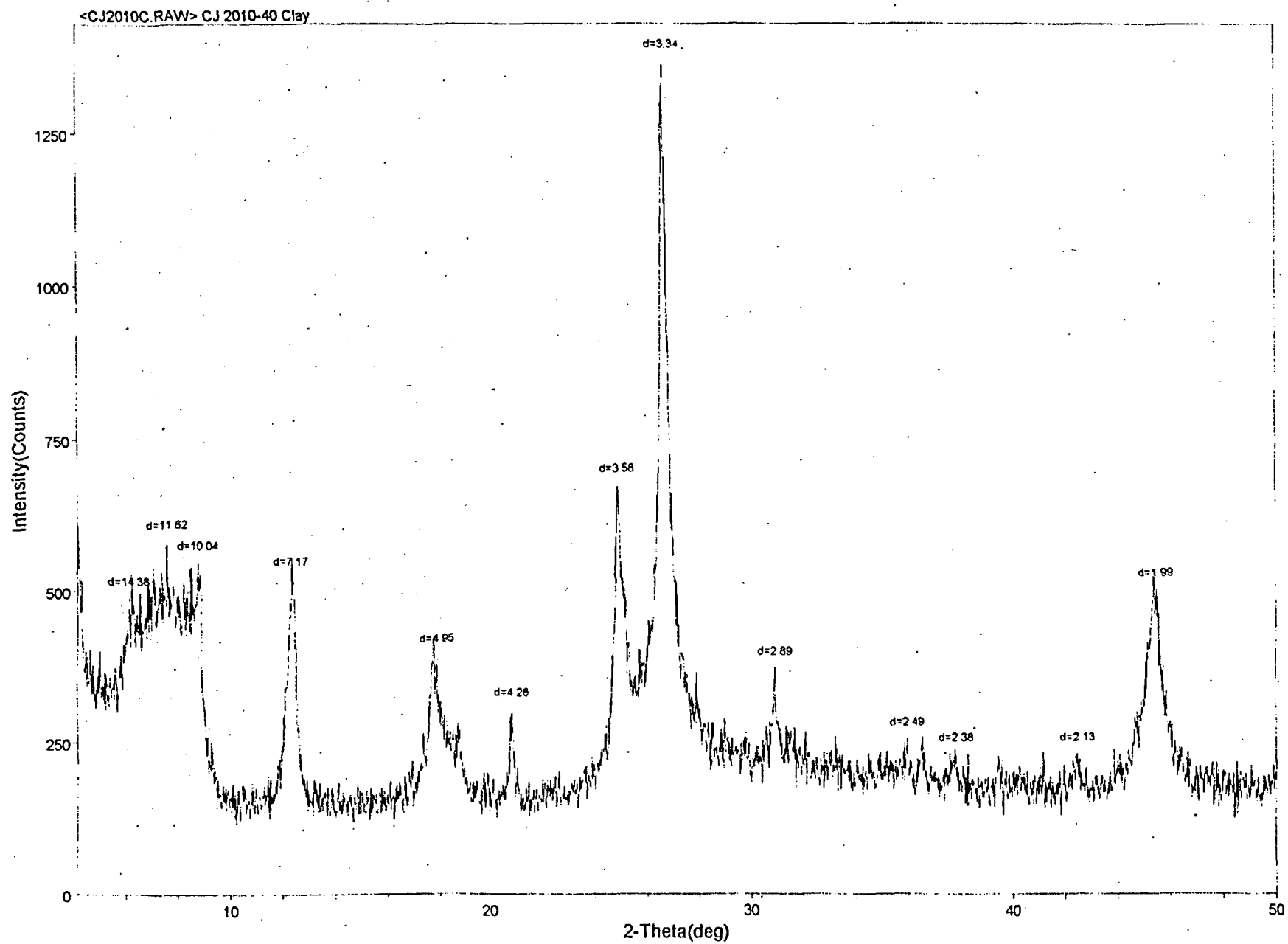
<CJ209HL.RAW> CJ209-40 H300

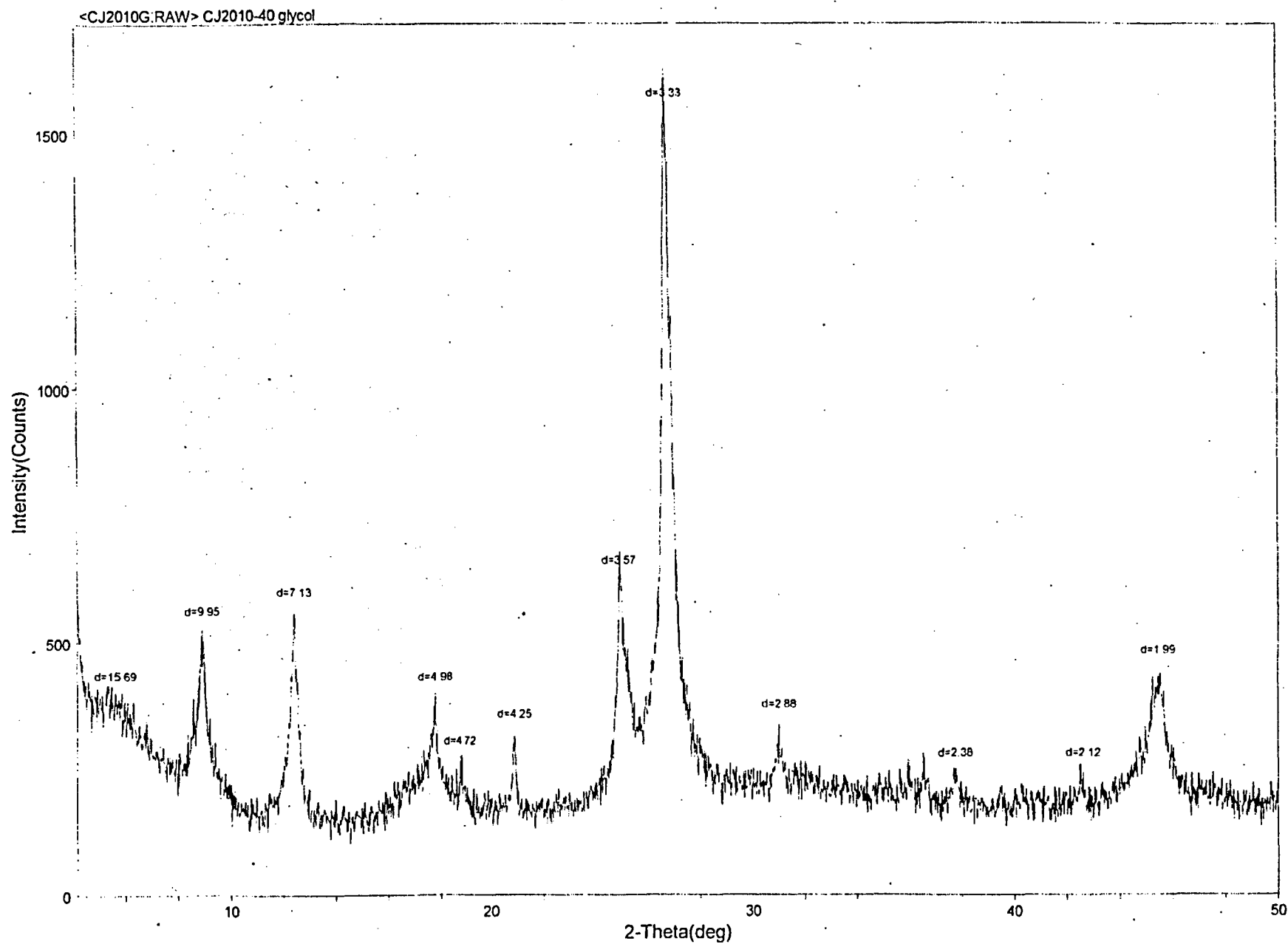


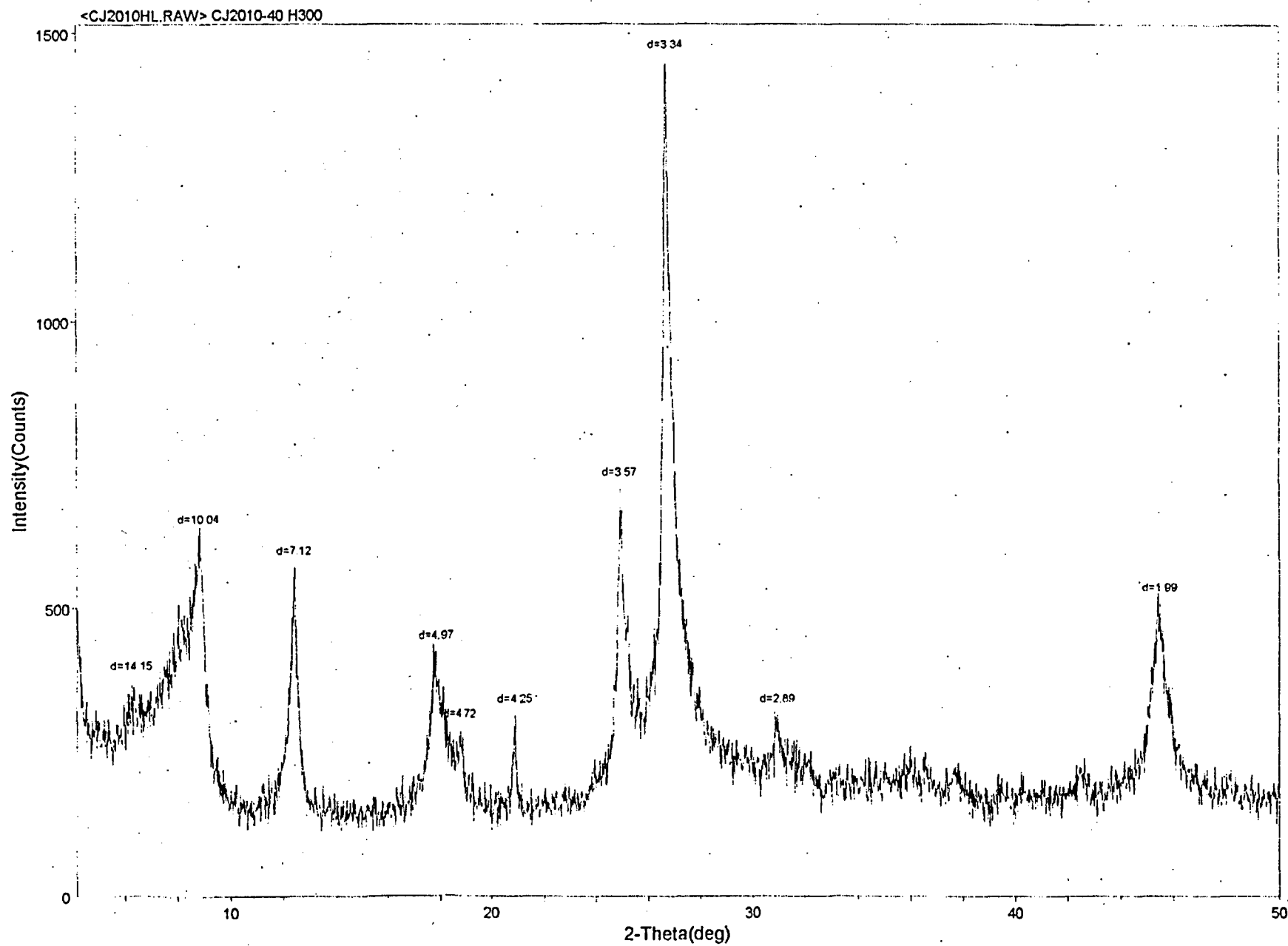


<CJ209HH.RAW> CJ209-40 H550

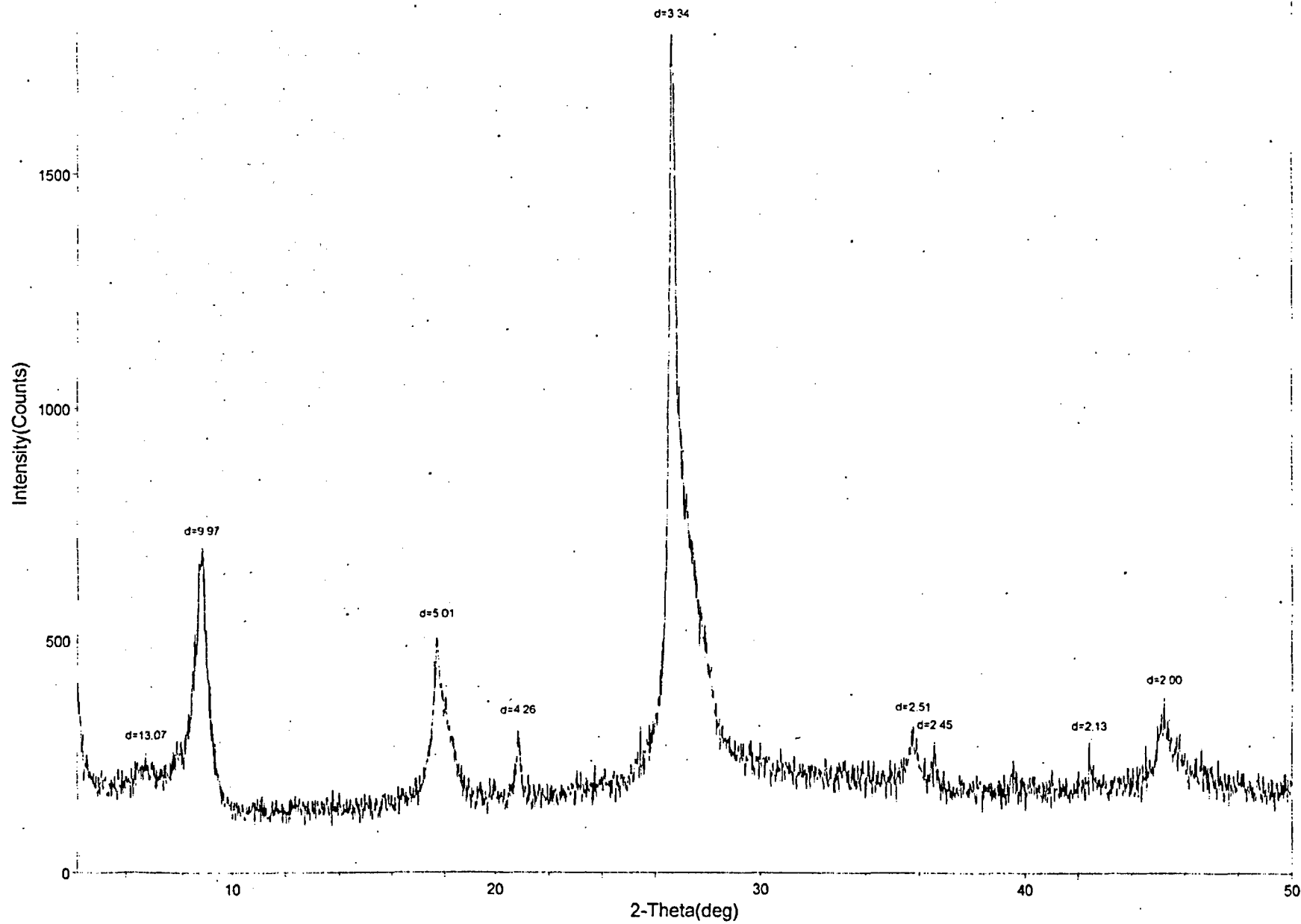








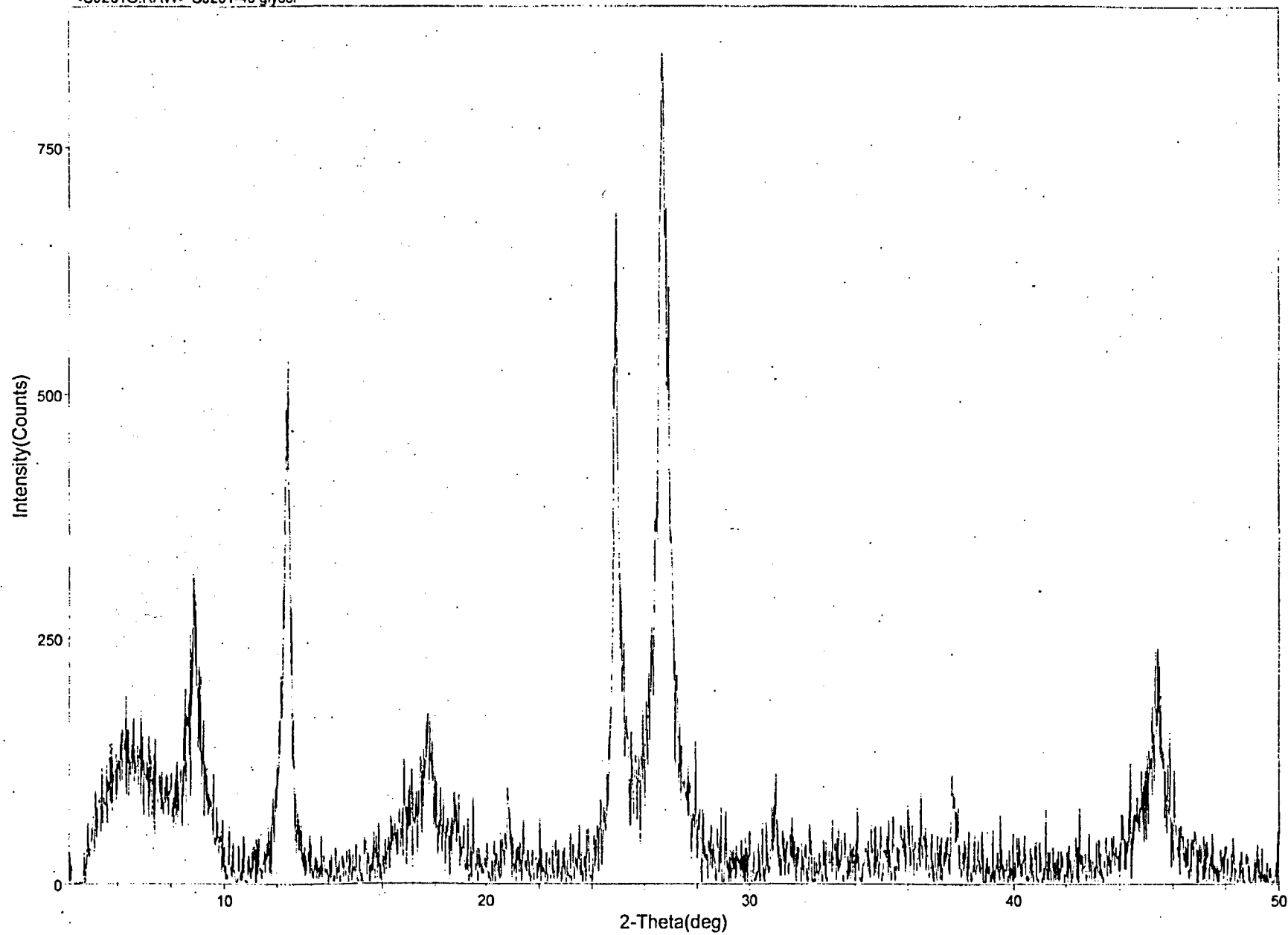
<CJ2010HH.RAW> CJ2010-40 H550



**Appendix 7.**

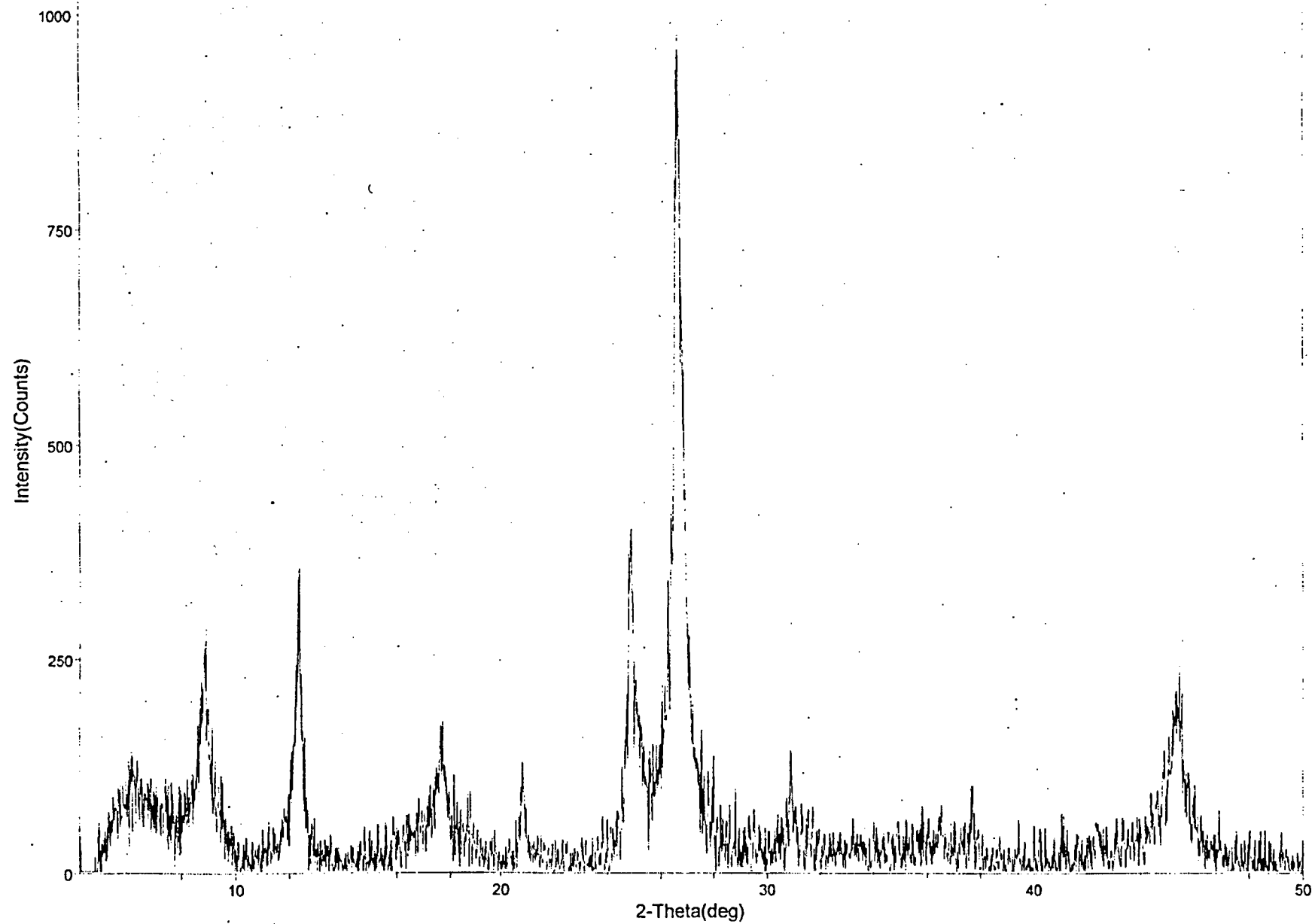
**X-ray diffraction patterns of glycol solvated clays with background removed**

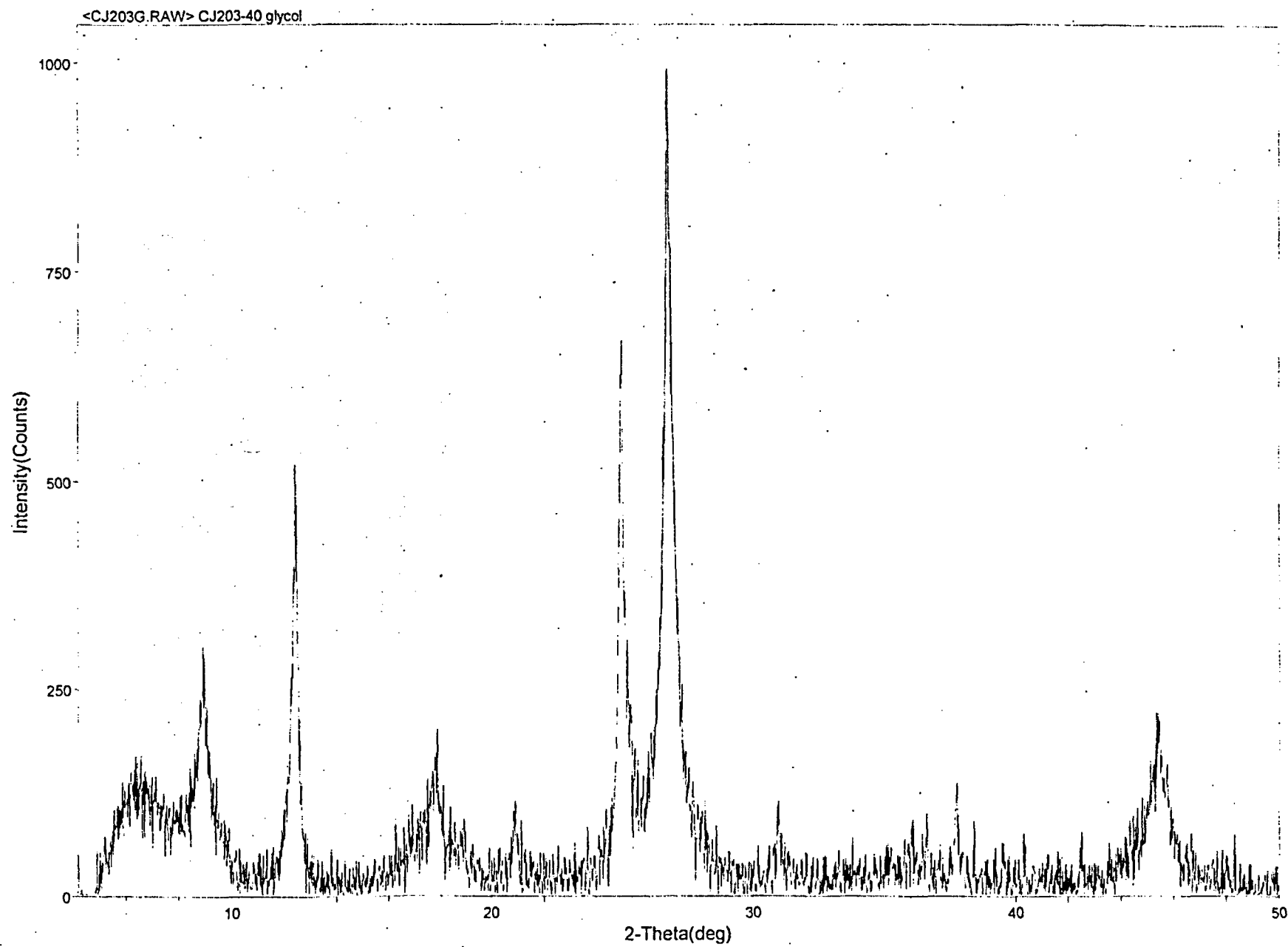
<CJ201G.RAW> CJ201-40 glycol

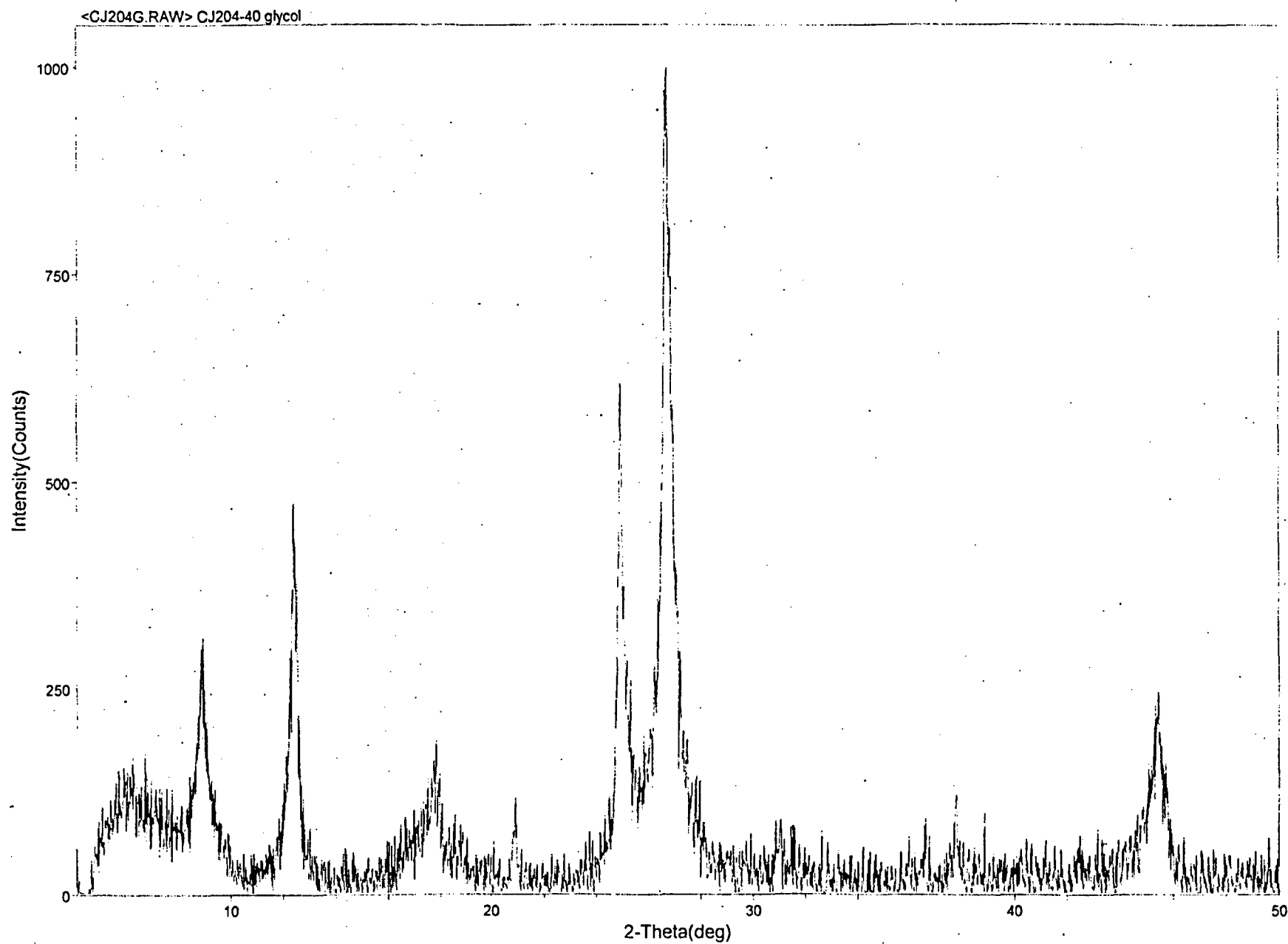


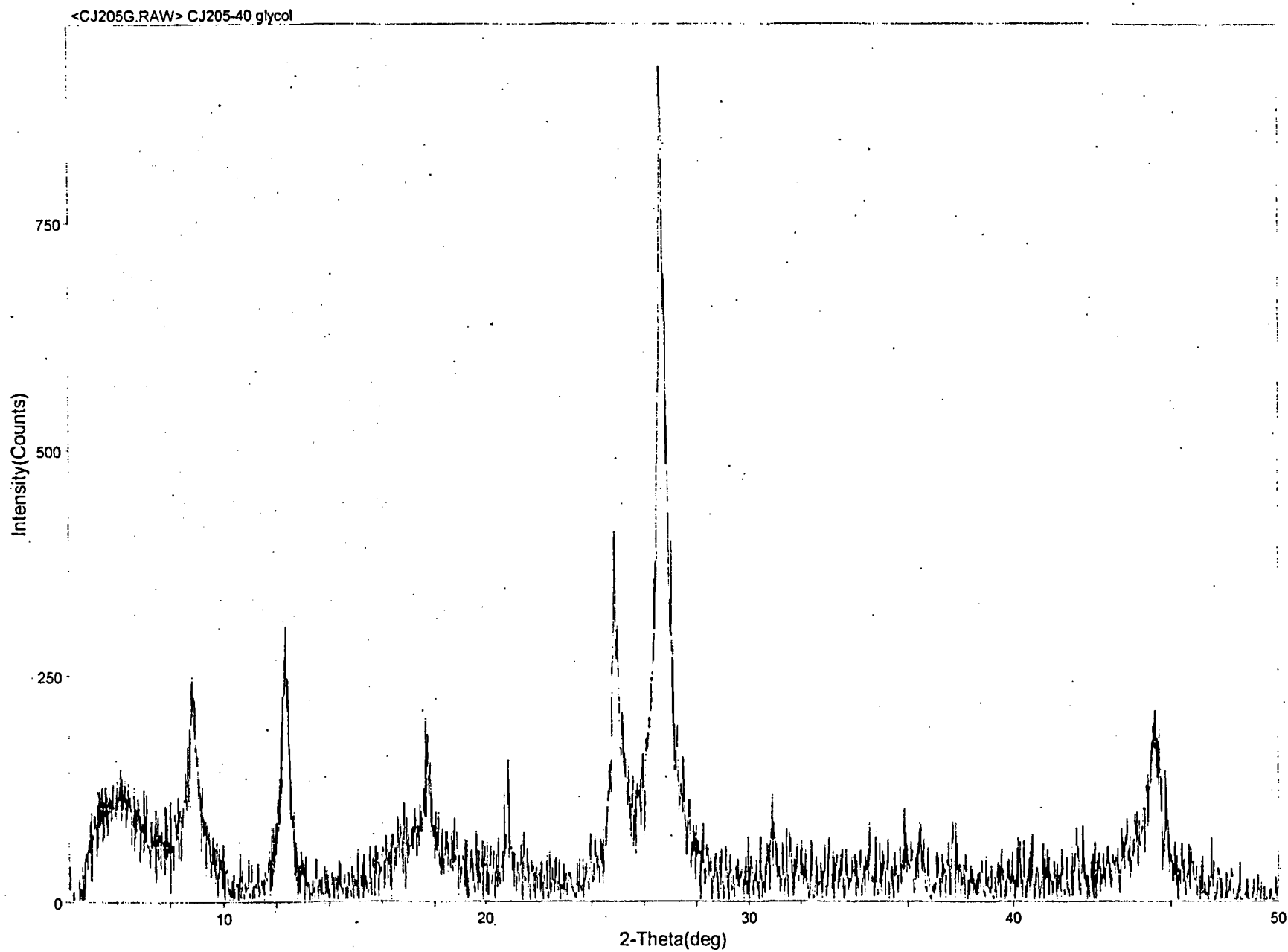


<CJ202G.RAW> CJ202-40 glycol

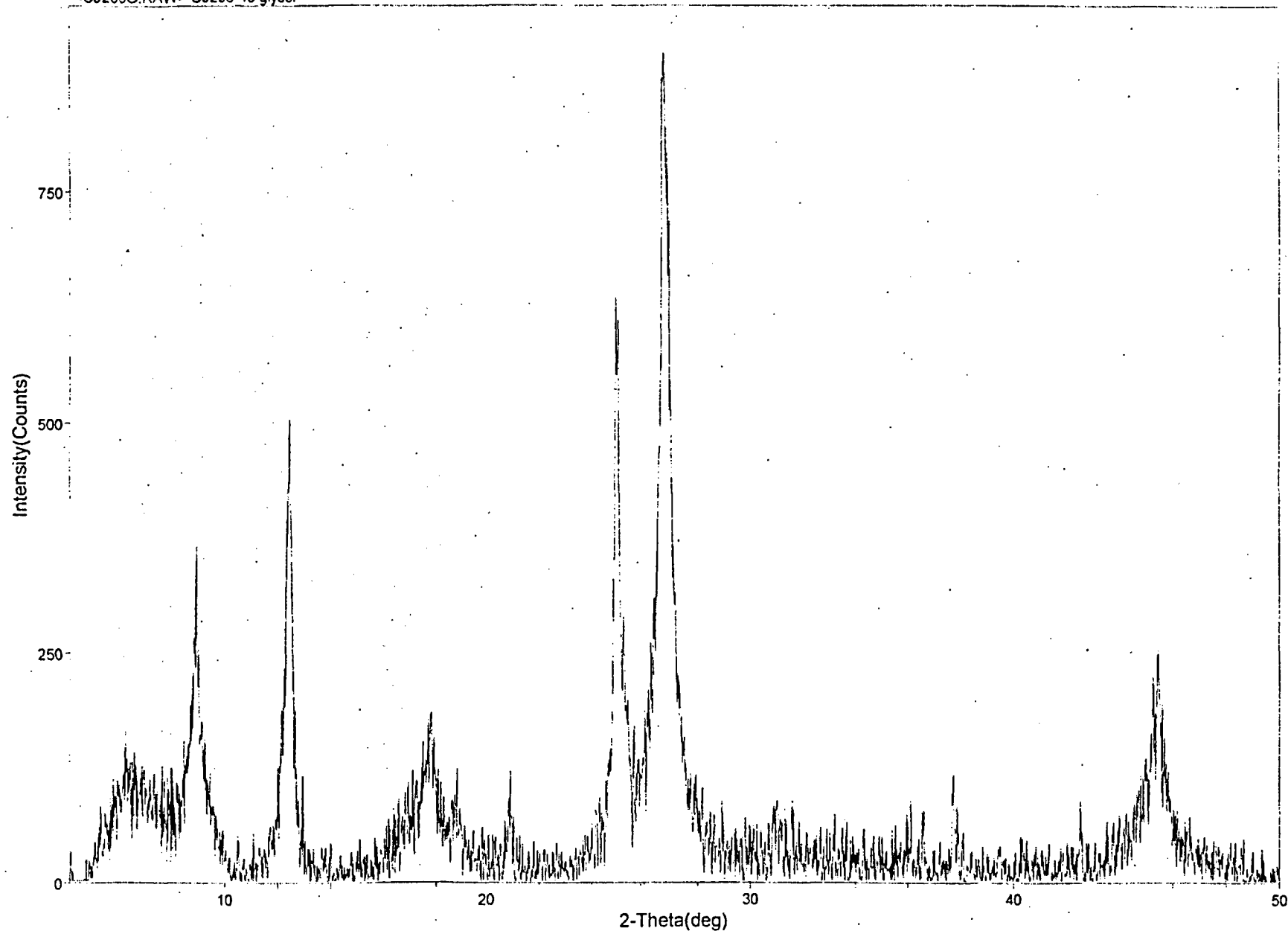


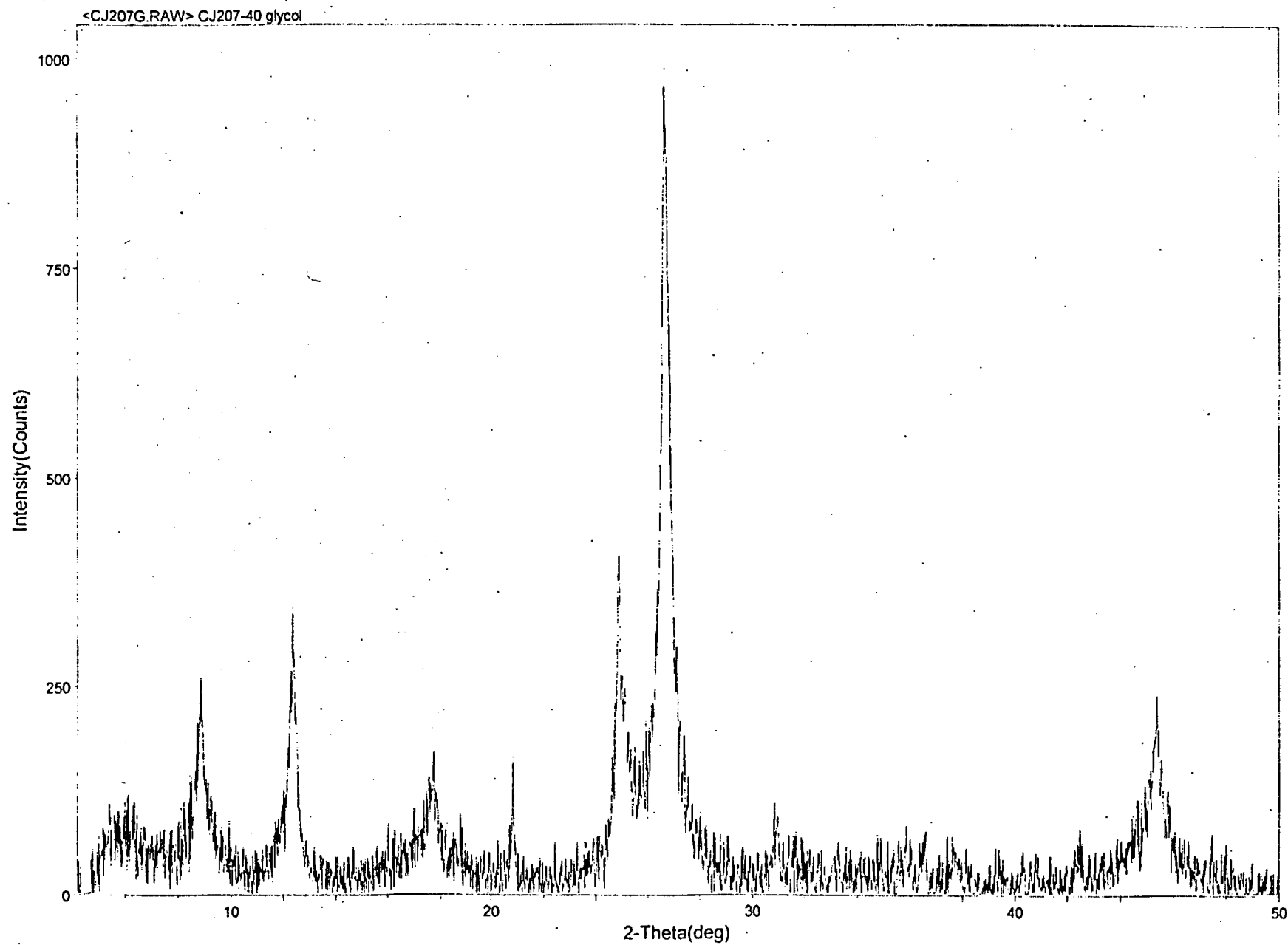


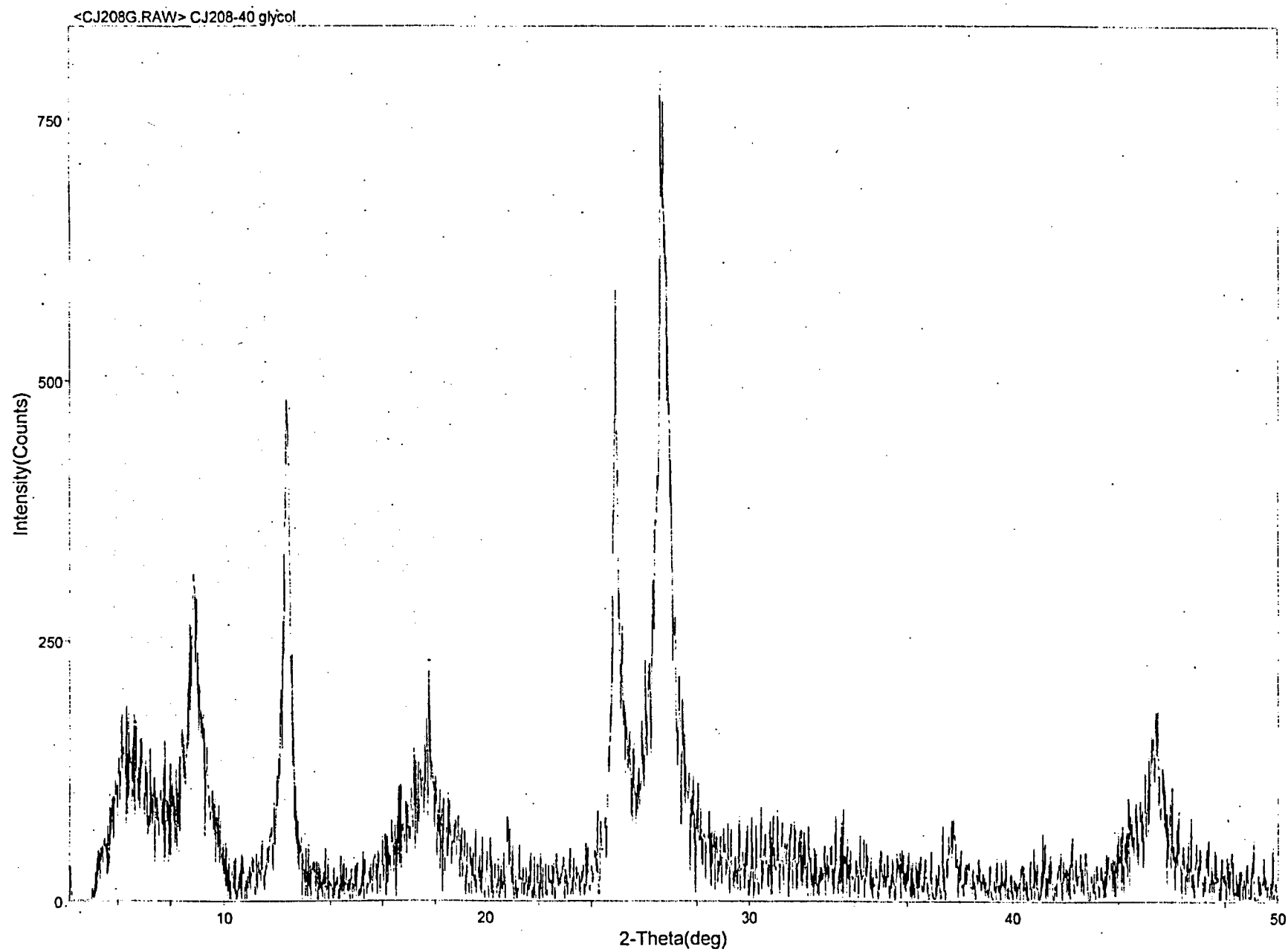




<CJ206G RAW> CJ206-40 glycol

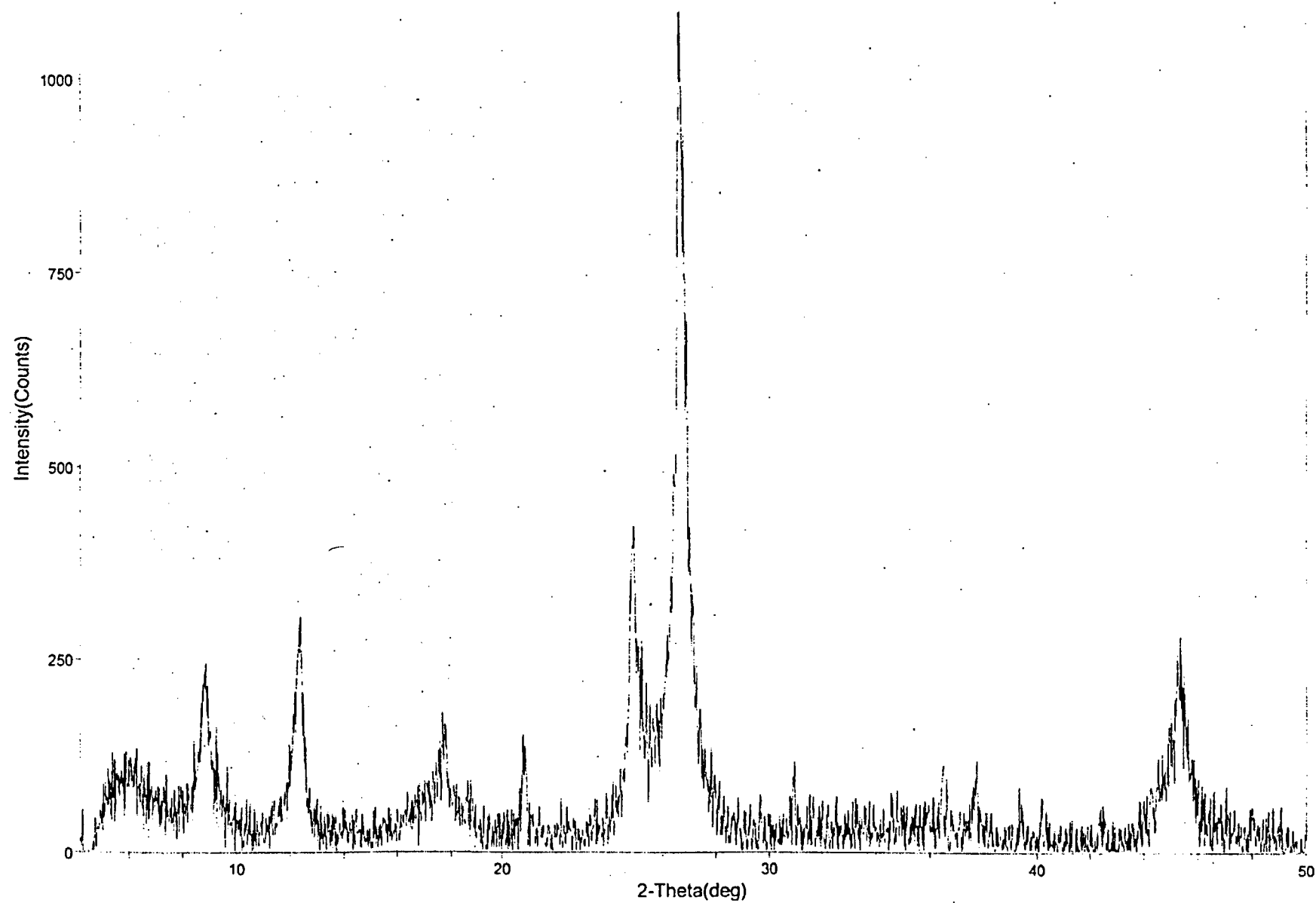




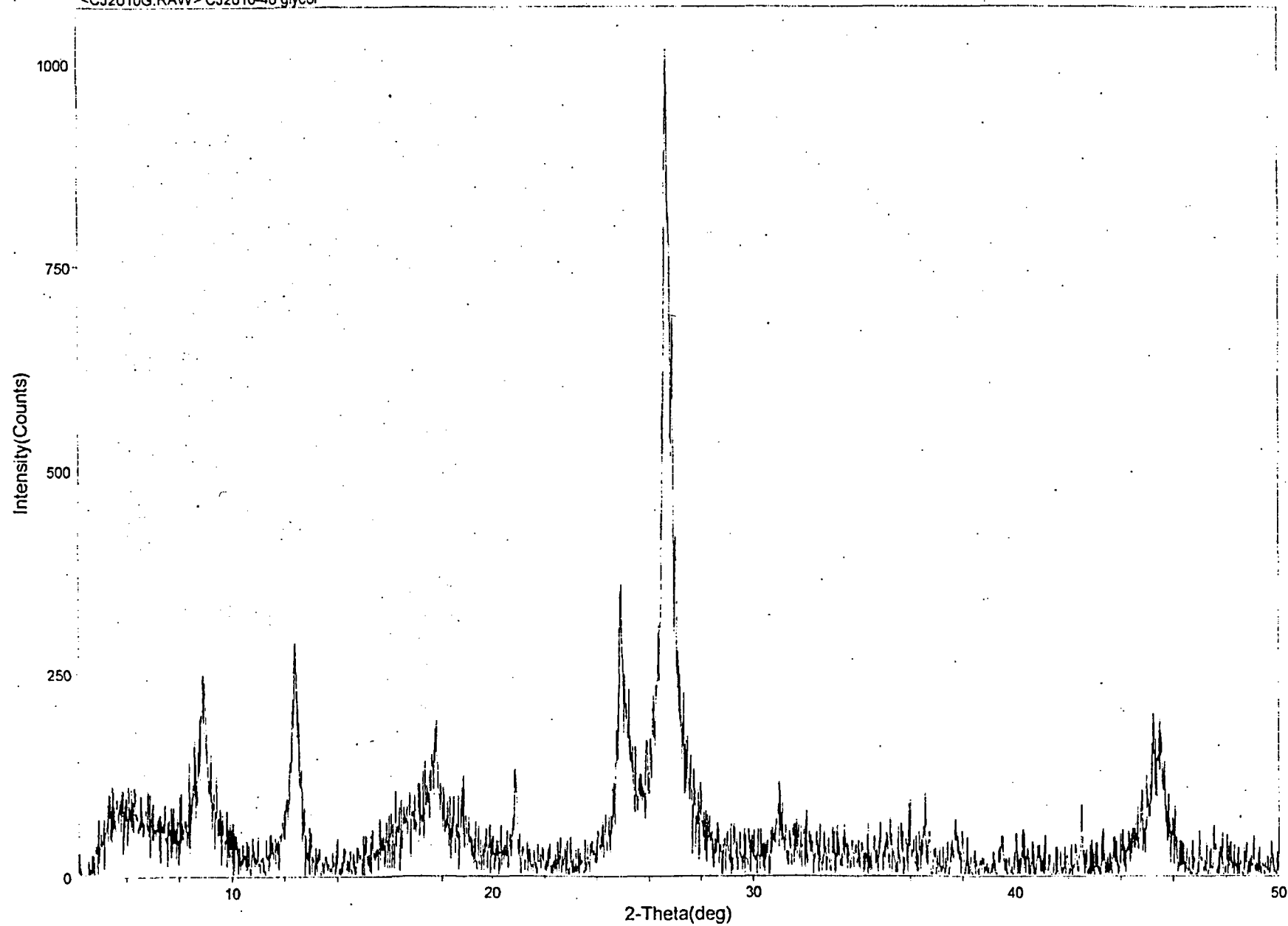




<CJ209G.RAW> CJ209-40 glycol



<CJ2010G.RAW> CJ2010-40 glycol



## **Appendix E**

### **Copies of Analytical Reports of BET Surface Area Analysis**

**Prepared by Micromeritics Analytical Services  
Norcross, Georgia**

TriStar 3000 V6.05.01 A

Unit 1 Port 1

Serial #: 1098

Page 1

Sample: CJ-201-40 06-0210 3/3  
 Operator: MJP  
 Submitter: S.M.Stoller  
 File: C:\\_101JAN06-0210.SMP

Started: 2/1/2006 12:27:55PM  
 Completed: 2/1/2006 3:23:59PM  
 Report Time: 2/1/2006 3:24:00PM  
 Warm Free Space: 5.1716 cm<sup>3</sup> Measured  
 Equilibration Interval: 10 s  
 Sample Density: 1.000 g/cm<sup>3</sup>

Analysis Adsorptive: N2  
 Analysis Bath Temp.: 77.300 K  
 Sample Mass: 4.2757 g  
 Cold Free Space: 14.2717 cm<sup>3</sup> Measured  
 Low Pressure Dose: None  
 Automatic Degas: Yes

Sample Prep: Stage	Soak Temperature (°C)	Ramp Rate (°C/min)	Soak Time (min)
1	100	10	960

**Isotherm Tabular Report**

Relative Pressure (P/Po)	Absolute Pressure (mmHg)	Quantity Adsorbed (cm <sup>3</sup> /g STP)	Elapsed Time (h:min)	Saturation Pressure (mmHg)
			01:10	735.79211
0.048910454	35.98793	2.2822	01:49	
0.077386655	56.94049	2.4522	01:59	
0.095083473	69.96167	2.5421	02:08	
0.123883388	91.15242	2.6734	02:15	
0.148628264	109.35950	2.7840	02:22	
0.173850205	127.91761	2.8924	02:28	
0.199214129	146.58018	2.9983	02:33	
0.224543969	165.21768	3.1044	02:39	
0.250010120	183.95547	3.2120	02:44	
0.275550098	202.74759	3.3213	02:50	
0.301305895	221.69850	3.4329	02:55	

TriStar 3000 V6.05.01 A

Unit 1 Port 1

Serial #: 1098

Page 2

Sample: CJ-201-40 06-0210 3/3  
 Operator: MJP  
 Submitter: S.M.Stoller  
 File: C:\...01JAN06-0210.SMP

Started: 2/1/2006 12:27:55PM  
 Completed: 2/1/2006 3:23:59PM  
 Report Time: 2/1/2006 3:24:00PM  
 Warm Free Space: 5.1716 cm<sup>3</sup> Measured  
 Equilibration Interval: 10 s  
 Sample Density: 1.000 g/cm<sup>3</sup>

Analysis Adsorptive: N<sub>2</sub>  
 Analysis Bath Temp.: 77.300 K  
 Sample Mass: 4.2757 g  
 Cold Free Space: 14.2717 cm<sup>3</sup> Measured  
 Low Pressure Dose: None  
 Automatic Degas: Yes

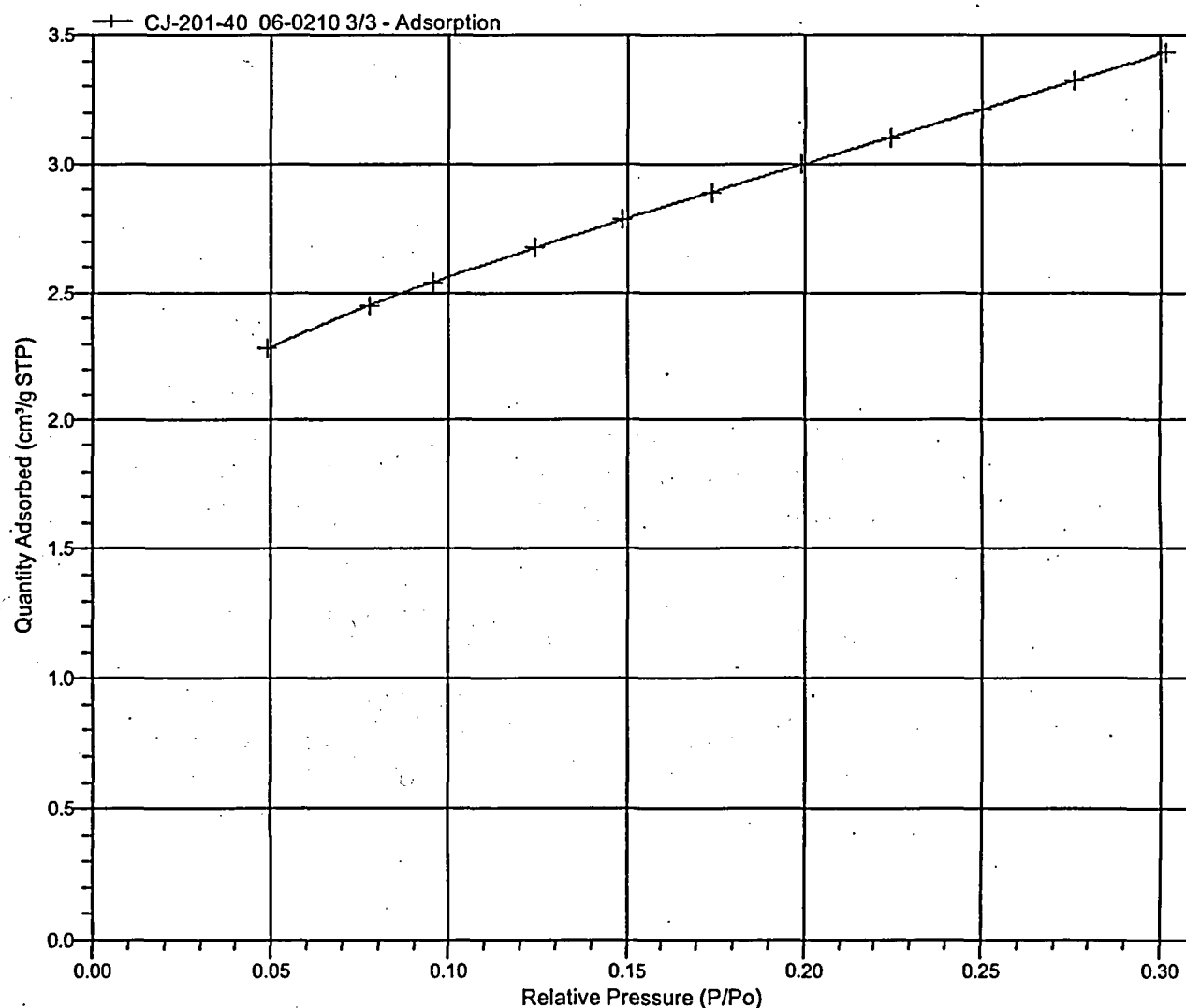
Sample Prep: Stage  
 1

Soak Temperature (°C)  
 100

Ramp Rate (°C/min)  
 10

Soak Time (min)  
 960

Isotherm Linear Plot



TriStar 3000 V6.05.01 A

Unit 1 Port 1

Serial #: 1098

Page 3

Sample: CJ-201-40 06-0210 3/3  
 Operator: MJP  
 Submitter: S.M.Stoller  
 File: C:\...101JAN06-0210.SMP

Started: 2/1/2006 12:27:55PM  
 Completed: 2/1/2006 3:23:59PM  
 Report Time: 2/1/2006 3:24:00PM  
 Warm Free Space: 5.1716 cm<sup>3</sup> Measured  
 Equilibration Interval: 10 s  
 Sample Density: 1.000 g/cm<sup>3</sup>

Analysis Adsorptive: N2  
 Analysis Bath Temp.: 77.300 K  
 Sample Mass: 4.2757 g  
 Cold Free Space: 14.2717 cm<sup>3</sup> Measured  
 Low Pressure Dose: None  
 Automatic Degas: Yes

Sample Prep: Stage  
 1

Soak Temperature (°C)  
 100

Ramp Rate (°C/min)  
 10

Soak Time (min)  
 960

**BET Surface Area Report**

BET Surface Area: 10.6561 ± 0.0383 m<sup>2</sup>/g  
 Slope: 0.405995 ± 0.001443 g/cm<sup>3</sup> STP  
 Y-Intercept: 0.002523 ± 0.000277 g/cm<sup>3</sup> STP  
 C: 161.941253  
 Qm: 2.4479 cm<sup>3</sup>/g STP  
 Correlation Coefficient: 0.9999432  
 Molecular Cross-Sectional Area: 0.1620 nm<sup>2</sup>

Relative Pressure (P/Po)	Quantity Adsorbed (cm <sup>3</sup> /g STP)	1/[Q(Po/P - 1)]
0.048910454	2.2822	0.022534
0.077386655	2.4522	0.034206
0.095083473	2.5421	0.041333
0.123883388	2.6734	0.052891
0.148628264	2.7840	0.062706
0.173850205	2.8924	0.072755
0.199214129	2.9983	0.082971
0.224543969	3.1044	0.093277
0.250010120	3.2120	0.103784
0.275550098	3.3213	0.114520
0.301305895	3.4329	0.125620

TriStar 3000 V6.05.01 A

Unit 1 Port 1

Serial #: 1098

Page 4

Sample: CJ-201-40 06-0210 3/3  
 Operator: MJP  
 Submitter: S.M.Stoller  
 File: C:\...\01JAN06-0210.SMP

Started: 2/1/2006 12:27:55PM  
 Completed: 2/1/2006 3:23:59PM  
 Report Time: 2/1/2006 3:24:00PM  
 Warm Free Space: 5.1716 cm<sup>3</sup> Measured  
 Equilibration Interval: 10 s  
 Sample Density: 1.000 g/cm<sup>3</sup>

Analysis Adsorptive: N2  
 Analysis Bath Temp: 77.300 K  
 Sample Mass: 4.2757 g  
 Cold Free Space: 14.2717 cm<sup>3</sup> Measured  
 Low Pressure Dose: None  
 Automatic Degas: Yes

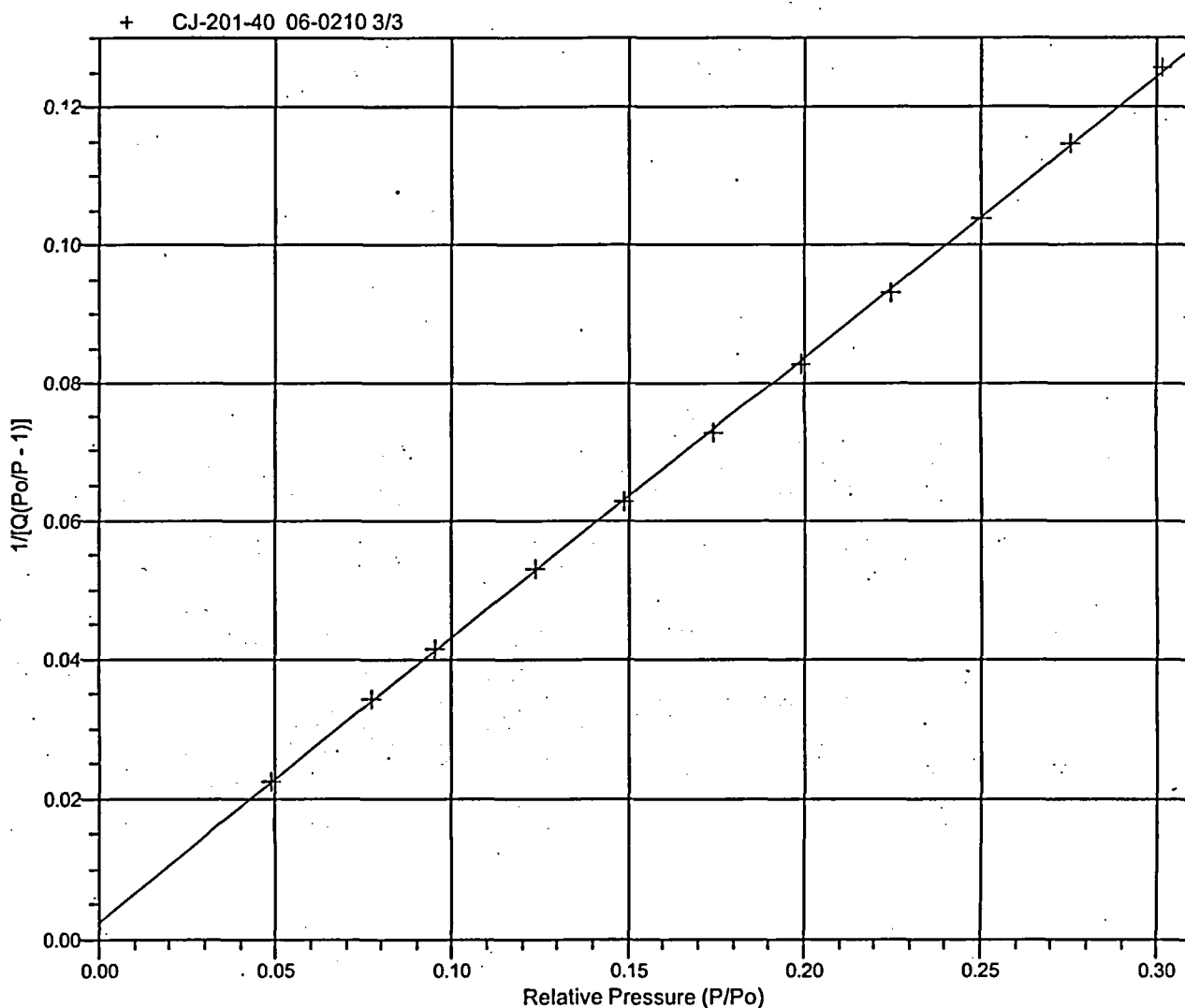
Sample Prep: Stage  
 1

Soak Temperature (°C)  
 100

Ramp Rate (°C/min)  
 10

Soak Time (min)  
 960

BET Surface Area Plot





TriStar 3000 V6.05.01 A

Unit 1 Port 1

Serial #: 1098

Page 5

Sample: CJ-201-40 06-0210 3/3  
Operator: MJP  
Submitter: S.M.Stoller  
File: C:\...01JAN06-0210.SMP

Started: 2/1/2006 12:27:55PM  
Completed: 2/1/2006 3:23:59PM  
Report Time: 2/1/2006 3:24:00PM  
Warm Free Space: 5.1716 cm<sup>3</sup> Measured  
Equilibration Interval: 10 s  
Sample Density: 1.000 g/cm<sup>3</sup>

Analysis Adsorptive: N2  
Analysis Bath Temp.: 77.300 K  
Sample Mass: 4.2757 g  
Cold Free Space: 14.2717 cm<sup>3</sup> Measured  
Low Pressure Dose: None  
Automatic Degas: Yes

Sample Prep: Stage  
1

Soak Temperature (°C)  
100

Ramp Rate (°C/min)  
10

Soak Time (min)  
960

#### Summary Report

##### Surface Area

Single point surface area at P/Po = 0.301305895: 10.4413 m<sup>2</sup>/g

BET Surface Area: 10.6561 m<sup>2</sup>/g

TriStar 3000 V6.05.01 A

Unit 1 Port 2

Serial #: 1098

Page 1

Sample: CJ-202-40 06-0211 38/38  
 Operator: MJP  
 Submitter: S.M.Stoller  
 File: C:\...101JAN06-0211.SMP

Started: 2/1/2006 12:27:55PM  
 Completed: 2/1/2006 3:23:59PM  
 Report Time: 2/1/2006 3:42:29PM  
 Warm Free Space: 6.0917 cm<sup>3</sup> Measured  
 Equilibration Interval: 10 s  
 Sample Density: 1.000 g/cm<sup>3</sup>

Analysis Adsorptive: N2  
 Analysis Bath Temp.: 77.300 K  
 Sample Mass: 4.8504 g  
 Cold Free Space: 17.8637 cm<sup>3</sup> Measured  
 Low Pressure Dose: None  
 Automatic Degas: Yes

Sample Prep: Stage 1      Soak Temperature (°C) 100      Ramp Rate (°C/min) 10      Soak Time (min) 960

**Isotherm Tabular Report**

Relative Pressure (P/Po)	Absolute Pressure (mmHg)	Quantity Adsorbed (cm <sup>3</sup> /g STP)	Elapsed Time (h:min)	Saturation Pressure (mmHg)
			01:10	735.79211
0.048188998	35.45708	2.6084	01:46	
0.075697008	55.69726	2.8007	01:58	
0.105261690	77.45072	2.9694	02:08	
0.124125949	91.33089	3.0685	02:13	
0.148686061	109.40203	3.1933	02:20	
0.174005999	128.03224	3.3160	02:27	
0.199663001	146.91046	3.4353	02:32	
0.225068618	165.60371	3.5540	02:38	
0.250788476	184.52818	3.6731	02:43	
0.276325488	203.31812	3.7943	02:49	
0.302319564	222.44435	3.9175	02:54	

TriStar 3000 V6.05.01 A

Unit 1 Port 2

Serial #: 1098

Page 2

Sample: CJ-202-40 06-0211 38/38  
 Operator: MJP  
 Submitter: S.M.Stoller  
 File: C:\...01JAN06-0211.SMP

Started: 2/1/2006 12:27:55PM  
 Completed: 2/1/2006 3:23:59PM  
 Report Time: 2/1/2006 3:42:29PM  
 Warm Free Space: 6.0917 cm<sup>3</sup> Measured  
 Equilibration Interval: 10 s  
 Sample Density: 1.000 g/cm<sup>3</sup>

Analysis Adsorptive: N2  
 Analysis Bath Temp.: 77.300 K  
 Sample Mass: 4.8504 g  
 Cold Free Space: 17.8637 cm<sup>3</sup> Measured  
 Low Pressure Dose: None  
 Automatic Degas: Yes

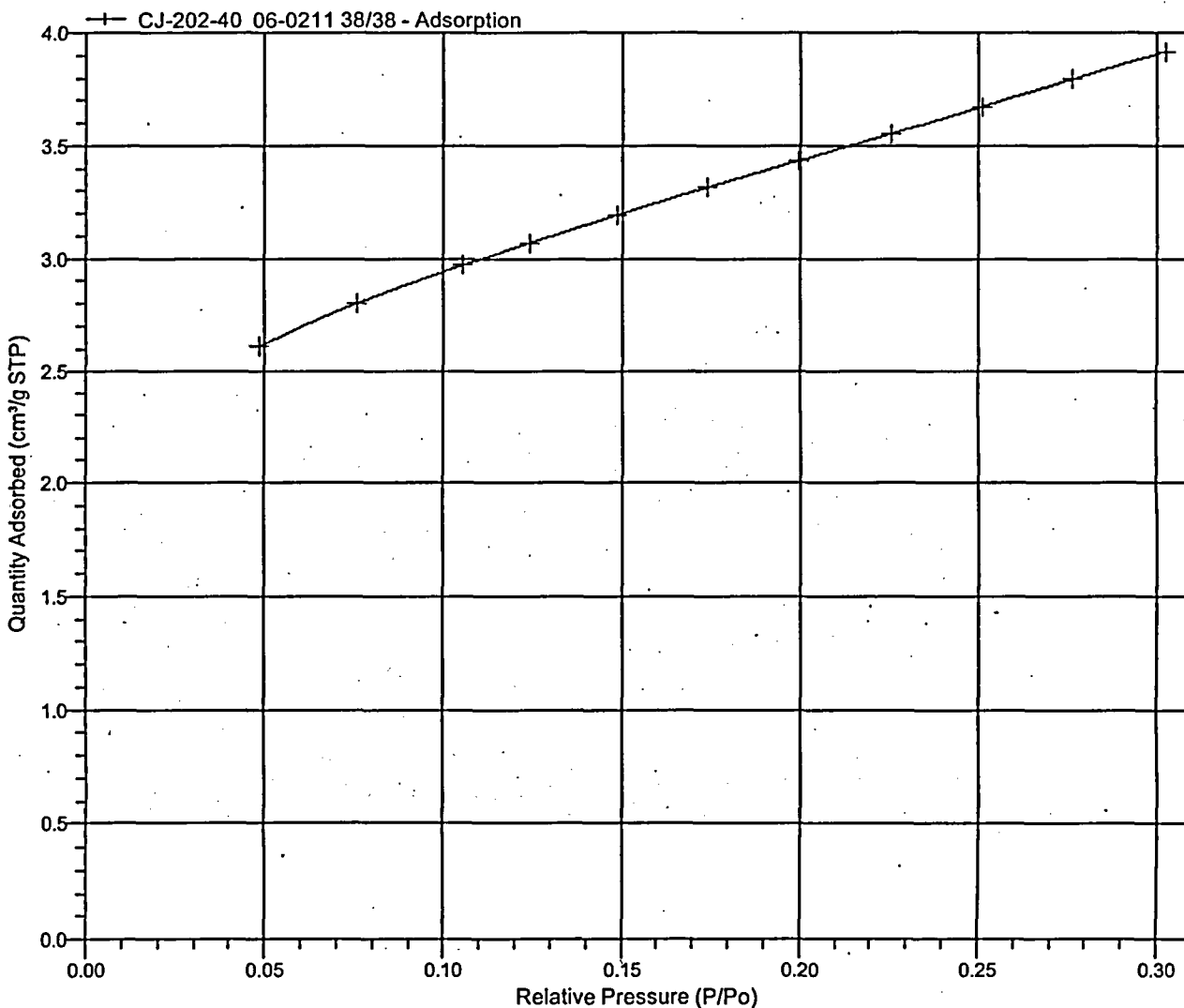
Sample Prep: Stage  
 1

Soak Temperature (°C)  
 100

Ramp Rate (°C/min)  
 10

Soak Time (min)  
 960

Isotherm Linear Plot



TriStar 3000 V6.05.01 A

Unit 1 Port 2

Serial #: 1098

Page 3

Sample: CJ-202-40 06-0211 38/38  
 Operator: MJP  
 Submitter: S.M.Stoller  
 File: C:\...101JAN06-0211.SMP

Started: 2/1/2006 12:27:55PM  
 Completed: 2/1/2006 3:23:59PM  
 Report Time: 2/1/2006 3:42:29PM  
 Warm Free Space: 6.0917 cm<sup>3</sup> Measured  
 Equilibration Interval: 10 s  
 Sample Density: 1.000 g/cm<sup>3</sup>

Analysis Adsorptive: N<sub>2</sub>  
 Analysis Bath Temp.: 77.300 K  
 Sample Mass: 4.8504 g  
 Cold Free Space: 17.8637 cm<sup>3</sup> Measured  
 Low Pressure Dose: None  
 Automatic Degas: Yes

Sample Prep: Stage  
 1

Soak Temperature (°C)  
 100

Ramp Rate (°C/min)  
 10

Soak Time (min)  
 960

**BET Surface Area Report**

BET Surface Area: 12.2117 ± 0.0440 m<sup>2</sup>/g  
 Slope: 0.354268 ± 0.001265 g/cm<sup>3</sup> STP  
 Y-Intercept: 0.002211 ± 0.000225 g/cm<sup>3</sup> STP  
 C: 161.265813  
 Qm: 2.8052 cm<sup>3</sup>/g STP  
 Correlation Coefficient: 0.9999490  
 Molecular Cross-Sectional Area: 0.1620 nm<sup>2</sup>

Relative Pressure (P/P <sub>0</sub> )	Quantity Adsorbed (cm <sup>3</sup> /g STP)	1/[Q(P <sub>0</sub> /P - 1)]
0.048188998	2.6084	0.019410
0.075697008	2.8007	0.029241
0.105261690	2.9694	0.039619
0.124125949	3.0685	0.046185
0.148686061	3.1933	0.054694
0.174005999	3.3160	0.063529
0.199663001	3.4353	0.072621
0.225068618	3.5540	0.081722
0.250788476	3.6731	0.091131
0.276325488	3.7943	0.100635

TriStar 3000 V6.05.01 A

Unit 1 Port 2

Serial #: 1098

Page 4

Sample: CJ-202-40 06-0211 38/38

Operator: MJP

Submitter: S.MStoller

File: C:\...01JAN06-0211.SMP

Started: 2/1/2006 12:27:55PM

Completed: 2/1/2006 3:23:59PM

Report Time: 2/1/2006 3:42:29PM

Warm Free Space: 6.0917 cm<sup>3</sup> Measured

Equilibration Interval: 10 s

Sample Density: 1.000 g/cm<sup>3</sup>

Analysis Adsorptive: N<sub>2</sub>

Analysis Bath Temp.: 77.300 K

Sample Mass: 4.8504 g

Cold Free Space: 17.8637 cm<sup>3</sup> Measured

Low Pressure Dose: None

Automatic Degas: Yes

Sample Prep: Stage

1

Soak Temperature (°C)

100

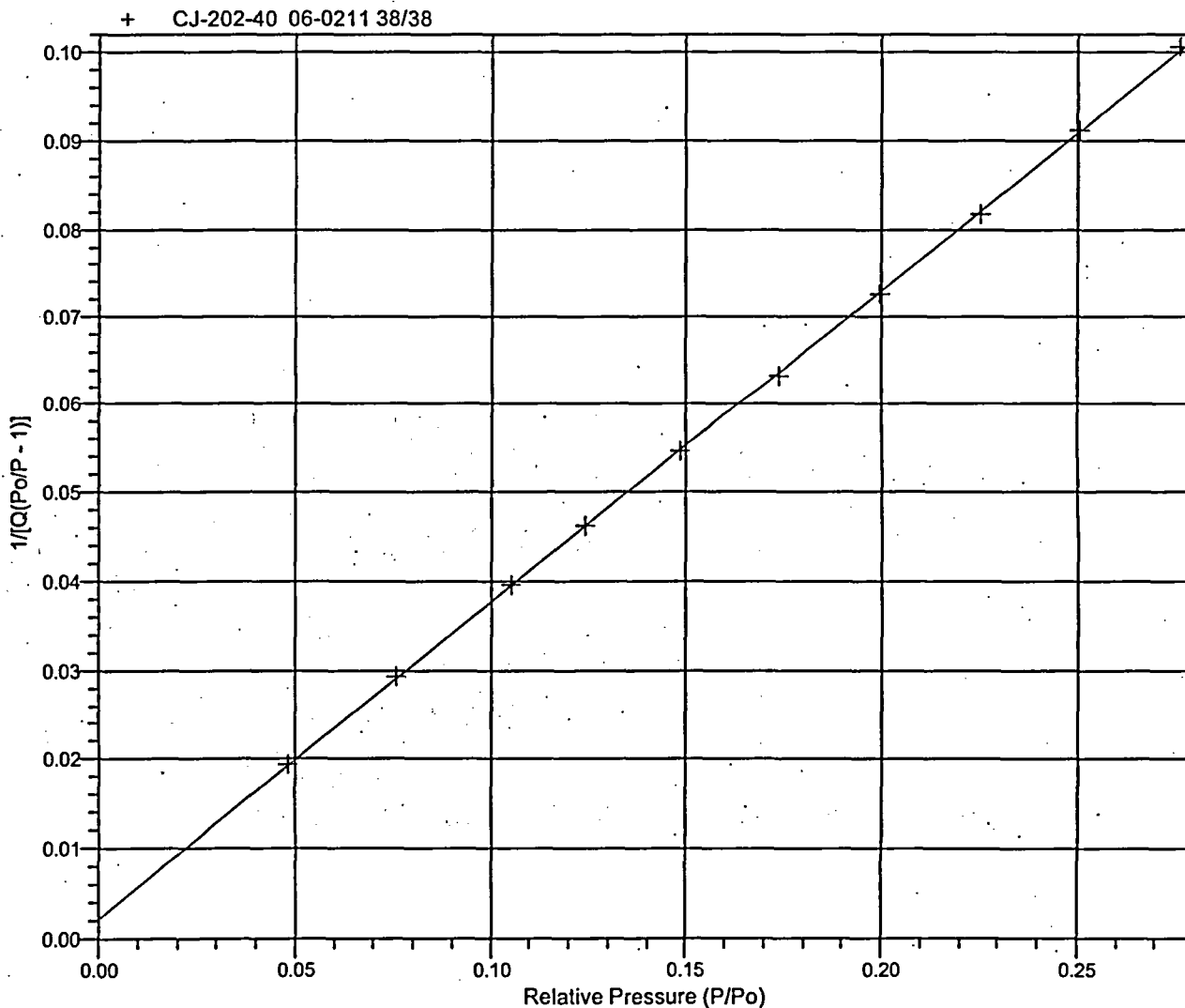
Ramp Rate (°C/min)

10

Soak Time (min)

960

**BET Surface Area Plot**





TriStar 3000 V6.05.01 A

Unit 1 Port 2

Serial #: 1098

Page 5

Sample: CJ-202-40 06-0211 38/38  
Operator: MJP  
Submitter: S.M.Stoller  
File: C:\...01JAN06-0211.SMP

Started: 2/1/2006 12:27:55PM  
Completed: 2/1/2006 3:23:59PM  
Report Time: 2/1/2006 3:42:29PM  
Warm Free Space: 6.0917 cm<sup>3</sup> Measured  
Equilibration Interval: 10 s  
Sample Density: 1.000 g/cm<sup>3</sup>

Analysis Adsorptive: N<sub>2</sub>  
Analysis Bath Temp: 77.300 K  
Sample Mass: 4.8504 g  
Cold Free Space: 17.8637 cm<sup>3</sup> Measured  
Low Pressure Dose: None  
Automatic Degas: Yes

Sample Prep: Stage	Soak Temperature (°C)	Ramp Rate (°C/min)	Soak Time (min)
1	100	10	960

#### Summary Report

##### Surface Area

Single point surface area at P/Po = 0.276325488: 11.9531 m<sup>2</sup>/g

BET Surface Area: 12.2117 m<sup>2</sup>/g

# MICROMERITICS ANALYTICAL SERVICES

The Particle  
Testing  
Authority

TriStar 3000 V6.05.01 A

Unit 1 Port 3

Serial #: 1098

Page 1

Sample: CJ-203-40 06-0212 815/815  
Operator: MJP  
Submitter: S.M.Stoller  
File: C:\...\01JAN06-0212.SMP

Started: 2/1/2006 12:27:55PM  
Completed: 2/1/2006 3:23:59PM  
Report Time: 2/1/2006 3:24:02PM  
Warm Free Space: 5.8383 cm<sup>3</sup> Measured  
Equilibration Interval: 10 s  
Sample Density: 1.000 g/cm<sup>3</sup>

Analysis Adsorptive: N2  
Analysis Bath Temp.: 77.300 K  
Sample Mass: 4.9651 g  
Cold Free Space: 16.8406 cm<sup>3</sup> Measured  
Low Pressure Dose: None  
Automatic Degas: Yes

Sample Prep: Stage	Soak Temperature (°C)	Ramp Rate (°C/min)	Soak Time (min)
1	100	10	960

## Isotherm Tabular Report

Relative Pressure (P/Po)	Absolute Pressure (mmHg)	Quantity Adsorbed (cm <sup>3</sup> /g STP)	Elapsed Time (h:min)	Saturation Pressure (mmHg)
			01:10	735.79211
0.048868273	35.95689	1.8390	01:39	
0.078725572	57.92566	1.9854	01:49	
0.095925972	70.58157	2.0561	01:54	
0.123915770	91.17625	2.1632	02:00	
0.148682981	109.39977	2.2569	02:06	
0.173643780	127.76572	2.3496	02:11	
0.198912019	146.35789	2.4415	02:16	
0.224032241	164.84116	2.5341	02:22	
0.249180936	183.34537	2.6292	02:26	
0.274443482	201.93335	2.7267	02:32	
0.299973650	220.71825	2.8268	02:36	

TriStar 3000 V6.05.01 A

Unit 1 Port 3

Serial #: 1098

Page 2

Sample: CJ-203-40 06-0212 815/815  
 Operator: MJP  
 Submitter: S.M.Stoller  
 File: C:\...101JAN06-0212.SMP

Started: 2/1/2006 12:27:55PM  
 Completed: 2/1/2006 3:23:59PM  
 Report Time: 2/1/2006 3:24:02PM  
 Warm Free Space: 5.8383 cm<sup>3</sup> Measured  
 Equilibration Interval: 10 s  
 Sample Density: 1.000 g/cm<sup>3</sup>

Analysis Adsorptive: N<sub>2</sub>  
 Analysis Bath Temp.: 77.300 K  
 Sample Mass: 4.9651 g  
 Cold Free Space: 16.8406 cm<sup>3</sup> Measured  
 Low Pressure Dose: None  
 Automatic Degas: Yes

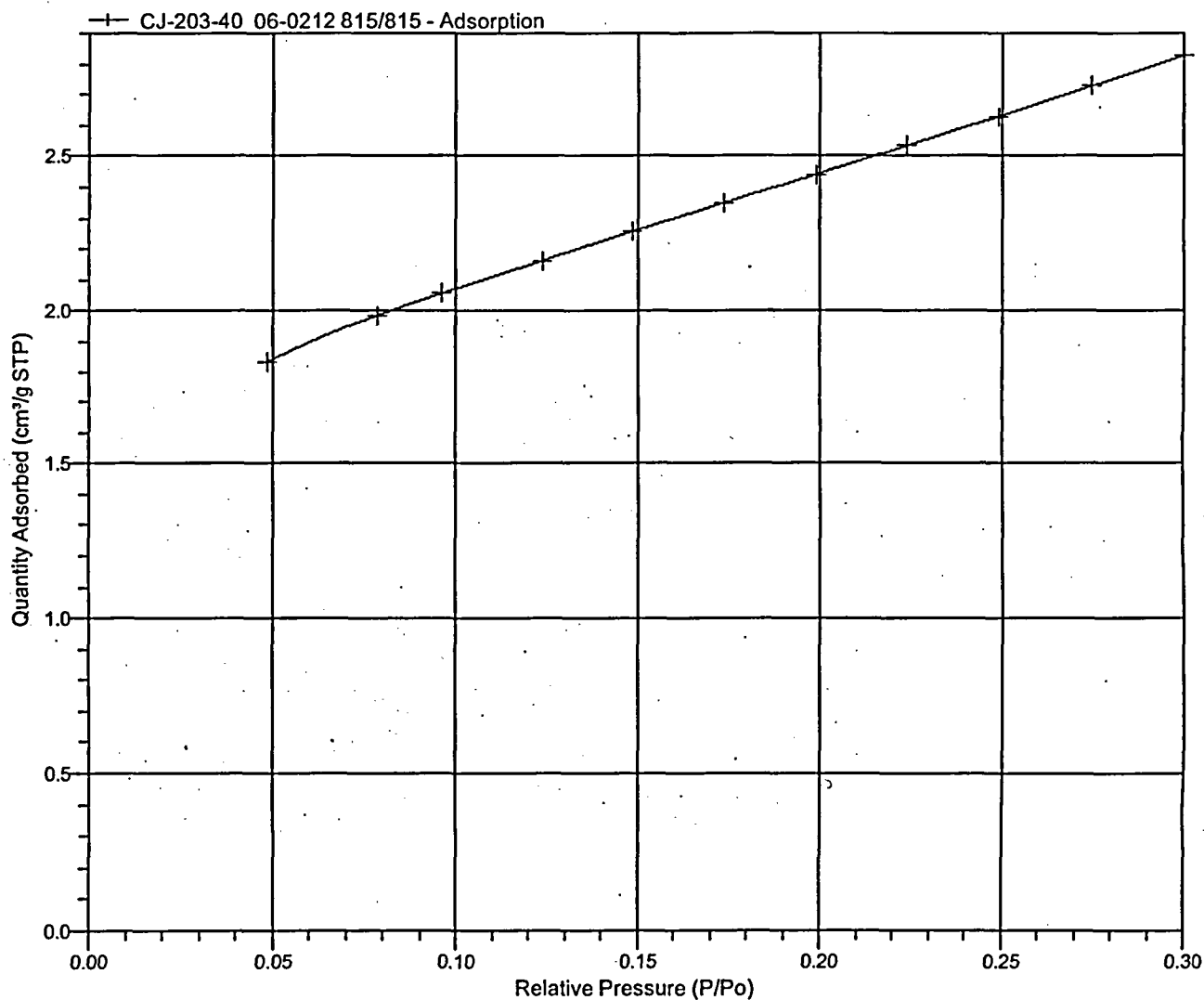
Sample Prep: Stage  
 1

Soak Temperature (°C)  
 100

Ramp Rate (°C/min)  
 10

Soak Time (min)  
 960

Isotherm Linear Plot





TriStar 3000 V6.05.01 A

Unit 1 Port 3

Serial #: 1098

Page 3

Sample: CJ-203-40 06-0212 815/815  
 Operator: MJP  
 Submitter: S.M.Stoller  
 File: C:\...101JAN06-0212.SMP

Started: 2/1/2006 12:27:55PM  
 Completed: 2/1/2006 3:23:59PM  
 Report Time: 2/1/2006 3:24:02PM  
 Warm Free Space: 5.8383 cm<sup>3</sup> Measured  
 Equilibration Interval: 10 s  
 Sample Density: 1.000 g/cm<sup>3</sup>

Analysis Adsorptive: N<sub>2</sub>  
 Analysis Bath Temp.: 77.300 K  
 Sample Mass: 4.9651 g  
 Cold Free Space: 16.8406 cm<sup>3</sup> Measured  
 Low Pressure Dose: None  
 Automatic Degas: Yes

Sample Prep: Stage  
 1

Soak Temperature (°C)  
 100

Ramp Rate (°C/min)  
 10

Soak Time (min)  
 960

**BET Surface Area Report**

BET Surface Area: 8.8087 ± 0.0164 m<sup>2</sup>/g  
 Slope: 0.489798 ± 0.000906 g/cm<sup>3</sup> STP  
 Y-Intercept: 0.004396 ± 0.000173 g/cm<sup>3</sup> STP  
 C: 112.409201  
 Qm: 2.0235 cm<sup>3</sup>/g STP  
 Correlation Coefficient: 0.9999846  
 Molecular Cross-Sectional Area: 0.1620 nm<sup>2</sup>

Relative Pressure (P/Po)	Quantity Adsorbed (cm <sup>3</sup> /g STP)	1/[Q(Po/P - 1)]
0.048868273	1.8390	0.027939
0.078725572	1.9854	0.043041
0.095925972	2.0561	0.051604
0.123915770	2.1632	0.065385
0.148682981	2.2569	0.077385
0.173643780	2.3496	0.089433
0.198912019	2.4415	0.101703
0.224032241	2.5341	0.113929
0.249180936	2.6292	0.126228
0.274443482	2.7267	0.138723
0.299973650	2.8268	0.151593

TriStar 3000 V6.05.01 A

Unit 1 Port 3

Serial #: 1098

Page 4

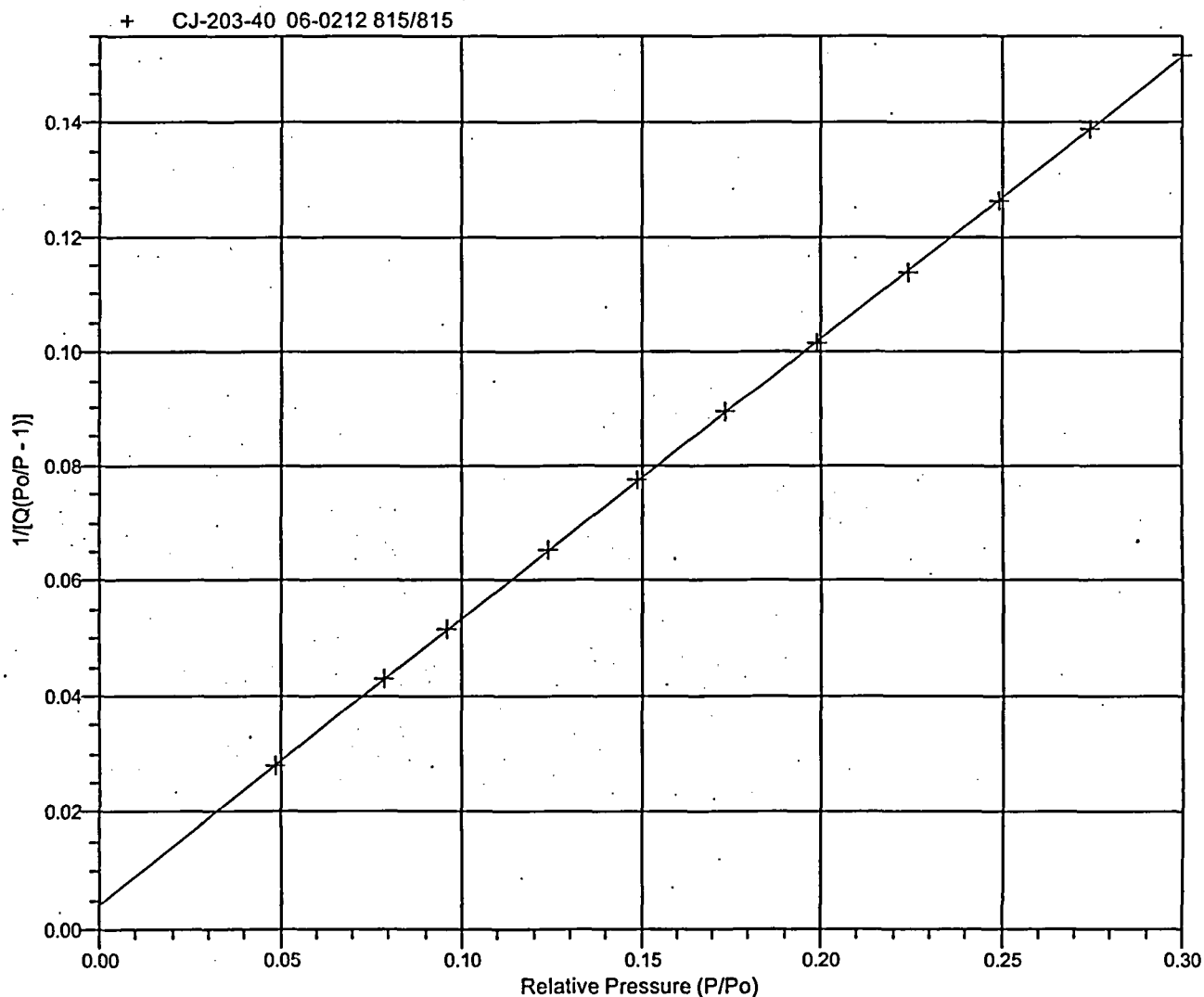
Sample: CJ-203-40 06-0212 815/815  
 Operator: MJP  
 Submitter: S.M.Stoller  
 File: C:\...101JAN06-0212.SMP

Started: 2/1/2006 12:27:55PM  
 Completed: 2/1/2006 3:23:59PM  
 Report Time: 2/1/2006 3:24:02PM  
 Warm Free Space: 5.8383 cm<sup>3</sup> Measured  
 Equilibration Interval: 10 s  
 Sample Density: 1.000 g/cm<sup>3</sup>

Analysis Adsorptive: N<sub>2</sub>  
 Analysis Bath Temp: 77.300 K  
 Sample Mass: 4.9651 g  
 Cold Free Space: 16.8406 cm<sup>3</sup> Measured  
 Low Pressure Dose: None  
 Automatic Degas: Yes

Sample Prep: Stage	Soak Temperature (°C)	Ramp Rate (°C/min)	Soak Time (min)
1	100	10	960

**BET Surface Area Plot**



TriStar 3000 V6.05.01 A

Unit 1 Port 3

Serial #: 1098

Page 5

Sample: CJ-203-40 06-0212 815/815  
Operator: MJP  
Submitter: S.M.Stoller  
File: C:\...01JAN06-0212.SMP

Started: 2/1/2006 12:27:55PM  
Completed: 2/1/2006 3:23:59PM  
Report Time: 2/1/2006 3:24:02PM  
Warm Free Space: 5.8383 cm<sup>3</sup> Measured  
Equilibration Interval: 10 s  
Sample Density: 1.000 g/cm<sup>3</sup>

Analysis Adsorptive: N2  
Analysis Bath Temp.: 77.300 K  
Sample Mass: 4.9651 g  
Cold Free Space: 16.8406 cm<sup>3</sup> Measured  
Low Pressure Dose: None  
Automatic Degas: Yes

Sample Prep: Stage  
1

Soak Temperature (°C)  
100

Ramp Rate (°C/min)  
10

Soak Time (min)  
960

#### Summary Report

##### Surface Area

Single point surface area at P/Po = 0.299973650: 8.6142 m<sup>2</sup>/g

BET Surface Area: 8.8087 m<sup>2</sup>/g

# MICROMERITICS ANALYTICAL SERVICES

The Particle  
Testing  
Authority

TriStar 3000 V6.05.01 A

Unit 2 Port 1

Serial #: 1449

Page 1

Sample: CJ-204-40 06-0213 G1/G1  
Operator: MJP  
Submitter: S.M.Stoller  
File: C:\...01JAN06-0213.SMP

Started: 2/1/2006 12:24:05PM  
Completed: 2/1/2006 3:16:44PM  
Report Time: 2/1/2006 3:43:34PM  
Warm Free Space: 5.6492 cm<sup>3</sup> Measured  
Equilibration Interval: 10 s  
Sample Density: 1.000 g/cm<sup>3</sup>

Analysis Adsorptive: N2  
Analysis Bath Temp.: 77.300 K  
Sample Mass: 4.4734 g  
Cold Free Space: 16.0508 cm<sup>3</sup> Measured  
Low Pressure Dose: None  
Automatic Degas: Yes

Sample Prep: Stage	Soak Temperature (°C)	Ramp Rate (°C/min)	Soak Time (min)
1	100	10	960

## Isotherm Tabular Report

Relative Pressure (P/Po)	Absolute Pressure (mmHg)	Quantity Adsorbed (cm <sup>3</sup> /g STP)	Elapsed Time (h:min)	Saturation Pressure (mmHg)
			01:13	734.31885
0.051070929	37.50235	2.8265	01:47	
0.076067257	55.85762	3.0041	01:58	
0.098670631	72.45570	3.1361	02:04	
0.123344049	90.57386	3.2685	02:12	
0.148242354	108.85715	3.3977	02:18	
0.173544281	127.43684	3.5242	02:24	
0.199226794	146.29599	3.6479	02:30	
0.224759373	165.04504	3.7714	02:36	
0.250534137	183.97194	3.8965	02:41	
0.276424207	202.98351	4.0230	02:46	
0.302354651	222.02472	4.1525	02:51	

TriStar 3000 V6.05.01 A

Unit 2 Port 1

Serial #: 1449

Page 2

Sample: CJ-204-40 06-0213 G1/G1  
 Operator: MJP  
 Submitter: S.M.Stoller  
 File: C:\...101JAN06-0213.SMP

Started: 2/1/2006 12:24:05PM  
 Completed: 2/1/2006 3:16:44PM  
 Report Time: 2/1/2006 3:43:34PM  
 Warm Free Space: 5.6492 cm<sup>3</sup> Measured  
 Equilibration Interval: 10 s  
 Sample Density: 1.000 g/cm<sup>3</sup>

Analysis Adsorptive: N2  
 Analysis Bath Temp.: 77.300 K  
 Sample Mass: 4.4734 g  
 Cold Free Space: 16.0508 cm<sup>3</sup> Measured  
 Low Pressure Dose: None  
 Automatic Degas: Yes

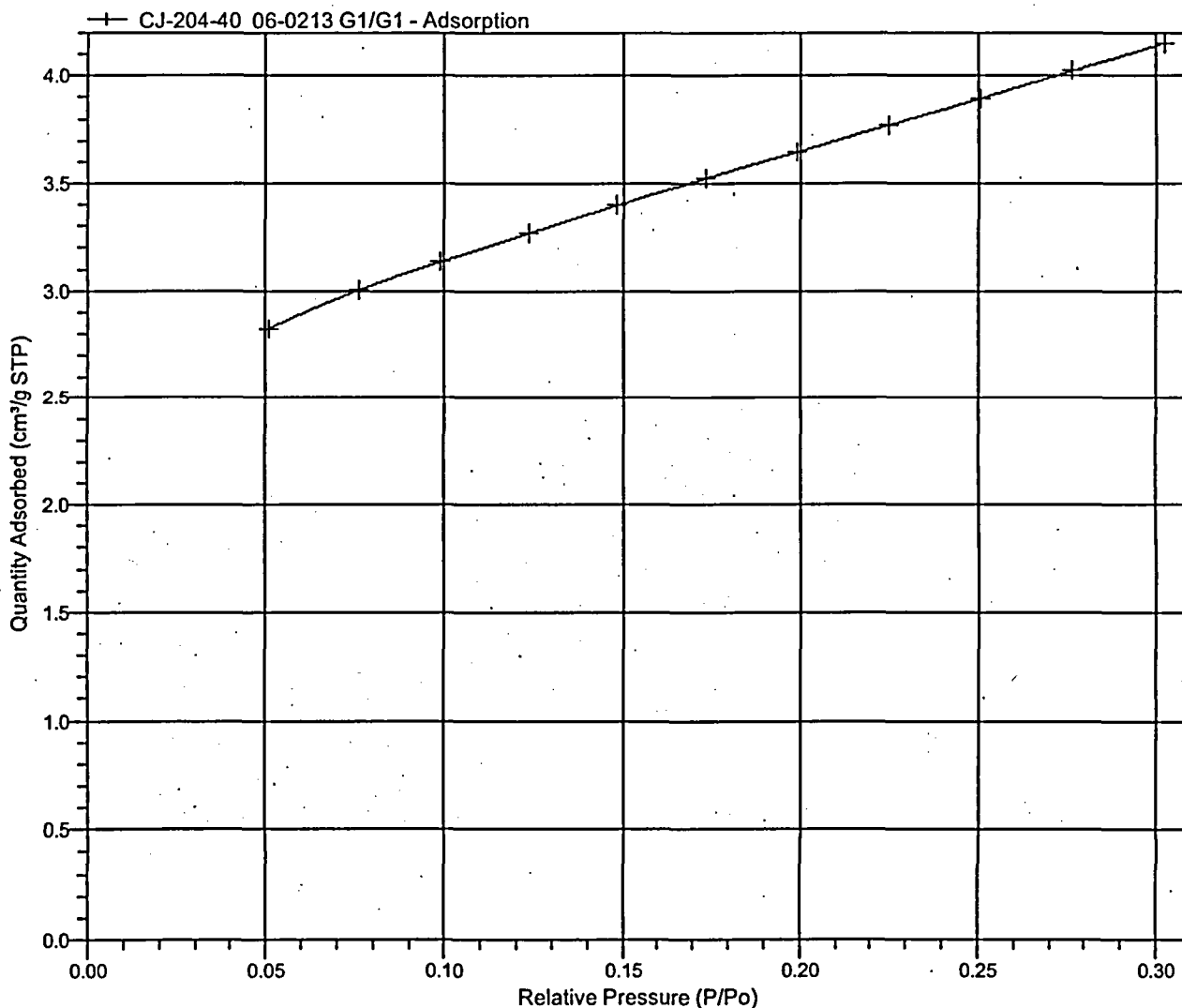
Sample Prep: Stage  
 1

Soak Temperature (°C)  
 100

Ramp Rate (°C/min)  
 10

Soak Time (min)  
 960

Isotherm Linear Plot



TriStar 3000 V6.05.01 A

Unit 2 Port 1

Serial #: 1449

Page 3

Sample: CJ-204-40 06-0213 G1/G1  
 Operator: MJP  
 Submitter: S.M.Stoller  
 File: C:\...101JAN06-0213.SMP

Started: 2/1/2006 12:24:05PM  
 Completed: 2/1/2006 3:16:44PM  
 Report Time: 2/1/2006 3:43:34PM  
 Warm Free Space: 5.6492 cm<sup>3</sup> Measured  
 Equilibration Interval: 10 s  
 Sample Density: 1.000 g/cm<sup>3</sup>

Analysis Adsorptive: N2  
 Analysis Bath Temp.: 77.300 K  
 Sample Mass: 4.4734 g  
 Cold Free Space: 16.0508 cm<sup>3</sup> Measured  
 Low Pressure Dose: None  
 Automatic Degas: Yes

Sample Prep: Stage	Soak Temperature (°C)	Ramp Rate (°C/min)	Soak Time (min)
1	100	10	960

**BET Surface Area Report**

BET Surface Area: 12.9162 ± 0.0501 m<sup>2</sup>/g  
 Slope: 0.335315 ± 0.001288 g/cm<sup>3</sup> STP  
 Y-Intercept: 0.001719 ± 0.000229 g/cm<sup>3</sup> STP  
 C: 196.026540  
 Qm: 2.9671 cm<sup>3</sup>/g STP  
 Correlation Coefficient: 0.9999410  
 Molecular Cross-Sectional Area: 0.1620 nm<sup>2</sup>

Relative Pressure (P/Po)	Quantity Adsorbed (cm <sup>3</sup> /g STP)	1/[Q(Po/P - 1)]
0.051070929	2.8265	0.019041
0.076067257	3.0041	0.027406
0.098670631	3.1361	0.034908
0.123344049	3.2685	0.043047
0.148242354	3.3977	0.051223
0.173544281	3.5242	0.059584
0.199226794	3.6479	0.068202
0.224759373	3.7714	0.076873
0.250534137	3.8965	0.085791
0.276424207	4.0230	0.094960

TriStar 3000 V6.05.01 A

Unit 2 Port 1

Serial #: 1449

Page 4

Sample: CJ-204-40 06-0213 G1/G1  
 Operator: MJP  
 Submitter: S.M.Stoller  
 File: C:\L\01JAN06-0213.SMP

Started: 2/1/2006 12:24:05PM  
 Completed: 2/1/2006 3:16:44PM  
 Report Time: 2/1/2006 3:43:34PM  
 Warm Free Space: 5.6492 cm<sup>3</sup> Measured  
 Equilibration Interval: 10 s  
 Sample Density: 1.000 g/cm<sup>3</sup>

Analysis Adsorptive: N2  
 Analysis Bath Temp.: 77.300 K  
 Sample Mass: 4.4734 g  
 Cold Free Space: 16.0508 cm<sup>3</sup> Measured  
 Low Pressure Dose: None  
 Automatic Degas: Yes

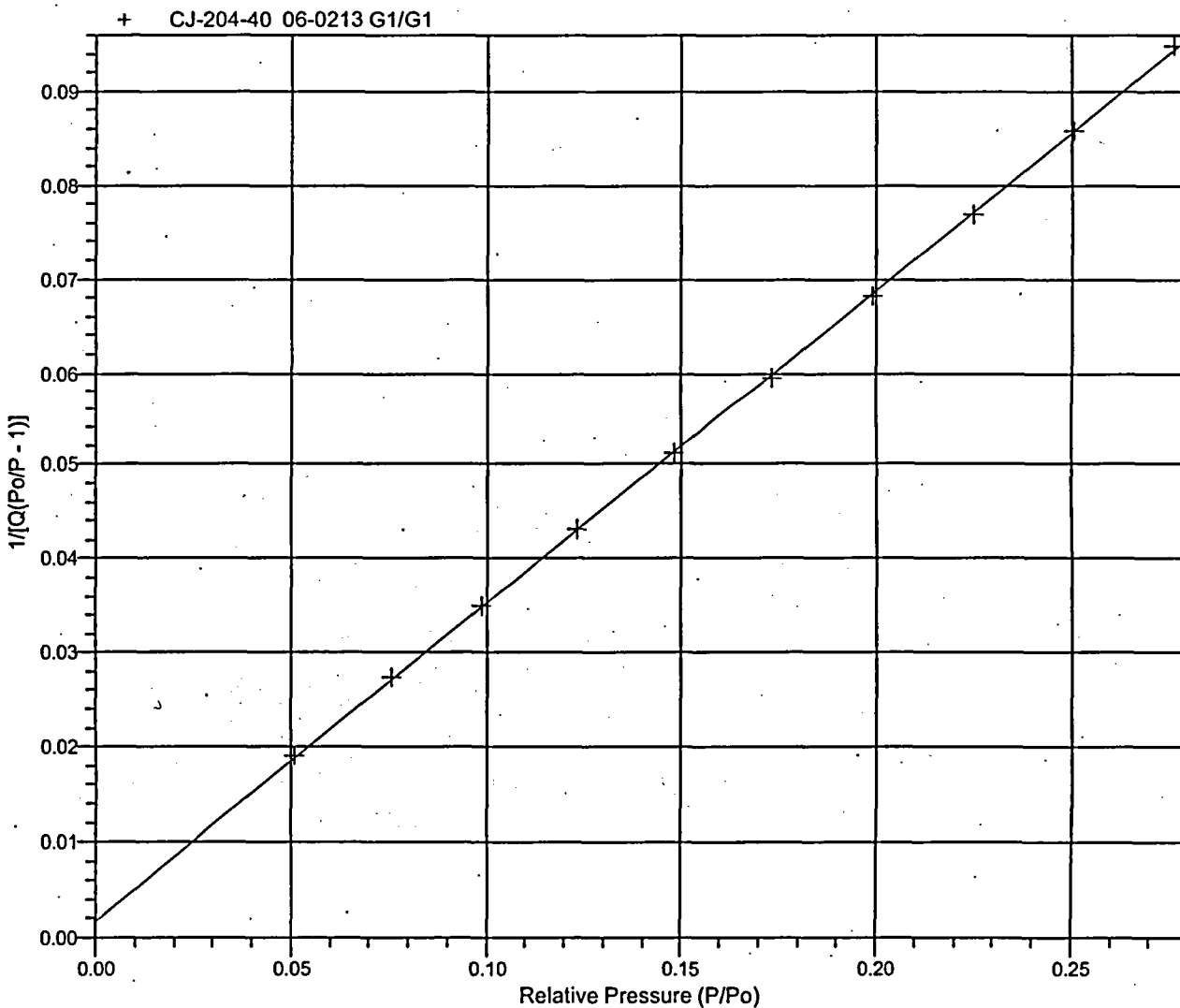
Sample Prep: Stage  
 1

Soak Temperature (°C)  
 100

Ramp Rate (°C/min)  
 10

Soak Time (min)  
 960

BET Surface Area Plot



TriStar 3000 V6.05.01 A

Unit 2 Port 1

Serial #: 1449

Page 5

Sample: CJ-204-40 06-0213 G1/G1  
Operator: MJP  
Submitter: S.M.Stoller  
File: C:\...01JAN06-0213.SMP

Started: 2/1/2006 12:24:05PM  
Completed: 2/1/2006 3:16:44PM  
Report Time: 2/1/2006 3:43:34PM  
Warm Free Space: 5.6492 cm<sup>3</sup> Measured  
Equilibration Interval: 10 s  
Sample Density: 1.000 g/cm<sup>3</sup>

Analysis Adsorptive: N2  
Analysis Bath Temp.: 77.300 K  
Sample Mass: 4.4734 g  
Cold Free Space: 16.0508 cm<sup>3</sup> Measured  
Low Pressure Dose: None  
Automatic Degas: Yes

Sample Prep: Stage  
1

Soak Temperature (°C)  
100

Ramp Rate (°C/min)  
10

Soak Time (min)  
960

#### Summary Report

##### Surface Area

Single point surface area at P/Po = 0.276424207: 12.6720 m<sup>2</sup>/g

BET Surface Area: 12.9162 m<sup>2</sup>/g



TriStar 3000 V6.05.01 A

Unit 2 Port 2

Serial #: 1449

Page 1

Sample: CJ-205-40 06-0214 G2/G2  
 Operator: MJP  
 Submitter: S.M.Stoller  
 File: C:\...01JAN06-0214.SMP

Started: 2/1/2006 12:24:05PM  
 Completed: 2/1/2006 3:16:44PM  
 Report Time: 2/1/2006 3:16:49PM  
 Warm Free Space: 5.6027 cm<sup>3</sup> Measured  
 Equilibration Interval: 10 s  
 Sample Density: 1.000 g/cm<sup>3</sup>

Analysis Adsorptive: N2  
 Analysis Bath Temp.: 77.300 K  
 Sample Mass: 4.2657 g  
 Cold Free Space: 15.9013 cm<sup>3</sup> Measured  
 Low Pressure Dose: None  
 Automatic Degas: Yes

Sample Prep: Stage	Soak Temperature (°C)	Ramp Rate (°C/min)	Soak Time (min)
1	100	10	960

**Isotherm Tabular Report**

Relative Pressure (P/Po)	Absolute Pressure (mmHg)	Quantity Adsorbed (cm <sup>3</sup> /g STP)	Elapsed Time (h:min)	Saturation Pressure (mmHg)
			01:13	734.31885
0.049028719	36.00271	2.0965	01:39	
0.078428859	57.59179	2.2602	01:46	
0.095402314	70.05572	2.3412	01:53	
0.123514763	90.69922	2.4647	02:01	
0.148487792	109.03738	2.5710	02:06	
0.173677332	127.53454	2.6739	02:11	
0.198861179	146.02751	2.7753	02:16	
0.224033607	164.51210	2.8776	02:21	
0.249320011	183.08038	2.9817	02:26	
0.274777348	201.77419	3.0875	02:31	
0.300337231	220.54329	3.1959	02:36	

TriStar 3000 V6.05.01 A

Unit 2 Port 2

Serial #: 1449

Page 2

Sample: CJ-205-40 06-0214 G2/G2  
 Operator: MJP  
 Submitter: S.M.Stoller  
 File: C:\...\01JAN06-0214.SMP

Started: 2/1/2006 12:24:05PM  
 Completed: 2/1/2006 3:16:44PM  
 Report Time: 2/1/2006 3:16:49PM  
 Warm Free Space: 5.6027 cm<sup>3</sup> Measured  
 Equilibration Interval: \*10 s  
 Sample Density: 1.000 g/cm<sup>3</sup>

Analysis Adsorptive: N2  
 Analysis Bath Temp.: 77.300 K  
 Sample Mass: 4.2657 g  
 Cold Free Space: 15.9013 cm<sup>3</sup> Measured  
 Low Pressure Dose: None  
 Automatic Degas: Yes

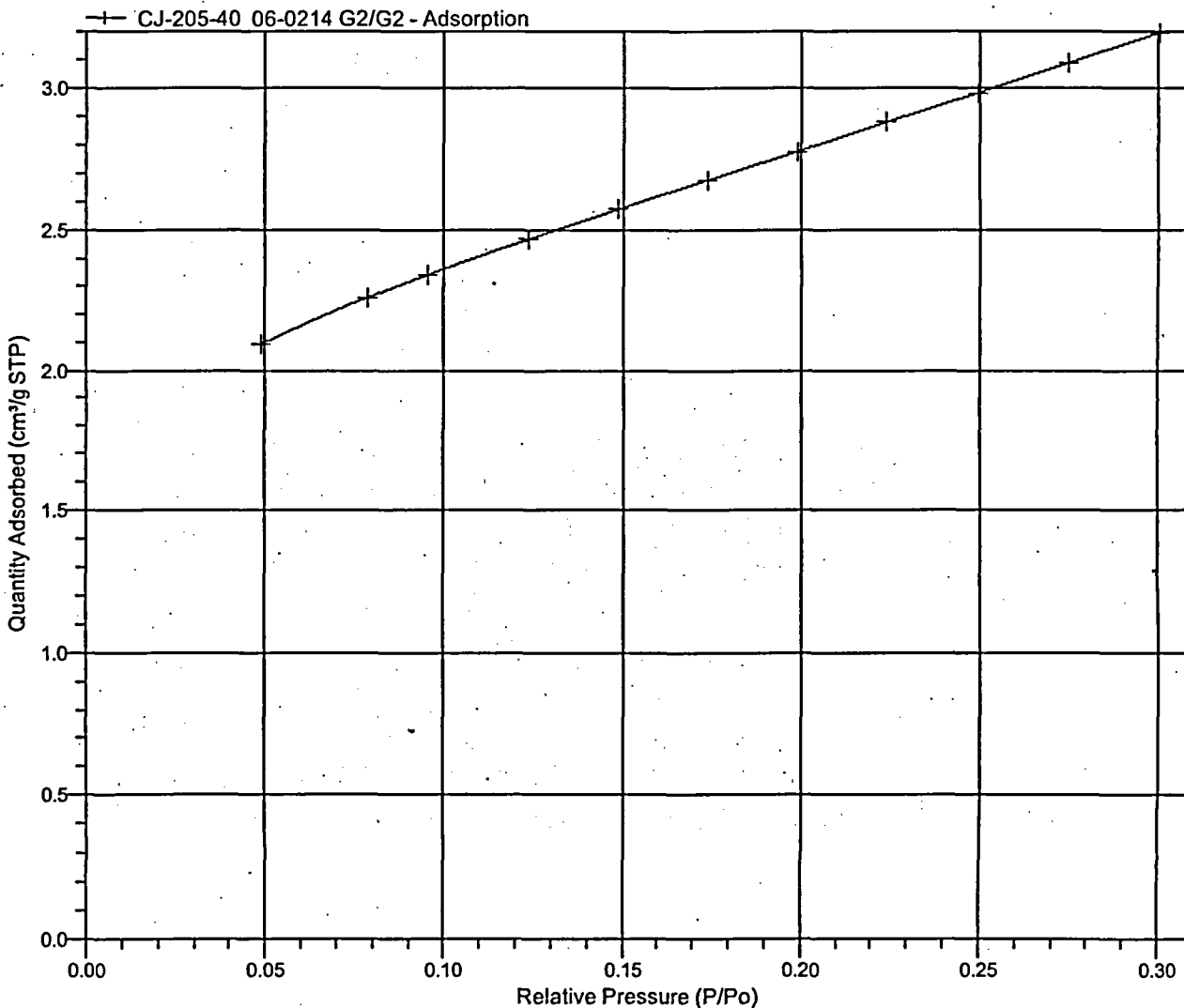
Sample Prep: Stage  
 1

Soak Temperature (°C)  
 100

Ramp Rate (°C/min)  
 10

Soak Time (min)  
 960

Isotherm Linear Plot



TriStar 3000 V6.05.01 A

Unit 2 Port 2

Serial #: 1449

Page 3

Sample: CJ-205-40 06-0214 G2/G2  
 Operator: MJP  
 Submitter: S.M.Stoller  
 File: C:\...01JAN06-0214.SMP

Started: 2/1/2006 12:24:05PM  
 Completed: 2/1/2006 3:16:44PM  
 Report Time: 2/1/2006 3:16:49PM  
 Warm Free Space: 5.6027 cm<sup>3</sup> Measured  
 Equilibration Interval: 10 s  
 Sample Density: 1.000 g/cm<sup>3</sup>

Analysis Adsorptive: N2  
 Analysis Bath Temp.: 77.300 K  
 Sample Mass: 4.2657 g  
 Cold Free Space: 15.9013 cm<sup>3</sup> Measured  
 Low Pressure Dose: None  
 Automatic Degas: Yes

Sample Prep: Stage	Soak Temperature (°C)	Ramp Rate (°C/min)	Soak Time (min)
1	100	10	960

**BET Surface Area Report**

BET Surface Area: 9.9511 ± 0.0246 m<sup>2</sup>/g  
 Slope: 0.434049 ± 0.001061 g/cm<sup>3</sup> STP  
 Y-Intercept: 0.003410 ± 0.000203 g/cm<sup>3</sup> STP  
 C: 128.300420  
 Qm: 2.2859 cm<sup>3</sup>/g STP  
 Correlation Coefficient: 0.9999731  
 Molecular Cross-Sectional Area: 0.1620 nm<sup>2</sup>

Relative Pressure (P/Po)	Quantity Adsorbed (cm <sup>3</sup> /g STP)	1/[Q(Po/P - 1)]
0.049028719	2.0965	0.024591
0.078428859	2.2602	0.037652
0.095402314	2.3412	0.045048
0.123514763	2.4647	0.057175
0.148487792	2.5710	0.067826
0.173677332	2.6739	0.078604
0.198861179	2.7753	0.089441
0.224033607	2.8776	0.100333
0.249320011	2.9817	0.111387
0.274777348	3.0875	0.122716
0.300337231	3.1959	0.134314

TriStar 3000 V6.05.01 A

Unit 2 Port 2

Serial #: 1449

Page 4

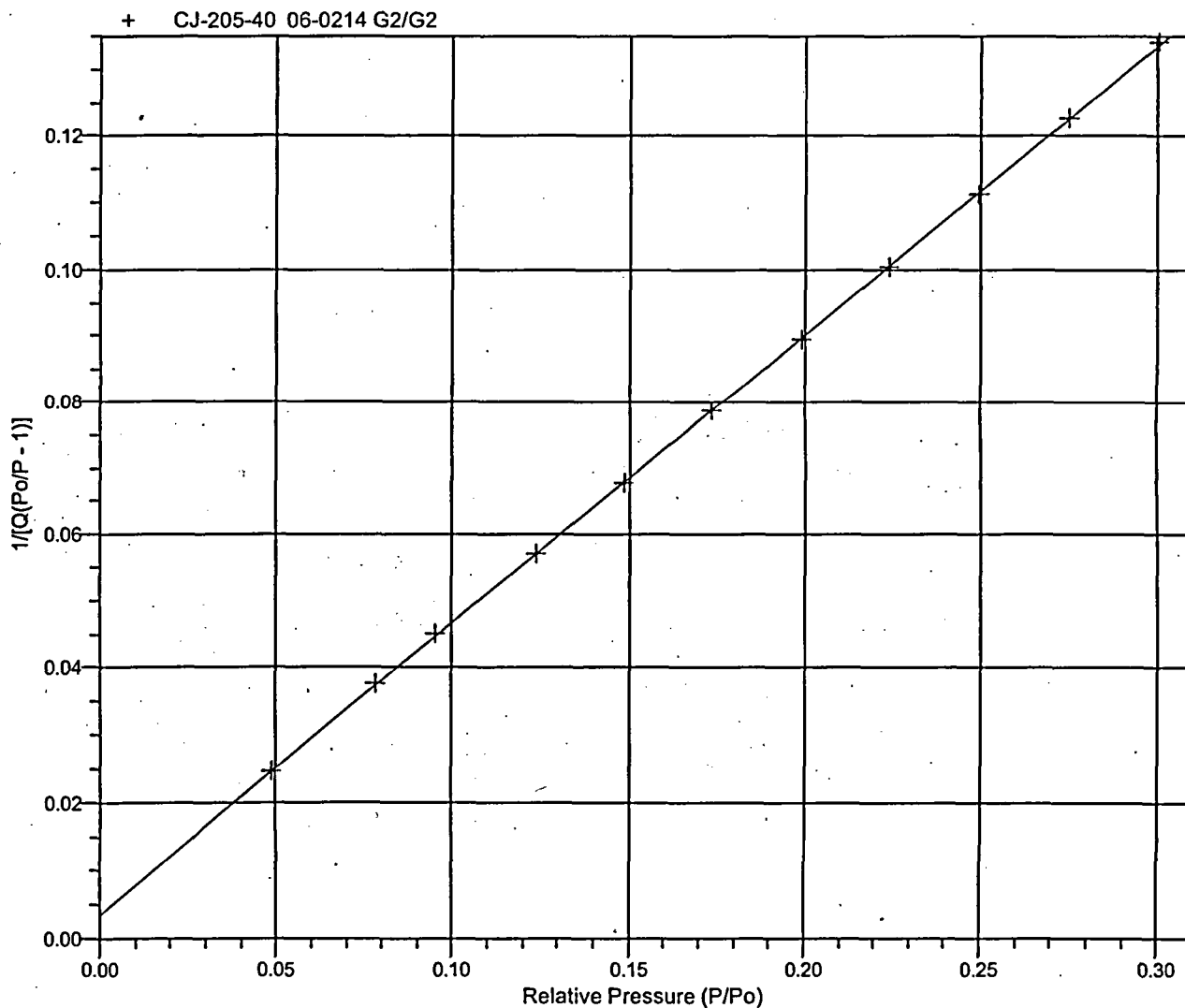
Sample: CJ-205-40 06-0214 G2/G2  
 Operator: MJP  
 Submitter: S.M.Stoller  
 File: C:\...\01JAN06-0214.SMP

Started: 2/1/2006 12:24:05PM  
 Completed: 2/1/2006 3:16:44PM  
 Report Time: 2/1/2006 3:16:49PM  
 Warm Free Space: 5.6027 cm<sup>3</sup> Measured  
 Equilibration Interval: 10 s  
 Sample Density: 1.000 g/cm<sup>3</sup>

Analysis Adsorptive: N2  
 Analysis Bath Temp.: 77.300 K  
 Sample Mass: 4.2657 g  
 Cold Free Space: 15.9013 cm<sup>3</sup> Measured  
 Low Pressure Dose: None  
 Automatic Degas: Yes

Sample Prep: Stage	Soak Temperature (°C)	Ramp Rate (°C/min)	Soak Time (min)
1	100	10	960

BET Surface Area Plot



TriStar 3000 V6.05.01 A

Unit 2 Port 2

Serial #: 1449

Page 5

Sample: CJ-205-40 06-0214 G2/G2  
Operator: MJP  
Submitter: S.M.Stoller  
File: C:\...\01JAN06-0214.SMP

Started: 2/1/2006 12:24:05PM  
Completed: 2/1/2006 3:16:44PM  
Report Time: 2/1/2006 3:16:49PM  
Warm Free Space: 5.6027 cm<sup>3</sup> Measured  
Equilibration Interval: 10 s  
Sample Density: 1.000 g/cm<sup>3</sup>

Analysis Adsorptive: N2  
Analysis Bath Temp.: 77.300 K  
Sample Mass: 4.2657 g  
Cold Free Space: 15.9013 cm<sup>3</sup> Measured  
Low Pressure Dose: None  
Automatic Degas: Yes

Sample Prep: Stage  
1

Soak Temperature (°C)  
100

Ramp Rate (°C/min)  
10

Soak Time (min)  
960

### Summary Report

#### Surface Area

Single point surface area at P/Po = 0.300337231: 9.7341 m<sup>2</sup>/g

BET Surface Area: 9.9511 m<sup>2</sup>/g

# **MICROMERITICS** **ANALYTICAL SERVICES** *The Particle Testing Authority*

TriStar 3000 V6.05.01 A

Unit 2 Port 3

Serial #: 1449

Page 1

Sample: CJ-205-40-P 06-0215 G3/G3  
 Operator: MJP  
 Submitter: S.M.Stoller  
 File: C:\...101JAN06-0215.SMP

Started: 2/1/2006 12:24:05PM  
 Completed: 2/1/2006 3:16:44PM  
 Report Time: 2/1/2006 3:16:50PM  
 Warm Free Space: 5.8945 cm<sup>3</sup> Measured  
 Equilibration Interval: 10 s  
 Sample Density: 1.000 g/cm<sup>3</sup>

Analysis Adsorptive: N2  
 Analysis Bath Temp.: 77.300 K  
 Sample Mass: 4.4765 g  
 Cold Free Space: 17.0075 cm<sup>3</sup> Measured  
 Low Pressure Dose: None  
 Automatic Degas: Yes

Sample Prep: Stage	Soak Temperature (°C)	Ramp Rate (°C/min)	Soak Time (min)
1	100	10	960

## Isotherm Tabular Report

Relative Pressure (P/Po)	Absolute Pressure (mmHg)	Quantity Adsorbed (cm <sup>3</sup> /g STP)	Elapsed Time (h:min)	Saturation Pressure (mmHg)
			01:13	734.31885
0.051768373	38.01449	2.2498	01:43	
0.077711856	57.06528	2.4063	01:52	
0.098809999	72.55804	2.5137	01:57	
0.123341660	90.57211	2.6296	02:02	
0.148014517	108.68985	2.7437	02:07	
0.173110903	127.11860	2.8561	02:12	
0.198399312	145.68835	2.9674	02:17	
0.223636885	164.22078	3.0796	02:21	
0.249010002	182.85274	3.1938	02:25	
0.274450881	201.53445	3.3106	02:30	
0.300168460	220.41936	3.4299	02:34	

TriStar 3000 V6.05.01 A

Unit 2 Port 3

Serial #: 1449

Page 2

Sample: CJ-205-40-P 06-0215 G3/G3  
 Operator: MJP  
 Submitter: S.MStoller  
 File: C:\...101JAN06-0215.SMP

Started: 2/1/2006 12:24:05PM  
 Completed: 2/1/2006 3:16:44PM  
 Report Time: 2/1/2006 3:16:50PM  
 Warm Free Space: 5.8945 cm<sup>3</sup> Measured  
 Equilibration Interval: 10 s  
 Sample Density: 1.000 g/cm<sup>3</sup>

Analysis Adsorptive: N<sub>2</sub>  
 Analysis Bath Temp.: 77.300 K  
 Sample Mass: 4.4765 g  
 Cold Free Space: 17.0075 cm<sup>3</sup> Measured  
 Low Pressure Dose: None  
 Automatic Degas: Yes

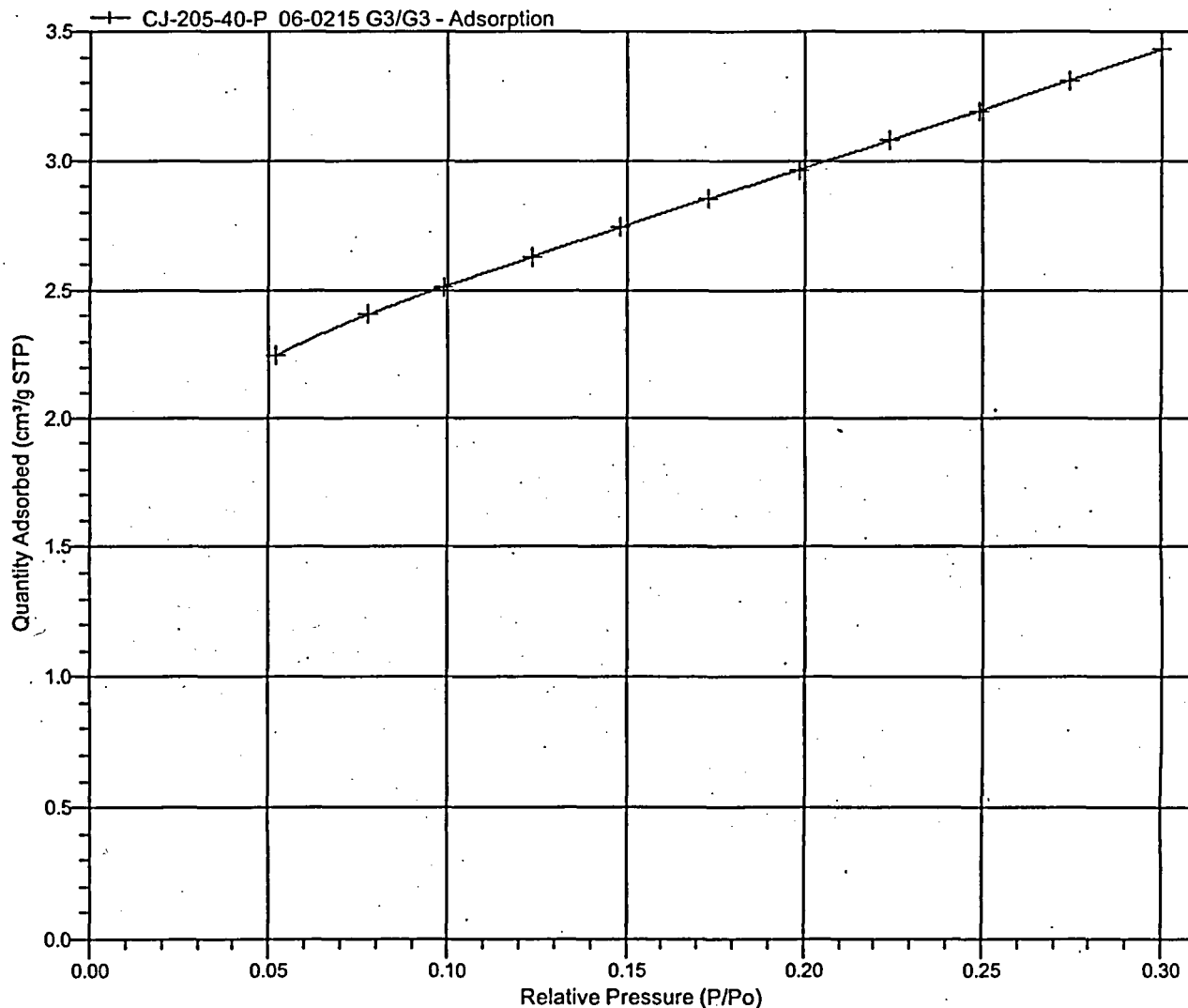
Sample Prep: Stage  
 1

Soak Temperature (°C)  
 100

Ramp Rate (°C/min)  
 10

Soak Time (min)  
 960

Isotherm Linear Plot



TriStar 3000 V6.05.01 A

Unit 2 Port 3

Serial #: 1449

Page 3

Sample: CJ-205-40-P 06-0215 G3/G3  
 Operator: MJP  
 Submitter: S.M.Stoller  
 File: C:\...01JAN06-0215.SMP

Started: 2/1/2006 12:24:05PM  
 Completed: 2/1/2006 3:16:44PM  
 Report Time: 2/1/2006 3:16:50PM  
 Warm Free Space: 5.8945 cm<sup>3</sup> Measured  
 Equilibration Interval: 10 s  
 Sample Density: 1.000 g/cm<sup>3</sup>

Analysis Adsorptive: N2  
 Analysis Bath Temp.: 77.300 K  
 Sample Mass: 4.4765 g  
 Cold Free Space: 17.0075 cm<sup>3</sup> Measured  
 Low Pressure Dose: None  
 Automatic Degas: Yes

Sample Prep: Stage	Soak Temperature (°C)	Ramp Rate (°C/min)	Soak Time (min)
1	100	10	960

**BET Surface Area Report**

BET Surface Area: 10.6955 ± 0.0222 m<sup>2</sup>/g  
 Slope: 0.403460 ± 0.000830 g/cm<sup>3</sup> STP  
 Y-Intercept: 0.003553 ± 0.000159 g/cm<sup>3</sup> STP  
 C: 114.541452  
 Qm: 2.4569 cm<sup>3</sup>/g STP  
 Correlation Coefficient: 0.9999810  
 Molecular Cross-Sectional Area: 0.1620 nm<sup>2</sup>

Relative Pressure (P/Po)	Quantity Adsorbed (cm <sup>3</sup> /g STP)	1/[Q(Po/P - 1)]
0.051768373	2.2498	0.024266
0.077711856	2.4063	0.035016
0.098809999	2.5137	0.043619
0.123341660	2.6296	0.053505
0.148014517	2.7437	0.063319
0.173110903	2.8561	0.073300
0.198399312	2.9674	0.083407
0.223636885	3.0796	0.093537
0.249010002	3.1938	0.103817
0.274450881	3.3106	0.114260
0.300168460	3.4299	0.125050



TriStar 3000 V6.05.01 A

Unit 2 Port 3

Serial #: 1449

Page 4

Sample: CJ-205-40-P 06-0215 G3/G3

Operator: MJP

Submitter: S.M.Stoller

File: C:\...101JAN06-0215.SMP

Started: 2/1/2006 12:24:05PM

Completed: 2/1/2006 3:16:44PM

Report Time: 2/1/2006 3:16:50PM

Warm Free Space: 5.8945 cm<sup>3</sup> Measured

Equilibration Interval: 10 s

Sample Density: 1.000 g/cm<sup>3</sup>

Analysis Adsorptive: N2

Analysis Bath Temp.: 77.300 K

Sample Mass: 4.4765 g

Cold Free Space: 17.0075 cm<sup>3</sup> Measured

Low Pressure Dose: None

Automatic Degas: Yes

Sample Prep: Stage

1

Soak Temperature (°C)

100

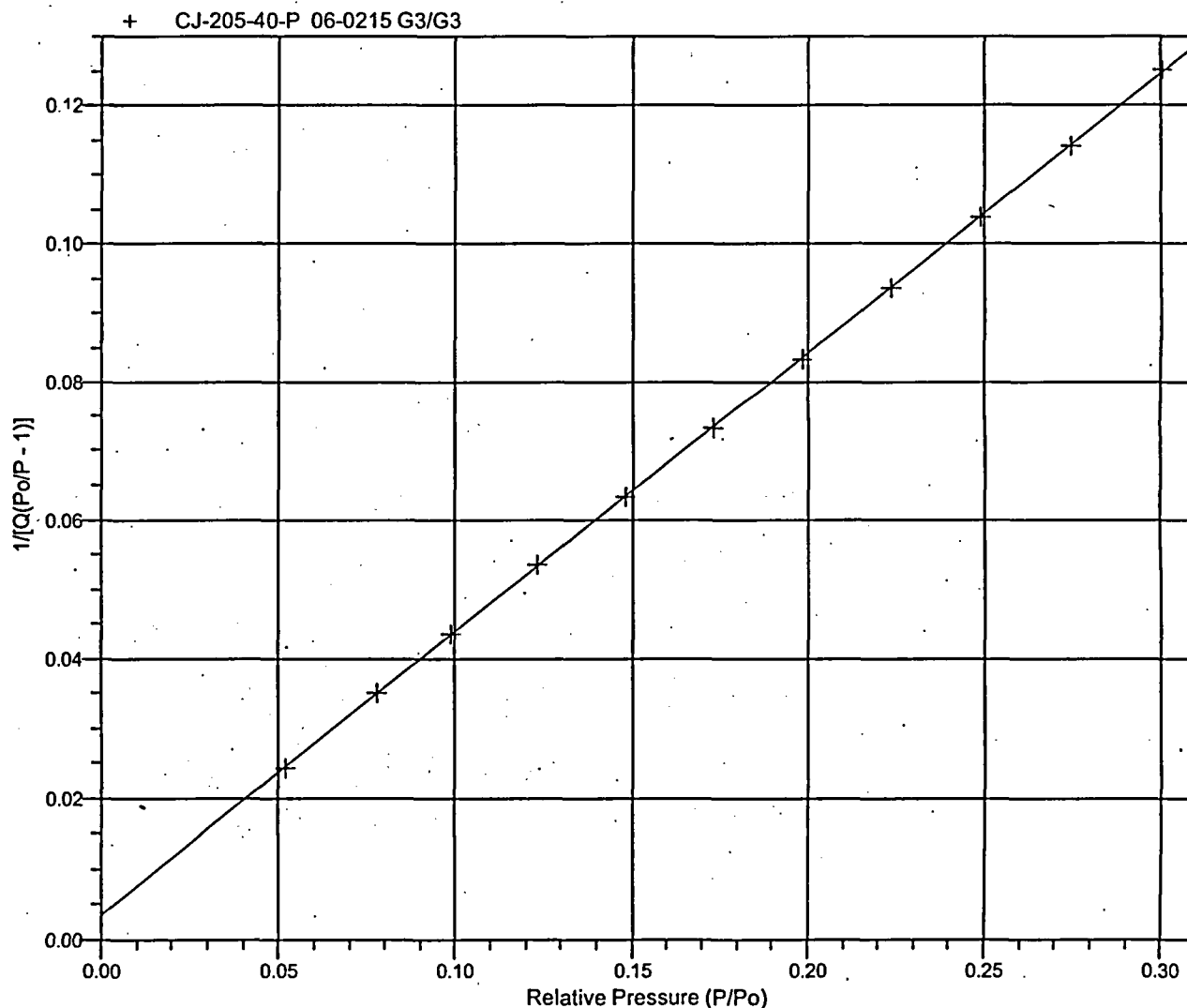
Ramp Rate (°C/min)

10

Soak Time (min)

960

**BET Surface Area Plot**



TriStar 3000 V6.05.01 A

Unit 2 Port 3

Serial #: 1449

Page 5

Sample: CJ-205-40-P 06-0215 G3/G3  
Operator: MJP  
Submitter: S.M.Stoller  
File: C:\...101JAN06-0215.SMP

Started: 2/1/2006 12:24:05PM  
Completed: 2/1/2006 3:16:44PM  
Report Time: 2/1/2006 3:16:50PM  
Warm Free Space: 5.8945 cm<sup>3</sup> Measured  
Equilibration Interval: 10 s  
Sample Density: 1.000 g/cm<sup>3</sup>

Analysis Adsorptive: N2  
Analysis Bath Temp.: 77.300 K  
Sample Mass: 4.4765 g  
Cold Free Space: 17.0075 cm<sup>3</sup> Measured  
Low Pressure Dose: None  
Automatic Degas: Yes

Sample Prep: Stage  
1

Soak Temperature (°C)  
100

Ramp Rate (°C/min)  
10

Soak Time (min)  
960

#### Summary Report

##### Surface Area

Single point surface area at P/Po = 0.300168460: 10.4494 m<sup>2</sup>/g

BET Surface Area: 10.6955 m<sup>2</sup>/g

TriStar 3000 V6.05.01 A

Unit 1 Port 1

Serial #: 1098

Page 1

Sample: CJ-206-40 06-0216 F3/F3  
 Operator: MJP  
 Submitter: S.M.Stoller  
 File: C:\...01JAN06-0216.SMP

Started: 2/1/2006 4:22:41PM  
 Completed: 2/1/2006 8:12:53PM  
 Report Time: 2/1/2006 8:12:54PM  
 Warm Free Space: 5.3716 cm<sup>3</sup> Measured  
 Equilibration Interval: 10 s  
 Sample Density: 1.000 g/cm<sup>3</sup>

Analysis Adsorptive: N2  
 Analysis Bath Temp.: 77.300 K  
 Sample Mass: 4.8010 g  
 Cold Free Space: 15.0468 cm<sup>3</sup> Measured  
 Low Pressure Dose: None  
 Automatic Degas: Yes

Sample Prep: Stage 1      Soak Temperature (°C) 100      Ramp Rate (°C/min) 10      Soak Time (min) 960

**Isotherm Tabular Report**

Relative Pressure (P/Po)	Absolute Pressure (mmHg)	Quantity Adsorbed (cm <sup>3</sup> /g STP)	Elapsed Time (h:min)	Saturation Pressure (mmHg)
			01:08	736.94562
0.050766839	37.41240	1.9969	01:39	
0.077301212	56.96679	2.1382	01:50	
0.098732820	72.76072	2.2335	01:57	
0.123413197	90.94881	2.3341	02:04	
0.147980169	109.05334	2.4337	02:10	
0.172864649	127.39185	2.5332	02:17	
0.198418174	146.22340	2.6309	02:22	
0.223756218	164.89616	2.7288	02:27	
0.248980899	183.48538	2.8292	02:32	
0.274404000	202.22083	2.9321	02:37	
0.300121926	221.17354	3.0374	02:41	

TriStar 3000 V6.05.01 A

Unit 1 Port 1

Serial #: 1098

Page 2

Sample: CJ-206-40 06-0216 F3/F3  
 Operator: MJP  
 Submitter: S.M.Stoller  
 File: C:\...01JAN06-0216.SMP

Started: 2/1/2006 4:22:41PM  
 Completed: 2/1/2006 8:12:53PM  
 Report Time: 2/1/2006 8:12:54PM  
 Warm Free Space: 5.3716 cm<sup>3</sup> Measured  
 Equilibration Interval: 10 s  
 Sample Density: 1.000 g/cm<sup>3</sup>

Analysis Adsorptive: N<sub>2</sub>  
 Analysis Bath Temp.: 77.300 K  
 Sample Mass: 4.8010 g  
 Cold Free Space: 15.0468 cm<sup>3</sup> Measured  
 Low Pressure Dose: None  
 Automatic Degas: Yes

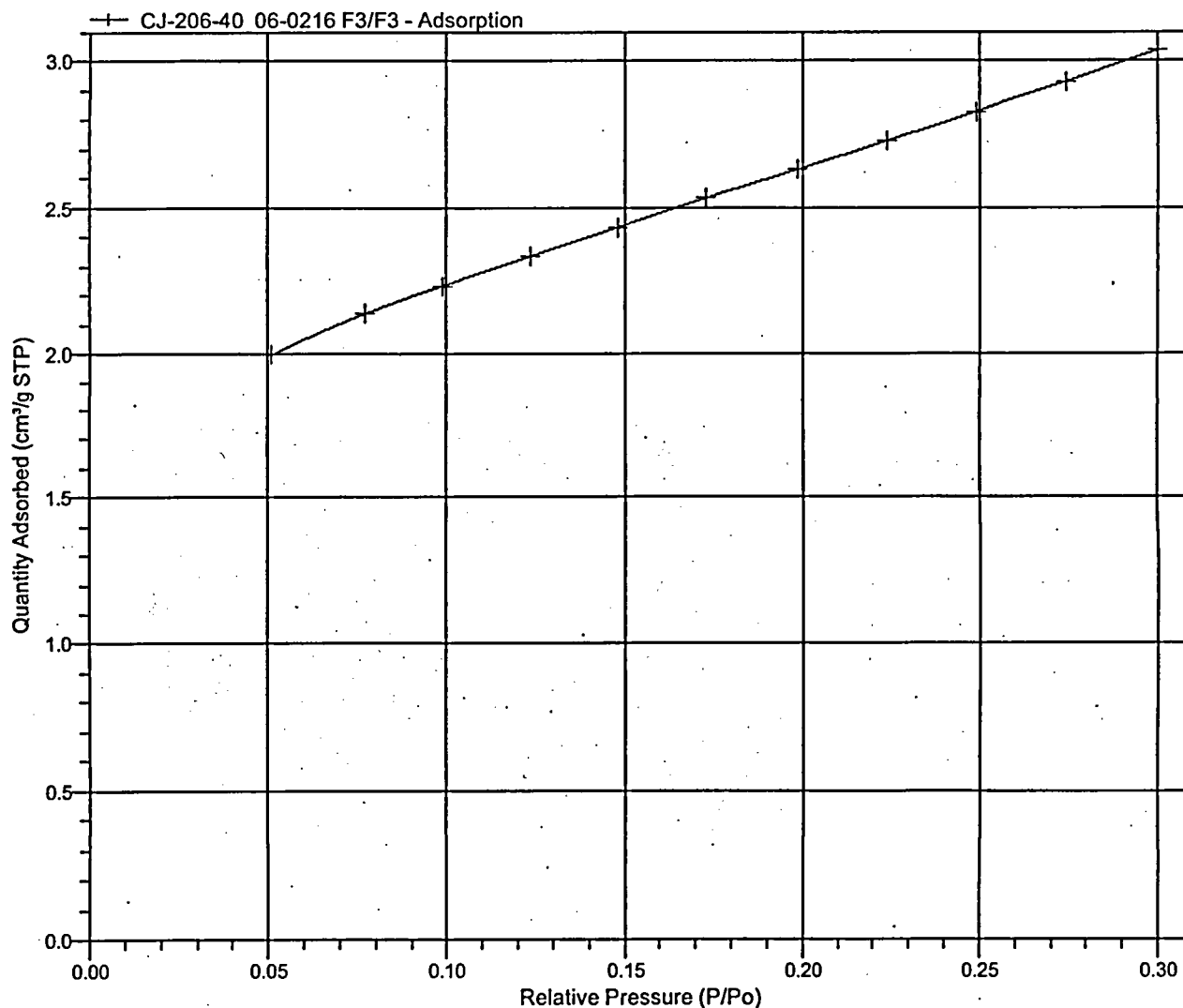
Sample Prep: Stage  
 1

Soak Temperature (°C)  
 100

Ramp Rate (°C/min)  
 10

Soak Time (min)  
 960

Isotherm Linear Plot



TriStar 3000 V6.05.01 A

Unit 1 Port 1

Serial #: 1098

Page 3

Sample: CJ-206-40 06-0216 F3/F3  
 Operator: MJP  
 Submitter: S.M.Stoller  
 File: C:\...01JAN06-0216.SMP

Started: 2/1/2006 4:22:41PM  
 Completed: 2/1/2006 8:12:53PM  
 Report Time: 2/1/2006 8:12:54PM  
 Warm Free Space: 5.3716 cm<sup>3</sup> Measured  
 Equilibration Interval: 10 s  
 Sample Density: 1.000 g/cm<sup>3</sup>

Analysis Adsorptive: N2  
 Analysis Bath Temp.: 77.300 K  
 Sample Mass: 4.8010 g  
 Cold Free Space: 15.0468 cm<sup>3</sup> Measured  
 Low Pressure Dose: None  
 Automatic Degas: Yes

Sample Prep: Stage  
 1

Soak Temperature (°C)  
 100

Ramp Rate (°C/min)  
 10

Soak Time (min)  
 960

**BET Surface Area Report**

BET Surface Area: 9.4615 ± 0.0195 m<sup>2</sup>/g  
 Slope: 0.456311 ± 0.000930 g/cm<sup>3</sup> STP  
 Y-Intercept: 0.003784 ± 0.000178 g/cm<sup>3</sup> STP  
 C: 121.597783  
 Qm: 2.1735 cm<sup>3</sup>/g STP  
 Correlation Coefficient: 0.9999813  
 Molecular Cross-Sectional Area: 0.1620 nm<sup>2</sup>

Relative Pressure (P/Po)	Quantity Adsorbed (cm <sup>3</sup> /g STP)	1/[Q(Po/P - 1)]
0.050766839	1.9969	0.026782
0.077301212	2.1382	0.039182
0.098732820	2.2335	0.049047
0.123413197	2.3341	0.060317
0.147980169	2.4337	0.071364
0.172864649	2.5332	0.082501
0.198418174	2.6309	0.094087
0.223756218	2.7288	0.105634
0.248980899	2.8292	0.117180
0.274404000	2.9321	0.128978
0.300121926	3.0374	0.141178

TriStar 3000 V6.05.01 A

Unit 1 Port 1

Serial #: 1098

Page 4

Sample: CJ-206-40 06-0216 F3/F3  
 Operator: MJP  
 Submitter: S.M.Stoller  
 File: C:\...101JAN06-0216.SMP

Started: 2/1/2006 4:22:41PM  
 Completed: 2/1/2006 8:12:53PM  
 Report Time: 2/1/2006 8:12:54PM  
 Warm Free Space: 5.3716 cm<sup>3</sup> Measured  
 Equilibration Interval: 10 s  
 Sample Density: 1.000 g/cm<sup>3</sup>

Analysis Adsorptive: N2  
 Analysis Bath Temp: 77.300 K  
 Sample Mass: 4.8010 g  
 Cold Free Space: 15.0468 cm<sup>3</sup> Measured  
 Low Pressure Dose: None  
 Automatic Degas: Yes

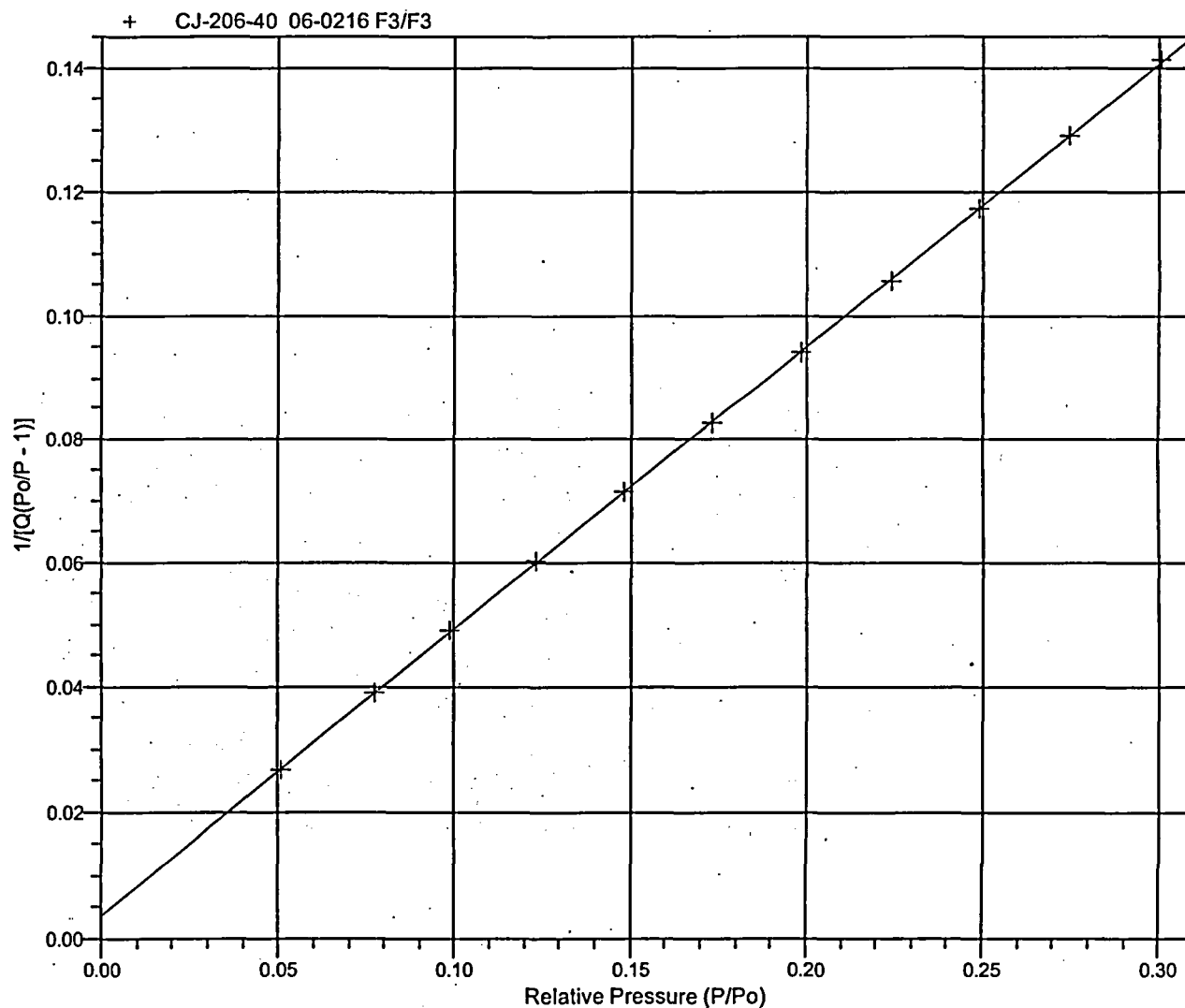
Sample Prep: Stage  
 1

Soak Temperature (°C)  
 100

Ramp Rate (°C/min)  
 10

Soak Time (min)  
 960

**BET Surface Area Plot**



TriStar 3000 V6.05.01 A

Unit 1 Port 1

Serial #: 1098

Page 5

Sample: CJ-206-40 06-0216 F3/F3  
Operator: MJP  
Submitter: S.M.Stoller  
File: C:\...101JAN06-0216.SMP

Started: 2/1/2006 4:22:41PM  
Completed: 2/1/2006 8:12:53PM  
Report Time: 2/1/2006 8:12:54PM  
Warm Free Space: 5.3716 cm<sup>3</sup> Measured  
Equilibration Interval: 10 s  
Sample Density: 1.000 g/cm<sup>3</sup>

Analysis Adsorptive: N2  
Analysis Bath Temp.: 77.300 K  
Sample Mass: 4.8010 g  
Cold Free Space: 15.0468 cm<sup>3</sup> Measured  
Low Pressure Dose: None  
Automatic Degas: Yes

Sample Prep: Stage	Soak Temperature (°C)	Ramp Rate (°C/min)	Soak Time (min)
1	100	10	960

#### Summary Report

##### Surface Area

Single point surface area at P/Po = 0.300121926: 9.2542 m<sup>2</sup>/g

BET Surface Area: 9.4615 m<sup>2</sup>/g

# MICROMERITICS ANALYTICAL SERVICES

The Particle  
Testing  
Authority

TriStar 3000 V6.05.01 A

Unit 1 Port 2

Serial #: 1098

Page 1

Sample: CJ-207-40 06-0217 N1/N1  
Operator: MJP  
Submitter: S.M.Stoller  
File: C:\...101JAN06-0217.SMP

Started: 2/1/2006 4:22:41PM  
Completed: 2/1/2006 8:12:53PM  
Report Time: 2/2/2006 7:50:36AM  
Warm Free Space: 5.5902 cm<sup>3</sup> Measured  
Equilibration Interval: 10 s  
Sample Density: 1.000 g/cm<sup>3</sup>

Analysis Adsorptive: N2  
Analysis Bath Temp.: 77.300 K  
Sample Mass: 4.3543 g  
Cold Free Space: 15.9894 cm<sup>3</sup> Measured  
Low Pressure Dose: None  
Automatic Degas: Yes

Sample Prep: Stage	Soak Temperature (°C)	Ramp Rate (°C/min)	Soak Time (min)
1	100	10	960

## Isotherm Tabular Report

Relative Pressure (P/Po)	Absolute Pressure (mmHg)	Quantity Adsorbed (cm <sup>3</sup> /g STP)	Elapsed Time (h:min)	Saturation Pressure (mmHg)
0.051121487	37.68829	2.8779	01:08	736.94562
0.075556860	55.71075	3.0562	02:10	
0.098313891	72.49754	3.1924	02:33	
0.123338473	90.95711	3.3267	02:49	
			03:00	737.50061
			03:09	
0.148133515	109.24856	3.4562	03:09	
0.173619345	128.04437	3.5836	03:16	
0.199105163	146.84018	3.7082	03:23	
0.224676473	165.69904	3.8333	03:30	
0.250356073	184.63776	3.9600	03:37	
0.276132543	203.64792	4.0890	03:43	
0.302022993	222.74214	4.2212	03:49	



TriStar 3000 V6.05.01 A

Unit 1 Port 2

Serial #: 1098

Page 2

Sample: CJ-207-40 06-0217 N1/N1  
 Operator: MJP  
 Submitter: S.M.Stoller  
 File: C:\...01JAN06-0217.SMP

Started: 2/1/2006 4:22:41PM  
 Completed: 2/1/2006 8:12:53PM  
 Report Time: 2/2/2006 7:50:36AM  
 Warm Free Space: 5.5902 cm<sup>3</sup> Measured  
 Equilibration Interval: 10 s  
 Sample Density: 1.000 g/cm<sup>3</sup>

Analysis Adsorptive: N2  
 Analysis Bath Temp.: 77.300 K  
 Sample Mass: 4.3543 g  
 Cold Free Space: 15.9894 cm<sup>3</sup> Measured  
 Low Pressure Dose: None  
 Automatic Degas: Yes

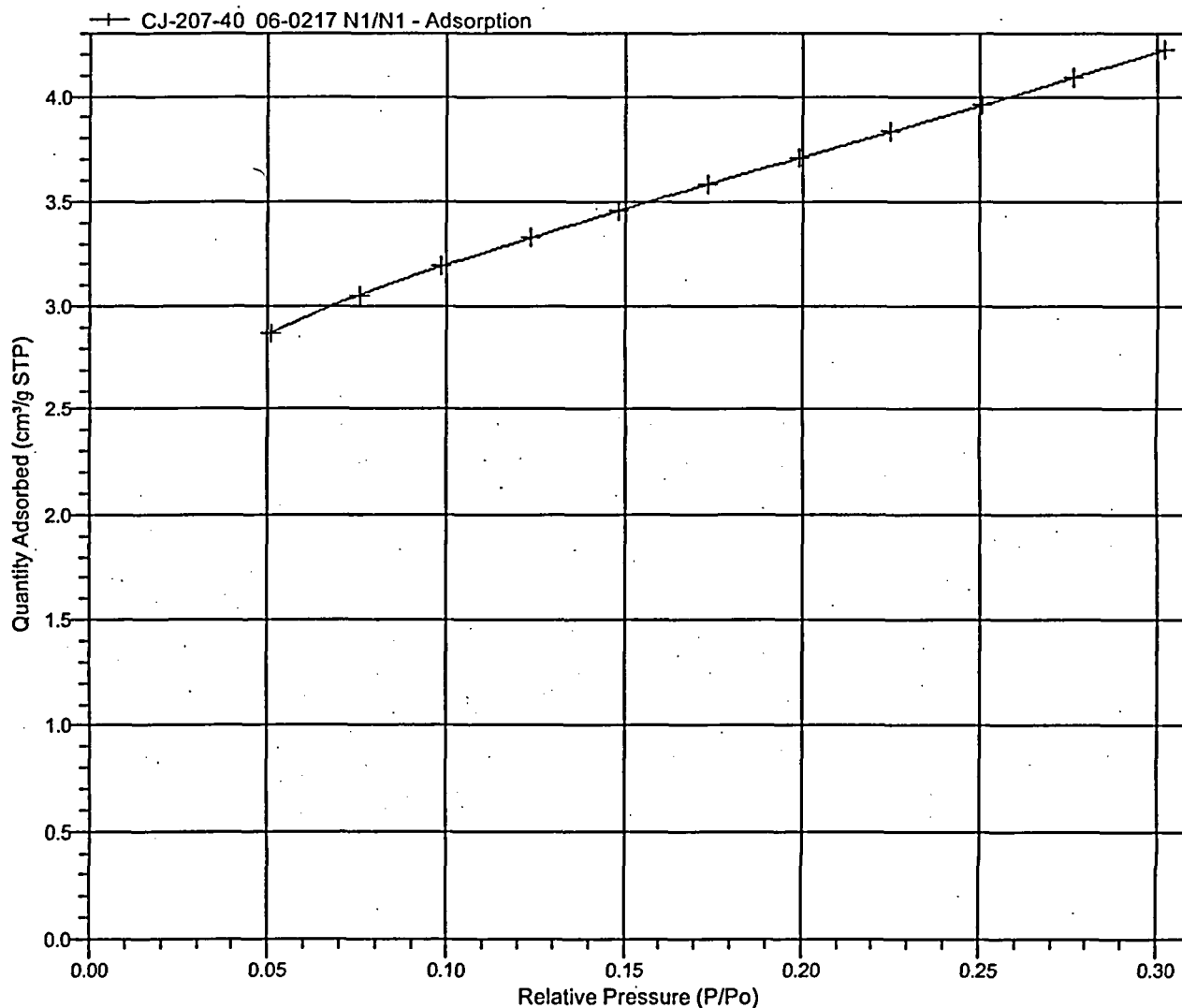
Sample Prep: Stage  
 1

Soak Temperature (°C)  
 100

Ramp Rate (°C/min)  
 10

Soak Time (min)  
 960

Isotherm Linear Plot



TriStar 3000 V6.05.01 A

Unit 1 Port 2

Serial #: 1098

Page 3

Sample: CJ-207-40 06-0217 N1/N1  
 Operator: MJP  
 Submitter: S.M.Stoller  
 File: C:\...101JAN06-0217.SMP

Started: 2/1/2006 4:22:41PM  
 Completed: 2/1/2006 8:12:53PM  
 Report Time: 2/2/2006 7:50:36AM  
 Warm Free Space: 5.5902 cm<sup>3</sup> Measured  
 Equilibration Interval: 10 s  
 Sample Density: 1.000 g/cm<sup>3</sup>

Analysis Adsorptive: N2  
 Analysis Bath Temp: 77.300 K  
 Sample Mass: 4.3543 g  
 Cold Free Space: 15.9894 cm<sup>3</sup> Measured  
 Low Pressure Dose: None  
 Automatic Degas: Yes

Sample Prep: Stage	Soak Temperature (°C)	Ramp Rate (°C/min)	Soak Time (min)
1	100	10	960

**BET Surface Area Report**

BET Surface Area: 13.1245 ± 0.0495 m<sup>2</sup>/g  
 Slope: 0.330055 ± 0.001233 g/cm<sup>3</sup> STP  
 Y-Intercept: 0.001631 ± 0.000219 g/cm<sup>3</sup> STP  
 C: 203.384811  
 Qm: 3.0149 cm<sup>3</sup>/g STP  
 Correlation Coefficient: 0.9999442  
 Molecular Cross-Sectional Area: 0.1620 nm<sup>2</sup>

Relative Pressure (P/Po)	Quantity Adsorbed (cm <sup>3</sup> /g STP)	1/[Q(Po/P - 1)]
0.051121487	2.8779	0.018721
0.075556860	3.0562	0.026743
0.098313891	3.1924	0.034154
0.123338473	3.3267	0.042292
0.148133515	3.4562	0.050313
0.173619345	3.5836	0.058627
0.199105163	3.7082	0.067041
0.224676473	3.8333	0.075597
0.250356073	3.9600	0.084335
0.276132543	4.0890	0.093290

TriStar 3000 V6.05.01 A

Unit 1 Port 2

Serial #: 1098

Page 4

Sample: CJ-207-40 06-0217 N1/N1  
 Operator: MJP  
 Submitter: S.M.Stoller  
 File: C:\...01JAN06-0217.SMP

Started: 2/1/2006 4:22:41PM  
 Completed: 2/1/2006 8:12:53PM  
 Report Time: 2/2/2006 7:50:36AM  
 Warm Free Space: 5.5902 cm<sup>3</sup> Measured  
 Equilibration Interval: 10 s  
 Sample Density: 1.000 g/cm<sup>3</sup>

Analysis Adsorptive: N2  
 Analysis Bath Temp.: 77.300 K  
 Sample Mass: 4.3543 g  
 Cold Free Space: 15.9894 cm<sup>3</sup> Measured  
 Low Pressure Dose: None  
 Automatic Degas: Yes

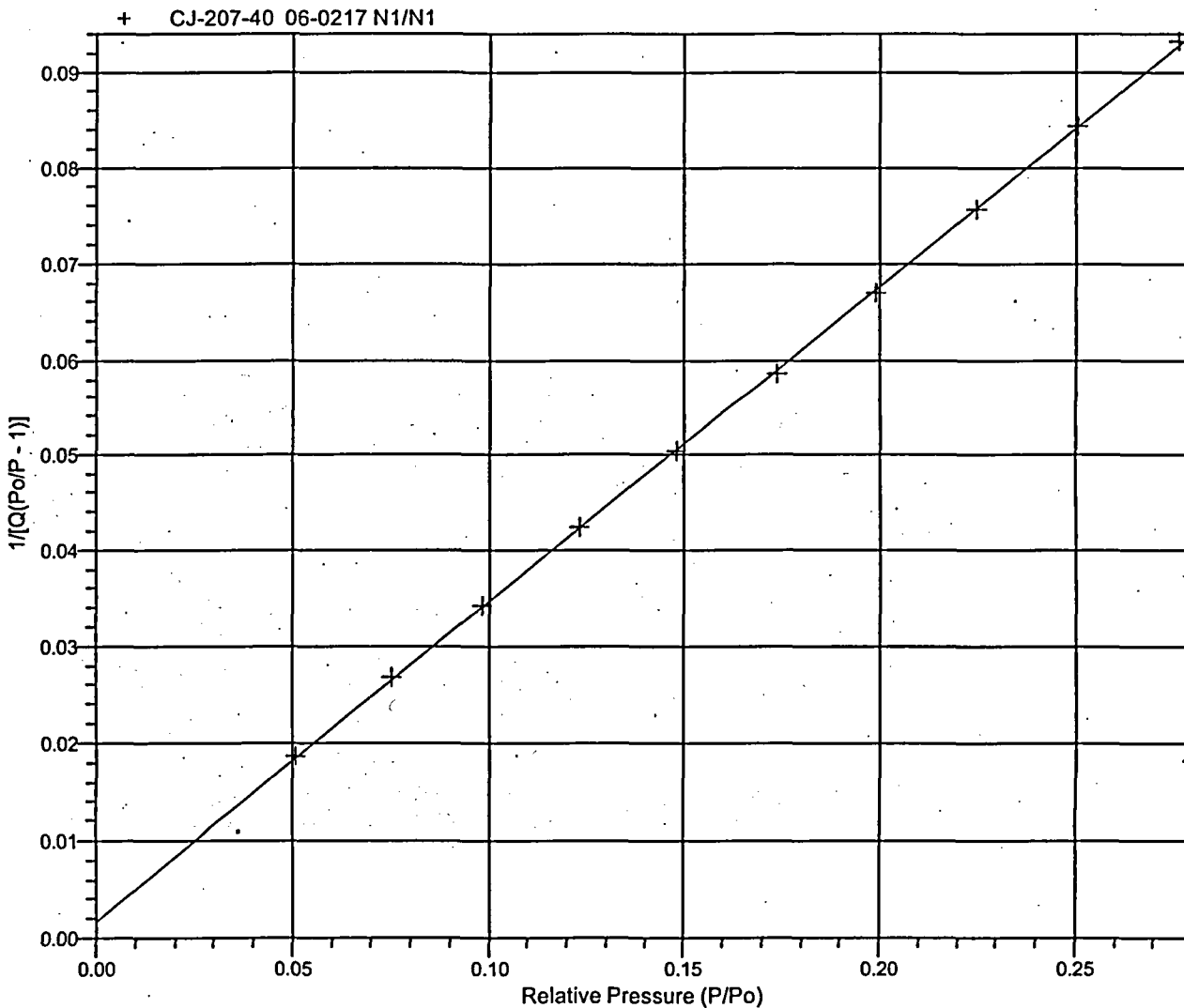
Sample Prep: Stage  
 1

Soak Temperature (°C)  
 100

Ramp Rate (°C/min)  
 10

Soak Time (min)  
 960

BET Surface Area Plot



TriStar 3000 V6.05.01 A

Unit 1 Port 2

Serial #: 1098

Page 5

Sample: CJ-207-40 06-0217 N1/N1  
Operator: MJP  
Submitter: S.M.Stoller  
File: C:\...01JAN06-0217.SMP

Started: 2/1/2006 4:22:41PM  
Completed: 2/1/2006 8:12:53PM  
Report Time: 2/2/2006 7:50:36AM  
Warm Free Space: 5.5902 cm<sup>3</sup> Measured  
Equilibration Interval: 10 s  
Sample Density: 1.000 g/cm<sup>3</sup>

Analysis Adsorptive: N2  
Analysis Bath Temp.: 77.300 K  
Sample Mass: 4.3543 g  
Cold Free Space: 15.9894 cm<sup>3</sup> Measured  
Low Pressure Dose: None  
Automatic Degas: Yes

Sample Prep: Stage  
1

Soak Temperature (°C)  
100

Ramp Rate (°C/min)  
10

Soak Time (min)  
960

#### Summary Report

##### Surface Area

Single point surface area at P/Po = 0.276132543: 12.8851 m<sup>2</sup>/g

BET Surface Area: 13.1245 m<sup>2</sup>/g

# MICROMERITICS ANALYTICAL SERVICES

The Portlano  
Testing  
Authority

TriStar 3000 V6.05.01 A

Unit 1 Port 3

Serial #: 1098

Page 1

Sample: CJ-208-40 06-0218 N2/N2  
Operator: MJP  
Submitter: S.M.Stoller  
File: C:\...01JAN06-0218.SMP

Started: 2/1/2006 4:22:41PM  
Completed: 2/1/2006 8:12:53PM  
Report Time: 2/1/2006 8:12:55PM  
Warm Free Space: 5.7202 cm<sup>3</sup> Measured  
Equilibration Interval: 10 s  
Sample Density: 1.000 g/cm<sup>3</sup>

Analysis Adsorptive: N2  
Analysis Bath Temp.: 77.300 K  
Sample Mass: 4.3662 g  
Cold Free Space: 16.4086 cm<sup>3</sup> Measured  
Low Pressure Dose: None  
Automatic Degas: Yes

Sample Prep: Stage	Soak Temperature (°C)	Ramp Rate (°C/min)	Soak Time (min)
1	100	10	960

## Isotherm Tabular Report

Relative Pressure (P/Po)	Absolute Pressure (mmHg)	Quantity Adsorbed (cm <sup>3</sup> /g STP)	Elapsed Time (h:min)	Saturation Pressure (mmHg)
			01:08	736.94562
0.050132413	36.94486	1.9911	01:38	
0.078159955	57.59964	2.1391	01:47	
0.098735843	72.76295	2.2310	01:57	
0.123546271	91.04688	2.3313	02:03	
0.148265749	109.26379	2.4301	02:08	
0.173383114	127.77393	2.5273	02:13	
0.198727824	146.45160	2.6228	02:18	
0.224004352	165.07903	2.7188	02:24	
0.249400225	183.79440	2.8166	02:28	
0.274898405	202.58517	2.9161	02:33	
0.300589849	221.51837	3.0177	02:38	

TriStar 3000 V6.05.01 A

Unit 1, Port 3

Serial #: 1098

Page 2

Sample: CJ-208-40 06-0218 N2/N2  
 Operator: MJP  
 Submitter: S.M.Stoller  
 File: C:\...01JAN06-0218.SMP

Started: 2/1/2006 4:22:41PM  
 Completed: 2/1/2006 8:12:53PM  
 Report Time: 2/1/2006 8:12:55PM  
 Warm Free Space: 5.7202 cm<sup>3</sup> Measured  
 Equilibration Interval: 10 s  
 Sample Density: 1.000 g/cm<sup>3</sup>

Analysis Adsorptive: N2  
 Analysis Bath Temp.: 77.300 K  
 Sample Mass: 4.3662 g  
 Cold Free Space: 16.4086 cm<sup>3</sup> Measured  
 Low Pressure Dose: None  
 Automatic Degas: Yes

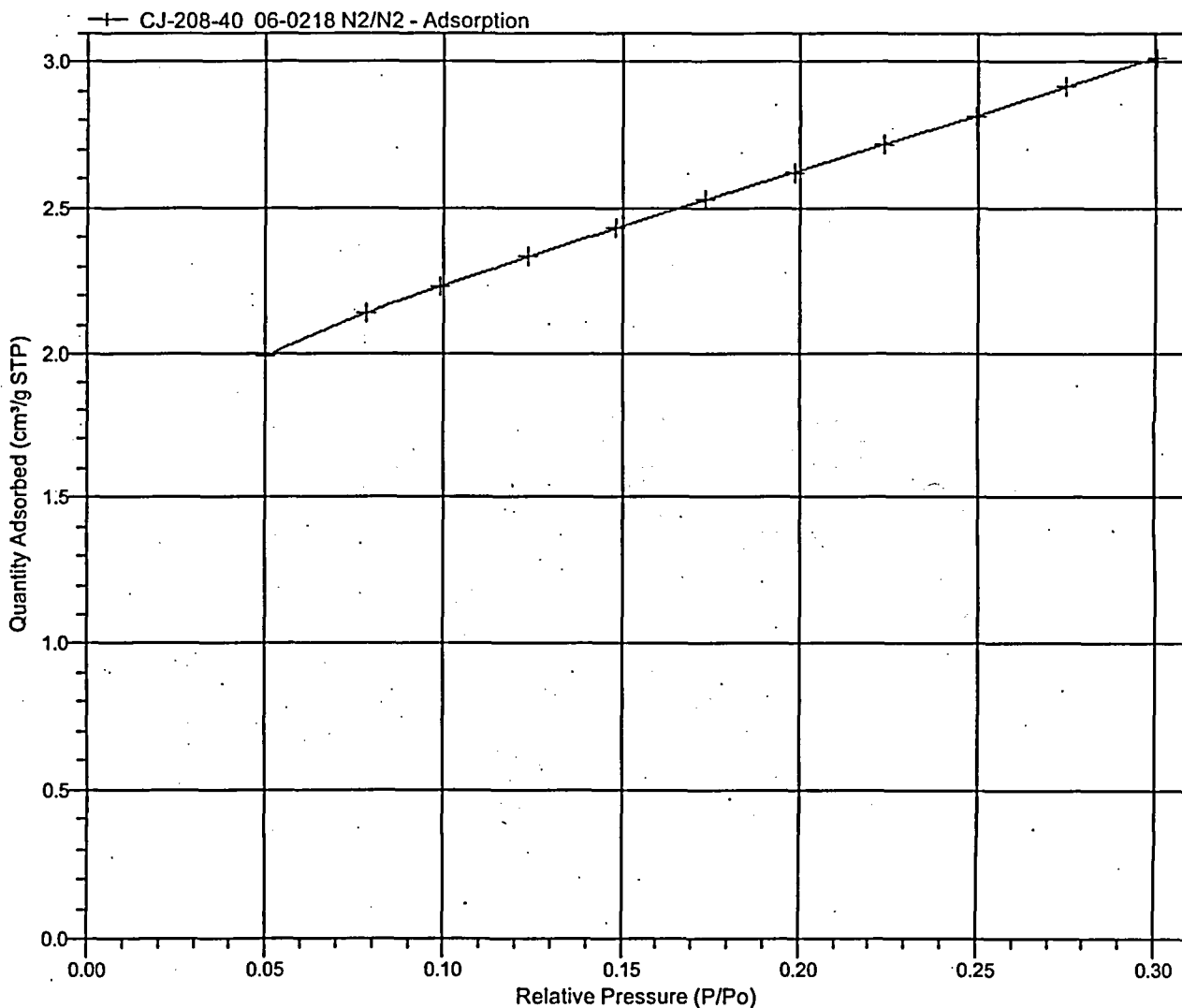
Sample Prep: Stage  
 1

Soak Temperature (°C)  
 100

Ramp Rate (°C/min)  
 10

Soak Time (min)  
 960

Isotherm Linear Plot



TriStar 3000 V6.05.01 A

Unit 1 Port 3

Serial #: 1098

Page 3

Sample: CJ-208-40 06-0218 N2/N2  
 Operator: MJP  
 Submitter: S.M.Stoller  
 File: C:\...01JAN06-0218.SMP

Started: 2/1/2006 4:22:41PM  
 Completed: 2/1/2006 8:12:53PM  
 Report Time: 2/1/2006 8:12:55PM  
 Warm Free Space: 5.7202 cm<sup>3</sup> Measured  
 Equilibration Interval: 10 s  
 Sample Density: 1.000 g/cm<sup>3</sup>

Analysis Adsorptive: N2  
 Analysis Bath Temp.: 77.300 K  
 Sample Mass: 4.3662 g  
 Cold Free Space: 16.4086 cm<sup>3</sup> Measured  
 Low Pressure Dose: None  
 Automatic Degas: Yes

Sample Prep: Stage	Soak Temperature (°C)	Ramp Rate (°C/min)	Soak Time (min)
1	100	10	960

**BET Surface Area Report**

BET Surface Area: 9.3897 ± 0.0250 m<sup>2</sup>/g  
 Slope: 0.460156 ± 0.001212 g/cm<sup>3</sup> STP  
 Y-Intercept: 0.003458 ± 0.000232 g/cm<sup>3</sup> STP  
 C: 134.056409  
 Qm: 2.1570 cm<sup>3</sup>/g STP  
 Correlation Coefficient: 0.9999688  
 Molecular Cross-Sectional Area: 0.1620 nm<sup>2</sup>

Relative Pressure (P/Po)	Quantity Adsorbed (cm <sup>3</sup> /g STP)	1/[Q(Po/P - 1)]
0.050132413	1.9911	0.026507
0.078159955	2.1391	0.039637
0.098735843	2.2310	0.049105
0.123546271	2.3313	0.060466
0.148265749	2.4301	0.071634
0.173383114	2.5273	0.082995
0.198727824	2.6228	0.094562
0.224004352	2.7188	0.106174
0.249400225	2.8166	0.117966
0.274898405	2.9161	0.130006
0.300589849	3.0177	0.142417

TriStar 3000 V6.05.01 A

Unit 1 Port 3

Serial #: 1098

Page 4

Sample: CJ-208-40 06-0218 N2/N2  
 Operator: MJP  
 Submitter: S.M.Stoller  
 File: C:\...01JAN06-0218.SMP

Started: 2/1/2006 4:22:41PM  
 Completed: 2/1/2006 8:12:53PM  
 Report Time: 2/1/2006 8:12:55PM  
 Warm Free Space: 5.7202 cm<sup>3</sup> Measured  
 Equilibration Interval: 10 s  
 Sample Density: 1.000 g/cm<sup>3</sup>

Analysis Adsorptive: N2  
 Analysis Bath Temp.: 77.300 K  
 Sample Mass: 4.3662 g  
 Cold Free Space: 16.4086 cm<sup>3</sup> Measured  
 Low Pressure Dose: None  
 Automatic Degas: Yes

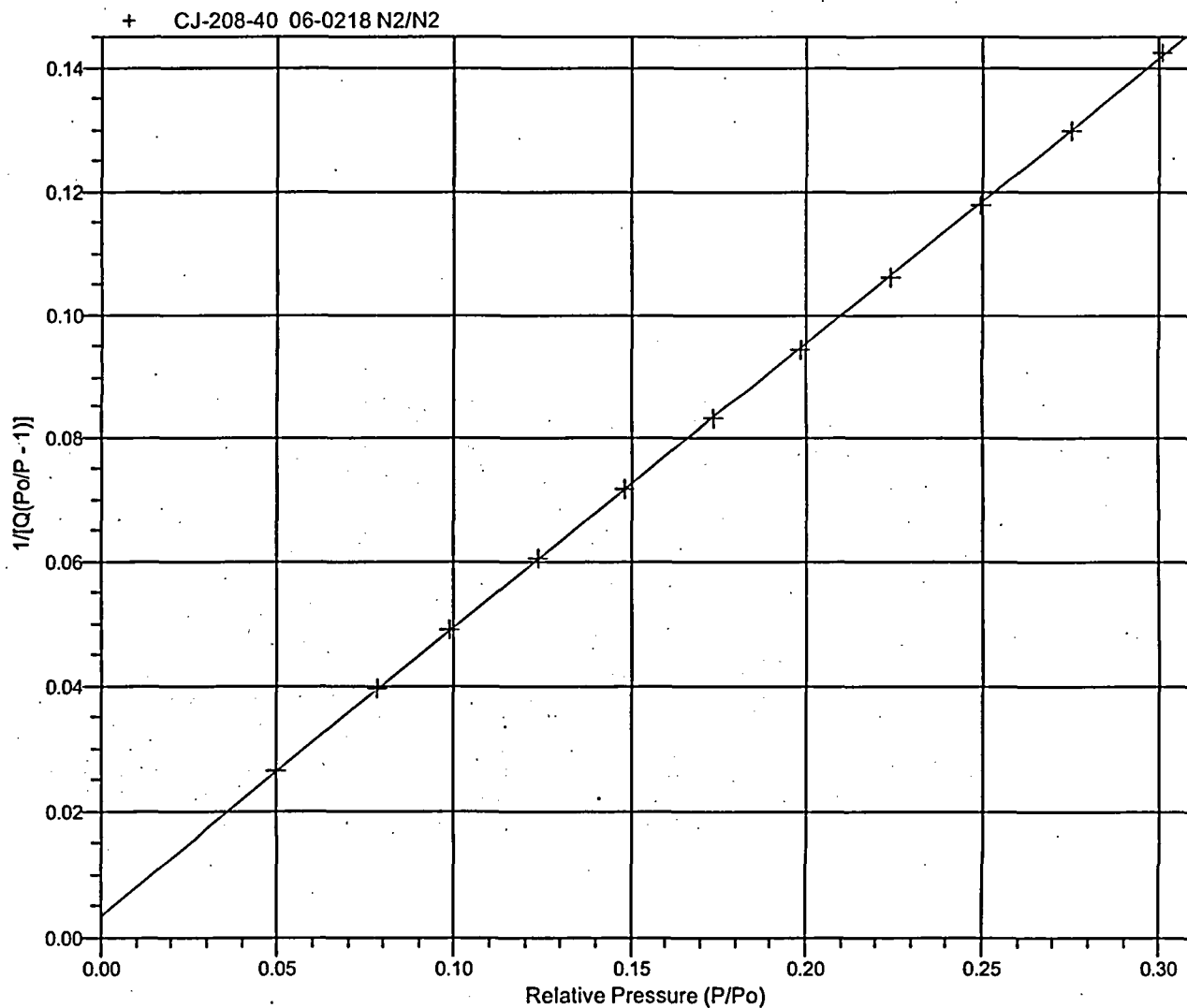
Sample Prep: Stage  
 1

Soak Temperature (°C)  
 100

Ramp Rate (°C/min)  
 10

Soak Time (min)  
 960

**BET Surface Area Plot**





TriStar 3000 V6.05.01 A

Unit 1 Port 3

Serial #: 1098

Page 5

Sample: CJ-208-40 06-0218 N2/N2  
Operator: MJP  
Submitter: S.M.Stoller  
File: C:\...01JAN06-0218.SMP

Started: 2/1/2006 4:22:41PM  
Completed: 2/1/2006 8:12:53PM  
Report Time: 2/1/2006 8:12:55PM  
Warm Free Space: 5.7202 cm<sup>3</sup> Measured  
Equilibration Interval: 10 s  
Sample Density: 1.000 g/cm<sup>3</sup>

Analysis Adsorptive: N2  
Analysis Bath Temp.: 77.300 K  
Sample Mass: 4.3662 g  
Cold Free Space: 16.4086 cm<sup>3</sup> Measured  
Low Pressure Dose: None  
Automatic Degas: Yes

Sample Prep: Stage  
1

Soak Temperature (°C)  
100

Ramp Rate (°C/min)  
10

Soak Time (min)  
960

#### Summary Report

##### Surface Area

Single point surface area at P/Po = 0.300589849: 9.1880 m<sup>2</sup>/g

BET Surface Area: 9.3897 m<sup>2</sup>/g

TriStar 3000 V6.05.01 A

Unit 2 Port 1

Serial #: 1449

Page 1

Sample: CJ-209-40 06-0219 N5/N5  
 Operator: MJP  
 Submitter: S.M.Stoller  
 File: C:\...01JAN06-0219.SMP

Started: 2/1/2006 4:23:29PM  
 Completed: 2/1/2006 7:40:08PM  
 Report Time: 2/1/2006 7:40:06PM  
 Warm Free Space: 5.4357 cm<sup>3</sup> Measured  
 Equilibration Interval: 10 s  
 Sample Density: 1.000 g/cm<sup>3</sup>

Analysis Adsorptive: N2  
 Analysis Bath Temp.: 77.300 K  
 Sample Mass: 5.1155 g  
 Cold Free Space: 15.2828 cm<sup>3</sup> Measured  
 Low Pressure Dose: None  
 Automatic Degas: Yes

Sample Prep: Stage	Soak Temperature (°C)	Ramp Rate (°C/min)	Soak Time (min)
1	100	10	960

**Isotherm Tabular Report**

Relative Pressure (P/Po)	Absolute Pressure (mmHg)	Quantity Adsorbed (cm <sup>3</sup> /g STP)	Elapsed Time (h:min)	Saturation Pressure (mmHg)
0.051788686	38.12119	2.1947	01:10	736.09106
0.076204501	56.09345	2.3405	01:36	
0.098370893	72.40993	2.4519	01:47	
0.122832732	90.41608	2.5662	01:55	
0.147622492	108.66360	2.6782	02:03	
0.172751686	127.16097	2.7882	02:09	
0.197898138	145.67105	2.8976	02:15	
0.223314975	164.38016	2.9762	02:21	
0.248559218	182.96222	3.0077	02:27	
0.274240708	201.86613	3.1200	02:32	
0.300100534	220.90132	3.2344	02:37	
		3.3510	02:42	

TriStar 3000 V6.05.01 A

Unit 2 Port 1

Serial #: 1449

Page 2

Sample: CJ-209-40 06-0219 N5/N5  
 Operator: MJP  
 Submitter: S.M.Stoller  
 File: C:\...01JAN06-0219.SMP

Started: 2/1/2006 4:23:29PM  
 Completed: 2/1/2006 7:40:08PM  
 Report Time: 2/1/2006 7:40:06PM  
 Warm Free Space: 5.4357 cm<sup>3</sup> Measured  
 Equilibration Interval: 10 s  
 Sample Density: 1.000 g/cm<sup>3</sup>

Analysis Adsorptive: N2  
 Analysis Bath Temp.: 77.300 K  
 Sample Mass: 5.1155 g  
 Cold Free Space: 15.2828 cm<sup>3</sup> Measured  
 Low Pressure Dose: None  
 Automatic Degas: Yes

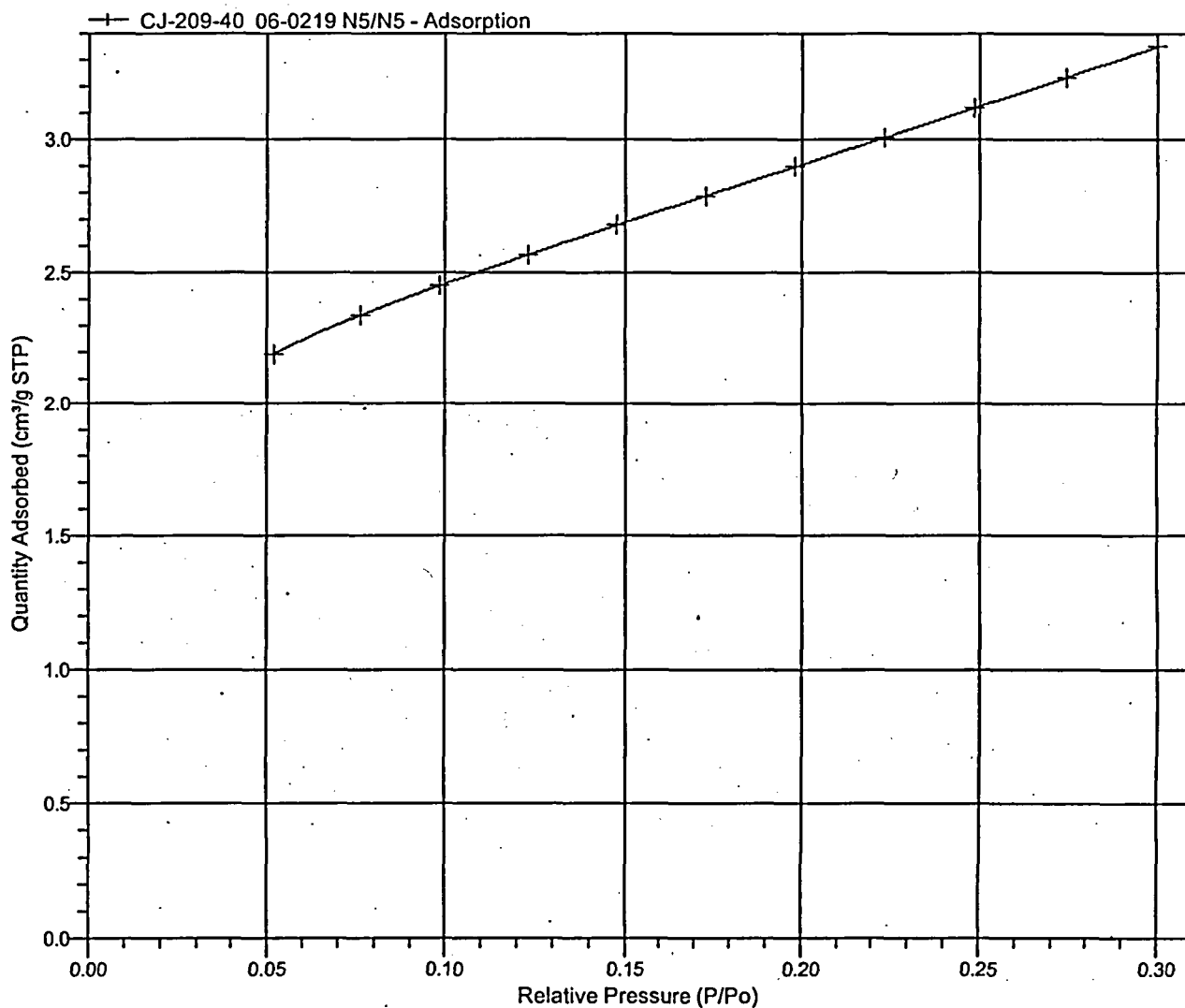
Sample Prep: Stage  
 1

Soak Temperature (°C)  
 100

Ramp Rate (°C/min)  
 10

Soak Time (min)  
 960

Isotherm Linear Plot



TriStar 3000 V6.05.01 A

Unit 2 Port 1

Serial #: 1449

Page 3

Sample: CJ-209-40 06-0219 N5/N5  
 Operator: MJP  
 Submitter: S.M.Stoller  
 File: C:\...\01JAN06-0219.SMP

Started: 2/1/2006 4:23:29PM  
 Completed: 2/1/2006 7:40:08PM  
 Report Time: 2/1/2006 7:40:06PM  
 Warm Free Space: 5.4357 cm<sup>3</sup> Measured  
 Equilibration Interval: 10 s  
 Sample Density: 1.000 g/cm<sup>3</sup>

Analysis Adsorptive: N2  
 Analysis Bath Temp.: 77.300 K  
 Sample Mass: 5.1155 g  
 Cold Free Space: 15.2828 cm<sup>3</sup> Measured  
 Low Pressure Dose: None  
 Automatic Degas: Yes

Sample Prep: Stage  
 1

Soak Temperature (°C)  
 100

Ramp Rate (°C/min)  
 10

Soak Time (min)  
 960

**BET Surface Area Report**

BET Surface Area: 10.4560 ± 0.0226 m<sup>2</sup>/g  
 Slope: 0.412643 ± 0.000883 g/cm<sup>3</sup> STP  
 Y-Intercept: 0.003694 ± 0.000169 g/cm<sup>3</sup> STP  
 C: 112.707884  
 Qm: 2.4019 cm<sup>3</sup>/g STP  
 Correlation Coefficient: 0.9999794  
 Molecular Cross-Sectional Area: 0.1620 nm<sup>2</sup>

Relative Pressure (P/Po)	Quantity Adsorbed (cm <sup>3</sup> /g STP)	1/[Q(Po/P - 1)]
0.051788686	2.1947	0.024886
0.076204501	2.3405	0.035244
0.098370893	2.4519	0.044498
0.122832732	2.5662	0.054568
0.147622492	2.6782	0.064665
0.172751686	2.7882	0.074897
0.197898138	2.8976	0.085148
0.223314975	3.0077	0.095596
0.248559218	3.1200	0.106018
0.274240708	3.2344	0.116828
0.300100534	3.3510	0.127954

TriStar 3000 V6.05.01 A

Unit 2 Port 1

Serial #: 1449

Page 4

Sample: CJ-209-40 06-0219 N5/N5  
 Operator: MJP  
 Submitter: S.M.Stoller  
 File: C:\...01JAN06-0219.SMP

Started: 2/1/2006 4:23:29PM  
 Completed: 2/1/2006 7:40:08PM  
 Report Time: 2/1/2006 7:40:06PM  
 Warm Free Space: 5.4357 cm<sup>3</sup> Measured  
 Equilibration Interval: 10 s  
 Sample Density: 1.000 g/cm<sup>3</sup>

Analysis Adsorptive: N2  
 Analysis Bath Temp.: 77.300 K  
 Sample Mass: 5.1155 g  
 Cold Free Space: 15.2828 cm<sup>3</sup> Measured  
 Low Pressure Dose: None  
 Automatic Degas: Yes

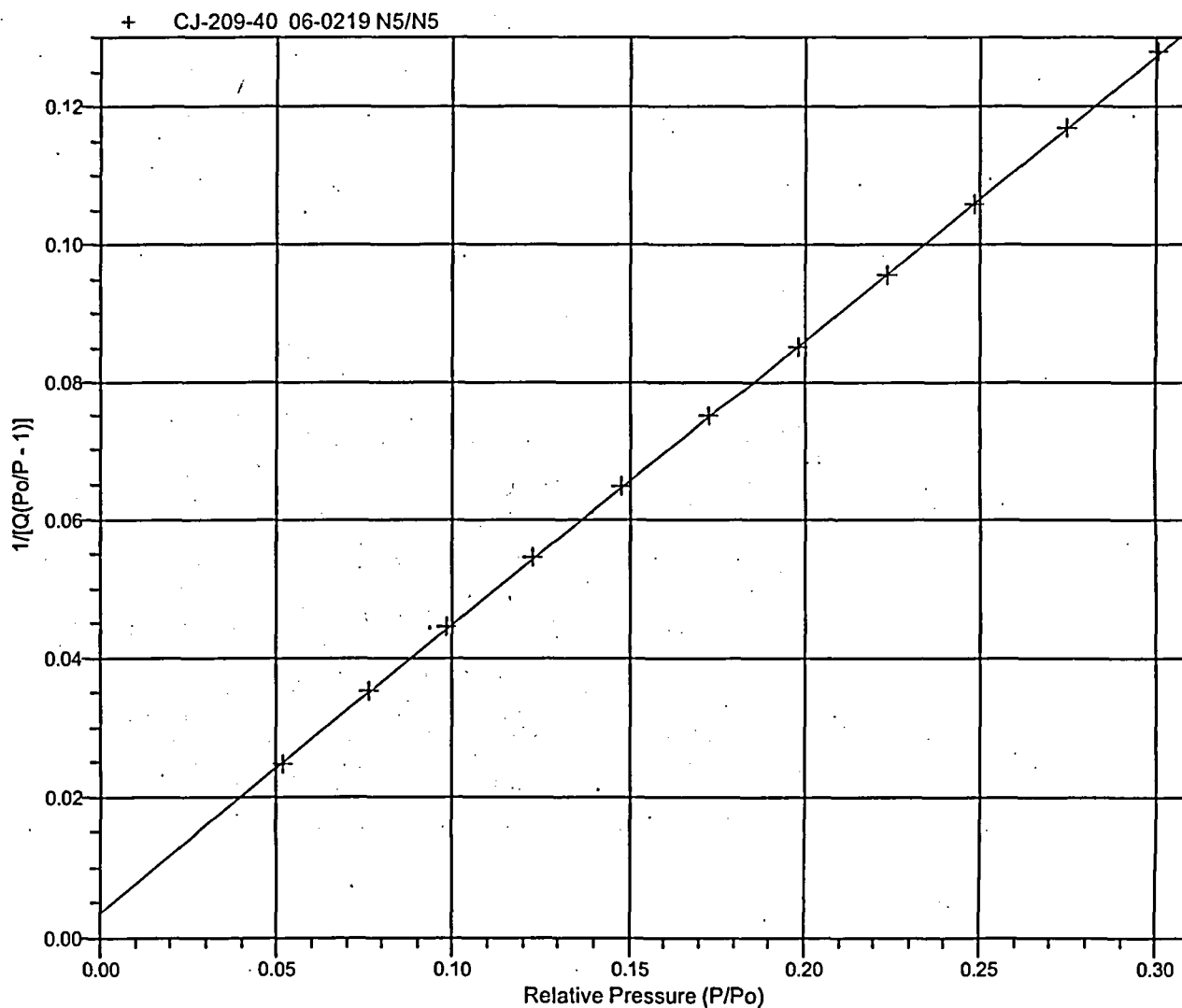
Sample Prep: Stage  
 1

Soak Temperature (°C)  
 100

Ramp Rate (°C/min)  
 10

Soak Time (min)  
 960

**BET Surface Area Plot**



TriStar 3000 V6.05.01 A

Unit 2 Port 1

Serial #: 1449

Page 5

Sample: CJ-209-40 06-0219 N5/N5  
Operator: MJP  
Submitter: S.M.Stoller  
File: C:\...101JAN06-0219.SMP

Started: 2/1/2006 4:23:29PM  
Completed: 2/1/2006 7:40:08PM  
Report Time: 2/1/2006 7:40:06PM  
Warm Free Space: 5.4357 cm<sup>3</sup> Measured  
Equilibration Interval: 10 s  
Sample Density: 1.000 g/cm<sup>3</sup>

Analysis Adsorptive: N2  
Analysis Bath Temp.: 77.300 K  
Sample Mass: 5.1155 g  
Cold Free Space: 15.2828 cm<sup>3</sup> Measured  
Low Pressure Dose: None  
Automatic Degas: Yes

Sample Prep: Stage  
1

Soak Temperature (°C)  
100

Ramp Rate (°C/min)  
10

Soak Time (min)  
960

#### Summary Report

##### Surface Area

Single point surface area at P/Po = 0.300100534: 10.2099 m<sup>2</sup>/g

BET Surface Area: 10.4560 m<sup>2</sup>/g

TriStar 3000 V6.05.01 A

Unit 2 Port 2

Serial #: 1449

Page 1

Sample: CJ-210-40 06-0220 N6/N6  
 Operator: MJP  
 Submitter: S.M.Stoller  
 File: C:\...101JAN06-0220.SMP

Started: 2/1/2006 4:23:29PM  
 Completed: 2/1/2006 7:40:08PM  
 Report Time: 2/2/2006 7:51:21AM  
 Warm Free Space: 5.6495 cm<sup>3</sup> Measured  
 Equilibration Interval: 10 s  
 Sample Density: 1.000 g/cm<sup>3</sup>

Analysis Adsorptive: N2  
 Analysis Bath Temp.: 77.300 K  
 Sample Mass: 5.1428 g  
 Cold Free Space: 16.1759 cm<sup>3</sup> Measured  
 Low Pressure Dose: None  
 Automatic Degas: Yes

Sample Prep: Stage 1      Soak Temperature (°C) 100      Ramp Rate (°C/min) 10      Soak Time (min) 960

**Isotherm Tabular Report**

Relative Pressure (P/Po)	Absolute Pressure (mmHg)	Quantity Adsorbed (cm <sup>3</sup> /g STP)	Elapsed Time (h:min)	Saturation Pressure (mmHg)
0.049305304	36.29458	2.8912	01:10	736.09106
0.073760837	54.29753	3.0722	01:51	
0.103302563	76.04499	3.2499	02:06	
0.123540210	90.94355	3.3609	02:19	
0.148244880	109.13059	3.4916	02:29	
0.173779264	127.92847	3.6198	02:37	
0.199364321	146.76399	3.7447	02:43	
0.224954724	165.60370	3.8690	02:50	
0.250692811	184.55220	3.9948	02:57	
0.276623808	203.64293	4.1218	03:03	
			03:09	736.17419
			03:11	
0.302748904	222.87593	4.2511	03:15	

TriStar 3000 V6.05.01 A

Unit 2 Port 2

Serial #: 1449

Page 2

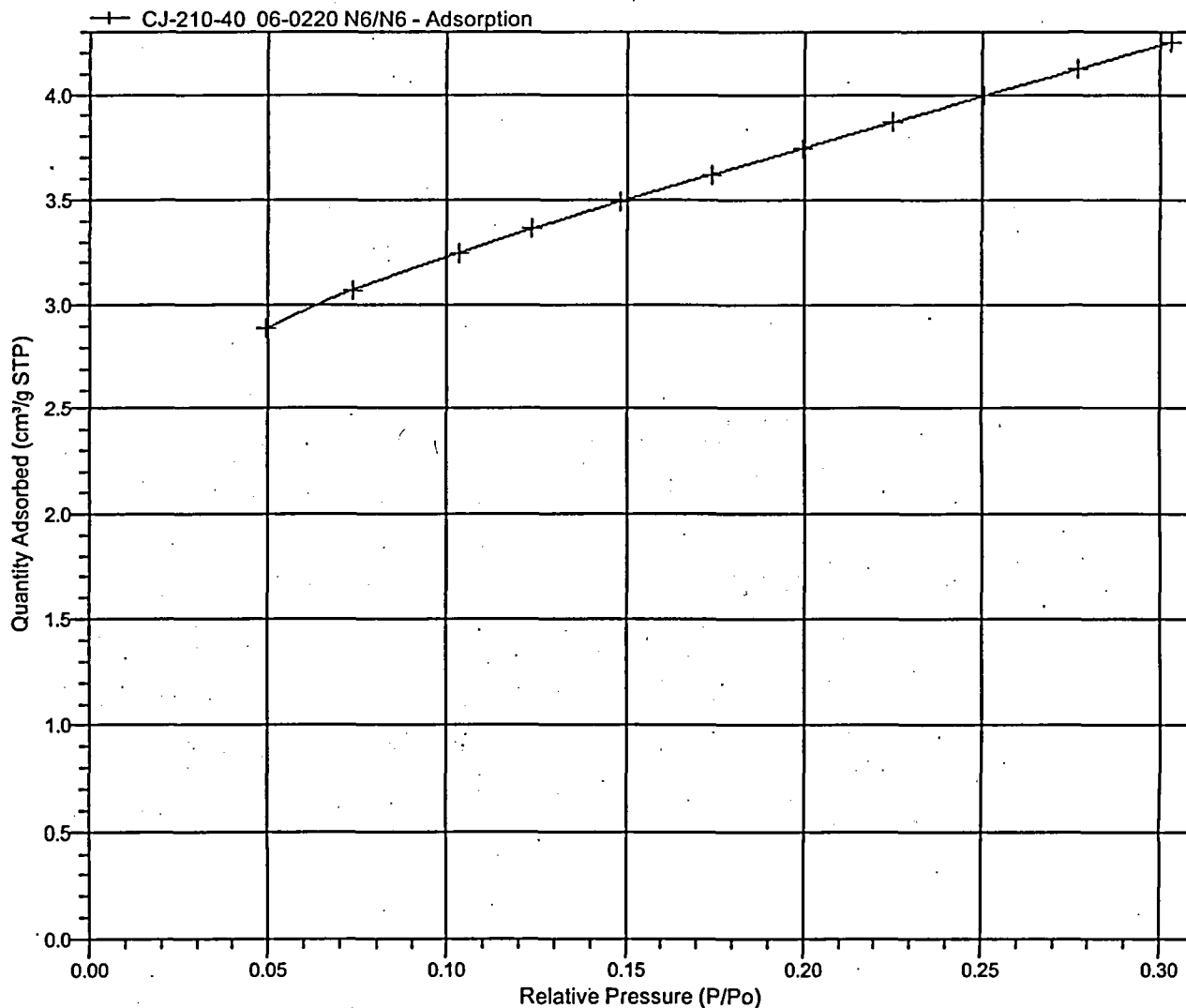
Sample: CJ-210-40 06-0220 N6/N6  
 Operator: MJP  
 Submitter: S.M.Stoller  
 File: C:\...101JAN06-0220.SMP

Started: 2/1/2006 4:23:29PM  
 Completed: 2/1/2006 7:40:08PM  
 Report Time: 2/2/2006 7:51:21AM  
 Warm Free Space: 5.6495 cm<sup>3</sup> Measured  
 Equilibration Interval: 10 s  
 Sample Density: 1.000 g/cm<sup>3</sup>

Analysis Adsorptive: N2  
 Analysis Bath Temp: 77.300 K  
 Sample Mass: 5.1428 g  
 Cold Free Space: 16.1759 cm<sup>3</sup> Measured  
 Low Pressure Dose: None  
 Automatic Degas: Yes

Sample Prep: Stage	Soak Temperature (°C)	Ramp Rate (°C/min)	Soak Time (min)
1	100	10	960

Isotherm Linear Plot





TriStar 3000 V6.05.01 A

Unit 2 Port 2

Serial #: 1449

Page 3

Sample: CJ-210-40 06-0220 N6/N6  
 Operator: MJP  
 Submitter: S.M.Stoller  
 File: C:\..101JAN06-0220.SMP

Started: 2/1/2006 4:23:29PM  
 Completed: 2/1/2006 7:40:08PM  
 Report Time: 2/2/2006 7:51:21AM  
 Warm Free Space: 5.6495 cm<sup>3</sup> Measured  
 Equilibration Interval: 10 s  
 Sample Density: 1.000 g/cm<sup>3</sup>

Analysis Adsorptive: N2  
 Analysis Bath Temp.: 77.300 K  
 Sample Mass: 5.1428 g  
 Cold Free Space: 16.1759 cm<sup>3</sup> Measured  
 Low Pressure Dose: None  
 Automatic Degas: Yes

Sample Prep: Stage	Soak Temperature (°C)	Ramp Rate (°C/min)	Soak Time (min)
1	100	10	960

**BET Surface Area Report**

BET Surface Area: 13.2247 ± 0.0591 m<sup>2</sup>/g  
 Slope: 0.327644 ± 0.001449 g/cm<sup>3</sup> STP  
 Y-Intercept: 0.001529 ± 0.000258 g/cm<sup>3</sup> STP  
 C: 215.310851  
 Qm: 3.0379 cm<sup>3</sup>/g STP  
 Correlation Coefficient: 0.9999217  
 Molecular Cross-Sectional Area: 0.1620 nm<sup>2</sup>

Relative Pressure (P/Po)	Quantity Adsorbed (cm <sup>3</sup> /g STP)	1/[Q(Po/P - 1)]
0.049305304	2.8912	0.017938
0.073760837	3.0722	0.025921
0.103302563	3.2499	0.035448
0.123540210	3.3609	0.041939
0.148244880	3.4916	0.049847
0.173779264	3.6198	0.058106
0.199364321	3.7447	0.066495
0.224954724	3.8690	0.075018
0.250692811	3.9948	0.083751
0.276623808	4.1218	0.092777

TriStar 3000 V6.05.01 A

Unit 2 Port 2

Serial #: 1449

Page 4

Sample: CJ-210-40 06-0220 N6/N6  
 Operator: MJP  
 Submitter: S.M.Stoller  
 File: C:\...101JAN06-0220.SMP

Started: 2/1/2006 4:23:29PM  
 Completed: 2/1/2006 7:40:08PM  
 Report Time: 2/2/2006 7:51:21AM  
 Warm Free Space: 5.6495 cm<sup>3</sup> Measured  
 Equilibration Interval: 10 s  
 Sample Density: 1.000 g/cm<sup>3</sup>

Analysis Adsorptive: N2  
 Analysis Bath Temp.: 77.300 K  
 Sample Mass: 5.1428 g  
 Cold Free Space: 16.1759 cm<sup>3</sup> Measured  
 Low Pressure Dose: None  
 Automatic Degas: Yes

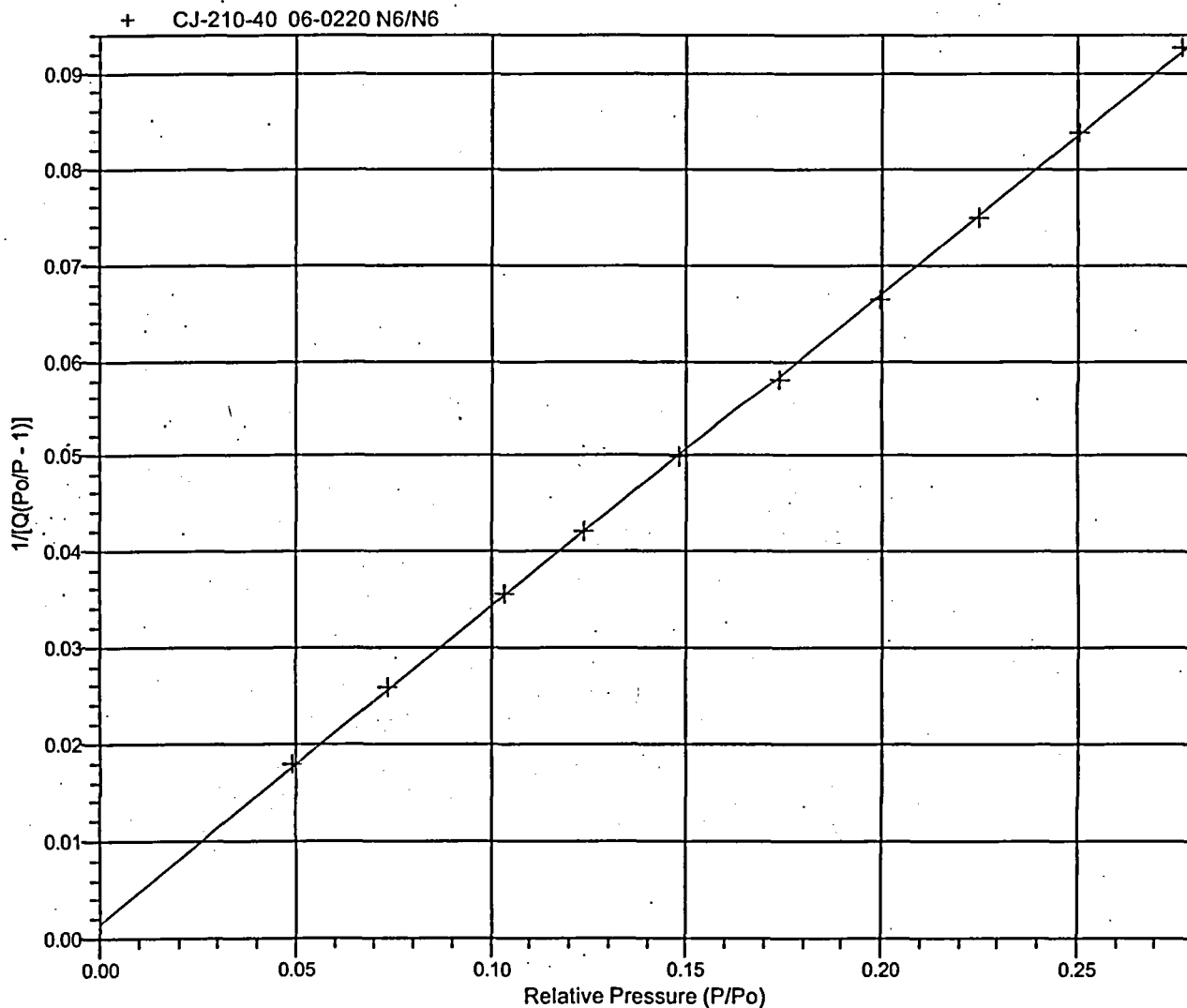
Sample Prep: Stage  
 1

Soak Temperature (°C)  
 100

Ramp Rate (°C/min)  
 10

Soak Time (min)  
 960

**BET Surface Area Plot**



TriStar 3000 V6.05.01 A

Unit 2 Port 2

Serial #: 1449

Page 5

Sample: CJ-210-40 06-0220 N6/N6  
Operator: MJP  
Submitter: S.M.Stoller  
File: C:\...01JAN06-0220.SMP

Started: 2/1/2006 4:23:29PM  
Completed: 2/1/2006 7:40:08PM  
Report Time: 2/2/2006 7:51:21AM  
Warm Free Space: 5.6495 cm<sup>3</sup> Measured  
Equilibration Interval: 10 s  
Sample Density: 1.000 g/cm<sup>3</sup>

Analysis Adsorptive: N2  
Analysis Bath Temp.: 77.300 K  
Sample Mass: 5.1428 g  
Cold Free Space: 16.1759 cm<sup>3</sup> Measured  
Low Pressure Dose: None  
Automatic Degas: Yes

Sample Prep: Stage  
1

Soak Temperature (°C)  
100

Ramp Rate (°C/min)  
10

Soak Time (min)  
960

#### Summary Report

##### Surface Area

Single point surface area at P/Po = 0.276623808: 12.9795 m<sup>2</sup>/g

BET Surface Area: 13.2247 m<sup>2</sup>/g

## **Appendix F**

### **PHREEQC Input Files for Sequential Batch Reaction Models**

#### List of Files

- (1) *Transport\_seq\_batch\_horizontal*
- (2) *Transport\_seq\_batch\_vertical*

# Transport\_seq\_batch\_horizontal

TITLE Crescent Junction Transport Model - Horizontal Transport in Sequential Batch Test

# Includes Mineral PPT, adsorption, and IX  
 # Transport of Tailings Water through Mancos Shale  
 # Database "Phreeqc\_Davis\_Naturita\_GC\_Short.txt"  
 # GC (Generalized Composite) Adsorption Model (to match Davis and Curtis Figure 5.6)  
 # React in 3 separate batch steps using "fresh" Mancos (from 40-ft depth) each step  
 # Use BH210 gw only to set the IX and adsorption sites  
 # Added U to BH210 to get the right amount adsorbed to show the measured U increase  
 SOLUTION 0 SPF-1 (Tailings Fluid). Using final control values from batch tests.

temp	25	
pH	7.85	
pe	7	
redox	pe	
units	mg/L	
Alkalinity	510.0	as CaCO3
Amm	2000	
Ca	196	
Na	5300	
Mg	310	
K	129	
S(6)	18272	as SO4
Cl	1018	

SOLUTION 1 Groundwater from C3 BH 210. Initial solution for exchange sites  
 # Groundwater chemistry from Borehole 210 (C3)  
 # sampled 11/7/05. This sample is considered representative of Mancos groundwater  
 # This composition sets the initial conditions for the exchange sites

units	mg/L	
temp	25.0	
pH	7.23	
pe	12.5	
Alkalinity	634	as CaCO3
Amm	0	
Ca	180	
Na	12000	
Mg	140	
K	58	
S(6)	1700	as SO4
Cl	23000	
U		0.2

END

## EXCHANGE 1

equilibrate with solution 1  
 # Used 400 mL fluid with 100g rock, ie. R/W = 250g/L  
 # Mean measured CEC=11.23 meq/L  
 # Exchange Sites = 250 g/L x 11.23 meq/100g x 1 eq/1000 meq = 0.028 eq/L  
 X 0.028

## SURFACE 1

# Site Density = (1.92 umoles hydroxyl sites)/m^2 (assumed bidentate bonds)  
 # from Davis and Kent (1990) and  
 # used in Davis and Curtis (2003) Naturita GC Model  
 # Surface area (Mean of 10 values from 1-2 mm fraction) = 11.02 m^2/g (BET Measurement)  
 # Used 250 g rock/L gw  
 # Of Total Sites: Very Strong Sites = 0.01 %, Strong Sites = 1.2 % (Davis and Curtis)  
 # Total Sites = 5290 umol sites/L gw (from 250\*11.02\*1.92)  
 # Very Strong Sites = 0.0001\*5290 = 0.53 umoles/L (5.3e-7 mol/L)  
 # Strong Sites = 0.012 \* 5290 = 63.5 umoles/L (6.35e-5 mol/L)  
 # Weak Sites = 0.9879 \* 5290 = 5226 umoles/L (5.226e-3 mol/L)

-equilibrate with solution 1			
Hfo_WOH	5.226e-3	11.02	250.0

	Transport_seq_batch_horizontal		
Hfo_SOH	6.35e-5	11.02	250.0
Hfo_VOH	5.3e-7	11.02	250.0
-no_edl			

End

```

Use Solution 0
Use Exchange 1
Use Surface 1
Equilibrium_Phases 1
# The total no. of moles is based on water soluble and XRD tests of Mancos Shale
# For verticle transport through deeper Mancos (in mol/Lgw):Gypsum 6.67e-4,
Nahcolite 0.017
# For horizontal transport through shallower Mancos (in mol/Lgw):Gypsum 0.017,
Nahcolite 6.67e-3
# Calcite 1 wgt % = 0.025 mol/Lgw for all depths. Calcite was not completely
dissolved in tests.
# Halite 6.67e-4 mol/Lgw for all depths
  Calcite 0.0      0.025
  Gypsum  0.0      0.017
  Nahcolite 0.0      6.67e-3
  Halite  0.0      6.67e-4

```

PRINT

```

  -reset      true
SELECTED_OUTPUT
  -file      transport_seq_batch_horizontal.sel
  -totals    Na Amm K Ca Cl U S(6)
  -molalities NaX AmmHX KX CaX2

```

Save Solution 0

END

```

Use Solution 0
Use Exchange 1
Use Surface 1
Equilibrium_Phases 1
# The total no. of moles is based on water soluble and XRD tests of Mancos Shale
# For verticle transport through deeper Mancos (in mol/Lgw):Gypsum 6.67e-4,
Nahcolite 0.017
# For horizontal transport through shallower Mancos (in mol/Lgw):Gypsum 0.017,
Nahcolite 6.67e-3
# Calcite 1 wgt % = 0.025 mol/Lgw for all depths. Calcite was not completely
dissolved in tests.
# Halite 6.67e-4 mol/Lgw for all depths
  Calcite 0.0      0.025
  Gypsum  0.0      0.017
  Nahcolite 0.0      6.67e-3
  Halite  0.0      6.67e-4

```

PRINT

```

  -reset      true
SELECTED_OUTPUT
  -file      transport_seq_batch_horizontal.sel
  -totals    Na Amm K Ca Cl U S(6)
  -molalities NaX AmmHX KX CaX2

```

Save Solution 0

END

```

Use Solution 0
Use Exchange 1
Use Surface 1
Equilibrium_Phases 1
# The total no. of moles is based on water soluble and XRD tests of Mancos Shale
# For verticle transport through deeper Mancos (in mol/Lgw):Gypsum 6.67e-4,
Nahcolite 0.017
# For horizontal transport through shallower Mancos (in mol/Lgw):Gypsum 0.017,

```

Transport\_seq\_batch\_horizontal

Nahcolite 6.67e-3

# Calcite 1 wgt % = 0.025 mol/Lgw for all depths. Calcite was not completely dissolved in tests.

# Halite 6.67e-4 mol/Lgw for all depths

Calcite	0.0	0.025	
Gypsum	0.0	0.017	
Nahcolite	0.0	6.67e-3	
Halite	0.0	6.67e-4	

PRINT

-reset

true

SELECTED\_OUTPUT

-file

transport\_seq\_batch\_horizontal.sel

-totals

Na Amm K Ca Cl U S(6)

-molalities

NaX AmmHX KX CaX2

END

# Transport\_seq\_batch\_verticle

TITLE Crescent Junction Transport Model - Verticle Transport in Sequential Batch Test

# Includes Mineral PPT, adsorption, and IX  
 # Transport of Tailings Water through Mancos Shale  
 # Database "Phreeqc\_Davis\_Naturita\_GC\_Short.txt"  
 # GC (Generalized Composite) Adsorption Model (to match Davis and Curtis Figure 5.6)  
 # React in 5 separate batch steps using "fresh" Mancos (from 40-ft depth) at first step  
 # then, "fresh" Mancos from deeper (lower gypsum) for remaining steps  
 # Use BH210 gw only to set the IX and adsorption sites  
 # Added U to BH210 to get the right amount adsorbed to show the measured U increase  
 SOLUTION 0 SPF-1 (Tailings Fluid). Using final control values from batch tests.

temp	25	
pH	6.63	
pe	7	
redox	pe	
units	mg/L	
Alkalinity	510.0	as CaCO3
Amm	2000	
Ca	196	
Na	5300	
Mg	310	
K	129	
S(6)	18272	as SO4
Cl	1018	

SOLUTION 1 Groundwater from CJ BH 210. Initial solution for exchange sites  
 # Groundwater chemistry from Borehole 210 (CJ)  
 # sampled 11/7/05. This sample is considered representative of Mancos groundwater  
 # This composition sets the initial conditions for the exchange sites

units	mg/L
temp	25.0
pH	7.23
pe	12.5
Alkalinity	634 as CaCO3
Amm	0
Ca	180
Na	12000
Mg	140
K	58
S(6)	1700 as SO4
Cl	23000
U	0.2

END

## EXCHANGE 1

equilibrate with solution 1

# Used 400 mL fluid with 100g rock, ie. R/W = 250g/L  
 # Mean measured CEC=11.23 meq/L  
 # Exchange Sites = 250 g/L x 11.23 meq/100g x 1 eq/1000 meq = 0.028 eq/L  
 X 0.028

## SURFACE 1

# Site Density = (1.92 umoles hydroxyl sites)/m^2 (assumed bidentate bonds)  
 # from Davis and Kent (1990) and  
 # used in Davis and Curtis (2003) Naturita GC Model  
 # Surface area (Mean of 10 values from 1-2 mm fraction) = 11.02 m^2/g (BET Measurement)  
 # Used 250 g rock/L gw  
 # Of Total Sites: Very Strong Sites = 0.01 %, Strong Sites = 1.2 % (Davis and Curtis)  
 # Total Sites = 5290 umol sites/L gw (from 250\*11.02\*1.92)  
 # Very Strong Sites = 0.0001\*5290 = 0.53 umoles/L (5.3e-7 mol/L)  
 # Strong Sites = 0.012 \* 5290 = 63.5 umoles/L (6.35e-5 mol/L)  
 # Weak Sites = 0.9879 \* 5290 = 5226 umoles/L (5.226e-3 mol/L)



	Transport_seq_batch_verticle		
-equilibrate with solution 1			
Hfo_WOH	5.226e-3	11.02	250.0
Hfo_SOH	6.35e-5	11.02	250.0
Hfo_VOH	5.3e-7	11.02	250.0
-no_edl			

End

# Reaction with 40-ft depth sample

Use Solution 0

Use Exchange 1

Use Surface 1

#PHASES

# Fix\_H+

# H+ = H+

# log\_k 0.0

Equilibrium\_Phases 1

# The total no. of moles is based on water soluble and XRD tests of Mancos Shale

# For verticle transport through deeper Mancos (in mol/Lgw):Gypsum 6.67e-4,

Nahcolite 0.017

# For horizontal transport through shallower Mancos (in mol/Lgw):Gypsum 0.017,

Nahcolite 6.67e-3

# Calcite 1 wgt % = 0.025 mol/Lgw for all depths. Calcite was not completely dissolved in tests.

# Halite 6.67e-4 mol/Lgw for all depths

Calcite	0.0	0.025
---------	-----	-------

Gypsum	0.0	0.01
--------	-----	------

Nahcolite	0.0	6.67e-3
-----------	-----	---------

Halite	0.0	6.67e-4
--------	-----	---------

# CO2(g)	-2.1	1.0
----------	------	-----

# Fix_H+	-7.73	CO2(g)	10.0
----------	-------	--------	------

PRINT

-reset	true
--------	------

Save Solution 0

END

# Reaction with 105-ft depth sample

Use Solution 0

Use Exchange 1

Use Surface 1

Equilibrium\_Phases 1

# The total no. of moles is based on water soluble and XRD tests of Mancos Shale

# For verticle transport through deeper Mancos (in mol/Lgw):Gypsum 6.67e-4,

Nahcolite 0.017

# For horizontal transport through shallower Mancos (in mol/Lgw):Gypsum 0.017,

Nahcolite 6.67e-3

# Calcite 1 wgt % = 0.025 mol/Lgw for all depths. Calcite was not completely dissolved in tests.

# Halite 6.67e-4 mol/Lgw for all depths

Calcite	0.0	0.025
---------	-----	-------

Gypsum	0.0	6.67e-4
--------	-----	---------

Nahcolite	0.0	0.017
-----------	-----	-------

Halite	0.0	6.67e-4
--------	-----	---------

PRINT

-reset	true
--------	------

Save Solution 0

END

# Reaction with 170-ft sample

Use Solution 0

Use Exchange 1

Use Surface 1

Equilibrium\_Phases 1

# The total no. of moles is based on water soluble and XRD tests of Mancos Shale

# Transport\_seq\_batch\_verticle

```
# For verticle transport through deeper Mancos (in mol/Lgw):Gypsum 6.67e-4,
Nahcolite 0.017
# For horizontal transport through shallower Mancos (in mol/Lgw):Gypsum 0.017,
Nahcolite 6.67e-3
# Calcite 1 wgt % = 0.025 mol/Lgw for all depths. Calcite was not completely
dissolved in tests.
# Halite 6.67e-4 mol/Lgw for all depths
      Calcite      0.0      0.025
      Gypsum       0.0      6.67e-4
      Nahcolite    0.0      0.017
      Halite       0.0      6.67e-4
```

```
PRINT
      -reset      true
Save Solution 0
END
```

## # Reaction with 235-ft sample

```
Use Solution 0
Use Exchange 1
Use Surface 1
Equilibrium_Phases 1
# The total no. of moles is based on water soluble and XRD tests of Mancos shale
# For verticle transport through deeper Mancos (in mol/Lgw):Gypsum 6.67e-4,
Nahcolite 0.017
# For horizontal transport through shallower Mancos (in mol/Lgw):Gypsum 0.017,
Nahcolite 6.67e-3
# Calcite 1 wgt % = 0.025 mol/Lgw for all depths. Calcite was not completely
dissolved in tests.
# Halite 6.67e-4 mol/Lgw for all depths
      Calcite      0.0      0.025
      Gypsum       0.0      6.67e-4
      Nahcolite    0.0      0.017
      Halite       0.0      6.67e-4
```

```
PRINT
      -reset      true
Save Solution 0
END
```

## # Reaction with 300-ft sample

```
Use Solution 0
Use Exchange 1
Use Surface 1
Equilibrium_Phases 1
# The total no. of moles is based on water soluble and XRD tests of Mancos shale
# For verticle transport through deeper Mancos (in mol/Lgw):Gypsum 6.67e-4,
Nahcolite 0.017
# For horizontal transport through shallower Mancos (in mol/Lgw):Gypsum 0.017,
Nahcolite 6.67e-3
# Calcite 1 wgt % = 0.025 mol/Lgw for all depths. Calcite was not completely
dissolved in tests.
# Halite 6.67e-4 mol/Lgw for all depths
      Calcite      0.0      0.025
      Gypsum       0.0      6.67e-4
      Nahcolite    0.0      0.017
      Halite       0.0      6.67e-4
```

```
PRINT
      -reset      true
Save Solution 0
END
```

## **Appendix G**

### **PHREEQC Input Files for Transport Models**

#### List of Files

- (1) *Transport\_horizontal*
- (2) *Transport\_vertical*

# Transport\_horizontal

TITLE Crescent Junction Transport Model - Horizontal Transport Through Mancos Shale  
 # Includes Mineral PPT, adsorption, and IX  
 # Transport of Tailings Water through Mancos Shale  
 # Database "Phreeqc\_Davis\_Naturita\_GC\_Short.txt"  
 # GC (Generalized Composite) Adsorption Model (to match Davis and Curtis Figure 5.6)  
 #  
 #

## SOLUTION 0 SPF-1 (Tailings Fluid)

temp 25  
 pH 6.63  
 pe 7  
 redox pe  
 units mg/L  
 Alkalinity 570.0 as CaCO3  
 Amm 2181.82  
 Ca 209.62  
 Na 5781.41  
 Mg 315.71  
 K 112.23  
 S(6) 17454.37 as SO4  
 Cl 910.26  
 U 4.0

## SOLUTION 1-40 Groundwater from CJ BH 210. Initial solution for column

# Groundwater chemistry from Borehole 210 (CJ)  
 # sampled 11/7/05. This sample is considered representative of Mancos groundwater

units mg/L  
 temp 25.0  
 pH 7.23  
 pe 12.5  
 Alkalinity 634 as CaCO3  
 Amm 0  
 Ca 180  
 Na 12000  
 Mg 140  
 K 58  
 S(6) 1700 as SO4  
 Cl 23000

# Uranium concentration was calibrated by seq batch test model to produce  
 # the amount of required adsorption.  $0.2 / 30 = 0.0067 \text{ mg/L}$   
 U 0.0067

END

# Equilibrate BH 210 Fluid with Calcite and Gypsum

USE solution 1

Equilibrium\_Phases

Calcite 0.0 10.0  
 Gypsum 0.0 10.0

Save solution 1

End

# Equilibrate soln 1 (BH 210) with exchange sites and Minerals

EXCHANGE 1-20

equilibrate with solution 1

# R/W = 7500 g/L

# Mean measured CEC=11.23 meq/100g

# Exchange Sites =  $7500 \text{ g/L} \times 11.23 \text{ meq/100g} \times 1 \text{ eq/1000 meq} = 0.842 \text{ eq/L}$   
 x 0.842

Equilibrium\_Phases 1-20

# The total no. of moles is based on water soluble and XRD tests of Mancos shale  
 # For vertical transport through deeper Mancos (in mol/Lgw):Gypsum 0.02, Nahcolite 0.5

# For horizontal transport through shallower Mancos (in mol/Lgw):Gypsum 0.5, Nahcolite 0.2

# Calcite 1 wgt % = 0.75 mol/Lgw for all depths. Calcite was not completely

# Transport\_horizontal

dissolved in tests.

# Halite 0.02 mol/Lgw for all depths

Calcite 0.0 0.75

Gypsum 0.0 0.5

Nahcolite 0.0 0.2

Halite 0.0 0.02

SURFACE 1-20

# Site Density = (1.92 umoles hydroxyl sites)/m<sup>2</sup> (assumed bidentate bonds)

# from Davis and Kent (1990) and

# used in Davis and Curtis (2003) Naturita GC Model

# Surface area (Mean of 10 values from 1-2 mm fraction) = 11.02 m<sup>2</sup>/g (BET Measurement)

# Used 7500 g rock/Lgw

# Of Total Sites: Very Strong Sites = 0.01 %, Strong Sites = 1.2 % (Davis and Curtis)

# Total Sites = 158,688 umol sites/L gw (from 7500\*11.02\*1.92)

# Very Strong Sites = 0.0001\*158688 = 15.87 umoles/L (SJM Calculation)

# Strong Sites = 0.012 \* 158688 = 1904 umoles/L (SJM Calculation)

# Weak Sites = 0.9879 \* 158688 = 156768 umoles/L (SJM Calculation)

-equilibrate 1

Hfo\_WOH 1.568e-1 11.02 7500.0

Hfo\_SOH 1.904e-3 11.02 7500.0

Hfo\_VOH 1.587e-5 11.02 7500.0

-no\_ed1

PRINT

-reset true

ADVECTION

-cells 20

-shifts 200

-punch 20

# -punch 10 20

-punch\_frequency 1

-print 20

-print\_frequency 50

USER\_GRAPH

-headings PV Na C NH4\*5 Ca\*10 Cl SO4 U\*1000 KD\*25000 pH\*1000

# -headings PV TOTADS CS TOT("U") KD

-chart\_title "Crescent Junction Horizontal Transport Model"

-axis\_titles "PORE VOLUME" "Effluent Concentration (mg/L)"

-axis\_scale x\_axis 0 10 1 0.1

-axis\_scale y\_axis 0 25000.0 1000.0

-initial\_solutions false

-plot\_concentration\_vs time

-start

5 TOTADS = MOL("Hfo\_WOUO2OH") + MOL("Hfo\_SOUO2CO3-") + MOL("Hfo\_VOUO2OH") +

MOL("Hfo\_VOUO2CO3-")

6 CS = TOTADS/7500

7 KD = (CS/TOT("U"))\*1000

10 GRAPH\_X (STEP\_NO + 0.5) / 20

20 GRAPH\_Y TOT("Na")\*23000, TOT("C")\*12000, TOT("Amm")\*18000\*5,

TOT("Ca")\*40000\*10, TOT("Cl")\*35900, TOT("S(6)")\*96000, TOT("U")\*238000\*1000, KD\*25000, 1000\*(-LA"H+")

# 20 GRAPH\_Y TOT("U")\*238000\*1000, KD\*25000

-end

PRINT

-user\_graph true

SELECTED\_OUTPUT

-file CJ\_transport.sel

-totals Na Amm K Ca Cl

-molalities NaX AmmHX KX CaX2

END

# Transport\_vertical

TITLE Crescent Junction Transport Model - Vertical Transport Through Mancos Shale  
 # Includes Mineral PPT, adsorption, and IX  
 # Transport of Tailings Water through Mancos Shale  
 # Database "Phreeqc\_Davis\_Naturita\_GC\_Short.txt"  
 # GC (Generalized Composite) Adsorption Model (to match Davis and Curtis Figure 5.6)  
 #  
 #

SOLUTION 0 SPF-1 (Tailings Fluid). From means in SOWP Table 9

temp	25	
pH	6.63	
pe	7	
redox	pe	
units	mg/L	
Alkalinity	570.0	as CaCO3
Amm	2181.82	
Ca	209.62	
Na	5781.41	
Mg	315.71	
K	112.23	
S(6)	17454.37	as SO4
Cl	910.26	
U	4.0	

SOLUTION 1-20 Groundwater from CJ BH 210. Initial solution for streamtube.

# Groundwater chemistry from Borehole 210 (CJ)

# sampled 11/7/05. This sample is considered representative of Mancos groundwater

units	mg/L
temp	25.0
pH	7.23
pe	12.5
Alkalinity	634 as CaCO3
Amm	0
Ca	180
Na	12000
Mg	140
K	58
S(6)	1700 as SO4
Cl	23000

# U value is 0.2 (used in model of Seq Batch) divided by 30 (W/R factor)  
 U 6.67e-3

END

# Equilibrate Tailings Fluid with Calcite

USE solution 0

PHASES

Fix_H+			
H+ = H+			
log_k	0.0		
Equilibrium_Phases			
Calcite	0.0	10.0	
Fix_H+	-6.63	NaOH	10.0

Save solution 0

End

# Equilibrate BH 210 Fluid with Calcite

USE solution 1

Equilibrium\_Phases

Calcite	0.0	10.0	
Fix_H+	-7.23	NaOH	10.0
Gypsum	0.0	10.0	

#

Save solution 1

End

# Equilibrate soln 1 (BH 210) with exchange sites and Minerals

EXCHANGE 1-20

equilibrate with solution 1

# Transport\_vertical

```

# R/W = 7500 g/L
# Mean measured CEC=11.23 meq/100g
# Exchange Sites = 7500 g/L x 11.23 meq/100g x 1 eq/1000 meq = 0.842 eq/L
#
# Equilibrium_Phases 1-20
# The total no. of moles is based on water soluble and XRD tests of Mancos Shale.
# For verticle transport through deeper Mancos (in mol/Lgw):Gypsum 0.02, Nahcolite
0.5
# For horizontal transport through shallower Mancos (in mol/Lgw):Gypsum 0.5,
Nahcolite 0.2
# Calcite 1 wgt % = 0.75 mol/Lgw for all depths. Calcite was not completely
dissolved in tests.
# Halite 0.02 mol/Lgw for all depths
#
# Calcite 0.0 0.75
# Gypsum 0.0 0.02
# Nahcolite 0.0 0.5
# Halite 0.0 0.02
SURFACE 1-20
# Site Density = (1.92 umoles hydroxyl sites)/m^2 (assumed bidentate bonds)
# from Davis and Kent (1990) and
# used in Davis and Curtis (2003) Naturita GC Model
# Surface area (Mean of 10 values from 1-2 mm fraction) = 11.02 m^2/g (BET
Measurement)
# Used 7500 g rock/Lgw
# Of Total Sites: Very Strong Sites = 0.01 %, Strong Sites = 1.2 % (Davis and
Curtis)
# Total Sites = 158,688 umol sites/L gw (from 7500*11.02*1.92)
# Very Strong Sites = 0.0001*158688 = 15.87 umoles/L (SJM Calculation)
# Strong Sites = 0.012 * 158688 = 1904. umoles/L (SJM Calculation)
# Weak Sites = 0.9879 * 158688 = 156768 umoles/L (SJM Calculation)
#
# -equilibrate 1
# Hfo_WOH 1.568e-1 11.02 7500.0
# Hfo_SOH 1.904e-3 11.02 7500.0
# Hfo_VOH 1.587e-5 11.02 7500.0
# -no_edl
PRINT
# -reset true
ADVECTION
# -cells 20
# -shifts 200
# -punch 20
# -punch 10 20
# -punch_frequency 1
# -print 20
# -print_frequency 50
USER_GRAPH
# -headings PV Na C NH4*5 Ca*10 Cl SO4 U*1000 KD*25000 pH*1000
# -headings PV TOTADS CS TOT("U") KD
# -chart_title "Crescent Junction Vertical Transport Model"
# -axis_titles "PORE VOLUME" "Effluent Concentration (mg/L)"
# -axis_scale x_axis 0 10 1 0.1
# -axis_scale y_axis 0 25000.0 1000.0
# -initial_solutions false
# -plot_concentration_vs time
# -start
# 5 TOTADS = MOL("Hfo_WOUO2OH") + MOL("Hfo_SOUO2CO3-") + MOL("Hfo_VOUO2OH") +
MOL("Hfo_VOUO2CO3-")
# 6 CS = TOTADS/7500
# 7 KD = (CS/TOT("U"))*1000
# 10 GRAPH_X (STEP_NO + 0.5) / 20
# 20 GRAPH_Y TOT("Na")*23000, TOT("C")*12000, TOT("Amm")*18000*5,
TOT("Ca")*40000*10, TOT("Cl")*35900, TOT("S(6)")*96000, TOT("U")*238000*1000,
KD*25000, 1000*(-LA"H+")

```

```

# 20 GRAPH_Y TOT("U")*238000*1000, KD*25000
      Transport_vertical
      -end
PRINT
      -user_graph true
SELECTED_OUTPUT
      -file      CJ_transport.sel
      -totals    Na Amm K Ca Cl
      -molalities      NaX AmmHX KX CaX2
END
```



## **Appendix H**

### **Thermodynamic Database Used for PHREEQC Models**

# Phreeqc\_Davis\_Naturita\_GC\_Short

## SOLUTION\_MASTER\_SPECIES

# PHREEQC Database modified with Jim Davis model used in Naturita GC Model.

# See Davis and Curtis (2003)

# Removed all elements/species not used in models

#element	species	alk	gfw_formula	element_gfw
#				
H	H+	-1.0	H	1.008
H(0)	H2	0.0	H	
H(1)	H+	-1.0	0.0	
E	e-	0.0	0.0	0.0
O	H2O	0.0	O	16.0
O(0)	O2	0.0	O	
O(-2)	H2O	0.0	0.0	
Ca	Ca+2	0.0	Ca	40.08
Mg	Mg+2	0.0	Mg	24.312
Na	Na+	0.0	Na	22.9898
K	K+	0.0	K	39.102
Cl	Cl-	0.0	Cl	35.453
C	CO3-2	2.0	HCO3	12.0111
C(+4)	CO3-2	2.0	HCO3	
Alkalinity	CO3-2	1.0	Ca0.5(CO3)0.5	50.05
S	SO4-2	0.0	SO4	32.064
S(6)	SO4-2	0.0	SO4	
N	NO3-	0.0	N	14.0067
N(+5)	NO3-	0.0	N	
Amm	AmmH+	0.0	AmmH	17.0
U	UO2+2	0.0	238.0290	238.0290
U(6)	UO2+2	0.0	238.0290	238.0290

## SOLUTION\_SPECIES

H+ = H+	log_k	0.0	
	-gamma	9.0	0.0
e- = e-	log_k	0.0	
H2O = H2O	log_k	0.0	
Ca+2 = Ca+2	log_k	0.0	
	-gamma	5.0	0.1650
Mg+2 = Mg+2	log_k	0.0	
	-gamma	5.5	0.20
Na+ = Na+	log_k	0.0	
	-gamma	4.0	0.075
K+ = K+	log_k	0.0	
	-gamma	3.5	0.015
Cl- = Cl-	log_k	0.0	
	-gamma	3.5	0.015
CO3-2 = CO3-2	log_k	0.0	

Phreeqc\_Davis\_Naturita\_GC\_Short

-gamma 5.4 0.0

SO4-2 = SO4-2  
log\_k 0.0  
-gamma 5.0 -0.04

NO3- = NO3-  
log\_k 0.0  
-gamma 3.0 0.0

AmmH+ = AmmH+  
log\_k 0.0  
-gamma 2.5 0.0

#UO2+2 primary master species  
UO2+2 = UO2+2  
log\_k 0.0

H2O = OH- + H+  
log\_k -14.0  
delta\_h 13.362 kcal  
-analytic -283.971 -0.05069842 13323.0 102.24447  
-1119669.0  
-gamma 3.5 0.0

#O2 secondary master species  
2H2O = O2 + 4H+ + 4e-  
log\_k -86.08  
delta\_h 134.79 kcal

#H2 secondary master species  
2 H+ + 2 e- = H2  
log\_k -3.15  
delta\_h -1.759

#####

#MAJOR ION SPECIES FROM DAVIS AND CURTIS NRC REPORT TABLE 2-1. 2003

CO3-2 + H+ = HCO3-  
log\_k 10.329

CO3-2 + 2 H+ = CO2 + H2O  
log\_k 16.683

SO4-2 + H+ = HSO4-  
log\_k 1.98

#####

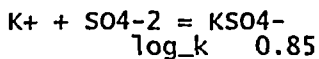
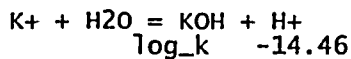
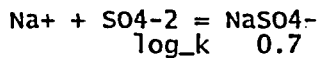
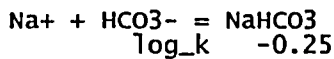
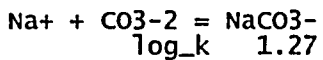
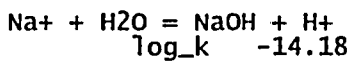
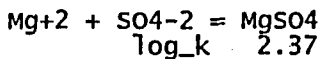
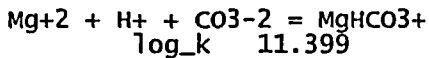
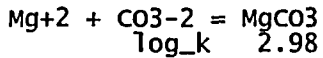
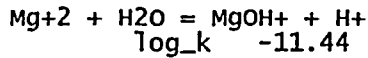
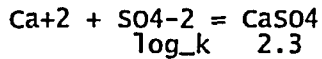
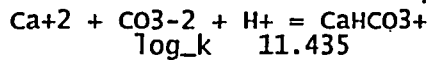
AmmH+ = Amm + H+  
log\_k -9.252  
delta\_h 12.48 kcal

AmmH+ + SO4-2 = AmmHSO4-  
log\_k 1.11

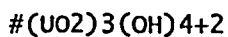
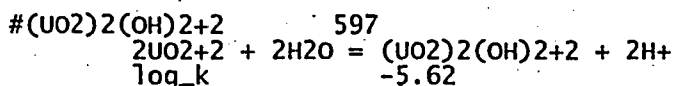
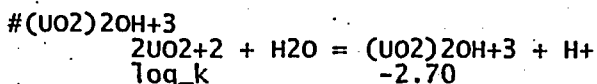
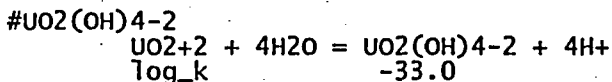
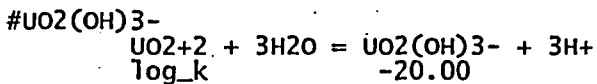
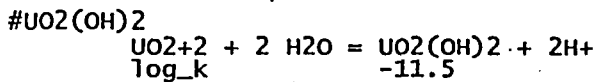
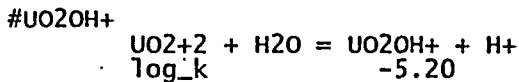
Ca+2 + H2O = CaOH+ + H+  
log\_k -12.78

Ca+2 + CO3-2 = CaCO3  
log\_k 3.224

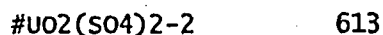
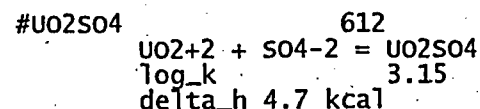
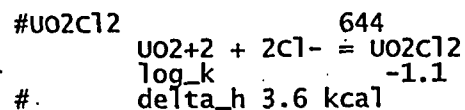
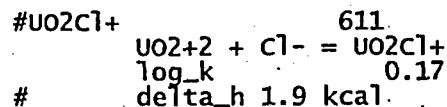
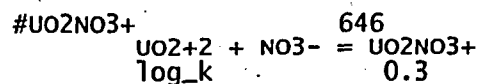
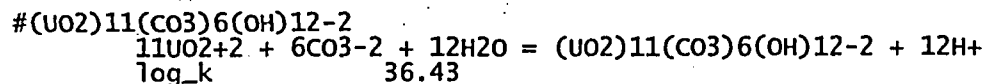
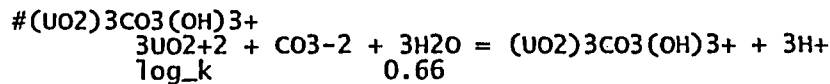
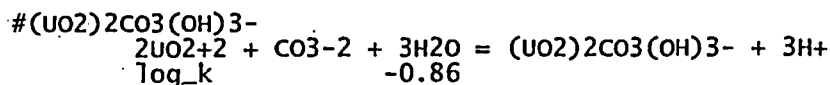
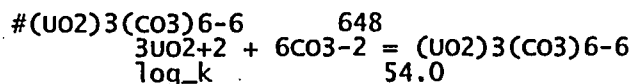
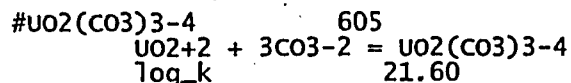
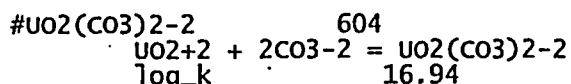
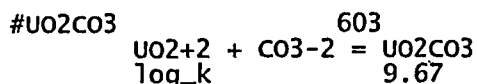
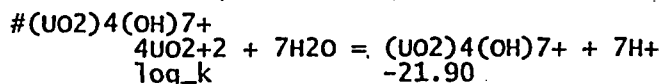
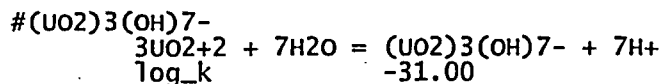
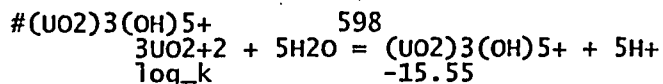
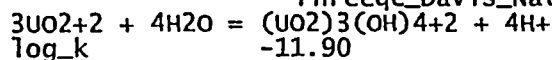
Phreeqc\_Davis\_Naturita\_GC\_Short



#URANIUM SPECIES FROM TABLE 2-1 DAVIS AND CURTIS NRC REPORT 2003



Phreeqc\_Davis\_Naturita\_GC\_Short



Phreeqc\_Davis\_Naturita\_GC\_Short  
 $\text{UO}_2 + 2\text{SO}_4 = \text{UO}_2(\text{SO}_4)_2$   
log\_k 4.14  
delta\_h 8.4 kcal

# PHASES

## Calcite

$\text{CaCO}_3 = \text{CO}_3^{2-} + \text{Ca}^{2+}$   
log\_k -8.48  
delta\_h -2.297 kcal  
-analytic -171.9065 -0.077993 2839.319 71.595

## Aragonite

$\text{CaCO}_3 = \text{CO}_3^{2-} + \text{Ca}^{2+}$   
log\_k -8.336  
delta\_h -2.589 kcal  
-analytic -171.9773 -0.077993 2903.293 71.595

## Dolomite

$\text{CaMg}(\text{CO}_3)_2 = \text{Ca}^{2+} + \text{Mg}^{2+} + 2\text{CO}_3^{2-}$   
log\_k -17.09  
delta\_h -9.436 kcal

## Gypsum

$\text{CaSO}_4 \cdot 2\text{H}_2\text{O} = \text{Ca}^{2+} + \text{SO}_4^{2-} + 2\text{H}_2\text{O}$   
log\_k -4.58  
delta\_h -0.109 kcal  
-analytic 68.2401 0.0 -3221.51 -25.0627

## Anhydrite

$\text{CaSO}_4 = \text{Ca}^{2+} + \text{SO}_4^{2-}$   
log\_k -4.36  
delta\_h -1.710 kcal  
-analytic 197.52 0.0 -8669.8 -69.835

## Halite

64  
 $\text{NaCl} = \text{Na}^+ + \text{Cl}^-$   
log\_k 1.582  
delta\_h 0.918 kcal

## Thenardite

65  
 $\text{Na}_2\text{SO}_4 = 2\text{Na}^+ + \text{SO}_4^{2-}$   
log\_k -0.179  
delta\_h -0.572 kcal

## Nahcolite

58  
 $\text{NaHCO}_3 = \text{Na}^+ + \text{HCO}_3^-$   
log\_k -0.548  
delta\_h 3.720 kcal

## Trona

59  
 $\text{NaHCO}_3 \cdot \text{Na}_2\text{CO}_3 \cdot 2\text{H}_2\text{O} = 2\text{H}_2\text{O} + 3\text{Na}^+ + \text{CO}_3^{2-} + \text{HCO}_3^-$   
log\_k -0.795  
delta\_h -18.0 kcal

## Natron

60  
 $\text{Na}_2\text{CO}_3 \cdot 10\text{H}_2\text{O} = 2\text{Na}^+ + \text{CO}_3^{2-} + 10\text{H}_2\text{O}$   
log\_k -1.311  
delta\_h 15.745 kcal

## Thermonatrite

61  
 $\text{Na}_2\text{CO}_3 \cdot \text{H}_2\text{O} = 2\text{Na}^+ + \text{CO}_3^{2-} + \text{H}_2\text{O}$

Phreeqc\_Davis\_Naturita\_GC\_Short

log\_k 0.125  
delta\_h -2.802 kcal

#####  
# Uranium Mineral FROM TABLE 2-2 DAVIS AND CURTIS NRC REPORT 2003

Schoepite 602  
 $\text{UO}_2(\text{OH})_2 + 2\text{H}^+ = \text{UO}_2 + 2\text{H}_2\text{O}$   
log\_k 4.93

Rutherfordine 606  
 $\text{UO}_2\text{CO}_3 = \text{UO}_2 + \text{CO}_3 - 2$   
log\_k -14.49

Gummite 600  
 $\text{UO}_3 + 2\text{H}^+ = \text{UO}_2 + \text{H}_2\text{O}$   
log\_k 10.403  
delta\_h -23.015 kcal

$\text{UO}_3(\text{gamma})$  599  
 $\text{UO}_3 + 2\text{H}^+ = \text{UO}_2 + \text{H}_2\text{O}$   
log\_k 7.719  
delta\_h -19.315 kcal

#####

$\text{Na}_4\text{UO}_2(\text{CO}_3)_3$  571  
 $\text{Na}_4\text{UO}_2(\text{CO}_3)_3 = 4\text{Na}^+ + \text{UO}_2 + 3\text{CO}_3 - 2$   
log\_k -16.290

B-UO<sub>2</sub>(OH)<sub>2</sub> 601  
 $\text{UO}_2(\text{OH})_2 + 2\text{H}^+ = \text{UO}_2 + 2\text{H}_2\text{O}$   
log\_k 5.544  
delta\_h -13.730 kcal

#####  
# CO<sub>2</sub> gas FROM TABLE 2-1 DAVIS AND CURTIS NRC REPORT 2003

CO<sub>2</sub>(g)  
CO<sub>2</sub> = CO<sub>2</sub>  
log\_k -1.472  
# delta\_h -4.776 kcal  
# -analytic 108.3865 0.01985076 -6919.53 -40.45154  
669365.0  
#####

H<sub>2</sub>O(g)  
H<sub>2</sub>O = H<sub>2</sub>O  
log\_k 1.51  
delta\_h -44.03 kJ  
# Stumm and Morgan, from NBS and Robie, Hemmingway, and Fischer (1978)  
# Gases from LLNL.dat...

Amm(g)  
Amm = Amm  
log\_k 1.7966

EXCHANGE\_MASTER\_SPECIES  
X X-

Phreeqc\_Davis\_Naturita\_GC\_Short

EXCHANGE\_SPECIES

X- = X-  
log\_k 0.0

Na+ + X- = NaX  
log\_k 0.0  
-gamma 4.0 0.075

K+ + X- = KX  
log\_k 0.7  
-gamma 3.5 0.015  
delta\_h -4.3 # Jardine & Sparks, 1984

# !!!!!

# H+ + X- = HX  
log\_k 1.0  
-gamma 9.0 0.0

AmmH+ + X- = AmmHX  
log\_k 0.6  
-gamma 2.5 0.0  
delta\_h -2.4 # Laudelout et al., 1968

Ca+2 + 2X- = CaX2  
log\_k 0.8  
-gamma 5.0 0.165  
delta\_h 7.2 # Van Bladel & Gheyl, 1980

Mg+2 + 2X- = MgX2  
log\_k 0.6  
-gamma 5.5 0.2  
delta\_h 7.4 # Laudelout et al., 1968

#####  
# Surface Species FROM TABLE 5.4 DAVIS AND CURTIS NRC REPORT 2003

SURFACE\_MASTER\_SPECIES

Hfo\_v Hfo\_vOH  
Hfo\_s Hfo\_sOH  
Hfo\_w Hfo\_wOH

#####  
SURFACE\_SPECIES

# Very strong binding site Hfo\_ss  
# Strong binding site Hfo\_s  
# Weak binding site Hfo\_w

Hfo\_vOH = Hfo\_vOH  
log\_k 0.0

Hfo\_sOH = Hfo\_sOH  
log\_k 0.0

Hfo\_wOH = Hfo\_wOH  
log\_k 0.0

#####  
# Uranium Surface Species FROM TABLE 5.4 DAVIS AND CURTIS NRC REPORT 2003  
# Uranyl

Hfo\_wOH + UO2+2 + H2O = Hfo\_wOUO2OH + 2H+  
log\_k -6.74

Hfo\_sOH + UO2+2 + CO2 + H2O = Hfo\_sOUO2CO3- + 3H+  
log\_k -8.00



Phreeqc\_Davis\_Naturita\_GC\_Short

Hfo\_vOH + UO2+2 + H2O = Hfo\_vOUO2OH + 2H+  
log\_k -2.06

Hfo\_vOH + UO2+2 + CO2 + H2O = Hfo\_vOUO2CO3- + 3H+  
log\_k -6.36

#####

END